Exceptional preservation of soft tissues in Mesozoic coleoid cephalopods : the keys to a story

Alison J. Rowe

Sorbonne Université

Ecole doctorale 398 : Géosciences, Ressources Naturelles et Environnent

Centre de Recherche en Paléontologie – Paris – (CR2P) UMR 7207

Conservation exceptionnelle des tissus mous de céphalopodes coléoïdes mésozoïques : les clés d'une histoire

Exceptional preservation of soft tissues in Mesozoic coleoid cephalopods: The keys to a story

Par Alison J. Rowe

Thèse de doctorat en Biogéoscience

Co-dirigée Dirigée par Loïc Villier et Isabelle Rouget

et co-encadrée par Isabelle Kruta

Devant un jury composé de :

M. Jorge Cubo Garcia, Professeur, Sorbonne Université – Président

M. Martin Košťák, Professeur, Karlova University – Rapporteur

M. Pascal Neige, Professeur, Université de Bourgogne – Rapporteur

M. Arnaud Brayard, Directeur de Recherche CNRS, Université de Bourgogne – Examinateur

M. Dirk Fuchs, Doctor, Bayerische Staatssammlung für Paläontologie und Geologie – Examinateur

M. Loïc Villier, Professeur, Sorbonne Université – Co-Directeur de thèse

Ms. Isabelle Rouget, Professeur, Muséum national d'Histoire naturelle – Co-Directeur de thèse

Ms. Isabelle Kruta, Maître de Conférences, Sorbonne Université - Co-Directeur de thèse

To my younger self who thought this wasn't possible.

And for the 'village' that helped me to do it.

ACKNOWLEDGEMENTS:

When I first began my undergraduate program in 2014, I never imagined that almost 10 years later I would be submitting a PhD thesis and preparing to defend it. None of this would have been possible without my 'village' – the community of people who have supported me in this process and contributed to this achievement - and it is to them I owe a debt of gratitude. Reflecting on this journey, I am first transported back to writing the initial application letters for various undergraduate programs. Though this was a big step into the unknown for me, the abundance of support I received from those around me (despite the changes it would mean for them, too) enabled me to pursue my dream. As I sit with a final draft of my PhD thesis on my desk, I am aware of just how much my life has changed. The journey was difficult at times, but I am grateful for all it has taught me.

Searching for the right words to express the extent of my gratitude to my friends and mentors is not an easy task. Though I was reminded of something I learned during my master's program at the University of Bristol: If you are stuck, keep reading. (And even if you are not stuck, keep reading!) So, I did. Not a paper, but I picked up a book that I've been wanting to read for a while. Flipping through the pages, I came across a citation that interested me and as I found the relevant page in the back, I saw the name it was associated with: Neil Landman. This, to me, was significant as Neil has been one of my mentors from almost the beginning of my journey. It seemed fitting that when I was seeking help and inspiration, it was Neil's name I found. Looking further through the book I also found two of my current advisors, members of my thesis jury, and co-authors I have worked with. This moment reminded me that the giants upon whose shoulders we stand are very real people, and I was grateful that these giants have been part of my journey. But I need to go back further, as there are other people that were there at the beginning and kickstarted 'all things cephalopod'. Academically, I am indebted to David Seidemann, and the very first 'radiator chat' at the Brooklyn College advisory session, and of course, to Matt Garb who was the person to introduce me to cephalopods. The available spot in your lab, and the matter-of-fact belief you had in me, enriched the opportunities and experiences I had at an undergrad level, and led to a world where a masters and a PhD were a reality. And James Witts, I still hear your voice in my head, "it's time to stop collecting data and start writing it up". To Neil, Seidemann, Matt, James, Kirk, as well as the members, and honorary members, of Landman's Cretaceous Crew, thank you. You made me feel part of something very special.

Sincere thanks, too, to Mike Benton, Armin Elsler, Tom Stubbs, and Suresh Sing for their patience and guidance as I ventured into the world of vertebrate paleontology for my masters.

Fast forward to today, and I am indebted to the amazing advisors that have been guiding me for the last three years, Isabelle Rouget, Isabelle Kruta, and Loïc Villier. I am incredibly fortunate to be a part of such a great team and have learned so much from each of them. My sincere thanks. Despite the abundance of their own work, they have patiently addressed my questions, fostered discussion, offered new perspectives, given me structure, supported me throughout this PhD, and had a huge impact on me professionally. They have also undertaken the painstaking task of reading and suggesting edits on the proofs of this manuscript – any mistakes that may remain are due to my own oversight.

Sincere thanks also to those who have been part of my thesis committee (in alphabetical order: Arnaud Brayard, Jorge Cubo Garcia, Dirk Fuchs, Henk-Jan Hoving, Romain Jattiot) and the external members of my thesis jury (Arnaud Brayard, Dirk Fuchs, Martin Košťák, Pascal Neige), who have given their expertise and valuable time to my PhD. Thank you, too, to my friends in the CR2P lab who have welcomed me and been so patient with my very poor French. To Alexandre Lethiers, who has brought 'my' fossil coleoids to life so beautifully, to Pierre Gueriau, Olivier Bethoux, and Natalie Poulet who have taught me how to work with the imaging methods I've relied on in this thesis, to Florent Goussard who provided help every time I have asked, to Didier Merle for accommodating me in the museum collections, and to Lilian Cazes for the beautiful photographs of specimens.

Finally, to my family – both biological, and found. You are a fundamental part of this process. You've supported me, celebrated, and commiserated with me and, when needed, carried me. Gran, I've felt your presence more acutely than normal the past month or two, and I am reminded that you are still with me despite not physically being here. Mum, Jess, Hugh, Dad, and Kathleen, you are foundational to this entire journey, believing in me when I didn't think I could, giving me perspective, but most of all providing unwavering support. Thank you for your love and strength. Thank you, too, to my friends that have been following the same university path. Kayla, Lisa, Broph, Jone, Ellie, Adrian. I don't think I would be here without you. And to my very own Golden Girls, Charlotte and Nat. Thank you. For everything. And forever. Finally, Mat, Buddy, and Holly, thank you for being by my side in this marathon and for holding my hand across the finishing line. Now everything is easy 'cause of you.

Table of Contents

CHAPTER 3

CHAPTER 4

ANNEX

Foreword

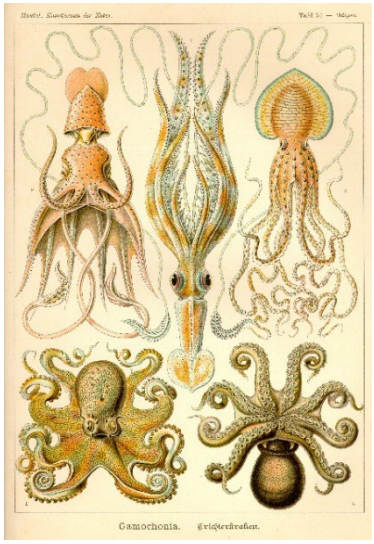

Haeckel (1904)

Cephalopods are some of the ocean's most charismatic and enigmatic creatures and have long held a fascination for humankind. Aristotle is well known for his work on the shallow-water forms, both marveling at their mesmerizing color changes and describing the male hectocotylus for the first time; coleoids from the deep sea have inspired myths and legends for centuries, with the Kraken terrorizing folkloric seafarers. Coleoids have also inspired biomedical and bio- and material engineering advances, leading to groundbreaking work on nerve cell function, and applications for robotic engineering (Hanlon *et al.* 2018). Today, there are more than 800 described coleoid cephalopod species which are widely diverse and inhabit almost all marine habitats. Their sophisticated visual illusions - skin patterning, rapid coloration changes, and an almost jewel-like appearance with bioluminescence - make them some of the most beautiful animals on the earth. They have developed the most complex brains among invertebrate animals and the ability to perform sophisticated behaviors; they also play a key role in modern oceans and food webs (Boyle & Rodhouse 2008).

Arising during the Cambrian (Strugnell *et al.* 2006; Kröger *et al.* 2011; Tanner *et al.* 2017; Uribe & Zardoya 2017; Sanchez *et al.* 2018; Hildenbrand *et al.* 2021), cephalopods have a long evolutionary history that spans almost 500 million years. Molecular studies show that the internally shelled forms, the coleoids, diverged from the Nautiloidea in the early Devonian

(Tanner *et al.* 2017, López-Córdova *et al.* 2022). Current coleoid diversity is more recent, and crown groups originated in the Mesozoic (Tanner *et al.* 2017, López-Córdova *et al.* 2022) though the evolutionary pathways are not clear. As such, there is a real need to understand their evolutionary history, drivers of their diversification, and the timing of their adaptations. Fossils have a key role to play in finding answers to these questions. Not only do they provide tangible evidence to correlate with estimated molecular divergence dates, but they also reveal the timing of morphological innovations. By understanding these innovations, we can infer associated behaviors and their roles in past ecosystems.

However, coleoids are rarely preserved in the fossil record. The majority of known fossil taxa come from deposits of exceptional preservation (Lagerstätten). The internalized shell (gladius) is the most common structure to preserve and as a result, systematic studies of fossils have been mainly based on gladius morphology. In the last two decades, the use of new imaging methods has enabled us to visualize the remains of soft tissues and include them to a greater extent. As a result, they have begun to be used in phylogenetic reconstructions (Sutton *et al.* 2016; Whalen & Landman 2022), and to interpret lifestyles (e.g. Klug *et al.* 2021). These high-resolution imaging methods (e.g., UV, X-ray computed tomography, μXRF major-to-trace elemental mapping) are increasingly used in paleontological studies and have proven successful in recording anatomical features of cephalopods that are not visible using traditional methods (Kruta *et al.* 2011, 2013, 2016; Gueriau *et al*. 2018).

Among the known Mesozoic Lagerstätten preserving a wealth of coleoid material with exceptionally preserved soft tissues, the localities of La Voulte-sur-Rhône (Jurassic) and Lebanon (Cretaceous) were chosen as primary targets for this work. Each had a different depositional environment and preservation style, and they represent two important periods in cephalopod evolution.

This material provides the perfect opportunity to exploit a variety of imaging techniques, revealing information on these important fossilized soft tissues. The quality and completeness of anatomical data obtained enables meaningful morphological comparison with extant forms and contributes to the current state of coleoid systematics.

The main objectives of this thesis are to utilize the large panel of imaging techniques to:

- Identify, reconstruct, and describe previously unknown, or poorly known soft tissues and internal organs of Mesozoic coleoid taxa.

- Provide higher resolution taxa descriptions and allow comparative analyses between Mesozoic and extant forms.
- Identify the morphological innovations and interpret associated behaviors and potential habitats occupied within the framework of the ecology of the dynamic Mesozoic marine ecosystems.

The outline of this manuscript follows the thesis goals and draws attention to the importance of anatomical studies. The first chapter provides a short overview the diversity of Extant cephalopods, specifically coleoids, as well as their Bauplan and ecology. This is followed by an introduction to the systematics of Mesozoic fossil gladius bearing coleoids, and a description of the main Mesozoic Lagerstätten where they are found.

The second chapter highlights the value of comparative anatomy with Extant taxa, which is essential for grasping the complex fossil structures observed in the following chapters. The first virtual dissection of *V. infernalis* is provided and shows that even with the popularization of X-Ray imaging techniques, data are still lacking on rare groups or taxa.

The third chapter focuses on the study of the Octobrachia from La Voulte sur Rhone. Non-invasive imaging techniques provided new anatomical data on fossil coleoids preserved in 3D, which enabled high resolution taxa descriptions and the identification of a new species.

The fourth chapter takes a different approach and combines physico-chemical imaging and morphological measurements on 54 specimens of the same coleoid species. The results highlight a significant variability in the morphology of the gladii and arm size, and generated discussion on diagnostic and ontogenetic features of the species, but questions remain about the extent of the impact of taphonomic biases.

Finally, a conclusion summarizes the main results and suggests perspectives for future studies.

BIBLIOGRAPHY

BOYLE, P. and RODHOUSE, P. 2008. *Cephalopods: ecology and fisheries*. John Wiley & Sons.

GUERIAU, P., JAUVION, C. and MOCUTA, C. 2018. Show me your yttrium, and I will tell you who you are: implications for fossil imaging. *Palaeontology*, **61**, 981–990.

HAECKEL, E., 1998. Kunstformen der Natur (1904). Prestel, München.

HANLON, R., VECCHIONE, M. and ALLCOCK, L. 2018. *Octopus, Squid, and Cuttlefish: A visual, scientific guide to the oceans' most advanced invertebrates*. University of Chicago Press.

HILDENBRAND, A., AUSTERMANN, G., FUCHS, D., BENGTSON, P. and STINNESBECK, W. 2021. A potential cephalopod from the early Cambrian of eastern Newfoundland, Canada. *Communications Biology*, **4**, 1–11.

KRÔGER B, VINTHER, J. and FUCHS, D. 2011. Cephalopod origin and evolution: A congruent picture emerging from fossils, development and molecules: Extant cephalopods are younger than previously realised and were under major selection to become agile, shell-less predators. *BioEssays*, **33**, 602–613.

KRUTA, I., LANDMAN, N., ROUGET, I., CECCA, F. and TAFFOREAU, P. 2011. The role of ammonites in the Mesozoic marine food web revealed by jaw preservation. *Science*, **331**, 70–72.

———, ———, ———, ——— and ———. 2013. The radula of the Late Cretaceous scaphitid ammonite *Rhaeboceras halli* (Meek and Hayden, 1856). *Palaeontology*, **56**, 9–14.

———, ROUGET, I., CHARBONNIER, S., BARDIN, J., FERNANDEZ, V., GERMAIN, D., BRAYARD, A. and LANDMAN, N. 2016. *Proteroctopus ribeti* in coleoid evolution. *Palaeontology*, **59**, 767–773.

LÓPEZ-CÓRDOVA, D. A., AVARIA-LLAUTUREO, J., ULLOA, P. M., BRAID, H. E., REVELL, L. J., FUCHS, D. and IBÁÑEZ, C. M. 2022. Mesozoic origin of coleoid cephalopods and their abrupt shifts of diversification patterns. *Molecular Phylogenetics and Evolution*, **166**, 107331.

SANCHEZ, G., SETIAMARGA, D. H. E., TUANAPAYA, S., TONGTHERM, K., WINKELMANN, I. E., SCHMIDBAUR, H., UMINO, T., ALBERTIN, C., ALLCOCK, L., PERALES-RAYA, C., GLEADALL, I., STRUGNELL, J. M., SIMAKOV, O. and NABHITABHATA, J. 2018. Genus-level phylogeny of cephalopods using molecular markers: current status and problematic areas. *PeerJ*, **6**, e4331

STRUGNELL, J., JACKSON, J., DRUMMOND, A. J. and COOPER, A. 2006. Divergence time estimates for major cephalopod groups: evidence from multiple genes. *Cladistics*, **22**, 89–96.

SUTTON, M., PERALES-RAYA, C. and GILBERT, I. 2016. A phylogeny of fossil and living neocoleoid cephalopods. *Cladistics*, **32**, 297–307.

TANNER, A. R., FUCHS, D., WINKELMANN, I. E., GILBERT, M. T. P., PANKEY, M. S., RIBEIRO, Â. M., KOCOT, K. M., HALANYCH, K. M., OAKLEY, T. H., DA FONSECA, R. R., PISANI, D. and VINTHER, J. 2017. Molecular clocks indicate turnover and diversification of modern coleoid cephalopods during the Mesozoic Marine Revolution. *Proceedings of the Royal Society B: Biological Sciences*, **284**, 20162818.

URIBE, J. E. and ZARDOYA, R. 2017. Revisiting the phylogeny of Cephalopoda using complete mitochondrial genomes. *Journal of Molluscan Studies*, **83**, 133–144.

WHALEN, C. D. and LANDMAN, N. H. 2022. Fossil coleoid cephalopod from the Mississippian Bear Gulch Lagerstätte sheds light on early vampyropod evolution. *Nature Communications*, **13**, 1107.

CHAPTER 1: CEPHALOPOD PRESENT & PAST: AN OVERVIEW

1.1 ~ Extant Cephalopod Diversity

Current cephalopods belong to two subclasses: the Nautiloidea (Fig. 1.1A), who possess external, chambered shells, and the Coleoidea (Fig 1.1B-G), whose shells are internalized. These internal shells are chambered in cuttlefishes (Fig. 1.1E) and Spirula (Fig. 1.1G) or reduced to an organic vestige (e. g. the squid 'pen' (Fig. 1.1F), the delicate, ovoid-shaped gladius of Idiosepius, and the stylets and U, V- or saddle- shaped shells of certain Cirrate (Fig. 1.1C) and Incirrate octopods. Some forms (certain Incirrate octopods like Amphioctopus (Fig. 1.1D) have lost them altogether (Boyle & Rodhouse 2008; Bizikov & Toll 2016; Ponder *et al.* 2020). Though Nautiloidea prospered in the early Palaeozoic, today they are represented by just two extant genera belonging to the order Nautilida (Pohle *et al.* 2022), *Nautilus* and *Allonautilus* (Boyle & Rodhouse 2008). As a result, Coleoidea represent most of the extant cephalopod species in modern oceans (Nesis *et al.* 1987; Jereb & Roper 2005, 2010; Kröger *et al.* 2011; Jereb *et al.* 2016; Tanner *et al.* 2017; Jaitly *et al.* 2022).

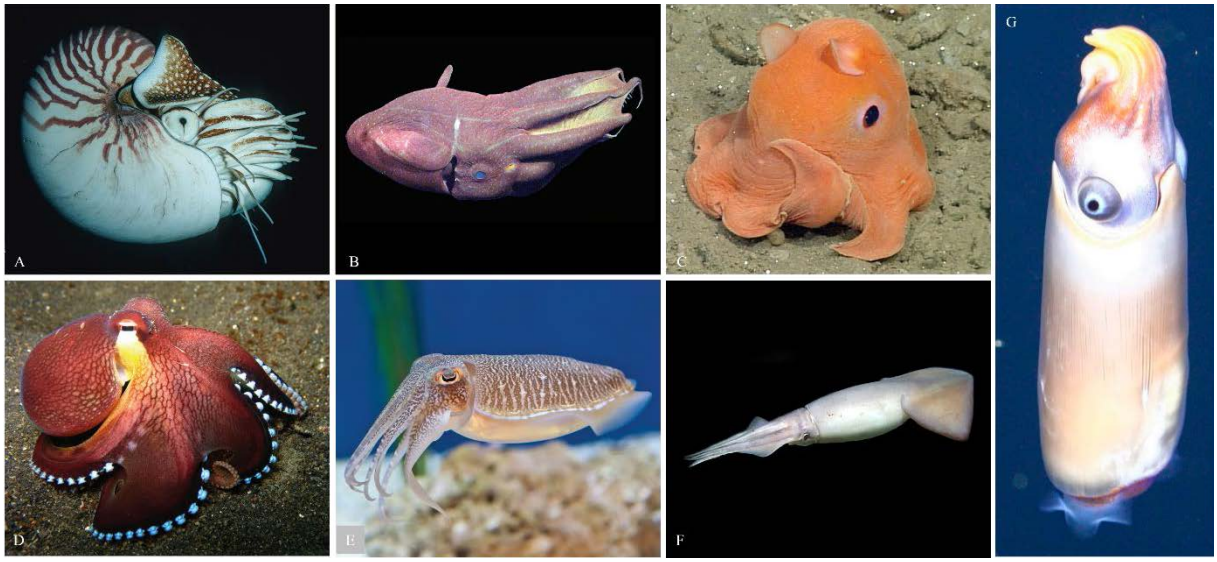

Figure 1.1: Examples of modern cephalopods. Photographs: Ponder et al. 2020 (A-F), & Lindsay et al. 2020 (G). *Nautilus belauensis*, Saunders 1981 (Nautilidae), Palau. © Gerald and Buff Corsi/Focus on Nature, Inc (A). *Vampyroteuthis infernalis* Chun 1903 (Vampyroteuthidae), California. © 2007 MBARI (B). *Opisthoteuthis sp*. (Opisthoteuthidae), Monterey Bay, California. © 2013 MBARI (Cirrate Octopod) (C). *Amphioctopus marginatus* (Taki 1964) (Amphitretidae), Indonesia. © Christine Huffard (Incirrate Octopod) (D). *Sepia pharaonic* Ehrenberg 1831 (Sepiidae, western Indian Ocean. © Gerald and Buff Corsi/Focus on Nature, Inc (E). *Dosidicus gigas* (d'Orbigny 1835) (Ommastrephidae. © 2009 MBARI (F). *Spirula spirula* (Linnaeus 1758) (Spirulidae) (G).

Coleoids are comprised of two superorders (Fig. 1.2): Decabrachia (cuttlefish and squid), whose ten arms include a differentiated elongate pair of tentacles in the ventro-lateral position (arm pair IV), and Octobrachia, which have either eight arms (octopuses) or, as in the case of the modern vampire squid Vampyroteuthis, eight arms and a pair of retractable filaments in the

dorso-lateral position; these represent a modified arm pair II (Young 1967; Vecchione *et al.* 2000; Nixon & Young 2003; Nishiguchi & Mapes 2008; Nixon 2011a; Ponder *et al.* 2020). Modern octopuses include cirrate forms (Fig. 1.1C) that possess fins and sensory filamentous appendages on their arms (cirri), and incirrate forms (Fig. 1.1D), which lack these features.

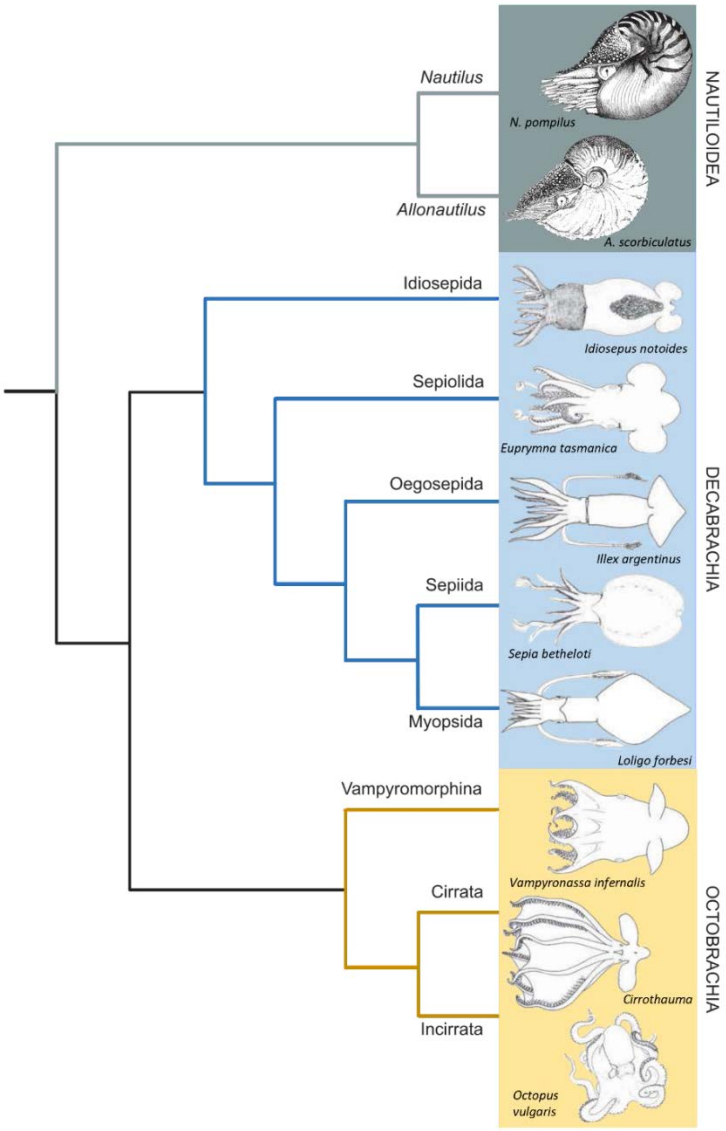

Figure 1.2: Simplified relationships of the extant cephalopods (based on Anderson & Lindgren 2021). Nautiloidea (*Nautilus* and *Allonautilus*) are a sister taxon to the Coleoidea (Decabrachia and Octobrachia). The 10-armed decabrachians include the Idiosepida (pygmy squid), Oegopsida (mainly pelagic squids), Sepiids (cuttlefish) and Myopsida (neritic squids). Note that Spirulida is not included in this tree. Octobrachia includes the Vampyromorphina (*V. infernalis*), and the Octopoda (Cirrata and Incirrata, finned, and non-finned groups respectively). Silhouettes are from Jereb & Roper (2005).

1.1.1 ~ Diversity of Decabrachia and Octobrachia

There are ~800 species of coleoid and they reflect a wide range of morphological diversity (Jereb & Roper 2005, 2010; Jereb *et al.* 2016). This varies from elongated forms with

streamlined dynamics (Fig. 1.1F, G), to groups with a slightly bulbous and rounded appearance (Fig. 1.1C, D). There are genera whose mantles are just a few millimeters in length, and those that are more than two meters (Jereb & Roper 2010; Nixon 2011a, *b*; Jereb *et al.* 2016; Guerra 2019; Ponder *et al.* 2020). Examples of this size difference can be seen in both suborders. In Decabrachia, the tiny Pygmy cuttlefish (*Idiosepius*) has a maximum mantle length of 20 mm (Jereb & Roper 2010) in contrast with the *Architeuthis dux* Steenstrup 1857, the giant squid, which can reach around 13 meters from the posterior part of the mantle to the anterior tip of the arm crown (Nixon 2011*b*; Hanlon & Messenger 2018; Ponder *et al.,* 2020). In Octobrachia, *Octopus wolfi* (Wülker 1913) has a maximum total length of 45 mm (Jereb & Roper 2010), while the Giant Pacific Octopus (*Enteroctopus dofleini* (Wülker 1910)) is generally at least three meters in total body length (including arms) and can potentially reach up to six meters (Jereb & Roper 2010; Ponder *et al.* 2020).

1.1.2 ~ Bauplan

The bodies of all coleoids are defined by two distinct sections (Fig. 1.3): the anterior cephalopodium, which includes the head, arm crown, and funnel, and the visceropalium, which comprises the mantle, mantle cavity, internal organs, shell, and any fins (Nixon 2011*a*; Ponder *et al.* 2020). The arm crown (Fig. 1.4) of all living coleoids has several distinctive features that are used to determine taxonomic relationships (Nixon 2011*a*). This includes the number of arms as previously mentioned, as well as the armature (Fuchs *et al.* 2021). The suckers are also a distinctive form of armature on all living Coleoidea, though the morphology differs between Decabrachia and Octobrachia (Kier & Smith 1990; Nixon & Young 2003, Nixon 2011*a*; Ponder *et al.* 2020; Fuchs *et al.* 2021). Decabrachian suckers are attached to the arms by narrow pedunculate stalks and have a proteinous, rigid ring lining the inside of the sucker (sucker ring). In some groups these rings have a smooth oral surface (e.g., Sepiolida), or blunt or sharp teeth (e.g., Sepiida, and Loliginida, Oegopsida respectively), and in several Oegopsid families these rings develop into hooks (Fuchs *et al.* 2021). Octobrachia lack this ring, and their symmetrical suckers are attached to the arm with broad, non-pedunculate bases (Nixon 2011*a*; Ponder *et al.*

2020; Fuchs *et al.* 2021). Cirri are a characteristic feature of Cirrata and Vampyromorpha. These slender sensory filaments are paired on the arms and positioned laterally to the suckers.

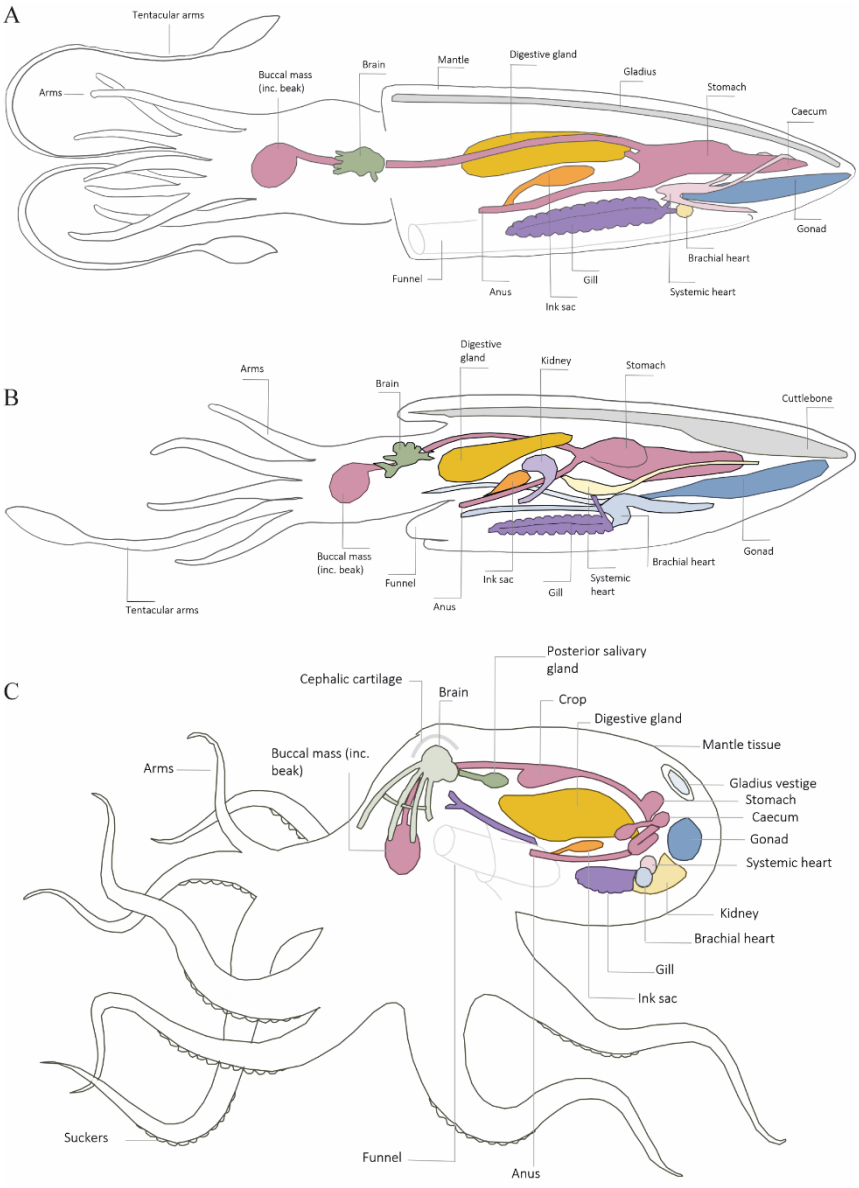

Figure 1.3: Simplified anatomy of a modern squid (Decabrachia), cuttlefish (Decabrachia) and octopus (Octobrachia) showing the arm configuration and internal organs. Modified from Hanlon & Messenger 2018. The anterior cephalopodium includes the head, arm crown, and funnel; the visceropalium comprises the mantle, mantle cavity, internal organs, shell, and fins (if present).

Internalization of the cephalopod shell within the mantle is linked with key innovations in the coleoid body plan. It has enabled more active life modes, increased potential for habitat transitions, and contributed to the modern diversity of the group (Mangold & Young 1998; Bizikov 2004; Kröger *et al.* 2011, Nixon 2011*a*; Bizikov & Toll 2016, Fuchs *et al.* 2016*a*;

Ponder *et al.* 2020; Jaitly *et al.* 2022). Its structure and morphology vary considerably (Bizikov & Toll 2016). The calcified chambered shell of the cuttlefish (Fig. 1.1E) and coiled shell of the Spirula (Fig. 1.1G) help the animals regulate their buoyancy in the water (Bizikov 2004; Bizikov & Toll 2016; Fuchs *et al.* 2016*a*). However, most major groups of extant coleoids (loliginids, oegopsids, vampyroteuhids, sepiolids, and the cirrate and incirrate octopods) have decalcified shell vestiges made from a composition of beta chitins and proteins (Hunt & Nixon 1981; Toll 1988; Bizikov & Toll 2016). These are commonly known as a gladius (plural: gladii) and serve both to support the soft body and provide muscular attachment sites (Bizikov & Toll 2016, Fuchs *et al.* 2016a). Several coleoid groups (including some sepiolida, Idiosepiidae, and incirrate octopods, Argonautoidea, Bolitenoidea, and some Octopodidae) have lost the shell entirely (Voight 1997; Bizikov 2004; Bizikov & Toll 2016).

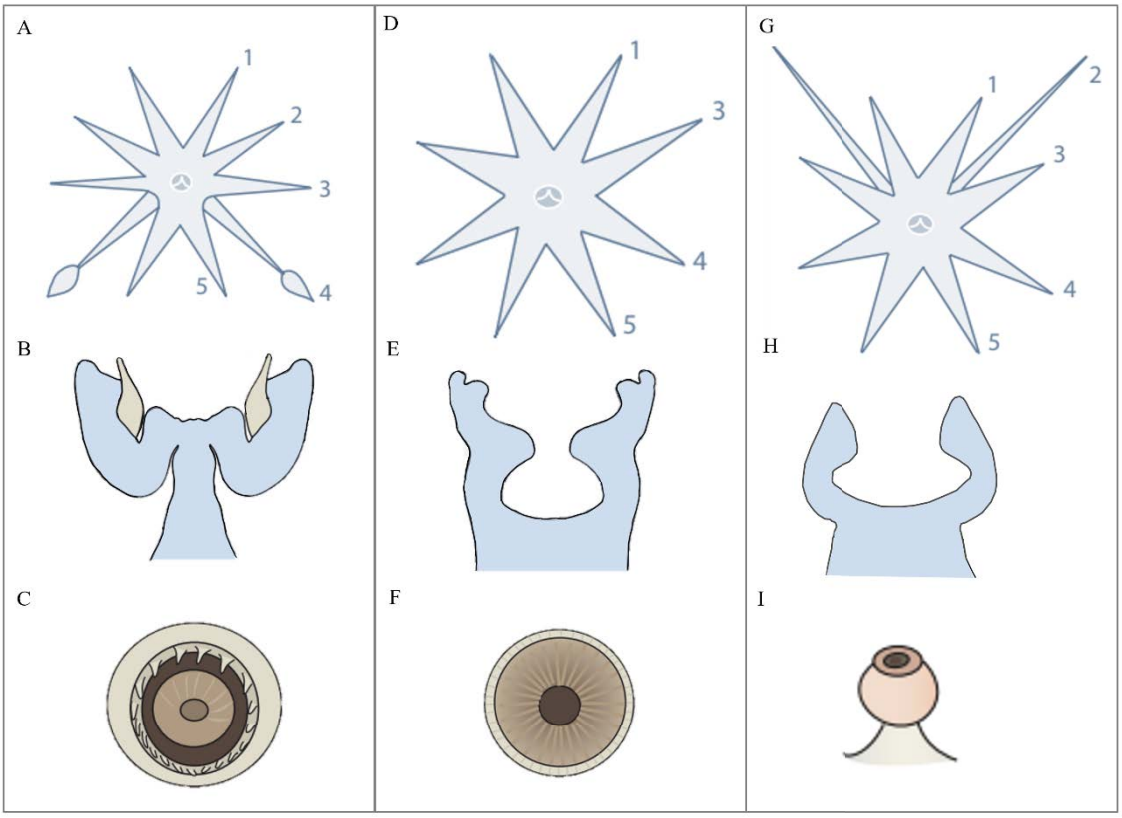

Figure 1.4: Arm configuration and sucker morphology for Decabrachia (A-C): showing the tentacular arm pair (arm pair 4) in ventro-lateral position (A), pedunculated sucker stalk and profile of the sucker ring (B), and oral view of the sucker showing the teeth on the sucker ring(C); Octobrachia (D-F): Note the absence of the tentacular arm pair (D), the absence of sucker ring in profile and oral views (E, F); *Vampyroteuthis* (G-I): showing the filamentous arm pair (arm pair 2) in dorso-lateral position (G), and the sucker in profile view (H, J). Modified from Ponder *et al.* 2020.

The Octobrachia gladius is reduced in size in multiple lineages. The vestigial gladius in living Cirrata (U-shaped in opisthoteuthids and grimpoteuthids (Fig. 1.1C), V-shaped in cirroctopodids, and saddle-shaped in cirroteuthids) provides support for the fins, which are the primary means of locomotion (Bizikov 2004; Collins & Villanueva 2006; Bizikov & Toll 2016; Vecchione *et al.* 2016) for these abyssal species. Cirrata employ a variety of lifestyles from benthic (opisthoteuthids), to benthopelagic (grimpoteuthids and cirroctopodids) with occasional pelagic excursions (cirroteuthids). In the Incirrata (Fig. 1.1D), the most common forms (Octopodidae) are benthic, and they use their arms to crawl over the substrate and manipulate objects (Bizikov 2004). Their spindle-shaped stylets serve as an attachment site for the funnel muscles, which enables their jetting behavior (Bizikov 2004; Nixon 2011*a*; Bizikov & Toll 2016; Ponder *et al.* 2020). Some shallow-water octopods have lost these stylets and the ability to jet-swim (Voight 1997; Ponder *et al.* 2020). However, the progressive reduction, or loss, enabled more flexibility and plasticity in the mantle. This was a beneficial exaptation to benthic life as it allowed octopuses to exploit small crevices while hunting or avoiding predators (Bizikov 2004; Boyle & Rodhouse 2008; Hanlon & Messenger 2018; Ponder *et al.* 2020).

1.2 ~ Extant Coleoid Ecology

Today, modern coleoids (Fig. 1.1) have a wide range of morphological diversity (Jereb & Roper 2005, 2010; Sanchez *et al.* 2018). Both superorders (Decabrachia and Octobrachia), are generally active predators that inhabit all the world's oceans, and they occupy a wide range of benthic and pelagic habitats (Voss & Sweeney 1998; Boyle & Rodhouse 2008; Nixon 2011b; Jaitly *et al.* 2022). Despite this ubiquity, many species are listed as Data Deficient on the IUCN Red List (Kemp *et al.* 2012; Xavier *et al.* 2015). Indeed, of the ~800 coleoid species that have been described (Xavier *et al.* 2015; Guerra 2019), there is only sufficient data to understand the life habits (e.g., feeding ecology, habitat, distribution, reproductive biology) of about 60 (Jereb & Roper 2005, 2010; Xavier *et al.* 2015; Jereb *et al.* 2016).

The greatest known diversity of coleoid cephalopods is from coastal forms (oceanic and mesopelagic), while the biology of offshore species is lesser known (Boyle & Rodhouse 2008; Hoving *et al.* 2014; Xavier *et al.* 2015). In pelagic taxa, active locomotion is produced by jet propulsion, as well as fins, which help the animal to maneuver (Boyle & Rodhouse 2008). Benthic groups, such as coastal octopuses use jet propulsion only for rapid escape or predatory movements and use their suckered arms to move through their habitat (Hanlon & Messenger

2018). Demersal forms generally have a more rounded body and advanced crypsis techniques including aposematic colors, or other decoy behaviors (Strugnell *et al.* 2014). Pelagic taxa are more fusiform in shape, with photophores for crypsis and communication, and fins for propulsion and maneuverability (Lindgren *et al.* 2004, Fuchs *et al.* 2016a). These behaviors are supported by a sophisticated nervous system, comparable to that of vertebrates (Nixon & Young 2003; Grasso & Basil 2009; Hanlon & Messenger 2018; Shigeno *et al.* 2018; Jaitly *et al.* 2022; Klug *et al.* 2023). Their advanced cognitive abilities and sensory systems are used for crypsis, defense, predation, and communication. These behaviors include changes in skin coloration, patterning, or texture camouflage, countershading, inking, and jet propulsion (Mcfall-Ngai 1990; Budelmann 1996; Nixon & Young 2003; Bush & Robison 2007; Hanlon 2007; Nishiguchi & Mapes 2008; Derby 2014; Villanueva *et al.* 2017; Ponder *et al.* 2020; Jaitly *et al.* 2022).

Coleoids play a key role in modern marine trophic webs (Clarke & Clarke 1997; Boyle & Rodhouse 2008; Hoving *et al.* 2014; Xavier *et al.* 2015; Villanueva *et al.*2017) and are typically voracious, opportunistic predators in coastal and pelagic ecosystems (Rodhouse & Nigmatullin 1996; Ibáñez *et al.*2021a). Stomach contents are direct evidence to understand diet (Rodhouse & Nigmatullin 1996; Ibáñez *et al.* 2021a). In fossil forms this has also been understood though 'frozen behavior', where two animals died in the act of predation (Klug *et al.* 2021a) as well as mechanical evidence, such as drill holes (Klompmaker & Kittle 2021; Klompmaker & Landman 2021). Stable isotope analysis of beaks is a common tool to determine trophic level and reconstruct their position in the marine food web (Cherel & Hobson 2005; Hobson & Cherel 2006; Xavier *et al.* 2022). Coleoids consume a variety of fish, crustaceans, and other invertebrates, while also being consumed by higher predators including fish, marine mammals, and birds (Boyle & Rodhouse 2008; Villanueva *et al.* 2017; Mapes *et al.* 2019; Ibáñez *et al.* 2021b). Cannibalism has also been documented in both extant and fossil forms (Mapes *et al.* 2019). Predation is generally visual with rapid forward strike and then the arms and tentacles are used to move the prey to the mouth (Boyle & Rodhouse 2008). Decabrachia tend to use their beak to bite into the soft tissues while Octobrachia have developed methods of prey handling that utilize toxins and enzymes before consumption (Boyle & Rodhouse 2008). Cephalopods, particularly oceanic squids, are active mesopredators occupying the same niche as fishes (Tanner *et al.* 2017). However, a well-known exception to this is the iconic vampire squid, *Vampyroteuthis infernalis*, the only extant vampyromorph (Fig. 1.1B). Its ecology is unique among coleoids as it is a passive, opportunistic detritivore. *V. infernalis* often inhabit

the oxygen minimum zone of the deep ocean, using their retractable filaments (Fig. 1.4G) to gather the falling detritus (Pickford 1949; Hoving & Robison 2012; Hoving *et al.* 2014; Golikov *et al.* 2019; Košťák *et al.* 2021). It is unclear when this contrasting feeding strategy and lifestyle first appeared. Fossil Vampyromorpha are known to have inhabited epicontinental seas, though their fossil record terminates in the anoxic sediments of the Lower Aptian OAE1 at Heligoland; the first record of a post-Mesozoic vampyromorph is Oligocene in age (Košťák *et al.* 2021). As this vampyromorph also employed a bathyal, low-oxygen lifestyle, Košťák *et al.* 2021 suggest that the lineage may have already been adapted to hypoxic conditions in the Mesozoic.

1.3 ~ Evolutionary History

Molecular calibration indicates that the original divergence of cephalopods from other molluscs occurred during the Cambrian (Strugnell *et al.* 2006; Kröger *et al.* 2011; Tanner *et al.* 2017; Uribe & Zardoya 2017; Sanchez *et al.* 2018; Hildenbrand *et al.* 2021). These earliest cephalopods are generally understood to be members of the order Plectronocerida (Kröger 2005; Kröger *et al.* 2011; Hildenbrand *et al.* 2021) and diverged from a monoplacophoran ancestor (Kocot *et al.* 2020) that had a high, conical shell with septa in the apical section (Kröger *et al.* 2011). There have been three overarching phases of Cephalopod evolution during the last 540 Ma: 1) the adaptation of the shell to be used as a buoyancy mechanism, 2) the ability for free swimming, and 3) for coleoids, an overall internalization and reduction of the mineralized shell following diversification in the Ordovician (Kröger *et al.* 2011; Tanner *et al.* 2017).

The first known cephalopod forms preserved the external septate shell (Yochelson *et al.* 1973) and gained a ventral siphuncle, which allowed their chambered shells to become gas-filled (Yochelson *et al.* 1973; Hildenbrand *et al.* 2021). Though the chambered shell was not yet adapted for jet propulsion, it enabled them to regulate buoyancy and elevate themselves vertically from the sediment (Yochelson *et al.* 1973; Mutvei *et al.* 2007).

Free swimming forms were present by the latest Cambrian. They experienced pulses of diversification during the Ordivician and radiated into several lineages (Kröger & Yun-Bai 2009; Tanner *et al.* 2017; Pohle *et al.* 2022). The external shells underwent considerable morphological alteration, with the emergence of long, straight orthoconic shapes as well as coiled forms, first in nautiloids and then in ammonoids (Jaitly *et al.* 2022). They were also able to expand their habitats from shallow marine- to almost all marine environments (Kröger & Yun-Bai 2009; Kröger *et al.* 2009). The habitat and niche expansions, and pulsed radiations,

have been linked with increasing complexity of ecosystems and competition from contemporaneous taxa (Kröger & Yun-Bai 2009). Their expansion into the pelagic environment is linked with an increase of food resources in the pelagic zone, and a more stable trophic web (Kröger & Yun-Bai 2009; Kroger *et al.* 2009). Indeed, cephalopods were top predators in these marine environments and were the largest swimming organisms in the Ordovician, reaching several meters in size and likely employing a macrophagous feeding strategy (Westermann & Savazzi 1999; Kröger & Yun-Bai 2009).

Crown cephalopods, Coleoidea and Nautiloidea, are estimated to have diverged in the late Palaeozoic (Voight 1997; Young *et al.* 1998; Lindgren *et al.* 2004; Strugnell *et al.* 2006; Kröger *et al.* 2011; Tanner *et al.* 2017; Klug *et al.* 2019; Mapes *et al.* 2019; López-Córdova *et al.* 2022; Pohle *et al.* 2022) either around the Silurian-Devonian boundary, or in the earliest Devonian (~415 Ma). This is coincident with the appearance of jawed fishes in the late Palaeozoic (Kröger 2005). This divergence time is supported by the fossil record for known stem group coleoids (Kröger & Mapes 2007; De Baets *et al.* 2013; Klug *et al.* 2015a; Tanner *et al.* 2017) and nautiloids (Warszawa & Korn 1992; Tanner *et al.* 2017). The first record of coleoid beaks, coincident with the emergence of crown cephalopods, indicates the shift in predator-prey dynamics observed during the Devonian Nekton Revolution and the radiation of jawed vertebrates (Klug *et al.* 2010b; Tanner *et al.* 2017).

Molecular estimates show that the current coleoid diversity can be traced to the Mesozoic, a period that also saw the radiation of ray-finned fish groups and marine vertebrates (Tanner *et al.* 2017). Co-evolution and competition with teleost fishes (bony fish) for productive marine environments (Packard, 1972; Boyle & Rodhouse 2008; Tanner *et al.* 2017; Jaitly *et al.* 2022) is postulated to have driven the radiation and cognitive advancements of coleoids in the Mesozoic. This competition instigated the adaptations of multiple complex behaviors related to communication, defense, and reproduction (Hanlon & Messenger 2018), many of which are ecologically similar to modern fishes (Nishiguchi & Mapes 2008).

The diversity of current taxa has been argued using two competing hypotheses. The first suggests rapid diversification following the K-Pg boundary, as coleoids faced less predatory pressures and were able to successfully exploit the niches left empty by ammonites and belemnites. The second cites broad ecological change in the Mid-Cenozoic related to distributional changes under new climate conditions and biotic interactions (López-Córdova *et al.* 2022). There is support for both hypotheses as the rate of coleoid diversification has been shown to increase before the K-Pg boundary and in the Cenozoic (López-Córdova *et al.* 2022).

This PhD will focus on the Mesozoic, the period in which the main coleoid lineages emerged and, more specifically, the morphological and ecological innovations on Octobrachia during this time. During the Mesozoic, Octobrachia bore a superficial resemblance to modern squid (Mapes *et al.* 2019) - the fusiform shape of pelagic Decabrachia and fishes (Lindgren *et al.* 2012). However, the reduction or loss of the gladius in most modern forms, as well as variation in extant body morphology, complicates the comparison between fossil and extant groups (Lindgren *et al.* 2004; Donovan & Fuchs 2012; Kruta *et al.* 2016; Sutton *et al.* 2016). Another challenge is that one of the major fossil lineages, Vampyromorpha, is today, only represented by one species (*Vampyroteuthis infernalis*), which possesses a unique range of morphological characters including a well-developed gladius (Pickford 1936, 1949; Allcock *et al.* 2014). As a result, the Octobrachia fossil record provides only limited insight into the evolution of this group and more generally in the evolution of coleoids (Strugnell & Nishiguchi 2007; Kröger *et al.* 2011; Tanner *et al.* 2017). High-resolution data on fossil morphology (soft tissues and gladius) is therefore essential to build a more complete picture of coleoid evolutionary history (Kruta *et al.* 2016).

1.4 ~ Mesozoic Fossil Gladius-Bearing Coleoids

The configuration of internal organs in recent coleoids varies importantly at high taxonomic rank (Fig. 1.3) and, along with the morphology of soft tissues, it provides insight into their ecology and mode of life. However, as soft tissues are rarely preserved in the fossil record, most fossil coleoids are known primarily from their internal shell which is often not well preserved and difficult to classify (Jeletzky 1966; Engeser & Bandel 1988; Doyle *et al.* 1994; Fuchs 2006b; Donovan & Fuchs 2012; Sutton *et al.* 2016; Fuchs 2020). As a result, morphological homologies and ancestral conditions are difficult to establish (Voight 1997; Vecchione *et al.* 2000; Allcock *et al.* 2011; Lindgren *et al.* 2012; Xavier *et al.* 2015; Guerra 2019). Historically, only a few computational phylogenies on extant, fossil and extant, or just fossil taxa have included morphological data (Young & Vecchione 1996; Voight 1997; Lindgren *et al.* 2004; Kruta *et al.* 2016; Sutton *et al.* 2016; Fuchs 2020; Fuchs *et al.* 2020; Whalen & Landman 2022). Today, molecular methods predominate in phylogenetic analyses of extant cephalopods (e.g., Lindgren *et al.* 2004, 2012; Strugnell *et al.* 2005; Allcock *et al.* 2011; Strugnell & Nishiguchi 2007; Sanchez et al 2018; Lindgren *et al.* 2012; Uribe & Zardoya 2017; Lindgren & Anderson 2018; Anderson & Lindgren 2021; Fernández-Álvarez *et al.* 2022;

López-Córdova *et al.* 2022; Pohle *et al.* 2022; Roscian *et al.* 2022), though purely paleontological analyses of coleoid relationships are dominated by the morphology of the gladius (Fig. 1.5) and gladius vestige (e.g., Fuchs 2006a, Fuchs *et al.* 2007a,b; Fuchs & Weis 2008, 2009, 2010; Fuchs 2009; Donovan & Fuchs 2012; Sutton *et al.* 2016; Fuchs 2020; Fuchs *et al.* 2020) as it has a relatively high potential for preservation (Lindgren *et al.* 2004; Donovan & Fuchs 2012; Kruta *et al.* 2016; Sutton *et al.* 2016) and decays more slowly than soft tissue (Kear *et al.* 1995). The original composition of the fossil coleoid gladius has been debated. It is found in different facies preserved in calcium phosphate (francolite) which indicates an original calcium carbonate composition. However, this calcium phosphate is now understood to be a diagenetic product of the same chinito-protein complex possessed by present-day squid (Doguzhaeva & Mutvei 2006; Donovan 2016).

There are three main types of fossil gladius (Fig. 1.5), each corresponding with one of the three Octobrachia suborders, Prototeuthina, Loligosepiina, and Teudopseina (Fuchs 2016, 2020). Overall, each appears arrow-like in shape though the median fields (Fig. 5) vary in form between the lineages. The anterior margins of these range from tapered to broad, and the posterior lateral fields and associated hyperbolar zones vary from very short and narrow, to large and long. These important variations in morphologies are the basis for fossil coleoid systematics (Fig. 1.5). Very simply, the Prototeuthina gladius is slender with a triangular-shaped median field. The Loligosepiina and Teudopseina both have developed lateral fields, though the median field of the Teudopseina is spindle-shaped with an anteriorly tapered median margin; in Loligosepiina it has a more triangular shape. At the subordinal level, each has a generally homogeneous morphotype, though considerable variation occurs within each lineage (Fig. 1.6) (Fuchs 2016, 2020).

Due to the similarity in shape between many of these fossil gladii, and the gladius in extant Decabrachia, early studies on Mesozoic coleoids assigned all but a few specimens (four specimens of the incirrate *Palaeoctopus* from the Upper Cretaceous, and a few argonaut egg cases from the Cenozoic to the 10-armed subgroup (e.g., Rüppell 1829; Naef 1922; Jeletzky 1965, 1966; Donovan 1977; Fuchs 2020). However, an evaluation of *Plesioteuthis* (prototeuthid), *Leptoteuthis* (Loligosepiina) and *Trachyteuthis* (Teudopseina) by Bandel & Leach (1986) identified that each of the studied genera only had eight arms, not ten, and therefore described them with closer affinities to Vampyromorpha. As such, a new classification scheme was erected, whereby ‘Vampyromorphoidea’ contained two lineages: Octopoda and Vampyromorpha (Engeser & Bandel 1988), and many of the Mesozoic coleoids

previously assigned to Decabrachia were reclassified and included as part of the eight-armed group (Doyle *et al.* 1994; Haas 2002; Bizikov 2004; Fuchs 2006*a*, *b*, 2020, Fuchs *et al.* 2007*a*, 2009, 2010; Fuchs & Weis 2009; Fuchs & Larson 2011*a*, *b*; Fuchs & Iba 2015; Klug *et al.* 2015*b*; Donovan & Fuchs 2016).

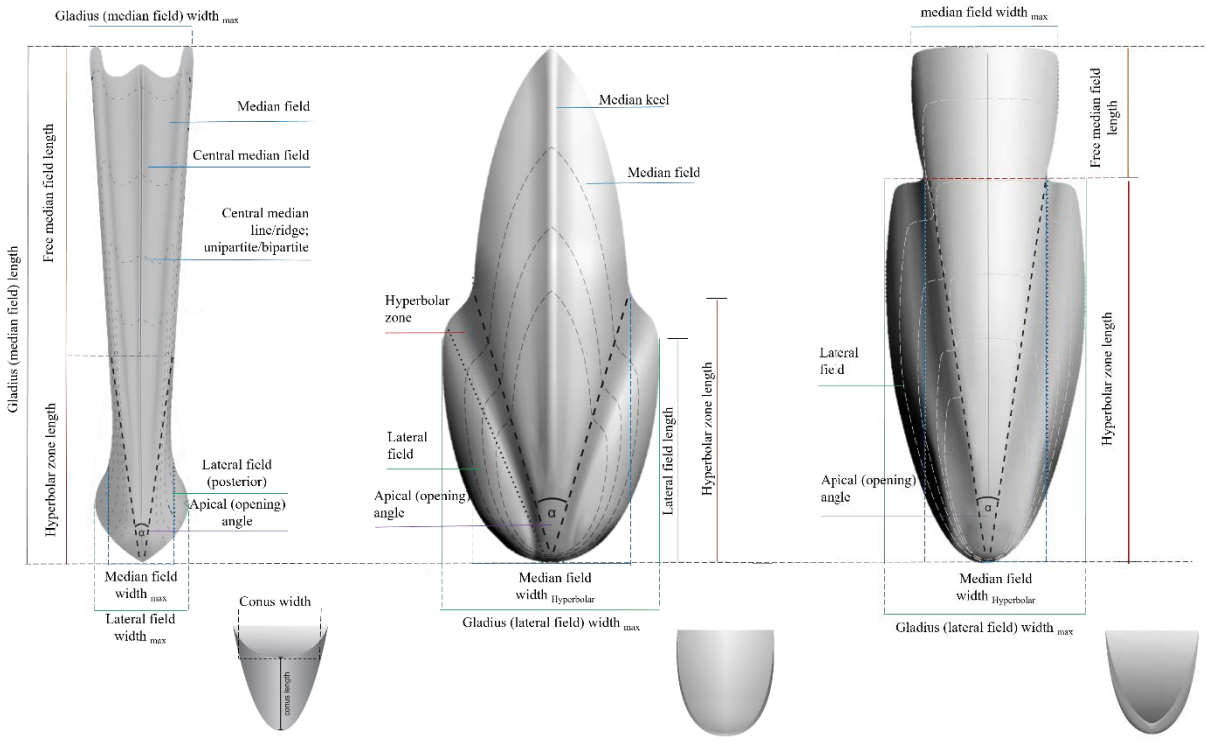

Figure 1.5: Illustrations of the three types of fossil gladii. From left to right: Prototeuthina, Teudopseina, and Loligosepiina. Though the morphology is somewhat homogenous at this subordinal level, there is considerable variation at the genera and species level. This variation forms the basis for the systematics of fossil coleoids. Modified from Fuchs & Larson 2011a, Fuchs 2016.

In our current understanding, Octobrachia dominates the Mesozoic coleoid fossil record (e.g., Fuchs 2006*a*, *b*; Fuchs *et al.* 2010; Clements *et al.* 2017; Klug *et al.* 2023) (Fig. 1.6). Experimental studies (e.g., Clements *et al.* 2017) point to a taphonomic bias to explain the limited number of occurrences of fossil Decabrachia, identifying that the high ammonia content in the decabrachian muscular tissue - used to regulate their buoyancy - made pH levels too high to be conducive for phosphatization (e.g., Allison 1988; Briggs *et al.* 1993; Briggs & Wilby 1996; Clements *et al.* 2017, 2022; Klug *et al.* 2023).

Due to the similar shape of the body and gladius, the Loligosepiina suborder (the Loligosepiidae, Geopeltidae, Leptoteuthidae, Mastigophoridae families) are recognized as part of the Vampyromorpha order (Haas 2002; Fuchs 2006*a*, *b*, 2020). Vampyromorphina (family: Vampyroteuthidae), which contains the Modern *V. infernalis*, is also a suborder of the

Vampyromorpha. A simplified visual representation of these relationships is outlined in Fig. 1.6. The gladius vestiges in modern Octopoda, particularly the unpaired rudiments in Cirrata, are recognized as reduced forms of the Teudopseid gladius (Order: Octopoda, Suborder: Teudopseina). As such, the Teudopseina are described as the stem group of the Octopoda (Haas 2002; Bizikov 2004; Fuchs 2009, 2020; Fuchs & Schweigert 2018).

The systematic position of Prototeuthina has been debated as the morphology of the gladius has led to different interpretations (e.g., Doyle *et al.* 1994; Young *et al.* 1998; Haas 2002; Fuchs *et al.* 2007*a*). Indeed, Jeletzky (1966, p. 35), Donovan (1977, p. 43), Doyle *et al.* (1994, p. 4), and Fuchs (2006*a,* p. 121) suggested that the loligosepiid-style gladius configuration (median field, lateral fields, and conus) is derived from the somewhat similar, but older pro-ostracum of the Triassic phragmoteuthid. As such, they proposed that the loligosepiid forms subsequently gave rise to the Prototeuthina and Teudopsiid forms. However, work by Fuchs, Klinghammer, and Keupp (2007*a*) and Schweigert & Fuchs (2012) challenged this interpretation. They identified the oldest known gladii as belonging to the Prototeuthina suborder. They discounted the phragmoteuthid origin as the prototeuthid form differs and possesses relatively short lateral fields and poorly developed hyperbolar zones (Figs 1.5, 1.6). This interpretation is in line with Fuchs (2006*b*) who suggested that the prototeuthid gladius was the most ancestral as it retained a true conus (Fig. 1.5), and therefore the wider, more open conus of loligosepiid and teudopsid forms were more derived. In this work we follow the view of Fuchs (2020) positioning Prototeuthina as a stem Octobrachia.

It has not yet been possible to construct an undisputed phylogeny that includes fossil and extant Coleoidea (Lindgren *et al.* 2004; Kröger *et al.* 2011; Kruta *et al.* 2016; Sutton *et al.* 2016). Inherent difficulties include the morphological variety in modern forms, limited fossil record, uncertain homologies, and differing evolutionary rates across the groups (Young & Vecchione 1996; Lindgren *et al.* 2004; Allcock *et al.* 2014; Tanner *et al.* 2017). To date, only 3 studies have combined homologous fossil and extant morphological characters in a cladistic format. The original matrix to combine these data was published by Sutton *et al.* (2016). This was minimally modified for *Proteroctopus* by Kruta *et al.* (2016), and then underwent a more extensive revision by Whalen & Landman (2022). This recent analysis of the systematics of fossil and extant coleoids (Whalen & Landman 2022) has 153 characters in the matrix. Of these, the gladius contributes approximately half (n=75) of the character states, despite many of the details being poorly resolved.

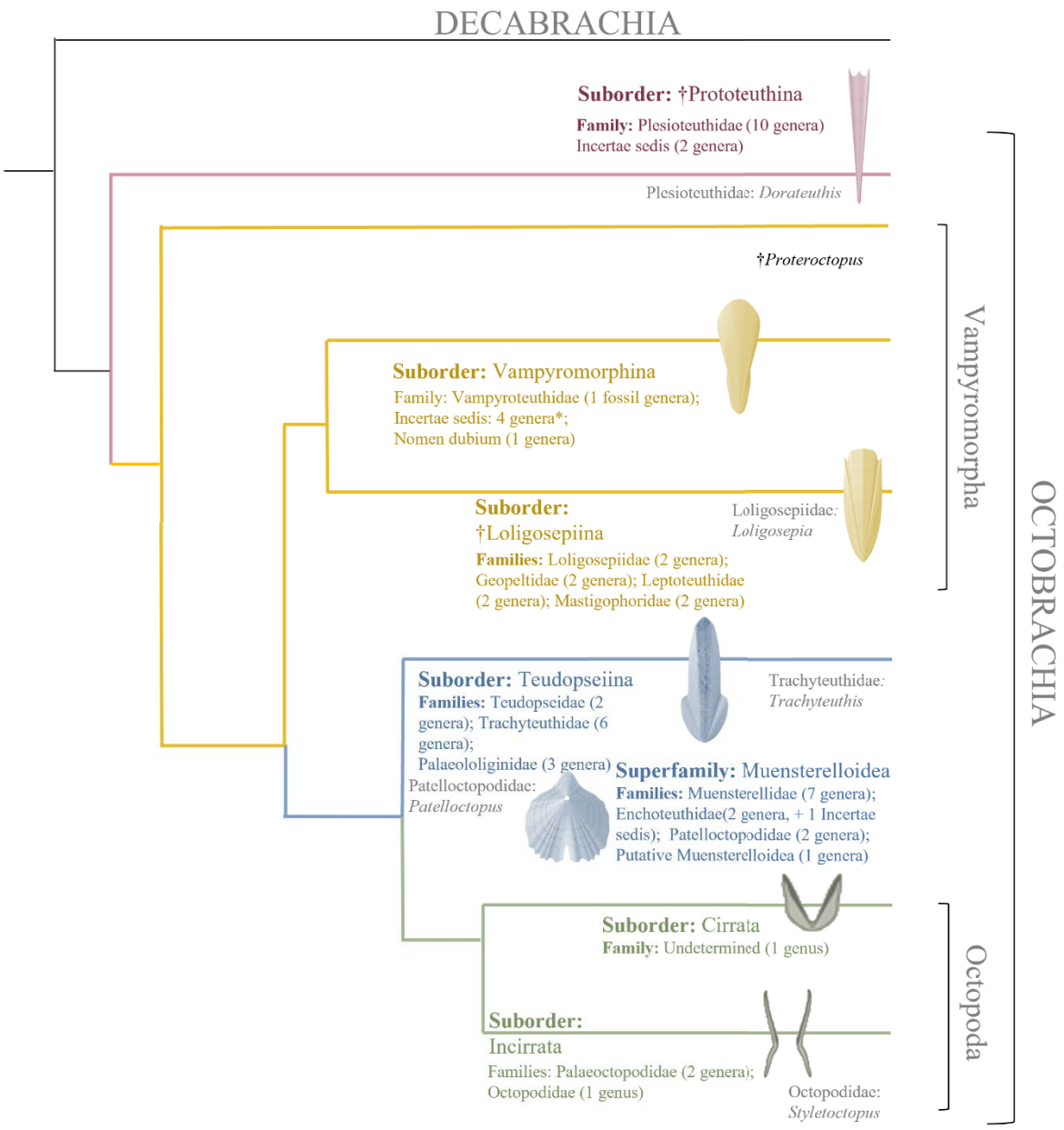

Figure 1.6: Phylogenetic hypothesis for Octobrachia including main fossil suborders and families, and the number of associated genera. Adapted from Fuchs 2006b and Fuchs 2020. Gladius illustrations modified from Fuchs 2020 and Whalen & Landman 2022 (Cirrata, and Incirrata).

The original classification of the two coleoid superorders was based on the number of arms in the arm crown. These were Decapoda (ten-arm) and (Octopoda) eight-armed forms (Leach 1817). Later, Owen (1836) divided the Cephalopoda based on gill anatomy. He gave the name Tetrabranchia to reflect the two gill-pair conditions seen in nautilus, and Dibranchia to represent the single gill pair seen in Octobrachia and Decabrachia (Donovan & Fuchs 2012). Haeckel (1866) retained Tetrabranchia and Dibranchia as subclasses of Cephalopoda, though avoided using the Order, Decapoda Leach 1817 as Decapoda Latrielle 1802 was already in use for

crustaceans. Instead, Haeckel (1886) introduced Decabrachia and Octobrachia. Younger homonyms have also been suggested for the 10-armed forms including Decapodiformes Young, Vecchione & Donovan 1998, which is commonly used in the literature. See Hoffmann 2015 for a detailed review of Decabrachia names.

Subdivisions within Octobrachia have also been based on anatomy (Fuchs 2020). When Octopoda was first described (Leach 1817), it reflected eight-armed forms without fins and cirri. Keferstein (1866) and Haeckel (1866) proposed the family name Cirroteuthidae to reflect those with cirri and fins, and assigned finless, and cirri-less forms to the families Eledonidena and Phylonexiden. Later, Grimpe (1916) would introduce Cirrata and Incirrata to delineate between finned, and non-finned taxa. An additional subdivision of Octobrachia was proposed by Pickford (1936), who argued for an ordinal assignment for Vampyromorpha. Today, this is represented by just one genus, *Vampyroteuthis,* and species *V. infernalis*. The position and rank of *Vampyroteuthis* has been heavily debated due to the mosaic of characters that are not shared with either Octobrachia or Decabrachia (Fuchs 2020). However, its close relationship with Octobrachia has been confirmed by recent phylogenies (Strugnell & Nishiguchi 2007; Uribe & Zardoya 2017; Lindgren & Anderson 2018; Sanchez *et al.* 2018; Anderson & Lindgren 2021; Roscian *et al.* 2022), and various names have been proposed for the group that includes Octobrachia and Vampyromorpha (Fuchs 2020). These include Octopodiformes, Vampyromorphoidea, Octobrachia, Vampyropoda, and Octobrachiomorpha (Berthold & Engeser 1987; Engeser & Bandel 1988; Boletzky 1992; Doyle, Donovan, and Nixon 1994; Haas 2002). Here, we follow the classification of Fuchs (2020) and use Octobrachia and Decabrachia (Fig. 1.6) to reflect the two suborders. Vampyromorpha is included with Octobrachia. A table of the existing fossil Octobrachia and their systematic placement is provided in the annex of this manuscript.

1.5 ~ Mesozoic Gladius-Bearing Lagerstätten

Though the record of Mesozoic Octobrachia is dominated by fossil gladii, a limited number of Lagerstätten deposits (Fig. 1.7) retain evidence of exceptionally preserved soft tissues (Supplementary Table 1.1). These provide an unparalleled window into the life and diversity of ancient coleoid cephalopods (e.g., Fischer & Riou 1982*a*, *b*, 2002; Fischer 2003; Fuchs 2006*a*, 2014; Charbonnier *et al.* 2007*b*; Charbonnier 2009; Fuchs *et al.* 2009; Fuchs & Weis 2009; Klug *et al.* 2010*a*, 2015*b*, 2021*a*; Fuchs & Larson 2011*a, b*; Kruta *et al.* 2016; Martindale

et al. 2017; Hoffmann *et al.* 2020). It is beyond the scope of this thesis to provide an exhaustive list of Mesozoic coleoid-bearing localities, however those discussed here include the celebrated Lower Jurassic Posidonia Shale (Holzmaden, Germany), the Upper Jurassic Plattenkalks of Nusplingen (Upper Kimmeridgian) and Solnhofen (Lower Tithonian), Germany (e.g. Klug *et al.* 2005, 2015*b*, 2021*a*; Fuchs 2007, Fuchs *et al.* 2007*a*, *b,* 2010, 2013), and the Upper Cretaceous Plattenkalks of the Lebanese (Cenomanian and Santonian) localities of Haqel, Hjoula and Sahel Aalma (Bottjer *et al.* 2002; Fuchs 2006*a*; Fuchs & Larson 2011*a, b*; Jattiot *et al.* 2015; Fuchs *et al.* 2016*b*). The record of coleoids from the Mid-Jurassic cephalopods is less well known, and mainly represented by the Callovian-aged Lagerstätten of Christian Malford, UK (Wilby *et al.* 2004, 2008; Hart *et al.* 2016) and La Voulte-sur-Rhône, France (Fischer & Riou 1982*a*, *b*, 2002; Fischer 2003; Charbonnier *et al.* 2014; Fuchs 2014; Kruta *et al.* 2016). These conservation deposits (Seilacher 1982) provide unique windows into the evolutionary timeline and morphological detail of the mainly soft-bodied coleoids (Klug *et al.* 2005, 2015*b*; Fuchs 2006*a*; Fuchs & Larson 2011*a*; Donovan & Fuchs 2016; Fuchs *et al.* 2016*b*; Kruta *et al.* 2016; Mapes *et al.* 2019).

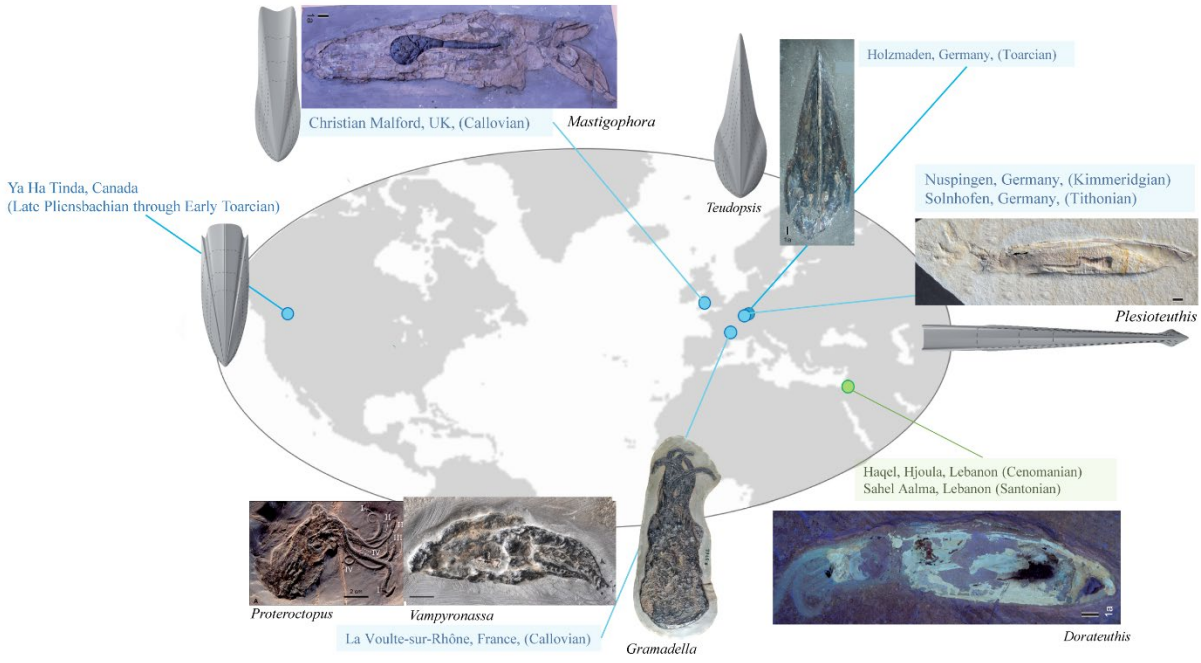

Figure 1.7: A representation of key Mesozoic Lagerstätten. In the Lower Jurassic (Pliensbachian–Toarcian) these Lagerstätten include the black shales of the Ya Ha Tinda Lagerstätte (Alberta, Canada) and the Posidonia shales which mainly outcrop in southern Germany. Middle Jurassic (Callovian) deposits include the laminated clays and mudstones associated with the Oxfordian Clay Formation at Christian Malford (Wiltshire, England) and the laminated marls of the La Voulte Lagerstätte (Ardeche, France). The Upper Cretaceous includes the lithographic limestones of Haqel, Hjoula, and Sahel Aalma (Lebanon). All images from Fuchs (2020). Scale bars are 10 mm unless otherwise indicated.

1.5.1 ~ Lower Jurassic

The Early Jurassic was a period of significant environmental and biotic perturbation, that included the ~183 Ma Toarcian Oceanic Anoxic Event (TOAE) (Little & Benton 1995). Organic-rich black shale deposition was driven by increased primary productivity in the ocean and low oxygen conditions (Caruthers *et al.* 2013).

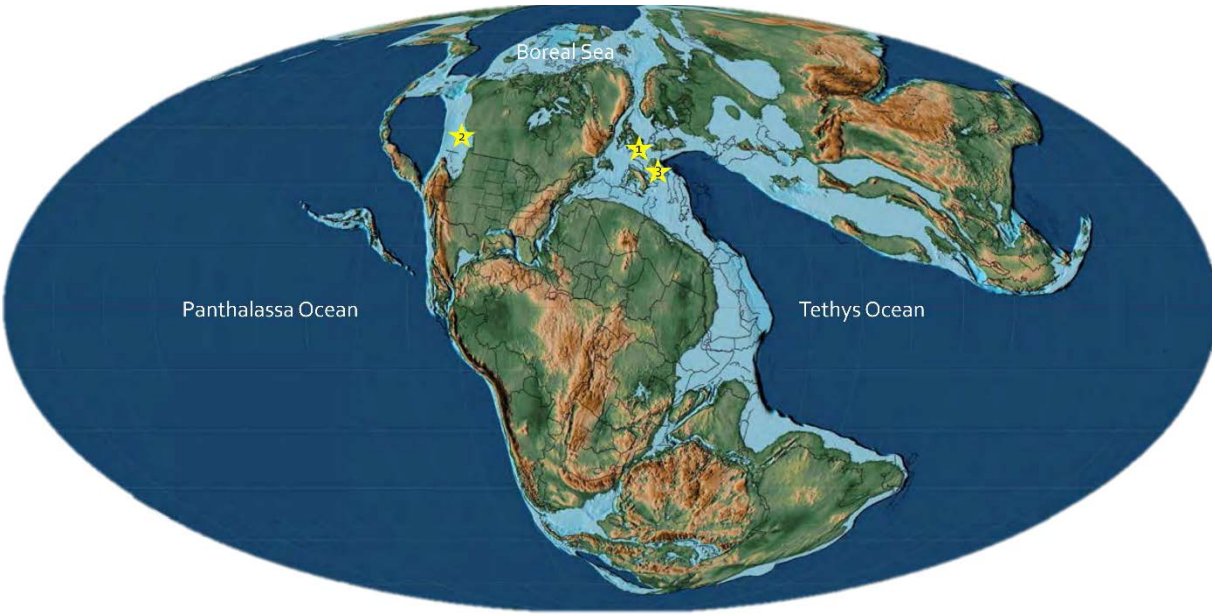

Figure 1.8: Early Jurassic (Toarcian) 179.3 Ma. Showing the Posidonia Shales, Germany (1), Ya Ha Tinda, Canada (2) and Strawberry Bank, England (3). Map modified from CR Scotese, PALEOMAP Project (Map 39), Maximum flooding surface. Mollwide Projection.

Key Lagerstätten in Lower Jurassic deposits are represented by the Posidonia Shale (Seilacher 1982; Röhl *et al.* 2001), the Ya Ha Tinda (lower Fernie Formation) in Alberta, Canada (Martindale *et al.* 2017), and the Strawberry Bank (Beacon Limestone Formation, UK) (Williams *et al.* 2015). The Strawberry Bank (Toarcian) is interpreted to be a shallow marine lagoon deposit (Williams *et al.* 2015), potentially in brackish water environments (Muscente *et al.* 2019). Both the Ya Ha Tinda (Pleinsbachian – Toarcian) and Posidonia Shale (Toarcian) Lagerstätten record deeper marine settings, where anoxic bottom-water conditions were punctuated by intermittent oxic and suboxic conditions (Seilacher 1982; Röhl *et al.* 2001; Martindale *et al.* 2017; Muscente *et al.* 2019; Sinha *et al.* 2021). Each were positioned on epicontinental shelves (Fig. 1.8) in the Panthalassa and Tethys Oceans during the TOAE (e.g. (Muscente *et al.* 2019, 2023; Košťák *et al.* 2021; Sinha *et al.* 2021). Despite being paleogeographically separate, each has a similar fauna (e.g., ichthyosaurs, ray-finned fishes, gladius-bearing coleoids, crustaceans, ammonites, bivalves, and crinoids) though the species

typically vary between the ocean basins. The faunal similarities suggest these localities had similar ecosystems (Muscente *et al.* 2017), though the preservational pathways differ between these depositional environments (Muscente *et al.* 2019). There are six coleoid genera from these Lagerstätten, which belong to the Prototeuthina (*Paraplesioteuthis),* Loligosepiina (*Loligosepia Jeletzkyteuthis, Geopeltis*, *Parabelopeltis*), and Teudopseina (*Teudopsis*).

Posidonia Shale Lagerstätte: The famous Posidonia shales (Posidonienschiefer Formation) belong to the Lias Group of western and northern Europe, which outcrop as bituminous 'oil' shales in numerous Lagerstätten deposits (northeastern and southwestern Germany, southern Luxembourg, northwestern Austria, and the Netherlands) (Muscente *et al.* 2023). Deposition of these sediments (generally marls and marly clays with a few intercalated limestone horizons) occurred in multiple basins of the European epicontinental sea on the northwestern side of the Tethys (e.g., the Paris, Yorkshire/Cleveland, Northwestern German, and Southwestern German basins). During the deposition of the Posidonienschiefer Fm., bottom water anoxia prevailed in the Southwestern German Basin (Muscente *et al.* 2023) and was punctuated by short term oxic pulses (Röhl *et al.* 2001) that were driven by sea-level changes (seasonal variations superimposed on long-term trends) (Röhl *et al.* 2001).

The classic 'Posidonia Shale Konservatlagerstätte' outcrops in the Holzmaden region in southern Germany, where the exceptionally preserved marine fauna primarily occur, primarily in the Falciferum biozone (Member II). The faunal assemblage includes marine reptiles and fishes (Maxwell & Martindale 2017; Lindgren & Anderson 2018), ammonoids, coleoids (Jenny *et al.* 2019; Klug *et al.* 2021*b*), crustaceans (Klug *et al.* 2021*b*), crinoids (Hess 1999; Matzke & Maisch 2019), benthic bivalves and brachiopods (Röhl *et al.* 2001). Many of the organisms preserved are pelagic, though the benthic communities correspond with the periods of oxygenation.

Most coleoids come from the bioturbated beds (Fleins) (Sinha *et al.* 2021) and are co-occurring with ichthyosaur fossils. The coleoid gladii are typically phosphatized (apatite), though some poorly preserved specimens are composed of calcite and carbonaceous material (Muscente *et al.* 2023). Pyritized fossils are also fairly common (Littke *et al.* 1991; Muscente *et al.* 2019). Work by Muscente *et al.* (2023) shows that phosphatization occurred early in the diagenetic process prior to burial compaction, and around the oxic/anoxic boundary, which was located within the sediment. They suggest that animals were preserved during episodes of oxygenation in the basin and in environments on the margins of anoxic bodies of water.

The lack of terrestrial sediments in the microlaminated mudstones indicate the paleo depositional environment was far from the coastline in a low energy environment, below wave base (Muscente *et al.* 2023). The articulated remains indicate little transportation, rapid burial in the fine-grained sediments (Muscente *et al.* 2023).

Ya Ha Tinda: Contemporaneous in age, the black shales and organic-rich (shaley) siltstones of the Fernie Formation of Ya Ha Tinda Lagerstätte (Alberta, Canada) represent a more expanded time interval (Martindale *et al.* 2017) than Strawberry Bank and the Posidonia Shales (Martindale *et al.* 2017). The Members include the Red Deer (platy calcareous shales interbedded with fine siltstones and black limestone) and Poker Chip Shale (poorly cemented, black calcareous shales and mudstones interbedded locally with bituminous limestones) and represent the first Pliensbachian–Toarcian Lagerstätte outside of Europe, and the only Jurassic Lagerstätte in North America (Martindale *et al.* 2017; Muscente *et al.* 2017; Sinha *et al.* 2021). Soft tissue preservation extends from the Kunae (Pliensbachian) to Planulata (Toarcian) biozones (Martindale *et al.* 2017) which correlates with the Margaritatus to Bifrons biozones of Europe (Martindale *et al.* 2017). The faunal assemblage includes articulated vertebrates (ichthyosaurs and fishes), ammonites, crustaceans, crinoids, brachiopods, gastropods, bivalves, wood, and microfossils (e.g., Martindale & Aberhan 2017; Martindale *et al.* 2017; Maxwell & Martindale 2017; Muscente *et al.* 2019; Sinha *et al.* 2021). Coleoid gladii, ink sacs, and mantle tissues (Marroquín *et al.* 2018) are also present, though represent just 2% of the fossil population (Muscente *et al.* 2019). These are predominantly phosphatized (apatite), though some fossils do contain carbonaceous material (Muscente *et al.* 2019).

The geochemistry and lithology of the finely laminated sediments, and articulation of the fossil specimens indicate a deep-water (below wave base) open marine setting that was generally deposited under anoxic conditions. However, as seen in the Posidonia Shales, the benthic communities confirm periods of oxygenation.

Strawberry Bank: The Strawberry Bank Lagerstätte was deposited on the northwestern margin of the Tethys Ocean and forms part of the Lower Jurassic Lias Group. Located near Ilminster in Somerset (England) the local deposits consist of interbedded nodular limestones and silty-clays (Williams *et al.* 2015; Sinha *et al.* 2021; Jamison-Todd *et al.* 2022) and represent the Falciferum (Serpentinum) ammonite biozone (Sinha *et al.* 2021). The majority of fossils from this now inaccessible locality were collected between 1840 and 1860 by Charles Moore

(Williams *et al.* 2015; Sinha *et al.* 2021; Jamison-Todd *et al.* 2022). Few studies were conducted on the specimens he described, but recent research has focused on the vertebrate fauna (Caine & Benton 2011; Jamison-Todd *et al.* 2022). In addition to the vertebrates (e.g., articulated fishes and reptiles), the faunal assemblage includes cephalopods, crustaceans, and insects, which were mainly preserved in carbonate concretions (Williams *et al.* 2015; Sinha *et al.* 2021). This combination of marine and terrestrial taxa suggests that the depositional environment was near the palaeocoastline (Williams *et al.* 2015; Sinha *et al.* 2021), likely in a localized lagoon, mud flat, or similar quiet-water environment (Sinha *et al.* 2021).

1.5.2 ~ Middle Jurassic

The Callovian stage was initiated by a major transgressive phase, which resulted in widespread marine facies deposition across much of northwest Europe (Fig 1.9) (Allison 1988*a*). Middle Jurassic (Callovian) deposits include the laminated clays and mudstones associated with the Oxfordian Clay Formation at Christian Malford (Wiltshire, England) and the marls of the La Voulte Lagerstätte (Ardeche, France). Ten coleoid genera have been described from these Lagerstätten and belong to the Prototeuthina (*Romaniteuthis*, *Rhomboteuthis*), Loligosepiina (*Mastigophora*), Teudopseina (*Trachyteuthis*, *Muensterellina*, *Pearceiteuthis*, *Teudopsis*), and *incertae sedis* members of the Vampyromorphina family (*Gramadella*, *Proteroctopus*, *Vampyronassa*).

Christian Malford: The Christian Malford Lagerstätte is part of the Peterborough Member of the Oxford Clay Formation (Callovian–Oxfordian) in Wiltshire, England (Allison 1988*b*; Martill & Hudson 1991; Wilby *et al.* 2004, 2008; Hart *et al.* 2016, 2019). Originally discovered during railway construction in 1840, local collectors actively worked the site until 1857, finding thousands of exceptionally preserved ammonites, fish, and crustacean specimens that are mainly attributed to the Athleta Zone, Phaeinum Subzone. However, the Lagerstätte became famous for the coleoids (e.g., belemnites and Octobrachia) that were preserved there, many of which retained their soft tissues and ink sacs (Owen 1844; Donovan 1983, Allison 1988*b*; Martill & Hudson 1991; Donovan & Crane 1992; Wilby *et al.* 2004, 2008; Hart *et al.* 2016, 2019). Indeed, the fossil fauna is diverse and abundant (Wilby *et al.* 2004), retaining both soft tissues, and hard aragonitic features.

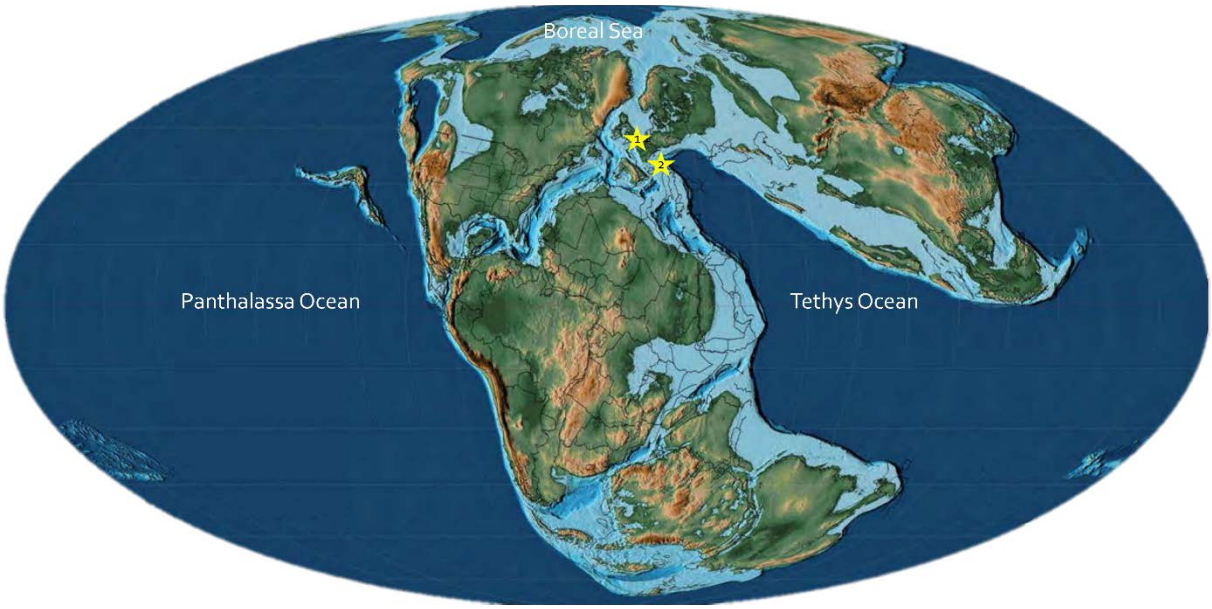

Figure 1.9: Middle Jurassic (Callovian) 164.5 Ma. Showing the localities of Christian Malford, England (1), and La Voulte-sur-Rhône, France (2). Modified from CR Scotese, PALEOMAP Project (Map 36). Mollweide Projection. Transgressive systems tract.

Paleogeographically, Christian Malford provided an epicontinental link between the Boreal and Tethyan oceans (Martill & Hudson 1991; Hart *et al.* 2019). There is no clear consensus as to whether Christian Malford (Lower Oxford Clay,) represents a relatively shallow (e.g., Wilby *et al.* 2004; Price *et al.* 2015), or relatively deep (e.g., Hart *et al.* 2019) depositional environment, though based on the fossil assemblage Hart *et al.* (2019) supposed it was relatively deep, with restricted circulation. Indeed, the organic-rich, fine-grained mudstone succession from the locality records episodic oxic/anoxic conditions. The bottom water conditions were commonly inhospitable, though the overlying water column was highly productive and supported a diverse fauna (Wilby *et al.* 2008). The laminated mudstones of the Peterborough Member are greatly compacted (by 70 %–80 %) (Price *et al.* 2015; Hart *et al.* 2016, 2019), and alternate between being fissile and organic-rich, and massive, shelly, and organically poor (Price *et al.* 2015). Nektonic fossils dominate the organic-rich horizons, while those with less organics retain diverse assemblages of infaunal and epifaunal bivalves and gastropods (Price *et al.* 2015). Importantly for the phosphatization process, the soft substrate allowed the organisms to sink below the sediment-water interface and begin rapid diagenesis (Wilby *et al.* 2004). The exceptional phosphatic preservation (aragonite) of the coleoid fauna indicates any postmortem disturbance was minimal (Hart *et al.* 2019).

La Voulte-sur-Rhône: The Lower Callovian Lagerstätte of La Voulte-sur-Rhône (Gracilis

Biozone) (Elmi 1967) is in south-eastern France (Ardèche) adjacent to the Rhône River. Reconstructions of Callovian paleogeography place the locality on the western margin of the Tethys Ocean, adjacent to the submerged Massif Central (Wilby 2001; Charbonnier 2009; Charbonnier *et al.* 2014). Due to a series of heavy regional faulting, the Tethys margin east of La Voulte was characterized by a complex underwater topography of tilted blocks, and the heterogeneous conditions of La Voulte during the Callovian likely resembled escarpments and abrupt rocky bathymetry, similar to certain continental slopes today (e.g., Charbonnier 2009; Charbonnier *et al.* 2014).

The fossiliferous deposits of the La Voulte Lagerstätte crop out in a relatively thin interval (5-6 m) in the Mines Ravine (Charbonnier 2009; Charbonnier *et al.* 2014). The section is comprised of laminated, organic-rich marls, which are generally not bioturbated. They are capped by a thick (~15m) iron deposit. Sideritic concretions in the basal marls frequently preserve crustaceans and coleoids in three-dimension. Soft-bodied fossils are also preserved in the marl horizons, though have undergone compaction. Thin iron-rich carbonate layers repeat in succession and preserve an abundance of ophiuroids.

The macrofauna (arthropods, cephalopods, marine worms, echinoderms, marine vertebrates, bivalves, and brachiopods) (e.g., Charbonnier *et al.* 2007*a*, *b*, 2010, 2014, 2017; Villier *et al.* 2009; Audo & Charbonnier 2013; Audo *et al.* 2014*a*, 2019; Jauvion *et al.* 2016, 2017, 2020; Kruta *et al.* 2016; Vannier *et al.* 2016; Audo & Schweigert 2018; Jauvion 2020) were nearly exclusively pelagic, nectopelagic or mesopelagic, and included very few benthic organisms (Fischer 2003). The total assemblage represents bathymetrically distinct habitats (Audo *et al.* 2016; Košťák *et al.* 2021). Though the epipelagic waters of the Lagerstätte were likely well oxygenated, the rapid deposition in the sulphate-reduced soft sediment led to the iron-rich mineralization of the unique faunal assemblage (Charbonnier *et al.* 2010; Košťák *et al.* 2021). See Chapter 3 for further information on La Voulte-sur-Rhône.

1.5.3 ~ Late Jurassic

In the Late Jurassic, Europe was an archipelago surrounded by the northern Tethys (Fig. 1.10). Associated tropical – subtropical carbonate platforms were extensive and extended from southern France across Switzerland into Southern Germany (Villalobos-Segura *et al.* 2023). Southern Germany was positioned on the north-western Tethyan shelf and covered by an epicontinental sea (Schmid *et al.* 2005) and, in contrast to the predominantly dark clays of the

Lower and Middle Jurassic, a succession of light-colored limestones and marls (400-600 m) dominate (Schmid *et al.* 2005). Classic Upper Jurassic Lagerstätten in Germany include Nusplingen (Kimmeridgian – Tithonian), located in the Swabian Alb, and Schamhaupten (Kimmeridgian-Tithonian boundary) and Solnhofen (Lower Tithonian), which are both located in the lower section of the Franconian Alb. Collectively, these localities are commonly referred to as the Solnhofen Archipelago, or the Solnhofen Plattenkalks (Dietl & Schweigert 2004; Klug *et al.* 2005, 2021*a*; Donovan & Fuchs 2016; Schweigert & Roth 2021; Villalobos-Segura *et al.* 2023).

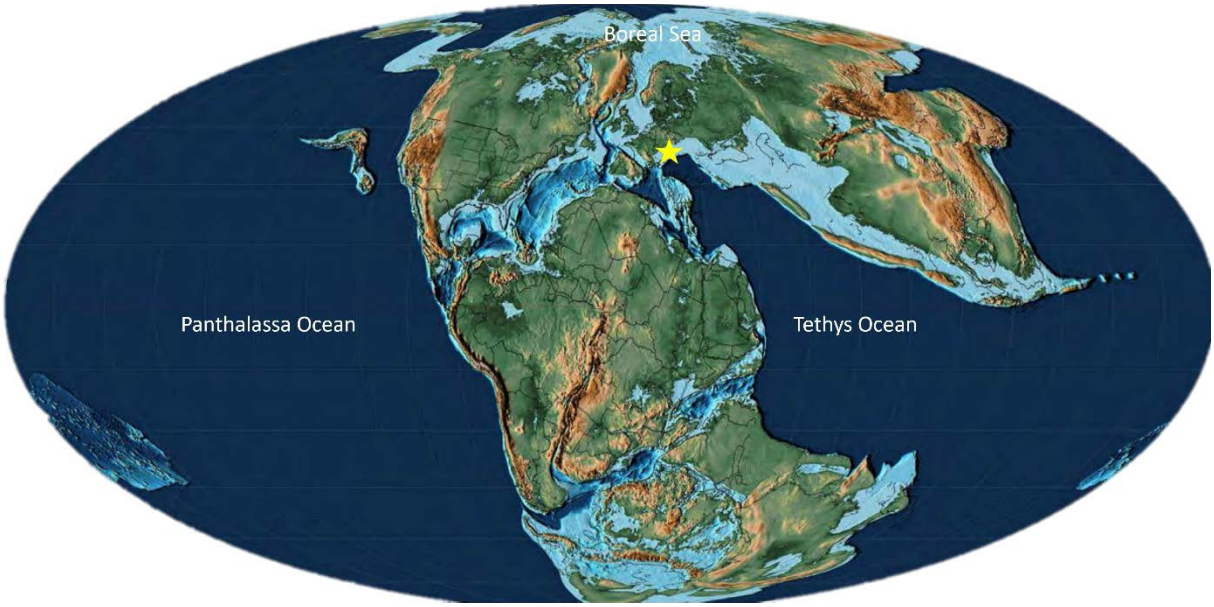

Figure 1.10: Late Jurassic (Tithonian) 148.2 Ma. Showing the locality of the Solnhofen Plattenkalks, Germany. Modified from CR 428 Scotese, PALAEOLAP Project (Map 33). Highstand System Track.

These plattenkalks represent deposition in an epicontinental sea, typically within restricted shallow-marine basins and semi-enclosed lagoons (Košťák *et al.* 2021), that were surrounded by extensive bioherms (Wilkin 2020). The Northern Tethys was often subject to large monsoonal storms that transported thousands of marine organisms into the complex lagoon system and generally inhospitable basins (Wilkin 2020). Characterized by hyper-salinity, and bacteria-driven, partially dysoxic bottom waters, each locality has a slightly different stratigraphy, lithology, taphonomy, and faunal assemblage (Donovan & Fuchs 2016).

The general lithology represents a series of very fine-grained lithographic limestones that preserve (phosphatize) various soft tissues and impressions (Bandel & Leich 1986; Fuchs *et al.* 2003, 2007*a*; Klug *et al.* 2005; Fuchs 2006*a*, *b*; Donovan & Fuchs 2016). The coleoids preserved from these Lower Jurassic German sites (fifteen known genera) are from the

Prototeuthina (*Boreopeltis Plesioteuthis*, *Senefelderiteuthis*), Loligosepiina (*Doryanthes*, *Leptotheuthis*, *Bavaripeltis*) and Teudopseina (*Patelloctopus*, *Tyrionella*, *Muensterella*, *Celaenoteuthis*, *Engeseriteuthis*, *Listroteuthis*, *Palaeololigo*, *Teudopsinia*, *Palaeololigo*) suborders.

Nusplingen: The Nusplingen Lithographic Limestones outcrop over two small quarries (Nusplingen and Egesheim quarries) near the village of Nusplingen. These expose 10 – 15m of finely laminated limestones in an area of area of about 2.5 km^2 (Villalobos-Segura *et al.* 2023). Fossils have been recorded from the site since the middle of the 19th century, and today the quarries are preserved as a national heritage site in the Swabian Alb Geopark (Dietl & Schweigert 2004, Klug *et al.* 2015*b*; Schweigert & Roth 2021). The deposits are Late Kimmeridgian in age, and belong to the Beckeri Zone, (Ulmense Subzone) (Dietl & Schweigert 2004, Klug *et al.* 2021*b*; Schweigert & Roth 2021; Villalobos-Segura *et al.* 2023). The conservation Lagerstätte (Klug *et al.* 2021*b*) was deposited in a locally restricted lagoon (<100 m) with stagnant bottom waters (Dietl & Schweigert 2004; Villalobos-Segura *et al.* 2023). The lagoon was surrounded by bioherms (sponge/microbial), some of which were tectonically lifted above sea level, forming small islands (Dietl & Schweigert 2004; Fuchs 2007; Schweigert & Roth 2021). There is a highly diverse assemblage of more than 400 fossil vertebrate, invertebrate, and plant taxa (Schweigert & Roth 2021; Villalobos-Segura *et al.* 2023). Despite the dysoxic seafloor, a few beds record a low diversity of endobenthic ichnofossils and traces of organisms interacting with the substrate (e.g. (Briggs 1995; Klein *et al.* 2016; Schweigert *et al.* 2016). However, the site is best known for well-preserved shark fossils and marine crocodilyformes (thalattosuchians) (Schweigert & Roth 2021). The most frequent invertebrate fossils are ammonites; belemnites are represented by one species; Vampyromorph coleoids are also present (Schweigert & Roth 2021). The predominantly allochthonous faunal assemblages record the shallow-water conditions of the surrounding epicontinental seas (Košťák *et al.* 2021).

Schamhaupten: The Lageratsätten is located in the southern Franconian Alb, near the village of Schamhaupten in the Eichstätt region (Viohl & Zapp 2007). The silicified plattenkalks were deposited in the Schamhaupten basin (>60 m) in a small carbonate depression, surrounded by massive carbonate rocks. This deposition occurred during a transgression that began in the early late Kimmeridgian and peaked in the early Tithonian. The basin reflects a stratified water column with hypersaline, dysaerobic bottom waters and microbial mats (Viohl & Zapp 2006,

2007). Two major types of facies are distinguishable: laminated limestones rich with articulated fossils, and coarser, detrital carbonates. Though there is no unequivocal biostratigraphic delineation, the Lagerstätte is part of the Painten Fm at the Kimmeridgian-Tithonian boundary (Viohl & Zapp 2006, 2007; Rauhut *et al.* 2018).

There is an abundance of autochthonous pelagic organisms (coccolithophorids, radiolarians, cephalopods, planktonic crinoids, fishes, and marine reptiles), indicating a link with the Tethys. All benthic and demersal organisms are interpreted to be allochthonous origin and were washed into the basin. Approximately 200 taxa have been identified. Cephalopods are represented in abundance by ammonites, a genus of belemnitid and belemnoteuthid, and ~10 undetermined Vampyropmorpha (Viohl & Zapp 2007).

Solnhofen: The Solnhofen Lithographic Limestones (Hybonotum zone) are possibly the most famous of the Jurassic plattenkalks. Located in the Altmühl Valley (southern Franconian Alb), they are comprised of the same laminated/thinly bedded limestones are intercalated thin marly layers (Etter 2002, Audo *et al.* 2014*b*), seen in the rest of the Solnhofen Archipelago. Like Nusplingen, these limestones were deposited in a lagoon environment (<200) (Audo *et al.* 2014*b*) that were surrounded by microbial/reef mounds, potentially uplifted above sea level (Fuchs 2007, Fuchs *et al.* 2007*b*)

The faunal assemblage from Solnhofen is extraordinarily diverse and exquisitely preserved. It represents both marine and terrestrial plants and animals, including Archaeopteryx (Villalobos-Segura *et al.* 2023). The Vampyromorph fauna in the Solnhofen limestones is highly diverse (e.g., Fuchs 2007, Fuchs *et al.* 2007*b*, *a*; Hoffmann *et al.* 2020, Klug *et al.* 2021*b*; Villalobos-Segura *et al.* 2023), though many older specimens lack specific locality information. Often attributed just to 'Solnhofen', they originated from various outcrops on the Solnhofen Archipelago (e.g., the Mörnsheim, Kelheim, Eichstätt, Langenaltheim, Painten). However, the morphology of these taxa appears homogeneous (Fuchs 2007).

1.5.4 ~ Upper Cretaceous

The lithographic limestones of the Lebanese Lagerstätten also reflect a shallow marine environment. Cretaceous-aged paleo-Lebanon was positioned on the African platform on the northern section of continental Gondwana (Figs 1.11, & 1.12). During this period, the area was subject to three overarching temporal sedimentary sequences (Ferry *et al.* 2007; Audo &

Charbonnier 2013): a series of depositional sequences bounded by unconformities (Valanginian to upper Aptian) and mild sea-level oscillations which emplaced large carbonate platforms (alternating shallow-water carbonate facies and finely-bedded and laminated mudstones) onto the Arabian craton on the platform (late Albian – Turonian); a deepening trend (Cenomanian/Turonian boundary – early Turonian) accelerated the drowning of the craton, depositing micritic limestones and chalks until the Eocene (Ferry *et al.* 2007; Audo & Charbonnier 2013). Equivalent coleoid-bearing limestones are unfortunately lacking between the Upper Jurassic and Cretaceous deposits (Fuchs *et al.* 2007*a*).

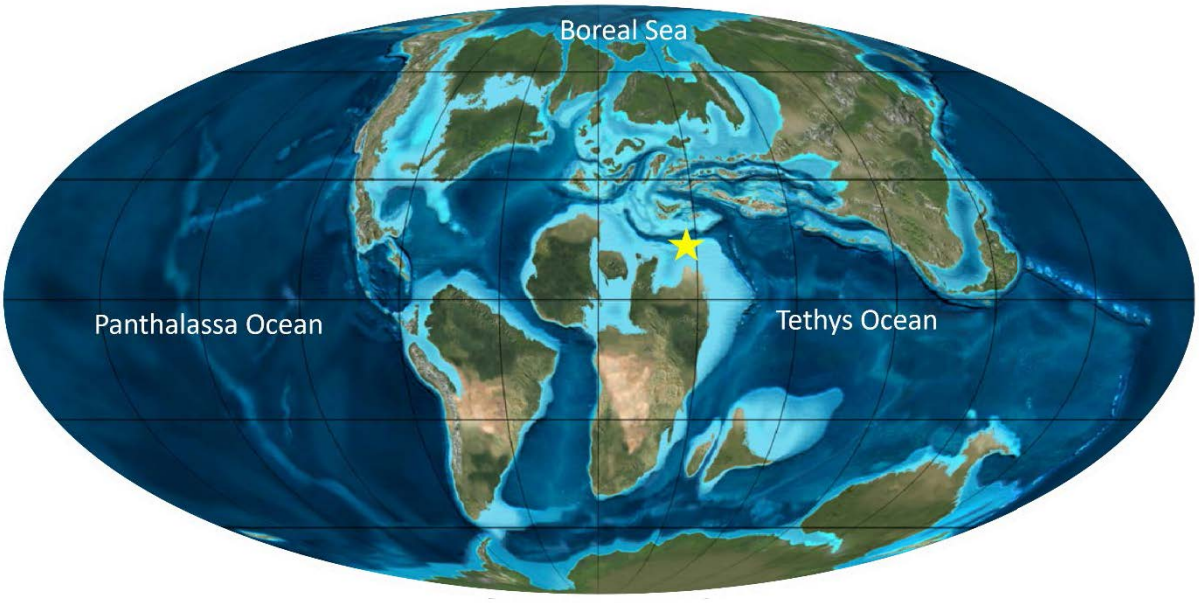

Figure 1.11: Late Cretaceous (Turonian - Coniacian) ~93.5 – 87 Ma. Showing the locality of the Lebanese Lagerstätten (Cenomanian, and Santonian). Modified from the global reconstruction (R. Blakey) from the TimeScale Creator software.

The main coleoid-bearing Lagerstätten in Lebanon are represented by three classic localities, Haqel, Hjoula from the Cenomanian, and Sahel Alma from the Santonian. These lithographic limestones are well-known for their fossil assemblages, which include fishes, reptiles, arthropods, annelids, and ammonoid and coleoid cephalopods (e.g., Dalla Vecchia *et al.* 2001; Forey *et al.* 2003; Wippich & Lehmann 2004; Bracchi & Alessandrello 2005; Fuchs 2006*a*, 2007; Fuchs *et al.* 2009; Fuchs & Weis 2009; Jattiot *et al.* 2015; Charbonnier *et al.* 2017; Cawley & Kriwet 2019; Audo *et al.* 2021; Klug *et al.* 2021*c*; El Hossny & Cavin 2023). A fourth locality, En Nammoura, is part of the same Cenomanian setting, though is less prolific in coleoids (Jattiot *et al.,* 2015).

Ten coleoid genera are known from these localities. These are from the Plesioteuthidae (*Boreopeltis*, *Dorateuthis*), and Teudopseina (*Teudopsinia*, *Glyphidopsis*, *Glyphiteuthis*, *Rachiteuthis*), and Incirrata (*Palaeoctopus*, *Keuppia*, *Styletoctopus*) suborders. These are preserved 2D compressions within the laminated limestones.

See Chapter 4 for further information on the Lebanese coleoid-bearing outcrops.

Haqel, Hjoula, and Sahel Aalma: The sub-lithographic, Sannine Limestone (~650 m max thickness) (Fuchs & Larson 2011*a*) of Haqel and Hjoula are located approximately 10 km east of Byblos (Jbail) (Charbonnier *et al.* 2017) and were deposited in small shallow basins (a few 100 m across) that correspond with depressions (Fuchs *et al.* 2009; Fuchs & Weis 2009; Audo & Charbonnier 2013; Charbonnier & Audo 2012; Jattiot *et al.* 2015). The age of these sediments has been constrained by foraminifera (Hückel 1970; Forey *et al.* 2003) and ammonites (Wippich & Lehmann 2004). Historically, the age determinations have wavered temporally between late Early Cenomanian to Late Cenomanian (Fuchs 2006*a*; Audo & Charbonnier 2013, Fuchs & Larson 2011*b*), though today the two outcrops are understood to represent the lower-upper Cenomanian (95 – 96 Ma) (Fuchs & Weis 2009; Fuchs & Larson 2011*a*; Jattiot *et al.* 2015). Hâdjoula is the slightly older of the two outcrops (Fuchs & Larson 2011*a*). The chalky laminated limestones of Sahel Alma are located approximately 20 km northeast of Beirut (Charbonnier & Audo 2012; Charbonnier *et al.* 2017; Azar *et al.* 2019). These sediments are Late Santonian in age and correspond with a deeper depositional environment than Hjoula or Haqel.

Much of what we know about Mesozoic Octobrachia stems from fossilized gladii and soft tissues preserved at these Lagerstätten localities. The earliest fossil Vampyromorph, *Loligosepia* (Fig. 1.5), is known from the Lower Jurassic Posidonia Shale Formation of Germany, as well as shales from France, Luxembourg, UK, and Canada (Alberta) (Fuchs 2020). The earliest known incirrate octopods (perhaps best known today by benthic Octopuses) are known from Late Cretaceous (Cenomanian and Santonian) deposits of the Lebanese Lagerstätte (Woodward 1883; Fuchs *et al.* 2009, 2016*a*; Fuchs 2020). Each of these three genera, *Palaeoctopus, Keuppia,* and *Styletoctopus,* evidence the heavily reduced, paired and unpaired gladius vestiges (Fuchs 2020).

Figure 1.12: Reconstruction of Hjoula (early Late Cretaceous). Image Huang Diving © in Azar *et al.* 2019.

1.6 ~ Gladius-bearing Coleoid Diversity in the Mesozoic

1.6.1 ~ A Patchy fossil record

The fossil record of Mesozoic coleoids is intermittent. It is not evenly distributed in time and space (Fig 1.13A, B), and typically is restricted to levels of exceptional conservation that are rare in the Triassic and the Cretaceous.

The Triassic has the least known diversity with just two described Prototeuthina genera, *Germanoteuthis* and *Reitneriteuthis*, both of which are *incertae sedis* within the suborder (Table 1.1). Overall, most genera are known from the Jurassic and Upper Cretaceous time bins (Fig. 1.13). These are typically from the Callovian locality of La Voulte-sur-Rhône in France, the Late Jurassic German Lagerstätten on the Solnhofen Archipelago, and the Upper Cretaceous lithographic limestones of Lebanon. The Upper Cretaceous has the most diversity overall with 23 genera. This reflects the diversity seen in the Lebanese Lagerstätten localities (10 genera), but also includes those that have been found elsewhere (e.g., *Eromangateuthis* which is known from the Upper Albian of Australia (Fuchs 2019), or *Niobrarateuthis* from the upper Santonian–lower Campanian of the USA (Miller, 1957).

Order			VAMPYRO-MORPHA	VAMPYRO-MORPHA	VAMPYRO-MORPHA	VAMPYRO-MORPHA	OCTOPODA	OCTOPODA	OCTOPODA	OCTOPODA
Suborder	PROTO-TEUTHINA	PROTO-TEUTHINA	LOLIGO-SEPIINA	LOLIGO-SEPIINA	VAMPYRO-MORPHINA		TEUDO-PSEINA	TEUDO-PSEINA	CIRRATA	INCIRRATA
		Incertae sedis		*Incertae sedis*		*Incertae sedis/Nomen dubium*		*Incertae sedis*		
Oligocene					1					
Upper Cretaceous	3					2	13	1	1	3
Lower Cretaceous	3		1							
Upper Jurassic	3		3	1			9			
Middle Jurassic	2		1			3	3			
Lower Jurassic	1		4				1			
Upper Triassic		1								
Middle Triassic		1								

Table 1.1: Simplified table to show the known gladius-bearing coleoid diversity by time bin (data from Fuchs 2020). This is represented by the Suborders Prototeuthina, Loligosepiina, Vampyromorphina, Teudopseina, Cirrata, and Incirrata, and includes *incertae sedis* and *Nomen dubium* genera. The included genera reflect all occurrences (also see Fig. 1.13A, B) as opposed to genera from the specific Lagerstätten discussed here. Additionally, as this table is grouped by time bin, a genus may be included more than once if it is present in more than one time bin. The Vampyromorphina from the Oligocene (*Necroteuthis*) is described as being related to extant Vampyroteuthis (Košťák *et al.* 2021) along with *Vampyronassa*, which is currently an *incertae sedis* Vampyromorph from the Mid-Jurassic.

At the Suborder-level Teudopseina has the highest diversity starting from one genus in the Lower Jurassic and increasing to 14 in the Late Cretaceous (Table 1.1). The Prototeuthina have the longest and most continuous fossil record, beginning in the early Triassic and extending to the End Cretaceous. Loligosepiina occur in the Lower Jurassic to Lower Cretaceous interval. Among the crown group suborders, Cirrata and Inciratta are not found before the Upper Cretaceous.

1.6.2 ~ Does fossil preservation offer sufficient details for broad scale comparisons?

Many of the diagnostic characteristics for coleoids are based on the morphology of the gladius, but soft tissues also have distinctive features that contribute to the understanding of systematic relationships. As discussed, these include the arm crown and the associated armature (e.g., suckers and their attachments, cirri, and sucker rings), as well as components of the digestive and respiratory systems. Though there is no complete record of the soft tissues for any Mesozoic Octobrachiate coleoid species, the collective amount of data (outlined in Supplementary Table 1.1), is growing. The ability to collect this data will only increase with the use of non-destructive imaging methods that reveal anatomy not visible with traditional

methods. This will enable more meaningful comparisons between fossil and extant coleoid taxa. Not only does this have systematic value, but it also provides a deeper understanding of the lifestyles of Mesozoic forms at a key time in their evolutionary history.

Chapters 3 and 4 of this manuscript will discuss some of the Vampyromorph and Prototeuthid coleoids from the Mid-Jurassic (La Voulte-sur-Rhône), and the Upper Cretaceous Lebanese localities, and how various imaging methods have enhanced the current knowledge about the soft tissues of Mesozoic Octobrachia.

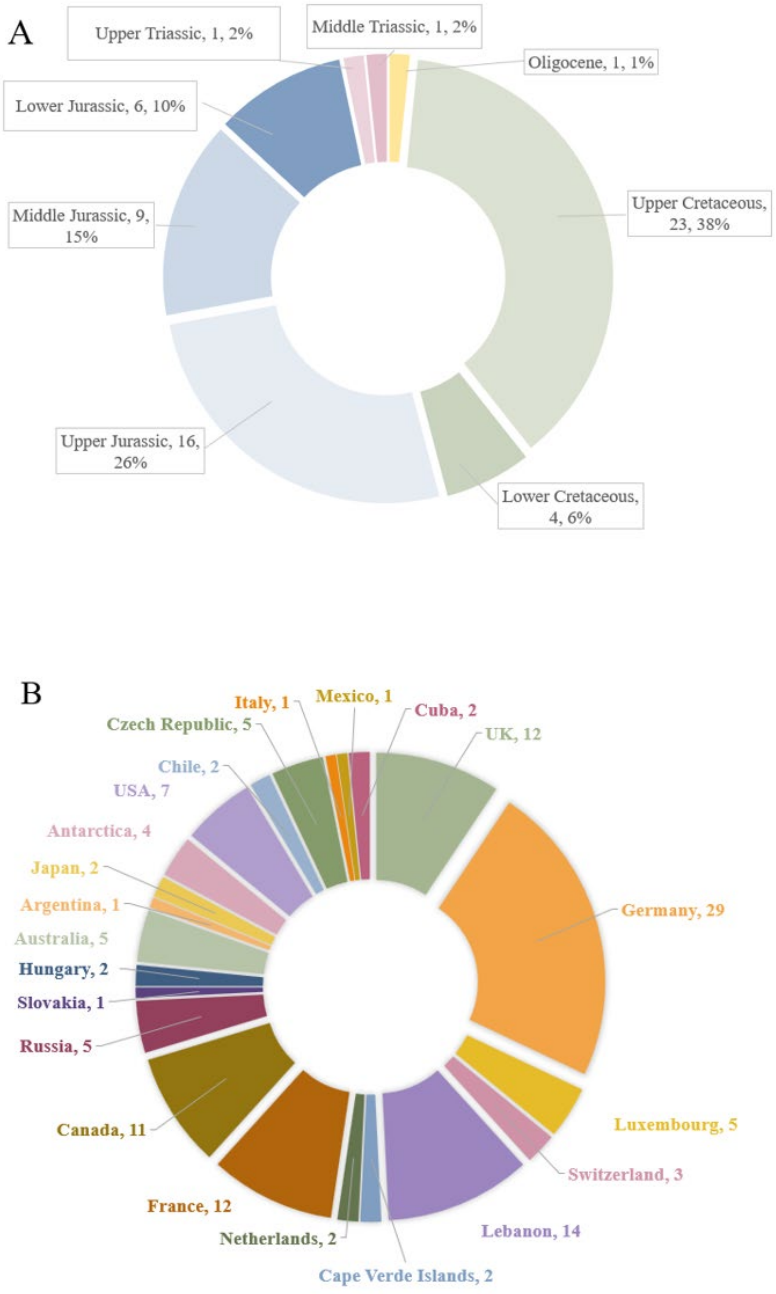

Figure 1.13: Time bin distribution of the described gladius-bearing coleoid genera (A), and number of gladius-bearing coleoid genera by global occurrence (B).

BIBLIOGRAPHY

ALLCOCK, A. L., COOKE, I. R. and STRUGNELL, J. M. 2011. What can the mitochondrial genome reveal about higher-level phylogeny of the molluscan class Cephalopoda?: HIGHER-LEVEL PHYLOGENY OF CEPHALOPODA. *Zoological Journal of the Linnean Society*, **161**, 573–586.

———, LINDGREN, A. and STRUGNELL, J. M. 2014. The contribution of molecular data to our understanding of cephalopod evolution and systematics: a review. *Journal of Natural History*, **49**, 1373–1421.

ALLISON, P. A. 1988*a*. *Konservat-Lagerstätten:* cause and classification. *Paleobiology*, **14**, 331–344.

———. 1988*b*. Phosphatized soft-bodied squids from the Jurassic Oxford Clay. *Lethaia*, **21**, 403–410.

ALTENA, C. O. R. and VAN, C. O. 1949. *Systematic catalogue of the palaeontological collection: sixth supplement (Teuthoidea)*. Teyler's Museum.

ANDERSON, F. E. and LINDGREN, A. R. 2021. Phylogenomic analyses recover a clade of large-bodied decapodiform cephalopods. *Molecular Phylogenetics and Evolution*, **156**, 107038.

AUDO, D. and CHARBONNIER, S. 2013. Late Cretaceous crest-bearing shrimps from the Sahel Alma Lagerstätte of Lebanon. *Acta Palaeontologica Polonica*, **58**, 335–349.

——— and SCHWEIGERT, G. 2018. Large polychelidan lobsters with a rounded carapace from the Middle Jurassic La Voulte-sur-Rhone Lagerstatte: taxonomic clarifications. *Geodiversitas*, **40**, 183–194.

———, WINKLER, N. and CHARBONNIER, S. 2021. *Pseudodrobna natator* n. comb., a new link between crustacean faunas from the Jurassic of Germany and Cretaceous of Lebanon. *Geodiversitas*, **43**, 209–218.

———, SCHWEIGERT, G., MARTIN, J.-P. S. and CHARBONNIER, S. 2014*a*. High biodiversity in Polychelida crustaceans from the Jurassic La Voulte-sur-Rhône Lagerstätte. *Geodiversitas*, **36**, 489–525.

———, ———, HAUG, J. T., HAUG, C., SAINT MARTIN, J.-P. and CHARBONNIER, S. 2014*b*. Diversity and palaeoecology of the enigmatic genus *Knebelia* (Eucrustacea, Decapoda, Eryonidae) from Upper Jurassic plattenkalks in southern Germany. *Palaeontology*, **57**, 397–416.

———., ———, ———, CHARBONNIER, S., SCHWEIGERT, G., MULLER, C. and HARZSCH, S. 2016. On the sighted ancestry of blindness - exceptionally preserved eyes of Mesozoic polychelidan lobsters. *Zoological Letters*, **2**.

——— ROBIN, N., LUQUE, J., KROBICKI, M., HAUG, J. T., HAUG, C., JAUVION, C. and CHARBONNIER, S. 2019. Palaeoecology of *Voulteryon parvulus* (Eucrustacea, Polychelida) from the Middle Jurassic of La Voulte-sur-Rhône Fossil-Lagerstätte (France). *Scientific Reports*, **9**, 5332.

AZAR, D., MAKSOUD, S., HUANG, D. and NEL, A. 2019. First Lebanese dragonflies (Insecta: Odonata, Aeshnoptera, Cavilabiata) from the Arabo-African mid-Cretaceous paleocontinent. *Cretaceous Research*, **93**, 78–89.

BANDEL, K. and LEICH, H. 1986. Jurassic Vampyromorpha (dibranchiate cephalopods). *Neues Jahrbuch für Geologie und Paläontologie-Monatshefte*, **3**, 129–148.

BERTHOLD, T. and ENGESER, T. 1987. Phylogenetic analysis and systematization of the Cephalopoda (Mollusca). Verh. Naturwiss. Ver. Hamburg 29, 187–220. *Cephalopods. Bull. Mar. Sci*, **64**, 57–76.

BIZIKOV, V. A. 2004. The shell in Vampyropoda (Cephalopoda): morphology, functional role and evolution. *Ruthenica*, 1–88.

——— and TOLL, R. B. 2016. Treatise Online no. 77: Part M, Chapter 9A: The Gladius and its Vestiges in Extant Coleoidea. *Treatise Online*.

BOLETZKY, S. von. 1992. Evolutionary aspects of development, life style, and reproductive mode in incirrate octopods (Mollusca, Cephalopoda). *Revue suisse de zoologie.*, **99**, 755–770.

BOTTJER, D. J., ETTER, W., HAGADORN, J. W. and TANG, C. M. 2002. Fossil-Lagerstätten: jewels of the fossil record. *Exceptional Fossil Preservation: A Unique View on the Evolution of Marine Life: Columbia University Press, New York*, 1–10.

BOYLE, P. and RODHOUSE, P. 2008. *Cephalopods: ecology and fisheries*. John Wiley & Sons.

BRACCHI, G. and ALESSANDRELLO, A. 2005. *Paleodiversity of the Free-living Polychaetes: (Annelida, Polychaeta) and Description of New Taxa from the Upper Cretaceous Lagerstätten of Haqel, Hadjula and Al-Namoura (Lebanon)*. Società Italiana di Scienze Naturali e Museo Civico di Storia Naturale.

BRIGGS, D. E. G. 1995. Experimental Taphonomy. *PALAIOS*, **10**, 539–550.

——— and WILBY, P. R. 1996. The role of the calcium carbonate-calcium phosphate switch in the mineralization of soft-bodied fossils. *Journal of the Geological Society*, **153**, 665–668.

———, KEAR, A. J., MARTILL, D. M. and WILBY, P. R. 1993. Phosphatization of soft-tissue in experiments and fossils. *Journal of the Geological Society*, **150**, 1035–1038.

BUDELMANN, B. 1996. Active marine predators: The sensory world of cephalopods. *Marine and Freshwater Behaviour and Physiology*, **27**, 59–75.

BUSH, S. and ROBISON, B. 2007. Ink utilization by mesopelagic squid. *Marine Biology*, **152**, 485–494.

CAINE, H. and BENTON, M. J. 2011. Ichthyosauria from the Upper Lias of Strawberry Bank, England. *Palaeontology*, **54**, 1069–1093.

CARUTHERS, A. H., SMITH, P. L. and GRÖCKE, D. R. 2013. The Pliensbachian–Toarcian (Early Jurassic) extinction, a global multi-phased event. *Palaeogeography, Palaeoclimatology, Palaeoecology*, **386**, 104–118.

CAWLEY, J. J. and KRIWET, J. 2019. A new genus and species of pycnodontid fish *Flagellipinna rhomboides*, gen. et sp. nov. (Neopterygii, Pycnodontiformes), from the Upper Cretaceous (Cenomanian) of Lebanon, with notes on juvenile form and ecology. *Journal of Vertebrate Paleontology*, **39**, e1614012.

CHARBONNIER, S. 2009. *Le Lagerstätte de La Voulte: un environnement bathyal au Jurassique*. *Mémoires Du Muséum National d'Histoire Naturelle*. Vol. 199. Publications scientifiques du Muséum Paris.

——— and AUDO, D. 2012. New nisto of slipper lobster (Decapoda: Scyllaridae) from the Hâdjoula Lagerstätte (Late Cretaceous, Lebanon). *Journal of Crustacean Biology*, **32**, 583–590.

——— VANNIER, J. and RIOU, B. 2007*a*. New Sea spiders from the Jurassic La Voulte-sur-Rhône Lagerstätte. *Proceedings of the Royal Society B: Biological Sciences*, **274**, 2555–2561.

———, ———., HANTZPERGUE, P. and GAILLARD, C. 2010. Ecological Significance of the Arthropod Fauna from the Jurassic (Callovian) La Voulte Lagerstätte. *Acta Palaeontologica Polonica*, **55**, 111–132.

———, AUDO, D., CAZE, B. and BIOT, V. 2014. The La Voulte-sur-Rhône Lagerstätte (Middle Jurassic, France). *Comptes Rendus Palevol*, **13**, 369–381.

———, VANNIER, J., GAILLARD, C., BOURSEAU, J.-P. and HANTZPERGUE, P. 2007*b*. The La Voulte Lagerstätte (Callovian): Evidence for a deep water setting from sponge and crinoid communities. *Palaeogeography, Palaeoclimatology, Palaeoecology*, **250**, 216–236.

———, TERUZZI, G., AUDO, D., LASSERON, M., HAUG, C. and HAUG, J. T. 2017. New thylacocephalans from the Cretaceous Lagerstätten of Lebanon. *Bulletin de la Société géologique de France*, **188**, 19.

CHEREL, Y., and HOBSON, K.A., 2005. Stable isotopes, beaks and predators: a new tool to study the trophic ecology of cephalopods, including giant and colossal squids. *Proceedings of the Royal Society B: Biological Sciences*, *272*(1572), pp.1601-1607.

CHUN, C., 1903. Aus den Tiefen des Weltmeeres. Gustav Fischer.

CLARKE, M. R. 1996. The Role of Cephalopods in the World's Oceans: An Introduction. *Philosophical Transactions: Biological Sciences*, **351**, 979–983.

——— and CLARKE, M. R. 1997. The role of cephalopods in the world's oceans: general conclusions and the future. *Philosophical Transactions of the Royal Society of London. Series B: Biological Sciences*, **351**, 1105–1112.

CLEMENTS, T., PURNELL, M. A. and GABBOTT, S. 2022. Experimental analysis of organ decay and pH gradients within a carcass and the implications for phosphatization of soft tissues. *Palaeontology*, **65**, e12617.

———, COLLEARY, C., DE BAETS, K. and VINTHER, J. 2017. Buoyancy mechanisms limit preservation of coleoid cephalopod soft tissues in Mesozoic Lagerstätten. *Palaeontology*, **60**, 1–14.

COLLINS, M. and VILLANUEVA, R. 2006. Taxonomy, ecology and behaviour of the Cirrate Octopods. *Oceanography and marine biology*, **44**, 277–322.

DALLA VECCHIA, F. M., ARDUINI, P. and KELLNER, A. W. A. 2001. The first pterosaur from the Cenomanian (Late Cretaceous) Lagerstätten of Lebanon. *Cretaceous Research*, **22**, 219–225.

DE BAETS, K., KLUG, C., KORN, D., BARTELS, C. and POSCHMANN, M. 2013. Emsian Ammonoidea and the age of the Hunsrück Slate (Rhenish Mountains, Western Germany). *Palaeontographica A*, **299**, 1–113.

DERBY, C. D. 2014. Cephalopod Ink: Production, Chemistry, Functions and Applications. *Marine Drugs*, **12**, 2700–2730.

DIETL, G. and SCHWEIGERT, G. 2004. The Nusplingen Lithographic Limestone-a "fossil lagerstaette" of late Kimmeridgian age from the Swabian Alb (Germany). *Rivista Italiana di Paleontologia e Stratigrafia*, **110**.

DOGUZHAEVA, L. A., & MUTVEI, H. 2006. Ultrastructural and chemical comparison between gladii in living coleoids and Aptian coleoids from Central Russia. Acta Universitatis Carolinae, Geologica, **49**, 83–93.

DONOVAN, D. 1977. Evolution of the dibranchiate Cephalopoda. **38**, 15–48.

———. 1983. Mastigophora Owen: A little known genus of Jurassic coleoid. *Neues Jahrbuch für Geologie und Paläontologie Abhandlungen*, **165**, 484–495.

DONOVAN, D.T., 2016. Part M., Chapter 9C: composition and structure of gladii in fossil Coleoidea. *Treatise Online*, *75*, pp.1-5.

——— and CRANE, M. 1992. The type material of the Jurassic cephalopod Belemnotheutis. *Palaeontology*, **35**, 273–296.

——— and FUCHS, D. 2012. Treatise Online no. 53: Part M, Chapter 14: History of higher classification of Coleoidea. *Treatise Online*.

——— and ———. 2016. Treatise Online no. 73: Part M, Chapter 13: Fossilized Soft Tissues in Coleoidea. *Treatise Online*.

——— and RIEGRAF, W. 2016. Treatise Online no. 78: Part M, Chapter 21: History of the Study of Fossil Coleoidea. *Treatise Online*.

D'ORBIGNY, A., 1835. In A. Ferussac & A. D'Orbigny (eds) Histoire Naturelle Générale et Particuliere des Céphalopodes Acétabulifères Vivants et Fossils. 2 vols. *Text and Atlas. Paris*.

DOYLE, P. 1990. Teuthid cephalopods from the Lower Jurassic of Yorkshire. *Palaeontology*, **33**, 193–207.

DOYLE, P., DONOVAN, D. T. and NIXON, M. 1994. Phylogeny and systematics of the Coleoidea.

EHRENBERG, C.G., 1831. Cephalopoda in mare rubro viventia. *Animalia invertebrata exclusis insectes. Symbolae physicae, seu icones et descriptiones Corparum Naturalium novorum aut minus cognitorum, quae ex itineribus per Libyam, Aegyptum, Nubiam, Dongalam, Syriam, Arabiam et Habessiniam, Pars zoologica, Hemprich, PC, and Ehrenberg, CG, Ed.,* Berlin, **4,** 6.

EL HOSSNY, T. and CAVIN, L. 2023. A New Enigmatic Teleost Fish from the Mid-Cretaceous of Lebanon. *Diversity*, **15**, 839.

ELMI, S. 1967. Le Lias supérieur et le Jurassique moyen de l'Ardèche (3e fascicule). *Travaux et Documents des Laboratoires de Géologie de Lyon*, **19**.

ENGESER, T. and BANDEL, K. 1988. Phylogenetic classification of coleoid cephalopods. 105–115.

ETTER, W. 2002. Solnhofen: plattenkalk preservation with Archaeopteryx. *Exceptional Fossil Preservation. A Unique View on the Evolution of Marine Life. Columbia University Press, New York*, 327–352.

FERNÁNDEZ-ÁLVAREZ, F. Á., TAITE, M., VECCHIONE, M., VILLANUEVA, R. and ALLCOCK, A. L. 2022. A phylogenomic look into the systematics of oceanic squids (order Oegopsida). *Zoological Journal of the Linnean Society*, **194**, 1212–1235.

FERRY, S., MERRAN, Y., GROSHENY, D. and MROUEH, M. 2007. The Cretaceous of Lebanon in the Middle East (levant) context. *Carnets de Géologie*, 38–42.

FISCHER, J.-C. 2003. Invertébrés remarquables du Callovien inférieur de la Voulte-sur-Rhône (Ardèche, France). *Annales de Paléontologie*, **89**, 223–252.

——— and RIOU, B. 1982*a*. Les teuthoïdes (Cephalopoda, Dibranchiata) du Callovien inférieur de la Voulte-sur-Rhône (Ardèche, France). *Annales de Paléontologie*, **68**, 295–325.

——— and ———. 1982*b*. Les Teuthoïdes (Cephalopoda, Dibranchiata) du Callovien inférieur de La Voulte− sur− Rhône (Ardèche, France). *Annales de Paléontologie*, **68**, 295–325.

——— and ———. 2002. *Vampyronassa rhodanica* nov. gen. nov sp., vampyromorphe (Cephalopoda, Coleoidea) du Callovien inférieur de la Voulte-sur-Rhône (Ardèche, France). *Annales de Paléontologie*, **88**, 1–17.

FOREY, P. L., YI, L., PATTERSON, C. and DAVIES, C. E. 2003. Fossil fishes from the Cenomanian (Upper Cretaceous) of Namoura, Lebanon. *Journal of Systematic palaeontology*, **1**, 227.

FUCHS, D. 2006*a*. Morphology, taxonomy and diversity of vampyropod coleoids (Cephalopoda) from the Upper Cretaceous of Lebanon. *Memorie della Società italiana di Scienze naturali e del Museo civico di Storia naturale di Milano*, **34**, 1–28.

———. 2006*b*. Fossil erhaltungsfahige Merkmalskomplexe der Coleoidea (Cephalopoda) und ihre phylogenetische Bedeutung. *Berliner Palaobiologische Abhandlungen*, **8**, 1–122.

———. 2007. Coleoid cephalopods from the plattenkalks of the Upper Jurassic of Southern Germany and from the Upper Cretaceous of Lebanon A faunal comparison. *Neues Jahrbuch für Geologie und Paläontologie - Abhandlungen*, **245**, 59–69.

———. 2009. Octobrachia—a diphyletic taxon. *Berliner Paläobiologische Abhandlungen*, **10**, 182–192.

———. 2014. First evidence of *Mastigophora* (Cephalopoda: Coleoidea) from the early Callovian of La Voulte-sur- Rhône (France). *Göttingen Contributions to Geosciences*, **77**, 21–27.

———. 2016. Treatise Online No. 83: Part M, Chapter 9B: The Gladius and Gladius Vestige in Fossil Coleoidea. *Treatise Online*.

———. 2020. Treatise Online no. 138: Part M, Chapter 23G: Systematic Descriptions: Octobrachia. *Treatise Online*.

———. 2019. *Eromangateuthis* N. Gen., a new genus for a Late Albian gladius-bearing giant octobrachian (Cephalopoda: Coleoidea). Paleontological Contributions, 21; 1-3

———. and R. WEIS. 2008. Taxonomy, morphology and phylogeny of Lower Jurassic loligosepiid coleoids (Cephalopoda). Neues Jahrbuch für Geologie und Paläontologie Abhandlungen, 249:93–112.

——— and ———. 2009. A new Cenomanian (Late Cretaceous) coleoid (Cephalopoda) from Hâdjoula, Lebanon. *Fossil Record*, **12**, 175–181.

——— and ———. 2010. Taxonomy, morphology and phylogeny of Lower Jurassic teudopseid coleoids (Cephalopoda). Neues Jahrbuch für Geologie und Paläontologie Abhandlungen, 257:351–366.

——— and LARSON, N. 2011*a*. Diversity, Morphology, and Phylogeny of Coleoid Cephalopods from the Upper Cretaceous Plattenkalks of Lebanon–Part II: Teudopseina. *Journal of Paleontology*, **85**, 815–834.

——— and ———. 2011*b*. Diversity, morphology, and phylogeny of coleoid cephalopods from the Upper Cretaceous Plattenkalks of Lebanon-Part I: Prototeuthidina. *Journal of Paleontology*, **85**, 234–249.

——— and IBA, Y. 2015. The gladiuses in coleoid cephalopods: homology, parallelism, or convergence? *Swiss Journal of Palaeontology*, **134**, 187–197.

——— and SCHWEIGERT, G. 2018. First Middle–Late Jurassic gladius vestiges provide new evidence on the detailed origin of incirrate and cirrate octopuses (Coleoidea). *PalZ*, **92**, 203–217.

———, KEUPP, H. and ENGESER, T. 2003. New records of soft parts of Muensterella scutellaris MUENSTER, 1842 (Coleoidea) from the Late Jurassic Plattenkalks of Eichstätt and their significance for octobrachian relationships. *Berliner Paläobiologische Abhandlungen*, **3**, 101–111.

———, KLINGHAMMER, A. and KEUPP, H. 2007*a*. Taxonomy, morphology and phylogeny of plesioteuthidid coleoids from the Upper Jurassic (Tithonian) Plattenkalks of Solnhofen. *Neues Jahrbuch für Geologie und Paläontologie - Abhandlungen*, **245**, 239–252.

———, ENGESER, T. and KEUPP, H. 2007*b*. Gladius shape variation in coleoid cephalopod Trachyteuthis from the Upper Jurassic Nusplingen and Solnhofen Plattenkalks. *Acta Palaeontol. Pol.*, **52**.

———, BRACCHI, G. and WEIS, R. 2009. New Octopods (Cephalopoda: Coleoidea) from the Late Cretaceous (Upper Cenomanian) of Häkel and Hädjoula, Lebanon. *Palaeontology*, **52**, 65–81.

———, VON BOLETZKY, S. and TISCHLINGER, H. 2010. New evidence of functional suckers in belemnoid coleoids (Cephalopoda) weakens support for the 'Neocoleoidea' concept. *Journal of Molluscan Studies*, **76**, 404–406.

———, KEUPP, H. and SCHWEIGERT, G. 2013. First record of a complete arm crown of the Early Jurassic coleoid *Loligosepia* (Cephalopoda). *Paläontologische Zeitschrift*, **87**, 431–435.

———, HOFFMANN, R. and KLUG, C. 2021. Evolutionary development of the cephalopod arm armature: a review. *Swiss Journal of Palaeontology*, **140**, 1–27.

———, IBA, Y., TISCHLINGER, H., KEUPP, H. and KLUG, C. 2016*a*. The locomotion system of Mesozoic Coleoidea (Cephalopoda) and its phylogenetic significance. *Lethaia*, **49**, 433–454.

———, WILBY, P. R., VON BOLETZKY, S., ABI-SAAD, P., KEUPP, H. and IBA, Y. 2016*b*. A nearly complete respiratory, circulatory, and excretory system preserved in small Late Cretaceous octopods (Cephalopoda) from Lebanon. *PalZ*, **90**, 299–305.

———, IBA, Y., HEYNG, A., IIJIMA, M., KLUG, C., LARSON, N. L. and SCHWEIGERT, G. 2020. The Muensterelloidea: phylogeny and character evolution of Mesozoic stem octopods. *Papers in Palaeontology*, **6**, 31–92.

GOLIKOV, A. V., CEIA, F. R., SABIROV, R. M., ABLETT, J. D., GLEADALL, I. G., GUDMUNDSSON, G., HOVING, H. J., JUDKINS, H., PÁLSSON, J., REID, A. L.,

ROSAS-LUIS, R., SHEA, E. K., SCHWARZ, R. and XAVIER, J. C. 2019. The first global deep-sea stable isotope assessment reveals the unique trophic ecology of Vampire Squid *Vampyroteuthis infernalis* (Cephalopoda). *Scientific Reports*, **9**, 19099.

GRASSO, F. W. and BASIL, J. A. 2009. The Evolution of Flexible Behavioral Repertoires in Cephalopod Molluscs. *Brain, Behavior and Evolution*, **74**, 231–245.

GRIMPE, G. 1916. *Chunioteuthis*: eine neue Cephalopodengattung. *Zoologischer Anzeiger*, **46**, 249.

GUERRA, Á. 2019. Functional Anatomy: Macroscopic Anatomy and Post-mortem Examination. *In* GESTAL, C., PASCUAL, S., GUERRA, Á., FIORITO, G. and VIEITES, J. M. (eds.) *Handbook of Pathogens and Diseases in Cephalopods*, Springer International Publishing, Cham, 11–38 pp.

HAAS, W. 2002. The evolutionary history of the eight-armed Coleoidea. In: Summesberger, H. *et al.* (eds.): *Cephalopods - Present & Past*: 341-351 (Abhandlungen der Geologischen Bundesanstalt 57)

HAECKEL, E. H. P. A. 1866. *Generelle morphologie der organismen. Allgemeine grundzüge der organischen formen-wissenschaft, mechanisch begründet durch die von Charles Darwin reformirte descendenztheorie, von Ernst Haeckel.* G. Reimer, Berlin.

HANLON, R. 2007. Cephalopod dynamic camouflage. *Current Biology*, **17**, R400–R404.

HANLON, R. T. and MESSENGER, J. B. 2018. *Cephalopod Behaviour*. Cambridge University Press.

HART, M. B., PAGE, K. N., PRICE, G. D. and SMART, C. W. 2019. Reconstructing the Christian Malford ecosystem in the Oxford Clay Formation (Callovian, Jurassic) of Wiltshire: exceptional preservation, taphonomy, burial and compaction. *Journal of Micropalaeontology*, **38**, 133–142.

———, DE JONGHE, A., PAGE, K. N., PRICE, G. D. and SMART, C. W. 2016. Exceptional accumulations of statoliths in association with the Christian Malford Lagerstätte (Callovian, Jurassic) in Wiltshire, United Kingdom. *Palaios*, **31**, 203–220.

HESS, H. 1999. Lower Jurassic Posidonia Shale of Southern Germany. *Fossil crinoids*, 183–196.

HILDENBRAND, A., AUSTERMANN, G., FUCHS, D., BENGTSON, P. and STINNESBECK, W. 2021. A potential cephalopod from the early Cambrian of eastern Newfoundland, Canada. *Communications Biology*, **4**, 1–11.

HOBSON, K.A. and CHEREL, Y., 2006. Isotopic reconstruction of marine food webs using cephalopod beaks: new insight from captively raised Sepia officinalis. *Canadian Journal of Zoology*, **84** (5), 766-770.

HOFFMANN, R. 2015. The correct taxon name, authorship, and publication date of extant ten-armed coleoids. *Paleontological Contributions*, **2015**, 1–4.

———, BESTWICK, J., BERNDT, G., BERNDT, R., FUCHS, D. and KLUG, C. 2020. Pterosaurs ate soft-bodied cephalopods (Coleoidea). *Scientific Reports*, **10**, 1230.

HOVING, H. J. T. and ROBISON, B. H. 2012. Vampire squid: detritivores in the oxygen minimum zone. *Proceedings of the Royal Society B: Biological Sciences*, **279**, 4559–4567.

———, PEREZ, J. A. A., BOLSTAD, K. S. R., BRAID, H. E., EVANS, A. B., FUCHS, D., JUDKINS, H., KELLY, J. T., MARIAN, J. E. A. R., NAKAJIMA, R., PIATKOWSKI, U., REID, A., VECCHIONE, M. and XAVIER, J. C. C. 2014. The study of deep-sea cephalopods. *In* VIDAL, E. A. G. (ed.) *Advances in Cephalopod Science: Biology, Ecology, Cultivation and Fisheries*, Vol. 67. Advances in Marine Biology, 235–359 pp.

HÜCKEL, U. 1970. Die Fischschiefer von Haqel und Hjoula in der Oberkreide des Libanon. *Neues Jahrbuch für Geologie und Paläontologie, Abhandlungen*, **135**, 113–149.

HUNT, S. and NIXON, M. 1981. A comparative study of protein composition in the chitin-protein complexes of the beak, pen, sucker disc, radula and oesophageal cuticle of cephalopods. *Comparative Biochemistry and Physiology Part B: Comparative Biochemistry*, **68**, 535–546.

IBÁÑEZ, C., DÍAZ-SANTANA-ITURRIOS, M., LÓPEZ-CÓRDOVA, D., CARRASCO, S., PARDO-GANDARILLAS, M., ROCHA, F. and VIDAL, E. 2021*a*. A phylogenetic approach to understand the evolution of reproduction in coleoid cephalopods. *Molecular Phylogenetics and Evolution*, **155: 106972**.

———, RIERA, R., LEITE, T., DÍAZ-SANTANA-ITURRIOS, M., ROSA, R. and PARDO-GANDARILLAS, M. C. 2021*b*. Stomach content analysis in cephalopods: past research, current challenges, and future directions. *Reviews in Fish Biology and Fisheries*, **31**, 505–522.

JAITLY, R., EHRNSTEN, E., HEDLUND, J., CANT, M., LEHMANN, P. and HAYWARD, A. 2022. The evolution of predator avoidance in cephalopods: A case of brain over brawn? *Frontiers in Marine Science*, **9**.

JAMISON-TODD, S., MOON, B. C., ROWE, A. J., WILLIAMS, M. and BENTON, M. J. 2022. Dietary niche partitioning in Early Jurassic ichthyosaurs from Strawberry Bank. *Journal of Anatomy*, **241**, 1409–1423.

JATTIOT, R., BRAYARD, A., FARA, E. and CHARBONNIER, S. 2015. Gladius-bearing coleoids from the Upper Cretaceous Lebanese Lagerstätten: Diversity, morphology, and phylogenetic implications. *Journal of Paleontology*, **89**, 148–167.

JAUVION, C. 2020. *De la vie à la pierre: préservation exceptionnelle d'arthropodes marins fossiles*. (Doctoral dissertation. Muséum National d'Histoire Naturelle, Paris).

———, CHARBONNIER, S. and BERNARD, S. 2017. A new look at the shrimps (Crustacea, Decapoda, Penaeoidea) from the Middle Jurassic La Voulte-sur-Rhone Lagerstatte. *Geodiversitas*, **39**, 705–716.

———, AUDO, D., CHARBONNIER, S. and VANNIER, J. 2016. Virtual dissection and lifestyle of a 165-million-year-old female polychelidan lobster. *Arthropod Structure & Development*, **45**, 122–132.

———, BERNARD, S., GUERIAU, P., MOCUTA, C., PONT, S., BENZERARA, K. and CHARBONNIER, S. 2020. Exceptional preservation requires fast biodegradation: thylacocephalan specimens from La Voulte-sur-Rhône (Callovian, Jurassic, France). *Palaeontology*, **63**, 395–413.

JELETZKY, J. A. 1965. Taxonomy and phylogeny of fossil Coleoidea (= Dibranchiata). *Geological Survey of Canada, Papers*, **65**, 76–78.

———, 1966. Comparative morphology, phylogeny, and classification of fossil Coleoidea. .

JENNY, D., FUCHS, D., ARKHIPKIN, A. I., HAUFF, R. B., FRITSCHI, B. and KLUG, C. 2019. Predatory behaviour and taphonomy of a Jurassic belemnoid coleoid (Diplobelida, Cephalopoda). *Scientific Reports*, **9**, 7944.

JEREB, P. and ROPER, C. F. E. 2005. *Cephalopods of the world. An Annotated and Illustrated catalogue of Cephalopod species known to date. Vol. 1. Chambered nautiluses and sepioids (Nautilidae, Sepiidae, Sepiolidae, Sepiadariidae, Idiosepiidae and Spirulidae)*. FAO Spec. Cat. Fish. Purp. 4(1), Rome, FAO, 262p.

——— and ROPER, C. F. 2010. *Cephalopods of the world-an annotated and illustrated catalogue of cephalopod species known to date. Vol 2. Myopsid and oegopsid squids*. FAO Species Catalogue for Fishery Purposes, No. 4, Vol. 2, Rome, FAO, 605p.

———, ———, Norman, M.D. and Finn J.K. 2016. *Cephalopods of the world. An Annotated and illustrated catalogue of Cephalopod species known to date. Vol. 3. Octopods and vampire squids.* FAO Spec. Cat. Fish. Purp. 4(3), Rome, FAO, 398p.

KEAR, A.J., BRIGGS, D.E. and DONOVAN, D.T., 1995. Decay and mineralization of non-mineralized tissue in coleoid cephalopods. *Palaeontology*, *38*, pp.105-131.

KEFERSTEIN, W. 1866. Kopftragende Weichthiere (Malacozoa cephalophora). *(No Title)*.

KEMP, R., PETERS, H., ALLCOCK, L., CARPENTER, K., OBURA, D., POLIDORO, B., RICHMAN, N., COLLEN, B., BÖHM, M. and BAILLIE, J. 2012. Marine invertebrate life. *Spineless: Status and trends of the world's invertebrates. Zoological Society of London, United Kingdom*, 34–45.

KIER, W. M. and SMITH, A. M. 1990. The Morphology and Mechanics of Octopus Suckers. *The Biological Bulletin*, **178**, 126–136.

KLEIN, N., SCHOCH, R. R. and SCHWEIGERT, G. 2016. A juvenile eurysternid turtle (Testudines: Eurysternidae) from the upper Kimmeridgian (Upper Jurassic) of Nusplingen (SW Germany). *Geobios*, **49**, 355–364.

KLOMPMAKER, A. A. and KITTLE, B. A. 2021. Inferring octopodoid and gastropod behavior from their Plio-Pleistocene cowrie prey (Gastropoda: Cypraeidae). *Palaeogeography, Palaeoclimatology, Palaeoecology*, **567**, 110251.

——— and LANDMAN, N. H. 2021. Octopodoidea as predators near the end of the Mesozoic Marine Revolution. *Biological Journal of the Linnean Society*, **132**, 894–899.

KLUG, C., SCHWEIGERT, G., DIETL, G. and FUCHS, D. 2005. Coleoid beaks from the Nusplingen Lithographic Limestone (Upper Kimmeridgian, SW Germany). *Lethaia*, **38**, 173–192.

———, ———, FUCHS, D. and DIETL, G. 2010*a*. First record of a belemnite preserved with beaks, arms and ink sac from the Nusplingen Lithographic Limestone (Kimmeridgian, SW Germany). *Lethaia*, **43**, 445–456.

———, ———, ——— and DE BAETS, K. 2021*a*. Distraction sinking and fossilized coleoid predatory behaviour from the German Early Jurassic. *Swiss Journal of Palaeontology*, **140**, 1–12.

———, ———, TISCHLINGER, H. and POCHMANN, H. 2021*b*. Failed prey or peculiar necrolysis? Isolated ammonite soft body from the Late Jurassic of Eichstätt (Germany) with complete digestive tract and male reproductive organs. *Swiss Journal of Palaeontology*, **140**, 3.

———, KRÖGER, B., VINTHER, J., FUCHS, D. and DE BAETS, K. 2015*a*. Ancestry, Origin and Early Evolution of Ammonoids. *In* KLUG, C., KORN, D., DE BAETS, K., KRUTA, I. and MAPES, R. H. (eds.) *Ammonoid Paleobiology: From Macroevolution to Paleogeography*, Vol. 44. Springer Netherlands, Dordrecht, 3–24 pp.

———, FUCHS, D., SCHWEIGERT, G., RÖPER, M. and TISCHLINGER, H. 2015*b*. New anatomical information on arms and fins from exceptionally preserved *Plesioteuthis* (Coleoidea) from the Late Jurassic of Germany. *Swiss Journal of Palaeontology*, **134**, 245–255.

———, POHLE, A., ROTH, R., HOFFMANN, R., WANI, R. and TAJIKA, A. 2021*c*. Preservation of nautilid soft parts inside and outside the conch interpreted as central nervous system, eyes, and renal concrements from the Lebanese Cenomanian. *Swiss Journal of Palaeontology*, **140**, 15.

———, KROEGER, B., KIESSLING, W., MULLINS, G. L., SERVAIS, T., FRÝDA, J., KORN, D. and TURNER, S. 2010*b*. The Devonian nekton revolution. *Lethaia*, **43**, 465–477.

———, LANDMAN, N., FUCHS, D., MAPES, R., POHLE, A., GUERIAU, P., REGUER, S. and HOFFMANN, R. 2019. Anatomy and evolution of the first Coleoidea in the Carboniferous. *Communications Biology*, **2**.

KLUG, C., HOFFMANN, R., TISCHLINGER, H. *et al.* 2023. 'Arm brains' (axial nerves) of Jurassic coleoids and the evolution of coleoid neuroanatomy. *Swiss J Palaeontol* **142**, 22

KOCOT, K. M., POUSTKA, A. J., STÖGER, I., HALANYCH, K. M. and SCHRÖDL, M. 2020. New data from Monoplacophora and a carefully-curated dataset resolve molluscan relationships. *Scientific Reports*, **10**, 101.

KOŠŤÁK, M., SCHLÖGL, J., FUCHS, D., HOLCOVÁ, K., HUDÁČKOVÁ, N., CULKA, A., FÖZY, I., TOMAŠOVÝCH, A., MILOVSKÝ, R., ŠURKA, J. and MAZUCH, M. 2021. Fossil evidence for vampire squid inhabiting oxygen-depleted ocean zones since at least the Oligocene. *Communications Biology*, **4**, 1–13.

KRÖGER, B. 2005. Adaptive evolution in Paleozoic coiled cephalopods. *Paleobiology*, **31**, 253–268.

——— and MAPES, R. H. 2007. On the origin of bactritoids (Cephalopoda). *Paläontologische Zeitschrift*, **81**, 316–327.

——— and YUN-BAI, Z. 2009. Pulsed cephalopod diversification during the Ordovician. *Palaeogeography, Palaeoclimatology, Palaeoecology*, **273**, 174–183.

KRÔGER B, SERVAIS T, ZHANG Y. 2009. The Origin and Initial Rise of Pelagic Cephalopods in the Ordovician. *PLoS ONE* 4(9), e7262.

———, VINTHER, J. and FUCHS, D. 2011. Cephalopod origin and evolution: A congruent picture emerging from fossils, development and molecules: Extant cephalopods are younger than previously realised and were under major selection to become agile, shell-less predators. *BioEssays*, **33**, 602–613.

KRUTA, I., ROUGET, I., CHARBONNIER, S., BARDIN, J., FERNANDEZ, V., GERMAIN, D., BRAYARD, A. and LANDMAN, N. 2016. *Proteroctopus ribeti* in coleoid evolution. *Palaeontology*, **59**, 767–773.

LEACH, W. E. 1817. Synopsis of the orders, families, and genera of the class Cephalopoda. *The Zoological Miscellany, being descriptions of new or interesting animals*, **3**, 137.

LINDGREN, A. R. and ANDERSON, F. E. 2018. Assessing the utility of transcriptome data for inferring phylogenetic relationships among coleoid cephalopods. *Molecular Phylogenetics and Evolution*, **118**, 330–342.

LINDGREN, A. R., GIRIBET, G. and NISHIGUCHI, M. K. 2004. A combined approach to the phylogeny of Cephalopoda (Mollusca). *Cladistics*, **20**, 454–486.

LINDGREN, A. R., PANKEY, M. S., HOCHBERG, F. G. and OAKLEY, T. H. 2012. A multi-gene phylogeny of Cephalopoda supports convergent morphological evolution in association with multiple habitat shifts in the marine environment. *BMC Evolutionary Biology*, **12**, 129.

LINDSAY, D.J., HUNT, J.C., MCNEIL, M., BEAMAN, R.J. and VECCHIONE, M., 2020. The first in situ observation of the ram's horn squid *Spirula spirula* turns "common knowledge" upside down. *Diversity*, **12**(12), 449.

LINNAEUS, C.V., 1758. Systema Naturae. Tomus 1. Editio decima, reformata. *Laurentii Salvi, Holmiae [Stockholm]*, 824.

LITTKE, R., LEYTHAEUSER, D., RULLKÖTTER, J. and BAKER, D. R. 1991. Keys to the depositional history of the Posidonia Shale (Toarcian) in the Hils Syncline, northern Germany. *Geological Society, London, Special Publications*, **58**, 311–333.

LITTLE, C. T. S. and BENTON, M. J. 1995. Early Jurassic mass extinction: A global long-term event. *Geology*, **23**, 495.

LÓPEZ-CÓRDOVA, D. A., AVARIA-LLAUTUREO, J., ULLOA, P. M., BRAID, H. E., REVELL, L. J., FUCHS, D. and IBÁÑEZ, C. M. 2022. Mesozoic origin of coleoid cephalopods and their abrupt shifts of diversification patterns. *Molecular Phylogenetics and Evolution*, **166**, 107331.

MANGOLD, K. M. and YOUNG, R. E. 1998. The systematic value of the digestive organs. *Smithsonian contributions to zoology*, 21–30.

MAPES, R. H., LANDMAN, N. H. and KLUG, C. 2019. Caught in the act? Distraction sinking in ammonoid cephalopods. *Swiss Journal of Palaeontology*, **138**, 141–149.

MARROQUÍN, S. M., MARTINDALE, R. C. and FUCHS, D. 2018. New records of the late Pliensbachian to early Toarcian (Early Jurassic) gladius-bearing coleoid cephalopods from the Ya Ha Tinda Lagerstätte, Canada. *Papers in Palaeontology*, **4**, 245–276.

MARTILL, D. M. and HUDSON, J. D. (eds.) 1991. Fossils of the Oxford Clay (Vol. 4). *In Field Guides to Fossils*. Palaeontological Association, London.

MARTINDALE, R. C. and ABERHAN, M. 2017. Response of macrobenthic communities to the Toarcian Oceanic Anoxic Event in northeastern Panthalassa (Ya Ha Tinda, Alberta, Canada). *Palaeogeography, Palaeoclimatology, Palaeoecology*, **478**, 103–120.

———, THEM, T. R., GILL, B. C., MARROQUÍN, S. M. and KNOLL, A. H. 2017. A new Early Jurassic (ca. 183 Ma) fossil *Lagerstätte* from Ya Ha Tinda, Alberta, Canada. *Geology*, **45**, 255–258.

MATZKE, A. T. and MAISCH, M. W. 2019. Palaeoecology and taphonomy of a Seirocrinus (Echinodermata: Crinoidea) colony from the Early Jurassic Posidonienschiefer Formation (Early Toarcian) of Dotternhausen (SW Germany). *Neues Jahrb. Geol. Paläontol.–Abh. Bd*, **291**, 89–107.

MAXWELL, E. E. and MARTINDALE, R. C. 2017. New *Saurorhynchus* (Actinopterygii: Saurichthyidae) material from the Early Jurassic of Alberta, Canada. *Canadian Journal of Earth Sciences*, **54**, 714–719.

MCFALL-NGAI, M. J. 1990. Crypsis in the Pelagic Environment. *American Zoologist*, **30**, 175–188.

MUSCENTE, A. D., MARTINDALE, R. C., SCHIFFBAUER, J. D., CREIGHTON, A. L. and BOGAN, B. A. 2019. Taphonomy of the Lower Jurassic Konservat-Lagerstätte at Ya Ha Tinda (Alberta, Canada) and its significance for exceptional fossil preservation during oceanic anoxic events. *PALAIOS*, **34**, 515–541.

———, VINNES, O., SINHA, S., SCHIFFBAUER, J. D., MAXWELL, E. E., SCHWEIGERT, G. and MARTINDALE, R. C. 2023. What role does anoxia play in exceptional fossil preservation? Lessons from the taphonomy of the Posidonia Shale (Germany). *Earth-Science Reviews*, **238**, 104323.

———, SCHIFFBAUER, J. D., BROCE, J., LAFLAMME, M., O'DONNELL, K., BOAG, T. H., MEYER, M., HAWKINS, A. D., HUNTLEY, J. W., MCNAMARA, M., MACKENZIE, L. A., STANLEY, G. D., HINMAN, N. W., HOFMANN, M. H. and XIAO, S. 2017. Exceptionally preserved fossil assemblages through geologic time and space. *Gondwana Research*, **48**, 164–188.

MUTVEI, H., ZHANG, Y.-B. and DUNCA, E. 2007. Late Cambrian Plectronocerid Nautiloids and Their Role in Cephalopod Evolution. *Palaeontology*, **50**, 1327–1333.

NAEF, A. 1921. Das System der dibranchiaten Cephalopoden und die mediterranen Arten derselben. *Mitt. Zool. Stn. Neapel*, **22**, 527–542.

———, 1922. *Die fossilen Tintenfische: eine paläozoologische Monographie*. Verlag von Gustav Fischer, Jena, Germany.

NESIS, K. N., LEVITOV, B. and BURGESS, L. A. 1987. *Cephalopods of the world: squids, cuttlefishes, octopuses, and allies*. (No title).

NISHIGUCHI, M. K. and MAPES, R. 2008. Cephalopoda. *In Phylogeny and Evolution of the Mollusca*, University of California Press, Berkeley, CA, 163–199 pp.

NIXON, M., 2011*a*. Treatise Online, no. 17, Part M, Chapter 3: Anatomy of Recent forms. *Treatise Online*.

———, 2011*b*. Treatise Online, no. 23: Part M, Chapter 7: Ecology and mode of life. *Treatise Online*.

——— and YOUNG, J. Z. 2003. *The Brains and Lives of Cephalopods*. Oxford University Press, Oxford.

OWEN, R. 1836. *The Cyclopaedia of Anatomy and Physiology: INS-PLA*. Vol. 3. Sherwood, Gilbert, and Piper.

———, 1844. VI. A description of certain Belemnites, preserved, with a great proportion of their soft parts, in the Oxford clay, at Christian-Malford, Wilts. *Philosophical Transactions of the Royal Society of London*, 65–85.

PACKARD, A., 1972. Cephalopods and fish: the limits of convergence. *Biological Reviews*, **47**(2), 241-307.

PICKFORD, G. 1936. A new order of dibranchiate cephalopods. *Anat. Rec*, **67**, 77.

PICKFORD, G. E. 1949. *Vampyroteuthis infernalis* Chun-An archaic dibranchiate cephalopod. II. External anatomy. *Dana Rep.*, **32**, 1–132.

POHLE, A., KRÖGER, B., WARNOCK, R., KING, A. H., EVANS, D. H., AUBRECHTOVÁ, M., CICHOWOLSKI, M., FANG, X. and KLUG, C. 2022. Early cephalopod evolution clarified through Bayesian phylogenetic inference. *BMC biology*, **20**, 1–30.

PONDER, W. F., LINDBERG, D. R. and PONDER, J. M. 2020. *Biology and Evolution of the Mollusca, Volume 2*. CRC Press.

PRICE, G. D., HART, M. B., WILBY, P. R. and PAGE, K. N. 2015. Isotopic analysis of Jurassic (Callovian) mollusks from the Christian Malford Lagerstätte (UK): Implications for ocean water temperature estimates based on belemnoids. *PALAIOS*, **30**, 645–654.

RAUHUT, O. W. M., FOTH, C. and TISCHLINGER, H. 2018. The oldest *Archaeopteryx* (Theropoda: Avialiae): a new specimen from the Kimmeridgian/Tithonian boundary of Schamhaupten, Bavaria. *PeerJ*, **6**, e4191.

RODHOUSE, P. G. and NIGMATULLIN, Ch. M. 1996. Role as Consumers. *Philosophical Transactions: Biological Sciences*, **351**, 1003–1022.

RÖHL, H.-J., SCHMID-RÖHL, A., OSCHMANN, W., FRIMMEL, A. and SCHWARK, L. 2001. The Posidonia Shale (Lower Toarcian) of SW-Germany: an oxygen-depleted ecosystem controlled by sea level and palaeoclimate. *Palaeogeography, Palaeoclimatology, Palaeoecology*, **165**, 27–52.

ROSCIAN, M., HERREL, A., ZAHARIAS, P., CORNETTE, R., FERNANDEZ, V., KRUTA, I., CHEREL, Y. and ROUGET, I. 2022. Every hooked beak is maintained by a prey: Ecological signal in cephalopod beak shape. *Functional Ecology*, **36**, 2015–2028.

RÜPPELL, E. 1829. *Abbildung und Beschreibung einiger neuen oder wenig gekannten Versteinerungen aus der Kalkschieferformation von Solenhofen*. Verlag der Brönner'schen buchhandlung,(S. Schmerber).

SANCHEZ, G., SETIAMARGA, D. H. E., TUANAPAYA, S., TONGTHERM, K., WINKELMANN, I. E., SCHMIDBAUR, H., UMINO, T., ALBERTIN, C., ALLCOCK, L., PERALES-RAYA, C., GLEADALL, I., STRUGNELL, J. M., SIMAKOV, O. and NABHITABHATA, J. 2018. Genus-level phylogeny of cephalopods using molecular markers: current status and problematic areas. *PeerJ*, **6**, e4331.

SAUNDERS, W.B. 1981. A new species of Nautilus from Palau. The Veliger, **24**(1): 1–7.

SCHMID, D. U., LEINFELDER, R. R. and SCHWEIGERT, G. 2005. Stratigraphy and palaeoenvironments of the Upper Jurassic of Southern Germany–a review. *Zitteliana*, 31–41.

SCHWEIGERT, G. and FUCHS, D. 2012. First record of a true coleoid cephalopod from the Germanic Triassic (Ladinian). *Neues Jahrbuch fur Geologie und Palaontologie-Abhandlungen*, **266**, 19.

SCHWEIGERT, G. and ROTH, S. 2021. The Nusplingen Plattenkalk – A Shark Lagoon in the Late Jurassic of the Swabian Alb Geopark. *Geoconservation Research*, **4**.

SCHWEIGERT, G., MAXWELL, E. and DIETL, G. 2016. First record of a true mortichnium produced by a fish. *Ichnos*, **23**, 71–76.

SEILACHER, A. 1982. *Posidonia Shales (Toarcian, S. Germany): stagnant basin model revalidated*. STEM Mucchi.

SHIGENO, S., ANDREWS, P. L. R., PONTE, G. and FIORITO, G. 2018. Cephalopod Brains: An Overview of Current Knowledge to Facilitate Comparison With Vertebrates. *Frontiers in Physiology*, **9**.

SINHA, S., MUSCENTE, A. D., SCHIFFBAUER, J. D., WILLIAMS, M., SCHWEIGERT, G. and MARTINDALE, R. C. 2021. Global controls on phosphatization of fossils during the Toarcian Oceanic Anoxic Event. *Scientific Reports*, **11**, 24087.

STRUGNELL, J. and NISHIGUCHI, M. K. 2007. Molecular phylogeny of coleoid cephalopods (Mollusca: Cephalopoda) inferred from three mitochondrial and six nuclear loci: a comparison of alignment, implied alignment and analysis methods. *Journal of Molluscan Studies*, **73**, 399–410.

———, NORMAN, M., JACKSON, J., DRUMMOND, A.J. and COOPER, A., 2005. Molecular phylogeny of coleoid cephalopods (Mollusca: Cephalopoda) using a multigene approach; the effect of data partitioning on resolving phylogenies in a Bayesian framework. *Molecular phylogenetics and evolution*, **37** (2), 426-441.

———, JACKSON, J., DRUMMOND, A. J. and COOPER, A. 2006. Divergence time estimates for major cephalopod groups: evidence from multiple genes. *Cladistics*, **22**, 89–96.

———, NORMAN, M. D., VECCHIONE, M., GUZIK, M. and ALLCOCK, A. L. 2014. The ink sac clouds octopod evolutionary history. *Hydrobiologia*, **725**, 215–235.

SUTTON, M., PERALES-RAYA, C. and GILBERT, I. 2016. A phylogeny of fossil and living neocoleoid cephalopods. *Cladistics*, **32**, 297–307.

TANNER, A. R., FUCHS, D., WINKELMANN, I. E., GILBERT, M. T. P., PANKEY, M. S., RIBEIRO, Â. M., KOCOT, K. M., HALANYCH, K. M., OAKLEY, T. H., DA FONSECA, R. R., PISANI, D. and VINTHER, J. 2017. Molecular clocks indicate turnover and diversification of modern coleoid cephalopods during the Mesozoic Marine Revolution. *Proceedings of the Royal Society B: Biological Sciences*, **284**, 20162818.

TAKI, I., 1965. Cephalopoda: 307–326. *OKADA et al.*

TOLL, R.B., 1982. The comparative morphology of the gladius in the order Teuthoidea (Mollusca: Cephalopoda) in relation to systematics and phylogeny. PhD Dissertation, University of Miami, FL.

TOLL, R.B., 1988. Functional morphology and adaptive patterns of the teuthoid gladius. In M. R. Clarke & E. R. Trueman (Eds.), *The Mollusca;* Form and function (pp. 167-182). New York: Academic Press.

URIBE, J. E. and ZARDOYA, R. 2017. Revisiting the phylogeny of Cephalopoda using complete mitochondrial genomes. *Journal of Molluscan Studies*, **83**, 133–144.

VANNIER, J., SCHOENEMANN, B., GILLOT, T., CHARBONNIER, S. and CLARKSON, E. 2016. Exceptional preservation of eye structure in arthropod visual predators from the Middle Jurassic. *Nature Communications*, **7**, 1–9.

VECCHIONE, M., YOUNG, R. E. and CARLINI, D. 2000. Reconstruction of ancestral character states in neocoleoid cephalopods based on parsimony. *American Malacological Bulletin*, **15**, 179–193.

———, MANGOLD, K. M. and YOUNG, R. E. 2016. *Cirrata Grimpe, 1916. Finned octopods*. http://tolweb.org/. Downloaded from http://tolweb.org/Cirrata/20086/2016.02.27 .

VILLALOBOS-SEGURA, E., STUMPF, S., TÜRTSCHER, J., JAMBURA, P. L., BEGAT, A., LÓPEZ-ROMERO, F. A., FISCHER, J. and KRIWET, J. 2023. A Synoptic Review of the Cartilaginous Fishes (Chondrichthyes: Holocephali, Elasmobranchii) from the Upper Jurassic Konservat-Lagerstätten of Southern Germany: Taxonomy, Diversity, and Faunal Relationships. *Diversity*, **15**, 386.

VILLANUEVA, R., PERRICONE, V. and FIORITO, G. 2017. Cephalopods as Predators: A Short Journey among Behavioral Flexibilities, Adaptions, and Feeding Habits. *Frontiers in Physiology*, **8**, 598.

VILLIER, L., CHARBONNIER, S. and RIOU, B. 2009. Sea stars from Middle Jurassic Lagerstätte of La Voulte-sur-Rhône (Ardèche, France). *Journal of Paleontology*, **83**, 389–398.

VIOHL, G. and ZAPP, M. 2006. Die Fossil-Lagerstätte Schamhaupten (oberstes Kimmeridgium, Südliche Frankenalb, Bayern). *Archaeopteryx*, **24**, 27–78.

——— and ——— 2007. Schamhaupten, an outstanding Fossil-Lagerstatte in a silicified Plattenkalk around the Kimmeridgian-Tithonian boundary (Southern Franconian Alb, Bavaria). *Neues Jahrbuch für Geologie und Paläontologie - Abhandlungen*, **245**, 127–142.

VOIGHT, J. R. 1997. CLADISTIC ANALYSIS OF THE OCTOPODS BASED ON ANATOMICAL CHARACTERS. *Journal of Molluscan Studies*, **63**, 311–325.

VOSS, N. A. and SWEENEY, M. J. 1998. Systematics and Biogeography of cephalopods. Volume I. *Smithsonian Contributions to Zoology*, 1–276.

WARSZAWA, J. D. and KORN, D. 1992. Devonian ancestors of Nautilus. *Paläontologische Zeitschrift*, **66**, 81–98.

WESTERMANN, G. and SAVAZZI, E. 1999. Life habits of nautiloids. *Functional morphology of the invertebrate skeleton*, 263–298.

WHALEN, C. D. and LANDMAN, N. H. 2022. Fossil coleoid cephalopod from the Mississippian Bear Gulch Lagerstätte sheds light on early vampyropod evolution. *Nature Communications*, **13**, 1107.

WILBY, P. R. 2001. La Voulte-Sur-Rhône. *In* BRIGGS, D. E. G. and CROWTHER, P. R. (eds.) *Palaeobiology II*, Blackwell Science Ltd, Malden, MA, USA, 349–351 pp.

———, HUDSON, J., CLEMENTS, R. and HOLLINGWORTH, N. 2004. Taphonomy and origin of an accumulate of soft-bodied cephalopods in the Oxford Clay Formation (Jurassic, England). *Palaeontology*, **47**, 1159–1180.

———, DUFF, K., PAGE, K. and MARTIN, S. 2008. Preserving the unpreservable: a lost world rediscovered at Christian Malford, UK. *Geology Today*, **24**, 95–98.

WILKIN, J. 2020. The south German Plattenkalks. *Geology Today*, **36**, 27–32.

WILLIAMS, M., BENTON, M. J. and ROSS, A. 2015. The Strawberry Bank Lagerstätte reveals insights into Early Jurassic life. *Journal of the Geological Society*, **172**, 683–692.

WIPPICH, M. G. E. and LEHMANN, J. 2004. *Allocrioceras* from the Cenomanian (mid-Cretaceous) of the Lebanon and its bearing on the palaeobiological interpretation of heteromorphic ammonites. *Palaeontology*, **47**, 1093–1107.

WOODWARD, H. 1883. I.—On a New Genus of Fossil "Calamary," from the Cretaceous Formation of Sahel Alma, near Beirût, Lebanon, Syria. *Geological Magazine*, **10**, 1–5.

Wülker, G., 1910. Über japanische cephalopoden: Beiträge zur kenntnis der systematik und anatomie der dibranchiaten. *(No Title)*.

XAVIER, J. C., ALLCOCK, A. L., CHEREL, Y., LIPINSKI, M. R., PIERCE, G. J., RODHOUSE, P. G. K., ROSA, R., SHEA, E. K., STRUGNELL, J. M., VIDAL, E. A. G., VILLANUEVA, R. and ZIEGLER, A. 2015. Future challenges in cephalopod research. *Journal of the Marine Biological Association of the United Kingdom*, **95**, 999–1015.

———, GOLIKOV, A. V., QUEIRÓS, J. P., PERALES-RAYA, C., ROSAS-LUIS, R., ABREU, J., BELLO, G., BUSTAMANTE, P., CAPAZ, J. C., DIMKOVIKJ, V. H., GONZÁLEZ, A. F., GUÍMARO, H., GUERRA-MARRERO, A., GOMES-PEREIRA, J. N., HERNÁNDEZ-URCERA, J., KUBODERA, T., LAPTIKHOVSKY, V., LEFKADITOU, E., LISHCHENKO, F., LUNA, A., LIU, B., PIERCE, G. J., PISSARRA, V., REVEILLAC, E., ROMANOV, E. V., ROSA, R., ROSCIAN, M., ROSE-MANN, L., ROUGET, I., SÁNCHEZ, P., SÁNCHEZ-MÁRQUEZ, A., SEIXAS, S., SOUQUET, L., VARELA, J., VIDAL, E. A. G. and CHEREL, Y. 2022. The significance of cephalopod beaks as a research tool: An update. *Frontiers in Physiology*, **13**.

YOCHELSON, E. L., FLOWER, R. H. and WEBERS, G. F. 1973. The bearing of the new Late Cambrian monoplacophoran genus *Knightoconus* upon the origin of the Cephalopoda. *Lethaia*, **6**, 275–309.

YOUNG, R. E. 1967. Homology of retractile filaments of vampire squid. *Science,* **156** (3782), 1633-4.

YOUNG, R. E. and VECCHIONE, M. 1996. Analysis of morphology to determine primary sister-taxon relationships within coleoid cephalopods. *American Malacological Bulletin*, **12**, 91–112.

YOUNG, R. E., VECCHIONE, M. and DONOVAN, D. T. 1998. The evolution of coleoid cephalopods and their present biodiversity and ecology. *South African Journal of Marine Science*, **20**, 393–420.

Chapter 1: Cephalopod present and past: an overview

Supplementary material

Cephalic Cartilage	Fin cartilage	Nucahl-and funel-locking cartilage	Buccal Mass	Beaks	Esophagus	Stomach	Crop	Respiratory system	Circulatory system	Excretory system	Repro. system
x			x	x		x		x			
			x			x		x			
x			x	x	x	x	x	x			?
			x			x		x			
						?					
? **				x **							
				x **							
			x								
			x	x							
				x				x			x
x	x		x	x		x		x			
			x								
x	x		x					x			
x	x					x	x				
x	x		x			x		x	?	?	?

		Muscular Mantle	Head mantle fusion	Arms	Filamentous arms**	Tentacles	Tentacular pockets	Circular Suckers	Onychites	Cirri-like appendages	Sucker rings	Arm web	Funnel	Fins
Prototeuthina	*Plesioteuthis*	x	?*	x		?		X		x		?	x	x
	Senefelderiteuthis	x		x										
	Dorateuthis	x		x										x
	Boreopeltis	x		x		?								x
	Rhomboteuthis	x		x		?		x				x		x
	Romaniteuthis	x		x		?		x						
Loligosepiina	*Vampyronassa*	x		x				x						x
	Proteroctopus	x	x	x										x
	Gramadella	x		x		?					?			
	Loligosepia	x		x	?**									
	Jelezkyteuthis	x		? **	?									? **
	Geopeltis	x												
	Parabelopoeltis	x												
	Mastigophora	x		x		?		x					x	x
	Doryanthes			?										
	Bavaripeltis	x												
	Leptoteuthis	x		x				x		?		?		
Teudopseina	*Trachyteuthis*	x		x		?				?		?		x
	Glyphiteuthis	x		x				x		x ***			?	x
	Glyphidopsis	x		x										
	Palaeololigo	x		x										
	Rachiteuthis	x	x	x									x	x
	Muensterella	x		x				x						x
	Keuppia	x		x				x						
	Palaeoctopus	x	x	x				x						
	Styletoctopus	x		x										

Supplementary Table 1.1 Fossilized soft tissues known in phragmocone- and gladius-bearing coleoid genera. X = known character; ? = Reported, but not confirmed. Modified from Donovan & Fuchs 2016, with additional information from *Hoffmann *et al.* 2020, **Klug *et al.* 2021, and ***Fuchs *et al.*, 2021.

Chapter 2: Comparative Anatomy of Recent Coleoids, The Backbone of Fossil Studies

INTRODUCTION

Comparative anatomy is an essential component of understanding the biology of organisms. Emerging in the 17th century, the approach was popularized by Cuvier (early 19th century) and rapidly spread in the community of biologists and paleontologists. It is a fundamental tool for recognizing homologies, resolving systematic questions, and interpreting the ecological implications of the various adaptations. Moreover, it is essential for interpreting fossil anatomy as soft tissues are generally only partially preserved in fossil Octobrachiate coleoids. As such, a knowledge of the anatomy of Recent relatives becomes crucial.

The organization of organs, how they are positioned in the body, as well as their size and texture is highly variable in present-day coleoids There are many anatomical descriptions available in the literature, but as Xavier *et al.* (2015) have pointed out, comparative anatomy becomes a rare specialty in organismic biology and the acquisition of detailed morphological data that can be shared between researchers remains a slow process. Earlier work does not always have high resolution or detailed enough illustrations, and more data is needed to enable us to observe anatomy at various scales (from the arrangement of organs in relation to each other to the organization of cell layers). In addition, species descriptions and investigations on the internal organization of soft-bodied animals conventionally rely on invasive techniques such as dissections or histological sampling (Kerbl *et al.* 2013; Ziegler & Sagorny 2021). These destructive methods are therefore not ideally suited to providing morphological or taxonomic descriptions of rare or fragile specimens (Ziegler & Sagorny 2021), and one of the major challenges in cephalopod research is identifying new approaches to study the morphology of cephalopods (Xavier *et al.* 2015). Indeed, many species are listed as Data Deficient on the IUCN Red List (Kemp *et al.* 2012; Xavier *et al.* 2015). Of the ~800 coleoid species that have been described (Xavier *et al.* 2015; Guerra 2019), there is only sufficient data to understand the life habits (e.g., feeding ecology, habitat, distribution, reproductive biology) of about 60 (Jereb & Roper 2005, 2010; Xavier *et al.* 2015; Jereb *et al.* 2016).

Cirrate octopods and the one extant Vampyromorph, *Vampyroteuthis infernalis* provide a good example of this problem, as what is known about these taxa comes from relatively few specimens (Collins & Villanueva 2006). These coleoids inhabit the deep sea and possess a semi-gelatinous body and are only caught in small numbers. They are extremely fragile, damage easily when captured, and often become distorted during preservation (Collins & Villanueva 2006; Ziegler & Sagorny 2021). As such, anatomical studies on rare, fragile taxa like these

benefit from a minimally invasive approach. This means the integrity of the sample can be retained (Ziegler & Sagorny 2021), while still obtaining an accurate account of soft tissue morphology (Xavier *et al.* 2015). Faced with the decline in anatomical work among biologists (Ziegler *et al.* 2018), acquiring or completing anatomical data on modern organisms is becoming a task increasingly transferred to paleontologists.

The aim of this chapter is to briefly outline digital methods in use for Recent forms and show how this primary information can be successfully used in the comparative anatomical study of fossil specimens. Digital imaging methods are particularly suited to the assessment of 3D organs and their position, which favors comparisons with fossils. The digital nature of the imaging techniques also enables robust amounts of data to be amassed and made openly available, contributing to the available information on lesser-known taxa.

Results illustrated in this chapter provide an overview of anatomical characters that are useful for phylogenetic resolution or ecology, and present new anatomical data acquired in tomography on *Vampyroteuthis*, a key taxon for understanding the Jurassic fossil groups.

2.1 ~ 3D IMAGING METHODS: THEORY AND APPLICATIONS

In the last few decades, an increased use of non-destructive scanning techniques has augmented the more traditional morphological methods of studies of extant cephalopods. There are now numerous 3D imaging methods that can be used to visualize animal morphology and anatomy in non-destructive ways (Hoffmann *et al.* 2014; Sutton *et al.* 2014; Xavier *et al.* 2015; Ziegler *et al.* 2018, 2021; Ziegler & Sagorny 2021). These digital three-dimensional imaging techniques permit analyses of entire specimens (Ziegler *et al.* 2018, 2021; Ziegler & Sagorny 2021) and an *in-situ* visualization of the internal organs and complex anatomical features that would otherwise not be visible without dissection (Ziegler *et al.* 2010, 2018; Hoffmann *et al.* 2014). As such, they are particularly beneficial for the study of rare, or important specimens (e.g., holotypes). The benefits and acquisition pathways of each method are dependent on the inherent constraints of the biological sample (e.g., size, material composition). Two well established methods for 3D imaging are magnetic resonance imaging (MRI) and X-ray computed tomography (CT), which map the attenuation of X-rays of heterogenous material (either by absorption or scattering) over a 360° rotating 3D sample (Sutton *et al.* 2014; Gueriau

et al. 2016; Ziegler *et al.* 2018). The methods are generally non-destructive, can be used on extant and fossil taxa, and require very little preparation of the sample.

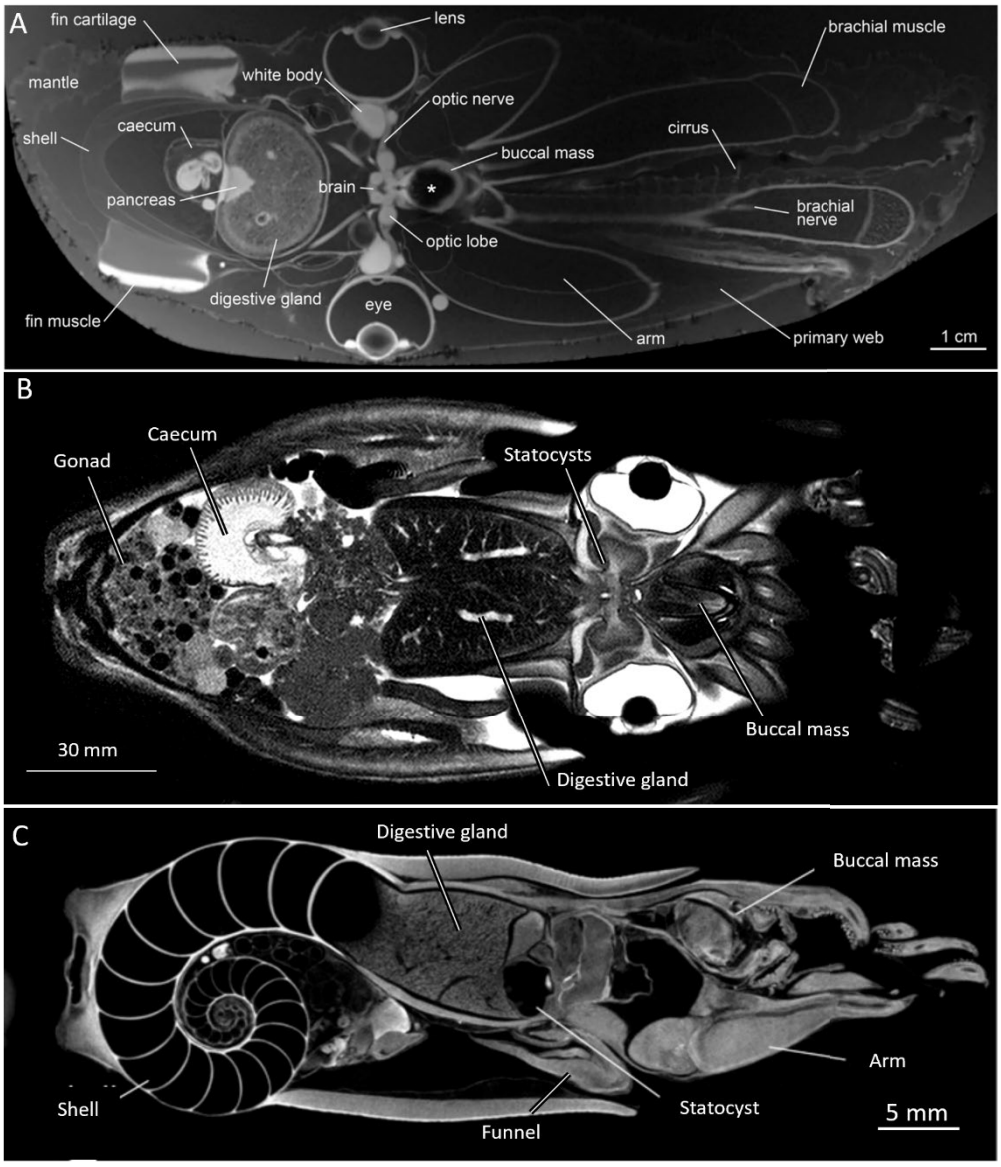

Figure 2.1: Tomographic slices showing features observed in the discussed techniques modified from Ziegler *et al*. 2018. (Anterior to the right. All are in dorsal view except C, which is sagittal). MRI of *Grimpoteuthis* Robson 1932, ZMB MOLL 240160, 280 µm isotropic voxel resolution. 290 mm total length. 20 min acquisition time (A). MRI of *Sepia officinalis* Linnaeus 1758, no collection number, 200 x 200 x 1,000 µm voxel resolution. 341 mm total length. 20 min acquisition time (B). Contrast-enhanced micro-computed tomography of *Spirula spirula* Linnaeus, 1758 (ZMK 405), 24 µm isotropic voxel resolution. 63 mm total length. Acquisition time, 5 h 29 min 18 s (C).

2.1.1 ~ Magnetic resonance imaging (MRI)

MRI is a form of tomography that uses strong magnetic fields to map the nuclei of light elements (typically hydrogen) in the specimen (Keevil 2001, Sutton 2008; Sutton *et al.*, 2014,

2016; Ziegler *et al.* 2018). As such, it is well suited to image soft tissues that contain hydrogen in the form of water molecules (Sutton *et al.* 2014). The prevalence of soft tissue in Modern coleoids makes them ideal candidates for MRI (Fig. 2.1) (Ziegler *et al.* 2011, 2018), while fossils can be more difficult given their low hydrogen composition (Sutton *et al.* 2014; Ziegler *et al.* 2018; Roscian *et al.* 2021). Acquisition times are highly variable and influenced by the size of the specimen (mm- to m-scale), water content, and imaging protocol. (See Zeigler *et al.* 2018, and 2021 for examples of its application on cephalopods). This scale range (Table 2.1) is well suited to coleoids who vary in size from a couple of centimeters in length (e.g., *Idiosepus*), to several meters, and has been successfully used in comparative anatomy studies (Chung & Marshall 2016, 2017; Ziegler *et al.* 2018; Chung *et al.* 2022). With the optimal scanning parameters, a resolution potential at the sub-millimeter scale can be achieved (Ziegler *et al.* 2011; Cunningham 2014; Sutton *et al.* 2014, 2016).

The MRI of the cuttlefish (*Sepia officinalis)* specimen (Fig. 2.1B) shows good differentiation of the major organ systems. However, Ziegler *et al.* (2018) notes that this is on both the non-mineralized, and mineralized structures. MRI is more optimally suited to hydrated tissues, so this result is in contrast with the expectation from this imaging technique.

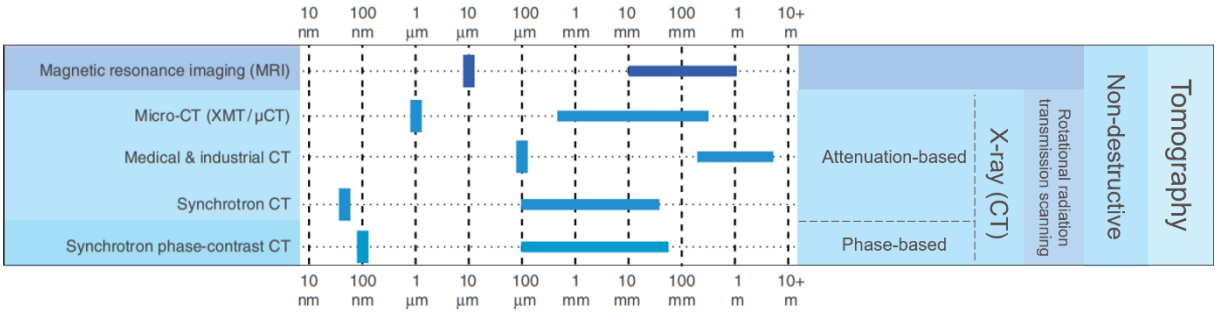

Table 2.1: Comparison of methods, and their size parameters. Thick horizontal lines show an approximate size range for the feature-of-interest. Thick vertical lines reflect the minimum approximate size of the resolvable feature. Modified from Sutton *et al.* 2014; 2016.

2.1.2 ~ X-ray computed tomography (CT)

CT-based techniques are particularly suited for rapid visualization of mineralized structures (Ziegler *et al.* 2010, 2018; Sutton *et al.* 2014) and are the most common tomographic technique for the study of fossils (Tafforeau *et al.* 2006, Kruta *et al.* 2011, Sutton *et al.* 2014). A medical, or laboratory-based CT scanner can image specimens that range in size from a few centimeters to a few meters (Table 2.1). With medical-based equipment, it is difficult to observe

structures <0.5mm, though laboratory CT imaging has a much higher spatial resolution and can reveal details at the micrometer scale (e.g., the thickness of dental enamel) (Tafforeau *et al*. 2006). µCT enables the imaging of internal or histological elements of small specimens (< 1mm) with finer discrimination than is possible than with CT (Table 2.1) and has been successfully used to reveal fine anatomical details on specimens encased in matrix (e.g., in cephalopods, the smallest cuspids of the radular teeth; Kruta *et al.* 2011). CT-techniques can also be used to image extant soft tissue material, though generally with the aid of a contrasting agent to enhance the visibility of the soft tissues. However, the success of the staining process is variable. Attempts to image extant chitinous structures (e.g., cephalopod beaks) have not always been optimal, even with common contrast solutions (PMA, PTA, and Osmium) (Metscher 2009; Sakurai & Ikeda 2019; Roscian *et al.* 2021, 2023).

One major limitation for fossil imaging is that the highly mineralized specimens generally exhibit low contrast in the preserved morphological features (Tafforeau *et al.* 2006). However, the advent of synchrotron X-ray tomography (Tafforeau *et al.* 2006; Kruta *et al.* 2011, 2013, 2016; Gueriau *et al.* 2016) has enabled the study of fossils with higher resolution, contrast, and fidelity than is possible with medical or laboratory-based scanners (Tafforeau *et al.* 2006; Ziegler *et al.* 2010, 2018; Kruta *et al.* 2011, 2013, 2016; Xavier *et al.* 2015; Gueriau *et al.* 2016; Roscian *et al.* 2021, 2022, 2023; Ziegler & Sagorny 2021; Goolaerts *et al.* 2022). For SR-CT scans, the X-ray beam intensity is orders of magnitude higher than that produced by X-ray tubes (Tafforeau *et al.* 2016).

When fossil tissue shares a similar density or composition with the surrounding matrix, it is often unable to be differentiated using attenuation methods (Tafforeau *et al*. 2006; Sutton *et al*. 2014). In these instances, propagation phase contrast synchrotron x-ray microcomputed tomography (PPC-SR-µCT) is of particular value (Tafforeau *et al.* 2006; Lak *et al.* 2008; Kruta 2010; Kruta *et al.* 2011; Sutton *et al.* 2014; Gueriau *et al*. 2016) is particularly beneficial. PPC-SR-µCT brings improved edge detection and makes it easier to discriminate between similarly absorbing materials (Gueriau *et al.* 2016). PPC-SR-µCT datasets are created by mapping the phase shift that the high-energy X-rays experience when they are passing through the sample instead (Tafforeau *et al.* 2006; Sutton *et al.* 2014); these can penetrate the material more effectively than lower-energy X-rays and have proved particularly useful for fossil cephalopods (Kruta *et al.* 2011, 2013, 2016; Rowe *et al.* 2022, 2023). This method affords the highest resolution, though the range is restricted to smaller sized samples. (See Sutton *et al.* 2014 for an overview and history of tomographic techniques used in paleontology).

2.2 ~ SAMPLE PREPARATION FOR OPTIMAL IMAGING

Though MRI and CT methods both permit the visualization of soft tissues and mineralized structures under certain conditions (Ziegler *et al.* 2018), MRI often performs poorly on solid materials (Sutton *et al.* 2014); likewise with CT on soft tissues. As such, MRI is not the optimal modality for visualizing fossil material in 3D (Sutton *et al.* 2014). As soft tissues (non-mineralized tissues) inherently have a lower contrast than mineralized tissues (Metscher 2009, 2010, 2013) contrasting agents (stains) are typically required for extant forms when acquiring µCT or CT data. By applying simple contrast stains prior to scanning, quantitative 3D images of coleoid soft tissues can be obtained (Metscher 2009; Pauwels *et al.* 2013; Gignac *et al.* 2016; Ziegler *et al.* 2018). Various stains exist for this purpose and absorption differs depending on the organs (Metscher 2009; Roscian *et al.* 2021). Stains that are commonly used are based on phosphomolybdic acid (PMA) (Pauwels *et al.* 2013), phosphotungstic acid (PTA) (Metscher 2009; Pauwels *et al.* 2013; Doost & Arnolda 2021), inorganic iodine (Metscher 2009; Doost & Arnolda 2021), and osmium tetroxide (Metscher 2009, 2013) and have enabled high-fidelity CT analyses of soft tissues (Gignac *et al.* 2016; Ziegler *et al.* 2018). The most broadly useful are inorganic iodine, phosphomolybdic acid (PMA) and phosphotungstic acid (PTA), which are much less toxic than osmium tetroxide (Metscher 2009). The amount of diffusion time required for staining varies on the size and density of the specimen, and the initial concentration of the stain (Ziegler *et al.* 2018). (See Metscher 2013, Table 1, for concentrations and staining times for the most commonly used contrast agents.)

A challenging aspect for extant species, and in particular gelatinous samples (e.g., *Vampyroteuthis*) is that during scanning, specimens must remain completely still on the mount to prevent artifacts from movement (Metscher 2009, 2010; Sutton *et al.* 2014; Ziegler *et al.* 2018). This is especially pertinent for smaller specimens as large specimens (>0.15m) can be placed in a container directly on the rotation stage during acquisition (Sutton *et al.* 2014). Mounting small specimens can be achieved by placing them in plastic tubes and surrounding them with malleable material with a low X-ray density (e.g., florists' foam, ethanol, or agar agar) (Metscher 2009; Sutton *et al.* 2014; Ziegler *et al.* 2018). See Metscher 2011 for mounting and staining techniques.

The 3D renderings that can be generated from these methods permit a much clearer interpretation of anatomical features than can be obtained from complex 2D line drawings (e.g., Fig. 1.3, Chapter 1) or photographs (e.g., Chung & Marshall 2016, 2017; Ziegler *et al.* 2018,

2021; Ziegler & Sagorny 2021). Additionally, they can form the basis of functional morphology studies including finite-element analysis (See Rayfield 2007) or hydrodynamic flow modelling (Sutton *et al.* 2014). These techniques have already facilitated comparative morphological analysis between fossil and extant forms (Kruta *et al.* 2011, 2016; Hoffmann *et al.* 2014), redescription of fossil holotypes (Kruta *et al.* 2016), and are being used to answer questions regarding taxonomic identification, diet, ecology, and evolutionary developments (Kruta *et al.* 2011; Lemanis *et al.* 2016; Goolaerts *et al.* 2022).

2.3 ~ Material studied for comparative anatomy

Multiple dissections of commercially purchased individuals (*Loligo* sp., *Octopus,* and *Sepia officinalis* Linnaeus 1758) were conducted to study the internal organs and configurations of extant coleoids (Figs 2.2 – 2.6). Following this, tomographic scans of six specimens were studied, and various anatomical components were rendered. This included four Modern Octobrachia species (two specimens of *V. infernalis* from museum collections at the American Museum of Natural History, NY, USA (AMNH IZC 361496) and from the Yale Peabody Museum, CT, USA (YPM IZ 18279), and one *Grimpoteuthis* sp. (ZMB 240160), as well as three Modern Decabrachia (*Spirula spirula,* ZMK 405) and two commercial Decabrachia (*Sepia officinalis,* and *Loligo* sp.). The *Grimpoteuthis* and *Spirula* were already digitized and downloaded from MorphoBank project #3107 (Ziegler *et al.* 2018).

Specimen	Species	Voxel (3D Pixel) resolution (scan)	Scan location	Scan type	Voxel resolution in file	Staining prior to scanning	Segmentation software
AMNH IZC 361496	*Vampyroteuthis infernalis*	36.29 µm isotropic	AMNH, NY	CT Scan	36.29 µm isotropic	1% PTA	Mimics
YPM IZ 18279	*Vampyroteuthis infernalis*	18.25 µm isotropic	AMNH, NY	CT Scan		1% PTA	Mimics
Commercial sample, squid	*Loligo vulgaris*	44.15 µm isotropic	AST-RX	CT Scan	44.15 µm isotropic	4% PTA solution	Mimics
Commercial sample, Sepia	*Sepia officinalis*	44.15 µm isotropic	AST-RX	CT Scan	44.15 µm isotropic	4% PTA solution	Mimics
ZMK 405	*Spirula spirula*	10 µm isotropic	SkyScan1272 (Bruker microCT, Kontich, Belgium)	CT Scan	10 µm isotropic	3% PTA solution	Drishti
ZMB MOLL 240160	*Grimpoteuthis*	280 µm isotropic	7 T MAGNETOM (SIEMENS Healthineers)	MRI	280 µm isotropic	-	Amira
No collection number	*Sepia officinalis*	200 x 200 x 1,000 µm	T Achieva (Philips Healthcare, Amsterdam, Netherlands)	MRI	200 x 200 x 1,000 µm	-	

Table 2.2: Acquisition parameters for the extant coleoids used in this chapter.

The two *V. infernalis* specimens were both scanned at the AMNH (NY, USA) with a voxel resolution of 36.29µm, and 15.25µm respectively. Each was stained in a 1% PTA solution prior to scanning to enhance the tissue contrast. The commercial samples of *Loligo* sp. and *Sepia officinalis* were stained with a 4% PTA solution and scanned on the AST-RX platform at the MNHN, (Paris, France) at a resolution of 44.15µm (Table 2.2).

Final scan files were reduced in size using the free and open-source image software, FIJI Image J. This involved removing tomographic slices and areas that contained no data, which enabled a faster processing time when working with the final file. The dataset was then segmented and rendered using the commercial Mimics software (v. 21.0, Materialise). The contrast in grayscale intensity of the stained soft tissues was utilized when rendering the anatomy.

2.4 ~ FROM DISSECTIONS TO VIRTUAL DISSECTIONS

Dissections are the foundation of comparative anatomy and remain essential to apprehend the overall anatomy. As such, they were conducted on commercial coleoid samples to understand the major differences in the anatomy of Recent groups (Figs 2.2 – 2.6). The observations were then compared with what could be identified in the CT scans. Though the relative 3D position of the organs is generally better reflected with X-ray based imaging (even if gelatinous samples do not always retain their shape), some key observations could only be gathered through dissections (e.g., delicate tissues like oviducts or gill glands). Comparing the results of these two observational methods allowed me to establish procedures for the examination of key morphological traits in fossil forms. These procedures were utilized in Rowe *et al.* 2022; 2023, included in this chapter, to interpret the anatomy of fossil coleoids.

As discussed in Chapter 1, morphology varies at high taxonomic level, and can be used to infer ecology. On the extant material, some of these features are clearly observable (e.g., arms, beaks), though the identification of other structures - the internal sucker configuration for example – is best observed with CT-scans prior to comparisons with fossil material.

The arm crown provides some of the defining characteristics for the main coleoid groups (Fig. 2.2). As noted in Chapter 1, octopuses have eight arms, while Decabrachians (squid and cuttlefish) have ten appendages: eight arms and two ventrolateral tentacular arms which have suckers on the distal ‘clubs’. The arm crown of *Vampyroteuthis* has eight arms and two

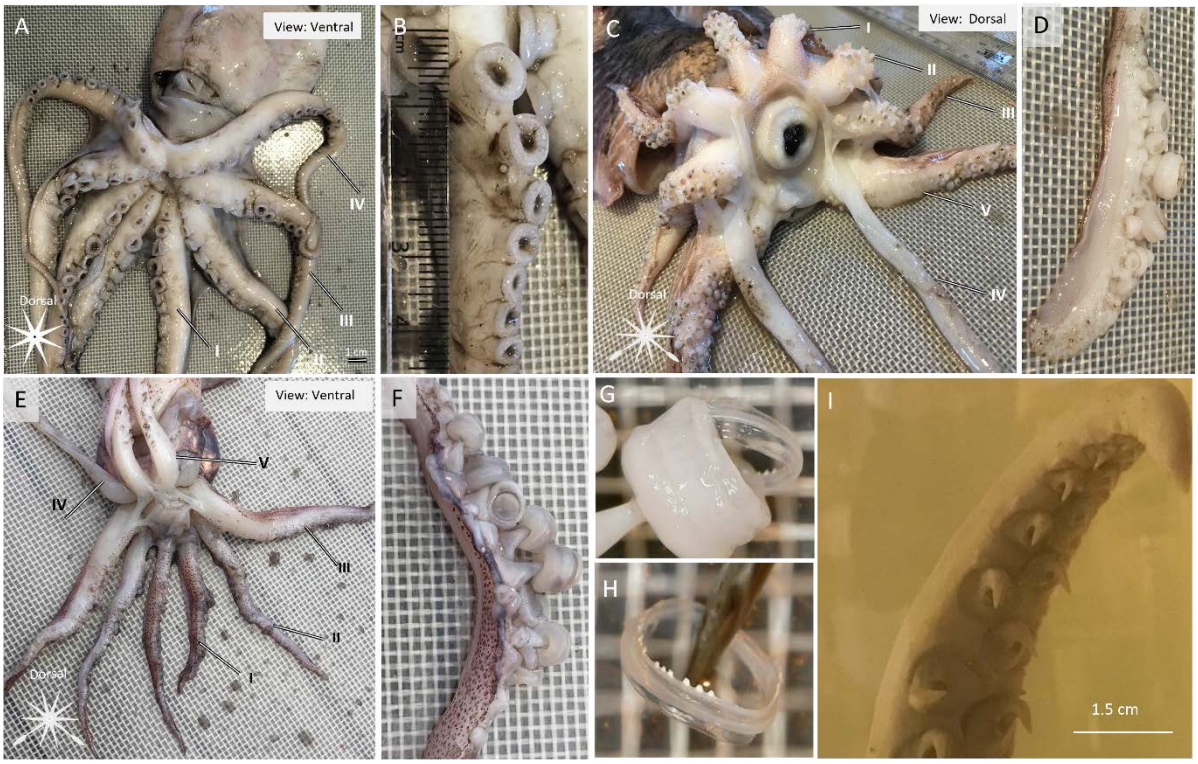

Figure 2.2: Dissection images of commercial coleoid specimens. *Eledone* sp. (Octobrachia), A, B; *Sepia officinalis* (Decabrachia), C, D; *Loligo* sp. (Decabrachia), E-H, and a distal tentacular club of *Mesonychoteuthis hamiltoni* Robson, 1925 (Decabrachia), I, Collected by Malcolm Clarke (Discovery Collections) reposited in the Natural History Museum, London, UK. The *Eledone* (A) is oriented in ventral view. The eight arms surround the buccal mass and are lined with uniserial suckers with broad bases to attach them to the arm (B). They show the characteristic radial symmetry of Octobrachia. *Sepia officinalis* showing the eight arms with numerous suckers (C), and the two tentacles, which only have suckers on the tentacular clubs (D). *Loligo* sp. (E) is oriented in ventral view. In life position, the paired tentacles (identified by IV) are ventro-lateral view as in the inset illustration. These tentacles also have pedunculated suckers on the tentacular distal clubs (F, G) that are lines with toothed sucker rings (G, H). Small suckers line the remaining arms (E). The oral view of the tentacular club of *Mesonychoteuthis* (I) shows the hooks. All dissection photographs were taken by the author, A. Rowe, unless otherwise indicated.

filamentous, retractable appendages in the dorsolateral position. These delicate long structures are not always preserved on collected extant specimens and, so far, have not been evidenced on fossil members assigned to their family, Vampyromorphina. Additional information such as the filament pockets can provide indirect evidence of their presence and can be observed with X-ray imaging. (See Chapter 1, Fig 1.6 for a simplified phylogenetic hypothesis of fossil forms).

In Octobrachia, suckers are radially symmetrical and attached to the arms by broad, cylindrical bases (Fig. 2.2A, B, J), and Decabrachia have pedunculate suckers that are bilateral in their symmetry and lined with a sucker ring (Fig. 2.2D-H). These may be smooth, or bear ‘teeth’, and are used to retain prey upon capture. In some Oegopsid families, the central tooth of this sucker ring has developed into a hook (Fig. 2.2 I). *Vampyroteuthis* suckers are symmetrical, have a conical-shaped attachment to the arm.

Figure 2.3: Dissection images of commercial coleoid specimens. *Eledone* sp. (Octobrachia), A; *Loligo* sp. (Decabrachia) B, C; *Sepia officinalis*. (Decabrachia), D, E. The dorsal head-mantle fusion is visible on the *Eledone* sp. (A). The *Loligo* (B, C) and *Sepia* (D, E) show the nuchal (C) and funnel locking cartilage (E).

The connection between the head and the mantle varies. In Octobrachia and some decabrachians (e.g., bobtail squids), the head and mantle tissue are fused dorsally (Fig. 2.3A). However, in most Decabrachia, the articulation between the head and mantle is provided by complimentary locking cartilages (nuchal, and funnel) (Fig. 2.3B-E). The cartilage is easily observable in dissection and appears denser than the surrounding tissues in CT scans. Fin cartilage can also be observed in Cirrate octopods and *Vampyroteuthis* and appears reticulate in CT scan images.

As mentioned in Chapter 1, the internal shells in extant coleoids show great variation between the groups. Cuttlefish and *Spirula* (Decabrachia) (Figs 2.1C, 2.6A, C) retain the chambered, gas-filled phragmocone, which helps regulate buoyancy in the water. The phragmocone can be easily identified in the CT-scans. However, most decabrachians have a 'pen' like gladius (Fig. 2.6B, D) that extends the length of the mantle. Cirrata have a greatly reduced gladius that provides fin support, and incirrates either have a pair of stylets that are muscle attachment sites,

or the gladius is absent. Due to the low absorption of staining in the gladius, the latter is hard to observe in CT scan.

Figure 2.4: Examples of a *Sepia* and *Loligo* (Decabrachia) gladius obtained during dissection (A, B, and illustrations of the same, modified from Bizikov &Toll (2016). Cuttlefish 'cuttlebone' in profile view (A) and dorsal illustration (C). *Loligo* gladius in dorsal view (B) and illustration (D).

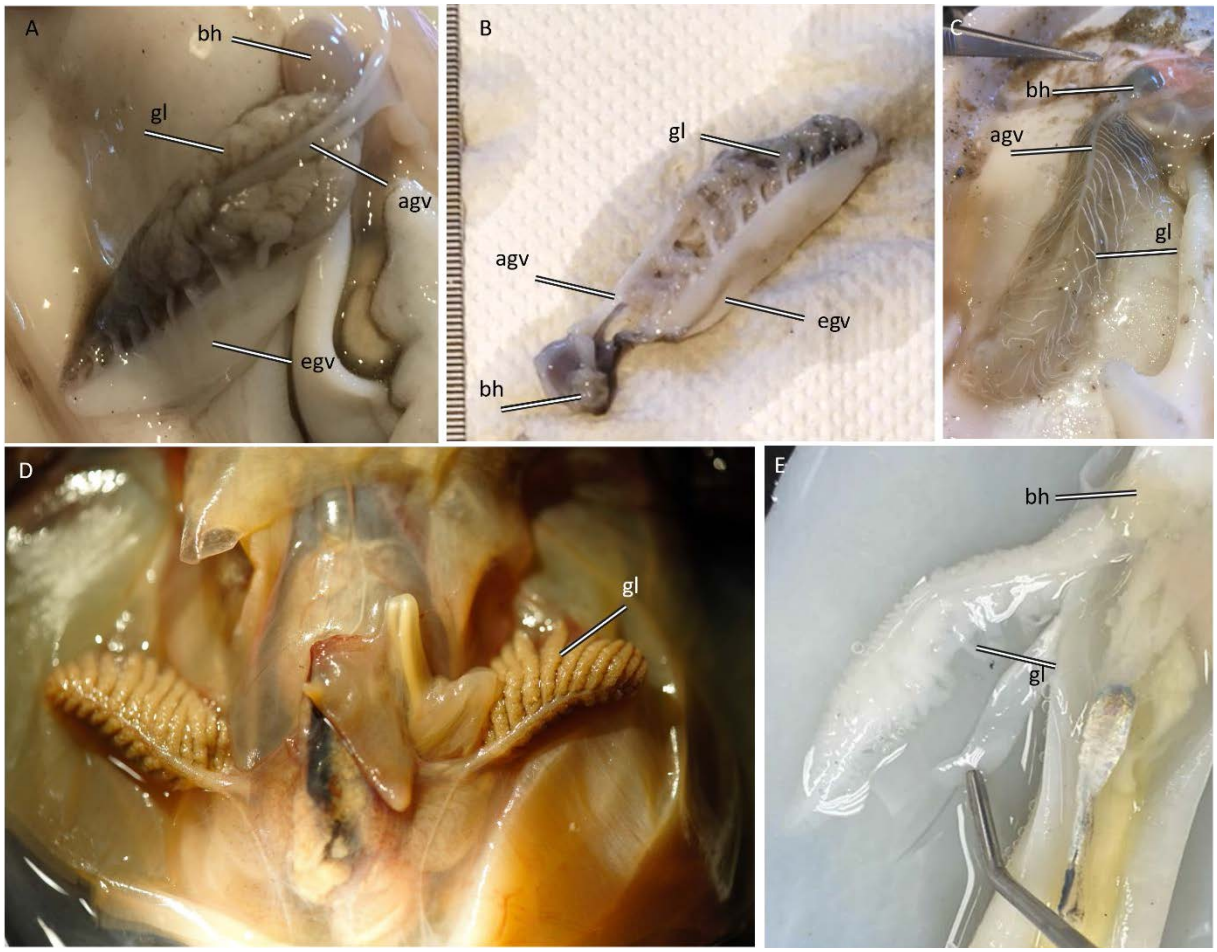

Figure 2.5: Photographs of gills obtained during dissection (A-C, E), and courtesy of Henk-Jan Hoving (D). *Eledone* (Octobrachia) A, B; *Sepia* (Decabrachia), C; *Vampyroteuthis infernalis* (Octobrachia), D; *Loligo* (Decabrachia), E. agf: afferent gill vessel, egv: efferent gill vessel, bh: branchial heart, gl: gill primary lamella.

Coleoids all possess one pair of gills that are positioned laterally in the mantle cavity, though the structure varies by major taxonomic group. Decabrachia have distally tapered forms with filamentous lamella protruding from the main afferent veins transport blood from the branchial heart to the gill, while the efferent vessel returns it to the systemic heart. This fine anatomical detail is difficult to observe CT scans. Nonetheless, this method can reveal the overall morphology of the gills and reveal if they are more brain-like in shape (Octobrachia), or filamentous (Decabrachia).

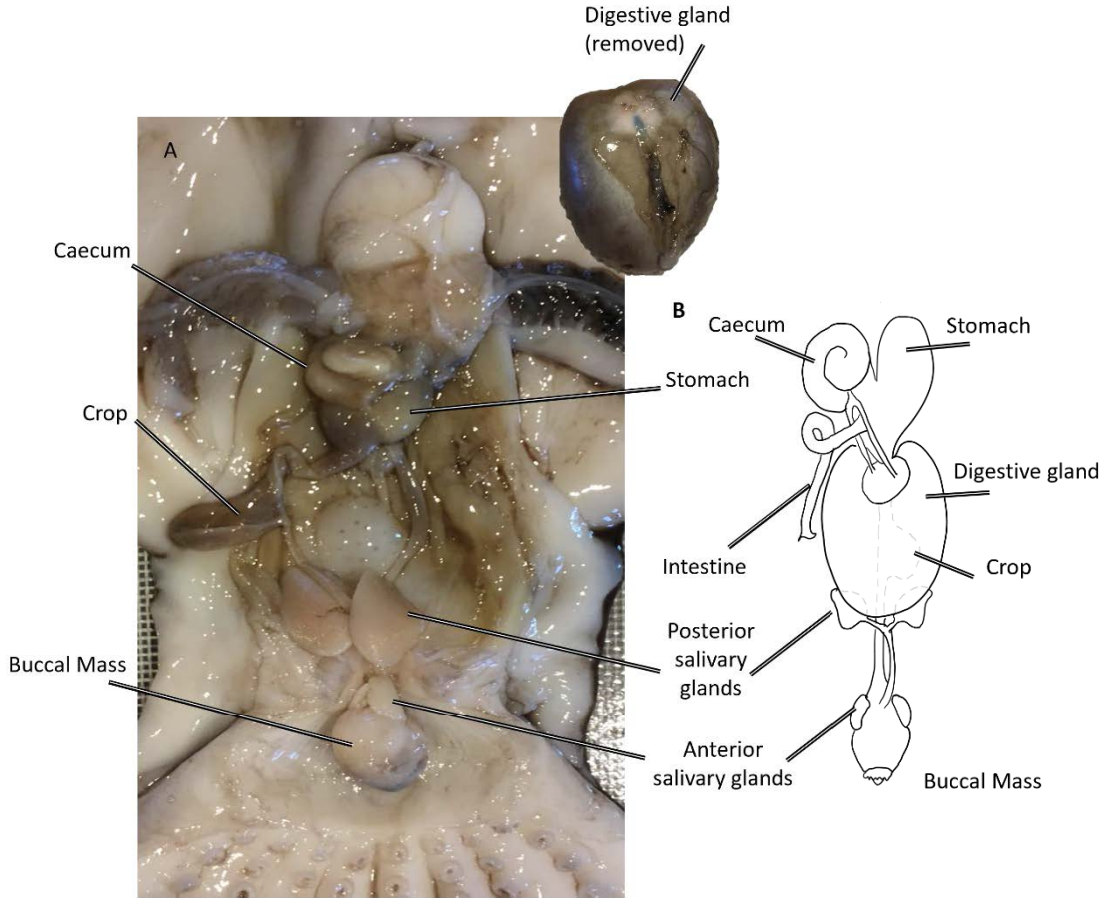

Figure 2.6: Commercial sample of an *Eledone* (Octobrachia) in ventral view, A, and illustration of the same, modified from Hanlon *et al.* 2018, B. The digestive gland has been removed from the specimen to reveal more internal anatomy.

In all coleoids, food is broken down by the beak and passed into the esophagus. This extends posteriorly to the stomach, which leads to the caecum and the intestine. The intestine then empties into the mantle cavity near the funnel. In Octobrachia (including *V. infernalis)*, the esophagus swells and forms a crop, enabling the storage of food before it reaches the stomach. The lamellar inner structure of the crop is easily observable on CT scans and is useful to determine if the digestive system reflects the Octobrachia or Decabrachia.

2.5 ~ 3D IMAGING AND THE ANATOMY OF DEEP-SEA SPECIES

Deep-sea specimens (e.g., *V. infernalis*) are also important for comparison with fossil material, though given their rarity could not be dissected here. An understanding of their anatomy could, therefore, only be made from comparing anatomical descriptions in the literature with CT files of individuals. This was carried out here for *Grimpoteuthis* and *V. infernalis*. The anatomical work on *V. infernalis* is included here as the first complete virtual dissection for the species and was presented in poster format at the Cephalopod International Advisory Council symposium in 2022. This is included in the Annex of this thesis.

2.5.1 ~ Grimpoteuthis

The MRI slices of *Grimpoteuthis* (Figs 2.1A, 2.7A-C) from Ziegler *et al.* (2018) clearly reveal structures associated with the digestive, reproductive, respiratory, and central nervous systems (Fig. 2.1A). The eyes, buccal mass and fin cartilage are also well defined. Where there is an absence of a sharp threshold boundary between the specimen and the scanning medium (e.g., the mantle tissue), creating a precise 3D volume rendering becomes more challenging. Though faint, the arm crown, uniserial suckers, and biserial cirri can be observed.

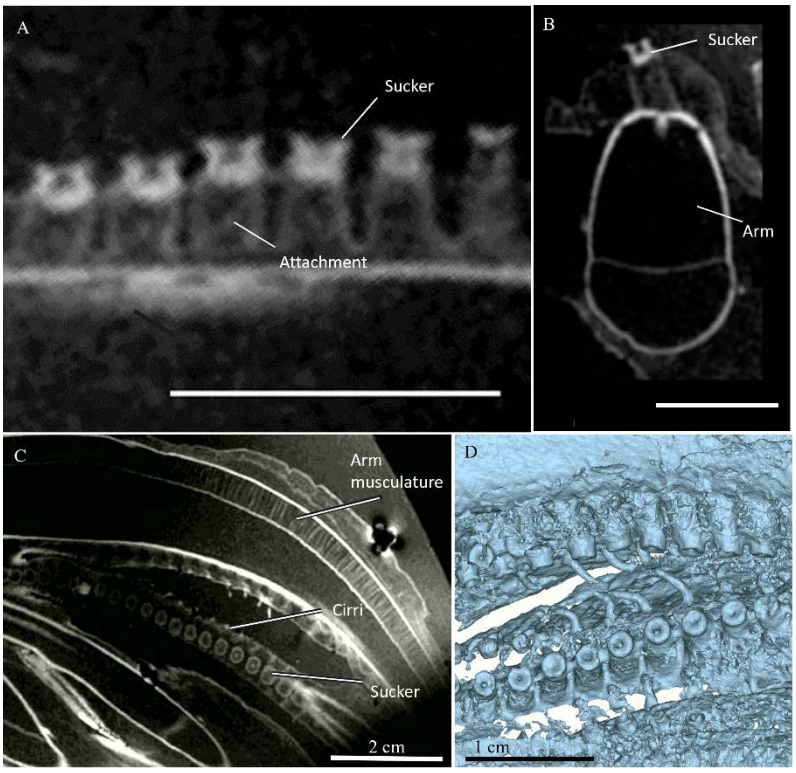

Figure 2.7: MRI slices showing the elements of the arm crown of *Grimpoteuthis* (ZMB MOLL 240160) from Ziegler *et al.* 2018. Sagittal view of the uniserial suckers (A), transverse slice of the arm and sucker (B), and arms, suckers, and cirri (C). 3D volume rendering of the arm crown showing the suckers and cirri (D).

2.4.2 ~ *Vampyroteuthis infernalis*

The CT scans of *V. infernalis* (Figs 2.8 - 2.12) revealed some of the characteristic soft tissues of these enigmatic Vampyromorphs, including the retractable filaments and their pockets, as well as the posterior luminous organs. The staining of this extant material successfully resulted in differential absorption depending on the organs and their composition, and impacted what was able to be successfully delineated and rendered.

In AMNH IZC 361496, the densely structured tissues show the most contrast and are therefore the most identifiable. This is visible in organs of the digestive system (Figs 2.8, 2.10, 2.11), including the digestive gland, stomach, and caecum. The beak and buccal musculature, eyes (Figs 2.8, 2.10), gills, fin cartilage, and luminous organs (Figs 2.8, 2.10, 2.11) are also well contrasted. Despite the good contrast shown in the fin cartilage, the cephalic cartilage and statocysts cartilage remains faint.

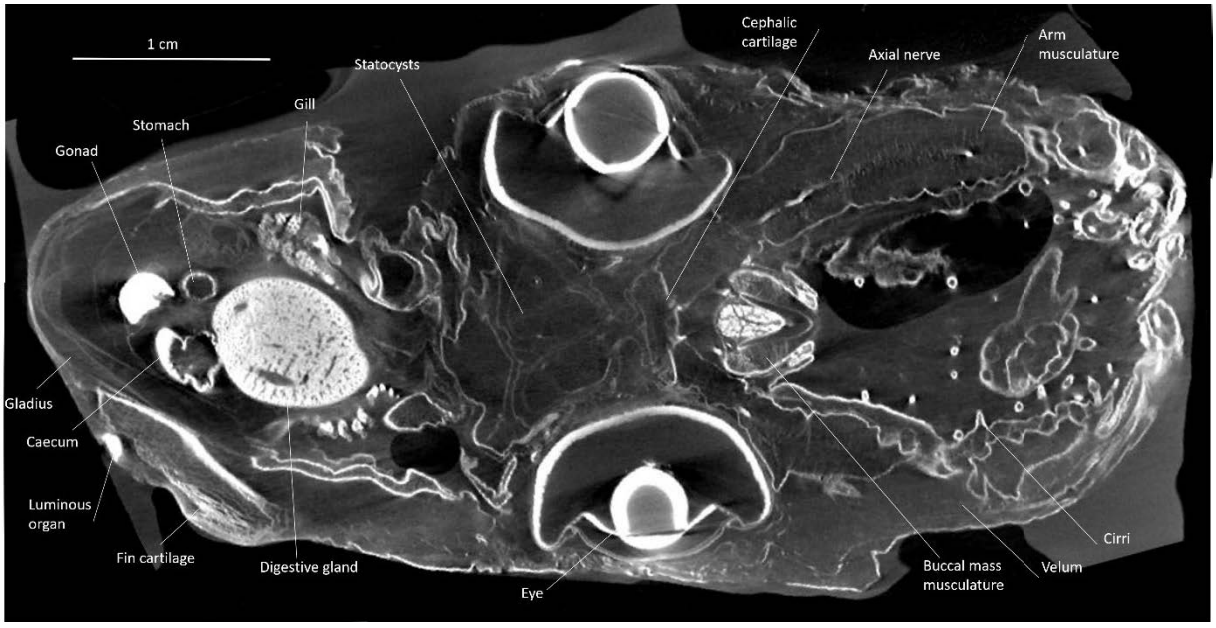

Figure 2.8: µCT slice (dorsal view) of *V. infernalis* (AMNH IZC 361496). Stained in a 1% PTA solution and scanned at the Microscopy and Imaging Facility of the AMNH. Voxel size: 38.40 µm. The same parameters are used in each of the figures of this specimen.

Elements of the arm crown (axial nerves, suckers, and cirri) can be identified (Figs 2.8, 2.9), although determining the boundaries of the individual arms is challenging as they overlap with each other distally. They are also surrounded by a deep velum that is indeterminable from the arm tissue in the scans. This is also the case for the smaller soft tissue elements (e.g., ducts, branchial hearts), and larger, unstructured features like the funnel, as they lack sharp threshold boundary.

The arm crown (Fig. 2.9) clearly shows the outline of eight arms and the two retractable filaments. It also reveals suckers and cirri (Fig. 2.9B, C), and the parts of the central nervous system, represented by an axial nerve running through the center of the arms (Fig. 2.9A-D). The axial nerves and filaments show more contrast than the arms indicating a differential absorption of staining agent. The pocket for the retractable filament (Fig. 2.9D) can also be observed in the dorso-ventral position (equivalent to arm pair II). Depending on the position of the slice along the specimen, it somewhat resembles an arm in transverse view, and could be mistaken for one if observations were based on individual slices of the local region. The velum appears pigmented in areas towards the external margin, indicating inconsistent staining.

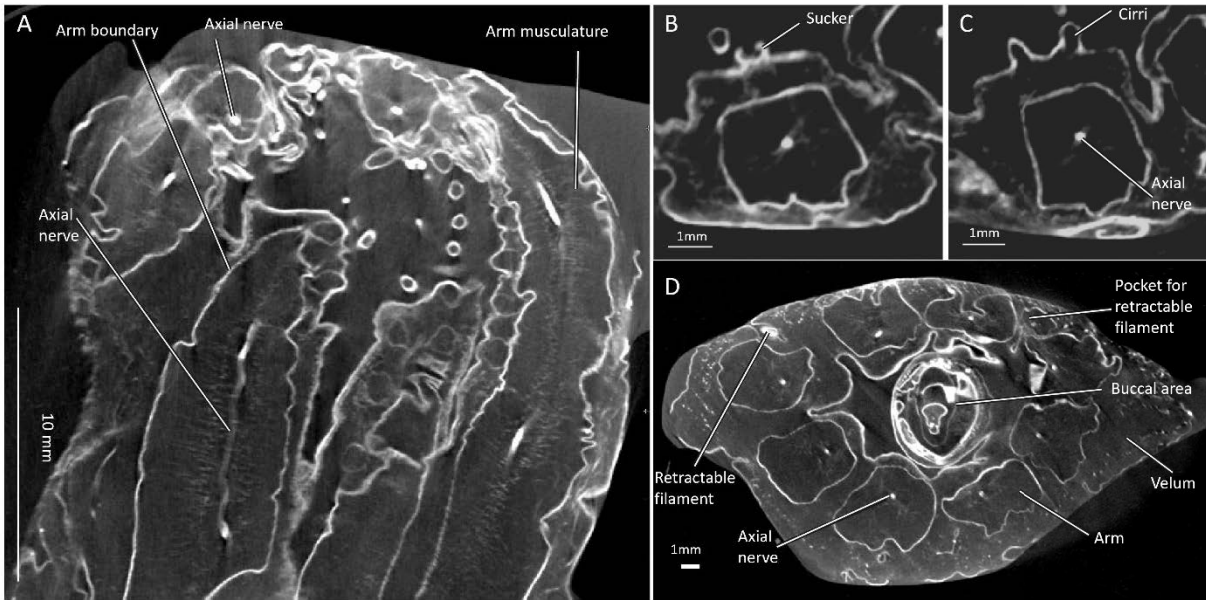

Figure 2.9: µCT slices of *V. infernalis* (AMNH IZC 361496). Elements of the central nervous system (axial nerves in the arms) are clearly visible (A-D). Here, the suckers and cirri are apparent in transverse views (B, C), they are not always simple to render given the overlapping tissues, and how the continuity of their appearance differs in dorsal (A), transverse (B, C) and sagittal views. The retractable filaments and the associated pockets are also observable in transverse view (D).

The buccal musculature has a high threshold boundary (Fig. 2.9D), and it is also possible to observe the rostral tip and outline of the beak (Fig. 2.10B). In between the optic lobes, the lobes of the brain and esophagus are well contrasted (Fig. 2.10A, C). The outline of the mantle and arm tissue is generally distinguishable by a thin white line. However, there are no clear boundaries to the internal margin of the mantle tissue, indicating that the staining agent has not penetrated the gelatinous tissue. Indeed, it has a visually similar density to the surrounding medium (Fig. 2.8 - 2.12).

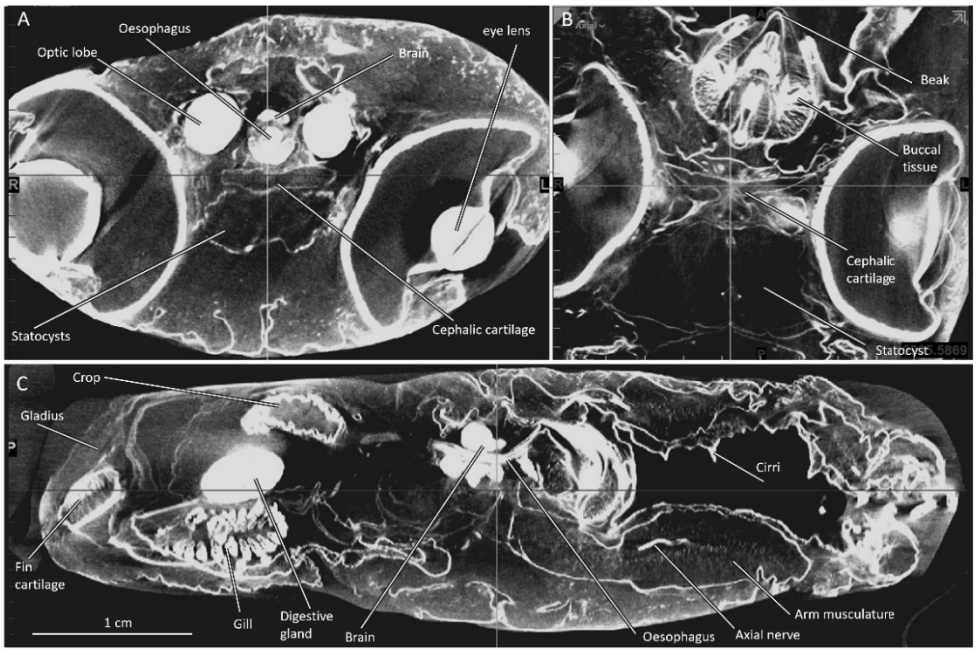

Figure 2.10: µCT slices of *V. infernalis* (AMNH IZC 361496) at the level of the cephalic cartilage. (Transverse: A, dorsal: B, and sagittal: C). The crossed lines show the correlation between the three different views. The optic lobes (A) eyes (A, B), cephalic cartilage, beak (B), esophagus, brain lobes, fin cartilage and elements of the digestive system are visible (C).

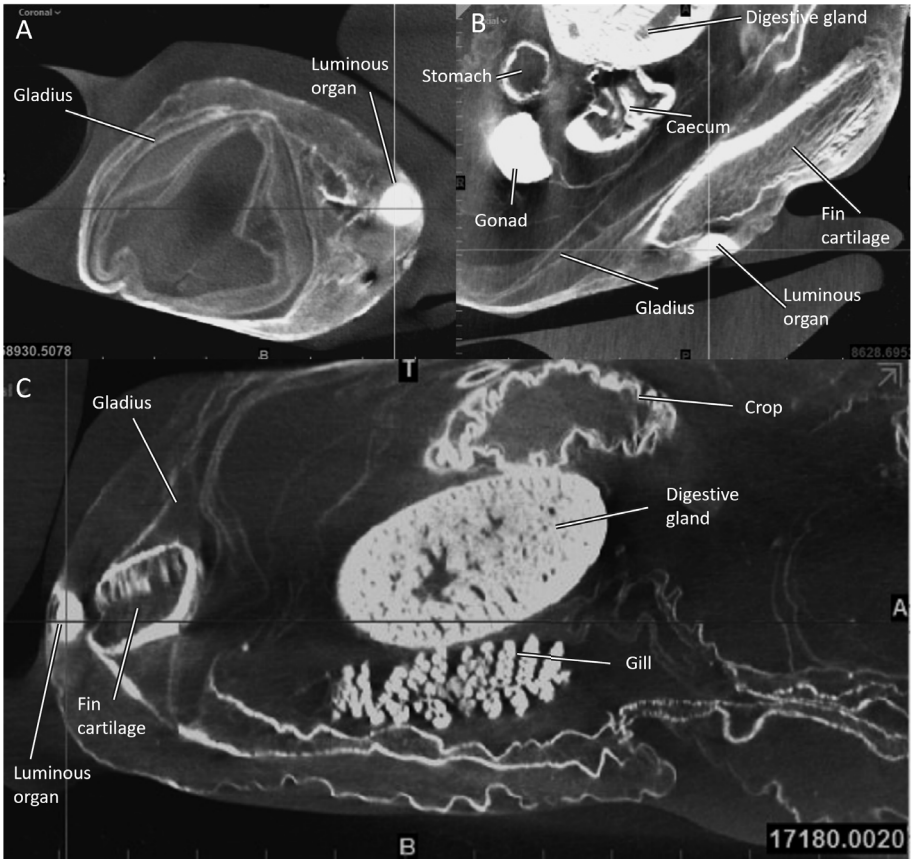

Figure 2.11: µCT slices of *V. infernalis* (AMNH IZC 361496) at the level of the posterior luminous organ. The crossed lines show the correlation between the three different views. Though the transverse view of the posterior section of the mantle (A) shows an outline of the gladius, the low threshold contrast and slight compression in the specimen contributes to the complexity of its rendering. There is minimal gladius contrast in dorsal (B) and sagittal (C) views.

Though the structural gladius provides the framework for the body, it does not have good contrast with the surrounding tissue, making it difficult to render. Its threshold contrast appears similar to that of the mantle (Fig. 2.8A, B) making it difficult to produce a precise threshold-based volume rendering. Similarly, the fin tissue does not have good contrast. This is in contrast with the fin and mantle tissues of *Sepia* and *Loligo* (Fig. 2.12B, C), which are more muscular. The internal texture of the digestive gland is clear (Fig. 2.11), as is the reticulated-like crop and gill lamellae, which are distinguishable at an individual level.

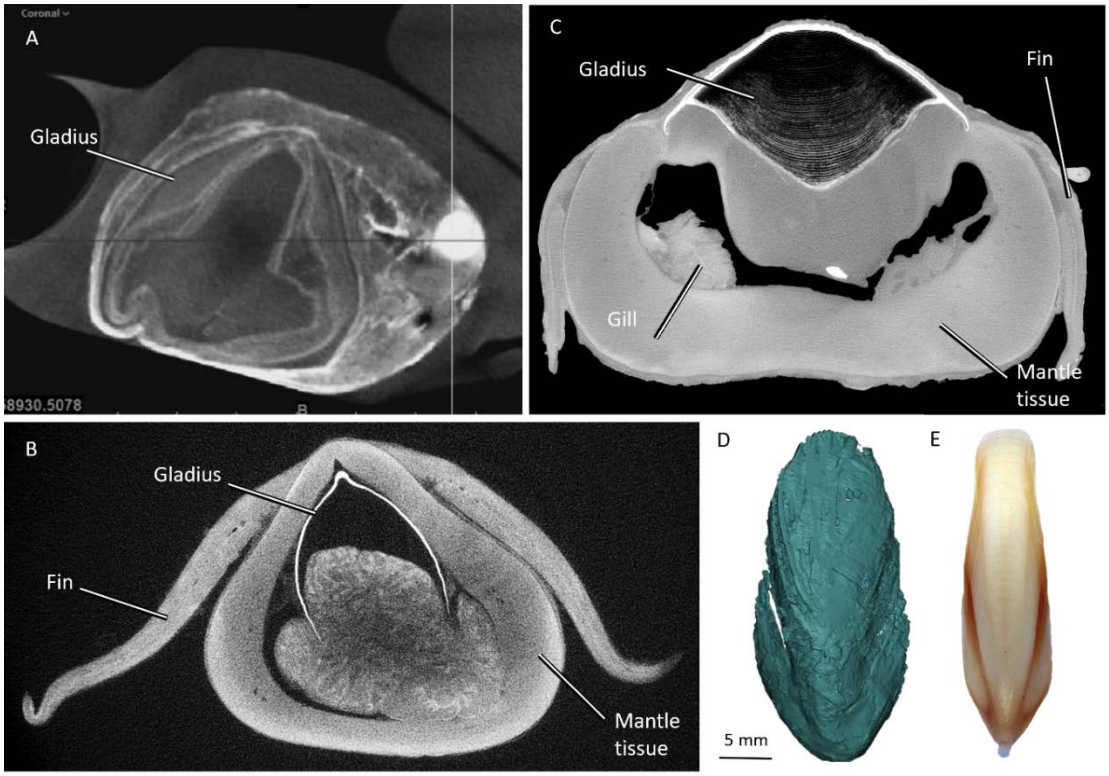

Figure 2.12: µCT slice of *V. infernalis* (AMNH IZC 361496), A. Transverse µCT slices of the posterior section of *Loligo* (B) and *Sepia* (C), both were stained in a 4% PTA solution prior to being scanned at the AST-RX platform (44.15 µm isotropic voxel resolution) at the MNHN. A rendering of the *V. infernalis* gladius from (AMNH IZC 361496) completed in Mimics (v. 21, Materialise), D; photograph of the *V. infernalis* gladius, modified from Bizikov & Toll 2016. The interpreted rendering is not an exact match with the actual gladius, highlighting the difficulty of interpreting the contrast boundaries. The gladii of *Loligo* and *Sepia* are clearly contrasted from the muscular tissue. The septa of the *Sepia* 'cuttlebone' are also visible indicating successful absorption of the staining agent.

This work enabled the 3D rendering of much of the anatomy of *V. infernalis* (Figs 2.13 – 2.17). This included the arm crown – the eight arms and two retractable filaments (Fig. 2.13), as well as the armature - the uniserial suckers and biserial cirri configuration on the oral surface of the arms (Fig. 2.14). The suckers were also able to be observed and rendered in profile view. These show the conical sucker attachment that is unique today in Modern *Vampyroteuthis*. Elements of the respiratory system (gills, branchial hearts, systemic heart, gland, possible digestive gland

appendages, and intestine), reproductive system (gonad) (Figs 2.15, 2.16), the eyes, optic lobes, brain, statocysts, and cephalic cartilage.

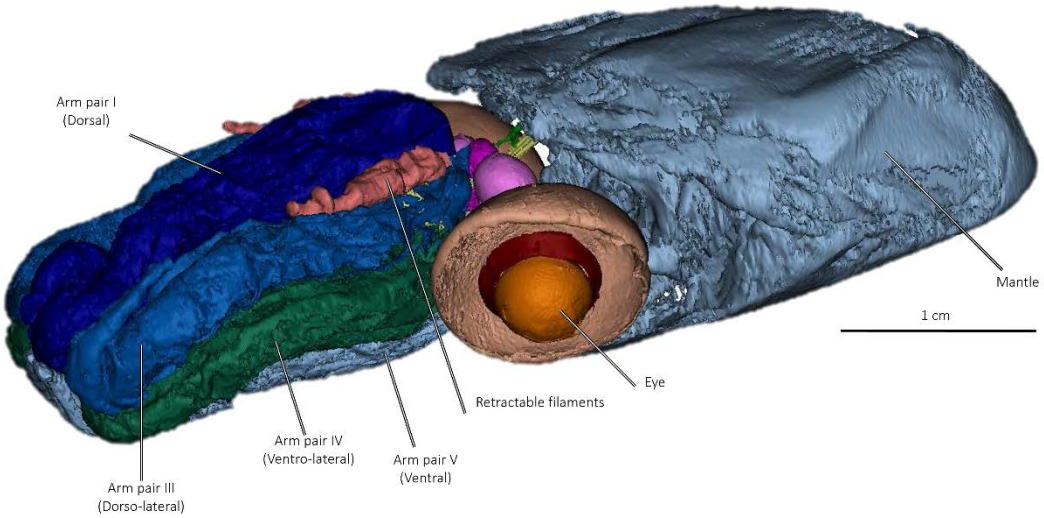

Figure 2.13: 3D volume rendering of *V. infernalis* (AMNH IZC 361496) showing the overall body plan, which includes eight arms, two retractable filaments, and a large pair of eyes.

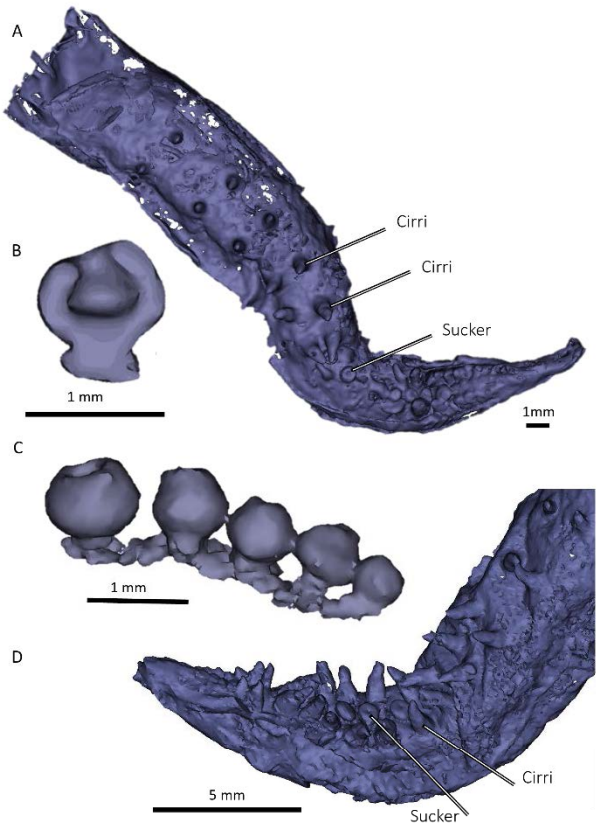

Figure 2.14: Two arms of *V. infernalis* (AMNH IZC 361496) showing the configuration of suckers and cirri (A, D). The suckers are positioned on the distal section of the arms and are flanked by biserial cirri, which have a sensory function. The suckers and sucker profile (B, C) are rendered from YPM 18279 and show the characteristic conical shaped attachment.

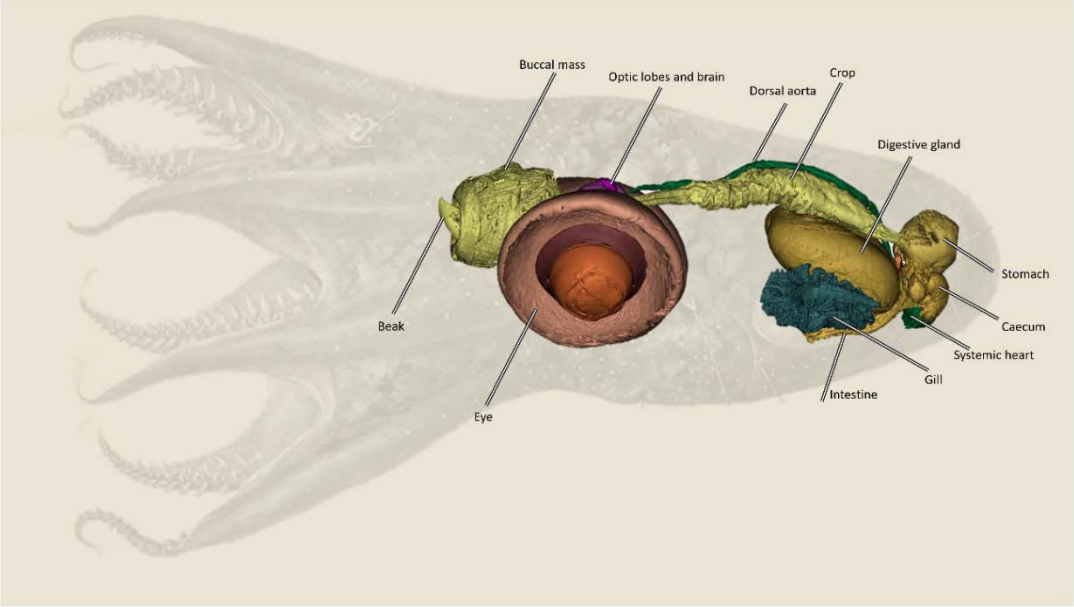

Figure 2.15: 3D rendering of digestive and respiratory elements of *V. infernalis* (AMNH IZC 361496) in sagittal view, superimposed onto an illustration of *V. infernalis* modified from Pickford 1946. The optic lobes and brain are just visible behind the eyes.

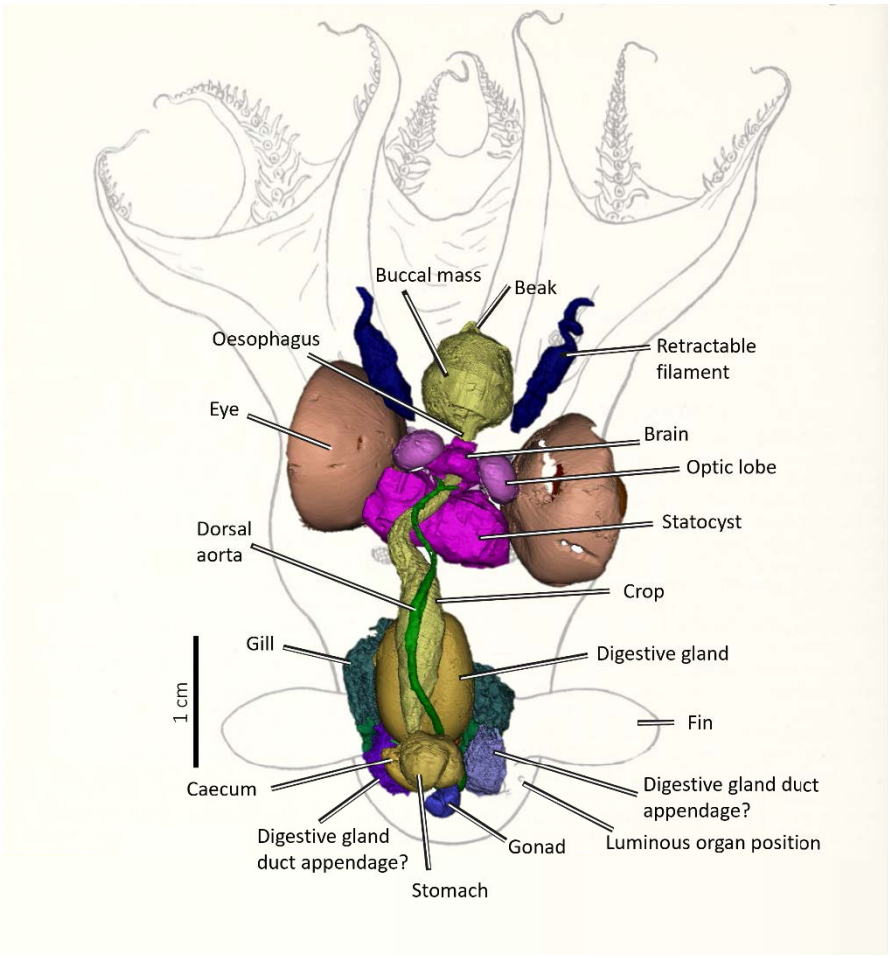

Figure 2.16: 3D rendering of internal elements of *V. infernalis (*AMNH IZC 361496) in dorsal view, superimposed onto an illustration of *V. infernalis* modified from Pickford 1946. This shows elements of the digestive, respiratory, and reproductive systems, as well as the optic lobes, brain, outline of statocysts, eyes, and retractable filaments.

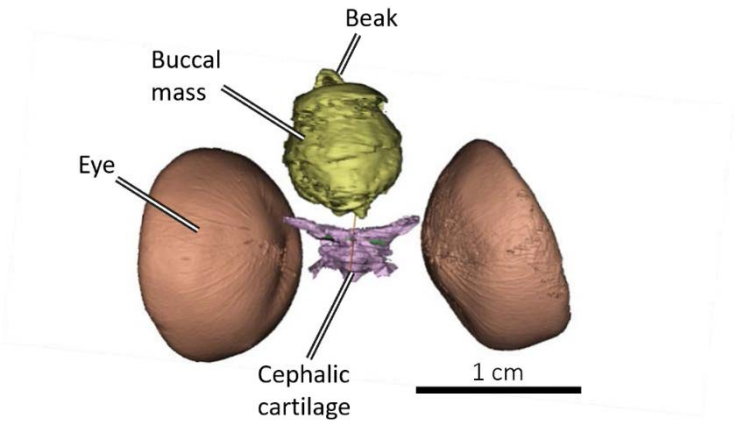

Figure 2.17: 3D rendering (dorsal view) of *V. infernalis* (AMNH IZC 361496) showing the buccal mass, rostral tip of the beak, and cephalic cartilage positioned between the eyes.

2.5 ~ Discussion

2.5.1 ~ Complementarity of dissections and 3D imaging methods

The use of 3D tomography in coleoid research is firmly established (e.g., Hoffmann *et al.* 2014; Sutton *et al.* 2014; Kruta *et al.* 2016; Roscian *et al.* 2021; Goolaerts *et al.* 2022). It is invaluable as a tool for morphological investigation, especially for rare or important specimens, as it allows the high-resolution imaging of internal structures in both fossil and extant forms that would have previously only been obtainable with destructive methods (Tafforeau *et al.* 2006).

Perhaps the greatest benefit of this type of imaging is that the data can be shared with a wider community (Kruta *et al.* 2011, 2013, 2016; Sutton *et al.* 2014; Hoffmann *et al.* 2021, Ziegler *et al.* 2021). As this approach enables the anatomy to be studied in detail without needing the physical specimen, 3D datasets have the potential to be accessed through digital museum collections or data repositories. These data can also be used for education and outreach (Rahman *et al.* 2012), collaborative analysis (Sutton *et al.* 2014), as well as forming a database of information that shifts the focus from the acquisition of data, to having data ready to analyze (Xavier *et al.* 2015; Ziegler *et al.* 2018). Further, these data and anatomical reconstructions also have applications in comparative, ecological, and functional studies. Indeed, within extant taxa, species or general-level variation could be explored by creating image stacks and datasets on multiple individuals of the same species or genera (Xavier *et al.* 2015). For systematic purposes some morphological traits can be investigated without the need for dissections, an asset particularly important for rare collection specimens. Indeed, if we refer to the latest

morphological computational phylogeny analysis (Whalen & Landman 2022), several of the characters used can be observed. In the matrix, the arm crown and suckers contribute thirty characters. In addition to the presence of either eight arms (Octobrachia), or ten (Decabrachia), this includes details on their comparative length and any modifications, as well as sucker location, attachment style and symmetry. Information on each of these characters can be attained with the tomographic methods as shown here (Figs 2.1 D, E, 2.9, 2.10, 2.11, 2.15, 2.16, 2.18). Yet, the data obtained through CT scans and staining showed that the level of detail that can be obtained on a key structure such as the gladius, representing >50% of the character matrix is variable (Fig. 2.9). For example, the rendering of the *V. infernalis* gladius demonstrates that while it is possible to have an overall sense of the structure, the low threshold contrast makes it difficult to reconstruct each of the character states that are observable on the physical gladius.

Despite its obvious benefits, there are also limitations to these methods. Certain tissues have similar X-ray densities after staining or fossilization, making it hard to discriminate between structures when they are positioned close to each other (Kerbl *et al.* 2013). For example, despite having excellent resolution on some of the anatomy of *V. infernalis* (e.g., digestive system elements, eyes, and gills), it was not possible to determine the boundaries of many of the non-dense soft tissues, like the funnel or ducts associated with the reproductive system, even with staining. A clearer picture of these elements would be gathered by dissections.

This study demonstrates anatomical features that are more likely to be identifiable using tomographic methods; what is observable and able to be rendered in extant forms provides a guide for what we may expect to see in fossil forms. The gelatinous mantle tissue of *V. infernalis* lacks the muscular structure of other forms (e.g., octopus, or squid) and the body appears slightly misshapen in the µCT images. The lack of rigidity contributes to the difficulty in determining the soft tissues, as organs are somewhat displaced and squashed. This is also an issue presented by fossil material as, inevitably, specimens have undergone compaction or rotation.

CONCLUSION

The study of coleoid tissues with 3D tomography represents a well-established and powerful set of tools, both for morphological analysis and dissemination of data (Sutton *et al.* 2014). Increased use of these non-destructive high-resolution imaging techniques will enable a clearer picture of morphology of the typically rare fossil and extant material (Kruta 2016) and

has the potential to give more insight into intraspecific variation. Used in conjunction with molecular techniques, digital morphological techniques have the potential to unlock the answers to numerous questions regarding cephalopod evolution. In this thesis, the virtual dissections of Cirrata and *V. infernalis* were the backbone for comparative studies of the Octobrachia from la Voulte-sur-Rhône that will be discussed in the following chapter.

BIBLIOGRAPHY

BIZIKOV, V. A. and TOLL, R. B. 2016. Treatise Online no. 77: Part M, Chapter 9A: The Gladius and its Vestiges in Extant Coleoidea. *Treatise Online*.

CHUNG, W.-S. and MARSHALL, N. J. 2016. Comparative visual ecology of cephalopods from different habitats. *Proceedings of the Royal Society B: Biological Sciences*, **283**, 20161346.

——— and ———. 2017. Complex visual adaptations in squid for specific tasks in different environments. *Frontiers in Physiology*, **8**, 105.

———, KURNIAWAN, N. D. and MARSHALL, N. J. 2022. Comparative brain structure and visual processing in octopus from different habitats. *Current Biology*, **32**, 97-110.e4.

COLLINS, M. and VILLANUEVA, R. 2006. Taxonomy, Ecology and Behaviour Of The Cirrate Octopods. *Oceanography and marine biology*, **44**, 277–322.

CUNNINGHAM, J. A., RAHMAN, I. A., LAUTENSCHLAGER, S., RAYFIELD, E. J. and DONOGHUE, P. C. J. 2014. A virtual world of paleontology. *Trends in Ecology & Evolution*, **29**, 347–357.

DOOST, A. and ARNOLDA, L. 2021. Iodine staining outperforms phosphotungstic acid in high-resolution micro-CT scanning of post-natal mice cardiac structures. *Journal of Medical Imaging*, **8**, 027001–027001.

GIGNAC, P. M., KLEY, N. J., CLARKE, J. A., COLBERT, M. W., MORHARDT, A. C., CERIO, D., COST, I. N., COX, P. G., DAZA, J. D. and EARLY, C. M. 2016. Diffusible iodine-based contrast-enhanced computed tomography (diceCT): an emerging tool for rapid, high-resolution, 3-D imaging of metazoan soft tissues. *Journal of anatomy*, **228**, 889–909.

GOOLAERTS, S., CHRISTIAENS, Y., H. MOLLEN, F., MOTTEQUIN, B. and STEURBAUT, E. 2022. Applying micro-CT Imaging in The Study of Historically And newly Collected specimens of Belosaepia (sepiida, coleoidea, Cephalopoda) from The Early Eocene (Ypresian) of Belgium. *Rivista Italiana di Paleontologia e Stratigrafia*, ***128***(3).

GUERIAU, P., BERNARD, S. and BERTRAND, L. 2016. Advanced Synchrotron Characterization of Paleontological Specimens. *Elements*, **12**, 45–50.

GUERRA, Á. 2019. Functional Anatomy: Macroscopic Anatomy and Post-mortem Examination. *In* GESTAL, C., PASCUAL, S., GUERRA, Á., FIORITO, G. and VIEITES, J. M. (eds.) *Handbook of Pathogens and Diseases in Cephalopods*, Springer International Publishing, Cham, 11–38 pp.

HANLON, R., VECCHIONE, M. and ALLCOCK, L. 2018. *Octopus, Squid, and Cuttlefish: A visual, scientific guide to the oceans' most advanced invertebrates*. University of Chicago Press.

HOFFMANN, R., SCHULTZ, J. A., SCHELLHORN, R., RYBACKI, E., KEUPP, H., GERDEN, S., LEMANIS, R. and ZACHOW, S. 2014. Non-invasive imaging methods

applied to neo-and paleo-ontological cephalopod research. *Biogeosciences*, **11**, 2721–2739.

———, SLATTERY, J. S., KRUTA, I., LINZMEIER, B. J., LEMANIS, R. E., MIRONENKO, A., GOOLAERTS, S., DE BAETS, K., PETERMAN, D. J. and KLUG, C. 2021. Recent advances in heteromorph ammonoid palaeobiology. *Biological Reviews*, **96**, 576–610.

JEREB, P. and ROPER, C. F. E. 2005. Cephalopods of the world. An Annotated and Illustrated catalogue of Cephalopod species known to date. Vol. 1. Chambered nautiluses and sepioids (Nautilidae, Sepiidae, Sepiolidae, Sepiadariidae, Idiosepiidae and Spirulidae). FAO Spec. Cat. Fish. Purp. 4(1), Rome, FAO, 262p.

——— and ROPER, C. F. 2010. Cephalopods of the world-an annotated and illustrated catalogue of cephalopod species known to date. Vol 2. Myopsid and oegopsid squids. FAO Species Catalogue for Fishery Purposes, No. 4, Vol. 2, Rome, FAO, 605p.

———, ———, NORMAN, M.D. and FINN J.K. 2016.Cephalopods of the world. An Annotated and illustrated catalogue of Cephalopod species known to date. Vol. 3. Octopods and vampire squids. FAO Spec. Cat. Fish. Purp. 4(3), Rome, FAO, 398p.

KEEVIL, S.F., 2001. Magnetic resonance imaging in medicine. *Physics Education*, *36*(6), p.476.

KEMP, R., PETERS, H., ALLCOCK, L., CARPENTER, K., OBURA, D., POLIDORO, B., RICHMAN, N., COLLEN, B., BÖHM, M. and BAILLIE, J. 2012. Marine invertebrate life. *Spineless: Status and trends of the world's invertebrates. Zoological Society of London, United Kingdom*, 34–45.

KERBL, A., HANDSCHUH, S., NÖDL, M.-T., METSCHER, B., WALZL, M. and WANNINGER, A. 2013. Micro-CT in cephalopod research: investigating the internal anatomy of a sepiolid squid using a non-destructive technique with special focus on the ganglionic system. *Journal of Experimental Marine Biology and Ecology*, **447**, 140–148.

KRUTA, I., 2011. *Étude de la masse buccale des ammonites: implications paléobiologiques et évolutives* (Doctoral dissertation, Muséum national d'histoire naturelle, Paris).

———, LANDMAN, N., ROUGET, I., CECCA, F. and TAFFOREAU, P. 2011. The role of ammonites in the Mesozoic marine food web revealed by jaw preservation. *Science*, **331**, 70–72.

———, ———, ———, ——— and ———. 2013. The radula of the Late Cretaceous scaphitid ammonite *Rhaeboceras halli* (Meek and Hayden, 1856). *Palaeontology*, **56**, 9–14.

———, ROUGET, I., CHARBONNIER, S., BARDIN, J., FERNANDEZ, V., GERMAIN, D., BRAYARD, A. and LANDMAN, N. 2016. *Proteroctopus ribeti* in coleoid evolution. *Palaeontology*, **59**, 767–773.

LEMANIS, R., KORN, D., ZACHOW, S., RYBACKI, E. and HOFFMANN, R. 2016. The evolution and development of cephalopod chambers and their shape. *PloS one*, **11**, e0151404.

LINNAEUS, C. 1789. *Systema Naturae per regna tria naturae, secundum classes, ordines, genera, species; cum characteribus, differentiis, synonymis, locis*. Vol. 1. apud JB Delamolliere.

METSCHER, B. D. 2009. MicroCT for comparative morphology: simple staining methods allow high-contrast 3D imaging of diverse non-mineralized animal tissues. *BMC Physiology*, **9**, 11.

——— 2011. *X-Ray Microtomographic Imaging of Vertebrate Embryos.* Cold Spring Harb Protoc, **12**.

——— 2013. Biological applications of X-ray microtomography: imaging microanatomy, molecular expression and organismal diversity. *Microsc Anal (Am Ed)*, **27**, 13–6.

PAUWELS, E., VAN LOO, D., CORNILLIE, P., BRABANT, L. and VAN HOOREBEKE, L. 2013. An exploratory study of contrast agents for soft tissue visualization by means of high resolution X-ray computed tomography imaging. *Journal of microscopy*, **250**, 21–31.

PICKFORD, G. E. 1946. *Vampyroteuthis infernalis* Chun, an archaic dibranchiate cephalopod. I. Natural history and distribution. Dana-report 29,40

RAHMAN, I. A., ADCOCK, K. and GARWOOD, R. J. 2012. Virtual fossils: a new resource for science communication in paleontology. *Evolution: Education and Outreach*, **5**, 635–641.

RAYFIELD, E. J. 2007. Finite element analysis and understanding the biomechanics and evolution of living and fossil organisms. *Annu. Rev. Earth Planet. Sci.*, **35**, 541–576.

ROBSON, G. 1925. On Mesonychoteuthis, a new genus of Oegopsid Cephalopoda. *Annals and Magazine of Natural History*. Ser. 9, 16: 272-277

——— 1932. A monograph of the recent Cephalopods. Part II. The Octopoda (excluding the Octopodinae). London: British Museum.

ROSCIAN, M., HERREL, A., CORNETTE, R., DELAPRÉ, A., CHEREL, Y. and ROUGET, I. 2021. Underwater photogrammetry for close-range 3D imaging of dry-sensitive objects: The case study of cephalopod beaks. *Ecology and Evolution*, **11**, 7730–7742.

———, SOUQUET, L., HERREL, A., UYENO, T., ADRIAENS, D., DE KEGEL, B. and ROUGET, I. 2023. Comparative anatomy and functional implications of variation in the buccal mass in coleoid cephalopods. *Journal of Morphology*, **284**, e21595.

———, HERREL, A., ZAHARIAS, P., CORNETTE, R., FERNANDEZ, V., KRUTA, I., CHEREL, Y. and ROUGET, I. 2022. Every hooked beak is maintained by a prey: Ecological signal in cephalopod beak shape. *Functional Ecology*, **36**, 2015–2028.

ROWE, A. J., KRUTA, I., VILLIER, L. and ROUGET, I. 2023. A new vampyromorph species from the Middle Jurassic La Voulte-sur-Rhône Lagerstätte. *Papers in Palaeontology*, **9**, e1511.

ROWE, A. J., KRUTA, I., LANDMAN, N. H., VILLIER, L., FERNANDEZ, V. and ROUGET, I. 2022. Exceptional soft-tissue preservation of Jurassic *Vampyronassa rhodanica* provides new insights on the evolution and palaeoecology of vampyroteuthids. *Scientific Reports*, **12**, 1–9.

SAKURAI, Y. and IKEDA, Y. 2019. Development of a contrast-enhanced micro computed tomography protocol for the oval squid (Sepioteuthis lessoniana) brain. *Microscopy Research and Technique*, **82**, 1941–1952.

SUTTON, M.D., 2008. Tomographic techniques for the study of exceptionally preserved fossils. *Proceedings of the Royal Society B: Biological Sciences*, *275*(1643), pp.1587-1593.

SUTTON, M. D., RAHMAN, I. A. and GARWOOD, R. J. 2014. *Techniques for virtual palaeontology*. Wiley Blackwell, Chichester, UK.

———, ——— and ——— 2016. Virtual Paleontology—An Overview. *Paleontological Society Papers*, **22**, 1–20.

TAFFOREAU, P., BOISTEL, R., BOLLER, E., BRAVIN, A., BRUNET, M., CHAIMANEE, Y., CLOETENS, P., FEIST, M., HOSZOWSKA, J., JAEGER, J.-J., KAY, R. F., LAZZARI, V., MARIVAUX, L., NEL, A., NEMOZ, C., THIBAULT, X., VIGNAUD, P. and ZABLER, S. 2006. Applications of X-ray synchrotron microtomography for non-destructive 3D studies of paleontological specimens. *Applied Physics A*, **83**, 195–202.

WHALEN, C. D. and LANDMAN, N. H. 2022. Fossil coleoid cephalopod from the Mississippian Bear Gulch Lagerstätte sheds light on early vampyropod evolution. *Nature Communications*, **13**, 1107.

XAVIER, J. C., ALLCOCK, A. L., CHEREL, Y., LIPINSKI, M. R., PIERCE, G. J., RODHOUSE, P. G. K., ROSA, R., SHEA, E. K., STRUGNELL, J. M., VIDAL, E. A. G., VILLANUEVA, R. and ZIEGLER, A. 2015. Future challenges in cephalopod research. *Journal of the Marine Biological Association of the United Kingdom*, **95**, 999–1015.

ZIEGLER, A. and SAGORNY, C. 2021. Holistic description of new deep-sea megafauna (Cephalopoda: Cirrata) using a minimally invasive approach. *BMC Biology*, **19**, 81.

———, MILLER, A. and NAGELMANN, N. 2021. Novel insights into early life stages of finned octopods (Octopoda: Cirrata). *Swiss Journal of Palaeontology*, **140**, 24.

———, OGURRECK, M., STEINKE, T., BECKMANN, F., PROHASKA, S. and ZIEGLER, A. 2010. Opportunities and challenges for digital morphology. *Biology Direct*, **5**, 45.

———, KUNTH, M., MUELLER, S., BOCK, C., POHMANN, R., SCHRÖDER, L., FABER, C. and GIRIBET, G. 2011. Application of magnetic resonance imaging in zoology. *Zoomorphology*, **130**, 227–254.

———, BOCK, C., KETTEN, D. R., MAIR, R. W., MUELLER, S., NAGELMANN, N., PRACHT, E. D. and SCHRÖDER, L. 2018. Digital Three-Dimensional Imaging Techniques Provide New Analytical Pathways for Malacological Research. *American Malacological Bulletin*, **36**, 248–273.

CHAPTER 3: VAMPYROMORPHA OF LA VOULTE-SUR-RHÔNE: SYSTEMATICS & ECOLOGICAL IMPLICATIONS

INTRODUCTION

Mesozoic coleoids are mainly known from the Lower Jurassic shales, and lithographic limestones of the Upper Jurassic and Upper Cretaceous. The Mid-Jurassic record is represented mainly by the Callovian-aged Lagerstätten of Christian Malford, UK (Wilby *et al.* 2004, 2008; Hart *et al.* 2019) and La Voulte-sur-Rhône, France (Fischer & Riou 1982*a*, *b*, 2002; Fischer 2003; Charbonnier 2009; Charbonnier *et al.* 2014; Fuchs 2014; Kruta *et al.* 2016). Each of the Mesozoic localities represent particular depositional environments (e. g., the dysoxic epicontinental seas of the Posidonia shales, or the shallow carbonate lagoons of Solnhofen and Lebanon) and have been a direct source of morphological information for Mesozoic coleoids. The Callovian-aged La Voulte-sur-Rhône Lagerstätte offers rare insight into a deeper marine-type setting (~200m) during this time (Charbonnier 2009).

In addition to the depositional setting, La Voulte-sur-Rhône is renowned for the diversity of coleoid genera – they represent more than a third of non-belemnoid genera from the Middle Jurassic (Fuchs 2020) that are uniquely preserved in three dimensions (Wilby *et al.* 1996; Charbonnier 2009; Charbonnier *et al.* 2014; Fuchs 2014; Kruta *et al.* 2016; Audo *et al.* 2019; Jauvion 2020). This makes La Voulte-sur-Rhône an important locality for the study of coleoid evolution.

3.1 GEOLOGICAL SETTING

Today, the Lagerstätte is an abandoned quarry in the Ravin des Mines (Fig. 3.1), near the town of La Voulte-sur-Rhône in Southeast France (Ardèche). The entire section is dated to the Lower Callovian age, specifically, the Gracilis Biozone (Elmi 1967). Paleogeographic reconstructions position the locality on the Ardèche margin, adjacent to the submerged Massif Central (=Hercynian crystalline basement) on the North-West and the Rhône basin on the South-East (Fig. 3.2). The main La Voulte fault (N54°) was very active throughout the area during the Callovian (Villier *et al.* 2009) and separates the fossiliferous outcrop from the basement. Indeed, the western margin is characterized by the complex submarine topography and steep bathymetric gradients caused by extensive and transverse reactivation of Hercynian faulting (Fischer 2003; Charbonnier 2009; Villier *et al.* 2009; Charbonnier *et al.* 2014).

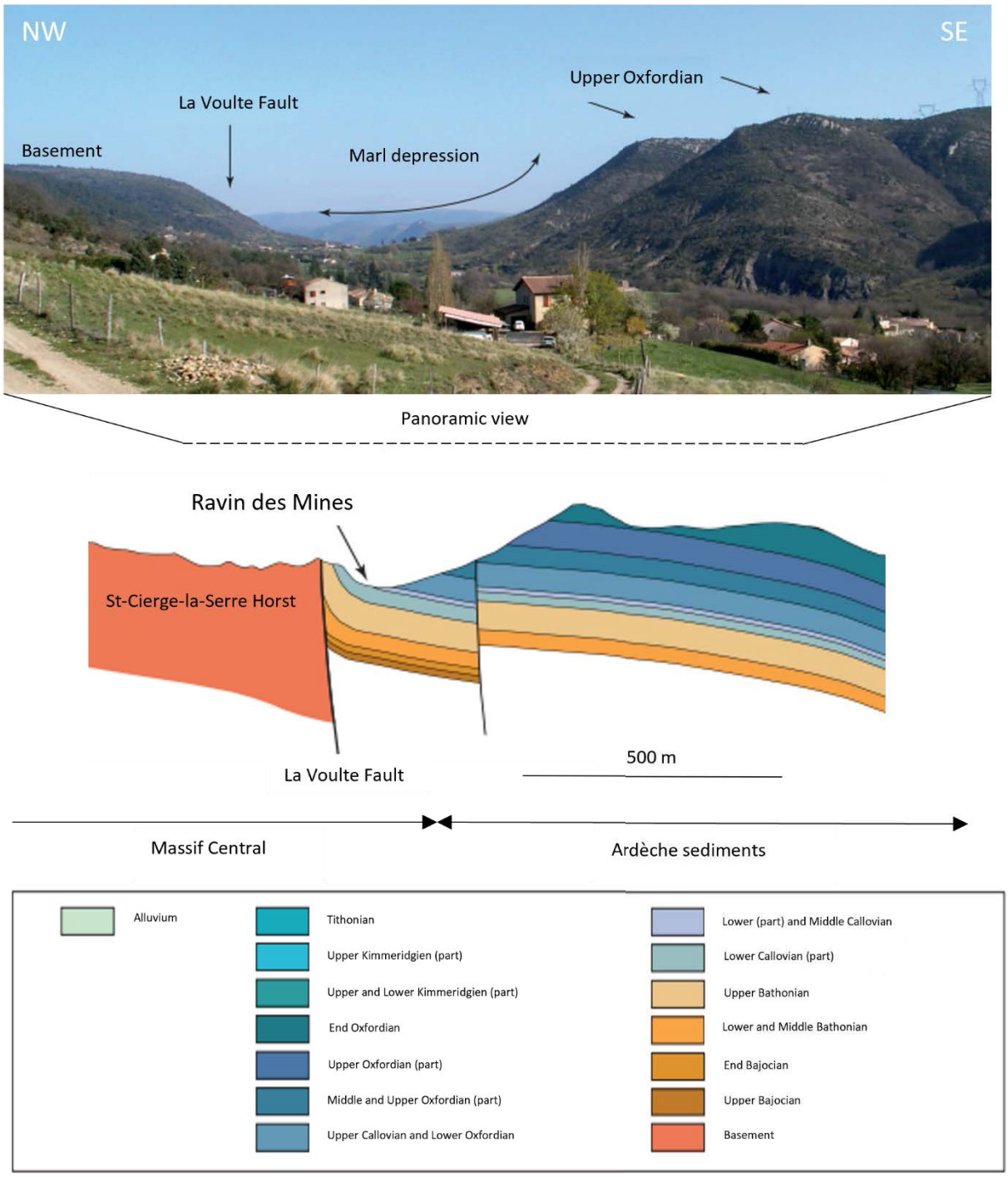

Figure 3.1: Overview of the La Voulte-sur-Rhône area (top) showing the existing topography of the Jurassic sediments. This corresponds with a geologic representation of the Ardèche palaeomargin (center) in cross section. Modified from Charbonnier 2009, Chapter 7, Fig. 38.

The lithology of La Voulte-sur-Rhône is dominated by marls (Fig. 3.3). The sediments came from the carbonate platforms, as well as submarine erosion of the basement blocks and the associated Early Mesozoic sediment cover (Charbonnier *et al.* 2007, 2014; Charbonnier 2009). These very fine sediments represent a depositional environment that was relatively calm, but

evidence of debris flow is also present, which correlates with slumping from the escarpments and rocky drop-offs from the mosaic of tilted blocks (Charbonnier 2009). The fossiliferous layers of the Lagerstätte outcrop in a small, relatively thin interval (5-6 m). These are overlain by about 15 m of iron deposits (Fig. 3.3), which were extensively mined in the 19th century (Charbonnier 2009; Villier *et al.* 2009; Charbonnier *et al.* 2014). Numerous sideritic concretions are present in the basal marls, and frequently contain three-dimensional soft-bodied fossils. Some marl horizons also have small pockets of more compacted soft-bodied specimens. These are interspersed with iron carbonate layers that are rich in ophiuroids (Charbonnier 2009; Villier *et al.* 2009; Charbonnier *et al.* 2014).

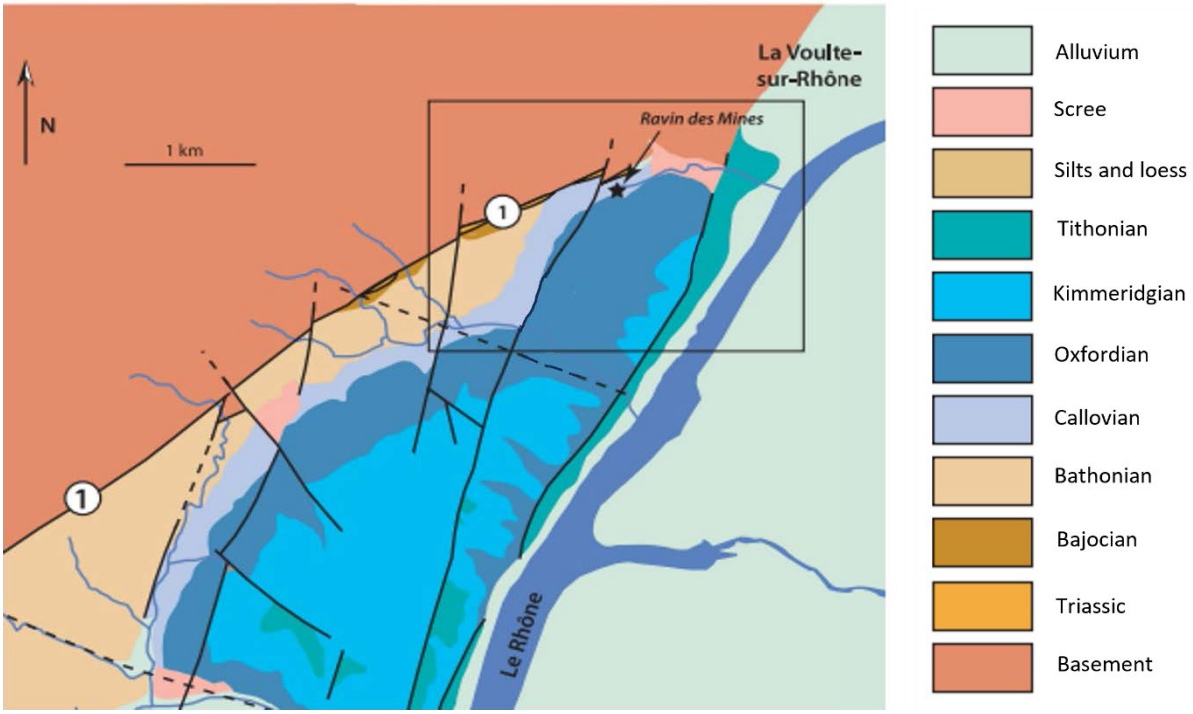

Figure 3.2: Simplified geologic representation of the northern Ardèche margin showing the faulting in the immediate area, including the La Voulte fault (represented by the number 1) that runs in a Hercynian direction (N 54°). Modified from Charbonnier 2009, Chapter 7, Fig. 39.

The exceptional 3D preservation of fossil material at La Voulte-sur-Rhône is a result of early replacement of soft tissues during a sequence of mineralization phases (Allison 1988; Briggs & Wilby 1996; Wilby *et al.* 1996; Wilby 2001; Jauvion 2020). Ordinarily in marine environments, calcium carbonate precipitates (Briggs & Wilby 1996; Wilby *et al.* 1996) but in the Jurassic La Voulte-sur-Rhône, rapid post-depositional microbial activity in the low oxygen setting reduced the pH, leading to authigenic precipitation of iron-rich minerals (Allison 1988; Briggs & Wilby 1996; Wilby *et al.* 1996; Jauvion 2020). In this scenario, the mineralization is localized, and the

organs and tissues may be replaced by different mineral phases making them mineralogically and chemically heterogeneous (Wilby *et al.* 1996; Jauvion 2020).

The initial replacement phases, which reproduce the anatomical structures, are by fluorapatite and pyrite (Jauvion 2020). As such, the organic composition of the organism's tissues is not preserved but are mineral replicas of the morphology on the scale of the whole organism scale to the subcellular scale in some cases (Jauvion 2020). Only the most resistant compounds (e.g., chitin, calcite) may be found in the fossil record (Jauvion 2020).

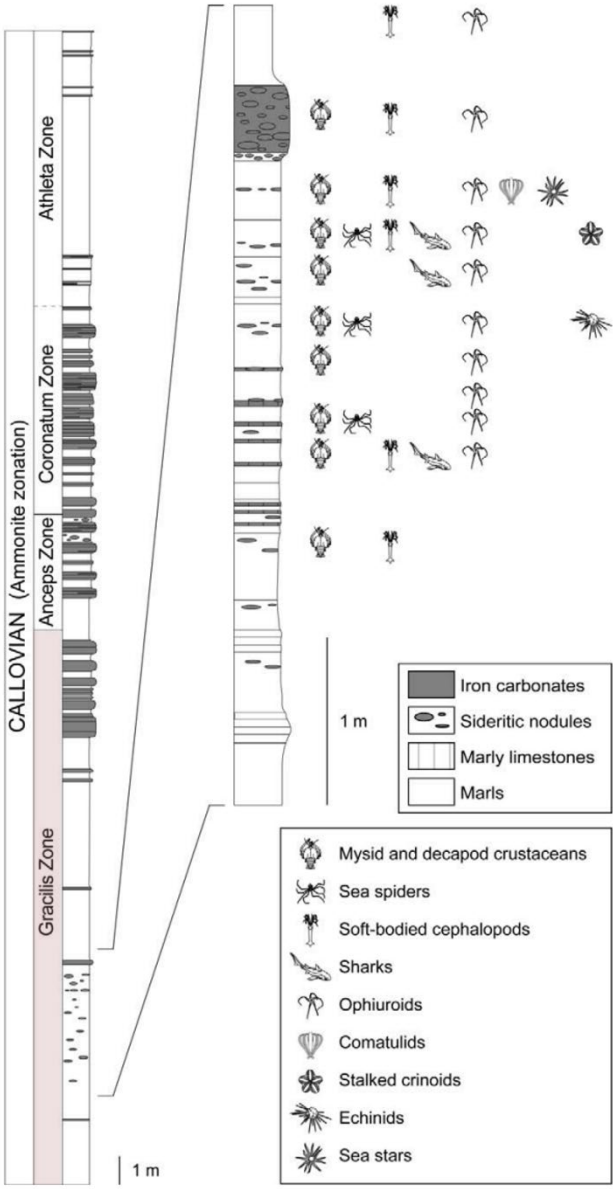

Figure 3.3: Stratigraphic column of the La Voulte-sur-Rhône Lagerstätte, showing the horizons of the major fossil occurrences in the Gracilis Zone. Modified from Villier *et al.* 2009.

3.2 BIODIVERSITY

The first paleontological studies at La Voulte-sur-Rhône were conducted around the mid-19th century and described a faunal assemblage that included brittle stars, brachiopods, ammonites. Indeed, it was ammonites that would later provide the biostratigraphic framework for the locality (Elmi 1967; Charbonnier 2009).

Today, around 60 fossil species are recognized from the faunal assemblage (Fig. 3.4). This is comprised of arthropods (~50%), coleoids (11%), marine worms and hemichordates (11%), echinoderms (10%), vertebrates (10-12%), bivalves (3%) and brachiopods (3%) (Charbonnier 2009; Charbonnier *et al.* 2014). The composition of this assemblage is generally original when compared with other Mesozoic Lagerstätten where biodiversity can be high. For example, more than 100 species are known from the Holzmaden shales, and there are more than 500 from the Solnhofen limestones (Charbonnier 2009). However, the differences in biodiversity between these sites needs to account for the sampling rate and outcrop area. At La Voulte-sur-Rhône, the fossiliferous layers outcrop over a few hectares, whereas the Solnhofen sediments outcrop over hundreds of km^2; they have also been quarried extensively for centuries. The paleoenvironment also contributes to differences in the preserved biodiversity. Indeed, Solnhofen organisms originate from open marine, reef, lagoonal, and continental environments, which maximizes the biodiversity of the fossil assemblages, while the sediments of La Voulte-sur-Rhône reflect less diverse ecosystems (Charbonnier 2009).

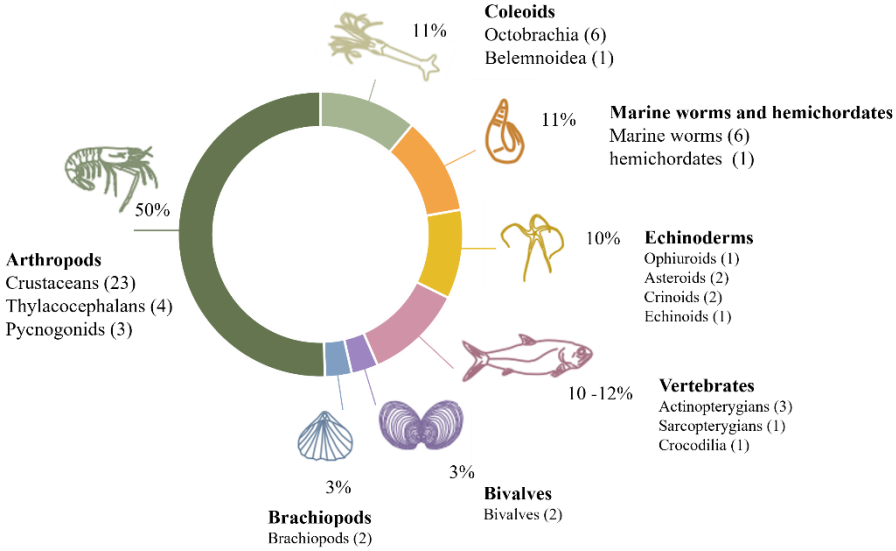

Figure 3.4: Faunal paleobiodiversity (groups, and number of species represented) in the La Voulte-sur-Rhône (Gracilis Zone). Adapted from Charbonnier 2009, Chapter 8, Tables 14 –20. Ammonites are not included in this summary.

3.3 Paleoenvironment

Much of the previous work on the La Voulte fauna has been generally systematic and descriptive in nature (Charbonnier 2009). Analyses by Fischer (2003) noted that the fauna from the locality was nearly exclusively pelagic, nectopelagic or mesopelagic, with very few benthic organisms. He estimated that the water depth would have reached roughly 200 m with well-oxygenated surface-and mid-water, and quiet, anoxic bottom water that was aphotic.

Charbonnier (2009) gave the first comprehensive assessment of faunal biodiversity from the locality and attempted to place it within a palaeoenvironmental and palaeoecological context. Comparisons between the fossils and present-day analogues indicated the paleoenvironment was bathyal, with a water depth of probably >200 m with low light penetration, and loose, muddy substrates. Further, the ecological conditions were stable enough such that populations could be sustained over time.

Without a definitive description, subsequent works (e.g., Audo *et al.* 2014 2019; Jauvion *et al.* 2016, 2017, 2020*a*, *b*) have continued to include palaeoecological information. Attempts to reconstruct the ecology and paleoenvironment of the site are still debated given the seemingly contradictory (photic and aphotic) habitat inferences of the faunal assemblage (Charbonnier *et al.* 2007, 2014; Charbonnier 2009; Jauvion *et al.* 2016; Audo *et al.* 2019).

3.4 Coleoid Diversity

The first mention of a coleoid from La Voulte-sur-Rhône was brief and part of a comprehensive synthesis of the geology and paleontology of the locality (Sayn & Roman 1928). In this monograph, Frédéric Roman described a "Cephalopoda" (part and counterpart, n° I.D.1743 and n° I.D.1744 respectively) and assigned it the name *Plesioteuthis gevreyi* Roman, 1928; (p. 112, pl. IV, fig. 1, 2). This specimen would later be redescribed with more clarity as *Romaniteuthis gevreyi* by Fischer & Riou (1982*b*).

In 1982, Fischer & Riou published two papers that are foundational to the study of coleoid cephalopods from La Voulte-sur-Rhône (Fischer & Riou 1982*a, b*), and described eight individuals that represented five new genera and species. These specimens were preserved both in nodules, and on the marl bedding planes. Those in the nodules had undergone some deformation, while specimens in the loose marls were more strongly compacted.

Using the classification nomenclature that was widespread at the time, these new taxa included the earliest known Octopod, *Proteroctopus ribeti* Fischer & Riou 1982a (suborder Palaeoctopodina, family Palaeoctopodidae, Fig. 3.5C) (Fischer & Riou 1982a), and six individuals assigned to the Order Teuthoidea (= Order: Decapoda of the Subclass Dibranchiata). They were further classified by the three Suborders that were commonly used, the prototeuthid (*Romaniteuthis gevreyi* (Fischer & Riou 1982b)), Fig. 3.5D*; Rhomboteuthis lehmani* Fischer & Riou 1982b, Fig. 3.5G), Mesoteuthoidea (*Teudopsis* sp., Fig. 3.5H), and Metateuthoidea (*Gramadella piveteaui* Fischer & Riou 1982b, Fig. 3.5B).

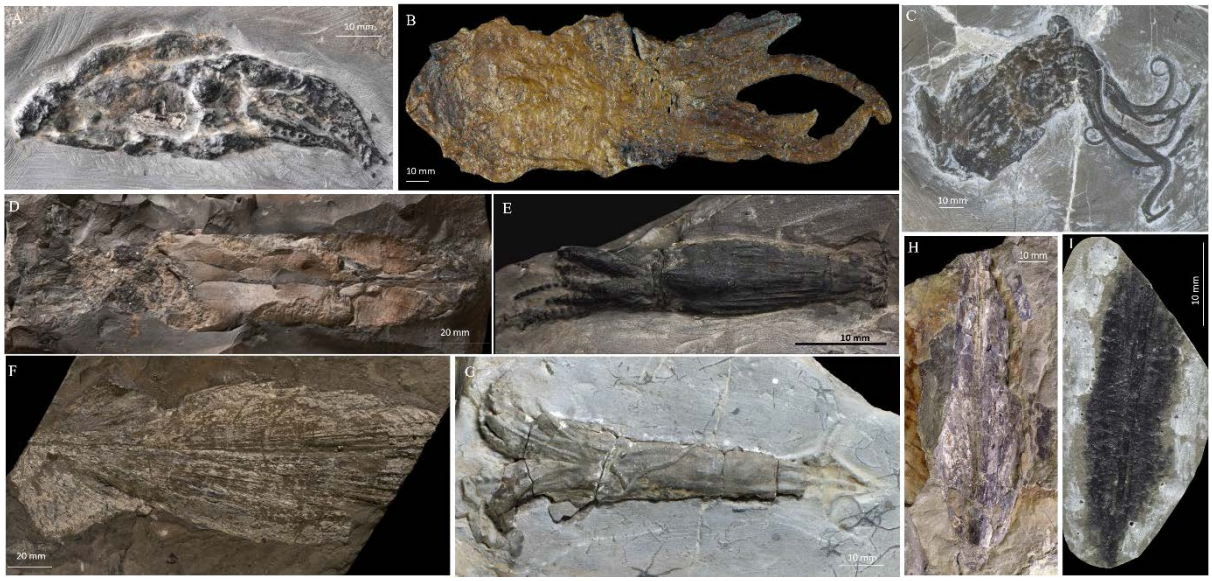

Figure 3.5: Representation of coleoid genera from La Voulte sur-Rhône. *Vampyronassa rhodanica*, holotype, MNHN.F.B74247 (A); *Gramadella piveteaui*, holotype, MNHN.F.R03760 (B); *Proteroctopus ribeti*, holotype, MNHN.F.R03801 (C); *Romaniteuthis gevreyi*, holotype MHNGr.PA.10277, preserved in a concretion (D); *Mastigophora aff. brevipennis*, holotype, MNHN.F.53379 (E); *incertae sedis* individual, MNHN.F.A29523 (F); *Rhomboteuthis lehmani*, MNHN.F.R03758 (G); *incertae sedis* individual, MNHN.F.A29585 (H); *Teudopsis* sp. MNHN.F.R03757 (I).

In 2002, Fischer & Riou described multiple individuals of *Vampyronassa rhodanica* Fischer & Riou 2002 (Fig. 3.5A, Fig. 3.6), a Jurassic Vampyromorph species from La Voulte-sur-Rhône, as part of the family of modern day *Vampyroteuthis infernalis*. Following the nomenclature used today, this species is classified in the family Vampyroteuthidae, order Vampyromorpha, subclass Coleoidea. *Mastigophora* aff. *brevipennis* (Fig. 3.5E) was described by Fuchs (2014) and assigned to the vampyromorph suborder Loligosepiina Jeletzky, 1965.

Proteroctopus was recently reappraised using PPC-SRμCT techniques (Kruta *et al.* 2016) revealing previously unknown information on the soft tissue anatomy and the gladius. However, there was not enough information on the gladius to determine systematic placement within

Vampyromorpha. Like *Gramadella* and *Vampyronassa, Proteroctopus* remains Vampyromorpha *incertae sedis.*

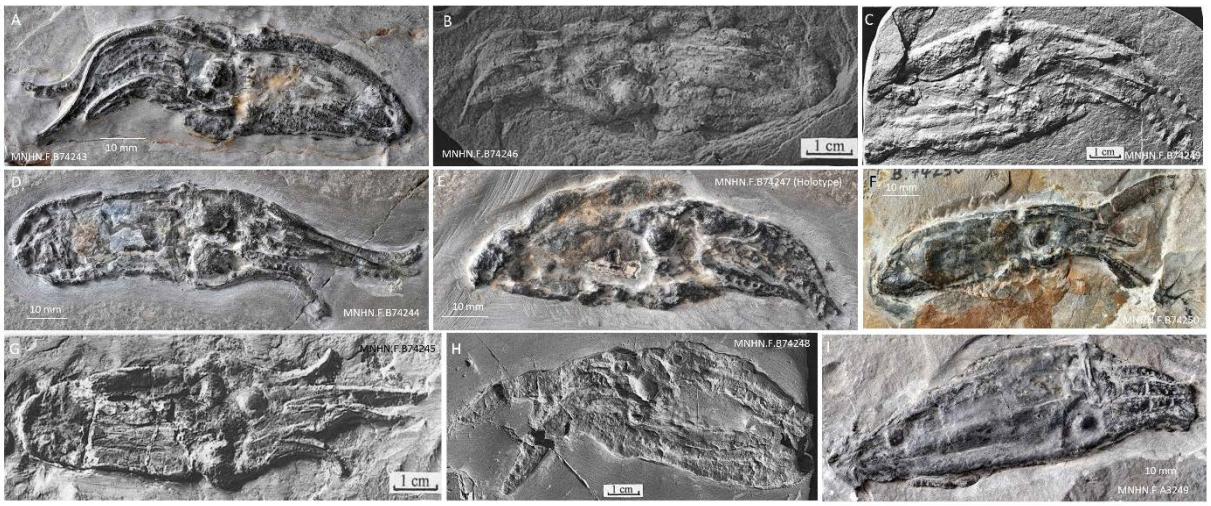

Figure 3.6: Specimens assigned to *Vampyronassa rhodanica*. The eight syntypes (A-H) described in Fischer & Riou 2002, and a previously undescribed coleoid specimen (I) tentatively assigned to the species. Specimens A, D, E, and I were reappraised in the two papers included in this chapter.

3.4.1 Overview

A recent systematic review by Fuchs (2020) classifies the taxa accordingly:

Superorder OCTOBRACHIA Haeckel, 1866
Suborder PROTOTEUTHINA Naef, 1921
Family PLESIOTEUTHIDAE Naef, 1921
Romaniteuthis Fischer & Riou, 1982a
Rhomboteuthis Fischer & Riou, 1982a

Order VAMPYROMORPHA Robson, 1929
Suborder LOLIGOSEPIINA Jeletzky, 1965
Family MASTIGOPHORIDAE Engeser & Reitner, 1985
Mastigophora Owen, 1856

VAMPYROMORPHA *INCERTAE SEDIS*
Gramadella Fischer & Riou, 1982a
Proteroctopus Fischer & Riou, 1982b
Vampyronassa Fischer & Riou, 2002

Order OCTOPODA Leach, 1817
Suborder TEUDOPSEINA Starobogatov, 1983
Family TEUDOPSEIDAE Regteren Altena, 1949
Teudopsis Eudes-Deslongchamps, 1835

The coleoid genera recognized from the site (Fischer & Riou 1982a, b, 2002; Fischer 2003; Charbonnier *et al.* 2007, 2014, Charbonnier 2009; Fuchs 2014; Kruta *et al.* 2016) are comprised of more than 70 individuals, not all of which have been described (Charbonnier 2009).

Three of the Octobrachia Superorder are represented in the La Voulte-sur-Rhône assemblage (Fuchs 2020) (Fig. 3.6 Table 3.1):

Superorder	ORDER	SUBORDER	FAMILY	GENERA	SPECIES	Specimen	Described in:
Stem OCTOBRACHIA		PROTOTEUTHINA Naef, 1921	PLESIOTEUTHIDAE Naef, 1921	*Romaniteuthis* Fischer & Riou, 1982a	*Romaniteuthis gevreyi*	MHNGr.PA.10277 (Holotype, part-and counterpart)*; MNHN.F.A29547	Fischer and Riou 1982b; Fuchs 2006b; Charbonnier 2009; Fuchs 2020
Stem OCTOBRACHIA		PROTOTEUTHINA Naef, 1921	PLESIOTEUTHIDAE Naef, 1921	*Rhomboteuthis* Fischer & Riou, 1982a	*Rhomboteuthis lemani*	MNHN.F.R03758 (Holotype); MNHN.F.R03761; MNHN.F.R03756; New**	Fischer and Riou 1982b; Fischer 2003; Fuchs 2006b; Charbonnier 2009, 2011; Charbonnier et al. 2014; Fuchs 2020
OCTOBRACHIA Haeckel, 1866	VAMPYROMORPHA Robson, 1929	LOLIGOSEPIINA Jeletzky, 1965	MASTIGOPHORIDAE Engeser & Reitner, 1985	*Mastigophora* Owen, 1856	*Mastigophora* aff. *brevipinnis*	MNHN.F.A53379***	Fuchs 2006*b*; 2014***
OCTOBRACHIA Haeckel, 1866	VAMPYROMORPHA Robson, 1929	VAMPYROMORPHINA Robson, 1929	INCERTAE SEDIS	*Gramadella* Fischer & Riou, 1982a	*Gramadella piveteaui*	MNHN.F.R03760 (Holotype); R03759; R03762	Fischer and Riou 1982b; Fuchs 2006b; Charbonnier 2009, 2011; Fuchs 2020
OCTOBRACHIA Haeckel, 1866	VAMPYROMORPHA Robson, 1929	VAMPYROMORPHINA Robson, 1929	INCERTAE SEDIS	*Proteroctopus* Fischer & Riou, 1982	*Proteroctopus ribeti*	MNHN R03801	Fischer & Riou 1982a; Fischer 2003; Charbonnier 2014; Kruta et al. 2016
OCTOBRACHIA Haeckel, 1866	VAMPYROMORPHA Robson, 1929	VAMPYROMORPHINA Robson, 1929	INCERTAE SEDIS	*Vampyronassa* Fischer & Riou, 2002	*Vampyronassa rhodanica*	MNHN.F.B74243; B74244; B74245; B74246; B74247 (Holotype); B74248; B74249; B74250	Fischer & Riou 2002; Fischer 2003; Charbonnier 2014
	OCTOPODA Leach, 1817	TEUDOPSEINA Starobogatov, 1983	TEUDOPSEIDAE Regteren Altena, 1949	*Teudopsis* Eudes-Deslongchamps, 1835	*Teudopsis* sp.	MNHN.F.R03757	Fischer and Ricu 1982b
		Incertae sedis	Teuthida	*Incertae sedis*	*Incertae sedis* sp.	MNHN.F.A29523	Charbonnier 2009
		Incertae sedis	Teuthida	*Incertae sedis*	*Incertae sedis* sp.	MNHN.F. A29585	Charbonnier 2009

Table 3.1: Gladius-bearing coleoid genera known from the La Voulte-sur-Rhône Lagerstätte. Information synthesized from Fischer & Riou 1982*a, b*; Fuchs 2006*b*; Fuchs 2014; Charbonnier 2009. * Listed as MHNGr.PA.10277 in Charbonnier 2009. Originally listed as I.P.M.-R.1743 and I.P.M.-R.1744 in Fischer & Riou 1982. ** Figured in Fuchs 2020 *** Correct collection number: MNHN.F.A53379. This table reflects the known taxa in La Voulte-sur-Rhône prior to the work in Rowe *et al.* 2022; 2023.

3.5 Re-appraisal of the Vampyromorpha specimens

Vampyronassa rhodanica, one of the four vampyromorph genera, represents the most speciose coleoid taxon at La Voulte-sur-Rhône, as 20 individuals were assigned to the species by Fischer & Riou (2002). Eight of these individuals were described as syntypes (Fig. 3.6 A-H). Using classic observational methods, Fischer & Riou (2002) described these specimens as possessing characteristic vampyromorph features (e.g., eight arms, laterally situated eyes, and posterior fins), and positioned the species as the oldest known family-level relative of *Vampyroteuthis infernalis.* The authors noted that the pyritic mineralization of the soft tissues added to the complexity of their anatomical assessments. For example, certain structures, like cirri, appeared more massive, and soft tissue contours of the fins and velum were not easy to

recognize. The presence of a gladius was interpreted from the color of the mineralized tissue, and the surrounding contours. However, as this has not been determined with certainty, it remains *incertae sedis* within the Vampyromorpha.

The described specimens were each preserved within the marl sediments, rather than inside concretions. As such, they experienced compaction and distortion. However, they still retain a level of 3D preservation that makes them ideal candidates for reappraisal using high-resolution X-ray tomographic imaging techniques.

These specimens provided an unparalleled opportunity to undertake a comparative morphological assessment between the fossil form and *V. infernalis* (see Chapter 1). Using the same imaging methods that were successfully applied to *Proteroctopus* (X-ray micro-computed tomography and propagation phase contrast synchrotron X-ray micro computed tomography) by Kruta *et al.* (2016) we generated detailed segmentation and renderings of internal and external anatomy. This enabled us to identify soft tissue innovations that were previously unknown in Jurassic vampyromorphs and discuss the ecological implications for coleoids within the complex La Voulte-sur-Rhône environment.

Three specimens of *V. rhodanica*, and a previously undescribed specimen assigned to *V. rhodanica* were assessed using the X-ray imaging methods outlined in Chapter 2. This resulted in two published papers which are included here. These are:

- Rowe, A.J., Kruta, I., Landman, N.H., Villier, L., Fernandez, V. and Rouget, I., 2022. Exceptional soft-tissue preservation of Jurassic Vampyronassa rhodanica provides new insights on the evolution and palaeoecology of vampyroteuthids. *Scientific Reports*, *12*(1), p.8292.
- Rowe, A.J., Kruta, I., Villier, L. and Rouget, I., 2023. A new vampyromorph species from the Middle Jurassic La Voulte-sur-Rhône Lagerstätte. *Papers in Palaeontology*, *9*(3), p.e1511.

The Supplementary information for Rowe *et al.* 2022 is included at the end of this chapter.

scientific reports

Check for updates

OPEN

Exceptional soft-tissue preservation of Jurassic *Vampyronassa rhodanica* provides new insights on the evolution and palaeoecology of vampyroteuthids

Alison J. Rowe[1]✉, Isabelle Kruta[1], Neil H. Landman[2], Loïc Villier[1], Vincent Fernandez[3,4] & Isabelle Rouget[1]

Although soft tissues of coleoid cephalopods record key evolutionary adaptations, they are rarely preserved in the fossil record. This prevents meaningful comparative analyses between extant and fossil forms, as well as the development of a relative timescale for morphological innovations. However, unique 3-D soft tissue preservation of *Vampyronassa rhodanica* (Vampyromorpha) from the Jurassic Lagerstätte of La Voulte-sur-Rhône (Ardèche, France) provides unparalleled opportunities for the observation of these tissues in the oldest likely relative of extant *Vampyroteuthis infernalis*. Synchrotron X-ray microtomography and reconstruction of *V. rhodanica* allowed, for the first time, a high-resolution re-examination of external and internal morphology, and comparison with other fossil and extant species, including *V. infernalis*. The new data obtained demonstrate that some key *V. infernalis* characters, such as its unique type of sucker attachment, were already present in Jurassic taxa. Nonetheless, compared with the extant form, which is considered to be an opportunistic detritivore and zooplanktivore, many characters in *V. rhodanica* indicate a pelagic predatory lifestyle. The contrast in trophic niches between the two taxa is consistent with the hypothesis that these forms diversified in continental shelf environments prior to the appearance of adaptations in the Oligocene leading to their modern deep-sea mode of life.

There is, to date, no undisputed phylogeny of the Cephalopoda that includes both extant and fossil taxa[1–4]. A scarcity of soft tissue preservation in fossil coleoids considerably restricts the number of characters available for comparison. Attempts at parsimony analyses highlight this significant imbalance, and the resulting bias limits the resolution and acceptance of existing phylogenetic trees[1,3].

Material from Konservat-Lagerstätten provide a unique opportunity to study these otherwise lost soft tissue details[5–9]. The Jurassic Lagerstätten of La Voulte-sur-Rhône (Callovian, Ardèche, France) represents a bathyal ecosystem in an offshore environment with steep, fault-controlled bathymetric gradients[10,11]. This site is unique for its three-dimensional fossil preservation of photic and aphotic taxa[10]. The assemblage is diverse and consists of mostly arthropods[11–13], as well as a few species of echinoderms[12,14], bivalves, brachiopods, and fish[11]. Cephalopods constitute 10% of the biodiversity[15] and approximately 20 specimens from the site have been assigned to the genus *Vampyronassa* by Fischer & Riou[16].

Considerable attention has been paid to the position of Vampyromorpha[2,4,17–23] as its only extant form, *Vampyroteuthis infernalis,* exhibits a mosaic of derived characters of both Octobrachia and Decabrachia[22]. It also has unique characters, including a well-developed gladius and two retractable filaments (arm pair II) in its arm crown which are not known in other extant cephalopods. After previously conflicting results regarding its

[1]Sorbonne Université-MNHN-CNRS-CR2P, 4 Pl. Jussieu, 75005 Paris, France. [2]American Museum of Natural History, 200 Central Park West, New York, NY 10024, USA. [3]The European Synchrotron—ESRF, CS40220, 38043 Grenoble, France. [4]Imaging and Analysis Centre, The Natural History Museum, London SW7 5BD, UK. ✉email: alison.rowe@sorbonne-universite.fr

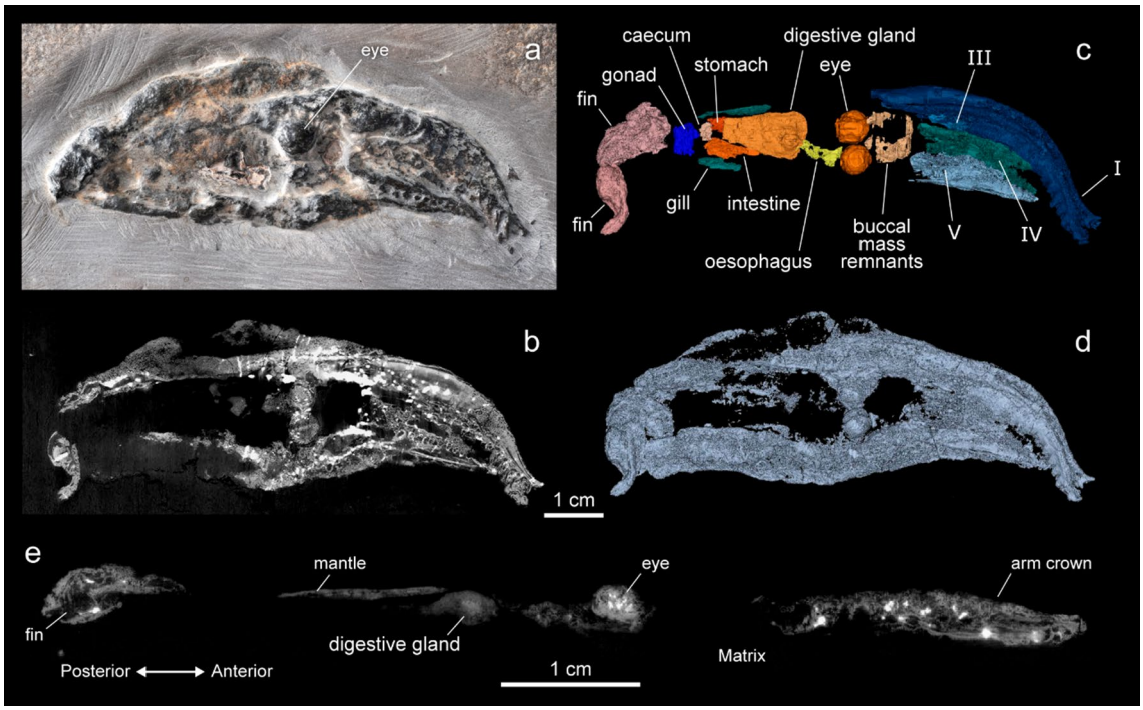

Figure 1. Images and reconstruction of the *V. rhodanica* holotype (MNHN.B.74247) acquired using PPC-SRμCT (voxel size: 12.64 μm), at the ESRF (Grenoble, France). (**a**) Photograph (P. Loubry, CR2P) of the specimen showing the 3-D preservation of the mineralised soft tissue. (**b**) PPC-SRμCT slice showing the contrast in the grey-scale image used to segment the specimen. This contrast results from the density variation among the various mineralised tissues. (**c**) 3D representation showing the arm crown (arm pair I, III, IV, and V), as well as other presumed internal elements (**d**) 3D reconstruction of the whole specimen (**e**) Sagittal slice showing the profile view.

affinity with Octobrachia or Decabrachia, the current consensus places *V. infernalis* as a basal member of the 8-armed Octobrachia[22–26]. *V. infernalis* is only known from deep-sea settings and is a detritivore, an opportunist consumer feeding on marine snow or zooplankton[27,28].

Two fossil taxa have been assigned to the same family Vampyroteuthidae: the bathyal *Necroteuthis* Kretzoi 1942 (Palaeogene)[29] known only from the gladius[22], and the Jurassic *Vampyronassa rhodanica*[16]. Eight well-preserved specimens of *V. rhodanica* have been described from La Voulte-sur-Rhône[16]. These individuals retain the exceptional 3-D preservation associated with this site and therefore play an important role in understanding character evolution in Vampyroteuthidae and Vampyromorpha (Loligosepiina and Vampyromorphina)[22].

Reanalysis of three *V. rhodanica* specimens using high-resolution imaging techniques provides a unique opportunity[30] to observe soft tissue characters of this family. For the first time, we have a detailed reconstruction of external and internal morphology of *V. rhodanica,* with specific attention paid to the characters on the arm crown. These new anatomical data provide insights into the character states of the fossil form and were incorporated into a morphological phylogeny[1]. The current analysis supports the sister relationship between *V. rhodanica* and *V. infernalis*. Through the comparative morphology of the two vampyromorph taxa, as well as other extant and fossil forms, we suggest a palaeoecological reconstruction for *V. rhodanica* as a pelagic predator.

Results

Laboratory X- ray micro-computed tomography (μCT) and propagation phase contrast synchrotron X-ray micro computed tomography (PPC-SRμCT) data allowed for a reappraisal of the morphology in each of the three *Vampyronassa* specimens. (See Supplementary Information for a redescription of each specimen and details on the CT acquisitions.) Externally, *V. rhodanica* is elongate with an oviform body (Fig. 1). The three specimens studied range in overall length (posterior-most part of the mantle to the anterior-most tip of the arms) from ~ 94–103 mm (See Supplementary Information for additional individual measurements). The mantle appears posteriorly rounded in dorso-ventral view (MNHN.F.74244 (paratype)) and posteriorly tapered in lateral view (MNHN.F.74247 (holotype); MNHN.F.74243 (paratype)) (Supplementary Fig. 1). Two densely outlined elliptical shapes are interpreted as mineralized fin cartilage in the posterior mantle (MNHN.F.74244). A small fin protrudes on the dorso-lateral posterior section of MNHN.F.74247 and corresponds with previously described fin placement[16].

The deep interconnecting velum, anteriorly extended funnel, and a cirri-like structure at the base of the dorsal arm described by Fischer & Riou[16] could not be confirmed during segmentation. There was no evidence of an ink sac, retractable filaments, or modification of arm pair IV. Hectocotylization was not observed. Topographic

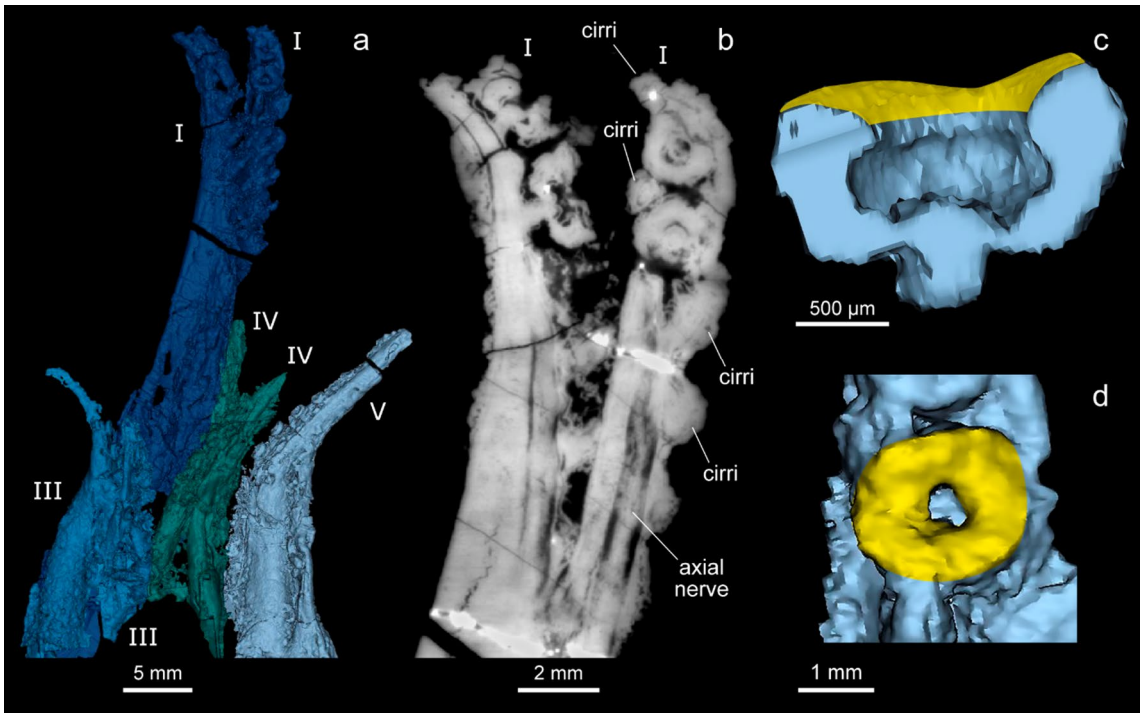

Figure 2. 3D reconstruction and image of the arm crown, and a sample dorsal sucker of *V. rhodanica* (MNHN.B.74244). (**a**) Reconstruction of the arm crown (Mimics software) showing 8 arms, with the longer dorsal arm pair (arm pair I). (**b**) PPC-SRμCT slice of arm pair I (voxel size: 12.64 µm) showing the armature (2 uniserial suckers and flanking pairs of cirri) at the distal section, and the axial nerves. (**c,d**) 3D reconstruction of a dorsal sucker in profile and oral view respectively. The yellow colour reflects the location of the infundibulum.

differences on the dorsal, posterior section of the specimens suggest remnants of the inner shell (gladius), though the type of X-ray imaging used here does not allow us to provide details on its state.

The luminous organs described by Fischer & Riou[16] could not be confirmed, though two dense, somewhat ovoid structures are located within the peripheral mantle tissue at the posterior-most area of the body in specimen MNHN.F.74244 (Supplementary Fig. 6). These dense structures are in a similar position to the luminous organs noted in the original description by Fischer & Riou[16], though are 4–5 times larger in MNHN.F.74244. They are only observable in the tomographic image and do not appear in the other two specimens.

Head-mantle fusion is evident, and the head is approximately half as wide as the length of the mantle. Mantle tissue extends out from the body margins in MNHN.F.74247 and MNHN.F.74244 (Supplementary Fig. 1). This tissue is not preserved in a splayed position in MNHN.F.74243.

The eyes of each specimen are preserved, though their position is relative due to the amount of distortion in the body prior to mineralization. They are subcircular, have undergone various amounts of compaction, and range in diameter from 5 to 7 mm (Fig. 1).

Elements in the arm crowns are particularly well preserved. Each has 8 tapered arms and distinct axial nerves (Fig. 2). The dorsal pair (arm pair I) is approximately equivalent in length to the mantle, and roughly twice the length of the sessile arms (arm pairs III–V).

Each dorsal arm has two uniserial, radially symmetrical suckers, and paired cirri positioned on the distal section (Fig. 2a,b). These suckers on the dorsal arms are attached by a muscular elongated neck, which protrudes into the acetabulum (Fig. 2c). The angle of the infundibulum is shallow and oriented somewhat parallel to the arm (Fig. 2c). Four, possibly five pairs of primary cirri (Fig. 2a,b) precede the most proximal sucker, and then alternate with the suckers towards the tip. Contrary to the description by Fischer & Riou[16], scans of the dorsal arms show no indication of proximal armature.

The remaining arms show very slight length variation with the arms preserved in ventral position (arm pair V) appearing marginally (a few millimetres) longer than the rest (arm pairs III and IV). It is not known if this is an artefact of preservation or a true character. Each of these arms has uniserial, radially symmetrical suckers and paired cirri (Supplementary Fig. 2). These features are present from the base to the tip of the arms. The suckers and cirri are similar in diameter, closely positioned and taper distally. Some suckers appear to be encircled by ovoid depressions in the peripheral tissue (Supplementary Fig. 3), though there is no evidence to indicate that these correspond with toothed sucker rings[31,32] found in some Decabrachia[2,33–35]. This detail appears in each of the *V. rhodanica* specimens, though it is not present on every sucker. The position of the depressions on the outer margins is not consistent with the feature being a remnant of the internally placed sucker rings in some Decabrachia[35], and there is no evidence of this character being present[32]. Similar looking tissue is visible elsewhere on the arms, including on the profile views of the cirri and suckers (Fig. 2b). Without further evidence to suggest otherwise, we suggest these depressions are a manifestation of degraded epithelium.

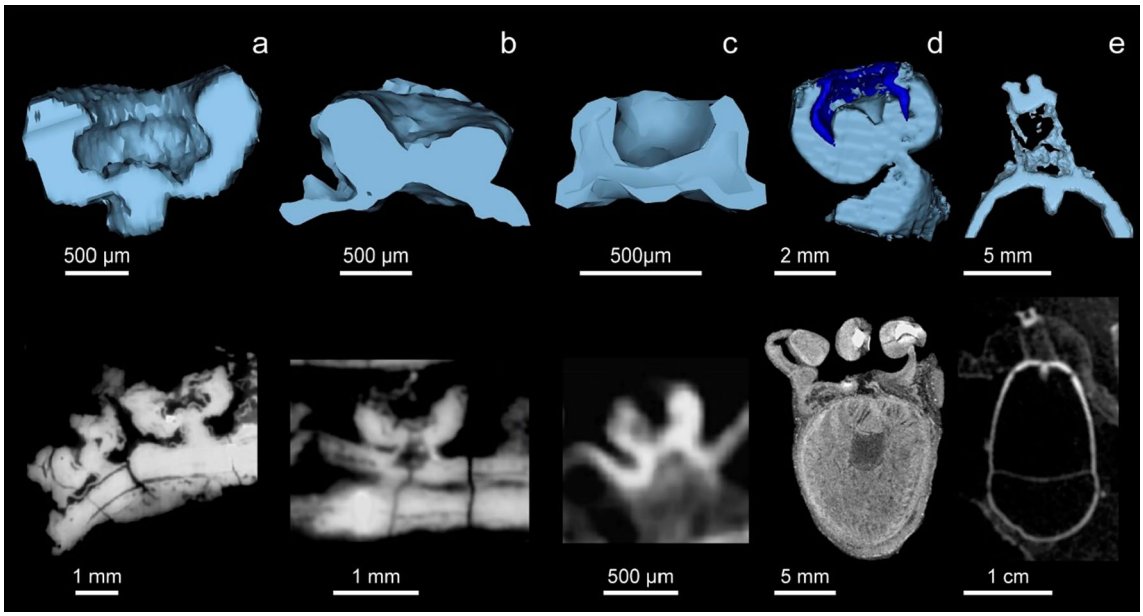

Figure 3. 3D reconstructions (top) and virtual slices (bottom) of sucker profiles. (**a,b**) Dorsal, and sessile sucker profiles of *V. rhodanica* MNHN.B.74244 respectively (PPC-SRµCT, ESRF). (**c**) *V. infernalis* (AMNH IZC 361496) (Vampyromorpha) (**d**) Commercial *Loligo* (Decabrachia) sample (µCT, AST-RX). (**e**) *Grimpoteuthis* (ZMB 240160) (Octobrachia) CT data from Ziegler et al.[58] and reconstructed for this study. Extant material (**d,e**) was stained prior to scanning.

All the suckers in the arm crown display a conical, *Vampyroteuthis*-like attachment (Fig. 3c, and Supplementary Fig. 4) and do not show a clear attachment to the arm muscle. There is slight variation between the sucker stalks on the dorsal arms and the rest of the arms in the arm crown (Fig. 3a,b respectively). The stalks connecting the two suckers to the dorsal arms are slightly longer and narrower than the more compact, triangular-shaped attachments that connect the suckers along the length of the sessile arms.

These new morphological data were incorporated into the existing phylogenetic matrix of Sutton et al.[3] that was modified by Kruta et al.[1]. The analyses returned 34 trees, and the data clarified four characters that were previously unresolved (#89-#92: Sucker symmetry; presence of sucker stalks; sucker lining, and the presence of proximal suckers, respectively. The consensus tree has the same topology as seen in Kruta et al.[1], with each of the state changes at node 134. This supports the hypothesis that *V. rhodanica* and *V. infernalis* are more closely related to each other than they are to any other taxon in this analysis (Supplementary Information Fig. 5). A radially symmetrical sucker state (character #89) was already known in *V. infernalis*. Our observations confirmed that this state is also reflected in *V. rhodanica*.

A character state was added to #91 to best reflect the shape of the stalks attached to the arm muscles. In Kruta et al.[1], this state is described as either a "conical pillar with base and neck" (state 0) consistent with modern Decabrachia, or a "cylinder" (state 1) consistent with modern Octobrachia. The shape of the sucker stalk in *V. rhodanica* resembles the attachment seen in modern *V. infernalis* (Fig. 3b,c). As such, character #91 was amended, adding a "base and plug"[34] state (state 2) to reflect the states outlined in Young & Vecchione[34]. For character #92[1], *V. rhodanica* showed no evidence of either a "horny" (state 1) or "cuticular [sucker] ring" (state 2) (see Fuchs et al.[35] for a full explanation of this character) on the inner lining of the sucker. In this study, both *V. infernalis* and *V. rhodanica* were coded as (state 0), to reflect the lack of this sucker lining. According to our results, (state 1) was common in Decabrachian taxa, and *V. infernalis* and *V. rhodanica* (state 2) were nestled within Octobrachia where this character was typically ambiguous. The type of muscular connection within the sucker attachment (character #90) proved to be of most interest. In *V. infernalis,* this state (state 2) is "present but not clearly attached to the arm muscles"[34]. This had previously been considered an autapomorphic character in *V. infernalis* though it is also present in *V. rhodanica*. It is, in fact, a synapomorphy of node 134 that links the two species and increases the robustness of the node.

Discussion

In their original description of *V. rhodanica*, Fischer & Riou[16] determined that the previously undescribed genus was a Jurassic relative of *V. infernalis*. This assignment was based on the configuration of the arm crown and armature, fin type, presence of luminous organs, lateral eyes, and the absence of an ink sac. Assuming this assignment is correct, then *V. rhodanica* is a member of the suborder Vampyromorphina, which includes the family Vampyroteuthidae[22,29].

Reappraisal of the anatomy shows that *V. rhodanica* and *V. infernalis* both have 8 arms and uniserial suckers flanked by cirri. They both possess *V. infernalis*-like sucker attachments[34,36], which are broader at the base and taper up to a radially symmetrical sucker.

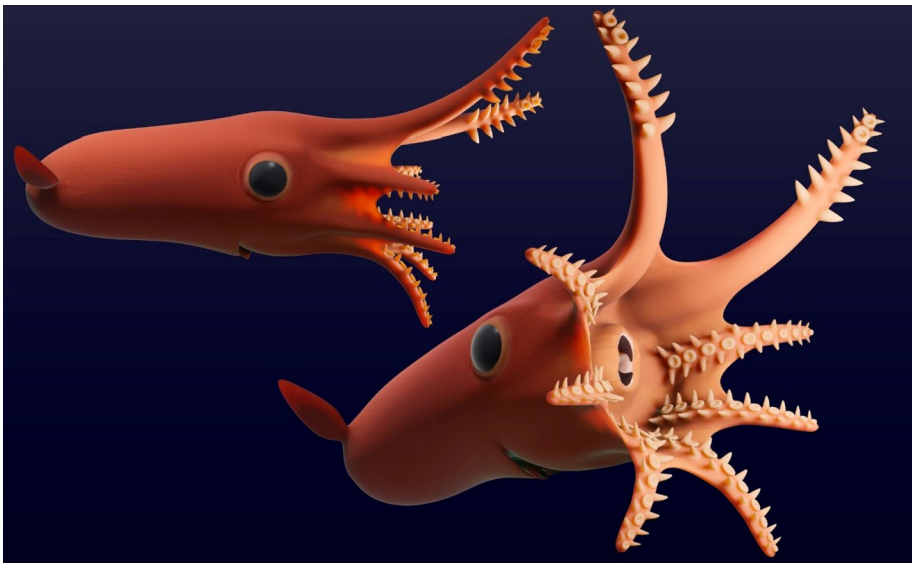

Figure 4. Hypothesised reconstruction of *V. rhodanica* based on the data from this study (A. Lethiers, CR2P). The scale is based on measurements from the holotype (MNHN.B.74247) and the arm crown is completed using dimensions from MNHN.B.74244.

Both species have distinctly modified arms though the morphology differs in each. *V. infernalis*, has retractable filaments in the position of arm pair II[27,33,34], though there is no evidence of these appendages in *V. rhodanica.* Instead, the species has elongate dorsal arms (arm pair I) with a unique configuration of suckers and cirri on the distal section.

The suckers and cirri of *V. rhodanica* are more numerous than those of *V. infernalis*[27,37]. They are also more closely positioned. Proportionally, the suckers of both species have a consistent ratio to mantle length[37], though the diameter of the cirri and infundibulum are greater in *V. rhodanica*. The *V. infernalis*-like attachment[1,3,34] is present in both species, though in *V. rhodanica*, the distal part of the neck protrudes into the acetabular cavity. Of note, the sucker stalks on the dorsal arms of *V. rhodanica* are more elongate than those on the other arms (Figs. 2b,c, and 3a,b). This variation in suckers and their attachments suggests a specialized function between the dorsal and sessile appendages. On the longer dorsal arms, the larger sucker diameter, and more elongate stalks (Figs. 2b and 4) indicate the potential for increased mobility over their extant relatives, and possibly facilitated additional manipulation and prey capture capability.

In addition to the arm crown specialization, *V. rhodanica* has a more streamlined shape than *V. infernalis*, which is caused by a proportionally narrower head. Their muscular body is narrower and more elongate than the gelatinous *V. infernalis*[16,27,37] suggesting a higher energy locomotory style. This is consistent with increased predation relative to the modern form. Observations in this study support many assertions of Fischer & Riou[16] about the characters in *V. rhodanica*, though the presence of luminous organs cannot be confirmed. Rather than luminous organs much larger than those present in the deep-sea, extant *V. infernalis*, it is possible that these structures represent displaced cartilage prior to fossilization (Supplementary Fig. 6).

Two other genera from the La Voulte-sur-Rhône locality, *Gramadella* and *Proteroctopus* are, like *V. rhodanica*, considered to be *Incertae sedis* Vampyromorpha[22]. All three share morphological similarities that include an elongated mantle fused with the head, and a longer dorsal arm pair with armature on the distal ends[1,16,22,38]. Neither the second nor fourth arm pair have been modified. Each has one pair of fins. In *Gramadella,* the fins are lateral and skirt-like[16,38]. In *V. rhodanica* and *Proteroctopus* these fins are located posteriorly[1,16].

V. rhodanica shows the greatest length variation between the dorsal and sessile arms (Fig. 4), though proportionally, *Gramadella,* and *Proteroctopus* have longer dorsal arms[1,31]. Fischer & Riou[31] and Kruta et al.[1] described biserial suckers in their descriptions of *Gramadella*, and *Proteroctopus,* respectively. In *Proteroctopus*, these suckers have a proportionally smaller diameter than the uniserial row in *V. rhodanica,* and do not exhibit the same tapered pattern.

None of these specimens shows evidence of an ink sac, though it is present in contemporaneous genera from the same assemblage (*Mastigophora, Rhomboteuthis* and *Romaniteuthis*)[8,16]. That this character occurs only in some taxa from the same assemblage suggests variation in ecology, possibly associated with the steep, bathymetric relief in the La Voulte-sur-Rhône paleoenvironment[11]. The mosaic of characters found within the coleoid taxa at La Voulte-sur-Rhône suggests that Mesozoic vampyromorphs co-occurred in different ecological niches during the mid-Jurassic.

Today, extant *V. infernalis* is uniquely adapted to a low-energy, deep-sea mode of life[27–29,39], though the timing of character acquisition and progression of this ecology is unclear[24]. It is hypothesised that the vampyromorph *Necroteuthis* Kretzoi 1942 was already exploiting this niche by the Oligocene[29], and that the initial shift to offshore environments was possibly driven by onshore competition[24,29]. The data obtained here suggests that

V. rhodanica, the purportedly oldest-known genus of the Vampyromorphina group, was an active predator following a pelagic mode of life.

Indeed, several anatomical details, mainly found in the brachial crown, seem to support this hypothesis. Though we cannot directly compare functionality of the arm crown elements with other Jurassic taxa, we can infer function based on observation in modern forms. In Octopoda, the sister group to Vampyromorpha, suckers are attached to the arm by a cylindrical layer of muscle, encircling oblique musculature[40,41], that connects the arm musculature and the lateral margin of the acetabulum[34,40–42]. This facilitates a variety of functions including locomotion, manipulation, and prey retention[43]. The sucker attaches by flattening the infundibulum against the surface and then the encircling epithelium creates a watertight seal[36,40–45]. Contraction of the radial acetabular muscles provides the pressure differential required to create the suction force[43,44,46].

The stalked sucker attachments[2,34] of decabrachians (Fig. 3d, and Supplementary Fig. 4) are muscular[35] and connect the musculature of the arm with the base of the sucker, forming part of the acetabulum[33,34]. Tension on the sucker stretches this muscular attachment, which pulls locally on the acetabular base. This facilitates a greater pressure differential inside the sucker, allowing the teeth on the sucker ring to maintain the hold[47].

Extant *V. infernalis* lack decabrachian-like stalks[2,18] and the neck of the attachment joins to the base of the acetabulum (Fig. 3c, and Supplementary Fig. 4), rather than being inserted into it[18]. The infundibulum is not distinct, and the suckers do not provide strong suction[27]. Instead, suckers function by secreting mucus to coat detritus—marine snow captured by retractable filaments—which is then moved to the mouth by cirri[7,27].

A mosaic of these characters is present in *V. rhodanica* (Fig. 3a,b), therefore, suggesting their potential for increased attachment and hold on prey over extant *V. infernalis*. These include a larger infundibular diameter, a neck attachment integrated with the acetabular muscles, and the elongated stalks of the dorsal suckers.

Additionally, the paired, filamentous cirri observed in extant cirrates[48] are present in *V. rhodanica* (Fig. 4, and Supplementary Fig. 2). In extant forms they are understood to have a sensory function and are used in the detection and capture of prey[48]. In *V. infernalis*, they serve to transport the food proximally along the arms to the mouth[27]. The greater diameters of cirri, and placement along the entire arm in *V. rhodanica* (Fig. 4), suggests an increased sensory function in these fossil forms.

The shape of the arms also contributes to the suction potential[49] in coleoids. Functional analysis in Octopoda highlights a positive correlation between distal tapering of the arms and their flexibility. A tapered, flexible arm facilitates more precise adhesion than a cylindrical-shaped one and requires a greater force for sucker detachment[49]. Suckers detach sequentially, rather than the more simultaneous release observed in models of arms with less taper variation. The tapered diameter of the suckers, like those seen on the sessile arms of *V. rhodanica*, potentially facilitated this kind of sequential detachment[49] allowing them more adherence force and flexibility. Though *V. rhodanica* has just two suckers on the distal tips of their dorsal arms, the most distal is marginally smaller in diameter than the proximal one. On the dorsal arms, this tapering is observed in conjunction with a well-developed axial nerve cord (Fig. 2b). In extant forms, the nerve cord facilitates complex motor functions[42]. The combination of these characters in *V. rhodanica* suggests their arms had increased potential to be actively used in prey capture[50] over extant *V. infernalis*.

Though arm crown characters offer insight on the ecology of *V. rhodanica*, in fossil coleoid phylogenies only a few characters are based on the suckers[1,3]. Two studies that have attempted to create a phylogeny using morphological characters that include both fossil and extant taxa return *V. rhodanica* and *V. infernalis* as sister taxa[1,3]. These matrices are, by necessity, heavily influenced by the gladius[51] and more than 50% of the characters are based on this feature[1,3]. Indeed, the authors[1] note that the lack of gladius data for some fossil forms, including *V. rhodanica,* creates an inherent bias in the phylogenetic matrix. Fischer & Riou[16] suggested that *V. rhodanica* and *V. infernalis* are related on the basis of the observable morphological characters in the family Vampyroteuthidae, though without morphological information on the gladius, a recent systematic synthesis of fossil Octobrachia[22] positioned *V. rhodanica* as Vampyromorpha *Incertae sedis*.

X-ray CT analysis in this study did not allow a reconstruction of the gladius. Nevertheless, it does provide new data on soft tissues, and permits comparisons between extant and fossil taxa. Specifically, we can add distinct states to 4 of the 132 characters in the existing phylogenetic matrix from Sutton et al.[3] that was modified and used in Kruta et al.[1]. These four characters (#89–#92) represent the suckers, and sucker attachments. Detailed examination revealed that the sessile and dorsal arms have the *Vampyroteuthis*-like attachment. In the dorsal arms, this is more elongated, though it cannot be considered pedunculate like those seen in modern decabrachians. Indeed, the attachment type (plug and base[34]) is the same, only the length varies. As previously discussed, this variation may have functional implications.

When updated with these new data, the matrix from this study returns the same topology seen in Kruta et al.[1] that supports the positioning of *V. rhodanica* and *V. infernalis* as sister taxa. Further, it strengthens their relationship as they both share a sucker attachment that is not clearly attached to the arm muscles, a state that was previously considered autapomorphic in *V. infernalis*. However, it is important to note that no additional characters were added for the gladius, which is the cornerstone of coleoid systematics[52]. Indeed, just 29 of the 132 matrix characters can so far be coded for *V. rhodanica*, with only 9 of these relating to the 74 states of the gladius.

Assuming the phylogenetic work so far is correct, then both species belong to the family Vampyromorphina, and are joined by the Oligocene fossil *Necroteuthis hungarica*[29]. While the lack of gladius characters precludes a full phylogenetic understanding of this group, preservation and observation of the soft tissues allow us to infer information regarding palaeobiology.

The data obtained in this study demonstrates that the characters observed in *V. infernalis,* including the sucker attachments and lack of ink sac, were present in Jurassic Vampyromorpha. Comparative anatomy of *V. rhodanica* and extant *V. infernalis* revealed that the fossil taxon displayed more morphological variation and were more diversified than previously understood. The assemblage of characters observed in *V. rhodanica* are consistent

with a pelagic predatory lifestyle and corroborate the likelihood of a distinctly different ecological niche. These findings support the hypothesis that a shift towards a deep-sea environment occurred prior to the Oligocene[5,29].

Methods and materials

Materials. Three fossil specimens of *V. rhodanica* (holotype MNHN.B.74247, and two paratypes MNHN.B.74244 and MNHN.B.74243) from La Voulte-sur-Rhône provided the basis for this study. These samples are reposited in the paleontological collections of the Muséum National d'Histoire Naturelle (Paris, France). Some anatomical features in these three specimens are absent due to distortion and tissue loss prior to mineralization, as well as during the preparatory process. Each specimen exhibits varying levels of deformation. Despite this, each has retained exceptional 3-D morphology.

This exceptional preservation was a result of soft tissue replacement during a sequence of mineralization phases[53]. Ordinarily, calcium carbonate precipitates in marine environments[54,55] but at La Voulte-sur-Rhône, rapid post-depositional microbial activity in the low oxygen setting reduced pH, leading to authigenic precipitation of iron-rich minerals[53,55–57]. Mineralization was localized in the organism, and the organs and tissues were potentially replaced by different mineral phases[54, 55]. Analyses of marine arthropods mineralized at La Voulte-sur-Rhône show that muscle tissue is replaced by fluorapatite and pyrite (and related sulphides)[53]. The same is assumed here for *V. rhodanica*. It is the density of these fossilized tissues that provides the grey-scale contrast observed in the tomographic imagery.

A subsequent reset of the pH reverted to calcite precipitating conditions[53,56,57] and allowed the preservation of fine morphological detail[55]. In some instances, calcium carbonate concretions formed around the specimens[53].

CT data of extant forms (*V. infernalis,* AMNH IZC 361496 and YPM IZ 018297.GP), and *Grimpoteuthis* and *Sepia* from MorphoBank project (#3107)[58] were also analysed for comparison.

Microtomography. The three *V. rhodanica* fossils were initially imaged using µCT at the AST-RX platform at the MNHN and then using PPC-SRµCT at the European Synchrotron Radiation Facility Synchrotron (ESRF, ID 19 beamline, Grenoble, France). PPC-SRµCT data have a voxel size of 12.64 µm (MHNH.B.74247, MHNH.B.74243 and MHNH.B.74244); AST-RX platform µCT data have a voxel size of 88.60 µm (MHNH.B.74244). Specimens of *V. infernalis* were analysed using µCT at the Microscopy and Imaging Facility of the American Museum of Natural History (New York, USA). The voxel size for each specimen analysed was 38.40 µm for AMNH IZC 361496, and 18.25 µm for YPM IZ 018297.GP. See Supplementary material for microtomography details.

Final CT data were reduced in size using ImageJ software (cropping and size reduction by binning $2 \times 2 \times 2$), and then segmented using Mimics software (Materialise NV, Belgium, Version 21.0). The contrasting densities of the mineralized soft tissues were utilized to identify anatomical features for segmentation. Morphological reconstructions were carried out for the three *V. rhodanica* specimens incorporating all possible internal and external soft tissues. A full reconstruction of *V. infernalis* was carried out on AMNH IZC 361496. Some suckers in YPM IZ 018297.GP had more clearly defined boundaries and these were integrated into the analysis to augment the data gathered from AMNH IZC 361496.

Phylogenetic analysis. New character state data obtained from the segmentation of *V. rhodanica* were incorporated into the phylogenetic matrix from Kruta et al.[1]. This matrix is built on 132 characters that describe morphological states of fossil and extant forms. More than 50% of these are based on the gladius. One new state was added to character 91 to reflect State 9 in Young and Vecchione[34]. Characters described by Fischer & Riou[16] that were not able to be observed by segmentation in this study, remain unchanged in the matrix. The dataset was analysed using TNT v.1.1[59] with implied weighting (concavity constant of $K = 3$). The monophyly of the decabrachians was constrained as in Sutton et al.[3].

Methods. Comparative studies were also conducted with fossil specimens, and descriptions and images were taken from the literature. Most of these character comparisons focussed on the arm crown, though the fins and ink sac were also included. The resulting fossil sample comprised three *Incertae sedis* Vampyromorpha, *Gramadella, Proteroctopus,* and *V. rhodanica*, as well as the loligosepiid *Mastigophora*.

Measurements for all specimens were collected using parameters outlined in Fig. 3 of Nixon 2011[36]. The mantle length was taken from the central lateral line of the eye to the most posterior part of the body. Arm length was taken from the central lateral line of the eye to the most anterior tip. As none of the specimens is preserved in anatomical position, all measurements are composite. Measurements followed the natural line of the form where possible.

The ratio calculations performed on these measurements were defined in Pickford[37] and are detailed in Supplementary Information. Pickford[37] provided a comprehensive account of measurements and ratios for *V. infernalis*, and the mean values provided were utilized for comparative analyses. The same ratios were used to calculate proportions in the fossil and extant forms where possible. Pickford[37] noted two equations to determine the length of longest arm: the arm length index and the mantle length index. The arm length index was used for the *V. infernalis* specimens, and therefore was used in this study. We used this formula also. Where possible, the various indices were calculated twice; once using measurements from the dorsal arms, and the others for the measurements taken from the shorter sessile arms. Ratios for elements within the suckers were not provided in Pickford[37] so an adaptation was used (Supplementary Information). From this, we calculated proportional values for the infundibular diameter, cirri diameter, and the acetabular cavity.

Received: 2 February 2022; Accepted: 26 April 2022
Published online: 23 June 2022

References

1. Kruta, I. *et al. Proteroctopus ribeti* in coleoid evolution. *Palaeontology* **59**, 767–773 (2016).
2. Lindgren, A. R., Giribet, G. & Nishiguchi, M. K. A combined approach to the phylogeny of Cephalopoda (Mollusca). *Cladistics* **20**, 454–486 (2004).
3. Sutton, M., Perales-Raya, C. & Gilbert, I. A phylogeny of fossil and living neocoleoid cephalopods. *Cladistics* **32**, 297–307 (2016).
4. Kröger, B., Vinther, J. & Fuchs, D. Cephalopod origin and evolution: A congruent picture emerging from fossils, development and molecules. *BioEssays* **33**, 602–613 (2011).
5. Klug, C., Schweigert, G., Fuchs, D. & De Baets, K. Distraction sinking and fossilized coleoid predatory behaviour from the German Early Jurassic. *Swiss J. Palaeontol.* **140**, 1–12 (2021).
6. Klug, C. *et al.* Anatomy and evolution of the first Coleoidea in the Carboniferous. *Commun. Biol.* **2**, 1–12 (2019).
7. Klug, C., Fuchs, D., Schweigert, G., Röper, M. & Tischlinger, H. New anatomical information on arms and fins from exceptionally preserved *Plesioteuthis* (Coleoidea) from the Late Jurassic of Germany. *Swiss J. Palaeontol.* **134**, 245–255 (2015).
8. Fuchs, D. First evidence of *Mastigophora* (Cephalopoda: Coleoidea) from the early Callovian of La Voulte-sur-Rhône (France). In *Göttingen Contributions to Geosciences* Vol. 77 (ed. Frank Wiese, M. R.) 21 (Universitätsverlag Göttingen, 2014).
9. Fuchs, D. *et al.* A nearly complete respiratory, circulatory, and excretory system preserved in small Late Cretaceous octopods (Cephalopoda) from Lebanon. *PalZ* **90**, 299–305 (2016).
10. Charbonnier, S. Le Lagerstätte de La Voulte: un environnement bathyal au Jurassique. *Publications scientifiques du Muséum Paris* (2009).
11. Charbonnier, S., Audo, D., Caze, B. & Biot, V. The La Voulte-sur-Rhône Lagerstätte (Middle Jurassic, France). *C.R. Palevol* **13**, 369–381 (2014).
12. Audo, D., Schweigert, G., Saint Martin, J. & Charbonnier, S. High biodiversity in Polychelida crustaceans from the Jurassic La Voulte-sur-Rhône Lagerstatte. *Geodiversitas* **36**, 489–525 (2014).
13. Jauvion, C., Charbonnier, S. & Bernard, S. A new look at the shrimps (Crustacea, Decapoda, Penaeoidea) from the Middle Jurassic La Voulte-sur-Rhône Lagerstatte. *Geodiversitas* **39**, 705–716 (2017).
14. Villier, L., Charbonnier, S. & Riou, B. Sea stars from Middle Jurassic Lagerstätte of La Voulte-sur-Rhône (Ardèche, France). *J. Palaeontol.* **83**, 389–398 (2009).
15. Charbonnier, S., Vannier, J., Gaillard, C., Bourseau, J. & Hantzpergue, P. The La Voulte Lagerstätte (Callovian): Evidence for a deep water setting from sponge and crinoid communities. *Palaeogeogr. Palaeoclimatol. Palaeoecol.* **250**, 216–236 (2007).
16. Fischer, J.-C. & Riou, B. *Vampyronassa rhodanica nov. gen. nov sp.*, vampyromorphe (Cephalopoda, Coleoidea) du Callovien inférieur de La Voulte-sur-Rhône (Ardèche, France). *Ann. de Paléontol.* **88**, 1–17 (2002).
17. Nishiguchi, M. K. & Mapes, R. Cephalopoda. In *Phylogeny and Evolution of the Mollusca* 163–199 (University of California Press, 2008).
18. Young, R. E., Vecchione, M. & Donovan, D. T. The evolution of coleoid cephalopods and their present biodiversity and ecology. *S. Afr. J. Mar. Sci.* **20**, 393–420 (1998).
19. Bonnaud, L., Boucher-Rodoni, R. & Monnerot, M. Phylogeny of cephalopods inferred from mitochondrial DNA sequences. *Mol. Phylogenet. Evo.* **7**, 44–54 (1997).
20. Strugnell, J., Norman, M., Jackson, J., Drummond, A. J. & Cooper, A. Molecular phylogeny of coleoid cephalopods (Mollusca: Cephalopoda) using a multigene approach; the effect of data partitioning on resolving phylogenies in a Bayesian framework. *Mol. Phylogenet. Evol.* **37**, 426–441 (2005).
21. Carlini, D. B., Reece, K. S. & Graves, J. E. Actin gene family evolution and the phylogeny of coleoid cephalopods (Mollusca: Cephalopoda). *Mol. Biol. Evo.* **17**, 1353–1370 (2000).
22. Fuchs, D. Treatise Online no. 138: Part M, Chapter 23G: Systematic Descriptions: Octobrachia. *Treatise Online* 1–52 (2020).
23. Carlini, D. B. Treatise Online no. 15: Part M, Chapter 15: Molecular Systematics of the Coleoidea. *Treatise Online* 1–8 (2010).
24. Tanner, A. R. *et al.* Molecular clocks indicate turnover and diversification of modern coleoid cephalopods during the Mesozoic Marine Revolution. *Proc. R. Soc. B* **284**, 2 (2017).
25. Anderson, F. E. & Lindgren, A. R. Phylogenomic analyses recover a clade of large-bodied decapodiform cephalopods. *Mol. Phylogenet. Evol.* **156**, 107038 (2021).
26. López-Córdova, D. A. *et al.* Mesozoic origin of coleoid cephalopods and their abrupt shifts of diversification patterns. *Mol. Phylogenet. Evol.* **166**, 107331 (2022).
27. Hoving, H. J. T. & Robison, B. H. Vampire squid: Detritivores in the oxygen minimum zone. *Proc. R. Soc. B* **279**, 4559–4567 (2012).
28. Golikov, A. V. *et al.* The first global deep-sea stable isotope assessment reveals the unique trophic ecology of Vampire Squid *Vampyroteuthis infernalis* (Cephalopoda). *Sci. Rep.* **9**, 2 (2019).
29. Košťák, M. *et al.* Fossil evidence for vampire squid inhabiting oxygen-depleted ocean zones since at least the Oligocene. *Comm. Biol.* **4**, 2 (2021).
30. Cunningham, J. A., Rahman, I. A., Lautenschlager, S., Rayfield, E. J. & Donoghue, P. C. J. A virtual world of paleontology. *Trends Ecol. Evol.* **29**, 347–357 (2014).
31. Fischer, J.-C. & Riou, B. Les Teuthoïdes (Cephalopoda, Dibranchiata) du Callovien inférieur de La Voulte– sur– Rhône (Ardèche, France). *Ann. de Paléontol.* **68**, 295–325 (1982).
32. Bandel, K. & Leich, H. Jurassic Vampyromorpha (dibranchiate cephalopods). *Neues Jahrb. für Geol. und Paläontologie-Monatshefte* **3**, 129–148 (1986).
33. Vecchione, M., Young, R. E. & Carlini, D. B. Reconstruction of ancestral character states in neocoleoid cephalopods based on parsimony. *Am. Malacol. Bull.* **15**, 179–193 (2000).
34. Young, R. E. & Vecchione, M. Analysis of morphology to determine primary sister-taxon relationships within coleoid cephalopods. *Am. Malacol. Bull.* **12**, 91–112 (1996).
35. Fuchs, D., Hoffmann, R. & Klug, C. Evolutionary development of the cephalopod arm armature: A review. *Swiss J. Palaeontol.* **140**, 1–18 (2021).
36. Nixon, M. Treatise Online no. 17: Part M, Chapter 3: Anatomy of Recent Forms. *Treatise Online* 1–49 (2011).
37. Pickford, G. E. *Vampyroteuthis infernalis* Chun-An archaic dibranchiate cephalopod II. External anatomy. *Dana Rep.* **32**, 1–132 (1949).
38. Donovan, D. T. & Fuchs, D. Treatise Online no. 73: Part M, Chapter 13: Fossilized Soft Tissues in Coleoidea. *Treatise Online* 1–30 (2016).
39. Hoving, H.-J. T. *et al.* The study of deep-sea cephalopods. In *Advances in Cephalopod Science: Biology, Ecology, Cultivation and Fisheries* (ed. Vidal, E. A. G.) vol. 67 235–359 (Advances in Marine Biology, 2014).
40. Kier, W. M. & Smith, A. M. The morphology and mechanics of octopus suckers. *Biol. Bull.* **178**, 126–136 (1990).
41. Kier, W. M. & Smith, A. M. The structure and adhesive mechanism of octopus suckers. *Am. Zool.* **41**, 1492–1492 (2001).
42. Kier, W. M. The musculature of coleoid cephalopod arms and tentacles. *Front. Cell Dev. Biol.* **4**, 2 (2016).

43. Kier, W. M. & Thompson, J. T. Muscle arrangement, function and specialization in recent coleoids. *Berliner Paläobiologische Abhandlungen* **3**, 141–162 (2003).
44. Tramacere, F. *et al.* The morphology and adhesion mechanism of *Octopus vulgaris* suckers. *PLoS ONE* **8**, 2 (2013).
45. Tramacere, F., Pugno, N. M., Kuba, M. J. & Mazzolai, B. Unveiling the morphology of the acetabulum in octopus suckers and its role in attachment. *Interface Focus* **5**, 2 (2015).
46. Grasso, F. W. & Setlur, P. Inspiration, simulation and design for smart robot manipulators from the sucker actuation mechanism of cephalopods. *Bioinspir. Biomim.* **2**, S170–S181 (2007).
47. Smith, A. M. Cephalopod sucker design and the physical limits to negative pressure. *J. Exp. Biol.* **199**, 949–958 (1996).
48. Collins, M. A. & Villanueva, R. Taxonomy, ecology and behaviour of the cirrate octopods. In *Oceanography and Marine Biology - an Annual Review* (eds. Gibson, R. N., Atkinson, R. J. A. & Gordon, J. D. M.) vol. 44 277–322 (Taylor & Francis, 2006).
49. Xie, Z. *et al.* Octopus arm-inspired tapered soft actuators with suckers for improved grasping. *Soft Rob.* **7**, 639–648 (2020).
50. Nödl, M.-T., Fossati, S. M., Domingues, P., Sánchez, F. J. & Zullo, L. The making of an octopus arm. *EvoDevo* **6**, 1–18 (2015).
51. Fuchs, D. *et al.* The Muensterelloidea: Phylogeny and character evolution of Mesozoic stem octopods. *Pap. Palaeontol.* **6**, 31–92 (2020).
52. Fuchs, D. & Weis, R. Taxonomy, morphology and phylogeny of Lower Jurassic teudopseid coleoids (Cephalopoda). *Neues Jahrb. für Geol. Paläontologie Abhandlungen* **257**, 351–366 (2010).
53. Jauvion, C. De la vie à la pierre: préservation exceptionnelle d'arthropodes marins fossiles. (PhD diss. Muséum National d'Histoire Naturelle, 2020).
54. Wilby, P. R., Briggs, D. E. G. & Riou, B. Mineralization of soft-bodied invertebrates in a Jurassic metalliferous deposit. *Geology* **24**, 847–850 (1996).
55. Clements, T., Colleary, C., De Baets, K. & Vinther, J. Buoyancy mechanisms limit preservation of coleoid cephalopod soft tissues in Mesozoic lagerstätten. *Palaeontology* **60**, 1–14 (2017).
56. Allison, P. A. Konservat-lagerstätten—cause and classification. *Paleobiology* **14**, 331–344 (1988).
57. Briggs, D. E. G. & Wilby, P. R. The role of the calcium carbonate calcium phosphate switch in the mineralization of soft-bodied fossils. *J. Geol. Soc.* **153**, 665–668 (1996).
58. Ziegler, A. *et al.* Digital three-dimensional imaging techniques provide new analytical pathways for malacological research. *Am. Mal. Bull.* **36**, 248–273 (2018).
59. Goloboff, P. A., Farris, J. S. & Nixon, K. C. TNT, a free program for phylogenetic analysis. *Cladistics* **24**, 774–786 (2008).

Acknowledgements

We thank A. Lethiers (CR2P) for the illustrations and hypothesised reconstruction of *V. rhodanica*, J. Bardin (CR2P) for phylogenetic analysis. We acknowledge ESRF for provision of synchrotron radiation facilities (proposal ES36) and thank P. Tafforeau for assistance using the Beamline ID19. We thank M. Chase for AMNH CT acquisition, L. Berniker and A. Rashkova for AMNH collections assistance, and M. Bellato for her advice regarding AST-RX CT. We thank H.J. Hoving and MBARI for donating the *V. infernalis* specimen to AMNH. We thank the YALE Peabody Museum Division of Invertebrate Zoology, for allowing us to stain material. We also thank Christian Klug and Dirk Fuchs for their reviews of this manuscript.

Author contributions

A.R. wrote the manuscript and performed the segmentation. I.K and I.R. designed the research topic. I.K is responsible for data acquisition (selection of specimens and CT acquisition) and lead ESRF Synchrotron proposal ES36. V.F. provided guidance during the Synchrotron proposal and reviewed and improved the data acquisitions section (Supplementary Information). All authors discussed the results and reviewed the manuscript.

Competing interests

The authors declare no competing interests.

Additional information

Supplementary Information The online version contains supplementary material available at https://doi.org/10.1038/s41598-022-12269-3.

Correspondence and requests for materials should be addressed to A.J.R.

Reprints and permissions information is available at www.nature.com/reprints.

Publisher's note Springer Nature remains neutral with regard to jurisdictional claims in published maps and institutional affiliations.

[Papers in Palaeontology, 2023, e1511]

A new vampyromorph species from the Middle Jurassic La Voulte-sur-Rhône Lagerstätte

by ALISON J. ROWE*, ISABELLE KRUTA, LOÏC VILLIER *and* ISABELLE ROUGET

Sorbonne Université-MNHN-CNRS-CR2P, 4 pl. Jussieu, 75005 Paris, France; alison.rowe@sorbonne-universite.fr
*Corresponding author

Typescript received 1 December 2022; accepted in revised form 17 April 2023

Abstract: Eight coleoid genera have so far been described from the Callovian-aged La Voulte-sur-Rhône Lagerstätte (*c.* 165 Ma; Ardèche, France), a locality noted for its unique three-dimensional preservation of soft tissues. Here, we used high resolution x-ray-based imaging methods, in conjunction with reflectance transformation imaging, to study the soft tissues of a previously undescribed coleoid from the La Voulte-sur-Rhône locality. This analysis identified both an ink sac and internal light organs, a combination of defence mechanisms present in the Recent, although not previously described from the coleoid fossil record, as well as the presence of Octobrachia-type arm musculature and *Vampyroteuthis*-like sucker attachments. The morphology of the gladius could not be attributed to any known coleoids and therefore justified the assignment of this single specimen to a new taxon: *Vampyrofugiens atramentum*. The addition of this new vampyromorph species not only increases the coleoid diversity known from the site, but also broadens the morphological variation observed in the co-occurring coleoid taxa. These findings suggest that there was a high diversity of cephalopods occupying differentiated communities during the Middle Jurassic.

Key words: soft-tissue preservation, Vampyromorpha, synchrotron microtomography, reflectance transformation imaging, coleoid, La Voulte-sur-Rhône Lagerstätte.

JURASSIC coleoid diversity is mostly recorded from the Lower Jurassic Lagerstätten such as the Posidonia Shales (Lower Toarcian, Holzmaden) as well as the Upper Jurassic (Kimmeridgian–Tithoninan) lithographic limestones of Nusplingen, and Solnhofen (southern Germany) (Klug *et al.* 2005, 2015, 2021; Fuchs 2007; Fuchs *et al.* 2007, 2010, 2013). The Middle Jurassic coleoid record (e.g. Christian Malford, UK (Wilby *et al.* 2004; Fuchs 2014) and La Voulte-sur-Rhône, France) (Fischer 2003) is less well known. More than one-third of the genera of non-belemnoid coleoids (Fuchs 2020) known from the Middle Jurassic are represented at La Voulte-sur-Rhône, making this an important site for understanding coleoid evolutionary history. Cephalopods constitute *c.* 11% of the diversity from the locality, with eight currently described coleoid genera (Fischer & Riou 2002; Fischer 2003; Charbonnier 2009; Fuchs 2014). Other groups include arthropods (Charbonnier 2009; Audo *et al.* 2014, 2019; Jauvion *et al.* 2016, 2017; Vannier *et al.* 2016), which comprise the majority (*c.* 50%) of the taxa, as well as echinoderms (Charbonnier *et al.* 2007; Charbonnier 2009; Villier *et al.* 2009), annelids, bivalves, brachiopods and a few vertebrate taxa (Crocodilia, Sarcopterygii and Actinopterygii) (Charbonnier 2009; Charbonnier *et al.* 2014).

Attempts to reconstruct the palaeoenvironment and ecology of the site have proven challenging. This is due both to its complex submarine topography, a result of the Callovian reactivation of a number of Hercynian faults (Charbonnier 2009; Charbonnier *et al.* 2014), and to the seemingly contradictory habitats of the faunal assemblage (Charbonnier *et al.* 2007, 2014; Charbonnier 2009; Vannier *et al.* 2016; Audo *et al.* 2019). Although based on a synthesis of the geology and fossil fauna of La Voulte-sur-Rhône, the fossil-bearing locality has been interpreted to represent a somewhat deep (200+ m) offshore environment (bathyal zone) around the slope–basin transition (Charbonnier 2009; Charbonnier *et al.* 2014).

The increased use of powerful imaging techniques over the last decade has enabled the reappraisal of many fossil specimens, including coleoids from La Voulte-sur-Rhône (Kruta *et al.* 2016; Rowe *et al.* 2022). The three-dimensional (3D) preservation seen in these coleoids is particularly well suited to x-ray-based approaches, which provide unparalleled opportunities for the observation of internal and external morphology (Jauvion *et al.* 2016, 2020; Kruta *et al.* 2016; Rowe *et al.* 2022). The exceptional preservation is a result of rapid replacement of the soft tissues with authigenic iron-rich minerals (see

doi: 10.1002/spp2.1511

Allison 1988, Wilby *et al.* 1996, Clements *et al.* 2017 and Jauvion 2020 for a description of the mineral replacement phases producing this level of preservation). Results from these studies have contributed to the discovery of previously unknown anatomical characters and also to palaeoecological and palaeoenvironmental interpretations of La Voulte-sur-Rhône.

Indeed, recent tomographic analysis of an arthropod specimen (Thylacocephalan, *Dollocaris*) (Vannier *et al.* 2016) contradicts the deep-water environment hypothesis for La Voulte-sur-Rhône. Analysis of its eyes and stomach contents indicates that *Dollocaris* was a visual ambush predator, which suggests that its palaeoenvironment was illuminated. Additionally, work on the vampyromorph coleoid *Vampyronassa rhodanica* (Rowe *et al.* 2022) from the locality has identified previously unknown morphologies in Jurassic taxa, which are indicative of a pelagic and predatory mode of life. This is in contrast to the deep-sea lifestyle of the extant coleoid *Vampyroteuthis infernalis*, which is positioned as its only extant relative.

Here, we describe a previously unpublished vampyromorph specimen (MNHN.F.A32491) from La Voulte-sur-Rhône, which was preliminarily assigned to *Vampyronassa rhodanica*. We used a variety of imaging techniques that enabled observation of the internal morphology, including many characters belonging to the arm crown. This appraisal demonstrates the benefits of these imaging methods to facilitate a clearer understanding of the morphology and lifestyle behaviours of Jurassic vampyromorph coleoids.

Although there is not, as yet, a definitive understanding of the palaeoecology at La Voulte-sur-Rhône, the increasing amount of gathered data is beginning to suggest that this locality represented a complex Jurassic ecosystem, with a larger coleoid diversity than previously understood.

MATERIAL AND METHOD

The specimen studied here (MNHN.F.A32491) is catalogued in the collections of the Muséum national d'Histoire naturelle (MNHN), Paris, France.

The specimen was imaged using propagation phase contrast synchrotron x-ray microcomputed tomography (PPC-SR-µCT) at the European Synchrotron Radiation Facility (ESRF, ID 19 beamline, Grenoble, France), at both a 12.64 µm (entire specimen) and 3.5 µm (arm crown) voxel size (see Rowe *et al.* 2022 for acquisition methods and http://paleo.esrf.fr/ for data and metadata). The resulting PPC-SR-µCT files were manipulated in ImageJ to reduce the size (binning and cropping) before segmentation, which was done using Mimics software (v.21.0; Materialise NV). Internal and external features for segmentation were identified using the density of the mineralized soft tissues, which appear as contrasting grayscale in the reconstructed files.

These data were then compared with three segmented and reconstructed *Vampyronassa rhodanica* specimens (MNHN.F.B74247; MNHN.F.B74244; MNHN.F.B74243) described in Rowe *et al.* (2022). The existing tomographic data of *V. rhodanica* enabled a direct comparison of features, specifically characters in the arm crown (arm length, sucker and cirri configuration). Additional comparisons were carried out on previously described fossil specimens (Fuchs 2020), including some from La Voulte-sur-Rhône, as well as extant taxa. Special attention was paid to the ink sac and luminous organs given that these were preserved in MNHN.F.A32491.

The specimen was also photographed using reflectance transformation imaging (RTI) at the MNHN to analyse the external morphology in relief from the matrix (Rouget *et al.* 2022).

Measurements of the specimen were taken following the delineations for Octobrachia shown in Nixon (2011, fig. 3), with the central lateral eye line marking the boundary between anterior and posterior sections. All measurements were composite and followed the natural line of the specimen where possible.

Using the RTI images and measurement parameters from Fuchs (2016, 2020), we attempted to reconstruct the gladius ratios and size for MNHN.F.A32491. A reconstruction of this was used to determine systematic placement (Fuchs 2020). Given that the specimen shows compaction and loss in certain areas, these results should be interpreted with appropriate caution.

Institutional abbreviations. AMNH, American Museum of Natural History, New York, USA; MNHN, Muséum national d'Histoire naturelle, Paris, France; ZMB, Museum für Naturkunde, Berlin, Germany.

SYSTEMATIC PALAEONTOLOGY

Superorder OCTOBRACHIA Haeckel, 1866
Order VAMPYROMORPHA Robson, 1929
Suborder LOLIGOSEPIINA Jeletzky, 1965
Family GEOPELTIDAE Regteren Altena, 1949
Genus VAMPYROFUGIENS nov.

LSID. https://zoobank.org/nomenclaturalacts/FA6A1790-3915-4F77-9452-E3CBDE01F48A

Type species. Vampyrofugiens atramentum.

Derivation of name. The name *Vampyrofugiens* is composed of the original Serbian word *Vampir* and the Latin *fugiens* (fleeing) to reflect the escape behaviours of this new vampyromorph taxon.

Diagnosis. As for type and only species.

Vampyrofugiens atramentum sp. nov.

LSID. https://zoobank.org/nomenclaturalacts/CF14CBF1-D8BF-4898-972A-A8E4AB71FA06

Holotype. MNHN.F.A32491.

Derivation of the name. The species name *atramentum* (Latin word for ink) is assigned and reflects the occurrence of an ink sac.

Diagnosis. Mantle bullet-shaped; arm length moderate (arm length : mantle length ratio of 0.6 although the distal tips are not preserved), no elongated arm pair; suckers radially symmetrical, uniserial, sucker rings absent; cirri biserial; head dorsally fused with mantle; ink sac present; luminous organs present internally; fins subterminal.

Type locality. La Voulte-sur-Rhône, France.

Type horizon. Middle Jurassic (Lower Callovian), *gracilis* Biozone.

Description

Body. MNHN.F.A32491 is positioned in dorsal view (Fig. 1A). The body and head region have undergone slight rotation and non-uniform compaction prior to fossilization. The distalmost part of the arms has been lost. The total preserved, measurable length (posterior part of the mantle to the preserved anterior tips of the arms) is *c.* 81 mm. The head and dorsal mantle are fused although the head is clearly outlined, suggesting that the anterior part of the mantle margin is positioned posterior to the eyes (Fig. 2). The mantle is posteriorly tapered and measures *c.* 55 mm in length from the central eye to the posteriormost margin. There is no evidence of mantle-locking cartilage. A funnel is visible in the PPC-SR-μCT slices (Fig. 1D) with the most anterior part terminating slightly posteroventrally to the eyes.

The combination of μCT and RTI reveals previously unseen internal and external morphological details, as well as showing topographic contouring on parts of the mantle. It is possible that these contours correspond, in part, to sections of the original gladius morphology (Fig. 2).

Fins. The specimen has one pair of posterior fins located in a subterminal position (Figs 1A–C, 3A, B, D, E), the tissue of which is draped across the posteriormost section of the mantle (Figs 1C, 3D). Not all of the tissue is preserved (Fig. 1A). What remains is narrowest in the posteriormost section and flares slightly anteriorly. The margins appear rounded. Here, we interpret the fins to be paddle-like in shape, similar to those of *Vampyroteuthis infernalis* (Pickford 1949). The internal fin cartilage is well preserved and appears clearly in the PPC-SR-μCT slices as defined linear structures in a paired lateral position (Fig. 3E).

Head. The head is fused to the mantle and measures *c.* 22 mm at its widest section. Both eyes are retained. The eyes are subspherical, *c.* 5 mm in diameter, and are located on different planes, which is consistent with the slight rotation of the specimen prior to fossilization. In cross-section, parts of the cephalic cartilage appear to be preserved (Fig. 3F).

Dorsally, a thin elongate structure (<1 mm in diameter) is draped perpendicular to the arm crown, just slightly anterior to the eyes (Figs 1A, 4). It is not continuous across the width of the head and does not appear to be fused with the tissue. Additionally, the internal composition of this element, visible in the PPC-SR-μCT slices, does not resemble a filamentous retractile appendage, or the internal musculature of the preserved arms. There is no evidence to suggest that this structure is part of the specimen, rather that it is a preserved piece of associated fauna, possibly a section of a brittle star arm (Fig. 4E), given that these are common taxa in the La Voulte-sur-Rhône locality (Charbonnier *et al.* 2014).

Arm crown. Eight arms are present in the arm crown, each with uniserial, radially symmetrical suckers and biserial cirri that are evident from the most proximal sections of the arms to the distal, truncated boundary (Figs 1A, 5). Without the distalmost parts it is not possible to define a precise length for each of the arms or determine with absolute certainty that there is no elongate pair. However, the extent of the preserved arms ranges from *c.* 24 mm to 29 mm. Although each shows evidence of compaction, they are all similar in dimension, morphology and tapering, which suggests that they all share a comparable length. The diameter of the arms measures *c.* 5–7 mm towards the base and *c.* 2–4 mm at the truncated distal section. Neither the PPC-SR-μCT nor the RTI data show evidence of an elongate pair of filamentous structures, or of hectocotylization. The internal musculature of the arms is clearly visible in the PPC-SR-μCT slices and has an Octobrachia-like configuration (Fig. 6). The muscle layers in the fossil form replicate the distinct gross musculature regions. An axial nerve chord is encircled by the transverse muscle, which in turn is surrounded by a band of longitudinal muscle. These appear striated in cross-section (Fig. 6A) and on coronal view (Fig. 6B).

Suckers. The uniserial suckers are radially symmetrical and present along the entire length of the arm (Fig. 5B, C). They show only slight variation in diameter (*c.* 1.2–1.9 mm), with those in the centre of the arm being marginally larger than those at the proximal and distal sections. Approximately 10 suckers are preserved on each arm and are flanked by interspersing cirri (Fig. 5C). Given that the arm tips are missing, it is likely that there were more on the living animal.

Each sucker is connected to the arm with a *Vampyroteuthis*-like attachment (Figs 7A–D, 8B–C). These attachments extend

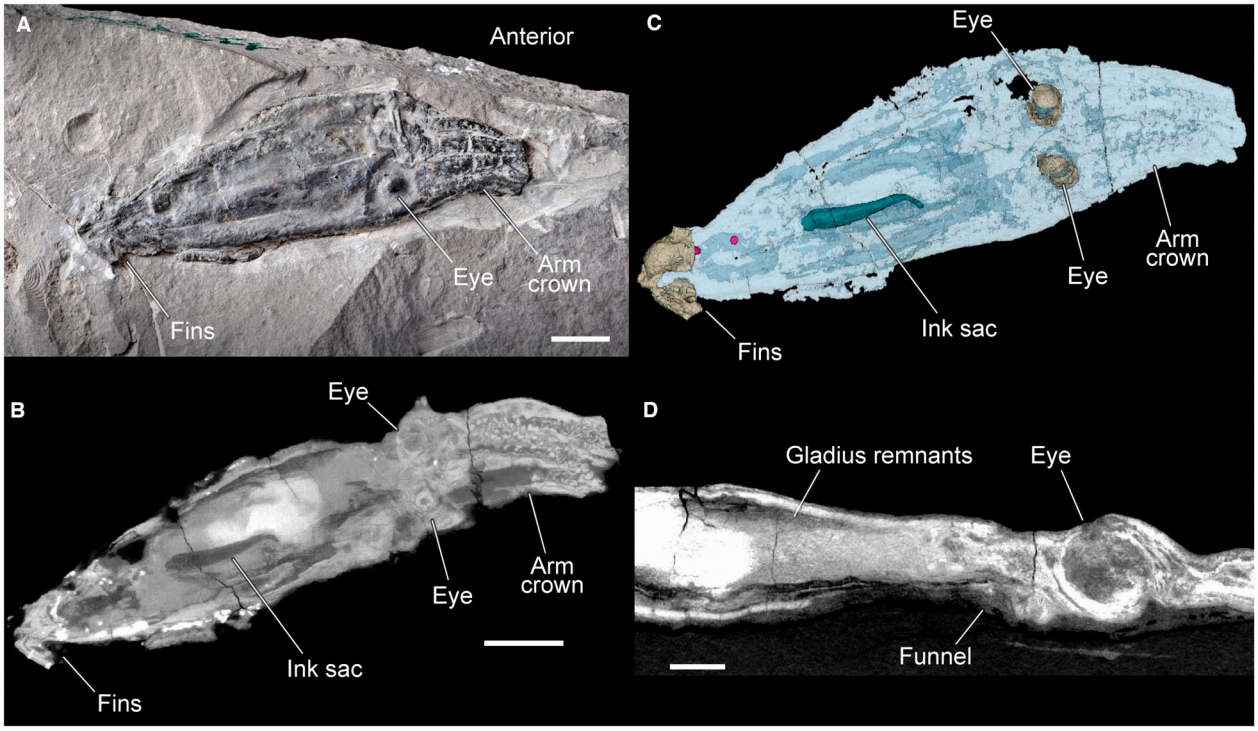

FIG. 1. Photograph, 3D rendering, and PPC-SR-μCT slices (binned dataset, voxel size: 25.28 μm) of the undescribed specimen (MNHN.F.A32491) acquired at the ESRF (Grenoble, France). A, photograph (P. Loubry, CR2P) of the specimen showing the 3D preservation of the mineralized soft tissue. B, composite of PPC-SR-μCT slices showing the greyscale contrast used to segment the specimen. C, 3D rendering showing the location of the fins (beige), ink sac (teal) and internal luminous organs (pink). D, longitudinal slice showing the location of the funnel, and an area interpreted to be remnants of the gladius in longitudinal view. Rendered in Mimics software (v.21.0). Scale bars represent: 10 mm (A–B); 2 mm (D).

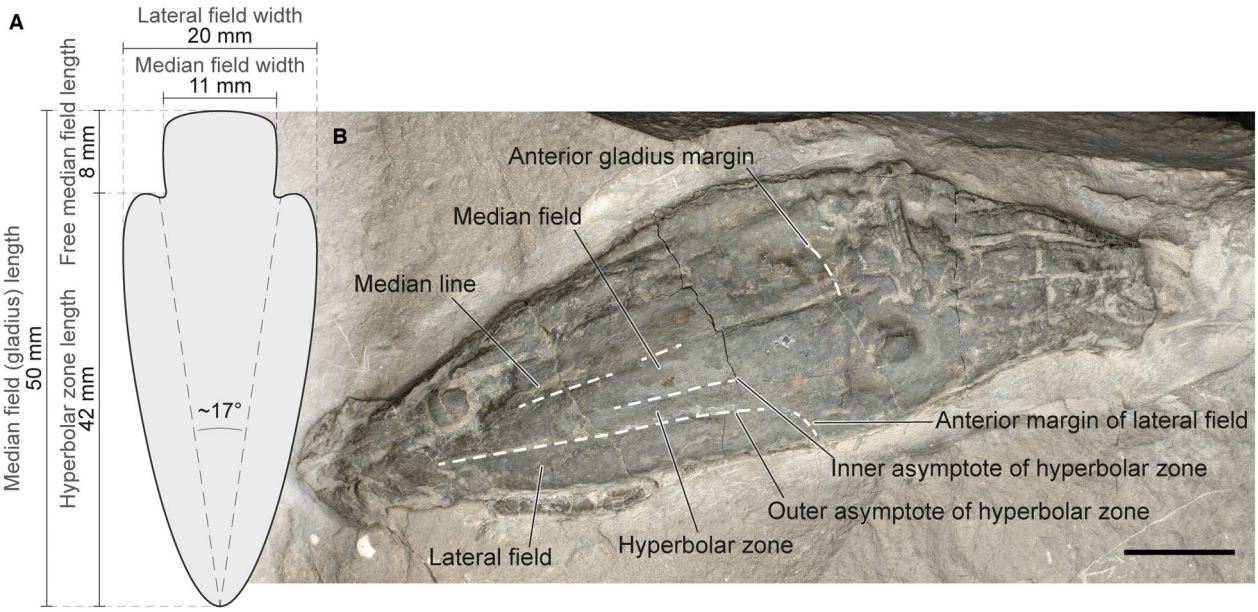

FIG. 2. A, hypothesized illustration of the gladius of *Vampyrofugiens atramentum* based on interpreted measurements and diagnostic indices. B, MNHN.F.A32491, highlighting some of the inferred elements and contours preserved on the gladius (photograph courtesy of P. Loubry, CR2P). Scale bar represents 10 mm.

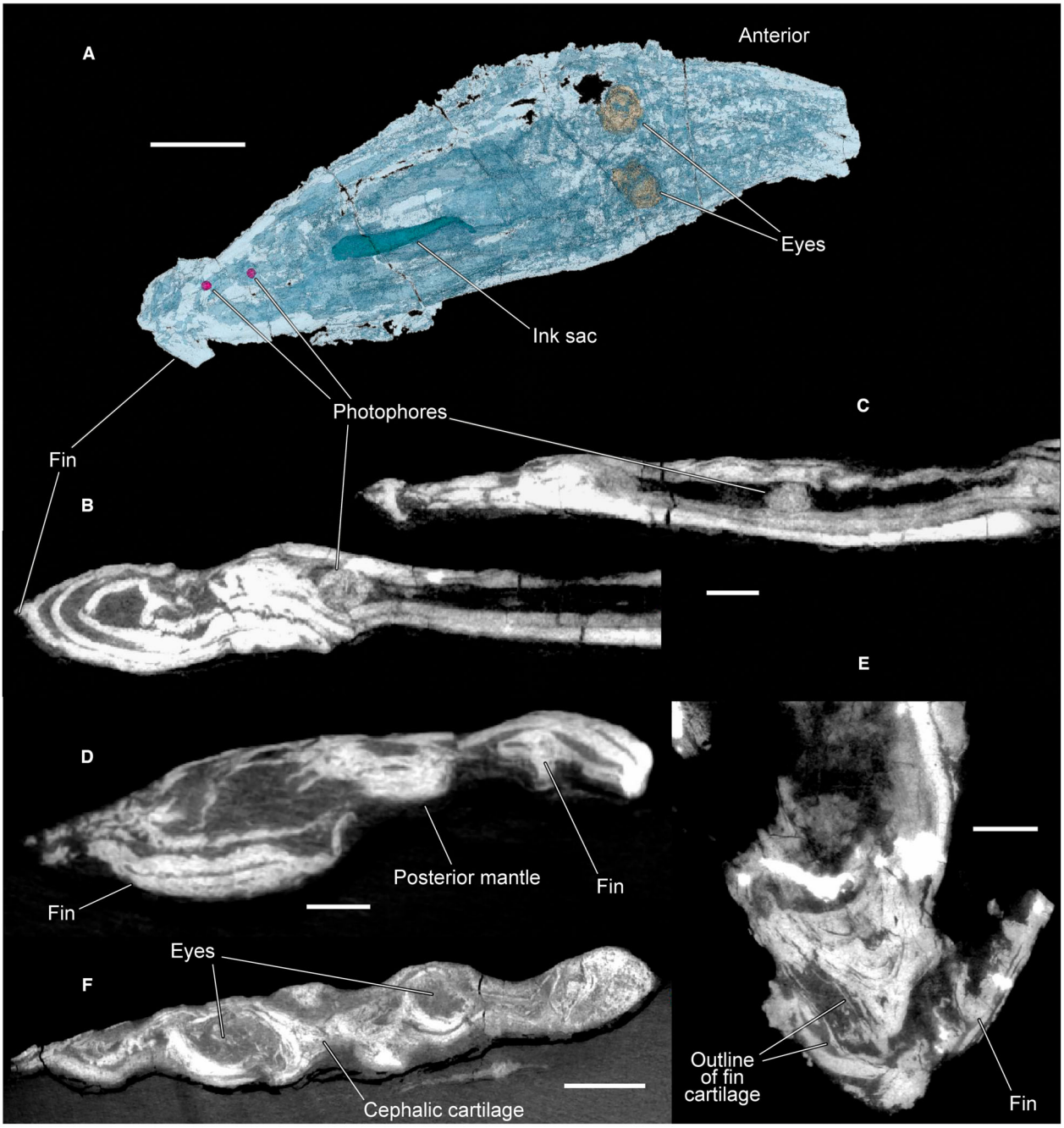

FIG. 3. 3D rendering and PPC-SR-μCT slices (binned dataset, voxel size: 25.28 μm) showing the internal luminous organs and preserved cartilaginous structures. A, overall rendering of the specimen indicating the anterior–posterior positioning of the photophores (pink). B–C, two longitudinal PPC-SR-μCT slices showing the photophores *in situ*. D, cross-section of the posteriormost section (looking anteriorly) showing the folded tissue of the laterally situated fins. E, coronal view of the posterior section showing the fin cartilage; here, it is visible on the left side of the image and appears as a faint white line encircling a dark, elongate area. F, cross-section of the head region showing the subcircular eyes and cephalic cartilage in an X shape between them. Rendered in Mimics software (v.21.0). Scale bars represent: 10 mm (A); 1 mm (B–C); 2 mm (D–E); 3 mm (F).

distally into the base of the acetabulum. Proximally, they are not clearly attached to the arm muscle. The infundibular muscle lines are also preserved on some of the suckers (Fig. 7A).

Pronounced ovoid cavities encircle the outer margins of most suckers. They are not uniform in size (they range up to *c.* 230 μm in diameter) and do not appear to be connected to each

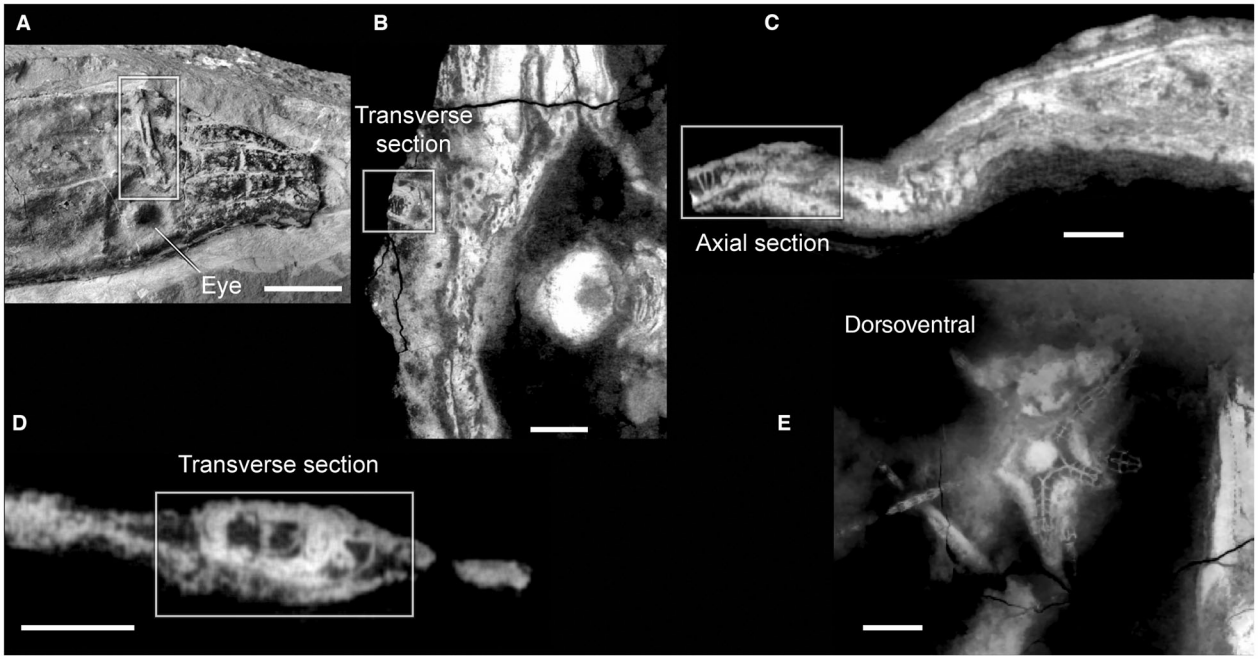

FIG. 4. A–D, images of MNHN.F.A32491 indicating the placement of the section of the supposed brittle star: A, photograph by P. Loubry (CR2P); B–D, PPC-SR-μCT slices (ESRF, binned dataset, voxel size: 25.28 μm); the assigned views represent the orientation of the brittle star, not the coleoid. E, example of a brittle star from the locality showing the preserved internal structure (PPC-SR-μCT slice; ESRF, binned dataset, voxel size: 25.28 μm). Scale bars represent: 10 mm (A); 2 mm (B, E); 1 mm (C–D).

other within the muscle layers of the sucker's soft tissue (Fig. 8A–C, E, F).

Ink sac. A clearly defined ink sac is positioned medioventrally in the mantle and appears as a cylindrically tapered, opaque black structure, *c.* 16 mm in length (Figs 1B, C, 3A). The smaller, anteriormost section of the ink sac is oriented toward the ventral margin of the body.

Luminous organs. Two uniformly spherical structures (*c.* 1 mm in diameter) are nestled inside the specimen, in a posterior cavity positioned just anterior to the fins (Fig. 3A–C). One sphere is anterior to the other and they both lie along the axial plane. The density of the structures is consistent with the variation seen in the rest of the preserved anatomy, and no other structures are located in the same cavity. We interpret these spheres as luminous organs rather than as other internal organs such as oocytes, which form clusters, or oviductal organs, which are laterally symmetrical. By their size and density they do not appear to be pyritic framboids, which have been described from La Voulte-sur-Rhône as being often >1 cm (Briggs & Crowther 2008).

Gladius. The PPC-SR-μCT data did not allow for concise visualization or full reconstruction of the gladius. However, the RTI data showed an external topographic relief that is consistent with the placement and shape of a gladius and is herein interpreted as such (Fig. 2). This external topography is supported by the preservation of internal mineralized sections visible anteriorly in the PPC-SR-μCT slices. Due to the lamellar composition and location (Fig. 1D), we conclude that these areas are preserved sections of the gladius.

The interpreted outline and parameters of the gladius remains formed the basis for a number of diagnostic measurements outlined in Fuchs (2020), and enabled a hypothesized reconstruction (Fig. 2). The length of the gladius (*c.* 50 mm) corresponds with that of the mantle and its width ratio (gladius $width_{max}$: gladius length) is moderate (0.4). The median field ratio (median field $width_{hypz}$: hyperbolar zone length) is slender (0.26) with an opening angle (between the inner asymptotes) of *c.* 17°. It features two very long hyperbolar zones (hyperbolar zone length :median field length ratio, 0.84) that extend into moderate lateral fields (lateral fields $width_{max}$: median field $width_{max}$ ratio, 1.8).

Given that it was not possible to make observations and measurements directly on the gladius, these interpretations should be viewed with caution.

DISCUSSION

Konservat-Lagerstätten, such as La Voulte-sur-Rhône, play a key role in the preservation of soft tissue, identification of behaviours and tracking of the timing of evolutionary innovations (Fuchs *et al.* 2010; Kruta *et al.* 2016; Klug *et al.* 2021). Despite the considerable amounts of morphological information retained, interpreting the

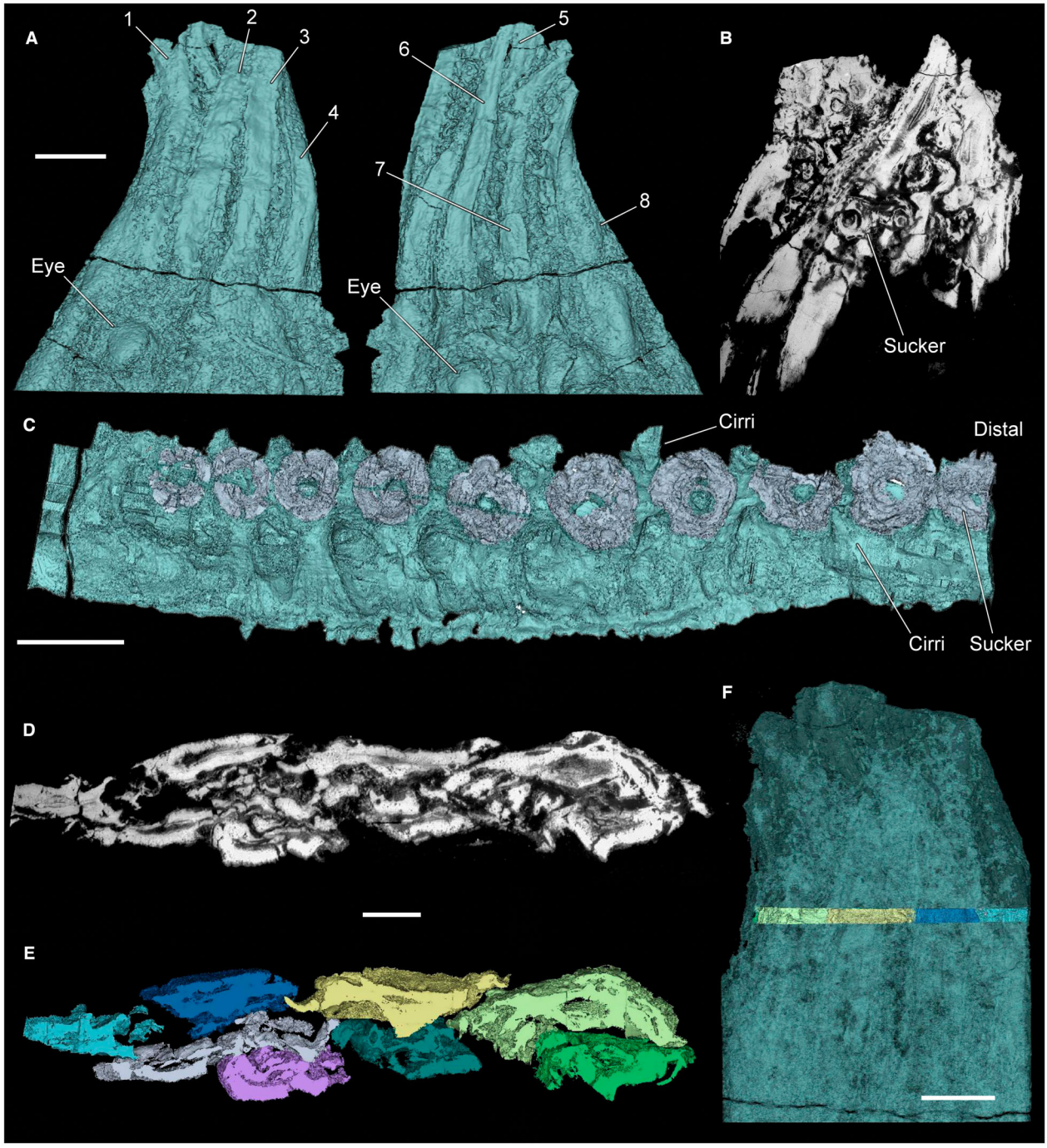

FIG. 5. 3D renderings and PPC-SR-μCT slices showing arm crown elements of MNHN.F.A32491 (binned dataset, voxel size: 7 μm). A, rendering of the arm crown in dorsal and ventral view showing eight arms in the undifferentiated arm crown. B, PPC-SR-μCT slice of the arm crown showing the radially symmetrical suckers, internal musculature and ovoid cavities in the soft tissues. C, 3D rendering of an arm showing the uniserial sucker row and biserial cirri configuration. D, PPC-SR-μCT slice in cross-section showing the eight arms. E, rendering of the cross-section in D; each arm is rendered in a different colour. F, semi-transparent rendering of the arm crown showing the location of the cross-section. Rendered in Mimics software (v. 21.0). Scale bars represent: 5 mm (A); 2 mm (C); 1 mm (D–E); 3 mm (F).

taxonomic and ecological implications of these characters can still be challenging. This is reflected in the new species described here.

Gladius. The gladius is the key diagnostic element used in fossil coleoid systematics; indeed, it forms the basis for the current taxonomy of Mesozoic coleoids (Young &

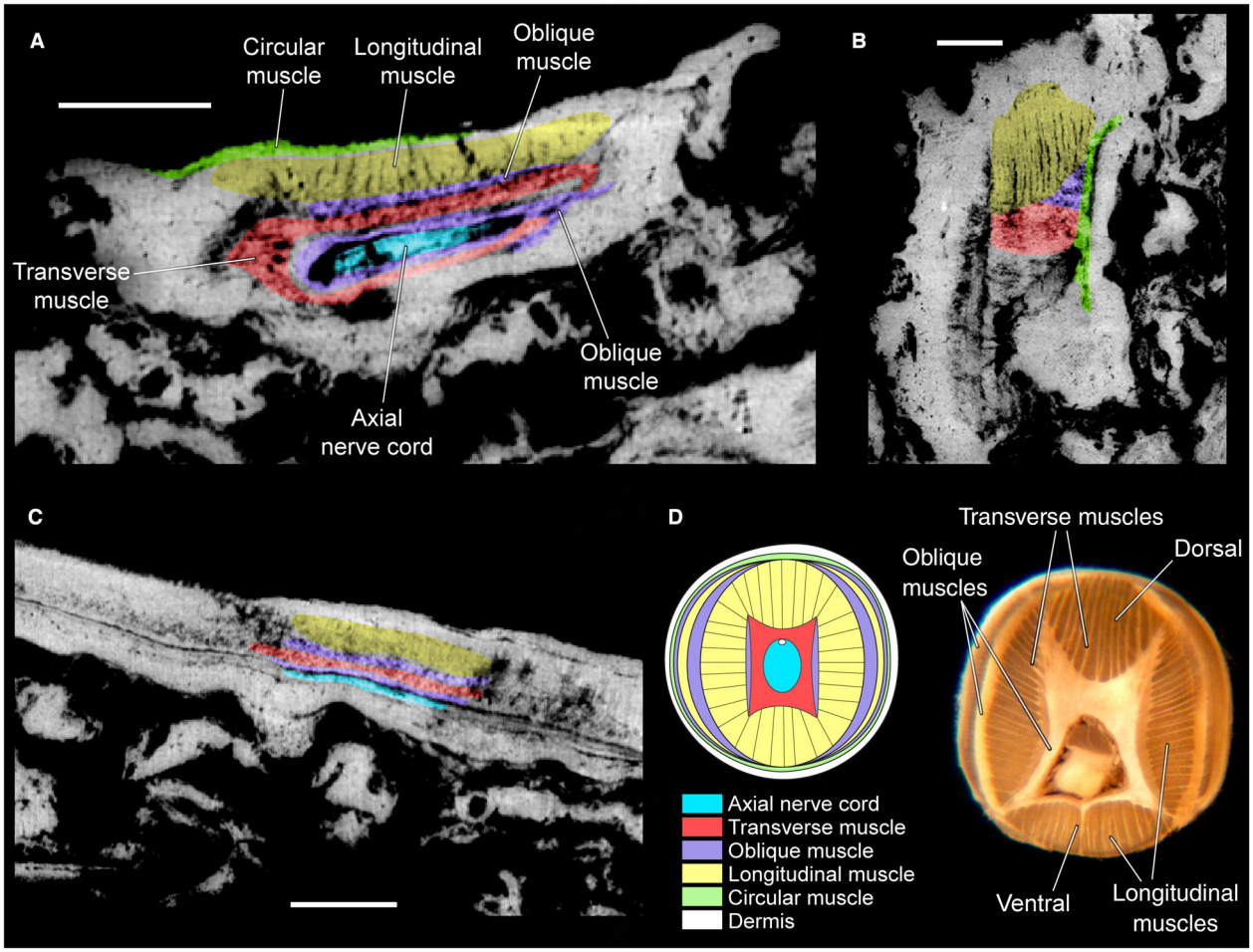

FIG. 6. A–C, slices (PPC-SR-μCT, binned dataset, voxel size: 7 μm) of an arm of MNHN.F.A32491 in: A, cross-section; B, coronal; C, longitudinal view. D, on the left, an illustration by Nödl (2015) outlines musculature regions and indicates the colours used in A–C; these bundled muscle groups reflect the different orientations and gross musculature seen in the cross-section of the extant octopus arm shown on the right (from Feinstein *et al.* 2011). In MNHN.F.A32491 the bundles of longitudinal muscle seem to be the best preserved. All scale bars represent 500 μm.

Vecchione 1996; Lindgren *et al.* 2004; Kruta *et al.* 2016; Sutton *et al.* 2016; Fuchs 2020). However, there are many inherent, widely recognized uncertainties in the present framework. These unknowns are a consequence of the limited sample size, which is constrained by the specific taphonomic conditions required for exceptional preservation (Marroquín *et al.* 2018). Additionally, the samples are preserved only in varying degrees and often show compaction or loss of taxonomic characters (Marroquín *et al.* 2018). These conservation parameters contribute to the limited understanding of the diagnostic characteristics and intraspecies-level variation and, as yet, it has not yet been possible to reconstruct a supported phylogeny (Lindgren *et al.* 2004; Kröger *et al.* 2011; Kruta *et al.* 2016; Sutton *et al.* 2016, Košťák *et al.* 2021).

One established diagnostic feature is the configuration of growth lines present on the gladius (Fuchs 2006; Fuchs & Weis 2008; Marroquín *et al.* 2018). Those located in the hyperbolic zone vary in levels of concavity and have been shown to be sufficient markers for the positive classification of fossil coleoids (Fuchs & Weis 2008). However, the mantle tissue preserved in MNHN.F.A32491 conceals the gladius and, therefore, any growth lines that could be used for diagnostic purposes.

The use of RTI uncovered details that were not seen on either μCT or visual observation. These enabled us to interpret the overall outline of the gladius (Fig. 2). Based on the interpreted morphology (apical angle, distinct hyperbolic zone, lack of lateral keels, and the width of median field) it is possible to rule this specimen out as a member of the Prototeuthid suborder (Fuchs 2016, 2020). In the Teudopseina suborder, the genera described in the corresponding biostratigraphic age range are the Teudopseidae, *Teudopsis* and *Teudopseina*, and the

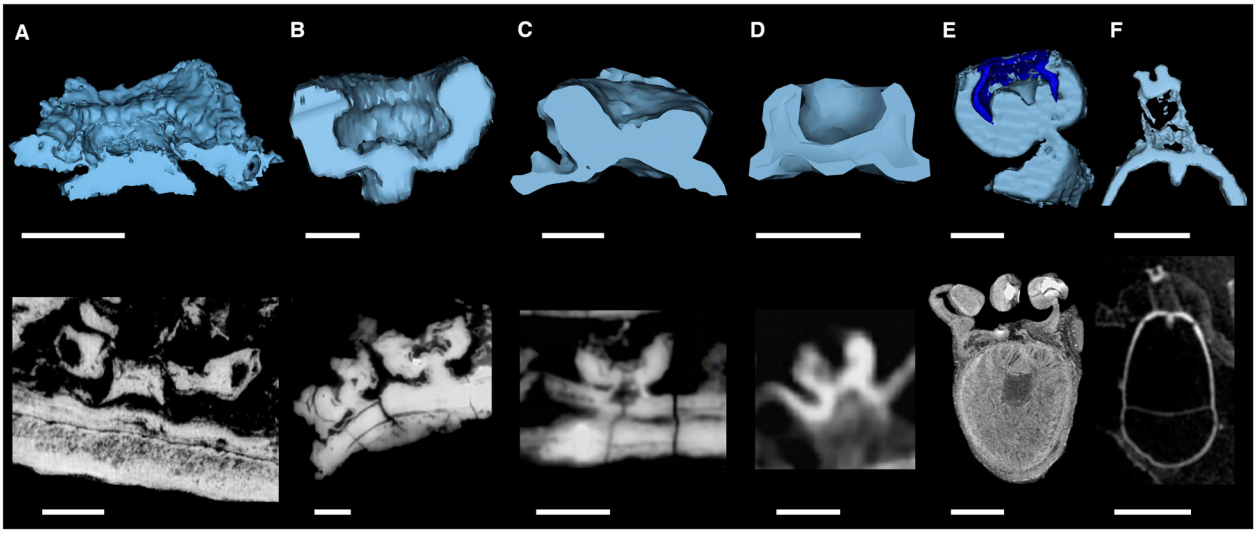

FIG. 7. 3D renderings (top) and PPC-SR-μCT, and μCT slices (bottom) of sucker profiles: A, *Vampyrofugiens atramentum*. PPC-SR-μCT slice (binned dataset, voxel size: 7 μm); B–C, dorsal (B) and non-dorsal (C) arms of *Vampyronassa rhodanica* (MNHN.F.B74244) (PPC-SR-μCT, binned dataset, voxel size: 25 μm); D, *Vampyroteuthis infernalis* (AMNH IZC 361496; μCT, voxel size 38.40 μm) (Vampyromorpha); E, commercial *Loligo* (Decabrachia) sample (μCT, AST-RX platform, MNHN); F, *Grimpoteuthis* (ZMB 240160) (Octobrachia) CT data reconstructed from (Ziegler *et al.* 2018); E–F, extant material was stained prior to scanning. Rendered in Mimics software (v.21.0). Scale bars represent (top row renderings): 500 μm (A–D); 2 mm (E); 5 mm (F); (bottom row PPC-SR-μCT and μCT slices) 400 μm (A); 1 mm (B–C); 500 μm (D); 5 mm (E); 10 mm (F).

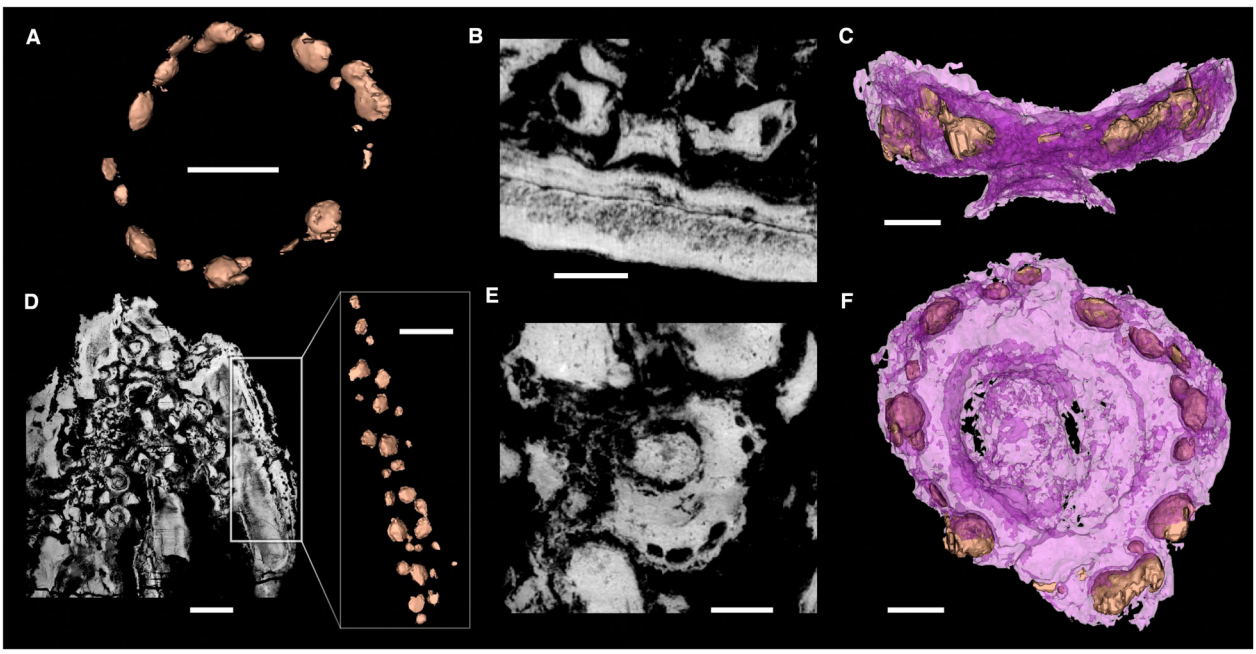

FIG. 8. PPC-SR-μCT slices (ESRF, binned dataset, voxel size: 7 μm) and 3D renderings of the ovoid cavities in the sucker (A–C, E, F) and arm tissue (D) of MNHN.F.A32491. A, coronal view showing a rendering of the cavities encircling the outer perimeter of the sucker. B, E, longitudinal and coronal view, respectively, of the sucker in the PPC-SR-μCT slice. C, F, rendering in longitudinal and coronal view, respectively, of the same sucker. D, PPC-SR-μCT slice of the ovoid cavities in the arm tissue, with an inset rendering of the cavities. Rendered in Mimics software (v.21.0). Scale bars represent: 400 μm (A–B, E); 200 μm (C, F); 2 mm (D); 500 μm (inset in D).

Trachyteuthidae, *Trachyteuthis* (Fuchs 2020). The gladius morphology of MNHN.F.A32491 is not consistent with any of these genera, nor indeed with members of the more derived cirrata or incirrata suborders. The gladius is also very different from the two specimens known from the Vampyromorphina suborder, extant *Vampyroteuthis* and the Oligocene-aged *Necroteuthis*. By process of elimination, the gladius belongs to a vampyromorph coleoid, probably in the Loligosepiina suborder.

The measurements of MNHN.F.A32491 do not fit exactly within the parameters listed for any of the genera in the four families of this suborder (Fuchs 2020), although they are most dissimilar to the families of Leptotheuthidae (*Leptotheuthis*, *Donovaniteuthis*) and Mastigophoridae (*Mastigophora*, *Doryanthes*). The genera of the Loligosepiidae family (*Loligosepia* and *Jeletzkyteuthis*) have longer hyperbolar zones than MNHN.F.A32491 and have anteriorly pointed lateral fields, which have not been seen in the new specimen (Fig. 9).

Of all of the members of Loligosepiina, the gladius reconstruction is closest to the geopeltid *Parabelopeltis*. It conforms to the diagnostic widths of both the gladius and median field, and is constrained by the upper limit of the hyperbolar zone length (Fig. 2). However, even here the measurements are not an exact match, given that the width of the lateral fields exceeds that of *Parabelopeltis*.

Additionally, the 'small' size of MNHN.F.A32491, as designated by the parameters outlined in Fuchs (2020), is not consistent with its placement in the 'medium-sized' Geopeltidae family. It is possible, however, that this specimen could be a sub-adult member.

Excluding the lateral field width and overall body size, all other known measurements are consistent with those of the genus *Parabelopeltis*. This genus is represented by only one Jurassic species, *P. flexuosa* (Fuchs 2020), from localities in Germany, Luxembourg, UK, Switzerland, Russia and Canada (Alberta) (Marroquín *et al.* 2018; Fuchs 2020).

Without direct observation of the gladius, the reconstructed shape (Fig. 2) was not sufficient to assign MNHN.F.A32491 to an already described species. Our hypothesized reconstruction indicates that although it could be close to *Parabelopeltis* (Fig. 9) there are some differences in its size and proportions, which justify a new species. As such, we suggest that MNHN.F.A32491 represents a new genera in the geopeltid family. Further discoveries will ideally provide additional information on the soft tissues of *Parabelopeltis*, or a better understanding of the gladius morphology in the newly assigned genus.

Ink sac. Like the gladius, the ink sac is included in the character matrix of fossil systematics (Young & Vecchione 1996; Lindgren *et al.* 2004; Kruta *et al.* 2016; Whalen & Landman 2022). However, the exceptional taphonomic conditions required for coleoid fossilization constrain our understanding of the extent of this feature in fossil taxa (Nishiguchi & Mapes 2008). Therefore, the presence of this character remains uncertain in many of the genera included in the morphology-based phylogenies (Young & Vecchione 1996; Lindgren *et al.* 2004; Kruta *et al.* 2016; Whalen & Landman 2022). However, Strugnell *et al.* (2014) have argued the volatility of this character and its suitability for determining high-level phylogenetic relationships, given that it has been lost in numerous lineages. As such, we refrain from attempting to contextualize the ink sac of the new species in a taxonomic framework, and instead we use it as an indicator of behaviour and of the implications for ecologic niche occupation.

Luminous organs. Although common and varied in families of extant Decabrachia, (Herring 1994; Herring *et al.* 1994) there are very few luminous genera in the extant Octobrachia (Herring 1988). Those known include two incirrate octopoda (*Japetella* and *Eledone*), as well as *Vampyroteuthis infernalis*, the only extant vampyromorph. This latter taxon has three sources of bioluminescence (Pickford 1949; Herring *et al.* 1994; Robison *et al.* 2003) including two photophores on the surface margin of the mantle, which are positioned dorsolaterally at the base of the pair of posterior fins (Herring 1988).

Photophores vary in structure and complexity, and there may be several types in one species. Their placement and variety differs between and within species, and can also be linked with sexual dimorphism (Herring 1988; Herring *et al.* 1992, 1994; Cavallaro *et al.* 2017). They can be distributed across the body (Cavallaro *et al.* 2017), where they potentially emit light from the arm crown, the eye and head region and mantle, or internally, where they are observed in brachial, anal and abdominal positions (Butcher *et al.* 1982; Nixon & Young 2003).

Unlike *Vampyroteuthis infernalis*, the luminous organs observed in MNHN.F.A32491 are internal and positioned with anterior–posterior symmetry. We interpret this to be the original orientation. Although the specimen does show evidence of some rotation prior to fossilization, the amount needed to reorient the symmetry of these structures seems inconsistent with what is observed.

Instead, the internal luminous organs of MNHN.F.A32491 are similar to the intestinal photophores specific only to a few species in extant Decabrachia (Nixon & Young 2003; Nixon 2011; Lindgren *et al.* 2019), although the medial anterior–posterior symmetry and visceral placement is not common (Jereb & Roper 2010). This alignment is found in some oegopsiids, specifically certain members of the enoploteuthid families, Lycoteuthidae and Pyroteuthidae (Jereb & Roper 2010).

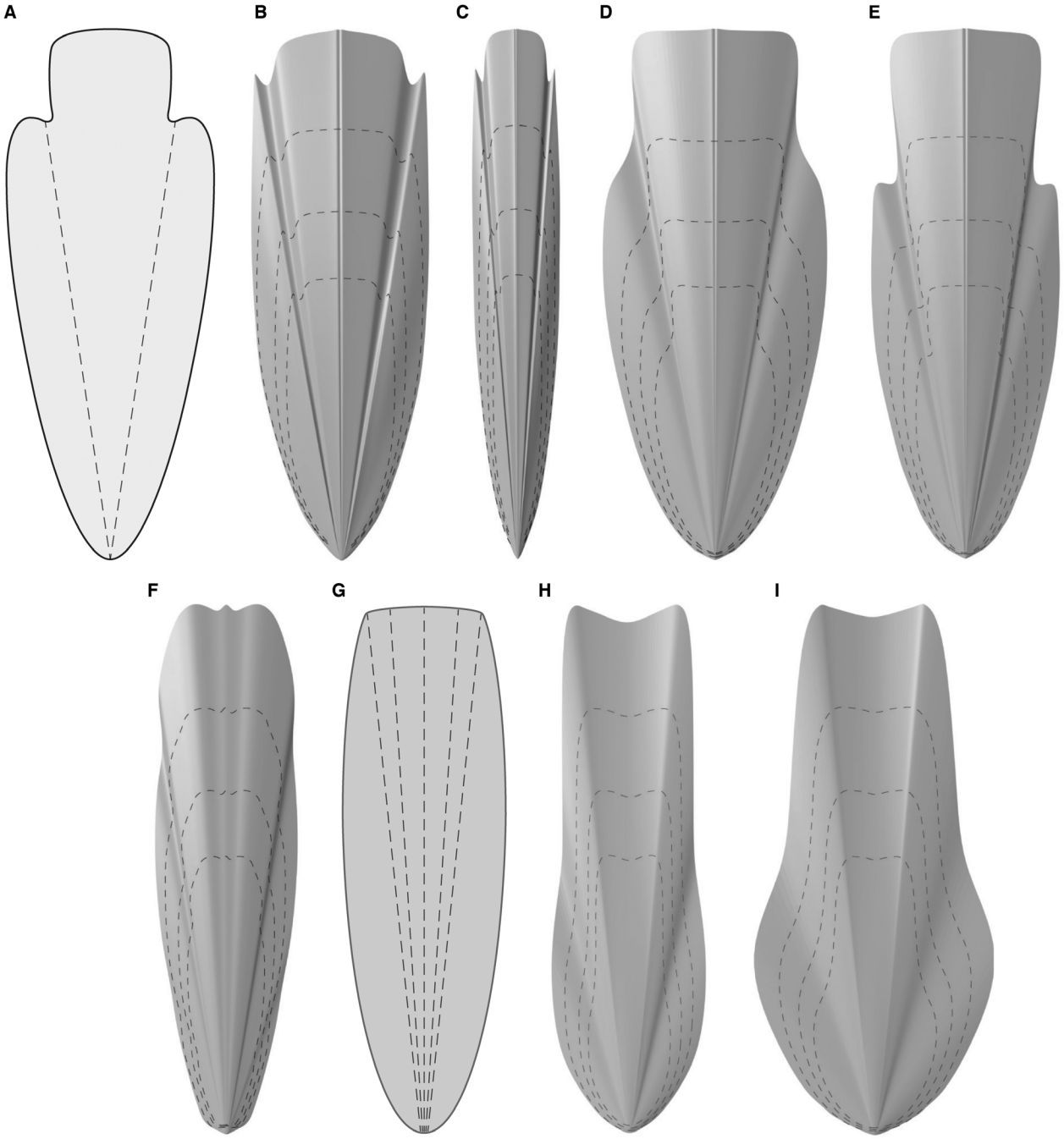

FIG. 9. Genus-level gladius illustrations from the Suborder Loligosepiina Jeletzky, 1965, adapted from Fuchs (2020), with the addition of the new species. A, *Vampyrofugiens atramentum* gen. et sp. nov. B–C, Family Loligosepiidae Regteren Altena, 1949: B, *Loligosepia* Quenstedt, 1839; C, *Jeletzkyteuthis* Doyle, 1990. D–E, Family Geopeltidae Regteren Altena, 1949: D, *Geopeltis* Regteren Altena, 1949; E, *Parabelopeltis* Naef, 1921. F–G, Family Leptotheuthidae Naef, 1921: F, *Leptotheuthis* Meyer, 1834; G, *Donovaniteuthis* Engeser & Keupp, 1997. H–I, Family Mastigoporidae Engeser & Reitner, 1985: H, *Mastigophora* Owen, 1856; I, *Doryanthes* Münster, 1846. Gladius illustrations are for morphological comparison and not to scale.

Species in these genera typically have multiple photophores on the body, although the position and axial symmetry of the two photophores seen in MNHN.F.A32491 (Fig. 3A–C) most closely resemble those of the abdominal light organs in the oegopsiid *P. microlampas* (Pyroteuthidae) (Lindgren *et al.* 2019). These are of a similar size and are positioned along the median line with one posterior to the other.

This symmetry is also seen in the onychoteuthid *Onychoteuthis banksii*, a species that is used in the phylogenies combining extant and fossil morphological characters (Lindgren *et al.* 2004; Kruta *et al.* 2016; Sutton *et al.* 2016; Rowe *et al.* 2022; Whalen & Landman 2022). However, in *O. banksii* the two photophores show a variation in size, with the anterior photophore being smaller than the posterior one by *c.* 75%, and they are more widely spaced along the intestine (Bolstad 2008; Jereb & Roper 2010; Bolstad *et al.* 2019).

Although luminous organs have been proposed in taxa from La Voulte-sur-Rhône (Fischer & Riou 2002), none has so far been positively identified using μCT (Kruta *et al.* 2016; Rowe *et al.* 2022). Furthermore, to our knowledge, this configuration of photophores is the only example of this arrangement observed in fossil coleoids. In extant forms, when the two internal anterior–posterior photophores are present they are accompanied by additional photophores elsewhere on the body (Jereb & Roper 2010).

Despite this uncommon symmetry, it is not possible to use this character for phylogenetic assertions because the high diversity of bioluminescence observed in extant cephalopods indicates that this feature has multiple independent evolutionary origins (Haddock *et al.* 2010). Within Octobrachia, bioluminescence has been identified as evolving independently in three lineages: in one incirrate family Bolitaenidae, the cirrates, and also in the *Vampyroteuthis* clade (Lindgren *et al.* 2012).

Lifestyle implications

Ink sac. The oldest confirmed record of the ink sac is linked with fossils from Upper Carboniferous Lagerstätte sediments (Nishiguchi & Mapes 2008; Doguzhaeva & Mapes 2017), indicating that inking behaviours have long been used in coleoid lineages. The use of ink is a distinctive part of extant coleoid behaviour, with taxa using concealment and confusion as a means to avoid predators (Bush & Robison 2007; Nixon 2011; Derby 2014). The use of ink has also been proposed as a chemical deterrent or disruptor (Bush & Robison 2007) or as a conspecific alarm cue (Derby 2014). The various forms of the ejected ink (including clouds, pseudomorphs and ropes), are associated with different defence strategies that include either direct escape or crypsis (Bush & Robison 2007).

Many taxa in extant lineages have lost their ink sac (Strugnell *et al.* 2014), including deep-water species, and a potential correlation between loss of ink sac and habitat depth has been explored (Allcock & Piertney 2002; Bush & Robison 2007). However, ink has been observed to be used by many coleoid species that inhabit dark, deep-sea conditions in addition to bright-light and low-light environments (10.6–1842.1 m) (Bush & Robison 2007; Derby 2014; Strugnell *et al.* 2014). Most occurrences are in the mesopelagic zone (200–1000 m), where *c.* 99% of the surface light is attenuated (Bush & Robison 2007). The use of ink in these aphotic conditions indicates that ink is not only a visual cue, but supports the hypothesis that its chemical composition also plays a role in predator evasion (Bush & Robison 2007; Miller *et al.* 2014; Strugnell *et al.* 2014). The loss of ink sac is also observed in some shallow-water forms. Rather than rely on this character for crypsis, these photic species use alternate methods of obfuscation such as aposematic colours, or other decoy behaviours (Strugnell *et al.* 2014).

Luminous organs. Extant coleoids also use bioluminescence as a form of crypsis, and as an effective visual cue and method of communication. It is common in groups that inhabit meso- and bathypelagic depths (Bush & Robison 2007), and shapes ecologic and social interactions (Young & Roper 1977; Young 1983; Herring 1988, 1994; McFall-Ngai 1990; Haddock *et al.* 2010). Unlike acoustic forms of signalling, bioluminescence can be directed (e.g. it is commonly ventrally located for countershading), and can be detected across great distances (Young & Roper 1977; Young 1983; Herring 1994).

The combination of ink and luminescence in the same animal is observed in some extant taxa. For example, some cranchids fill their transparent mantle cavities with ink and then use their photophores to counter-illuminate shadows from their eyes, digestive gland and ink sac to avoid predators below (Bush & Robison 2007). The presence of luminous organs and an ink sac in MNHN.F.A32491 indicates that these types of antipredation behaviours were also used in the Jurassic (Fig. 10).

Sucker cavities. The peripheral location of the ovoid-shaped sucker cavities suggests that they are not likely to be remnants of sucker rings, which are known from the internal perimeter of some decabrachians (Young & Vecchione 1996; Young *et al.* 1998; Fuchs *et al.* 2021). Indeed, no residual evidence of sucker rings is observed. Furthermore, the size and configuration seem inconsistent with the cavities being the remainder of infundibular pegs such as those seen on the oral sucker surface in some extant forms (Nixon & Young 2003). They have also been observed in the suckers of other fossil specimens from the La Voulte-sur-Rhône locality (Rowe *et al.* 2022). The cavities are not restricted only to the suckers in MNHN.F.A32491, but are also present in soft tissues of the arm crown (Figs 5B, 8).

These somewhat resemble Kölliker's organs seen in some extant octopod juveniles, however, in the extant forms the Kölliker's organs are present in both the arm

FIG. 10. Hypothesized reconstruction of *Vampyrofugiens atramentum* gen. et sp. nov. based on the data from this study (A. Lethiers, CR2P).

and mantle tissues, and disappear by the sub-adult stage (Brocco *et al.* 1974; Nixon & Young 2003; Villanueva *et al.* 2021). In MNHN.F.A32491 these are preserved only on the arm crown. Without further diagnostic information, we interpret the cavities on the suckers and the arms as a manifestation of degraded epithelial tissue.

Lifestyle implications for Vampyrofugiens atramentum. The mosaic of characters in MNHN.F.A32491 provide insight into the palaeoenvironment and complex ecological networks at La Voulte-sur-Rhône during the Middle Jurassic.

A synthesis of the geology and fossil fauna from the locality (Charbonnier 2009) indicated that it probably represented a deep, bathyal environment, probably situated around the slope–basin transition of the Ardèche margin to the Rhône basins. However, the diverse ecology of selected taxa from the site has raised questions regarding the palaeoenvironmental interpretation. These include work on *Dollocaris*, a thylacocephalan arthropod (Vannier *et al.* 2016), and *Voulteryon parvulus* (Audo *et al.* 2019), a polychelid lobster, both common to the locality. Specifically, *Dollocaris* has a combination of characters that indicate that it was a nektobenthic visual hunter, and therefore inhabited an illuminated setting. Similarly, a shallow-water palaeoenvironment is assumed for *Voulteryon parvulus*. However, the presence of episymbiotic thecideoid brachiopods, which are associated with dimly lit environments, on the carapace of the species suggests that La Voulte-sur-Rhône records a combination of settings that is consistent with its complex geology (Audo *et al.* 2019). Fossil assemblages from the site may reflect the various environments inhabited by the local fauna, while also recording temporal shifts in ecological affinities for some of the associated taxa. As an example, today stalked crinoids are restricted to deep marine environments, although during the Mesozoic they were living also in shallow marine settings (Charbonnier *et al.* 2014; Whittle *et al.* 2018).

A reappraisal of the soft tissues of three coleoid specimens (*Vampyronassa rhodanica*) identified a combination of morphological characters that indicate that the species had a pelagic lifestyle in the La Voulte-sur-Rhône setting, and occupied a predatory niche (Rowe *et al.* 2022). The mosaic of characters in *V. atramentum* highlight that it used both predatory and defensive strategies, with a combination of defence mechanisms so far unknown from the fossil record.

The presence of an ink sac (Figs 1B, C, 3A, 10) indicates that *V. atramentum* was likely to be prey to contemporaneous taxa and used concealment as a tool for evasion. Its photophores (Figs 3, 10) suggest that it used bioluminescence as a form of obfuscation and communication (Young & Roper 1977; Young 1983; Herring 1988, 1994; McFall-Ngai 1990; Bush & Robison 2007; Haddock *et al.* 2010). The anterior–posterior symmetry of these internal light organs has not previously been described from the fossil record and is limited today to only a few extant oegopsiid Decabrachia. These extant forms include *Onychoteuthis banksii* and

Pterygioteuthis microlampas, which are both known to inhabit epi-mesopelagic waters (Jereb & Roper 2010). Given the multiple evolutionary origins of bioluminescence and the convergent link with a pelagic lifestyle (Lindgren *et al.* 2012), it is possible that the photophores in these three species arose due to similar selective pressures.

The configuration of the arms and suckers in *V. atramentum* in conjunction with the sensory functionality of the cirri (Fig. 5A, C), suggests that it used both to detect and capture prey. The absence of a differentiated arm crown, like those seen in other genera (*Gramadella piveteaui*, *Proteroctopus ribeti* and *Vampyronassa rhodanica*) from the locality, however, indicates a less specialized usage (Fischer & Riou 1982, 2002; Kruta *et al.* 2016; Rowe *et al.* 2022). It is likely that the manipulation strategies used by *V. atramentum* were similar to those seen in extant Octobrachia given that the internal arm musculature mirrors that present in the extant eight-armed group (Fig. 6). This is the first evidence of this type of arm musculature preserved in Jurassic forms.

Not only does the description of this new taxon increase the known coleoid diversity at La Voulte-sur-Rhône, but the different co-occurring lifestyles seen in the coleoid fauna from the locality suggest a high diversity of ecological niches occupied by cephalopods. Of the octobrachiate coleoids from La Voulte-sur-Rhône, three of the seven genera have previously been described with an ink sac. As discussed by Kruta *et al.* (2016), taphonomy could play a role in whether or not this feature is preserved, but given the exceptional preservation at the site, it is likely that this reflects the original anatomy. The La Voulte-sur-Rhône genera described with an ink sac include two prototeuthids, *Romaniteuthis* and *Rhomboteuthis* (Family: Plesioteuthidae) (Fischer & Riou 1982; Fischer 2003) and the loligosepiid *Mastigophora* (Family: Mastigophoridae) (Fuchs 2014). The addition of this new loligosepiid, *V. atramentum*, indicates this character was more prevalent in this locality than previously understood. Furthermore, of the two diagnostic sucker attachments, those that are clearly attached to the arm musculature and those that are not (Young & Vecchione 1996; Lindgren *et al.* 2004; Whalen & Landman 2022), *V. atramentum* possessed the latter (Fig. 7A–D). Today, this is known in only one species, *Vampyroteuthis infernalis*, but the latter attachment type was also present in *Vampyronassa rhodanica* (Rowe *et al.* 2022). The presence of this character in two species from La Voulte-sur-Rhône shows that it was more widespread in Jurassic vampyromorphs than it is today.

If all of the coleoids described from La Voulte-sur-Rhône inhabited the same area, then the ecological network was highly structured, with well demarcated niches. Some species were more specialized to predatory behaviours, and others to defensive behaviours; those with high swimming abilities probably occupied pelagic settings, while others were more nektobenthic. The co-occurrence of forms with traits reflecting adaptation to varied light conditions emphasizes the complexity of the palaeoenvironments.

CONCLUSION

The use of high-resolution imaging techniques, PPC-SR-μCT and RTI, provides new observational data on the soft tissues, internal organs and gladius of an unpublished vampyromorph specimen (MNHN.F.A32491) from La Voulte-sur-Rhône.

The imaging shows that the individual had an Octobrachia-type arm configuration and musculature, *Vampyroteuthis*-like sucker attachments, an ink sac, and two internal light organs with anterior–posterior symmetry. The combination of the ink sac and internal luminous organs is known from the Recent, although not from fossil coleoids. Additionally, the observed gladius morphology in MNHN.F.A32491 differs from previously described coleoids and therefore justifies the assignment of this individual to a new taxon, *Vampyrofugiens atramentum* gen. et sp. nov.

Acknowledgements. We are grateful to Fernando Ángel Fernández-Álvarez for thoughtful discussion regarding extant Ommastrephidae, to Alexandre Lethiers (CR2P) for the figures, illustrations and hypothesized reconstruction, and to Evariste Monvoisin who contributed to the preliminary analysis of the scans, and to P. Loubry for the photograph of the specimen. Thanks also go to the team on the AST-RX platform (plateau d'Accès Scientifique à la Tomographie à Rayons X du MNHN, UAR 2700 2 AD CNRS) Paris, for providing the initial scans of MNHN.F.A32491. In addition to preliminary analyses, these were used to support the synchrotron proposal for further tomographic imaging. We acknowledge the European Synchrotron Radiation Facility for provision of synchrotron radiation facilities (Proposal ES36), and Vincent Fernandez for his help as a local contact during the acquisition and storing of the data. Additionally, we thank Olivier Bethoux and Valentin Buffa for assistance with the reflectance transformation imaging data collection. We also thank Christian Klug and Dirk Fuchs for their reviews of the manuscript.

Author contributions. **Conceptualization** I. Kruta (IK), I. Rouget (IR), A. J. Rowe (AJR); **Investigation** AJR; **Visualization** AJR, A. Lethiers, P. Loubry; **Writing – Original Draft Preparation** AJR; **Writing – Review & Editing** AJR, IK, IR, L. Villier.

DATA ARCHIVING STATEMENT

This published work and the nomenclatural acts it contains, have been registered in ZooBank: https://zoobank.org/References/49A109A7-4ED7-4106-AEFD-70750E1D4DB1.

PPC-SR-μCT scan data and μCT scan data for MNHN.F.A32491 are archived at the European Synchrotron Radiation Facility (ESRF), Grenoble (http://paleo.esrf.fr/), and the Muséum national d'Histoire naturelle (MNHN), Paris (http://coldb.mnhn.fr/catalognumber/mnhn/f/a32491), respectively. RTI data are available here: https://doi.org/10.48579/PRO/QIYKGW.

Editor. Dieter Korn

REFERENCES

ALLCOCK, A. L. and PIERTNEY, S. 2002. Evolutionary relationships of Southern Ocean Octopodidae (Cephalopoda: Octopoda) and a new diagnosis of *Pareledone*. *Marine Biology*, **140**, 129–135.

ALLISON, P. A. 1988. *Konservat-Lagerstätten:* cause and classification. *Paleobiology*, **14**, 331–344.

AUDO, D., SCHWEIGERT, G., MARTIN, J.-P. S. and CHARBONNIER, S. 2014. High biodiversity in Polychelida crustaceans from the Jurassic La Voulte-sur-Rhône Lagerstätte. *Geodiversitas*, **36**, 489–525.

AUDO, D., ROBIN, N., LUQUE, J., KROBICKI, M., HAUG, J. T., HAUG, C., JAUVION, C. and CHARBONNIER, S. 2019. Palaeoecology of *Voulteryon parvulus* (Eucrustacea, Polychelida) from the Middle Jurassic of La Voulte-sur-Rhône Fossil-Lagerstätte (France). *Scientific Reports*, **9**, 5332.

BOLSTAD, K. S. R. 2008. Systematics of the Onychoteuthidae Gray, 1847 (Cephalopoda: Oegopsida). PhD thesis, Auckland University of Technology, New Zealand, 259 pp.

BOLSTAD, K. S. R., VECCHIONE, M., YOUNG, R. E. and TSUCHIYA, K. 2019. *Onychoteuthis* Lichtenstein, 1818. The Tree of Life Web Project. http://tolweb.org/Onychoteuthis/19955/2019.03.26 [accessed 10 October 2022]

BRIGGS, D. E. and CROWTHER, P. R. 2008. *Palaeobiology II*. John Wiley & Sons.

BROCCO, S. L., O'CLAIR, R. M. and CLONEY, R. A. 1974. Cephalopod integument: the ultrastructure of Kölliker's organs and their relationship to setae. *Cell & Tissue Research*, **151**, 16.

BUSH, S. and ROBISON, B. 2007. Ink utilization by mesopelagic squid. *Marine Biology*, **152**, 485–494.

BUTCHER, S., DILLY, P. N. and HERRING, P. J. 1982. The comparative morphology of the photophores of the squid *Pyroteuthis margaritifera* (Cephalopoda: Enoploteuthidae). *Journal of Zoology*, **196**, 133–150.

CAVALLARO, M., BATTAGLIA, P., GUERRERA, M. C., ABBATE, F., LEVANTI, M. B., ANDALORO, F., GERMANÀ, A. and LAURÀ, R. 2017. New data on morphology and ultrastructure of skin photophores in the deep-sea squid *Histioteuthis bonnellii* (Férussac, 1834), Cephalopoda: Histioteuthidae. *Acta Zoologica*, **98**, 271–277.

CHARBONNIER, S. 2009. *Le Lagerstätte de La Voulte: Un environnement bathyal au Jurassique*, **199**. Mémoires du Muséum national d'Histoire naturelle.

CHARBONNIER, S., AUDO, D., CAZE, B. and BIOT, V. 2014. The La Voulte-sur-Rhône Lagerstätte (Middle Jurassic, France). *Comptes Rendus Palevol*, **13**, 369–381.

CHARBONNIER, S., VANNIER, J., GAILLARD, C., BOURSEAU, J.-P. and HANTZPERGUE, P. 2007. The La Voulte Lagerstätte (Callovian): evidence for a deep water setting from sponge and crinoid communities. *Palaeogeography, Palaeoclimatology, Palaeoecology*, **250**, 216–236.

CLEMENTS, T., COLLEARY, C., DE BAETS, K. and VINTHER, J. 2017. Buoyancy mechanisms limit preservation of coleoid cephalopod soft tissues in Mesozoic Lagerstätten. *Palaeontology*, **60**, 1–14.

DERBY, C. D. 2014. Cephalopod ink: production, chemistry, functions and applications. *Marine Drugs*, **12**, 2700–2730.

DOGUZHAEVA, L. A. and MAPES, R. H. 2017. A new late Carboniferous coleoid from Oklahoma, USA: implications for the early evolutionary history of the subclass Coleoidea (Cephalopoda). *Journal of Paleontology*, **92**, 157–169.

DOYLE, P. 1990. Teuthid cephalopods from the Lower Jurassic of Yorkshire. *Palaeontology*, **33**, 193–207.

ENGESER, T. and REITNER, J. 1985. Teuthiden aus dem Unterapt (»Töck«) von Helgoland (Schleswig-Holstein, Norddeutschland). Teuthids from the early aptian ("Töck") of Heligoland (Schleswig-Holstein, North Germany). *Paläontologische Zeitschrift*, **59**, 245–260.

ENGESER, T. and KEUPP, H. 1997. Zwei neue Gattungen und eine neue Art von vampyromorphen Tintenfischen (Coleoidea, Cephalopoda) aus dem Untertithonium von Eichstätt. *Archaeopteryx*, **15**, 47–58.

FEINSTEIN, N., NESHER, N. and HOCHNER, B. 2011. Functional morphology of the neuromuscular system of the *Octopus vulgaris* arm. *Vie et Milieu*, **61**, 219–229.

FISCHER, J.-C. 2003. Invertébrés remarquables du Callovien inférieur de la Voulte-sur-Rhône (Ardèche, France). *Annales de Paléontologie*, **89**, 223–252.

FISCHER, J.-C. and RIOU, B. 1982. Les teuthoïdes (Cephalopoda, Dibranchiata) du Callovien inférieur de la Voulte-sur-Rhône (Ardèche, France). *Annales de Paléontologie*, **68**, 295–325.

FISCHER, J.-C. and RIOU, B. 2002. *Vampyronassa rhodanica* nov. gen. nov. sp., vampyromorphe (Cephalopoda, Coleoidea) du Callovien inférieur de la Voulte-sur-Rhône (Ardèche, France). *Annales de Paléontologie*, **88**, 1–17.

FUCHS, D. 2006. Fossil erhaltungsfahige Merkmalskomplexe der Coleoidea (Cephalopoda) und ihre phylogenetische Bedeutung. *Berliner Palaobiologische Abhandlungen*, **8**, 1–122.

FUCHS, D. 2007. Coleoid cephalopods from the plattenkalks of the Upper Jurassic of Southern Germany and from the Upper Cretaceous of Lebanon: a faunal comparison. *Neues Jahrbuch für Geologie und Paläontologie – Abhandlungen*, **245**, 59–69.

FUCHS, D. 2014. First evidence of *Mastigophora* (Cephalopoda: Coleoidea) from the early Callovian of La Voulte-sur-Rhône (France). *Göttingen Contributions to Geosciences*, **77**, 21–27.

FUCHS, D. 2016. Part M: The gladius and gladius vestige in fossil coleoidea. *Treatise Online*, **83**, 1–23.

FUCHS, D. 2020. Part M: Systematic descriptions: Octobrachia. *Treatise Online*, **138**, 1–52.

FUCHS, D. and WEIS, R. 2008. Taxonomy, morphology and phylogeny of Lower Jurassic loligosepiid coleoids (Cephalopoda). *Neues Jahrbuch für Geologie und Paläontologie, Abhandlungen*, **249**, 93–112.

FUCHS, D., KLINGHAMMER, A. and KEUPP, H. 2007. Taxonomy, morphology and phylogeny of plesioteuthidid coleoids from the Upper Jurassic (Tithonian) Plattenkalks of Solnhofen. *Neues Jahrbuch für Geologie und Paläontologie, Abhandlungen*, **245**, 239–252.

FUCHS, D., VON BOLETZKY, S. and TISCHLINGER, H. 2010. New evidence of functional suckers in belemnoid coleoids (Cephalopoda) weakens support for the 'Neocoleoidea' concept. *Journal of Molluscan Studies*, **76**, 404–406.

FUCHS, D., KEUPP, H. and SCHWEIGERT, G. 2013. First record of a complete arm crown of the Early Jurassic coleoid Loligosepia (Cephalopoda). *Paläontologische Zeitschrift*, **87**, 431–435.

FUCHS, D., HOFFMANN, R. and KLUG, C. 2021. Evolutionary development of the cephalopod arm armature: a review. *Swiss Journal of Palaeontology*, **140**, 1–27.

HADDOCK, S. H. D., MOLINE, M. A. and CASE, J. F. 2010. Bioluminescence in the sea. *Annual Review of Marine Science*, **2**, 443–493.

HAECKEL, E. H. P. A. 1866. *Generelle morphologie der organismen. Allgemeine grundzüge der organischen formen-wissenschaft, mechanisch begründet durch die von Charles Darwin reformirte descendenztheorie, von Ernst Haeckel*. G. Reimer, Berlin.

HERRING, P. J. 1988. Luminescent organs. 449–489. *In* TRUEMAN, E. R. and CLARKE, M. R. (eds) *Form and function*, **11**. Academic Press.

HERRING, P. J. 1994. Reflective systems in aquatic animals. *Comparative Biochemistry & Physiology*, **109**, 513–546.

HERRING, P. J., DILLY, P. N. and COPE, C. 1992. Different types of photophore in the oceanic squids *Octopoteuthis* and *Taningia* (Cephalopoda: Octopoteuthidae). *Journal of Zoology*, **227**, 479–491.

HERRING, P. J., DILLY, P. N. and COPE, C. 1994. The bioluminescent organs of the deep-sea cephalopod *Vampyroteuthis infernalis* (Cephalopoda: Vampyromorpha). *Journal of Zoology*, **233**, 45–55.

JAUVION, C. 2020. De la vie à la pierre: préservation exceptionnelle d'arthropodes marins fossiles. PhD thesis, Muséum national d'Histoire naturelle, Paris, 223 pp.

JAUVION, C., AUDO, D., CHARBONNIER, S. and VANNIER, J. 2016. Virtual dissection and lifestyle of a 165-million-year-old female polychelidan lobster. *Arthropod Structure & Development*, **45**, 122–132.

JAUVION, C., CHARBONNIER, S. and BERNARD, S. 2017. A new look at the shrimps (Crustacea, Decapoda, Penaeoidea) from the Middle Jurassic La Voulte-sur-Rhone Lagerstatte. *Geodiversitas*, **39**, 705–716.

JAUVION, C., AUDO, D., BERNARD, S., VANNIER, J., DALEY, A. and CHARBONNIER, S. 2020. A new polychelidan lobster preserved with its eggs in a 165 Ma nodule. *Scientific Reports*, **10**, 3574.

JELETZKY, J. A. 1965. Taxonomy and phylogeny of fossil Coleoidea (= Dibranchiata). *Geological Survey of Canada, Papers*, **65**, 76–78.

JEREB, P. and ROPER, C. F. 2010. *Cephalopods of the world: An annotated and illustrated catalogue of cephalopod species known to date. Volume 2. Myopsid and oegopsid squids*. FAO Species Catalogue for Fishery Purposes, No. 4, Vol. 2., Rome.

KLUG, C., SCHWEIGERT, G., DIETL, G. and FUCHS, D. 2005. Coleoid beaks from the Nusplingen Lithographic Limestone (Upper Kimmeridgian, SW Germany). *Lethaia*, **38**, 173–192.

KLUG, C., FUCHS, D., SCHWEIGERT, G., RÖPER, M. and TISCHLINGER, H. 2015. New anatomical information on arms and fins from exceptionally preserved *Plesioteuthis* (Coleoidea) from the Late Jurassic of Germany. *Swiss Journal of Palaeontology*, **134**, 245–255.

KLUG, C., SCHWEIGERT, G., FUCHS, D. and DE BAETS, K. 2021. Distraction sinking and fossilized coleoid predatory behaviour from the German Early Jurassic. *Swiss Journal of Palaeontology*, **140**, 7.

KOŠŤÁK, M., SCHLÖGL, J., FUCHS, D., HOLCOVÁ, K., HUDÁČKOVÁ, N., CULKA, A., FÖZY, I., TOMAŠOVÝCH, A., MILOVSKÝ, R., ŠURKA, J. and MAZUCH, M. 2021. Fossil evidence for vampire squid inhabiting oxygen-depleted ocean zones since at least the Oligocene. *Communications Biology*, **4**, 216.

KRÖGER, B., VINTHER, J. and FUCHS, D. 2011. Cephalopod origin and evolution: a congruent picture emerging from fossils, development and molecules. *BioEssays*, **33**, 602–613.

KRUTA, I., ROUGET, I., CHARBONNIER, S., BARDIN, J., FERNANDEZ, V., GERMAIN, D., BRAYARD, A. and LANDMAN, N. 2016. *Proteroctopus ribeti* in coleoid evolution. *Palaeontology*, **59**, 767–773.

LINDGREN, A. R., GIRIBET, G. and NISHIGUCHI, M. K. 2004. A combined approach to the phylogeny of Cephalopoda (Mollusca). *Cladistics*, **20**, 454–486.

LINDGREN, A. R., PANKEY, M. S., HOCHBERG, F. G. and OAKLEY, T. H. 2012. A multi-gene phylogeny of Cephalopoda supports convergent morphological evolution in association with multiple habitat shifts in the marine environment. *BMC Evolutionary Biology*, **12**, 129.

LINDGREN, A. R., YOUNG, R. E. and MANGOLD, K. M. 2019. *Pyroteuthidae* Pfeffer, 1912. The fire squid. The Tree of Life Web Project. http://tolweb.org/Pyroteuthidae/19637/2019.03.26 [accessed 10 October 2022]

MARROQUÍN, S. M., MARTINDALE, R. C. and FUCHS, D. 2018. New records of the late Pliensbachian to early Toarcian (Early Jurassic) gladius-bearing coleoid cephalopods from the Ya Ha Tinda Lagerstätte, Canada. *Papers in Palaeontology*, **4**, 245–276.

McFALL-NGAI, M. J. 1990. Crypsis in the pelagic environment. *American Zoologist*, **30**, 175–188.

MEYER, H. V. 1834. *Leptoteuthis gigas. Museum Senckenbergianum, Abhandlungen*, **1**, 286–287.

MILLER, M., MIWA, T., MOCHIOKA, N., WATANABE, S., YAMADA, Y., FUKUBA, T. and TSUKAMOTO, K. 2014. Now you see me, now you don't: observation of a squid hiding in its ink trail. *Marine Biodiversity*, **45**, 149–150.

MÜNSTER, G. Z. 1846. Ueber die schalenlosen Cephalopoden des oberen Juragebirges, der lithographischen Kalkschiefern von Bayern. *Beiträge zur Petrefaktenkunde*, **7**, 51–65.

NAEF, A. 1921. Das System der dibranchiaten Cephalopoden und die mediterranen Arten derselben. *Mittheilungen aus der Zoologischen Station zu Neapal*, **22**, 527–542.

NISHIGUCHI, M. K. and MAPES, R. 2008. Cephalopoda. 163–199. *In* PONDER, W. (ed.) *Phylogeny and evolution of the Mollusca*. University of California Press.

NIXON, M. 2011. Part M: Anatomy of recent forms. *Treatise Online*, **17**, 1–49.

NIXON, M. and YOUNG, J. Z. 2003. *The brains and lives of cephalopods*. Oxford University Press.

NÖDL, M.-T., FOSSATI, S. M., DOMINGUES, P., SÁNCHEZ, F. J. and ZULLO, L. 2015. The making of an octopus arm. *EvoDevo*, **6**, 19.

OWEN, R. 1856. *Descriptive catalogue of the fossil organic remains of Invertebrata contained in the Museum of the Royal College of Surgeons of England*. Taylor & Francis.

PICKFORD, G. E. 1949. *Vampyroteuthis infernalis* Chun: an archaic dibranchiate cephalopod. II. External anatomy. *Dana Reports*, **32**, 1–132.

QUENSTEDT, F. A. 1839. *Loligo Bollensis* ist kein Belemniten-Organ. *Neues Jahrbuch für Mineralogie, Geognosie, Geologie und Petrefakten-Kunde*, **1839**, 156–167.

REGTEREN ALTENA, C. O. VAN 1949. *Systematic catalogue of the palaeontological collection: Sixth supplement (Teuthoidea)*. Teyler's Museum.

ROBISON, B. H., REISENBICHLER, K. R., HUNT, J. C. and HADDOCK, S. H. D. 2003. Light production by the arm tips of the deep-sea cephalopod *Vampyroteuthis infernalis*. *Biological Bulletin*, **205**, 102–109.

ROBSON, G. C. 1929. On the rare abyssal octopod *Melanoteuthis beebei* (sp. n.): a contribution to the phytogeny of the Octopoda. *Proceedings of the Zoological Society of London*, **99**, 469–486.

ROUGET, I., ROWE, A. and KRUTA, I. 2022. Image acquisition of specimen MNHN.F.A32491from La Voulte-sur-Rhône (*Vampyrofugiens* nov. gen. *atramentum* nov. sp.). https://doi.org/10.48579/PRO/QIYKGW

ROWE, A. J., KRUTA, I., LANDMAN, N. H., VILLIER, L., FERNANDEZ, V. and ROUGET, I. 2022. Exceptional soft-tissue preservation of Jurassic *Vampyronassa rhodanica* provides new insights on the evolution and palaeoecology of vampyroteuthids. *Scientific Reports*, **12**, 8292.

STRUGNELL, J. M., NORMAN, M. D., VECCHIONE, M., GUZIK, M. and ALLCOCK, A. L. 2014. The ink sac clouds octopod evolutionary history. *Hydrobiologia*, **725**, 215–235.

SUTTON, M., PERALES-RAYA, C. and GILBERT, I. 2016. A phylogeny of fossil and living neocoleoid cephalopods. *Cladistics*, **32**, 297–307.

VANNIER, J., SCHOENEMANN, B., GILLOT, T., CHARBONNIER, S. and CLARKSON, E. 2016. Exceptional preservation of eye structure in arthropod visual predators from the Middle Jurassic. *Nature Communications*, **7**, 10320.

VILLANUEVA, R., COLL-LLADÓ, M., BONNAUD-PONTICELLI, L., CARRASCO, S. A., ESCOLAR, O., FERNÁNDEZ-ÁLVAREZ, F. Á., GLEADALL, I. G., NABHITABHATA, J., ORTIZ, N., ROSAS, C., SÁNCHEZ, P., VOIGHT, J. R. and SWOGER, J. 2021. Born with bristles: new insights on the Kölliker's organs of octopus skin. *Frontiers in Marine Science*, **8**, 645738.

VILLIER, L., CHARBONNIER, S. and RIOU, B. 2009. Sea stars from Middle Jurassic Lagerstätte of La Voulte-sur-Rhône (Ardèche, France). *Journal of Paleontology*, **83**, 389–398.

WHALEN, C. D. and LANDMAN, N. H. 2022. Fossil coleoid cephalopod from the Mississippian Bear Gulch Lagerstätte sheds light on early vampyropod evolution. *Nature Communications*, **13**, 1107.

WHITTLE, R. J., HUNTER, A. W., CANTRILL, D. J. and McNAMARA, K. J. 2018. Globally discordant Isocrinida (Crinoidea) migration confirms asynchronous Marine Mesozoic Revolution. *Communications Biology*, **1**, 46.

WILBY, P. R., BRIGGS, D. E. G. and RIOU, B. 1996. Mineralization of soft-bodied invertebrates in a Jurassic metalliferous deposit. *Geology*, **24**, 847–850.

WILBY, P. R., HUDSON, J. D., CLEMENTS, R. G. and HOLLINGWORTH, N. T. J. 2004. Taphonomy and origin of an accumulate of soft-bodied cephalopods in the Oxford Clay Formation (Jurassic, England). *Palaeontology*, **47**, 1159–1180.

YOUNG, R. E. 1983. Oceanic bioluminescence: an overview of general functions. *Bulletin of Marine Science*, **33**, 829–845.

YOUNG, R. E. and ROPER, C. F. E. 1977. Intensity regulation of bioluminescence during countershading in living midwater animals. *Fishery Bulletin*, **75**, 239–252.

YOUNG, R. E. and VECCHIONE, M. 1996. Analysis of morphology to determine primary sister-taxon relationships within coleoid cephalopods. *American Malacological Bulletin*, **12**, 91–112.

YOUNG, R. E., VECCHIONE, M. and DONOVAN, D. T. 1998. The evolution of coleoid cephalopods and their present biodiversity and ecology. *South African Journal of Marine Science*, **20**, 393–420.

ZIEGLER, A., BOCK, C., KETTEN, D. R., MAIR, R. W., MUELLER, S., NAGELMANN, N., PRACHT, E. D. and SCHRÖDER, L. 2018. Digital three-dimensional imaging techniques provide new analytical pathways for malacological research. *American Malacological Bulletin*, **36**, 248–273.

DISCUSSION

3.6 ~ LIMITATION OF THE LAGERSTÄTTE FOSSILS AND THE IMAGING TOOLS

The work completed on *Vampyronassa* and *Vampyrofugiens* clearly shows the benefits of these 3D tomographic methods and the level of resolution they can uncover; however, these techniques also bring with them some limitations. In the studied specimens, the exact boundaries of internal structures were often difficult to determine. Larger and denser organs, such as the digestive gland, ink sac, luminous organs, and eyes, typically provided the clearest contrast boundaries for rendering, though some of the more detailed anatomy, the characters states of which are utilized in existing morphological matrices (e.g., gill lamellae attachment, or posterior salivary glands) (Kruta *et al.* 2016; Sutton *et al.* 2016; Whalen & Landman 2022), or habitat determination (e. g., Voss & Sweeney 1998; Nixon & Young 2003; Boyle & Rodhouse 2008; Hanlon & Messenger 2018), lacked the contrast for clear identification. This difficulty can be attributed to lack of preservation of the specimen, taphonomic processes (specimens are rarely preserved in an ideal lateral or dorsal anatomical position and are frequently compacted or twisted prior to fossilization), and the scan resolution on the sample.

In the most recent morphological matrix of Whalen & Landman (2022) 75 of the 153 characters are represented by the gladius (49%), and the remaining 78 (51%) relate to the soft tissues. In this matrix, the gladius of *V. rhodanica* is coded for 23 characters, and 22 are coded with a "?"; twenty soft tissues have coded character states, while 49 remain unknown ("?"). The work completed for Rowe *et al.* 2022 was able to add distinct states to 4 characters in the previous matrix (Sutton *et al*. 2016), that were all related to the suckers and sucker attachments. A new character (#95, the presence or absence of sucker hooks) in the matrix (Whalen & Landman 2022) can also be coded with the *V. rhodanica* data. The data gathered for the new taxon, *V. atramentum* provides information on 32 of the soft tissue character states.

It was not possible to contribute to character states of the gladius in *V. rhodanica* as the structure was not clearly visible in any of the individuals studied. Indeed, a limitation associated with gladius-bearing coleoids from La Voulte-sur-Rhône is the general poor visibility of gladius material. The combination of X-ray tomography and RTI imaging on *V. atramentum* was able to give enough gladius detail to contribute to the assignment of a new taxon (Rowe *et al.* 2023).

The tomography was able to identify internal remnants of the gladius structure, and the RTI enabled us to interpret the external topography. As discussed in Chapter 1, the absence of clear gladius morphology from the La Voulte-sur-Rhône contributes to the amount of *incertae sedis* taxa from the locality.

The morphology and tissues we identified in these two vampyromorph species were better suited to palaeoecological and behavioral interpretation. This work provided evidence that soft tissue characters were already morphologically diverse in the Jurassic and indicates a structured ecological network in the La Voulte-sur-Rhône environment. While the coleoid faunal assemblage constitutes considerate Mesozoic diversity, little is known about intraspecific variation. Except for *Vampyronassa*, all the coleoid taxa at La Voulte are represented by very few specimens.

3.7 New insight on ecology

The general anatomical disparity reflected in the La Voulte coleoids, and morphological comparisons with modern analogues, supports the hypothesis that ecological niches varied between the co-occurring species (Fischer & Riou 1982*a*, 2002; Fischer 2003, Charbonnier 2009; Fuchs 2014; Kruta *et al.* 2016; Rowe *et al.* 2022, 2023). For example, the two prototeuthids, *Romaniteuthis* and *Rhomboteuthis*, have a narrow fusiform body and well-developed posterior fins (Sayn & Roman 1928, Fischer & Riou 1982*b*; Charbonnier 2009; Fuchs 2020), and superficially resembled modern day squids (Decabrachia); indeed, both genera have been referred to as squid in the literature (e.g., Fischer 2003; Charbonnier 2009) though their eight arms dictate they are Octobrachia (Bandel & Leich 1986; Fuchs 2020). Their streamlined shape and posterior fins are typical today in epipelagic squid, which are fast swimmers (Fischer 2003) and active predators that prey mainly on fish and crustaceans (Fischer 2003; Boyle & Rodhouse 2008; Charbonnier 2009). Both species have also preserved an ink sac (Fischer & Riou 1982*a*; Fischer 2003) suggesting they also needed to employ crypsis to avoid prey. *Proteroctopus ribeti* has a more ovoid body shape with posterior fins, a differentiated arm crown with a longer dorsal pair, biserial suckers and cirri. Kruta *et al.* (2016) identified *P. ribeti* as an ancestral Octobrachia, which are described as somewhat morphologically similar to modern cirrates (Young & Vecchione 1996; Collins & Villanueva 2006). With the exception of two shallow water species, extant cirrates typically inhabit deeper

waters (> 300 m) living close to the sea floor (Collins & Villanueva 2006). They prey on small, slow swimming organisms including amphipods, polychaetes, and small bivalves (Boyle & Rodhouse 2008; Villanueva *et al.* 2017) and are predated on by sharks and teleost fishes (Collins & Villanueva 2006; Boyle & Rodhouse 2008).

As discussed by Rowe *et al.* (2022, 2023) *Vampyronassa* and *Vampyrofugiens* were also pelagic predatory species. The differentiated arm crown configuration in *Vampyronassa* indicates specialized function between the arms, and the lack of luminous organs and ink sac suggest it relied less on crypsis than *Vampyrofugiens,* which possessed both these features. Ink sacs are also described from *Mastigophora* (Fuchs 2014), the fusiform-shaped *Romaniteuthis* and *Rhomboteuthis* (Fischer & Riou 1982*a*), and *Gramadella* (Fischer & Riou 1982a) which also has differentiated arm crown (Fischer & Riou 1982*a*).

The abundance and exceptional preservation of the coleoid fauna at La Voulte suggests that the group was indigenous to the site and living in the water column (Fischer 2003, Charbonnier 2009). Multiple feeding strategies have been identified from the site based on the overall fauna, including filter feeders (bivalves), microphagy (brachiopods and ammonoid cephalopods); detritus feeders (e.g., annelids, crustaceans, echinoderms); sediment feeders (e.g., annelids, crustaceans) and predatory carnivores (e.g., coleoids, crustaceans, fish, and reptiles) (Fischer 2003; Charbonnier 2009). As part of the La Voulte-sur-Rhône palaeocosystem, gladius-bearing coleoids were likely predatory carnivores, preying upon the abundant crustacean fauna, small fish and other smaller coleoids. In turn the younger cephalopods were probably prey for the larger crustaceans, fish, and reptiles.

3.8. Perspectives

Only three of the coleoid taxa from La Voulte-sur-Rhône, *Proteroctopus ribeti*, *Vampyronassa rhodanica*, and *Vampyrofugiens atramentum*, have been reappraised using high-resolution imaging techniques (Kruta *et al.* 2016; Rowe *et al.* 2022, 2023). Given the large amounts of data preserved in these genera, it seems logical that future work should focus on reassessing the remaining coleoid taxa (*Romaniteuthis, Rhomboteuthis, Mastigophora, Gramadella*, and the undetermined Teudopsid forms) from the locality. Indeed, preliminary observations on existing tomographic scans reveal that the individuals would enhance the known diversity and contribute

to ecological interpretations. This has been the case with fossil arthropods from the locality, and tomographic work continues to reveal increasing novelties (e.g., Audo *et al.* 2014, 2019; Jauvion *et al.* 2016; Jauvion 2020). Descriptions of the unassigned Teudopsid gladii also indicate that we don't yet know the full extent of coleoid diversity at La Voulte-sur-Rhône.

The inherent issues with the current morphological matrix and lack of gladius information obtained from the locality, contributed to the decision to move away from phylogenetic assessment, and focus more on ecological and lifestyle questions. Further, the availability of specimens from the Lebanese limestones enabled the comparison of Mesozoic coleoids from a very different depositional environment. The large number of *Dorateuthis syriaca* Woodward 1883 individuals presented the opportunity to study not just the anatomy and behaviors of another species, but also allow for a robust study of intraspecific morphological variation.

BIBLIOGRAPHY

ALLISON, P. A. 1988. *Konservat-Lagerstätten:* cause and classification. *Paleobiology*, **14**, 331–344.

AUDO, D., SCHWEIGERT, G., MARTIN, J.-P. S. and CHARBONNIER, S. 2014. High biodiversity in Polychelida crustaceans from the Jurassic La Voulte-sur-Rhône Lagerstätte. *Geodiversitas*, **36**, 489–525.

———, ROBIN, N., LUQUE, J., KROBICKI, M., HAUG, J. T., HAUG, C., JAUVION, C. and CHARBONNIER, S. 2019. Palaeoecology of *Voulteryon parvulus* (Eucrustacea, Polychelida) from the Middle Jurassic of La Voulte-sur-Rhône Fossil-Lagerstätte (France). *Scientific Reports*, **9**, 5332.

BANDEL, K. and LEICH, H. 1986. Jurassic Vampyromorpha (dibranchiate cephalopods). *Neues Jahrbuch für Geologie und Paläontologie-Monatshefte*, **3**, 129–148.

BATHER, F. A. 1888. Shell-growth in Cephalopoda (Siphonopoda). *Journal of Natural History*, **1**, 298–309.

BRIGGS, D.E. and WILBY, P.R., 1996. The role of the calcium carbonate-calcium phosphate switch in the mineralization of soft-bodied fossils. *Journal of the Geological Society*, **153**(5), 665-668.

BOYLE, P. and RODHOUSE, P. 2008. *Cephalopods: ecology and fisheries*. John Wiley & Sons.

CHARBONNIER, S. 2009. *Le Lagerstätte de La Voulte: un environnement bathyal au Jurassique*. *Mémoires Du Muséum National d'Histoire Naturelle*. Vol. 199. Publications scientifiques du Muséum Paris.

———, AUDO, D., CAZE, B. and BIOT, V. 2014. The La Voulte-sur-Rhône Lagerstätte (Middle Jurassic, France). *Comptes Rendus Palevol*, **13**, 369–381.

———, VANNIER, J., GAILLARD, C., BOURSEAU, J.-P. and HANTZPERGUE, P. 2007. The La Voulte Lagerstätte (Callovian): Evidence for a deep water setting from sponge

and crinoid communities. *Palaeogeography, Palaeoclimatology, Palaeoecology*, **250**, 216–236.

COLLINS, M. and VILLANUEVA, R. 2006. Taxonomy, Ecology and Behaviour Of The Cirrate Octopods. *Oceanography and marine biology*, **44**, 277–322.

DOLLO, L. 1912. Les Céphalopodes adaptés à la vie nectique secondaire et benthique tertiaire. *Zoologisches Jahrbuch (Suppl.)* 15 (1): 105–140.

ELMI, S., 1967. Le Lias supérieur et le Jurassique moyen de l'Ardèche. *Documents des Laboratoires de Geolgie de la Faculte des Sciences de Lyon*, *19*,1-845.

ENGESER, T. and REITNER, J. 1985. Teuthiden aus dem Unterapt (»Töck«) von Helgoland (Schleswig-Holstein, Norddeutschland): Teuthids from the early aptian ("Töck") of heligoland (Schleswig-Holstein, North Germany). *Paläontologische Zeitschrift*, **59**, 245–260.

EUDES-DESLONGCHAMPS, M. 1835. Mémoire sur les Teudopsides, animaux fossiles, voisins des calmars. Mémoires de la Société Linnéenne de Normandie **5**:68–78.

FISCHER, J.-C. 2003. Invertébrés remarquables du Callovien inférieur de la Voulte-sur-Rhône (Ardèche, France). *Annales de Paléontologie*, **89**, 223–252.

——— and RIOU, B. 1982*a*. Le plus ancien octopode connu (Cephalopoda, Dibranchiata) : Proteroctopus ribeti nov. gen., nov. sp., du Callovien de l'Ardèche (France). Comptes Rendus de l'Académie des Sciences, Paris, 295 (II), 277–280.

——— and RIOU, B. 1982b. Les teuthoïdes (Cephalopoda, Dibranchiata) du Callovien inférieur de la Voulte-sur-Rhône (Ardèche, France). *Annales de Paléontologie*, **68**, 295–325.

——— and ———. 2002. *Vampyronassa rhodanica* nov. gen. nov sp., vampyromorphe (Cephalopoda, Coleoidea) du Callovien inférieur de la Voulte-sur-Rhône (Ardèche, France). *Annales de Paléontologie*, **88**, 1–17.

FUCHS, D. 2006*a*. Morphology, taxonomy and diversity of vampyropod coleoids (Cephalopoda) from the Upper Cretaceous of Lebanon. *Memorie della Società italiana di Scienze naturali e del Museo civico di Storia naturale di Milano*, **34**, 1–28.

———. 2006*b*. Fossil erhaltungsfahige Merkmalskomplexe der Coleoidea (Cephalopoda) und ihre phylogenetische Bedeutung. *Berliner Palaobiologische Abhandlungen*, **8**, 1–122.

FUCHS, D. 2014. First evidence of *Mastigophora* (Cephalopoda: Coleoidea) from the early Callovian of La Voulte-sur- Rhône (France). *Göttingen Contributions to Geosciences*, **77**, 21–27.

FUCHS, D. 2020. Treatise Online no. 138: Part M, Chapter 23G: Systematic Descriptions: Octobrachia. *Treatise Online*.

HAECKEL, E. H. P. A. 1866. *Generelle morphologie der organismen. Allgemeine grundzüge der organischen formen-wissenschaft, mechanisch begründet durch die von Charles Darwin reformirte descendenztheorie, von Ernst Haeckel.* G. Reimer, Berlin.

HANLON, R. T. and MESSENGER, J. B. 2018. *Cephalopod Behaviour*. Cambridge University Press.

HART, M. B., PAGE, K. N., PRICE, G. D. and SMART, C. W. 2019. Reconstructing the Christian Malford ecosystem in the Oxford Clay Formation (Callovian, Jurassic) of Wiltshire: exceptional preservation, taphonomy, burial and compaction. *Journal of Micropalaeontology*, **38**, 133–142.

JAUVION, C., CHARBONNIER, S. and BERNARD, S., 2017. A new look at the shrimps (Crustacea, Decapoda, Penaeoidea) from the Middle Jurassic La Voulte-sur-Rhône Lagerstätte. *Geodiversitas*, *39*(4), pp.705-716.

———, AUDO, D., CHARBONNIER, S. and VANNIER, J. 2016. Virtual dissection and lifestyle of a 165-million-year-old female polychelidan lobster. *Arthropod Structure & Development*, **45**, 122–132.

———, ———, BERNARD, S., VANNIER, J., DALEY, A. and CHARBONNIER, S. 2020. A new polychelidan lobster preserved with its eggs in a 165 Ma nodule. *Scientific Reports*, **10**, 1–7.

JELETZKY, J. A. 1965. Taxonomy and phylogeny of fossil Coleoidea (= Dibranchiata). *Geological Survey of Canada, Papers*, **65**, 76–78.

KRUTA, I., ROUGET, I., CHARBONNIER, S., BARDIN, J., FERNANDEZ, V., GERMAIN, D., BRAYARD, A. and LANDMAN, N. 2016. *Proteroctopus ribeti* in coleoid evolution. *Palaeontology*, **59**, 767–773.

LEACH, W. E. 1817. Synopsis of the orders, families, and genera of the class Cephalopoda. *The Zoological Miscellany, being descriptions of new or interesting animals*, **3**, 137.

NAEF, A., 1916. Systematische Ubersicht der mediterranen Cephalopoden. *Publ Staz Zool Napoli*, ***1***, 11-19.

NAEF, A., 1921. Das System der dibranchiaten Cephalopoden und die mediterranen Arten derselben. *Mitt. Zool. Stn. Neapel*, **22**, 527–542.

NIXON, M. and YOUNG, J. Z. 2003. *The Brains and Lives of Cephalopods*. Oxford University Press, Oxford.

OWEN, R. 1836. *The Cyclopaedia of Anatomy and Physiology: INS-PLA*. Vol. 3. Sherwood, Gilbert, and Piper.

REGTEREN ALTENA, C. O. VAN 1949. Systematic catalogue of the palaeontological collection: Sixth supplement (Teuthoidea). Teyler's Museum

ROBSON, G. C. 1929. On the rare Abyssal Octopod *Melanoteuthis beebei* (sp. n.): a Contribution to the Phytogeny of the Octopoda. *Proceedings of the Zoological Society of London*, **99**, 469–486.

ROMAN, F. 1928. Callovien Inférieur: Horizont a nodules de Crustacés et Poissons. In F. Roman, ed., Etudés sur les Callovien de la Vallée du Rhône. Lyon. p. 105–115.

ROWE, A. J., KRUTA, I., VILLIER, L. and ROUGET, I. 2023. A new vampyromorph species from the Middle Jurassic La Voulte-sur-Rhône Lagerstätte. *Papers in Palaeontology*, **9**, e1511.

ROWE, A. J., KRUTA, I., LANDMAN, N. H., VILLIER, L., FERNANDEZ, V. and ROUGET, I. 2022. Exceptional soft-tissue preservation of Jurassic Vampyronassa rhodanica provides new insights on the evolution and palaeoecology of vampyroteuthids. *Scientific Reports*, **12** 1-9.

THIELE in CHUN, C., 1915. Die Cephalopoden, II: Myopsida. Octopoda Wissenschaftliche Ergebnisse der Deutschen Tiefsee-Expedition auf dem Dampfer "Valdivia" 1898–1899, vol. 18. G. *Fischer. Jena*, pp.403-543.

SAYN, G. and ROMAN, F. 1928. Études sur le Callovien de la Vallée du Rhône. II Monographie stratigraphique et paléontologique du Jurassique moyen de la Voulte-sur-Rhône. 1er fascicule. 194.

STAROBOGATOV, Ya. I. 1983. Sistema Golovonogikh Molliuskov [Systematics of cephalopod molluscs]. In Ya. I. Starobogatov & Kir N. Nesis, eds., *Sistematika i Ekologiia Golovonogikh Molliuskov* [Taxonomy and Ecology of Cephalopod mollusks]. Zoological Institute of the USSR Academy of Sciences. Leningrad. p. 4–7

SUTTON, M., PERALES-RAYA, C. and GILBERT, I. 2016. A phylogeny of fossil and living neocoleoid cephalopods. *Cladistics*, **32**, 297–307.

VILLANUEVA, R., PERRICONE, V. and FIORITO, G. 2017. Cephalopods as Predators: A Short Journey among Behavioral Flexibilities, Adaptions, and Feeding Habits. *Frontiers in Physiology*, **8**, 598.

VILLIER, L., CHARBONNIER, S. and RIOU, B., 2009. Sea stars from Middle Jurassic Lagerstätte of La Voulte-sur-Rhône (Ardèche, France). *Journal of Paleontology*, **83**(3), 389-398.

VOSS, N. A. and SWEENEY, M. J. 1998. Systematics and Biogeography of cephalopods. Volume II. *Smithsonian Contributions to Zoology*, 277–599.

WHALEN, C. D. and LANDMAN, N. H. 2022. Fossil coleoid cephalopod from the Mississippian Bear Gulch Lagerstätte sheds light on early vampyropod evolution. *Nature Communications*, **13**, 1107.

WILBY, P., HUDSON, J., CLEMENTS, R. and HOLLINGWORTH, N. 2004. Taphonomy and origin of an accumulate of soft-bodied cephalopods in the Oxford Clay Formation (Jurassic, England). *Palaeontology*, **47**, 1159–1180.

WILBY, P. R. 2001. La Voulte-Sur-Rhône. *In* BRIGGS, D. E. G. and CROWTHER, P. R. (eds.) *Palaeobiology II*, Blackwell Science Ltd, Malden, MA, USA, 349–351 pp.

WILBY, P. R., BRIGGS, D. E. G. and RIOU, B. 1996. Mineralization of soft-bodied invertebrates in a Jurassic metalliferous deposit. *Geology*, **24**, 847–850.

———, DUFF, K., PAGE, K. and MARTIN, S. 2008. Preserving the unpreservable: a lost world rediscovered at Christian Malford, UK. *Geology Today*, **24**, 95–98.

WOODWARD, H., 1883. I.—On a New Genus of Fossil "Calamary," from the Cretaceous Formation of Sahel Alma, near Beirût, Lebanon, Syria. *Geological Magazine*, **10**(1), 1–5.

YOUNG, R. E. and VECCHIONE, M. 1996. Analysis of morphology to determine primary sister-taxon relationships within coleoid cephalopods. *American Malacological Bulletin*, **12**, 91–112.

THIELE in CHUN, C., 1915. Die Cephalopoden, II: Myopsida. Octopoda Wissenschaftliche Ergebnisse der Deutschen Tiefsee-Expedition auf dem Dampfer "Valdivia" 1898–1899, **18**:403-543.

SUPPLEMENTARY INFORMATION:

EXCEPTIONAL SOFT-TISSUE PRESERVATION OF JURASSIC *VAMPYRONASSA RHODANICA* PROVIDES NEW INSIGHTS ON THE EVOLUTION AND PALAEOECOLOGY OF VAMPYROTEUTHIDS

I) REDESCRIPTION OF *V. RHODANICA* SPECIMENS

Holotype: MNHN.B.74247

The holotype of *V. rhodanica,* MNHN.B.74247 (Fig.1) is fossilized in lateral view. It has an oviform, tapered mantle, and measures ~43 mm from the central line of the eye to the posterior tip.

Two small posterior fins are evident at the posterior of the mantle. One is displayed as a small projection extending outwards from the body. It is not possible to determine an exact shape, though given the positioning of the anterior-most part, it appears to have been attached only at the posterior section. The other fin is less apparent and seems to have been folded against the body prior to mineralization of the specimen. The associated fin cartilage is observed as two distorted ovoid shapes, with internal striated, curved strips that are denser than the surrounding tissue. The posterior section of the body has clearly been twisted as the two areas of fin cartilage are no longer on the original plane.

With the benefit of tomographic imaging, it is possible to identify a sinuous strip of soft tissue projecting along the margin that has been preserved in a dorsal position. This is denser than the surrounding matrix and has a somewhat mottled appearance. There is a distinct boundary on the outer edge of the tissue. It appears just in front of the right eye, extends almost all the way to the posterior, and tapers at both ends. There is no obvious corresponding counterpart splayed out on the other margin to indicate. Without further evidence it is not possible to determine the exact nature of this tissue, though here, we suggest it is splayed mantle tissue.

Elements of the digestive, respiratory, and reproductive systems are preserved, though the considerable compression and missing parts of the body makes it challenging to identify them with certainty. Additionally, despite topographic changes in the mantle indicative of a gladius, the X-ray imaging does not allow us to provide details on its presence or state. The holotype shows no evidence of an ink sac.

As in each of the specimens redescribed here, the head is short and represents the widest part of the body (~23 mm in the holotype). This appears to be fused to the mantle as no neck is evident. The eyes (~5-6 mm in diameter) are offset and preserved on different planes, reflecting some rotation of the head prior to mineralization.

MNHN.B.74247 retains 8 non-retractile (sessile) arms preserved in lateral view, the flesh of which tapers slightly toward the tip. Arm pair I are most dorsally situated in the arm crown and, as with the two other specimens, are the longest. Arm pair I (~49-51 mm) has armature only on the distal section of the arm. This is comprised of laterally paired cirri (no more than 2 mm in diameter as the base) and two, uniserial suckers (~2 mm in diameter) with radial symmetry. These have *Vampyroteuthis*-like attachments though are slightly more elongate that those on arms pairs III-V. There is no evidence of sucker rings.

Four, or perhaps five pairs of cirri precede the most proximal sucker, and an additional pair are positioned laterally between the proximal and distal sucker. No penultimate anterior pair of cirri are evident on the holotype, though a comparison of all three specimens (MNHN.B.74247; MNHN.B.74244; MNHN.B.74243) indicates that cirri are present in this location.

Arm pairs III to V range in size from approximately ~31 – 34 mm in composite length. They feature a single row of suckers on the oral surface which are present from the base to the tips of the arms. These taper distally and range in diameter from ~2 mm proximally to ~1 mm at the tip. Paired cirri are arranged on either side of the suckers (~13) along each arm. They have a maximum diameter of 2mm and taper in size toward the tip of the arms. Axial nerves can be identified in the arms and measure approximately 0.4 mm in diameter.

The suckers show a developed infundibulum and a *Vampyroteuthis*-like attachment that extends into the acetabular cavity. Additionally, some suckers are encircled by what appear to be small, ovoid holes in the soft tissue. There is no direct evidence to suggest that these are related morphologically with remnants of sucker lining seen in some decabrachians, rather we conclude that these are a result of degraded epithelial tissue.

MNHN.B.74244

This specimen is fossilized in dorsal view (Supplementary Fig. 1), heavily compacted, and the body is not as well preserved as the holotype. The mantle is posteriorly rounded, and measures ~46 mm in composite length. As with the holotype, the CT scan indicates the presence of tissue laterally surrounding the body. Two dense, ovoid structures are located at the posterior-most area of the body and appear to be enveloped by soft tissue. These measure ~5 mm at their longest transects. These are situated in a similar location to the luminous organs in the extant *V. infernalis*, though are much larger in size. This is the only specimen in which these structures are observed. It is not possible to say if they are luminous organs, though it is likely that they represent portions of displaced cartilage or tissue. There is no evidence of an ink sac, and it is not possible to observe a gladius.

The massive head is short and the two spherical eyes (~6 - 7 mm in diameter) are compacted and preserved on offset lateral planes. No neck is evident.

The arms have undergone rotation prior to fossilization and are positioned in a lateral view. As with each of the specimens, arm pair I, the longest of all the arms (~43 – 51 mm), are situated in the dorsal position, and their axial nerves are clearly visible in CT imagery (Fig. 2). The cirri and suckers display the same configuration as the other two specimens. On the dorsal arms, the cirri diameter tapers distally (~2 – 1 mm) and the two distal suckers (~2 mm diameter) have an elongated attachment like that of the holotype. In profile view it is possible to see that the distal end of the attachment extends into the acetabular chamber. No sucker lining is visible.

The other three arm pairs (III-V) are shorter in length (~24-36 mm) and lie more ventrally. Of the redescribed specimens, MNHN.B.74244 has the best-preserved armature. Each arm has a single row of suckers (up to 10 are visible per row) that run the length of the arm. These suckers also have a *Vampyroteuthis*-like attachment that extends into the acetabulum (Fig. 2). The suckers are framed by paired cirri, the diameter of which (suckers and cirri) is < 2mm. These both taper towards the tips of the arms. There is no evidence of a pair of retractable filaments (arm pair II) like those seen in *V. infernalis*.

MNHN.B.74243:

This specimen is the most poorly preserved of the three and considerable portions of the body and arm crown are missing. Fossilized in lateral view (Supplementary Fig. 1) it exhibits a tapered, fusiform shape and has a mantle length of ~46 mm.

As in the other two specimens, there is no internal organ that suggests that an ink sac was present, nor evidence of luminous organs. The extent of fins is particularly difficult to determine in this specimen. Posterior bulges, representative of internal fin cartilage, are present, though the CT scan shows these structures are distorted. Fin soft tissue is either not well retained or fossilized in such a way that it does not extend from the body. Soft tissue is present under the eye and terminates just in front of it. Fischer & Riou[1] suggested this was a long, muscular funnel, though we cannot confirm if this is funnel or mantle tissue.

It is apparent that the head has undergone considerable oblique twisting and compaction as the eyes are located almost on top of each other. They range in diameter from ~5 - 6 mm.

The dorsal arm pair (~53-57 mm) on MNHN.B.74243 are the longest of the three and have the same sucker and cirri configuration as the other two specimens. Some of the arm ornamentation is lost, though it is possible to make out a repetitive slight thickening pattern on the distal arm that corresponds with the basal parts of the cirri on the other two specimens.

Arm pairs III-V are shorter than the dorsal pair and are ~31-32 mm in length. As with the other two specimens, there is nothing to suggest there are any retractable filaments (arm pair II in *V. infernalis*). As it is not possible to identify the tips of the intermediate arms, they could possibly be longer. Many of the cirri and suckers on these arms are not preserved are not clearly able to be segmented. The exception to this is the most ventral arm pair, where the distal section displays a well-preserved sucker row flanked by cirri. The diameter of the few suckers that are measurable range between ~1 and ~2 mm. The smaller suckers are most distal. As with the holotype, there appear to be small holes surrounding some of the suckers.

II) MEASUREMENTS AND RATIOS

All measurements below are composite (following the contour of the element measured if possible) and based on what is preserved. Each element has potentially undergone compaction and/or distortion prior to fossilization. Measurements are listed in mm unless otherwise noted.

FOSSIL MATERIAL:

Supplementary Table S1: Overall measurements for the 3 *V. rhodanica* specimens (MNHN.B.74247; MNHN.B.74244; MNHN.B.74243)

	MNHN.B.74247	MNHN.B.74244	MNHN.B.74243
Dorsal arm length (longest)	51.2	50.5	57.2
Dorsal arm length (Shortest)	48.5	42.8	53.4
Sessile arm length (Longest)	33.5	35.9	32
Sessile arm length (Shortest)	30.7	23.6	30.5
Mantle (body) length (mid eye to posterior)	43	46	45.6
Total body length (body + longest dorsal arms)	94.2	96.5	102.6
Total body length (body + longest sessile arms)	76.3	82	77.4
Head width (widest part)	24.6	24	23.3
Sucker Diameter - dorsal (largest)	2.4	2.2	1.8
Sucker Diameter – dorsal (smallest)	1.9	2.1	1.5
Sucker Diameter – Sessile (largest)	1.7	1.6	1.7
Sucker Diameter – sessile (smallest)	0.8	0.8	0.7
Infundibulum width (max)		0.49	
Acetabular cavity width (max)			

Cirri height - sessile (longest)	1.6	1.8	N/A
Cirri height - sessile (Shortest)	0.5	0.9	N/A
Cirri diameter - sessile (largest)	1.8	1.8	0.8
Cirri diameter - sessile (smallest)	0.8	1	1
Cirri height - dorsal (longest)	1	2.2	1.1
Cirri height - dorsal (Shortest)	3.2	N/A	0.8
Cirri diameter - dorsal (largest)	0.8	1.6	0.8
Cirri diameter - dorsal (smallest)	1.7	0.7	0.4

Supplementary Table S2: Sample Arm (Arm pair V) measurements: *V. rhodanica* (MNHN.B.74244)

Sessile Arm	**Proximal**									**Distal**
Sucker Diameter	1.5	1.5	N/A	1.4	1.5	1.2	1.0	1.0	0.7	0.6
Distance btwn suckers	0.9	N/A	N/A	0.7	0.6	0.6	0.7	0.5	0.5	
Cirri diameter	1.4	1.7	1.4	1.6	1.2	1.4	0.9	0.9	0.8	0.6
Distance btwn cirri	0.2	0.3	0.5	0.7	0.7	0.7	0.9	0.7	0.6	
Infundibulum width	0.4	0.5	N/A	0.4	0.5	0.4	0.3	0.3	N/A	N/A
Acetabular cavity width	0.7	1.0	N/A	0.5	0.4	0.5	0.5	N/A	N/A	N/A
Sphincter distance	N/A	N/A	N/A	0.5	0.4	0.5	0.5	N/A	N/A	N/A
Sucker height (external)	0.7	0.7	N/A	0.8	0.7	0.5	0.5	N/A	N/A	N/A

Supplementary Table S3a: Sample Arm (Arm Pair I) sucker measurements: *V. rhodanica* (MNHN.B.74244)

Dorsal Arms (Sucker Measurements)	**Arm A**	**Arm A**	**Arm B**	**Arm B**
	Proximal	**Distal**	**Proximal**	**Distal**
Attachment diameter (base)	0.7	0.5	0.6	0.5
Attachment diameter (top)	0.6	0.6	0.6	0.5
Attachment diameter (below acetabulum)	0.5	0.4	0.5	0.4
Attachment length	0.9	0.7	0.7	0.7
Amount of attachment in acetabulum	0.5	0.5	0.4	0.4
Infundibulum diameter	0.9	0.5	0.7	0.7
Acetabular cavity diameter	1.0	0.8	0.8	0.9
Distance btwn sphincter	0.4	0.5	0.6	0.6
Sucker height (external)	0.9	0.9	0.8	0.9
Sucker height (internal)	0.7	0.7	0.6	0.6
Acetabular cavity base to sphincter	0.4	0.2	0.4	0.3
Sucker diameter	2.4	2.3	2.1	1.9
Distance btwn suckers (attachment base)		1.1	1.5	

Supplementary Table S3b: Sample Arm (Arm Pair I) cirri measurements: *V. rhodanica* (MNHN.B.74244)

Dorsal Arm Cirri: Diameter at base	**Proximal**					**Distal**
A	1.8	1.7	1.2	1.1	1.0	N/A
B	1.1	1.2	1.1	1.5	N/A	N/A

EXTANT MATERIAL:

Supplementary Table S4a: Sample arm (Arm Pair IV) sucker measurements: *V. infernalis* (AMNH IZC 361496)

Sample Arm (Suckers):	**Sucker 1 (Proximal)**	**Sucker 2**	**Sucker 3**	**Sucker 4**	**Sucker 5 (Distal)**
Infundibulum width	0.19	0.17	0.19	0.17	0.21
Acetabular cavity width	0.35	0.20	0.22	0.27	0.25
Sphincter distance	0.18	0.20	0.25	0.12	0.14
Sucker diameter	0.67	0.66	0.54	0.61	0.57

**Highlighted sucker measurements used in the comparison

Supplementary Table S4b: Sample arm (Arm Pair IV) cirri measurements: *V. infernalis* (AMNH IZC 361496)

Sample Arm (Cirri):	**Prox.**													**Dist.**
Cirri diameter at base	0.4	0.5	0.5	0.6	0.7	0.7	0.7	0.6	0.7	0.6	0.5	0.4	0.5	0.6
Distance btwn cirri	1.9	1.7	1.4	1.1	1.1	0.8	0.7	0.4	0.6	0.6	0.5	N/A	N/A	N/A

Supplementary Table S4c: Sample arm (Arm Pair IV) sucker measurements: *V. infernalis* (YPM IZ 18279.GP)

Sample Arm:	**Sucker 1 (Proximal)**	**Sucker 2**	**Sucker 3**	**Sucker 4**	**Sucker 5 (Distal)**
Infundibulum width	0.10	0.96	0.07	0.13	0.14
Acetabular cavity width	0.26	0.20	0.25	0.54	0.26
Sphincter distance	0.13	0.05	0.13	0.26	0.19
Sucker diameter	0.46	0.37	0.4	0.78	0.53

**Highlighted sucker measurements used in the comparison

Supplementary Table S5a: Ratios based on the composite measurements of *V. rhodanica* (this study), and mean values of *V. infernalis* from Pickford 1949[2].

	***V. rhodanica* MNHN.B.74247**	***V. rhodanica* MNHN.B.74244**	***V. rhodanica* MNHN.B.74243**	***V. infernalis* (Pickford[2]) Mean**
Absolute Size	43	46	46	49.2 (male); 59.5 (female)
Head Width Index	0.56	0.49	0.51	0.94
Length of Longest Arm (Dorsal)	54.4	52.3	55.6	
Length of Longest Arm (Sessile)	43.9	43.8	41.3	63
Longest:shortest arm (Dorsal)	59.9	46.7	53.3	
Longest:shortest arm (Sessile)	91.6	65.7	95.3	72
Sucker diameter index (Dorsal)	5.6	4.8	3.9	
Sucker diameter index (Sessile)	3.9	3.5	3.7	3.7
Cirri length index (Dorsal)	2.3	5.2	2.4	
Cirri length index (Sessile)	3.7	3.9	N/A	8.5
Arm:Mantle ratio (Dorsal)	0.8	0.9	0.8	
Arm:Mantle ratio (Sessile)	0.8	0.8	0.7	

The mean ratios for *V. infernalis* were taken directly from Pickford[2]. This table indicates that the head width of *V. rhodanica* is ~50% the length of the body, whereas the head width of *V. infernalis* is ~94%. See below for the ratio equations used. As *V. infernalis* does not have an elongated Arm Pair 1, the ratios were compared with the sessile arms in *V. rhodanica*. Ratios for the infundibulum diameter and cirri diameter were not listed in Pickford[2], so the ratio equations shown in Table 5b were utilized:

Supplementary Table S5b: Ratios based on the composite measurements of *V. rhodanica* (MNHN.B.74244) and *V. infernalis* (YPM IZ 18279.GP, and AMNH IZC 361496). Ratios were adapted from Pickford (1949)[2]

Sucker ratios:	**MNHN.B.74244**	**YPM IZ 18279.GP**	**AMNH IZC 361496**	**Ratio Equations**
Infundibulum size ratio	31	17	13	Largest measurement x 100/sucker diameter
Cirri diameter ratio	3.5	N/A	1.9	Largest measurement x 100/mantle length

RATIOS:

Absolute Size (*Mantle Length*):

V. infernalis sizes were taken from Pickford[2]. In that sample, the mean size was 49.2 (male), 59.5 (female). The range was 44 – 55 (male) (4 specimens) and 55 – 63 (female) (two specimens). The 3 *V. rhodanica* specimens MNHN.B.74247 (~43), MNHN.B.74244 (~46), and MNHN.B.74243 (~46) are consistent with the size range for individual male specimens of *V. infernalis*.

Head width index

V. rhodanica has a proportionally smaller head width than *V. infernalis*. This is expected as *V. infernalis* was described as having a wider head and a shorter mantle than *V. rhodanica* by Fischer & Riou[1]. The 3 MNHN specimens of *V. rhodanica* have a head width that is ~49 – 56% the length of the body. The range of head width ratios of *V. infernalis* described in Pickford[2] is 76 – 112%. The average head width is ~94% the length of the mantle. The head width of *V. rhodanica* is roughly half the mantle length.

Head Width X 100/Mantle Length

Length of longest arm

Pickford[2] noted two equations for this index, the arm length index, and the mantle length index. This study followed Pickford and used the arm length index for the *V. rhodanica* specimens. *V. infernalis* lacks the longer dorsal arm pair seen in *V. rhodanica*. While this index was calculated for both the dorsal arms, and arm pairs III-V in *V. rhodanica*, the ratios listed in Supplementary Table S5a utilized just arm pairs III – V.

When including the dorsal arms, the index for our *V. rhodanica* specimens range from ~52 – 56%. Using just the lengths of the sessile arms, the range is ~41 – 44%. Pickford[2] recorded that in *V. infernalis*, the mean value of the index was 63%, and ranged from 51 – 77%.

Arm length index: Length of longest arm x 100/ total length

Mantle length X 100/longest arm

Difference between longest and shortest arms:

This index shows the limits of variability in the arm crown. As for the Arm Length Index, calculations were performed on both the dorsal (Arm Pair I) and non-dorsal arms (arm pairs III – V), though only the non-dorsal arms are included in Supplementary Table S5a.

In the arm crown of *V. rhodanica*, the shortest sessile arms were roughly half the size of the longest dorsal arms (~47 – 60%). A comparison of just the non-dorsal arms showed less

variability with both the MNHN.B.74247, and MNHN.B.74243 expressing a range in the 90s (92, and 95% respectively). The index for specimen 74244 was 66%. This difference may reflect loss of length in arm pairs III-V. The mean index for *V. infernalis* is 72%. This is expected as the arm crown of *V. infernalis* shows less variability in dorsal arm length. The range, however, is wide and falls between 54 – 92%.

Length of the shortest arm x 100/length of longest arm

Sucker diameter index

This index reflects allometry with size. Again, this index was calculated both including, and excluding the dorsal arms. The range for *V. infernalis* is 2.0 – 4.8 % with a mean of 3.7%; this is consistent with the index returned for the sessile arms only (3.4 – 3.9%). Suckers on the dorsal arms of *V. rhodanica* have a slightly higher index and range from 3.9 – 5.6%.

Diameter of largest sucker x 100/ mantle-length

III) MICROTOMOGRAPHY

The three *V. rhodanica* fossils were initially imaged using X-ray Computed Tomography (µCT) at the AST-RX platform at the Muséum National d'Histoire Naturelle, Paris (MNHN, Paris, France), and then at the European Synchrotron Radiation Facility (ESRF, Grenoble, France). Acquisition at the AST-RX platform generated data with a voxel size of 88.60 µm. At the ESRF, the experiment was done at the ID19 beamline using propagation phase-contrast X-ray synchrotron microtomography (PPC-SRµCT). The experimental setup consisted of a filtered pink beam (Wiggler W150B gap: 55 mm; see Table S6 for filters) with detected total integrated energy ranging from 112 keV to 136.3 keV depending on the filter used; a sample-detector propagation distance of 16 m; and an indirect detector comprising a 500 mm LuAG:Ce crystal scintillator, a set of Hasselblad photographic lenses (Victor Hasselblad AB, Gothenburg, Sweden) providing a 1x magnification and a FReLoN-2k camera, generating data with an isotropic voxel size of 12.64 µm. Given the limited size of the X-ray beam with this setup (7.58 mm vertically and 25.89 mm horizontally), several acquisitions were necessary to cover the

specimens on the vertical axis with the motorised sample manipulator, keeping a 50% overlap between consecutive acquisitions. To overcome the limitation horizontally, the centre of rotation of the sample stage was set near the edge of the recorded projections, allowing to almost double the field of view in reconstructed data (i.e., so called half-acquisition[3]). For all specimens, each acquisition consisted of 4998 projections of 0.1 second exposure each, over a 360° rotation. The tomographic reconstruction was done with the PyHST2 software[4] using the single distance phase retrieval approach[5] generating stack of 32-bits files. Follow up post-processing included: ring corrections[6]; change of the dynamic range from 32-bit to 16-bit; vertical concatenation of the dataset using a weighted averaging; export of the concatenated dataset as stack of 16-bit tiff files.

Supplementary Table S6: List of parameters used for propagation phase-contrast X-ray synchrotron microtomography at the ID19 beamline of the ESRF.

Specimen	ID	gap	Filters	energy	ODD	voxel size	exposure	projection
MNHN.B.74247	W150B	55 mm	W: 0.5 mm Cu: 6 mm Al: 2.8 mm	136.3 keV	16 m	12.64 µm	0.1 s	4998
MNHN.B.74243	W150B	55 mm	W: 0.5 mm Cu: 6 mm Al: 2.8 mm	136.3 keV	16 m	12.64 µm	0.1 s	4998
MNHN.B.74244	W150B	55 mm	Cu: 8 mm Al 2.8 mm	112 keV	16 m	12.64 µm	0.1 s	4998

Imaging of extant *V. infernalis* were done using µCT at the Microscopy and Imaging Facility of the American Museum of Natural History (New York, USA). The resulting voxel size were 38.40 µm (AMNH IZC 361496) and 18.25 µm (YPM IZ18279.GP). Both specimens were stained in a 1% PTA solution prior to scanning.

Final CT data were reduced in size using ImageJ software (cropping and binning 2x2x2), and then segmented using Mimics software (Materialise NV, Belgium, Version 21.0). The contrasting densities of the mineralized soft tissues were utilized to identify anatomical features for segmentation. Morphological reconstructions were carried out for the three *V. rhodanica* specimens incorporating all possible internal and external soft tissues. A full reconstruction of *V. infernalis* was carried out on AMNH IZC 361496. Some sucker tissues in YPM IZ18279.GP had more clearly defined boundaries and these were integrated into the analysis to augment the data gathered from AMNH IZC 361496.

BIBLIOGRAPHY

1. Fischer, J.-C. & Riou, B. *Vampyronassa rhodanica nov. gen. nov sp*., vampyromorphe (Cephalopoda, Coleoidea) du Callovien inférieur de La Voulte-sur-Rhône (Ardèche, France). *Ann. de Paléontol.* **88**, 1–17 (2002).

2. Pickford, G. E. *Vampyroteuthis infernalis* Chun-An archaic dibranchiate cephalopod. II. External anatomy. *Dana Rep.* **32**, 1–132 (1949).

3. Carlson, K. J. *et al.* The endocast of MH1, *Australopithecus sediba*. *Science* **333**, 1402–1407 (2011).

4. Mirone, A., Brun, E., Gouillart, E., Tafforeau, P. & Kieffer, J. The PyHST2 hybrid distributed code for high speed tomographic reconstruction with iterative reconstruction and a priori knowledge capabilities. *Nuclear Instruments and Methods in Physics Research Section B: Beam Interactions with Materials and Atoms* **324**, 41–48 (2014).

5. Paganin, D., Mayo, S. C., Gureyev, T. E., Miller, P. R. & Wilkins, S. W. Simultaneous phase and amplitude extraction from a single defocused image of a homogeneous object. *Journal of microscopy* **206**, 33–40 (2002).

6. Lyckegaard, A., Johnson, G. & Tafforeau, P. Correction of ring artifacts in X-ray tomographic images. *Int. J. Tomo. Stat* **18**, 1–9 (2011).

7. Fuchs, D., Hoffmann, R. & Klug, C. Evolutionary development of the cephalopod arm armature: a review. *Swiss J. Palaeontol.* **140**, 1–18 (2021).

8. Young, R. E. & Vecchione, M. Analysis of morphology to determine primary sister-taxon relationships within coleoid cephalopods. *Am. Malacol. Bull.* **12**, 91–112 (1996).

9. Kruta, I. *et al. Proteroctopus ribeti* in coleoid evolution. *Palaeontology* **59**, 767–773 (2016).

10. Sutton, M., Perales-Raya, C. & Gilbert, I. A phylogeny of fossil and living neocoleoid cephalopods. *Cladistics* **32**, 297–307 (2016).

11. Goloboff, P. A., Farris, J. S. & Nixon, K. C. TNT, a free program for phylogenetic analysis. *Cladistics* **24**, 774–786 (2008).

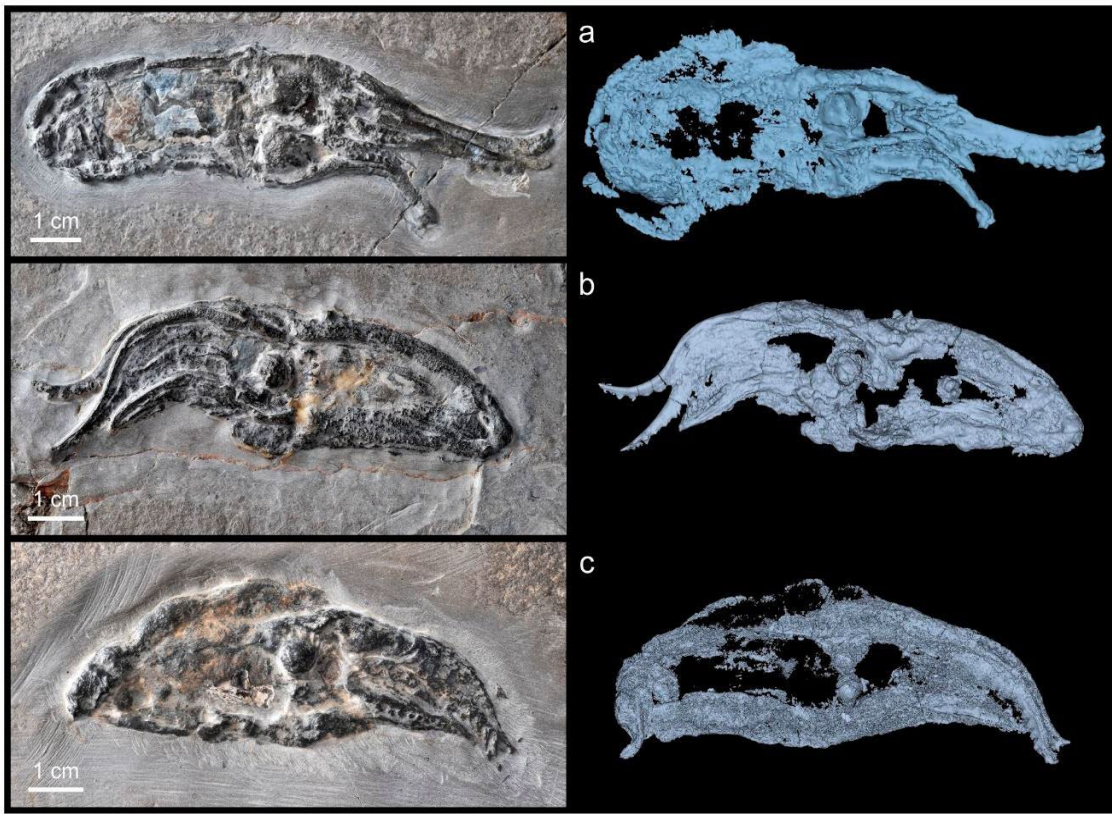

Supplementary Fig. 1. Photographs (left) by P. Loubry (CR2P), and 3D reconstructions (right) of the 3 V. rhodanica specimens. (a) MNHN.B.74244 (AST-RX). (b) MNHN.B.74243 (PPC-SR-µCT, ESRF). (c) MNHN.B.74247 (PPC-SR-µCT, ESRF). All reconstructions were created using Mimics software (Materialise NV, Belgium, Version 21.0).

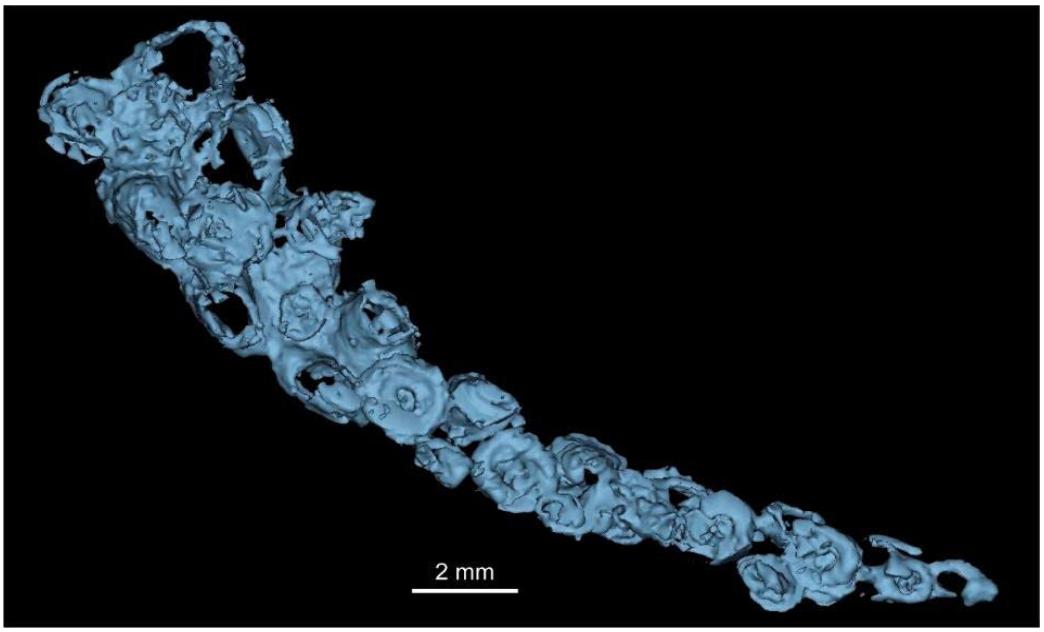

Supplementary Fig. 2. 3D reconstruction of a sessile arm (from arm pair V) of *V. rhodanica* MNHN.B.74244 showing the uniserial sucker row flanked by paired cirri. (PPC-SR-µCT, ESRF).

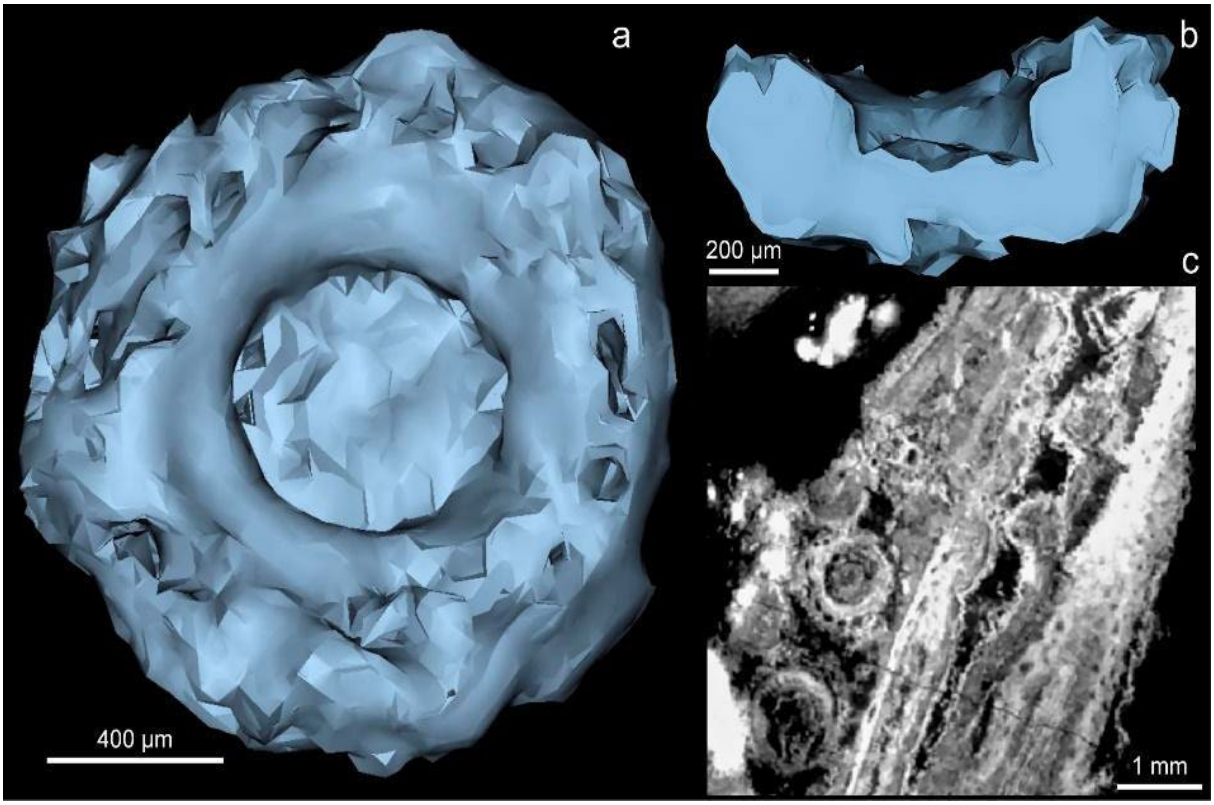

Supplementary Fig. 3. 3D Reconstruction of a sucker of MNHN.B.74243 showing the oval-shaped depressions. (**a**) Oral view showing the depressions encircling the outer perimeter of the sucker. (**b**) Profile view. (**c**) Slice (PPC-SR-µCT, ESRF) of the same sucker.

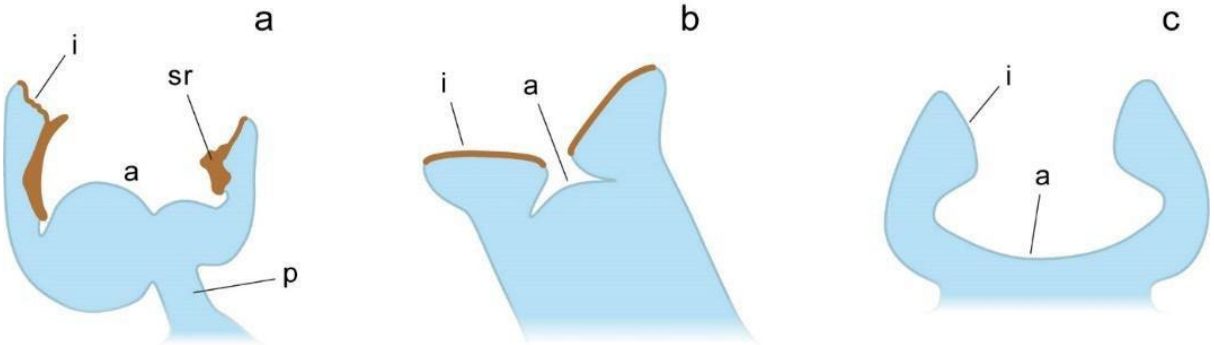

Supplementary Fig. 4. Simplified illustrations of the sucker and attachment types (in profile) of (**a**) Decabrachia, (**b**) Octobrachia, (**c**) Vampyromorpha. (**a,b**) adapted from Fuchs, Hoffmann, & Klug[7]. (**c**) adapted from Young & Vecchione[8]. (i) infundibulum, (a) acetabulum, (sr) sucker ring, (p) muscular, piston-like attachment.

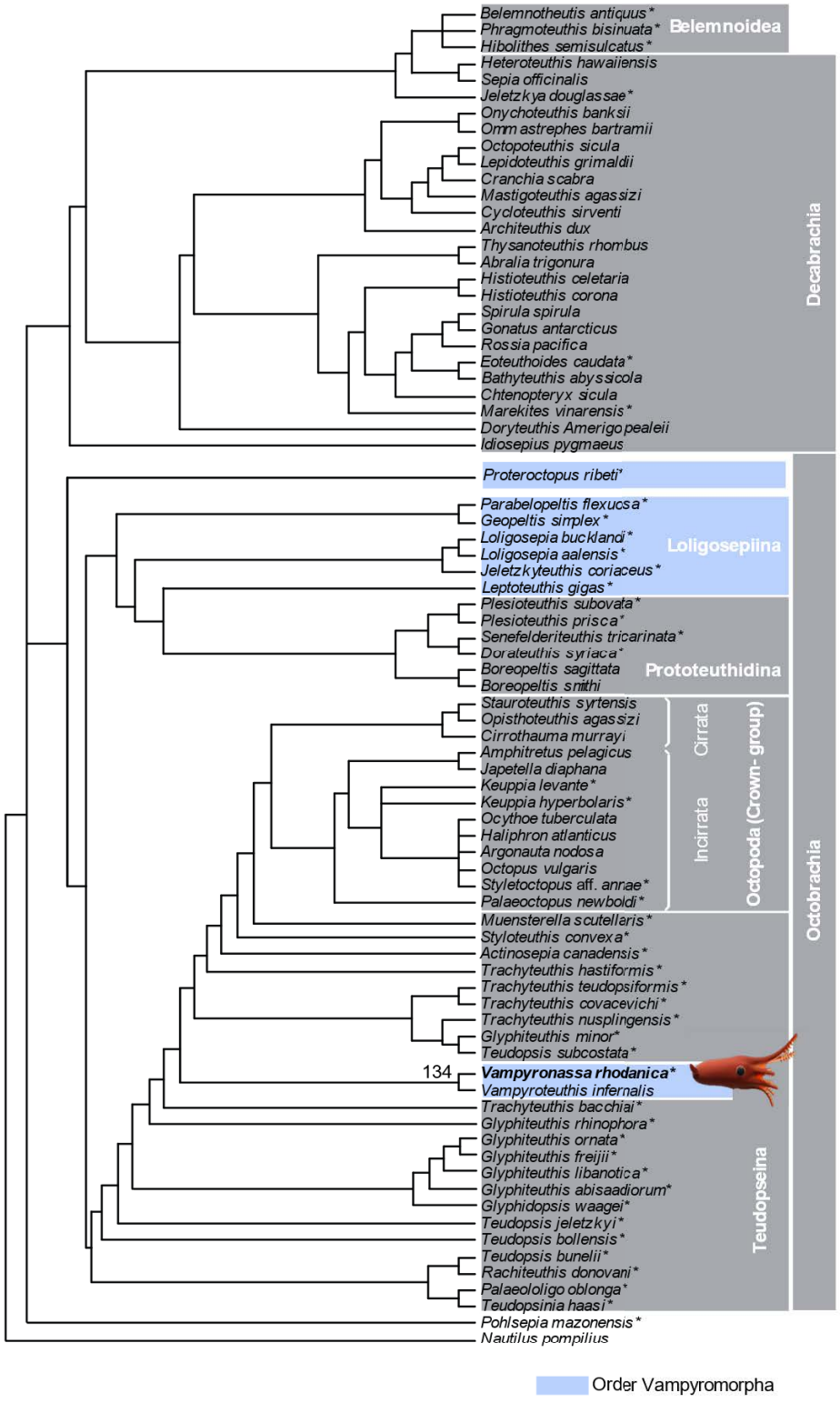

Supplementary Fig.5: Consensus tree obtained from 34 most parsimonious trees showing the relationship between *Vampyroteuthis infernalis* and *Vampyronassa rhodanica*. The matrix was modified from Kruta et al. [9], which was based on the matrix and parameters of Sutton et al.[10] (2016). Data were analysed using TNT[11]. The state of character 90 (sucker stalks that are present but not clearly attached to the arm muscles) at node 134 were previously autapomorphic in *V. infernalis*. This study shows that this state is present in *V. rhodanica* and therefore synapomorphic.

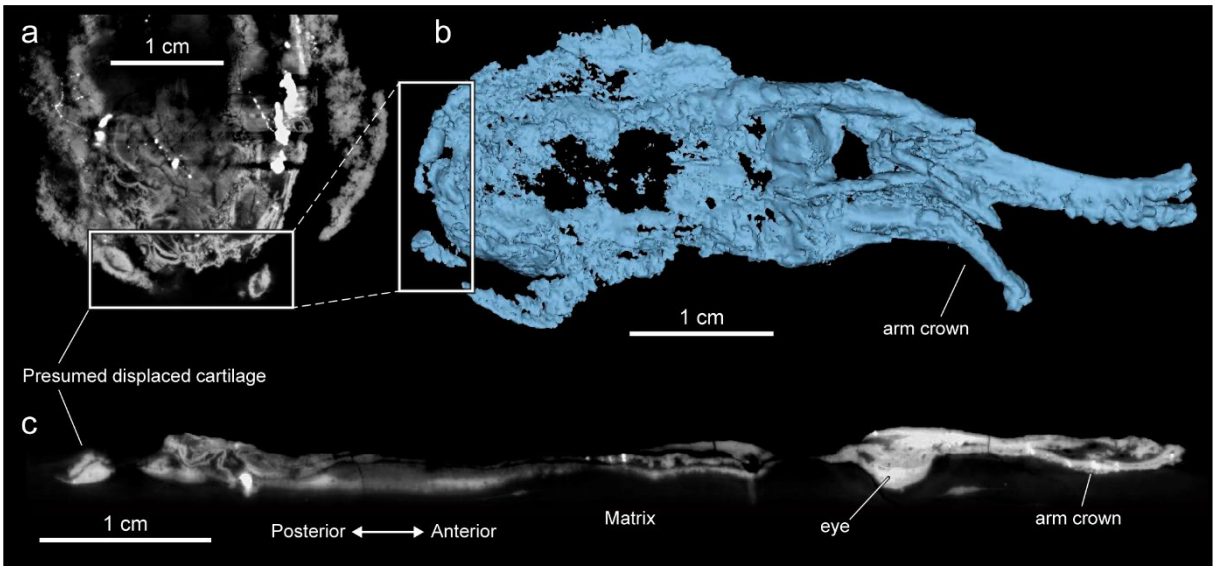

Supplementary Fig.6: **(a)** Axial slice (PPC-SR-µCT, ESRF) **(b)** 3D reconstruction and (**c**) sagittal slice (PPC-SR-µCT, ESRF) of MNHN.B.74244 showing the presumed displaced cartilage.

CHAPTER 4 : THE LEBANESE PLATTENKALKS: A WINDOW ON THE INTRASPECIFIC VARIATION OF FOSSIL OCTOBRACHIA

INTRODUCTION

The fossil-rich deposits of Lebanon have been famous for centuries and were written about by Herodotus as far back as 450 BCE. (Davis 1887; Woodward 1896, Fuchs & Larson 2011*a*; Audo & Charbonnier 2012; El Hossny & Cavin 2023). As noted in chapter one, the four Lagerstätten date from the Upper Cretaceous and are separated by around 9 to 10 million years: the Haqel, Hjoula and Nammoura deposits are from the Cenomanian and Sahel Aalma is Santonian in age. These localities are most well-known for the accumulation of fossil fishes – indeed, Chondrichthyes and Osteichthyes are found in large numbers on bedding planes (Forey *et al.* 2003; Audo & Charbonnier 2012; El Hossny & Cavin 2023) – but the assemblages also preserve numerous Crustaceans (Audo & Charbonnier 2012; Audo *et al.* 2017; Charbonnier *et al.* 2017) and exceptionally preserved soft-bodied organisms, including coleoids (Fuchs *et al.* 2009, 2016; Fuchs & Weis 2009, Fuchs & Larson 2011*a*, *b*; Jattiot *et al.* 2015).

Unlike the three-dimensional preservation seen at La Voulte-sur-Rhône – typically a result of precipitation of a concretion around the fossil - preservation in the Lebanese limestones (commonly known by the German word “Plattenkalks”) is two-dimensional (Jauvion 2020). In both localities, initial microbial activity on the organism produces a locally acidic environment and a rapid precipitation of calcium phosphate. As this acidity dissipates, there is a subsequent reversion to a more alkaline environment and calcium carbonate precipitates. At La Voulte-sur-Rhône, the carbonates commonly formed a concretion around the organism, whereas in Lebanon, the carbonates cemented the limestone sediments. In both settings, different minerals formed in parts of the same organism (Jauvion 2020). These processes are discussed in detail in Allison (1988), Briggs & Wilby (1996), and Jauvion (2020) and so not explored further here.

The Lebanese fossils are inherently highly suited to the investigation of the chemical composition of various tissues and organs. Unlike fossils preserved in 3D, their internal organs are exposed. This presents the opportunity to determine the composition of tissues (e.g., muscle, cartilage, and chitin) using multiple imaging techniques. These techniques are also powerful for identifying remnants of anatomical structures that are invisible through conventional observations (Gueriau *et al.* 2018). In Lebanon, such studies have already successfully been carried out on fish, crustaceans and coleoids (Gueriau *et al.* 2018; Jauvion 2020; Klug *et al.* 2021).

A great benefit of working on samples from these Lebanese deposits is the abundance of specimens from a single species. This is true for coleoids and has also been noted for other groups in the fossil assemblage (e.g., crustaceans). For example, *Paradollocaris vannieri* Charbonnier *et al.* (2017) is represented by 16 paratypes, and Audo & Charbonnier (2012) described 54 specimens of *Palaeobenthesicymus libanensis* (Brocchi 1875) in a single study. As highlighted in Chapter 1, deposits of exceptional preservation provide just a fragmented history of coleoid evolution, but the abundance of specimens in the Lebanese Lagerstätten make them important localities for obtaining key diagnostic data at the species scale. This species-level abundance enables detailed systematic work to be carried out that incorporates data on ontogenetic and intraspecific character variability. It also allows us to analyse the preservational potential of various anatomical characters from relatively similar depositional conditions. The Haqel, Hjoula and Sahel Aalma deposits therefore provide a textbook setting for this quantitative analysis.

The preservation of gladii and soft tissues varies in these Lebanese localities, but many elements of the fossils can be exploited for quantitative studies. The commonly preserved soft tissues are arm crowns, mantle tissues, ink sacs and gills, which are known for their high-quality. Stomach contents and buccal elements are also often retained (Lukeneder & Harzhauser 2004; Fuchs 2007; Fuchs *et al.* 2009, 2016; Fuchs & Weis 2009, Fuchs & Larson 2011*a*, *b*; Donovan & Fuchs 2016). The variability in soft tissue preservation is not yet fully known, though the increasing number of coleoid specimens from Lebanon enable the production of a core dataset that can be exploited for this purpose.

This chapter illustrates how an array of imaging techniques can be used to document the organ variability in an abundant coleoid taxon. After a brief overview of Octobrachian diversity in the Lebanese Lagerstätten, the core of the chapter is a reappraisal of *Dorateuthis syriaca*, revealing newly described intraspecific variation for the species, as well as implications for systematics and paleoecology. This is presented in Rowe *et al.* (in prep), which is included in this chapter.

Rowe A., Kruta I, Villier L., Gueriau P., Jattiot R., Fuchs D., Clements T., Charbonnier S., Rouget I. (in prep). Multimodal imaging reveals unknown intraspecific variation in the coleoid Dorateuthis syriaca Woodward, 1883 from the Lower Cretaceous of Lebanon. For submission to the *Journal of Systematic Palaeontology*

Two undescribed specimens of *Keuppia* were also studied as part of a co-supervised student project to begin exploring the variation of preservation within this early Incirrate genus. A brief description of these specimens is provided at the end of the chapter.

4.1 Overview of Coleoid Diversity

The fossil coleoid diversity from Lebanon comprises ten genera from the Octobrachia suborders, Prototeuthina, Teudopseina, and Incirrata (Fig. 4.1) (Fuchs 2020). No members of Loligosepiina are currently known from these localities.

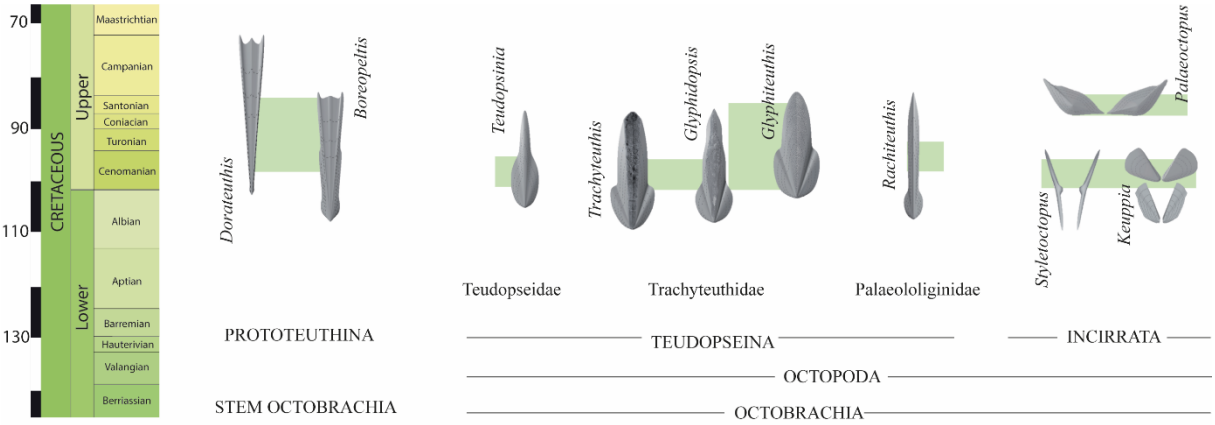

Figure 4.1 Overview of the genera present in the Lebanese sediments, and their stratigraphic distribution. Modified from Fuchs (2020). The gladius illustrations are not to scale and are for morphological comparison only.

A recent systematic review of fossil gladius-bearing coleoids (Fuchs 2020) classifies the taxa accordingly:

Superorder OCTOBRACHIA Haeckel, 1866
- Suborder PROTOTEUTHINA Naef, 1921
  - Family PLESIOTEUTHIDAE Naef, 1921
    - *Boreopeltis* Engeser & Reitner, 1985
    - *Dorateuthis* Woodward, 1883
- Order OCTOPODA Leach, 1817
  - Suborder TEUDOPSEINA Starobogatov, 1983
    - Family TEUDOPSEIDAE Regteren Altena, 1949
      - *Teudopsis* Eudes-Deslongchamps, 1835
    - Family TRACHYTEUTHIDAE Naef, 1921
      - *Trachyteuthis* Meyer, 1846
      - *Glyphidopsis* Fuchs & Larson, 2011b
      - *Glyphiteuthis* Reuss, 1854

Family PALAEOLOLIGINIDAE Naef, 1921
Rachiteuthis Fuchs, 2006b
Suborder INCIRRATA Grimpe, 1916
Family PALAEOCTOPODIDAE Dollo, 1912
Palaeoctopus Woodward, 1896a
Keuppia Fuchs, Bracchi, & Weis, 2009
Family OCTOPODIDAE d'Orbigny, 1840
Styletoctopus Fuchs, Bracchi, & Weis, 2009

Fifteen species (ten genera) have been described in the four Lebanon Lagerstätten (Table 4.1). Two species belong to the Prototeuthina, eight species are assigned to the Teudopseina, and four species are members of the Incirrata, which represent the oldest known fossil Incirrates. Fuchs *et al*. (2009), described a specimen of *Keuppia* sp. that could not unambiguously be assigned to a new species due to the preservation of the bipartite gladius. Jattiot *et al.* (2015) described a *Glyphiteuthis* sp. specimen from Nammoura with a singular combination of characters but did not establish it as a new species as the one specimen is not completely preserved. Two species have the provisional assignment of 'cf.', indicating that most of the diagnostic characters correspond to a given species, but some characters are unclear.

GENERA	SPECIES	LOCALITY
Boreopeltis Engeser & Reitner, 1985	*Boreopeltis smithi* Fuchs & Larson, 2011a [4]	Late Cenomanian-?Santonian
Dorateuthis Woodward, 1883	*Dorateuthis syriaca* Woodward, 1883 [1, 4, 6]	Haqel, Hjoula, Sahel Aalma
	Dorateuthis cf *syriaca* Woodward, 1883 [1]	Sahel Aalma
Teudopsinia Fuchs, 2010	*Teudopsinia haasi* Fuchs, 2010 [5, 7]	Haqel
Trachyteuthis Meyer, 1846	*Trachyteuthis bacchiai* Fuchs & Larson, 2011b [5]	Hjoula, Haqel
Glyphidopsis Fuchs & Larson, 2011b	*Glyphidopsis waagei* Fuchs & Larson, 2011b [5]	Haqel
Glyphiteuthis Reuss, 1854	*Glyphiteuthis libanotica* (Fraas, 1878) [1, 5, 6]	Hjoula, Haqel, ? Sahel Aalma
	Glyphiteuthis abisaadiorum Fuchs and Weis, 2009 [2, 5]	Hjoula, Haqel
	Glyphiteuthis freijii Fuchs & Larson, 2011b [5]	Hjoula, Haqel, En Nammoura
	Glyphiteuthis sp. [5, 6]	Hjoula, Haqel, En Nammoura
Rachiteuthis Fuchs, 2006b	*Rachiteuthis donovani* Fuchs, 2006b [1]	Hjoula, Haqel
	Rachiteuthis acutali Jattiot *et al*. 2015, [6]	Hjoula
Palaeoctopus Woodward, 1896a	*Palaeoctopus newboldi* (Woodward 1896) [8]	Sahel Aalma
Keuppia Fuchs, Bracchi, & Weis, 2009	*Keuppia levante* Fuchs, Bracchi, & Weis, 2009 [3]	Hjoula
	Keuppia hyperbolaris Fuchs, Bracchi, & Weis, 2009 [3]	Hjoula
	Keuppia sp. [3]	Hjoula
Styletoctopus Fuchs, Bracchi, & Weis, 2009	*Styletoctopus annae* Fuchs, Bracchi, & Weis, 2009 [3]	Haqel
	Styletoctopus aff. *Annae* [3]	Hjoula

Table 4.1 The 10 genera known from Lebanon comprise 14 species. Predominantly known from the Cenomanian localities of Haqel and Hjoula, they are also represented in Sahel Aalma and Nammoura: [1]Fuchs 2006, [2] Fuchs & Weis 2009, [3] Fuchs, Bracchi & Weis 2009, [4] Fuchs & Larson 2011a, [5] Fuchs & Larson 2011b, [6] Jattiot *et al.* 2015, [7] Fuchs 2010, [8] Fuchs 2020.

Among all the taxa described, *Dorateuthis syriaca* is the only one of the fifteen Lebanese species to be definitively known from both the Cenomanian and Santonian outcrops.

Boreopeltis smithi Fuchs & Larson 2011, and one species of *Glyphiteuthis libanotica* (Fraas, 1878) are known with certainty from the Cenomanian, and are possibly from the Santonian (Roger 1946, fig. 10; Fuchs 2011b). The remainder of the species are known from Haqel and Hjoula. As discussed earlier in the chapter and mentioned in Rowe *et al.* (in prep), these Cenomanian localities have been known for centuries and have provided the majority of the fossil coleoid specimens. One genus has been found at Nammoura.

4.2 Re-study of a key Cretaceous Octobrachia species: *Dorateuthis syriaca*

As outlined in the following manuscript, *Dorateuthis syriaca* is the most abundant gladius-bearing coleoid species in the Lebanese Lagerstätten. Morphological descriptions have varied in the literature and led to ambiguity regarding the diagnostic characters. However, access to imaging techniques particularly suited to the study of 2D fossil material offers a higher resolution picture of the anatomy. Applying these methods to a large sample of *D. syriaca*, we are able to offer the most comprehensive description of the species to date. This work provides the basis for Rowe *et al.* (in prep). Supplementary information for this work is included at the end of the chapter to facilitate reading.

Multimodal imaging reveals unknown intraspecific variation in the coleoid *Dorateuthis syriaca* Woodward, 1883 from the Lower Cretaceous of Lebanon

Alison J. Rowe [1], Isabelle Kruta [1], Loïc Villier [1], Pierre Gueriau [2, 3], Marie Radepont [4], Oulfa Belhadj [4], Katharina Müller [3], Romain Jattiot [5, 6], Dirk Fuchs [7], Thomas Clements [8], Sylvain Charbonnier [9], & Isabelle Rouget [1, 9]

[1] Sorbonne Université-MNHN-CNRS-CR2P, 4 Pl. Jussieu, 75005 Paris, France. [2] Institute of Earth Sciences, University of Lausanne, Géopolis, CH-1015 Lausanne, Switzerland. [3] Université Paris-Saclay, CNRS, ministère de la Culture, UVSQ, MNHN, UAR 3461 Institut photonique d'analyse non-destructive européen des matériaux anciens (IPANEMA), 91192, Saint-Aubin, France. [4] Centre de Recherche sur la Conservation – Paris (CRC), UAR 3224, MNHN, 36 rue Geoffroy St Hilaire, CP21, 75005 PARIS – France. [5] Centre de Recherche en Paléontologie – Paris (CR2P), UMR 7207, MNHN, CNRS, Sorbonne Université, 8 rue Buffon, CP 38, F-75005, Paris, France. [6] Biogéosciences, UMR6282, CNRS, Université Bourgogne, 6 Boulevard Gabriel, 21000 Dijon, France. [7] SNSB-Bayerische Staatssammlung für Paläontologie und Geologie, Richard-Wagner-Str. 10, 80333 Munich, Germany. [8] Friedrich-Alexander-Universität Erlangen-Nürnberg, Schloßplatz 4, 91054 Erlangen, Germany. [9] Muséum national d'Histoire naturelle de Paris, Centre de Recherche en Paléontologie –Paris, UMR CNRS 7207 CR2P, 57, rue Cuvier, 75005 Paris, France.

ABSTRACT

The Cretaceous Lebanese outcrops of Haqel, Hjoula (Cenomanian) and Sahel Aalma (Santonian) are renowned for their exceptional preservation of coleoid soft tissue and provide an unmatched opportunity to study a single species, *Dorateuthis syriaca*, across coeval shallow carbonate mud deposits. Despite being the most abundant coleoid from these deposits, the taxon lacks clear, unambiguous diagnostic characteristics of both the gladius, and soft tissue anatomy. The absence of a defined character complex for the species has led to inconsistencies in the literature and the need for a reappraisal.

This investigation represents the largest sample of *D. syriaca* studied with high-resolution, multi-imaging techniques, and has obtained a comprehensive morphological dataset of

measurements on this key taxon. This has allowed us to refine some of the character states used to understand the phylogeny of coleoids. Furthermore, we have identified morphological characters that were previously undescribed for the genus, including suckers, axial nerves, and possible retractor muscles, as well as provided confirmation of the circulatory and excretory systems, as well as an Octobrachia-type digestive system. We also discount the presence of tentacles, tentacular pockets, and onychites within the arm crown, and show that the species definition of *D. syriaca* is more complex than expected as our sample strongly suggests intraspecific variability is present in the gladius. We strongly support the hypothesis that it was an 8-armed coleoid that was likely an active visual predator.

INTRODUCTION

In the Mesozoic fossil record, coleoid soft tissues are known from just a few key Lagerstätten (Donovan & Fuchs 2016). In the Jurassic, these include the Pliensbachian–Toarcian Ya Ha Tinda Lagerstätte (Alberta, Canada), the Toarcian Posidonia shales of Holzmaden (Germany), the Callovian deposits of La Voulte-sur-Rhône (France), the Oxfordian Clay Formation at Christian Malford (England), and the Tithonian lithographic limestones of Solnhofen (Germany) (e.g., Wilby *et al.* 2004; Klug *et al.* 2005, 2015, 2021a,b; Fuchs 2007; Fuchs *et al.* 2007a,b, 2009, 2013, 2016; Charbonnier 2009; Charbonnier *et al.* 2014; Martindale *et al.* 2017; Marroquín *et al.* 2018; Hart *et al.* 2019; Muscente *et al.* 2019). Coleoid soft tissues in Cretaceous are famously known from the celebrated lithographic limestones of Lebanon (Fuchs *et al.* 2009; Fuchs & Weis 2009; Jattiot *et al.* 2015). In this Lebanese Lagerstätte, coleoids are most abundant in three outcrops: Haqel, Hjoula (Cenomanian) - also referred to in the literature as Hâdjoula, Hâkel - and the Santonian-aged Sahel Aalma (Woodward 1883, 1896; Roger 1946; Fuchs 2006a,b; Fuchs *et al.* 2009; Fuchs & Weis 2009; Fuchs & Larson 2011a,b). The coleoid assemblage is comprised of ten genera from the Octobrachia suborders, Prototeuthina, Teudopseiina, and Incirrata (Fuchs 2020); two of these genera, *Keuppia* and *Styletoctopus*, are positioned as the oldest known representatives of the Incirrata (Fuchs *et al.* 2009; Fuchs 2020). From a taphonomic perspective, the soft tissue preservation surpasses that of the celebrated Solnhofen Limestones (Fuchs 2006a, b; Fuchs *et al.* 2007; Fuchs & Weis 2009).

The prototeuthid *Dorateuthis syriaca* Woodward, 1883 is the most abundant coleoid in these Cretaceous-aged deposits (Fuchs & Larson, 2011a). Despite this, the species lacks unambiguous diagnostic characteristics (Fuchs & Larson 2011a; Jattiot *et al.* 2015). The

holotype has been noted to be poorly preserved (Fuchs 2006b), and many of its morphological characters are unclear and have been difficult to confirm using classical optical and UV photographic methods (Fuchs & Larson 2011a; Jattiot *et al.* 2015). The original species description by Woodward (1883) included some erroneous descriptions regarding the arm crown, fins, and gladius elements which has contributed to ambiguity regarding the exact diagnosis (Roger 1946; Fuchs 2006b, 2007; Fuchs & Larson 2011a; Jattiot *et al.* 2015), and systematic placement (Naef 1922; Roger 1946; Bandel & Leich 1986; Fuchs 2006b, 2007; Jattiot *et al.* 2015). The current genus-level taxonomic description is outlined in Fuchs (2020); Fuchs & Larson (2011a) provide the species-level description.

D. syriaca is known from three Lebanese localities Hjoula, Haqel (Cenomanian) and Sahel Aalma (Santonian), making the range of the species occurrence ca. 9–10 Ma. Multiple individuals have been figured (Woodward 1883; Naef 1922; Roger 1946; Fuchs 2006a,b, 2007, 2020; Fuchs & Larson 2011a; Jattiot *et al.* 2015; Donovan & Fuchs 2016; Klug *et al.* 2021b) as *D. syriaca*, or identified as such in international collections (e.g., MNHN, NHMUK, BHI). As *D. syriaca* is represented by a greater number of individuals than any other coleoid species from the Lebanese localities, it provides an unprecedented opportunity to study the intraspecific variation, and possible anatomical variance related to *post mortem* taphonomic processes.

This study represents the largest analysis on a single fossil species that combines precise morphological measurements complemented by an array of non-destructive and multimodal imaging techniques. In light of new imaging methods, the holotype of *D. syriaca* and 53 additional figured and previously undescribed individuals were examined. The new data reveal previous anatomical misinterpretations, resolve a number of novel character states for phylogenetic reconstructions (Whalen & Landman 2022), identify undescribed intraspecific variation, and provide insight into the lifestyle of the species. The resulting qualitative and quantitative dataset provides the most comprehensive understanding to date of the morphology of *D. syriaca*.

GEOLOGIC SETTING

During the Cretaceous, modern-day Lebanon (Fig. 1) was part of a large system of shallow carbonate platforms that were positioned on the Arabian craton (northeastern section of Gondwana) in the southern Tethys (Ferry *et al.* 2007; Fuchs *et al.* 2009; Fuchs & Weis 2009; Charbonnier & Audo 2012). Within these warm waters, oscillations in relative sea-level deposited fine grained, laminated, organic-rich lithographic limestones in restricted, intra-shelf

depressions (Fuchs 2006b; Ferry *et al.* 2007; Fuchs *et al.* 2009), and formed the renowned Lagerstätte deposits of Hjoula, Haqel, and Sahel Aalma. Each deposit shows some variation in the depositional environment and fossil assemblage.

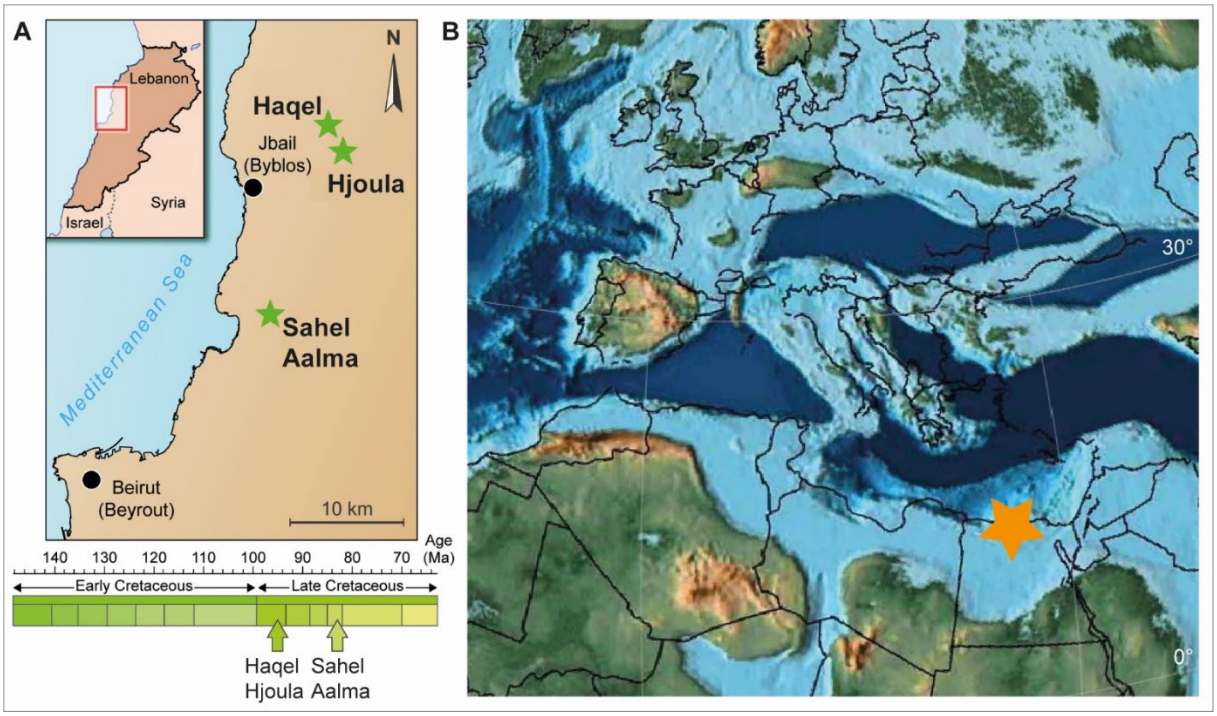

Figure 1: (A) Geographic location and stratigraphic position of the main coleoid-bearing localities of Haqel, Hjoula, and Sahel Aalma. Modified from Jattiot *et al.* (2015). (B) Simplified paleogeographic map of the Central Tethys during the Santonian, the time of deposition for Sahel Aalma. Created and modified from Scotese, C.R (2016). PALEOMAP PaleoAtlas for GPlates and the PaleoData Plotter Program, PALEOMAP Project.

Biostratigraphic data indicates that the older of the three sites, Haqel and Hjoula, formed somewhat contemporaneously in the late Cenomanian (George *et al.* in press; Wippich & Lehmann 2004; Fuchs *et al*. 2009). Though they are located geographically close to one another and share faunal similarities, they represent separate intra-shelf depressions (George *et al.* in press). Both outcrops are composed of highly fossiliferous lithographic limestones, though the sediments at Hjoula are more bituminous, have higher quantities of pyrite, and contain flint nodules (George *et al.* in press, Fuchs *et al.* 2009, Swinburne & Hemelben 1994). Each deposit has a high diversity of fossil organisms, though Hjoula is dominated by crustaceans while Haqel is renowned for the abundance of small teleost fish (El Hossny *et al.* 2023, Forey *et al*. 2003; George *et al.* in press).

The chalky laminated limestones of Sahel Aalma are constrained to the late Senonian (Santonian) (Ejel & Dubertret 1966; Fuchs 2006b), positioning it as ~10 My younger than the Cenomanian outcrops. In addition to the difference in lithology, Audo & Charbonnier (2012) identified deep water taxa in the faunal assemblage consistent with a deeper paleodepositional environment (Ferry *et al.* 2007; Fuchs *et al.* 2009; Fuchs & Larson 2011a; Audo & Charbonnier

2012), with a water depth most probably exceeding 150 m (Audo & Charbonnier 2012, George *et al.* in press).

Today, these three outcrops are located within a belt of Cretaceous sediments (NE-SW) in northwest Lebanon and each bear the name of the corresponding neighbouring town. Combined, these three deposits preserve exceptional faunal assemblages, including Upper Cretaceous fishes (Forey *et al.* 2003), arthropods (Roger 1946; Audo & Charbonnier 2012), annelids (Bracchi & Alessandrello 2005), echinoderms (Reich 2004), as well as coleoid, ammonoid, and nautilid cephalopods (Wippich & Lehmann 2004; Klug *et al.* 2021b). The Sahel Aalma outcrop is no longer accessible due to urban development (George *et al*. in press); therefore, most samples in this study are from the two Cenomanian sites.

INSTITUTIONAL ABBREVIATIONS

Muséum national d'Histoire naturelle, Paris, France (MNHN); Natural History Museum, London, England (NHMUK); Black Hills Institute of Geological Research, Hill City, USA (BHI); The University of Texas at Austin, Jackson School Museum of Earth History, Austin, USA (NPL); Naturhistorisches Museum Vienna, Austria (NHMW); Musée national d'histoire naturelle, Luxembourg City (MNHNL); Museo Civico di Storia Naturale di Milano, Italy (MSNM).

MATERIALS

The sample of *D. syriaca* used in this study includes 54 individuals selected from a larger group of 90 individuals, chosen as they preserved a generally complete gladius upon which diagnostic observations could be made. The individuals included are reposited in the collections of the Muséum national d'Histoire naturelle (MNHN), Paris (n = 11); Natural History Museum (NHMUK), London (n = 2); Black Hills Institute of Geological Research (BHI), Hill City (n = 29); The University of Texas at Austin, Jackson School Museum of Earth History (NPL), Austin (n = 1); Naturhistorisches Museum Vienna (NHMW), Vienna (n = 1); Musée national d'histoire naturelle (MNHNL), Luxembourg City (n = 1); Museo Civico di Storia Naturale di Milano (MSNM), Milan (n = 4), as well as 5 individuals from private collections. These were made available through photographs from co-author, DF. The provenance of the individuals is recorded as Haqel (n = 3), Hjoula (n = 36), and Sahel Aalma (n = 8). The remaining 7 individuals are also from the Lebanese Lagerstätten, though the precise

providence is not recorded. Supplementary Table 1 contains the locality and repository information for each individual considered and used for this study, and the analyses performed. This includes previously described and undescribed individuals.

METHODS

Multiple non-destructive, high-resolution imaging techniques were utilized to gather data, including:

- µXRF major-to-trace elemental mapping:
  - PUMA Beamline, SOLEIL Synchrotron, Saint-Aubin, France (6 individuals). Spectral interpretation on these data was carried out using PyMCA data-analysis freeware (Solé et al., 2007).
  - M6 Jetstream Bruker XRF, UAR 3224, Centre de Recherche sur la Conservation, MNHN, CNRS (2 individuals).
  - ATLAS M benchtop microEDXRF (micro XRF) spectrometer, iXRF, Austin, TX, USA (1 individual).
- Reflectance Transformation Imaging (RTI), MNHN, Paris, France (10 specimens).
- UV light photography (MNHN), (5 specimens).
- UV-visible-near infrared multi-spectral imaging (MSI), IPANEMA Platform, SOLEIL Synchrotron, Saint-Aubin, France (3 specimens).
- X-ray absorption spectroscopy (XAS), PUMA Beamline, SOLEIL Synchrotron, Saint-Aubin, France (1 specimen).

See Table 1 for the acquisition parameters of the figured specimens.

As a basis for the systematic revision, we used the diagnostic characteristics for *Dorateuthis* from Fuchs (2020) which provides a range of measurements for the genus, and the indices used to describe the various characters used in this reassessment. All measurements in this study were obtained using FIJI ImageJ software (Schindelin *et al.* 2012). Following common terminology, body length refers to the cumulative measurements of the mantle, head, and arms (posterior-most tip of the mantle to anterior-most tip of the longest preserved arms), while mantle length reflects the length of the mantle only.

Specimen	Imaging Type	Equipment/ Beamline	Illumination/ Excitation	Beam size/Full field	Acquisition/ Dwell time	Fig
BMNH C5017 (Holotype)	µXRF	M6 Jetstream Bruker XRF	Rhodium anode, 50 kV	100µm	2000 ms	3 A, B; 13 A
	RTI	-	-	-	-	3C - E
	Photograph (UV light)	-	-	-	-	3 F, G
	Photograph (Natural light)	-	-	-	-	4 E, F
BHI 2201	Photograph (Natural light)	-	-	-	-	4 A, B
MNHN.F.A 88588	Photograph (Natural light)	-	-	-	-	4 C, D
	µXRF	PUMA Beamline SOLEIL	monochrome 18.2 KeV	-	-	13 B; 14 B
BHI 2205	Photograph (Natural light)	-	-	-	-	4 G, H
	µXRF	iXRF	-	-	-	13 D
	Photograph (UV light)	-	-	-	-	14 F
private collection	Photograph (Natural light)	-	-	-	-	4 I, J
BHI 2229	Photograph (UV light)	-	-	-	-	8 A
BHI 5779	Photograph (UV light)	-	-	-	-	8 C
BHI 2203	Photograph (UV light)	-	-	-	-	8 E
NHMW1998z0105/0000	Photograph	Lukeneder & Harzhauser 2004	-	-	-	8 F
	Photograph	Lukeneder & Harzhauser 2004	-	-	-	9 F
MNHN.F.A 88589	µXRF	M6 Jetstream Bruker XRF	Rhodium anode, 50 kV	180 µm	500 ms	9 B; 13 C
	UV-visible-near infrared multispectral imaging	IPANEMA Platform	385 nm, green luminosity (514	-	30000 ms	9 C

	Photograph (Natural light)	-	-	-	-	11 A
	RTI	-	-	-	-	11 B-D, K-M; 12 A
	Photograph (UV light)	-	-	-	-	14 E
MNHN.F.50396	RTI	-	-	-	6 seconds	9 D
	Photograph	Jattiot *et al.* 2015	-	-	-	9 E
BHI 2222	Photograph (Natural light)	-	-	-	-	9 F
MNHN.F.A50400	RTI	-	-	F-stop: 10	25 seconds	9 I
MNHN.F.R06746	RTI	-	-	F-stop: 8	8 seconds	11 F, H
	Photograph (UV light)	-	-	-	-	11 G
BHI 2213	Photograph (Natural light)	-	-	-	-	11 I, J
MNHN.F.A88590	RTI	-	-	F-stop: 7	6 seconds	12 B
BHI 2219	Photograph (UV light)	-	-	-	-	12 E
NPL52121	Photograph (Natural light)	-	-	-	-	14 A
BHI 2212	Photograph (Natural light)	-	-	-	-	14 C
BHI 2227	Photograph (Natural light)	-	-	-	-	14 C

Table 1. Summary of the acquisition parameters for the each of the specimens figured. Note, this does not reflect all the individuals in the study sample (see supplementary material).

Initially, each individual was evaluated to determine if the gladius was complete or preserved in such a way that diagnostic measurements could be obtained. This was carried out either on the fossil, or by analyzing photographs of the individual (UV or natural light) in FIJI ImageJ software (Schindelin *et al.* 2012). Two key diagnostic measurements include the width and length of the gladius (Fig. 2, Supplementary Table 3). Additional measurements and observations on other gladius elements (e.g., apical angle and reinforcements) were then

obtained (Fig. 2 and Supplementary Table 3 for measurements, and Supplementary Table 4, and 5 for indices and characters respectively). Arm measurements were gathered for 22 individuals. Where the arms were visible, and the position of the eye could be determined, arms were measured from the central line of the eye, tracing the curve, to the anterior-most arm tip (Supplementary Table 3). This method follows the parameters for Octobrachia outlined in Nixon (2011, fig. 3). The arm pairs of *Dorateuthis* vary in length (Fuchs 2020) so where arm lengths have been used as indices, the maximum lengths have been utilized. The entire sample was evaluated for the presence and configuration of suckers, cirri, and the arrangement of the arm crown.

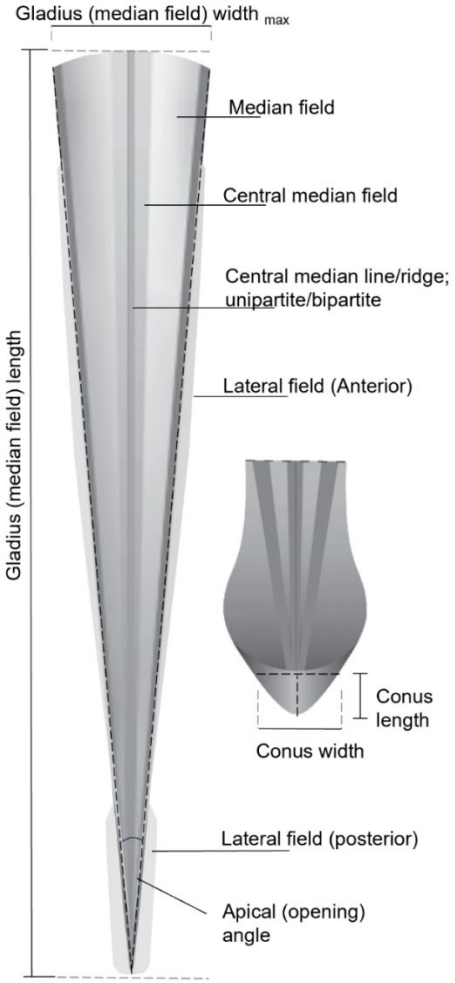

Figure 2: Illustration of hypothesized *D. Syriaca* gladius adapted from Fuchs (2006b, 2007, 2016, 2020) and Fuchs & Larson (2011a). The gladius has the triangular-shaped median field and funnel-like conus characteristic of the Suborder Prototeuthina. Pronounced lateral keels and a bipartite median ridge extend from the anterior to posterior margins; a median keel is not present in *Dorateuthis* (Fuchs 2020). The anterior margin is slightly convex. The apical angle is <12°. Both the observed anterior and posterior, lateral fields are indicated in this illustration.

Eyes were not visible in the holotype, so the length of the cephalic cartilage was used as a proxy for their diameter. Where the eyes and lenses were preserved, their maximum and minimum diameters were measured. Soft tissues and organs visible in the various imaging methods were recorded.

SYSTEMATIC PALAEONTOLOGY

Subclass COLEOIDEA Bather, 1888

Superorder OCTOBRACHIA Haeckel, 1866

Suborder PROTOTEUTHINA Naef, 1921

Family PLESIOTEUTHIDAE Naef, 1921

Genus DORATEUTHIS Woodward, 1883

Type species.—*Dorateuthis syriaca* Woodward, 1883 from the Cretaceous (Cenomanian-Santonian) lithographic limestones of Lebanon.

Included species.—*Dorateuthis syriaca* Woodward, 1883 is the only species that can be assigned with certainty. *''Neololigosepia'' stahleckeri* Reitner & Engeser, 1982 and *''Maioteuthis'' morroensis* Reitner and Engeser, 1982 (Barremian, Cape Verde Islands); *''Plesioteuthis''* sp. Engeser & Reitner, 1985 and *''Maioteuthis'' damesi* Engeser and Reitner, 1985 (Aptian, Heliogoland Germany); *''Plesioteuthis'' arcuata* von der Marck, 1873 (Campanian, Germany), and *''Plesioteuthis'' maestrichtensis* Binkhorst van den Binkhorst, 1861 (Maastrichtian, Netherlands) are all assigned to this genus based on their narrow gladius and continuous lateral keels, though they are represented by poorly preserved individuals.

Diagnosis.— Modified from Fuchs (2020)

Very small to medium-sized (mantle length <50–400 mm), gladius very slender to slender (gladius $width_{max}$ to gladius length 0.05–0.19). Central reinforcements variable; median line or ridge but no keel; uni-or bipartite. Median field very slender (opening angle <12°), median field area very large (median field area to gladius area >0.8). Anterior margin slightly convex. Lateral keels (reinforcements) pronounced, present from anterior to posterior margins; Lateral fields variable: absent, anterior (field length to gladius $length_{max}$ ratio 0.8–0.9), posterior (field length to gladius $length_{max}$ ratio ~0.3); narrow when present. Conus ventrally closed (conus $length_{max}$ to gladius $length_{max}$ ratio 0.03–0.05). Arm length moderate (arm length to mantle length ratio ~0.5); elongated dorsal pair. Cephalic cartilage ring shaped in lateral view. Fins anteriorly rounded; oar shaped.

Occurrence. Lower Cretaceous (Barremian)–Upper Cretaceous (Maastrichtian): Lebanon, northern Germany, Cape Verde Islands, the Netherlands.

DORATEUTHIS SYRIACA Woodward, 1883

1878 *Sepialites* Fraas: p. 346.

1883 *Dorateuthis syriaca* n. sp. Woodward: p. 1-5, pl. 1.

1888 *Curculionites senonicus* Kolbe: p. 135, pl. 11, fig. 8.

1896 *Sepialites*; Woodward, p. 231.

1922 *Dorateuthis syriaca*; Naef: p. 118.

1922 "*Plesioteuthis fraasi*" Naef: p. 133, fig. 50.

1922 "*Sepialites sahil-almae*" O. Fraas, 1878; Naef, p. 134, fig. 49c.

1943 *Sepialites sahil almae*; Klinghardt, p. 12, fig. 8.

1946 *Leptoteuthis syriaca*; Roger, pl. 4, figs. 5, 6, pl. 9, figs. 1, 2.

1952 *Sepialites Sahel-almae*; Roger, p. 738.

1952 *Leptoteuthis syriaca*; Roger, p. 739.

1986 *Dorateuthis sahilalmae*; Engeser & Reitner, p. 3, fig. 1, pl. 1, fig. 1.

1986 ?*Dorateuthis* sp.; Engeser and Reitner, p. 4, pl. 1, fig. 2.

1987 *Sepialites sahilalmae* (O. Fraas) Naef, 1922; Riegraf, p. 97.

1988 *Dorateuthis sahilalmae*; Engeser, p. 43.

2006a *Dorateuthis cf. syriaca*; Fuchs, p. 7, fig. 4, pl. 1–3.

2006b *Dorateuthis sahilalmae*; Fuchs, pl. 17H, pl. 22F.

2007 *Dorateuthis syriaca*; Fuchs, Klinghammer and Keupp, p. 246.

2007 *Dorateuthis sahilalmae*; Fuchs, Klinghammer and Keupp, p. 246.

2007 *Dorateuthis syriaca*; Fuchs, p. 64, fig. 4.

2007 *?Dorateuthis sahilalmae*; Fuchs, p. 64.

2011a *Dorateuthis syriaca*; Fuchs and Larson, p. 237, figs. 2–8, fig. 7.5.

2015 *Dorateuthis syriaca*; Nixon, p. 8, fig. 6a, c, d.

2015 *Dorateuthis syriaca*; Jattiot *et al.,* p.152, figs.4-6, 10, 11, fig.12.1-3, fig.13.2-3, fig. 14.

2016 *Dorateuthis syriaca*; Donovan and Fuchs, p. 20, figs. 12-15.

2016 *Dorateuthis syriaca*; Fuchs *et al*., p. 438, figs. 1, 9.

2018 *Dorateuthis syriaca*; Gueriau *et al*., p. 985, fig. 5.

2020 *Dorateuthis syriaca*; Fuchs, p. 11, fig. 3.

2021 *Dorateuthis syriaca*; Klug *et al.* 2021c, P. 7, Fig.5.

Holotype. —BMNH C5017, original of Woodward (1883, pl. 1)

Type locality.— Sahel Aalma, Lebanon

Occurrence.— late Cenomanian–late Santonian of Lebanon

Redescription of the holotype: The holotype of *D. syriaca* (Fig. 3) is preserved in ventral view. The entire length (the posterior mantle margin to the anterior tip of the arms) is ~68 mm. The length of the gladius is ~40 mm and corresponds with the length of the mantle. It has a triangular median field and convex (Fig. 3F, H) anterior margin (~4 mm wide). The gladius has well defined lateral reinforcements (keels) and a central bipartite ridge. All are continuous from the anterior to the posterior margin (Fig. 3 F, H). The lateral keels diverge at an angle of 6.3°. There is no evidence of a central median field encompassing the individual's bipartite ridge. There is no evidence of lateral fields, hyperbolar zones or conus.

µXRF mapping and UV photography enables the most precise assessment of arm length to date. The holotype has eight tapered arms (Fig. 3A, G, H). Six appear complete and range from 18 to 21 mm in length. Two lack their distal sections and have a preserved length of 15 and 17 mm. Using the index (arm length $_{max}$ to gladius length) outlined in Fuchs (2020) the arms are 'moderate' in size (a ratio of 0.53). The preserved diameter of seven of the arm bases varied between 0.5 and 1.4 mm. The arm with the smallest diameter (0.5 mm) is partially obscured by another arm, and therefore the original diameter was likely larger. There is no evidence of an additional tentacular pair, or any associated hooks that were noted in the original description by Woodward (1883). No suckers or cirri were observed.

µXRF elemental mapping reveals the cephalic cartilage (Fig. 3A), which is enriched in phosphorus and observed as two concave, semi-circular traces that flank the oesophagus in an anterior-posterior orientation. The cartilage is about 9 mm in length and is positioned between the posterior margin of the arm crown and the anterior lateral keels. The structures have a larger medial separation than is normally observed in dorsal view, and do not have the "pear" shape associated with ventral view (Fuchs & Larson 2011a*,* fig. 4), therefore we interpret what is preserved to be a central slice (Fig. 3A). The length of the cephalic cartilage was used as a proxy for eye diameter for the holotype. Relative to the length of the gladius (diameter $_{max}$ to gladius length), the eyes were ~0.23 the length. The cephalic cartilage flanks a mass of soft tissue that corresponds with the oesophagus and possibly the brain or optic lobes.

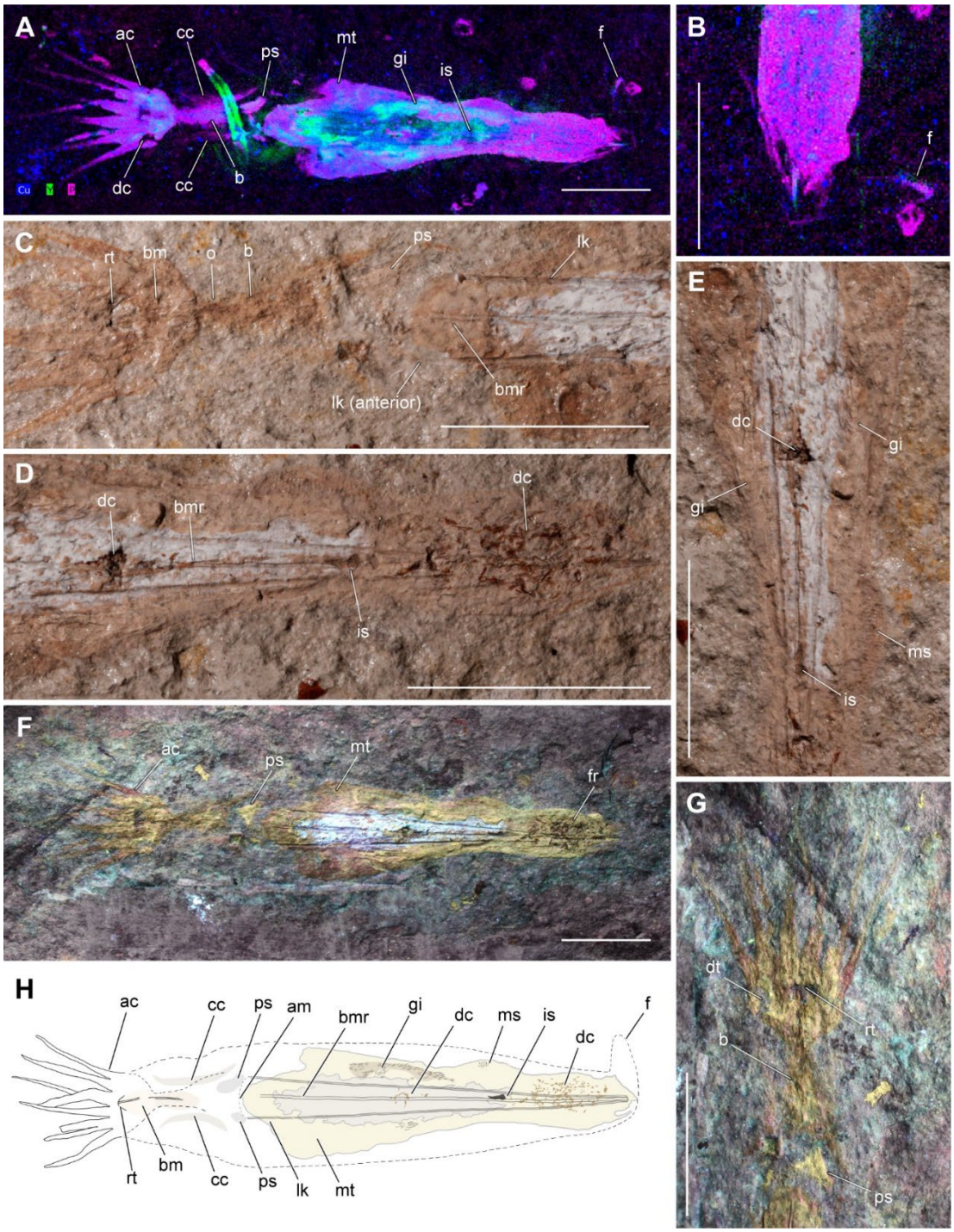

Figure 3: The holotype (BMNH C5017) of *D. syriaca* as illustrated by multiple non-destructive imaging techniques. (A) µXRF overlay of copper (blue), yttrium (green) and phosphorous (pink) distributions over the entire individual. Data collected with M6 Jetstream Bruker XRF (UAR 3224 CRC, MNHN); (B) Rotated close-up of the posterior section with the fin outline visible on the right (same acquisition); (C–E) Individual images from the Reflectance Transformation Imaging (RTI) stack showing (C) the anterior part of the body, head, and arm crown, (D) the posterior part of the body, and (E) the central part of the body; (F, G) UV photographs (L. Cazes, MNHN) of (F) the entire individual, and (G) the anterior part of the body, head, and arm crown; (H) Hypothesized illustration of the holotype (J. Gardner). The Y-enriched elongate feature in (A) is not considered part of the individual, but from a contemporaneous organism. Scale bars 10 mm. Abbreviations: ac – arm crown, am – anterior margin (gladius), b – brain, bm – buccal mass, bmr – bipartite median ridge, cc – cephalic cartilage, dc – digestive contents, f – fin, g – gill, is – ink sac, lk – lateral keel, ms – muscular striations, mt – mantle tissue, o – oesophagus, ps – paired structures, rt – rostrum tip.

The position of the cephalic cartilage is inconsistent with the eye position supposed by Woodward (1883). Indeed, imaging reveals their interpretation reflects degraded tissue at the base of the arm crown (Fig. 3A, G). Small protrusions, visible in the UV photographs and elemental maps, are positioned anteriorly to the lateral keels and represent cartilage or soft tissue (Fig. 3A, C, F- H). It is possible that these represent posterior salivary glands or are the remnants of retractor musculature. Two areas of digestive contents are visible (Fig. 3D, F, H). The anterior-most area was originally described as an ink sac (Woodward, 1883, pl. 1), however, our multimodal imaging reveals these structures are in fact digestive remnants. A random sampling of fragment sizes in these two digestive assemblages shows that the anterior remains are roughly 0.2–0.4 mm in length, while those in the posterior section have larger components (approximately 0.2–1.2 mm). A small ink sac is more posteriorly located (Fig 3D, H). RTI and μXRF mapping also reveal faint imprints of what we interpret to be elongate gill lamellae and a posterior fin (Fig. 3A, B, E, F). The contours of the fin revealed by elemental mapping (Fig. 3B) resemble the oar shape characteristic described for *Dorateuthis* (Fuchs 2020). As fins are otherwise unknown in individuals from Sahel Aalma (Fuchs & Larson 2011a), this represents the only known coleoid fin tissue preserved from this locality.

REDESCRIPTION OF *D. SYRIACA*

Size

The diagnostic mantle length for *Dorateuthis* is 201 - 400 mm (Fuchs 2020), which is categorised as “medium” in size. The mean mantle length in this study is smaller (~112mm, with a standard deviation of 35 mm), however, one of our measured samples did fall within the range for the medium sized mantle length. The rest are either small (n = 50, ~93%), or very small (n = 3, 6%). The body length (anterior tip of longest preserved arm to the posterior tip of the mantle) was able to be measured for 43% of the individuals in the whole sample. Of these, the majority, ~32%, had a body length that measured between 50 to 200 mm (mean length of ~141 mm and standard deviation of 43 mm). Five (9%) ranged between 201 to 400 mm in length (mean of 223 mm, and a standard deviation of 20 mm). One individual (not figured) had a body length of 241 mm.

Gladius size and shape

All the measured individuals have a triangular-shaped median field (Figs. 2 and 4A–F) with the widest section located at the anterior-most margin of the gladius. The shape of the anterior margin is slightly convex. This varies from the current diagnosis (Fuchs 2020), though it supports a previous, tentative interpretation (Fuchs 2006b, fig. 4). An anteriorly rounded imprint or contour on the ventro-medial section of the gladius is observed in four individuals (Fig. 4E–H). It is located just posterior to the anterior margin and bears a resemblance to the medial component of the head retractors seen in *Vampyroteuthis* (Bizikov & Toll 2016, fig. 12). As such, we suggest this feature corresponds with an attachment site for muscle tissue.

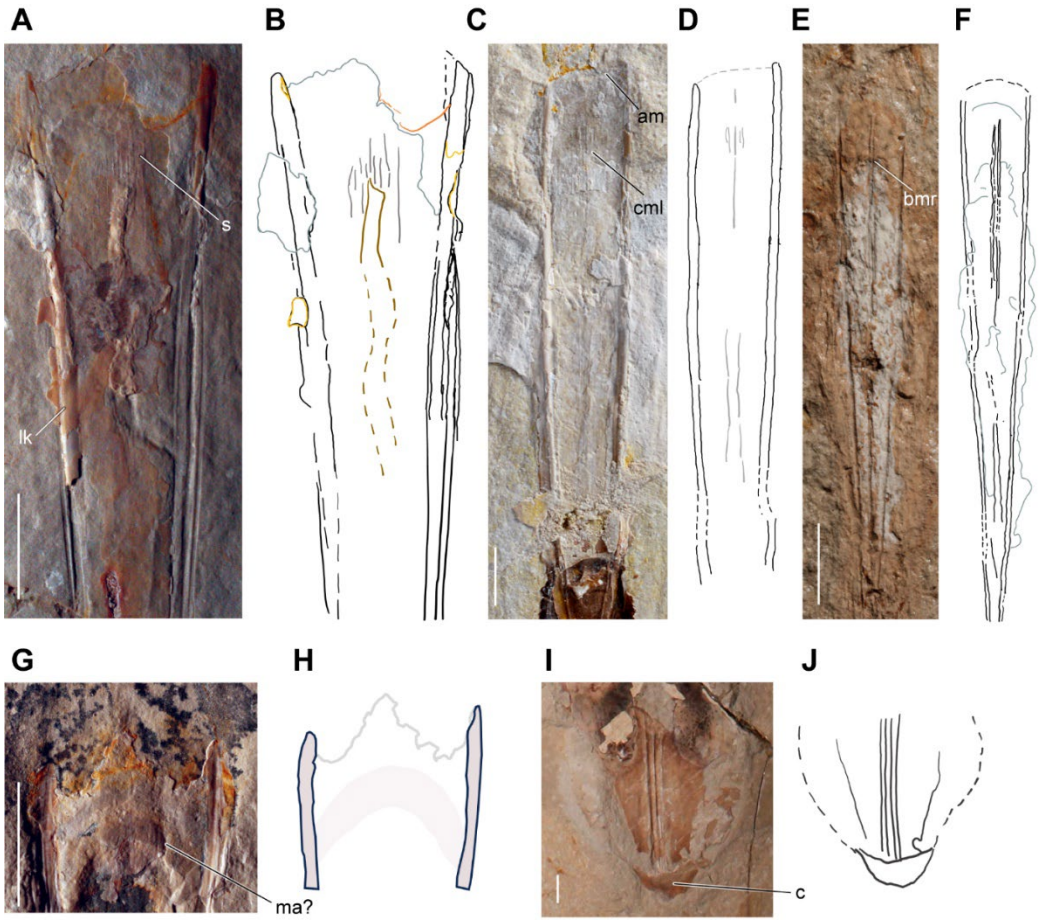

Figure 4: Photographs (natural light) and interpretative line drawings of gladius morphologies observed in *D. Syriaca.* (A–F). (A, B) BHI 2201, (C, D) MNHN.F.A88588, and (E, F) holotype BMNH C5017 showing the characteristic triangular-shaped median field, slightly convex anterior margin, and median reinforcement types. These median reinforcements take the form of a central median field that may have longitudinal striations (A, B). A central median line (C, D) or ridge (E, F) is also observable in the sample; these can be unipartite (C, D) or bipartite (E, F), and are observed with a central median field (C, D), and without (E, F). (G, H) BHI 2205 showing a semi-circular imprint that possibly reflects a muscle attachment site. (I, J) A ventrally closed conus, characteristic of Prototeuthina, observed in an individual from a private collection. Scale bars (A, C, E, G) 10 mm, (I) 5 mm. Abbreviations am – anterior margin of the gladius, bmr - bipartite median ridge, c - conus, cml - central median line, ma? - muscle attachment site?, s – striation.

87% of the individuals have the slender (gladius $width_{max}$ to gladius length) gladius proportions of *Dorateuthis* (Supplementary Table 4), though 13 % show a very slender gladius. All the individuals exhibit the requisite apical (opening) angle (<12°, mean of 6.9°). As not all the individuals measured are preserved in an ideal dorso-ventral position, this mean angle inherently incorporates some uncertainty. We found no significant correlation to link gladius size, shape, or total body size to any of the three specific localities (Fig. 5A, B). However, Sahel Aalma shows the most size disparity as the smallest (the holotype, with a mantle size of 40 mm) and largest (MNHN.F.A50402, 241 mm) individuals are from this outcrop.

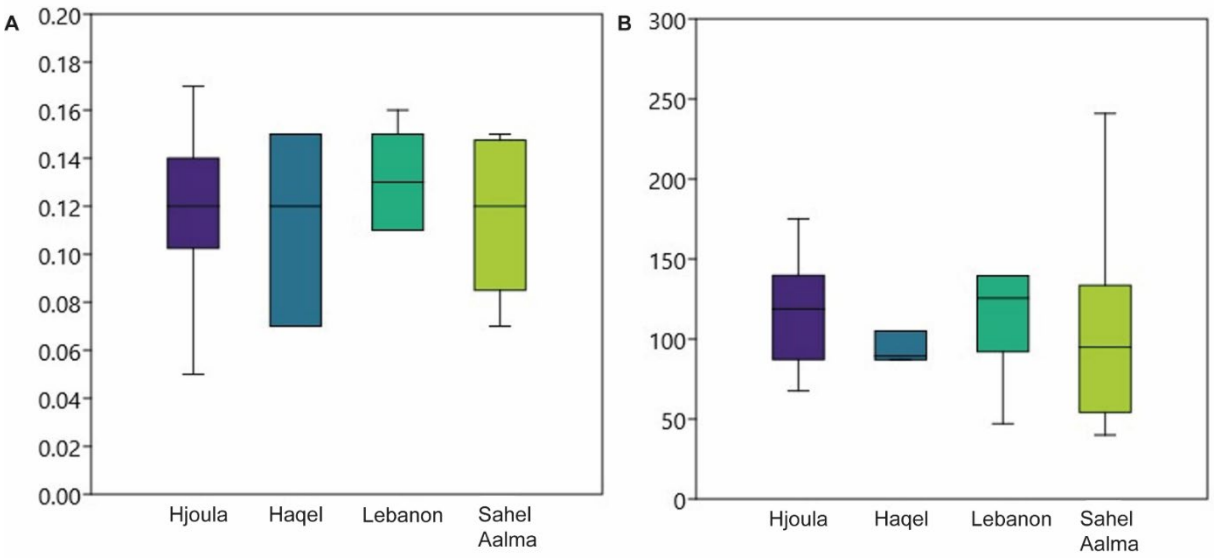

Figure 5: Size ranges were determined using (A) a gladius index and (B) gladius length. The gladius index is based on the ratio between gladius length and median field width, and then qualified by locality. *n* = 8 (15%) of the sample were noted to be from the Santonian-aged site of Sahel Aalma, and the older Cenomanian localities of Haqel (*n* = 3, ~6%), and Hjoula (*n* = 36, ~67%). As a small number of the individuals from these Lebanese outcrops lack their specific locality information (*n* = 7, ~13%), a more general grouping of 'Lebanon' was also included.

Gladius reinforcements, lateral fields, and median field area

Each of the 54 studied individuals has characteristic lateral reinforcements (keels) that are pronounced, and continuous from the anterior to the posterior margins of the gladius (Figs. 2, 4A–F). More than half of the sample (63%) exhibited some form of median reinforcements (Fig. 4A–F; Supplementary Table 5), longitudinally bisecting the gladius. These median reinforcements vary and take the form of either a central medial line (Figs. 2, 4C, D) or ridge (Figs. 2, 4E, F) which may be uni- or bi-partite. A central median field, an elongate area in the central section of the median field (Figs. 2, 4A, B) may also be visible and span the line or ridge; they are also observed without a line or ridge. Whether this variation is related solely to orientation is not clear. Longitudinal striations (Fig. 4A, B) were commonly observed in the

central median field in both dorsal and ventral view. These have previously been described in plesioteuthids, such as *Plesioteuthis prisca* (Naef, 1922, fig. 42b).

The gladius has three observed morphological variations (Fig. 6A–C) with two lateral field configurations. These include anterior (Fig. 6A) or posterior (Fig. 6B) lateral fields, though the most common type (78% of the sample) has a complete absence of lateral fields (Fig. 6C). Seven individuals have anteriorly positioned lateral fields (Fig. 6A) which represent 80% to 90% of the length of the gladius. They have no visible posterior lateral fields. Four have elongated posterior lateral fields (30% of the gladius length) with no evidence of anterior lateral fields (Fig. 6B). These gladius morphotypes could not be associated with other soft tissue characters (e.g. arm length, total body size, or locality) in the study sample. It is possible that the variation observed is due to *post mortem* processes (e.g. inconsistent mineral replacement across the gladii, disarticulation, or non-uniform compression), ontogenetic stage, or dimorphism (e.g. Toll 1998; Bizikov & Toll 2016).

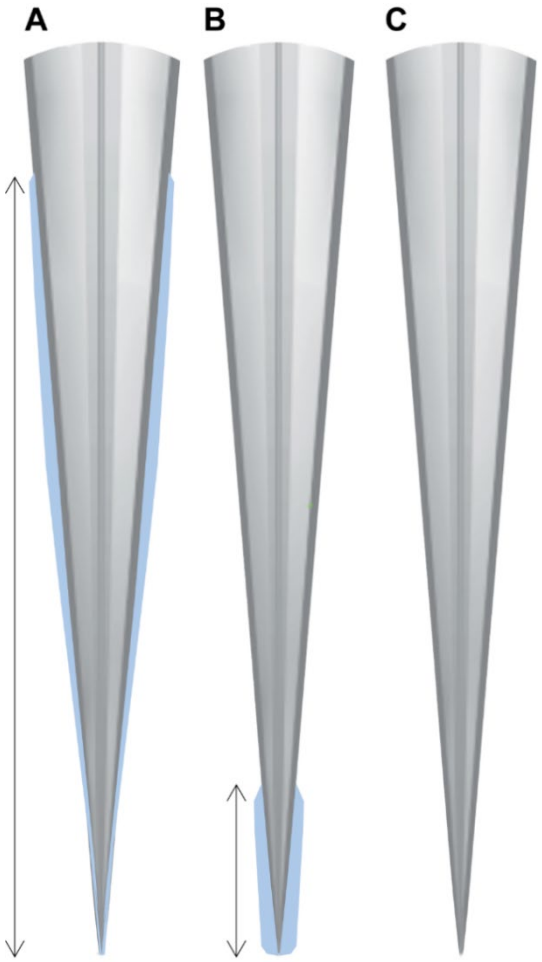

Figure 6: The morphological variation observed in the lateral fields (in blue) of D. syriaca: (A) anteriorly positioned, (B) posteriorly positioned, and (C) not visible. Modified from Fuchs (2006b, 2020).

Where lateral fields were observed, the area of the median field was calculated following the formula given in Fuchs (2020) (median field area to gladius area $_{total)}$, who notes this is "very large" (> 0.8) in *Dorateuthis*. All the individuals measured had a median field area >0.8 consistent with the diagnosis (Supplementary Table 4).

Conus

The conus is preserved in only two individuals, one in ventral view (Fig. 4I, J), the other in lateral. The length represents 3–5% of the gladius (Conus length $_{max}$ to Gladius length $_{max}$), and 80% of the width (Conus width$_{max}$ to Gladius width$_{max}$). No diagnostic indices currently exist for this character.

Arms

Twenty-two individuals (41%) provided the basis for arm measurements in this sample (see Methods). Each of these individuals preserve at least one arm; nineteen preserve two or more, and only two show a complete arm crown (Supplementary Table 5). Both the latter individuals show the diagnostic differentiation in arm length noted for the species: a more elongated dorsal arm pair, a relatively short ventral pair, and two intermediate-sized pairs in lateral position (Fuchs & Larson 2011a, fig. 3). The three smallest individuals (gladius <50 mm) in the sample, including the holotype, show very little variation in arm length (Supplementary Table 3; Fig. 3).

Comparisons between arm and gladius lengths were conducted (Fig. 7). These results indicated a general relative increase in relative arm length to mantle length as would be expected, supporting previous analyses that linked differentiation in the arm crown with allometry (Fuchs 2006b; Fuchs & Larson 2011a; Jattiot *et al.* 2015).

Chemical investigation reveals that the muscular mantle tissue reveals a diagenetic signature of strontium (Fig. 8) and yttrium. The presence of these elements is indicative of tissues preserved via authigenic replacement via calcium phosphate (apatite). Additionally, yttrium commonly substitutes for calcium during diagenesis (Gueriau *et al.* 2018), a mode of preservation common in Cretaceous Lebanese coleoid fossil soft tissues (Clements *et al.* 2020). Donovan & Fuchs (2016) supposed that arms were also preserved in apatite though they lacked analyses to confirm this. XRF data from the specimens showed that yttrium is present in both the arms and the (Fig. 8). The substitution of yttrium in varying soft tissues within a specimen has not been fully investigated, and this variation could be a diagenetic artifact, or could possibly reflect a bias of

phosphatization, which is known to be highly selective of particular tissues (as outlined in Clements *et al.* 2022).

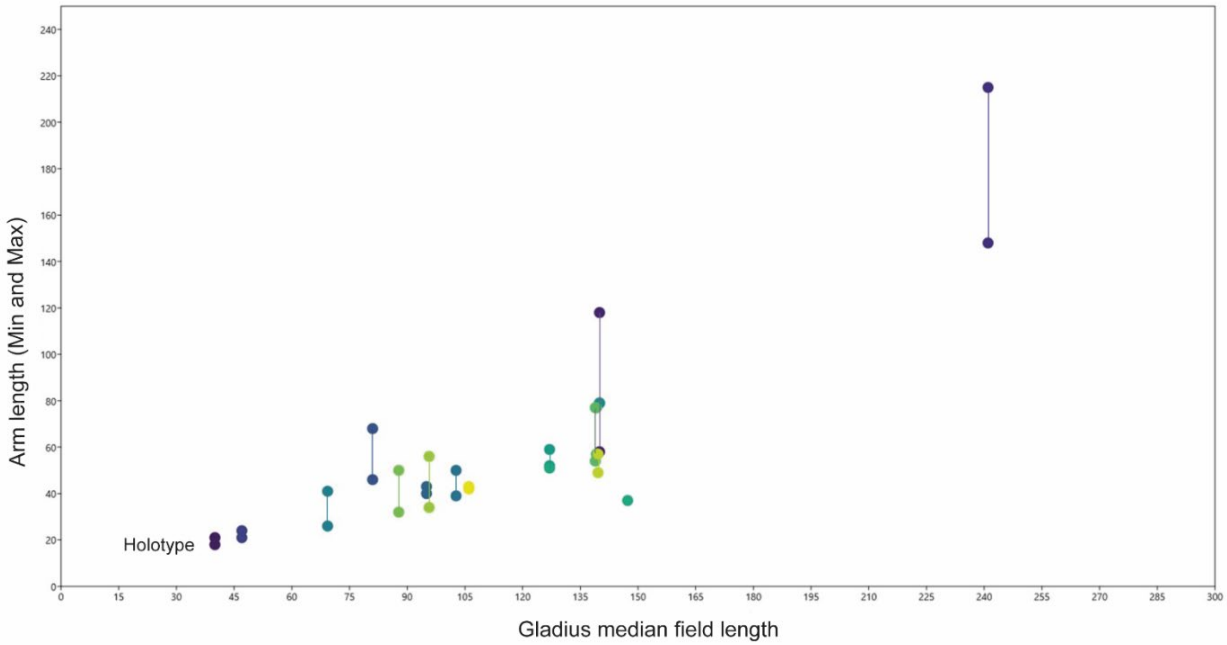

Figure 7: Arm length (Y-axis) vs. gladius median field length (X-axis) for the seventeen individuals that preserve at least two measurable arms, so maximum and minimum values could be obtained. These upper and lower values are represented by two longitudinally paired points; the colour of each pair marks one individual. The results here support a relative increase in arm length with mantle length, as well as increased differentiation in the arm crown with mantle length.

Armature

Eight individuals (15%) have retained evidence of suckers (Fig. 9A, B) ranging in diameter from ~1–2 mm. These appear uniserial and radially symmetrical when observed under UV light. Although no individual has an entire row observable, we infer they were present along the entire length since they are visible on proximal, medial, and distal portions of the arms in the separate specimens. There is no indication of attachment types, and no evidence of sucker linings, onychites, or cirri. Three individuals show remnants of the axial nervous system in the arm crown (Fig. 9C–D). These axial nerve elements (Rowe *et al.* 2023, Klug *et al.* 2023) are visible in UV light, and observed as delicate paired filaments, or dotted lines that follow the contours of the arms. Though one of these individuals have preserved the structure along the entire length of the arm, remnants are observed both proximally and medially (Fig 9C, D).

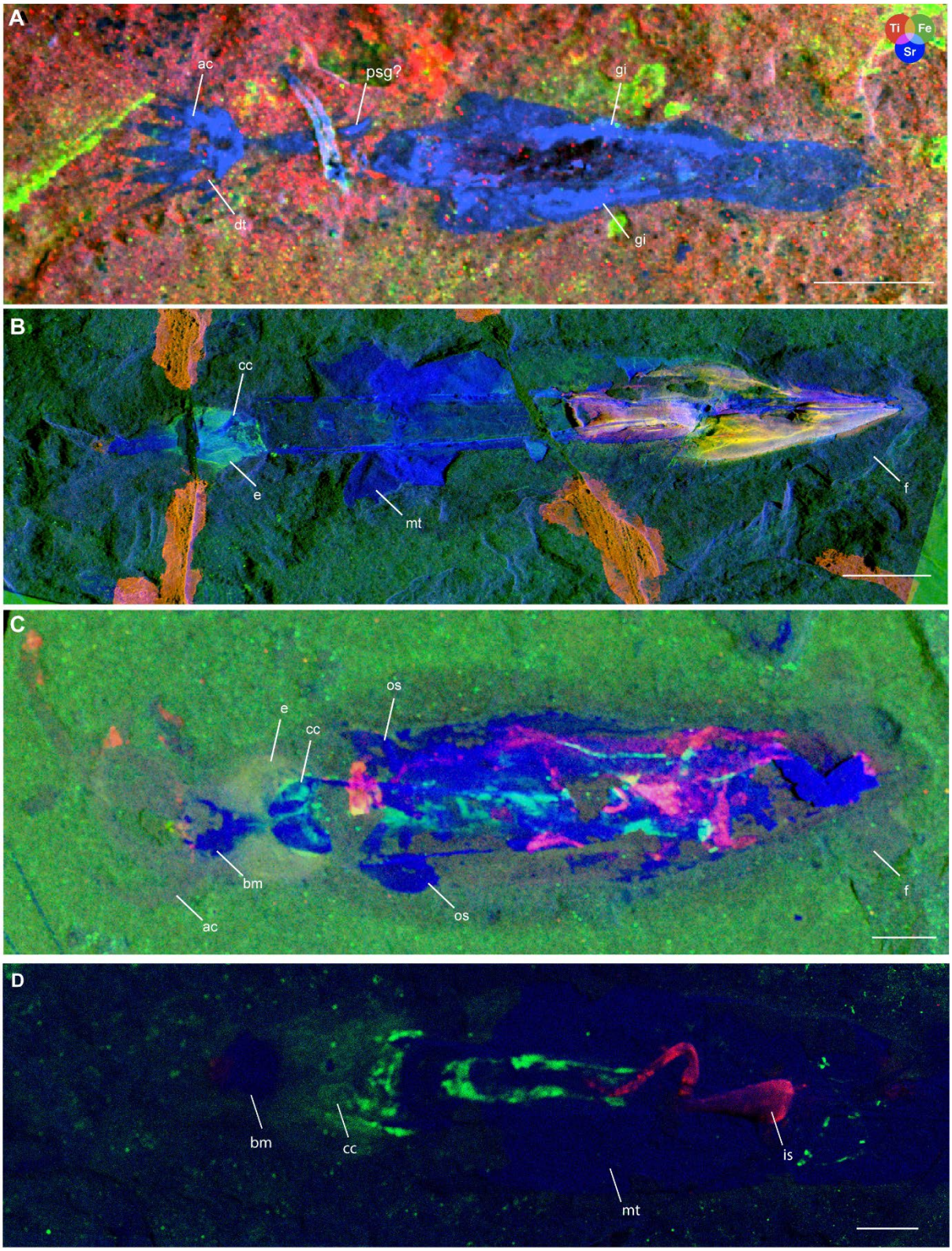

Figure 8: µXRF major-to-trace elemental mapping of 4 individuals of D. syriaca with overlays of titanium (red), iron (green) and strontium (blue) distributions (A) Holotype BMNH C5017; (B) MNHN.F.A88588 (C) MNHN.F.A88589 (D) BHI 2205. (A, C) collected using the M6 Jetstream Bruker XRF, UAR 3224 CRC, MNHN; (B) using the PUMA beamline, SOLEIL synchrotron, and (D) using Atlas X microXRF spectrometer equipped with a 5 micron polycapillary source, iXRF Systems, Austin, TX. Scale bars 10 mm (A), 10 mm (B–D). Abbreviations: ac – arm crown, an – axial nerve, bm – buccal mass, cc – cephalic cartilage, dt – degraded tissue, e – eye, f – fin, gi – gill, is – ink sac, mt – mantle tissue, os – ovoid structures, psg – posteriorly salivary gland.

Head

The cephalic cartilage (Fig. 9A-D) is evident in 31% of the individuals. Using the methodology for determining orientation of the cephalic cartilage as outlined by Fuchs and Larson (2011a), we determine that in our samples it is preserved both dorsoventrally and laterally. It is most clearly visible in the UV photographs and elemental maps where the phosphatized cartilage fluoresces (Fig. 9A, C). Structures interpreted as statocysts (Fig. 9C–E) are present on 4 individuals, just posterior to the cephalic cartilage. Internal calcareous statoliths (Boyle & Rodhouse 2008) are not observable.

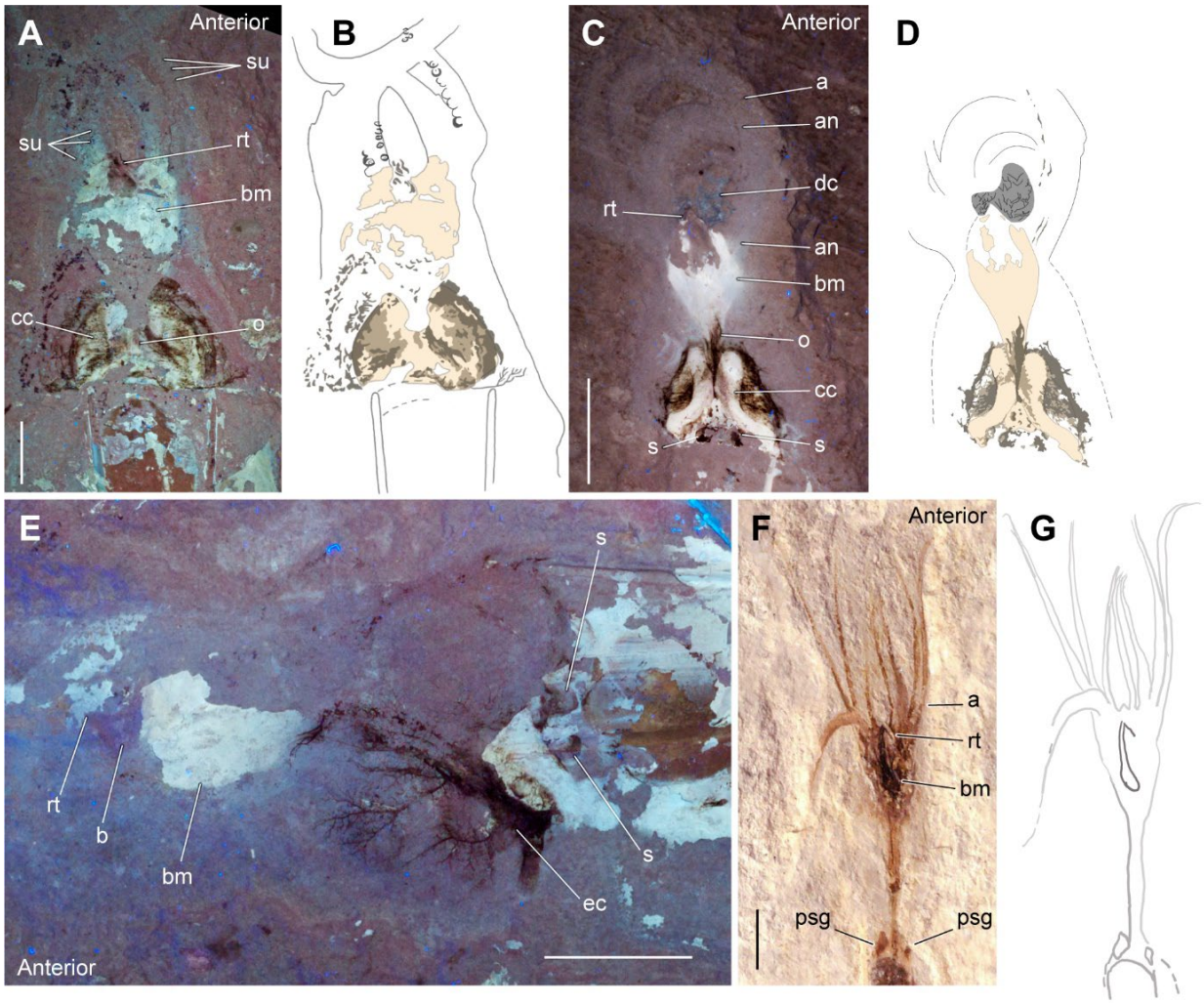

Figure 9: Photographs (UV, natural light), and interpretative line drawings of the head and arm crown region of *Dorateuthis*. (A-B) BHI 2229 and (C-D) BHI 5779 are oriented in ventral, and dorsal view respectively. Though not well preserved, suckers (A-B) and axial nerves (C-D) are identifiable. (E) BHI 2203, dorso-lateral view preserving eye capillaries, beak, and statocyst; (F, G) NHMW1998z0105/0000 retaining the entire arm crown and posterior salivary glands. Illustrations: J. Gardner (B, D), adaptation from Lukeneder & Harzhauser 2004 (F). Scale bars 10 mm. Abbreviations: a – arms, an – axial nerves, bm – buccal mass, cc – cephalic cartilage, dc – digestive contents, ec – eye capillaries, psg – posterior salivary glands, rt – rostrum tip, s – statocysts, su – suckers, o – oesophagus.

Eye measurements were obtained on 15 specimens (28% of the total individuals). As we had more precise measurements for the gladius, the gladius length was used to identify a ratio for

maximum eye diameter (0.13–0.25) rather than follow the index of Young & Vecchione (1996) which compares the eye radius to head width. Five individuals also preserve evidence of a central eye lens, which can be observed in Fig. 9E by the positioning of the capillary system in the eye (Donovan & Fuchs 2016; Fuchs *et al.* 2016a; Fuchs & Larson 2011a). This appears in natural light as delicate filaments of yellow staining in a reticulated pattern. This pattern appears dark under UV light (Fig. 9E).

Preservation of the buccal area is common and observed in ~72% of the individuals. The rostral tips, darker in colour than the rest of the beak chitin, are often visible under natural light. The muscular tissues of the buccal bulbs fluoresce under UV light (Fig. 9). µXRF analysis demonstrates that the muscular tissue has elevated yttrium traces compared with the matrix, indicating replacement of the original organic material by calcium phosphate (phosphatization) (as per Gueriau *et al.* 2018). The length of the buccal mass was measured in 31 individuals. The ratio of buccal mass length/gladius length ranges from 0.08 to 0.19. More detailed measurements of the buccal mass were taken on individuals NPL52121 (Fig. 10E-H) and BHI 2203 to capture the 2D shape, which were scaled to provide a reconstruction, the first of its kind for *D. syriaca* (see Fig. 11).

Posterior salivary glands and other paired structures

Previous descriptive works on *D. syriaca* have identified a pair of posterior salivary glands located next to the anterior-most parts of the lateral margins of the gladius (Lukeneder & Harzhauser 2004, Plate 2.2; Jattiot *et al.* 2015, fig 12.1; 12.2). Our study includes the two figured individuals of Lukeneder & Harzhauser (2004) and Jattiot *et al.* (2015) (Fig. 10D, F), which provides a comparator for this feature. The paired structures observed in the holotype closely resemble these posterior salivary glands.

Four individuals show paired structures that differ visually from the previously described posterior salivary glands (Fig. 10E-H, J-M). Two exhibit ovoid-shaped imprints in the region of the anterior lateral keels (Fig. 10A–C, E-H). In natural light, one of these structures is visible laterally to the anterior gladius margin in both individuals (shown here in NPL 52121, Fig. 10E-H). The XRF and MRI imagers reveal a corresponding ovoid area enriched in is visible on the opposing side of the gladius margin. But for the shape, there is no evidence to suggest that this is anything other than mantle tissue. As such, it is possible that this ovoid structure reflects the anterior section of a funnel. The other two individuals possess paired structures with a rope-like morphology (Fig. 10J-M). These are either visible as hemispherical projections anteriorly

angled towards the lateral keels (Fig. 10J, K), or medially angled inwards from the lateral keels (Fig. 10L, M), and are interpreted here as remnants of retractor muscles (Bizikov & Toll 2016; Fuchs *et al.* 2016b).

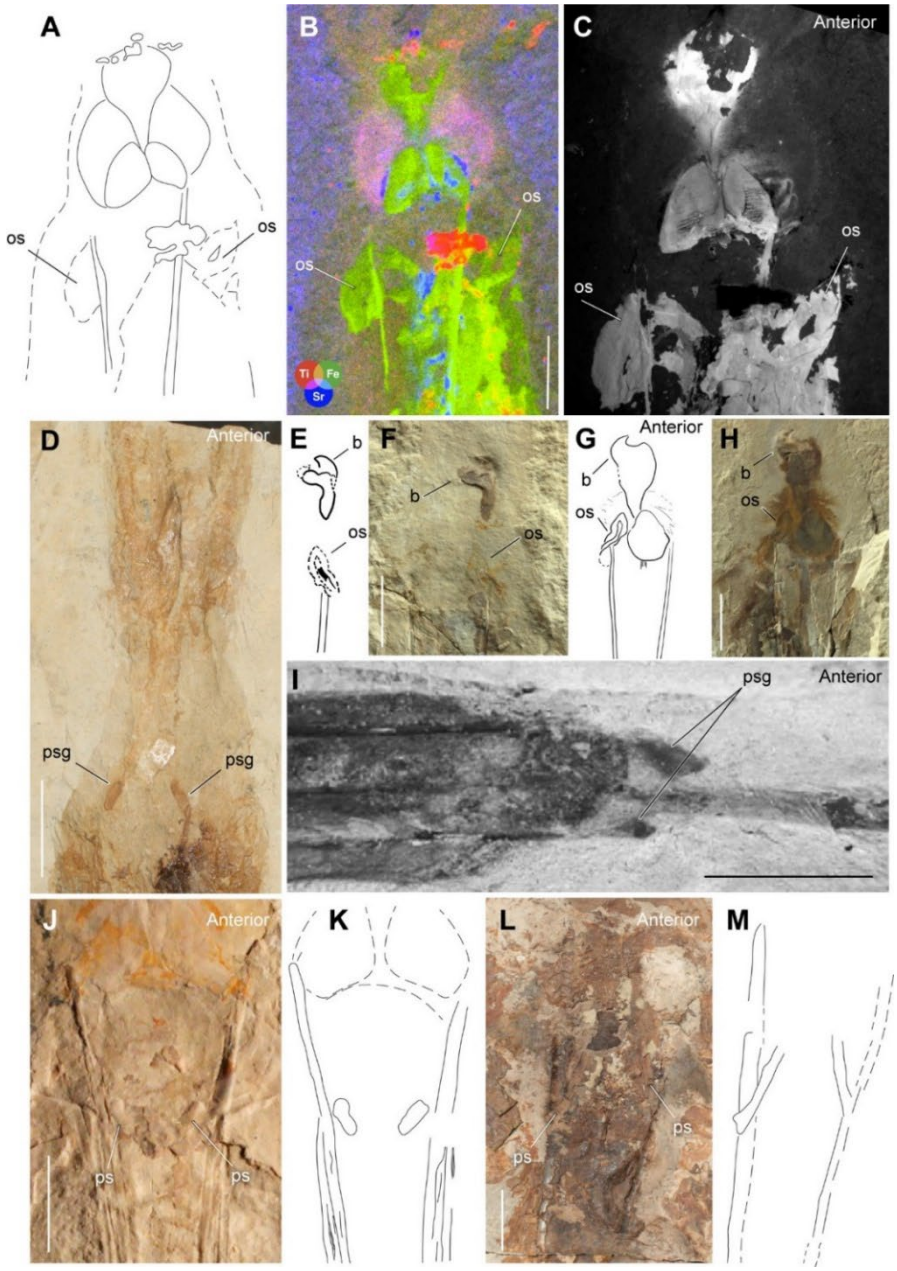

Figure 10: Variation in paired structures associated with the anterior part of the gladius of D. syriaca. (A–C) Individual MNHN.F.A88589: (A) interpretative line drawing, (B) µXRF overlay of titanium (red), yttrium (green) and iron (blue) distributions M6 Jetstream Bruker XRF, UAR 3224 CRC, MNHN) , and (C) luminescence emission at 385 nm under 514 nm illumination; UV-visible-near infrared multispectral imaging, UAR3461 IPANEMA; (D) MNHN.F.50396, individual image from the Reflectance Transformation Imaging (RTI) stack (also shown in fig. 12.1 of Jattiot *et al.* 2015); (E – H) NPL 52121 (part, and counterpart) illustrations and photographs in natural light showing the ovoid structure and beak. (I) Individual NHMW1998z0105/0000 from Lukeneder & Harzhauser (2004); (J, K) BHI 2222, (J) photograph in natural light and (K) interpretative line drawing; (L, M) Individual MNHN.F.A50400. (L) individual image from the Reflectance Transformation Imaging (RTI) stack and (M) interpretative line drawing. Note the two, pointed ovoid structures in A–C, and one pointed ovoid structure in E - H that are positioned adjacent to the external margins of the lateral keels. They appear different from the posterior salivary glands in MNHN.F.50396 (D, E) and NHMW1998z0105/0000 (F). BHI 2222 and MNHN.F.A50400 (G–J) possess rope-like structures positioned more posteriorly on the gladius visible in natural light. Scale bars 10 mm. Abbreviations: b – beak, os – ovoid structures, ps – paired structures, psg – posterior salivary glands.

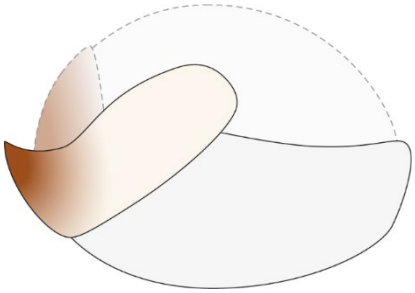

Figure 11: Hypothesized beak reconstruction for *D. syriaca* based on measurements from BHI 2203 and NPL52121 (see also Fig 9E-H). Illustration by A. Lethiers, CR2P.

Digestive system

Preserved digestive contents are observed in 19 individuals. Typically, the remains are ingested, and their relative position in the body enables comparison with the digestive organs in extant coleoids (Mangold & Young 1998; Wells 2011). One individual (MNHN.F.A88589) preserves remains in 3 areas (Fig. 12A–D): two are positioned in the posterior section of the mantle (Fig. 12A, C, D) and likely reflect the stomach and caecum. The composition of these remains varies which supports the different functions of these two digestive organs. The mass of digestive remains interpreted here to be stomach contents (Fig. 12C), contains an articulated ray fin and a pelvic girdle, likely from a teleost fish; the posterior-most mass (Fig. 12D) has a collection of less distinct, individual bones surrounded by a soft mass (Dr. Donald Davesne, pers. Com.) and likely represents caecal contents. The third mass of digestive remains (Fig. 12B) is positioned more anteriorly in the mantle, is tubular in shape, and also retains evidence of fish bones. The position and contents are consistent with the presence of a crop.

The individuals examined in the study enabled observation of almost all elements of the digestive system of *D. syriaca*. While the preservation of ingested food matter is not uncommon in organisms that are phosphatically preserved (see Clements *et al.* 2022*)*, phosphatization appears to be highly selective in terms of which tissues are replaced by apatite – and while ingested organics do seem to preferentially phosphatise, internal digestive integument is comparatively rare in the fossil record (Clements *et al*. 2022). This seems to be the case in *D. syriaca,* however, the relative positions of the ingested organics within the organism allows the determination of an Octobrachia-like gut configuration. One key character identified by this study is the crop of *D. syriaca*; the presence of a crop is known in Recent Vampyromorpha (Fig. 12E) and most Octopoda, but it is absent in modern Decabrachia (Mangold & Young 1998, fig. 1). As such, this configuration of the digestive system supports the assignment of *Dorateuthis* to Octobrachia.

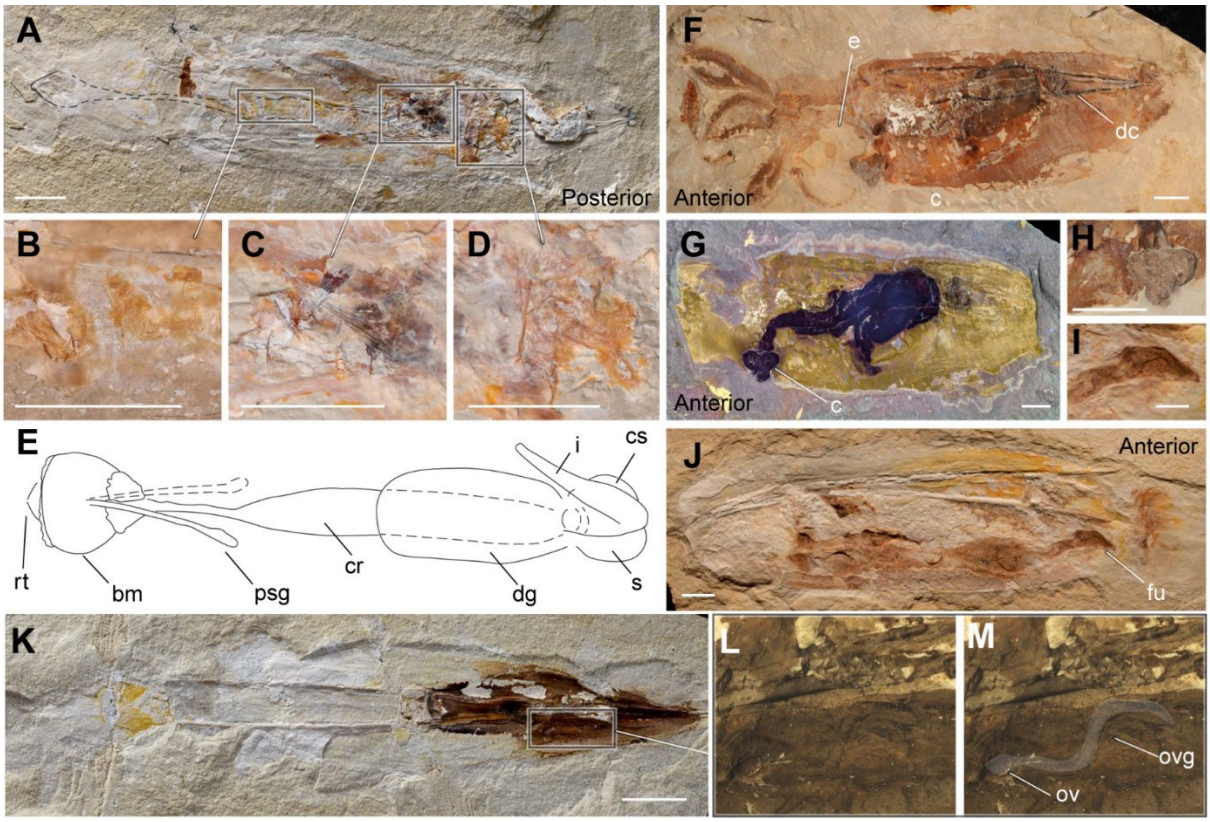

Figure 12: (A–D) Components of the digestive system, (G, I, J) funnel, and (K–M) possible reproductive elements of *D. syriaca.* (A–D) Individual MNHN.F.A88589 (A) in natural light, showing three separate areas preserving digestive contents, which indicates the presence of a crop, stomach, and caecum; (B-D) Close ups of the digestive contents from individual images of the Reflectance Transformation Imaging (RTI) stack. An illustration of the Vampyromorph digestive system is modified from Mangold & Young (1998) and provided here for reference (E). The vampyromorph, *Vampyroteuthis* is described with one posterior salivary gland, here, we observe two for *Dorateuthis*. (F-J) Funnel inferred in dorso-laterally preserved individuals MNHN.F.R06746 (F–H); (F, H) part, individual image from the RTI stack and (G) counterpart under UV light (UV photograph by L. Cazes, MNHN); (I, J) Photographs of BHI 2213 in natural light showing (I) a close up of the anterior-most part of the funnel, and (J) the entire mantle with the funnel in situ; (H) A coprolite is preserved at the anterior aperture of the funnel of MNHN.F.R06746. Individual image from the RTI stack; (K–M) individual MNHN.F A88589 in natural light showing the region of a possible oviduct and oviductal gland, and (L, M), close ups showing the impression (L) and overlay (M) of the same. Scale bars 10 mm. Abbreviations: bm – buccal mass, c – coprolite, cr – crop, cs – caecal sac, e – eye, dc – digestive contents, dg – digestive gland, fu – funnel, i – intestine, ov – oviduct, ovg – oviductal gland, psg – posterior salivary glands, rt – rostrum tip, s - stomach.

Funnel

A funnel can be inferred in two individuals (MNHN.F.R06746 and BHI 2213) that are both preserved in dorso-lateral view (Fig. 12F, G, I, J). The feature was not observed directly, though its presence was determined by a stained elongated mass within the boundaries of the mantle (Fig. 12F, G, J). The staining is interpreted here to delineate the internal part of the funnel. The anterior margin of this is located just posteriorly and ventrally to the head (Fig. 12G, J), consistent with the placement of the funnel in both fossil and modern coleoids.

Under natural and UV lights, this stained impression shows evidence of diagenetic circular structures (Fig. 12H–J) associated with the presence of ink (Klug *et al.* 2021b). These circular patterns are also present in individual MNHN.F.R06746 on an unresolved structure (Fig. 12G, H). Roger (1946) suggested it was a rectal bulb (translated from French), and Jattiot *et al.* (2015) indicated it may be a buccal mass. Given its location (Fig. 12F–H) and the presence of the diagenetic circular patterns, we interpret this structure to represent an accumulation of the long strings of pigmented faeces (coprolite) released from the mantle via the funnel (Boyle & Rodhouse 2008). As in BHI 2213 (Fig. 12I, J), the location of this indicates that the aperture of the funnel was positioned just posterior to the head in *D. syriaca.*

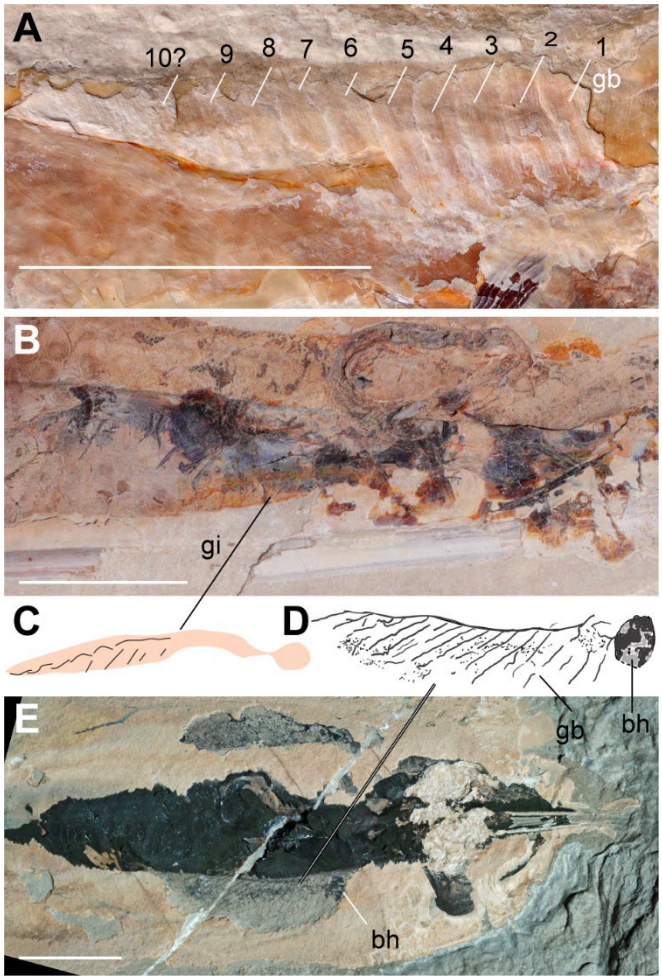

Figure 13: Gill preservation in *D. syriaca.* (A) Individual RTI image of MNHN.F.A88589 showing impressions of at least 10 gill blades; (B, C) Individual RTI image (B) and simplified illustration (C) of MNHN.F.A88590, showing preservation as orange pyritized stains; (D, E) BHI 2219 photographed in natural light. The gills appear black in colour, possibly a result of ink-staining. The branchial heart (E) is observable in the posterior part of the gill structure. Scale bars 10 mm. Abbreviations: bh – branchial heart, gb – gill blade, gi – gill.

Gills

Remains of gills are present in 12 individuals (22%). They are preserved either as impressions (Fig. 13A), orange pyritized stains (Fig. 13B, C) (Donovan & Fuchs, 2016), or

black ink-associated stains (Donovan & Fuchs, 2016) (Fig. 13D, E). The most complete gills (Fig. 13D, E) show the branchial heart (~2 mm length $_{max}$), the main efferent vessel (~14 mm), and a minimum of 17 gill blades. Combined, this represents ~21% of the gladius length. The associated lamellae are not preserved, though the filamentous, ink-stained gill blades taper distally (~4 mm to 1.3 mm). Lamellae (*n* = minimum of 9) and gill blades are present in MNHN.F. A88589 (Fig. 13A). Under natural light the blades are visible as orange filaments, and the lamellae are preserved as contoured relief. No main efferent vessel is observed.

Fins

The "oar shaped" fin described for *Dorateuthis* (Fuchs 2020, fig. 3,1e) is observed in the holotype from Sahel Aalma (Fig. 3A, B, H), as well as six (~11%) other individuals (Fig. 14) from the Cenomanian outcrops. It is preserved as a mineralized structure (Fig. 14A), an impression (Fig. 14C) or an orange-coloured stain (Fig. 14D), making it generally distinguishable from the matrix under natural light. Its visualization can be enhanced using µXFR elemental mapping (Figs. 8B, C and 14B) and/or UV photography (Fig. 14E, F).

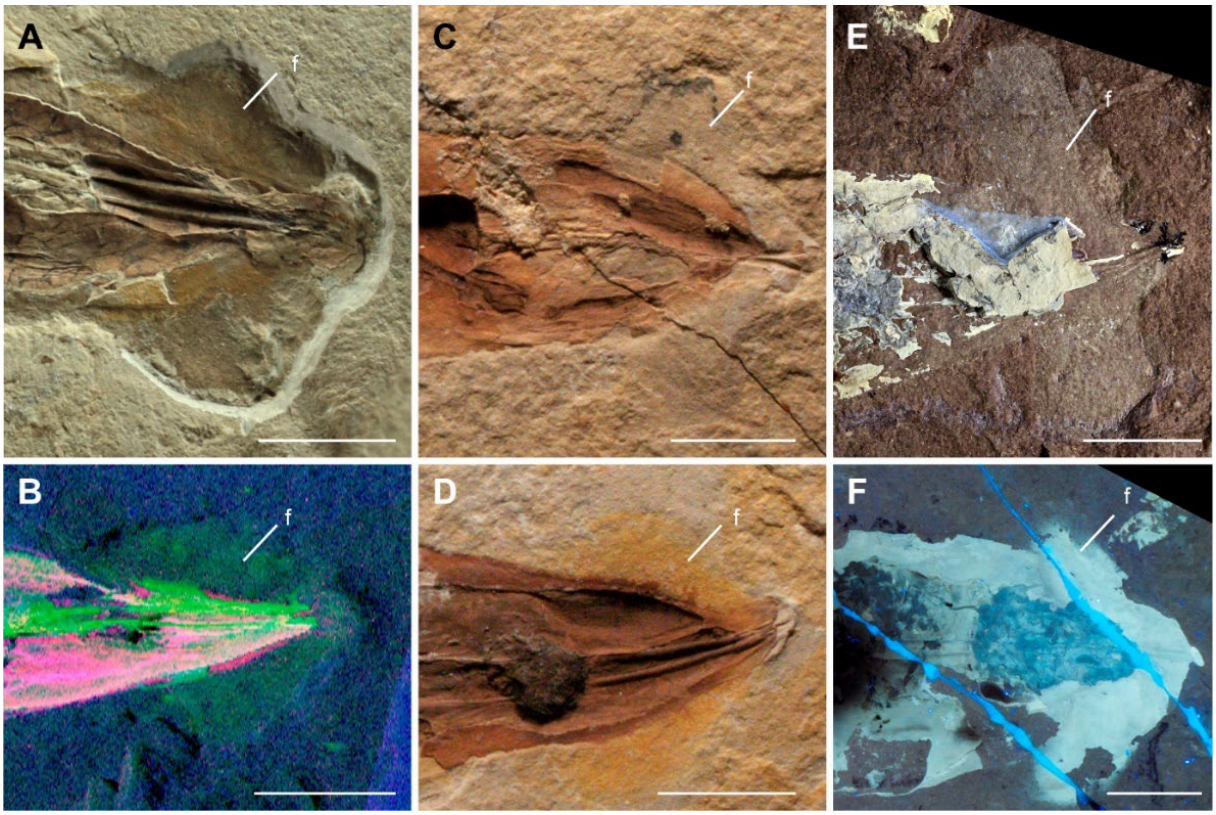

Figure 14: Oar-shaped fins of *D. syriaca.* (A) NPL52121, natural light; (B) MNHN.F.A88588, µXRF overlay of titanium (red), yttrium (green) and iron (blue) distributions; (C) BHI 2212, natural light; (D) BHI 2227, natural light; (E) MNHN.F.A88589, UV photograph (L. Cazes, MNHN); (F) BHI 2205, UV photograph. Scale bars 10 mm.

Reproductive system

Reproductive organs were tentatively included in a summary of known soft tissues in *D. syriaca* (Donovan & Fuchs 2016). This was based on a description by Roger (1946, fig. 7) of spermatophores in individual MNHN.F.R06746 (Fig. 12F). Observations on this individual show that what were interpreted to be spermatophores are, instead, stomach contents. However, there are impressions present in MNHN.F.A88588, corresponding with a larger, titanium-enriched area observable using µXRF mapping, which could possibly represent oviductal glands (Figs. 12K-M, 8B).

Novel anatomic characters of D. syriaca

The multimodal imaging approach and quantitative analyses performed in this work has enabled a revision of the summary of known soft tissues in *D. syriaca* (Supplementary Table 6) that were previously synthesized in Donovan & Fuchs (2016). Furthermore, we have identified morphological characters which are not previously described for the genus including paired retractor muscles, axial nerves in the arms, and an Octobrachia-type digestive system. For the first time we also provide clear evidence of a funnel, circulatory system, and excretory system. Lastly, we discount the presence of tentacles, tentacular pockets, and onychites within the arm crown, and confirm that *D. syriaca* possessed suckers.

DISCUSSION

Morphological variation in the gladius

Despite the exceptional preservation of coleoids from the Lebanese localities, it is vital to acknowledge that all fossils have undergone decay prior to fossilization, and therefore, do not represent an anatomically complete organism (e.g. Purnell *et al.* 2018; Clements *et al.* 2022 etc.). However, to elucidate the evolutionary history of coleoids, it is necessary to analyse fossil forms. Currently, especially in taxa found in the Lebanese Lagerstätten, the depositional environments and diagenetic processes are poorly understood (Geroge *et al.* in press). It is, therefore, difficult to establish an accurate taphonomic model that constrains the amount of decay that these organisms underwent prior to diagenesis, and while many of the soft tissues appear to be phosphatically preserved in *D. syriaca* (as per other Lebanese coleoid fossils), no comprehensive taphonomic model for coleoid fossils has yet been undertaken.

To further complicate our understanding of morphological variation, there are many uncertainties regarding the existing diagnostic characters of *Dorateuthis* and more specifically *D. syriaca* (Roger 1946; Woodward 1883; Fuchs 2006b, 2007; Fuchs & Larson 2011a; Jattiot *et al.* 2015). For example, previous observations on the posterior lateral fields have been conflicting, and both elongate (Fuchs 2006b, Pl. 1, fig. B) and rounded lateral fields (Fuchs & Larson 2011a, fig. 2.7) have been described. As such, there is no definitive diagnosis on the lateral fields in *Dorateuthis* (Fuchs 2020). Our observations of the elongated posterior lateral fields are consistent with the interpretation of Fuchs (2006b).

For the first time, this study describes long anterior lateral fields in *D. syriaca*, which resemble those seen in *Plesioteuthis* (Tithonian, Solnhofen) and the contemporaneous *Boreopeltis* (Fuchs & Larson 2011a; Fuchs 2020). A genus-level analysis of other prototeuthids, and taxa contemporaneous to *Dorateuthis* (Fuchs 2020), shows no evidence that this variation can be attributed to mistaken identity (Supplementary Table 7). As such, the polymorphism observed - the variation in the presence and location of the lateral fields, as well as the differences in the median reinforcements - adds to the complexity of what is known about this structure in *D. syriaca.* There are no clear links to local effects or the time difference between localities (Fig. 5). We interpret the observed morphological variation to be associated with either dimorphism or ontogenetic stage, as these are known to contribute to interspecific variation in extant gladii (e.g. Toll 1998; Bizikov & Toll 2016).

Size

The measurements obtained on the individuals in the sample enabled a hypothesized reconstruction for the holotype (likely a juvenile; see below), and an 'average-sized' individual of *D. syriaca* (Fig. 15). The two reconstructions show a large variation between the smallest and largest individual. The smaller size is not interpreted to be related to sexual dimorphism as our analyses show no distinctions indicative of more than one grouping (Supplementary Fig. 1A, B). Additionally, no correlation is observed between size and locality (Fig. 5A, B). Overall, the size of *D. syriaca* seems to be conservative despite the ~10 Ma age difference between the Cenomanian and Santonian sites. Despite having only eight individuals (15% of the total studied sample) from Sahel Aalma, the locality shows the most disparity as the smallest and largest outliers are from the site (Supplementary Fig. 1A, B). More individuals from this outcrop would need to be studied to determine if this was a real signal, or just a sampling bias.

The body size (including head and arms) was determined for 23 individuals. Even in the best-preserved individuals, precise measurements are difficult to obtain as boundaries in the 2D phosphatized individuals are not always clear. However, the characteristic configuration for *D. syriaca* – an elongate dorsal pair, a shorter ventral pair, and two intermediately sized lateral pairs (Fuchs & Larson 2011a) – is clearly present. This pattern was not observed in the three smallest individuals (mantle size <50 mm). Instead, they showed minimal length variation in the arm crown giving the appearance of arms that are all similar in length.

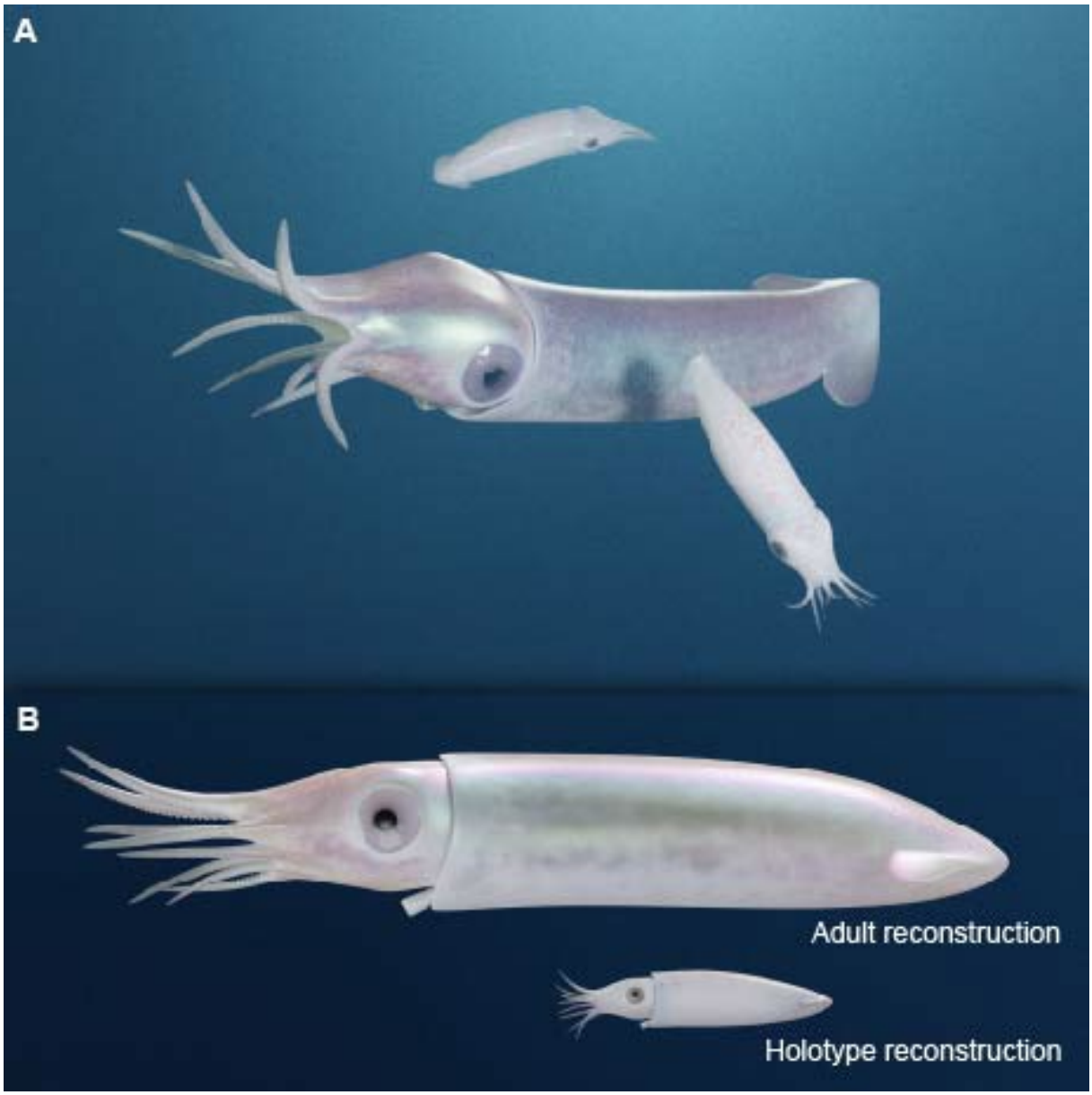

Figure 15: Hypothesized reconstructions of *D. syriaca*. (A) *D. syriaca* in inferred life positions, and (B) lateral view. (B) The larger individual (top) reflects an average, medium-sized D. syriaca. The smaller (bottom) is a reconstruction of the holotype, which is considered to be a juvenile. The reconstruction of the holotype was based on direct measurements of visible structures revealed by the µXRF, RTI, and UV imagery. As it was not possible to obtain measurements of all the preserved soft tissue on one individual, measurements from four individuals were used and scaled to the correct size. BHI 2232 provided the basis for the reconstruction. Scaled elements were obtained from BHI 2203 (eye and lens diameter), NHMW1998z01050000 (arm lengths), and BHI 2227 (fins). Reconstructions A. Lethiers, CR2P.

Seventeen individuals preserve two or more arms. Plotting the maximum and minimum arm lengths from these individuals shows a correlative increase in arm length to mantle length (Fig. 7). This supports the hypothesis that the relative arm length is linked with the ontogenetic stage (Fuchs, 2006b; Fuchs & Larson, 2011a; Jattiot *et al.,* 2015). Here, we suggest that the most parsimonious explanation of the smaller sizes observed in the entire study sample is that it is comprised mostly of juveniles, and the genera-level description in Fuchs (2020) included more mature individuals. Additionally, we hypothesize that the three smallest individuals, with minimal differentiation in the arm crown, represent young juveniles.

SYSTEMATIC AND PHYLOGENETIC IMPLICATIONS

D. syriaca is included in several published morphological matrices that contain both fossil and extant taxa. Initially published by Sutton *et al.* (2016), the matrix was minimally modified for *Proteroctopus* (Kruta *et al.* 2016) and *Vampyronassa* (Rowe *et al.* 2022) and underwent a more extensive revision by Whalen & Landman (2022). Our study provides new character state information on 20 of the 153-character states for *D. syriaca*, 5 of which are specific to the gladius. This increases our current understanding about this key coleoid species (Supplementary Table 8.)

Although the gladius of coleoids is a relatively simple structure, it contributes approximately half of the character states to the systematics of fossil and extant coleoids (Sutton *et al.* 2016; Whalen & Landman 2022). However, ambiguity regarding certain terminology introduces inherent issues, for example, when determining median reinforcements and fin shape. Currently, *D. syriaca* is coded as possessing a convex median keel (#55, Sutton *et al.* 2016; Whalen & Landman 2022). However, this is in contrast with descriptions in the literature for both the genus, which specifically notes the absence of a keel (Fuchs 2020, p. 10), and the species (Fuchs & Larson 2011, p. 238). Following these authors, the terms “line” or “ridge” were used here to reflect the level of robustness. Uncertainty around this definition can be seen in the original description of *D. syriaca*, in which Woodward (1883) uses both ridge and line seemingly interchangeably.

There is a similar vagueness around the classification of fin shapes; inconsistencies which have already been acknowledged (Sutton *et al*. 2016). The diagnostic shape for Dorateuthis is “oar-shaped” (Fuchs 2020), which is visually like the “rhomboid” shaped fin illustrated by Hanlon *et al.* (2018). Citing this issue, Sutton *et al.* (2016) coded only for two shapes, lobate

and rhomboidal. Currently Dorateuthis is coded as lobate. Determining the states for fin shape will continue to be limiting without a more concise terminology (Young *et al.* 2001). As the current systematic framework for Mesozoic coleoids has many inherent, widely recognized uncertainties (Young & Vecchione 1996; Lindgren *et al.* 2004; Kruta *et al.* 2016; Sutton *et al.* 2016; Fuchs 2020; Whalen & Landman 2022), a phylogenetic analysis was not conducted here.

LIFESTYLE IMPLICATIONS

The slender gladius morphology of *D. syriaca* was originally compared with that of modern *Ommastrephes* by Woodward (1883) and has subsequently been explored by Bizikov & Toll (2016) and Fuchs & Iba (2015). The data presented here supports those comparisons and offers insight into the lifestyle of *D. syriaca*. *Ommastrephes* are powerful pelagic swimmers that are found in continental shelf environments and in nutrient-rich upwelling zones, preying on fish and crustaceans (Jereb & Roper 2010). Ommastrephidae is a group of active visual hunters at all stages of ontogeny, generally fast growing, and vary in adult size based on relative growth rate in larval and juvenile stages (Jereb & Roper 2010).

The common muscular striations and elongated mantle indicate that *D. syriaca* also had the potential for active swimming. This would further be supported if the paired structures observed on the fossil individuals could be conclusively identified as head or funnel retractor musculature (Bizikov & Toll, 2016; Fuchs *et al.* 2016). The presence of prominent eyes suggest *D. syriaca* was also an active visual predator, and the volume and type of meal remains preserved in the digestive system indicates they were avid feeders with a diet consisting largely of fish. The arms, differentiated in size, likely facilitating the manipulation of their relatively large prey, which would have needed to be disarticulated with their sharp rostrum and buccal complex before being ingested (Lukeneder & Harzhauser 2004; Nixon 2015); this feeding strategy is adopted by Recent coleoids (Roscian *et al.* 2022). The expulsion of ink to conceal or confuse is a distinctive behavior in modern forms (Bush & Robison 2007; Nixon 2011; Derby 2014) and is observed in almost all the individuals in the fossil sample. The size of the ink sac varies, though this is not interpreted here as having a diagnostic value, rather reflects the amount of ink preserved in the organ (Fuchs 2006b). The presence of this character indicates they also utilized obfuscation techniques, likely to avoid predation.

ACKNOWLEDGMENTS

We thank SOLEIL synchrotron for provision of beamtime, Sebastian Schöder (SOLEIL synchrotron) for assistance at the PUMA beamline, and IXRF, Austin, TX, USA for the acquisition of the elemental maps. We thank Robert Farrar at the Black Hills Institute of Geological Research, South Dakota, USA for collections assistance and sample loans. We thank Olivier Bethoux (CR2P) for assistance with RTI acquisition, and Sorbonne University students Aimie Doriath-Döhler and Robin Piguet-Ruinet for their initial investigations on two specimens, MNHN.F.A88588 and MNHN.F.A88589 respectively, as part of an internship. We are also grateful to Alexandre Lethiers (CR2P) for the hypothesized reconstructions and figures, and L. Cazes (CR2P) for photographs of the specimens.

BIBLIOGRAPHY

AUDO, D. & CHARBONNIER, S. 2012. Late Cretaceous crest-bearing shrimps from the Sahel Alma Lagerstätte of Lebanon. *Acta Palaeontologica Polonica*, 58, 335–349.

BANDEL, K. & LEICH, H. 1986. Jurassic Vampyromorpha (dibranchiate cephalopods). *Neues Jahrbuch für Geologie und Paläontologie-Monatshefte*, 3, 129–148.

BATHER, F. A. 1888. Shell-growth in Cephalopoda (Siphonopoda). *Journal of Natural History*, 1, 298–309.

BINKHORST VAN DEN BINKHORST, J. 1861. Monographie des Gastropodes et Céphalopodes de la Craie Supérieure du Limburg. *Verlag Muquart, Verlag Müller, Brüssel, Maastricht*, 44 p.

BIZIKOV, V. A. & TOLL, R. B. 2016. Treatise Online no. 77: Part M, Chapter 9A: The Gladius and its Vestiges in Extant Coleoidea. *Treatise Online*, doi: 10.17161/to.v0i0.5728.

BOYLE, P. & RODHOUSE, P. 2008. *Cephalopods: Ecology and Fisheries*. John Wiley & Sons pp.

BRACCHI, G. & ALESSANDRELLO, A. 2005. *Paleodiversity of the Free-Living Polychaetes:(Annelida, Polychaeta) and Description of New Taxa from the Upper Cretaceous Lagerstätten of Haqel, Hadjula and Al-Namoura (Lebanon)*. Società Italiana di Scienze Naturali e Museo Civico di Storia Naturale pp

BUSH, S.L., & ROBISON, B. H. 2007. Ink utilization by mesopelagic squid. *Marine Biology*, *152*, 485-494.

CHARBONNIER, S. 2009. *Le Lagerstätte de La Voulte: Un Environnement Bathyal Au Jurassique*. Publications scientifiques du Muséum Paris, Mémoires du Muséum national d'Histoire naturelle, 272 pp.

CHARBONNIER, S. & AUDO, D. 2012. New nisto of slipper lobster (Decapoda: Scyllaridae) from the Hadjoula Lagerstätte (Late Cretaceous, Lebanon). *Journal of Crustacean Biology*, 32, 583–590, doi: 10.1163/193724012X634189.

CHARBONNIER, S., AUDO, D., CAZE, B. & BIOT, V. 2014. The La Voulte-sur-Rhône Lagerstätte (Middle Jurassic, France). *Comptes Rendus Palevol*, 13, 369–381, doi: 10.1016/j.crpv.2014.03.001.

CLEMENTS, T., PURNELL, M. A. & GABBOTT, S. 2022. Experimental analysis of organ decay and pH gradients within a carcass and the implications for phosphatization of soft tissues. *Palaeontology*, 65, e12617.

DERBY, C. D. 2014. Cephalopod Ink: Production, Chemistry, Functions and Applications. *Marine Drugs*, 12, 2700–2730, doi: 10.3390/md12052700.

DONOVAN, D. T. & FUCHS, D. 2016. Treatise Online no. 73: Part M, Chapter 13: Fossilized Soft Tissues in Coleoidea. *Treatise Online*, doi: 10.17161/to.v0i0.5675.

EJEL, F., & DUBERTRET, L. 1966. On the precise age of the Cretaceous fish and crustacean deposit of Sahel Alma (Lebanon). *Summary report of the sessions of the Geological Society of France*, *9*, 353-354.

EL HOSSNY, T.; CAVIN, L. 2023. A New Enigmatic Teleost Fish from the Mid-Cretaceous of Lebanon. *Diversity* 15(7), 839.

ENGESER, T. 1988. Vampyromorpha ("Fossile Teuthiden"). *In*: Westphal, F. (ed.) *Fossilium Catalogus. Animalia*. Kugler Publications, Amsterdam, 1–167.

ENGESER, T. & REITNER, J. 1985. Teuthiden aus dem Unterapt (»Töck«) von Helgoland (Schleswig-Holstein, Norddeutschland): Teuthids from the early aptian ("Töck") of heligoland (Schleswig-Holstein, North Germany). *Paläontologische Zeitschrift*, 59, 245–260, doi: 10.1007/BF02988811.

ENGESER, T. & REITNER, J. 1986. Coleoidenreste aus der Oberkreide des Libanon im Staatlichen Museum für Naturkunde in Stuttgart. *Stuttgarter Beiträge zur Naturkunde: Serie B Geologie und Paläontologie*, 124.

FERRY, S., MERRAN, Y., GROSHENY, D. & MROUEH, M. 2007. The Cretaceous of Lebanon in the Middle East (levant) context. *Carnets de Géologie*, 38–42.

FOREY, P. L., YI, L., PATTERSON, C. & DAVIES, C. E. 2003. Fossil fishes from the Cenomanian (Upper Cretaceous) of Namoura, Lebanon. *Journal of Systematic palaeontology*, 1, 227.

FRAAS, O. 1878. *Geologisches Aus Dem Libanon. Jahreshefte Des Vereins Für Vaterländische Naturkunde in Württemberg,*. Verlag nicht ermittelbar, 257–391 pp.

FUCHS, D. 2006a. Fossil erhaltungsfahige Merkmalskomplexe der Coleoidea (Cephalopoda) und ihre phylogenetische Bedeutung. *Berliner Palaobiologische Abhandlungen*, 8, 1–122.

FUCHS, D. 2006b. Morphology, taxonomy and diversity of vampyropod coleoids (Cephalopoda) from the Upper Cretaceous of Lebanon. *Memorie della Società italiana di Scienze naturali e del Museo civico di Storia naturale di Milano*, 34, 1–28.

FUCHS, D. 2007. Coleoid cephalopods from the plattenkalks of the Upper Jurassic of Southern Germany and from the Upper Cretaceous of Lebanon A faunal comparison. *Neues Jahrbuch für Geologie und Paläontologie - Abhandlungen*, 245, 59–69, doi: 10.1127/0077-7749/2007/0245-0059.

FUCHS, D. 2016. Treatise Online No. 83: Part M, Chapter 9B: The Gladius and Gladius Vestige in Fossil Coleoidea. *Treatise Online*.

FUCHS, D. 2020. Treatise Online no. 138: Part M, Chapter 23G: Systematic Descriptions: Octobrachia. *Treatise Online*, doi: 10.17161/to.vi.14661.

FUCHS, D. & IBA, Y. 2015. The gladiuses in coleoid cephalopods: homology, parallelism, or convergence? *Swiss Journal of Palaeontology*, 134, 187–197, doi: 10.1007/s13358-015-0100-3.

FUCHS, D. & LARSON, N. 2011a. Diversity, morphology, and phylogeny of coleoid cephalopods from the Upper Cretaceous Plattenkalks of Lebanon-Part I: Prototeuthidina. *Journal of Paleontology*, 85, 234–249, doi: 10.1666/10-089.1.

FUCHS, D. & LARSON, N. 2011b. Diversity, Morphology, and Phylogeny of Coleoid Cephalopods from the Upper Cretaceous Plattenkalks of Lebanon–Part II: Teudopseina. *Journal of Paleontology*, 85, 815–834, doi: 10.2307/23020132.

FUCHS, D. & WEIS, R. 2009. A new Cenomanian (Late Cretaceous) coleoid (Cephalopoda) from Hâdjoula, Lebanon. *Fossil Record*, 12, 175–181, doi: 10.1002/mmng.200900005.

FUCHS, D., ENGESER, T. & KEUPP, H. 2007a. Gladius shape variation in coleoid cephalopod Trachyteuthis from the Upper Jurassic Nusplingen and Solnhofen Plattenkalks. *Acta Palaeontol. Pol.*, 52.

FUCHS, D., KLINGHAMMER, A. & KEUPP, H. 2007. Taxonomy, morphology and phylogeny of plesioteuthidid coleoids from the Upper Jurassic (Tithonian) Plattenkalks of Solnhofen. *Neues Jahrbuch für Geologie und Paläontologie - Abhandlungen*, 245, 239–252, doi: 10.1127/0077-7749/2007/0245-0239.

FUCHS, D., BRACCHI, G. & WEIS, R. 2009. New Octopods (Cephalopoda: Coleoidea) from the Late Cretaceous (Upper Cenomanian) of Häkel and Hädjoula, Lebanon. *Palaeontology*, 52, 65–81, doi: 10.1111/j.1475-4983.2008.00828.x.

FUCHS, D., KEUPP, H. & SCHWEIGERT, G. 2013. First record of a complete arm crown of the Early Jurassic coleoid Loligosepia (Cephalopoda). *Paläontologische Zeitschrift*, 87, 431–435, doi: 10.1007/s12542-013-0182-4.

FUCHS, D., IBA, Y., TISCHLINGER, H., KEUPP, H. & KLUG, C. 2016b. The locomotion system of Mesozoic Coleoidea (Cephalopoda) and its phylogenetic significance. *Lethaia*, 49, 433–454, doi: 10.1111/let.12155.

FUCHS, D., WILBY, P. R., VON BOLETZKY, S., ABI-SAAD, P., KEUPP, H. & IBA, Y. 2016a. A nearly complete respiratory, circulatory, and excretory system preserved in small Late Cretaceous octopods (Cephalopoda) from Lebanon. *PalZ*, 90, 299–305, doi: 10.1007/s12542-015-0256-6.

GEORGE, H., BAZZI, M., EL HOSSNY, T., ASHRAF, N., ABI SAAD, P., CLEMENTS, T. (In press). The famous fish beds of Lebanon: the Upper Cretaceous LagerstÄtten of Haqel, Hjoula, Nammoura, and Sahel Aalma.

GUERIAU, P., JAUVION, C. & MOCUTA, C. 2018. Show me your yttrium, and I will tell you who you are: implications for fossil imaging. *Palaeontology*, 61, 981–990, doi: 10.1111/pala.12377.

GUILLERME, T., COOPER, N., BRUSATTE, S. L., DAVIS, K. E., JACKSON, A. L., GERBER, S., GOSWAMI, A., HEALY, K., HOPKINS, M. J. & JONES, M. E. 2020. Disparities in the analysis of morphological disparity. *Biology letters*, 16, 20200199.

HAECKEL, E. H. P. A. 1866. *Generelle Morphologie Der Organismen. Allgemeine Grundzüge Der Organischen Formen-Wissenschaft, Mechanisch Begründet Durch Die von Charles Darwin Reformirte Descendenztheorie, von Ernst Haeckel.* G. Reimer, Berlin, 1–617 pp., doi: 10.5962/bhl.title.3953.

HANLON, R., VECCHIONE, M. & ALLCOCK, L. 2018. *Octopus, Squid, and Cuttlefish: A Visual, Scientific Guide to the Oceans' Most Advanced Invertebrates*. University of Chicago Press pp.

HART, M. B., PAGE, K. N., PRICE, G. D. & SMART, C. W. 2019. Reconstructing the Christian Malford ecosystem in the Oxford Clay Formation (Callovian, Jurassic) of Wiltshire: exceptional preservation, taphonomy, burial and compaction. *Journal of Micropalaeontology*, 38, 133–142, doi: 10.5194/jm-38-133-2019.

JATTIOT, R., BRAYARD, A., FARA, E. & CHARBONNIER, S. 2015. Gladius-bearing coleoids from the Upper Cretaceous Lebanese Lagerstätten: Diversity, morphology, and phylogenetic implications. *Journal of Paleontology*, 89, 148–167, doi: 10.1017/jpa.2014.13.

JEREB, P. & ROPER, C. F. E. (eds). 2010. *Cephalopods of the World: An Annotated and Illustrated Catalogue of Cephalopod Species Known to Date. Vol. 2. Myopsid and Oegopsid Squids*. Food and Agriculture Organization of the United Nations, Rome, FAO species catalogue for fishery purposes, no. 4, 605 pp.

KLINGHARDT, F. 1943. Vergleichende untersuchungen über tintenfische und belemnitenähnliche weichtiere. *Sitzungsberichte der Gesellschaft naturforschender Freunde in Berlin*, 1942, 5–17.

KLUG, C., SCHWEIGERT, G., DIETL, G. & FUCHS, D. 2005. Coleoid beaks from the Nusplingen Lithographic Limestone (Upper Kimmeridgian, SW Germany). *Lethaia*, 38, 173–192, doi: 10.1080/00241160510013303.

KLUG, C., FUCHS, D., SCHWEIGERT, G., RÖPER, M. & TISCHLINGER, H. 2015. New anatomical information on arms and fins from exceptionally preserved Plesioteuthis

(Coleoidea) from the Late Jurassic of Germany. *Swiss Journal of Palaeontology*, 134, 245–255, doi: 10.1007/s13358-015-0093-y.

KLUG, C., SCHWEIGERT, G., FUCHS, D. & DE BAETS, K. 2021a. Distraction sinking and fossilized coleoid predatory behaviour from the German Early Jurassic. *Swiss Journal of Palaeontology*, 140, 1–12.

KLUG, C., POHLE, A., ROTH, R., HOFFMANN, R., WANI, R. & TAJIKA, A. 2021b. Preservation of nautilid soft parts inside and outside the conch interpreted as central nervous system, eyes, and renal concrements from the Lebanese Cenomanian. *Swiss Journal of Palaeontology*, 140, 15, doi: 10.1186/s13358-021-00229-9.

KLUG, C., DI SILVESTRO, G., HOFFMANN, R., SCHWEIGERT, G., FUCHS, D., CLEMENTS, T. & GUERIAU, P. 2021c. Taphonomic patterns mimic biologic structures: diagenetic Liesegang rings in Mesozoic coleoids and coprolites. *PeerJ*, 9, e10703.

KLUG, C., HOFFMANN, R., TISCHLINGER, H., FUCHS, D., POHLE, A., ROWE, A., ROUGET, I. AND KRUTA, I. 2023. 'Arm brains' (axial nerves) of Jurassic coleoids and the evolution of coleoid neuroanatomy. Swiss Journal of Palaeontology, 142(1), 22.

LINDGREN, A. R., GIRIBET, G. & NISHIGUCHI, M. K. 2004. A combined approach to the phylogeny of Cephalopoda (Mollusca). *Cladistics*, 20, 454–486, doi: 10.1111/j.1096-0031.2004.00032.x.

LUKENEDER, A. & HARZHAUSER, M. 2004. The Cretaceous coleoid Dorateuthis syriaca Woodward: morphology, feeding habits and phylogenetic implications. *Annalen des Naturhistorischen Museums in Wien. Serie A für Mineralogie und Petrographie, Geologie und Paläontologie, Anthropologie und Prähistorie*, 106, 213–225.

MANGOLD, K. M. & YOUNG, R. E. 1998. The systematic value of the digestive organs. *Smithsonian contributions to zoology*, 21–30.

MARROQUÍN, S. M., MARTINDALE, R. C. & FUCHS, D. 2018. New records of the late Pliensbachian to early Toarcian (Early Jurassic) gladius-bearing coleoid cephalopods from the Ya Ha Tinda Lagerstätte, Canada. *Papers in Palaeontology*, 4, 245–276, doi: 10.1002/spp2.1104.

MARTINDALE, R. C., THEM, T. R., GILL, B. C., MARROQUÍN, S. M. & KNOLL, A. H. 2017. A new Early Jurassic (ca. 183 Ma) fossil *Lagerstätte* from Ya Ha Tinda, Alberta, Canada. *Geology*, 45, 255–258, doi: 10.1130/G38808.1.

MUSCENTE, A. D., MARTINDALE, R. C., SCHIFFBAUER, J. D., CREIGHTON, A. L. & BOGAN, B. A. 2019. Taphonomy of the Lower Jurassic Konservat-Lagerstätte at Ya Ha Tinda (Alberta, Canada) and its significance for exceptional fossil preservation during oceanic anoxic events. *PALAIOS*, 34, 515–541, doi: 10.2110/palo.2019.050.

NAEF, A. 1921. Das System der dibranchiaten Cephalopoden und die mediterranen Arten derselben. *Mitt. Zool. Stn. Neapel*, 22, 527–542.

NAEF, A. 1922. *Die Fossilen Tintenfische: Eine Paläozoologische Monographie*. Verlag von Gustav Fischer, Jena, Germany, 322 pp.

NIXON, M. 2011. Treatise Online, no. 17, Part M, Chapter 3: Anatomy of Recent forms. *Treatise Online*, doi: 10.17161/to.v0i0.4087.

NIXON, M. 2015. Treatise Online no. 69: Part M, Chapter 12: The Buccal Apparatus of Recent and Fossil Forms. *Treatise Online*, doi: 10.17161/to.v0i0.5047

PURNELL, M.A., DONOGHUE, P.J., GABBOTT, S.E., MCNAMARA, M.E., MURDOCK, D.J. AND SANSOM, R.S., 2018. Experimental analysis of soft-tissue fossilization: opening the black box. *Palaeontology*, *61*(3), pp.317-323.

REICH, M. 2004. Holothurians from the Late Cretaceous 'Fish shales' of Lebanon. *In*: *Echinoderms: München*. A.A. Balkema, 487–488., doi: 10.1201/9780203970881-ch81.

REITNER, J. & ENGESER, T. 1982. Teuthiden aus dem barrême der insel maio (kapverdische inseln). *Paläontologische Zeitschrift*, 56, 209–216.

RIEGRAF, W. 1987. Plesioteuthis arcuata VON DER MARCK 1873 (Cephalopoda, Teuthida) from the Campanian (late Cretaceous) of Westfalia (NW Germany). *Münstersche Forschungen zur Geologie und Paläontologie*, 66, 95–110.

ROGER, J. 1946. Les invertébrés des couches à poisons du crétace supérieur du Liban: Mémoires de la Société Géologique de France. *Nouvelle Série*, 51, 1–92.

ROGER, J. 1952. Sous-classe des Dibranchiata OWEN 1836. *In*: Piveteau, J. (ed.) *Traité de Paléontologie*. Masson, Paris, 689–755.

ROSCIAN, M., HERREL, A., ZAHARIAS, P., CORNETTE, R., FERNANDEZ, V., KRUTA, I., CHEREL, Y. & ROUGET, I. 2022. Every hooked beak is maintained by a prey: Ecological signal in cephalopod beak shape. *Functional Ecology*, 36, 2015–2028.

ROWE, A. J., KRUTA, I., LANDMAN, N. H., VILLIER, L., FERNANDEZ, V. & ROUGET, I. 2022. Exceptional soft-tissue preservation of Jurassic *Vampyronassa rhodanica* provides new insights on the evolution and palaeoecology of vampyroteuthids. *Scientific Reports*, 12, 1–9, doi: 10.1038/s41598-022-12269-3.

ROWE, A. J., KRUTA, I., VILLIER, L., & ROUGET, I. 2023. A new vampyromorph species from the Middle Jurassic La Voulte-sur-Rhône Lagerstätte. *Papers in Palaeontology*, *9*(3), e1511

SCHINDELIN, J., ARGANDA-CARRERAS, I., FRISE, E., KAYNIG, V., LONGAIR, M., PIETZSCH, T., PREIBISCH, S., RUEDEN, C., SAALFELD, S. & SCHMID, B. 2012. Fiji: an open-source platform for biological-image analysis. *Nature methods*, 9, 676–682.

SCOTESE, C.R., 2016. PALEOMAP PaleoAtlas for GPlates and the PaleoData Plotter Program, PALEOMAP Project, http://www.earthbyte.org/paleomappaleoatlas-for-gplates/ DOI: 10.13140/RG2.2.34367.00166

SOLE, V. A., PAPILLON, E., COTTE, M., WALTER, P. & SUSINI, J. 2007. A multiplatform code for the analysis of energy-dispersive X-ray fluorescence spectra. *Spectrochimica Acta Part B: Atomic Spectroscopy*, 62, 63–68.

SUTTON, M., PERALES-RAYA, C. & GILBERT, I. 2016. A phylogeny of fossil and living neocoleoid cephalopods. *Cladistics*, 32, 297–307, doi: 10.1111/cla.12131.

SWINBURNE, N. H., & HEMLEBEN, C. 1994. The plattenkalk facies: A depositof several environments. *Geobios*, *27*, 313-320.

TOLL, R. B. (1988). Functional morphology and adaptive patterns of the teuthoid gladius. In *The Mollusca* (pp. 167-182). Academic Press.

WELLS, M. J. 2011. Treatise Online, no. 27: Part M, Chapter 4: Physiology of Coleoids. *Treatise Online*, doi: 10.17161/to.v0i0.4226.

WHALEN, C. D. & LANDMAN, N. H. 2022. Fossil coleoid cephalopod from the Mississippian Bear Gulch Lagerstätte sheds light on early vampyropod evolution. *Nature Communications*, 13, 1107.

WILBY, P., HUDSON, J., CLEMENTS, R. & HOLLINGWORTH, N. 2004. Taphonomy and origin of an accumulate of soft-bodied cephalopods in the Oxford Clay Formation (Jurassic, England). *Palaeontology*, 47, 1159–1180.

WIPPICH, M. G. E. & LEHMANN, J. 2004. Allocrioceras from the Cenomanian (mid-Cretaceous) of the Lebanon and its bearing on the palaeobiological interpretation of heteromorphic ammonites. *Palaeontology*, 47, 1093–1107, doi: 10.1111/j.0031-0239.2004.00408.x.

WOODWARD, H. 1883. I.—On a New Genus of Fossil “Calamary,” from the Cretaceous Formation of Sahel Alma, near Beirût, Lebanon, Syria. *Geological Magazine*, 10, 1–5, doi: 10.1017/S0016756800159667.

WOODWARD, H. 1896. On a Fossil Octopus (Calais Newboldi, J. De C. Sby. MS.) from the Cretaceous of the Lebanon. *Quarterly Journal of the Geological Society*, 52, 229-NP, doi: 10.1144/GSL.JGS.1896.052.01-04.12.

YOUNG, R. E. & VECCHIONE, M. 1996. Analysis of morphology to determine primary sister-taxon relationships within coleoid cephalopods. *American Malacological Bulletin*, 12, 91–112.

4.3 EXPLORING THE CHARACTERS OF EARLY INCIRRATA: *KEUPPIA*

Three previously undescribed individuals on loan from the American Museum of Natural History (AMNH, NY) were investigated during two short-term student internships I co-supervised in 2022 (undergraduate students SU M. Kandil, J. Dufour, and R. Piguet-Ruinet). The specimens are 135058 and 135059 (part and counterpart); 135060, and 117083 (part and counterpart) and from the Haqel deposit. The imaging acquisition methods are the same as those used for *D. syriaca*. Table 4.2 shows the type of imaging performed on each specimen.

	UV light	RTI	MSI	µXRF
135058	X			X
135059	X		X	X
135060	X			
117083a	X	X		
117083b	X		X	

Table 4.2: The Keuppia specimens from the AMNH were imaged using the same techniques used in Rowe et al. (in prep) and outlined here. These include UV-visible-near infrared multi-spectral imaging (MSI) at the SOLEIL Synchrotron, Saint-Aubin, France, Reflectance Transformation Imaging, and X-ray fluorescence spectroscopy (µXRF) (Centre de Recherche sur la Conservation, MNHN, CNRS). Optical microscopy and UV light methods were also used.

Two individuals, represented by AMNH 135058 and AMNH 135059 (part and counterpart), and AMNH 135060, have a well-preserved gladius, which enables identification to a species level. Each represents one of the two known species of the *Keuppia* genus, *K. levante*, and *K. hyperbolaris.* The other individual (AMNH 117083a, b) does not preserve the gladius vestige and an identification to genus or species level was not possible.

AMNH 135058 (Fig. 4.3) and AMNH 135059 (Fig. 4.4) can be identified as *K. levante*. In addition to the gladius, the specimen retains fin cartilage (Fig. 4.4C; 4.5B), which was also described for the holotype (Fuchs *et al*. 2009). The paired gladius vestige has a slightly semi-circular shape (Fig. 4.5A-C) and is located at the posterior-most section of the mantle. Growth lines (Fig. 4.3C; 4.5B) appear as transverse ridges on the dorsal surface of the gladius (AMNH 135059) and imprints on the ventral counterpart (AMNH 135058). Sucker impressions are clearly preserved on the arms and are best observed under UV light (Fig. 4.3D; 4.4D). Given

their concentration and their proximity to one another the suckers are interpreted to be biserial. No cirri are evident. These observations concur with those of Donovan & Fuchs (2016, fig. 8C) who describe a specimen of *K. levante* from Haqel with alternating circular suckers. The µXRF major-to-trace elemental mapping, show that the muscular tissue on the arms and mantle fluoresces in yttrium which denotes a composition of calcium phosphates. Trace metals such as iron and copper are initially involved in biomolecules with specific biological functions (Gueriau *et al.* 2018). Melanin from the ink sac reveals traces of copper, and the gills have an iron signature, which is common to blood vessels and capillaries (Donovan & Fuchs 2016).

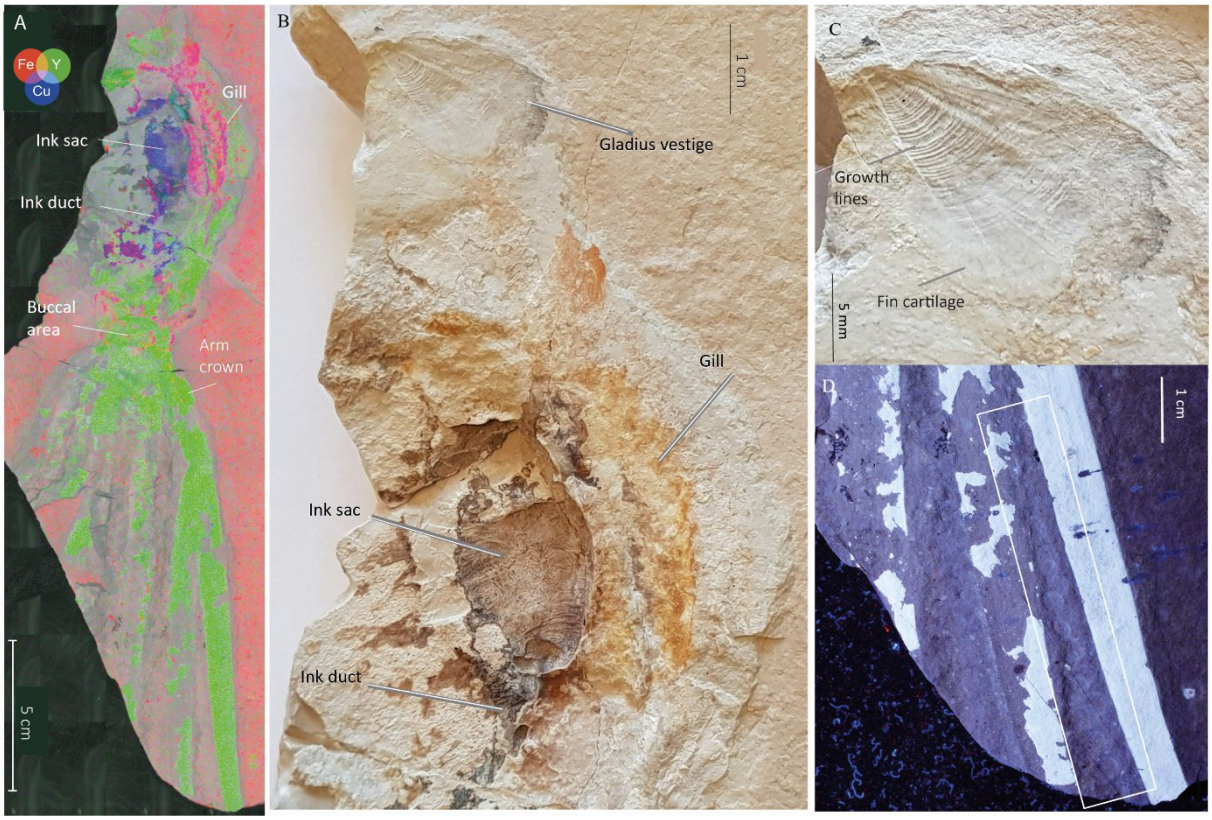

Figure 4.3: Images of AMNH 135058 (ventral view) showing the elemental map (A) resulting from µXRF major-to-trace elemental mapping, M6 Jetstream Bruker XRF, UAR 3224 CRC, MNHN, Fe (red) Y (green) and Cu (blue). Photograph of the posterior part of the specimen showing the ink sac, gill, and gladius vestige (B). Close up of the gladius vestige (C), and UV photograph of the sucker impressions (D) and phosphatized arm tissue. UV photograph by R. Piguet-Ruinet (SU Intern).

AMNH 135060 has the gladius vestige of *K. hyperbolaris* (Fig. 4.5A, B). The specimen shows the same biserial sucker row seen in the individual represented by AMNH 135058 and AMNH 135059. An axial nerve is clearly visible in natural light (Fig. 4.5C), though less visible in UV light (Fig. 4.5D).

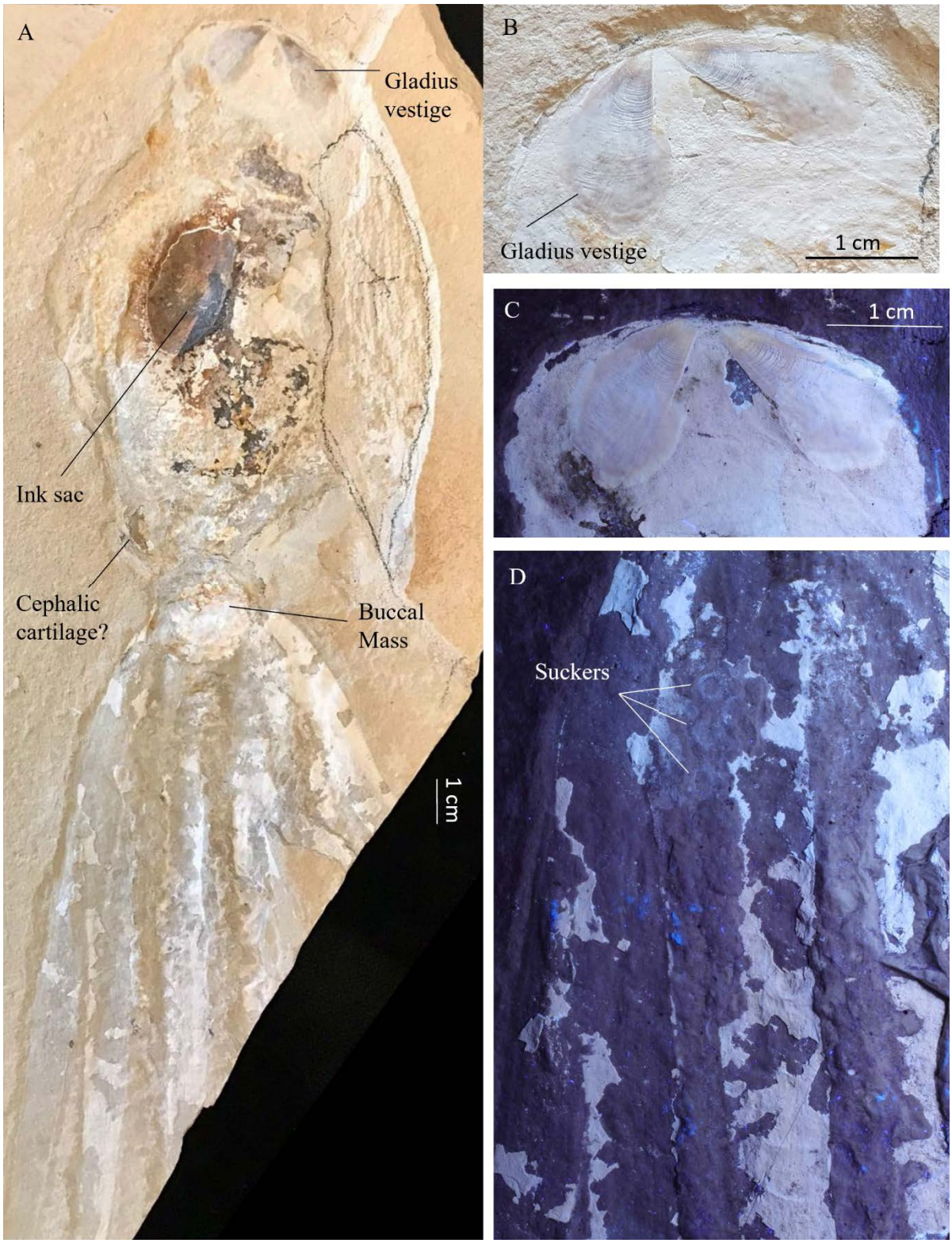

Figure 4.4: Photographs of AMNH 135059 (dorsal view) showing the extent of the preserved fossil in natural light (A). The area surrounded by pencil, with an X in the center is not exposed. Close up of the paired gladius vestige in natural light (B) and UV light (C). The transverse growth lines are clearly preserved. UV photograph of the suckers (D). UV photograph by R. Piguet-Ruinet (SU Intern).

Consistent with the species description for *K. hyperbolaris* (Fuchs *et al.* 2009), the two blades of the gladius vestige have a more subtriangular shape than those of *K. levante*. Additionally, there is a hyperbolar-like zone running longitudinally along each blade (Fig. 4.6A, E). In the description of the holotype, Fuchs *et al.* (2009) could not discern if the blades of the gladius vestige were weakly articulated or connected, or whether the vestige was paired as in *K. levante*. In AMNH 135060, the blades do appear to be connected (Fig. 4.5B).

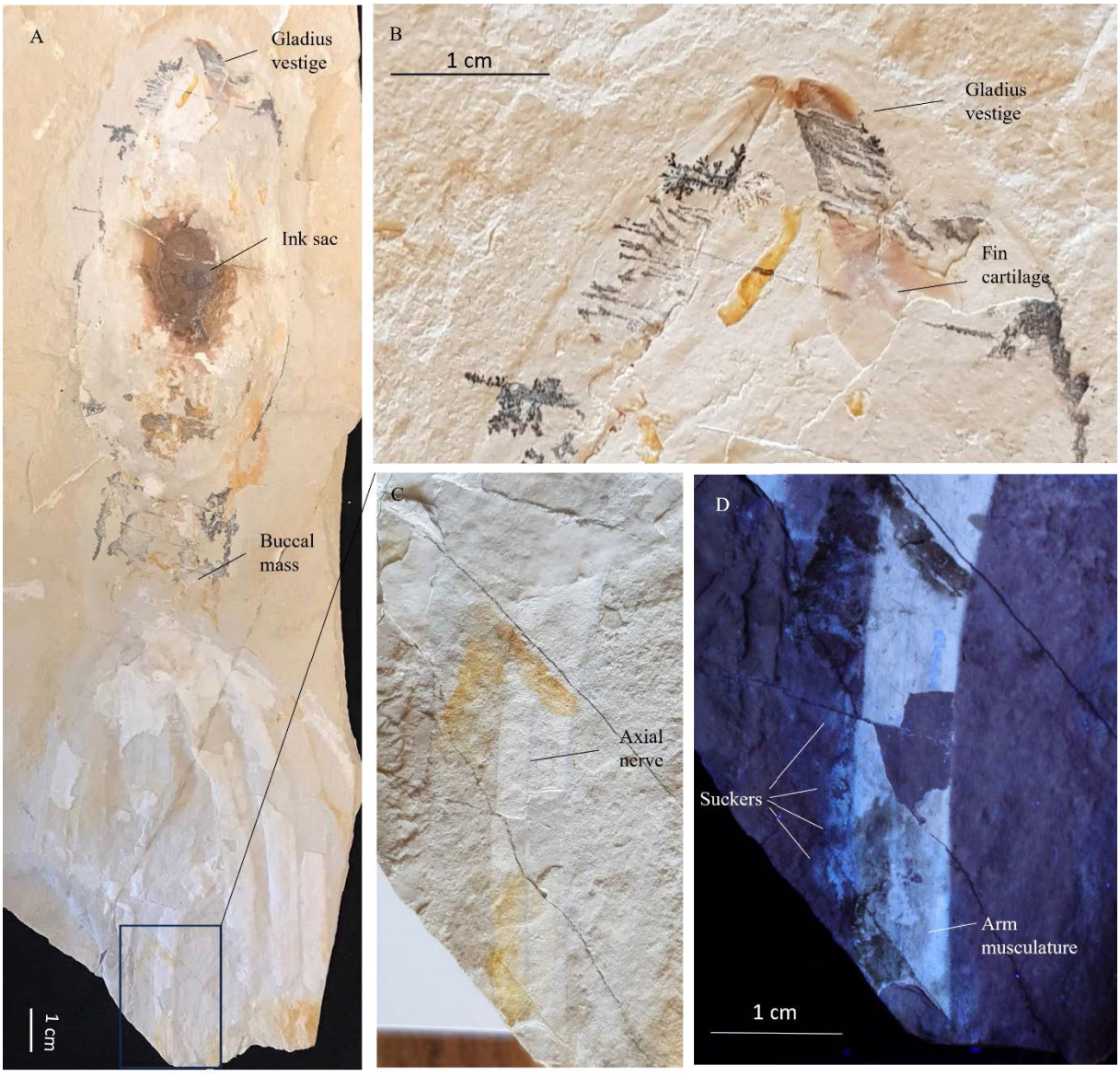

Figure 4.5: Photographs of AMNH 135060 showing the fossil in natural light (A). Close up of the gladius vestige (B) and arm showing the preserved axial nerve (C). The same arm in UV light (D) which shows phosphatized traces of the suckers and arm musculature. UV photograph by R. Piguet-Ruinet (SU Intern).

The gladius in AMNH 117083a, b (part, and counterpart) is not visible within the mantle outline (approximately 2.5cm in length). The mantle tissue appears as a pale white impression in the matrix that surrounds the internal organs (Fig. 4.7). The arm crown has the same preservation, which is most clearly viewed in UV light (Fig. 4.7C). The ink sac and duct are clearly visible, and a slightly heterogeneous mass (outlined in Fig. 4.7B in grey) is present in the posterior-most and lateral region. It is possible that this represents organs of the digestive system. The phosphatized remains of the buccal mass are best observed in UV, while the multi-spectral imaging (Fig. 4.7D) picks up on two overlapping circular structures in the head region. We interpret these to be the remains of compressed cephalic cartilage. Additionally, two circular shapes are positioned within the boundaries of the cephalic cartilage and possibly represent statocysts. Without the gladius, it is not possible to identify with certainty if this individual represents *Keuppia*, or a different taxon (e.g. *Styletoctopus*).

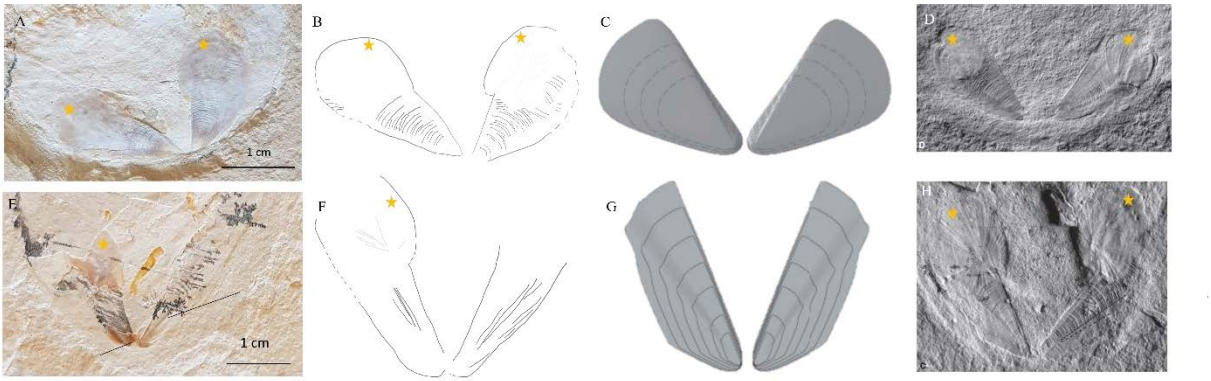

Figure 4.6: Photographs, drawings, and illustrations of AMNH 135058 (A – D), and AMNH 135060 (E – H). The illustrations (C, G) are from Fuchs (2020), and black and white photographs (D, H) are from Fuchs *et al.* (2009). The yellow stars indicate the position of fin attachments at the anterior-most parts of the gladius vestiges.

A better understanding of the soft tissues in *Keuppia* is desirable as the genus is among the first representatives of the suborder Incirrata. As shown in Fig. 4.4, and 4.5, structures such as axial nerves and suckers can be identified, which can provide insight into the evolution of the cephalopod nervous system. This is the subject of a recent paper by Klug *et al*. (2023) for which I was a co-author. Control of the suckers requires ganglia which are not yet known from the fossil record. An expanded study of these first Incirrata from Lebanon could provide insights on the evolutive history of the nervous system, as well as other soft tissues characters.

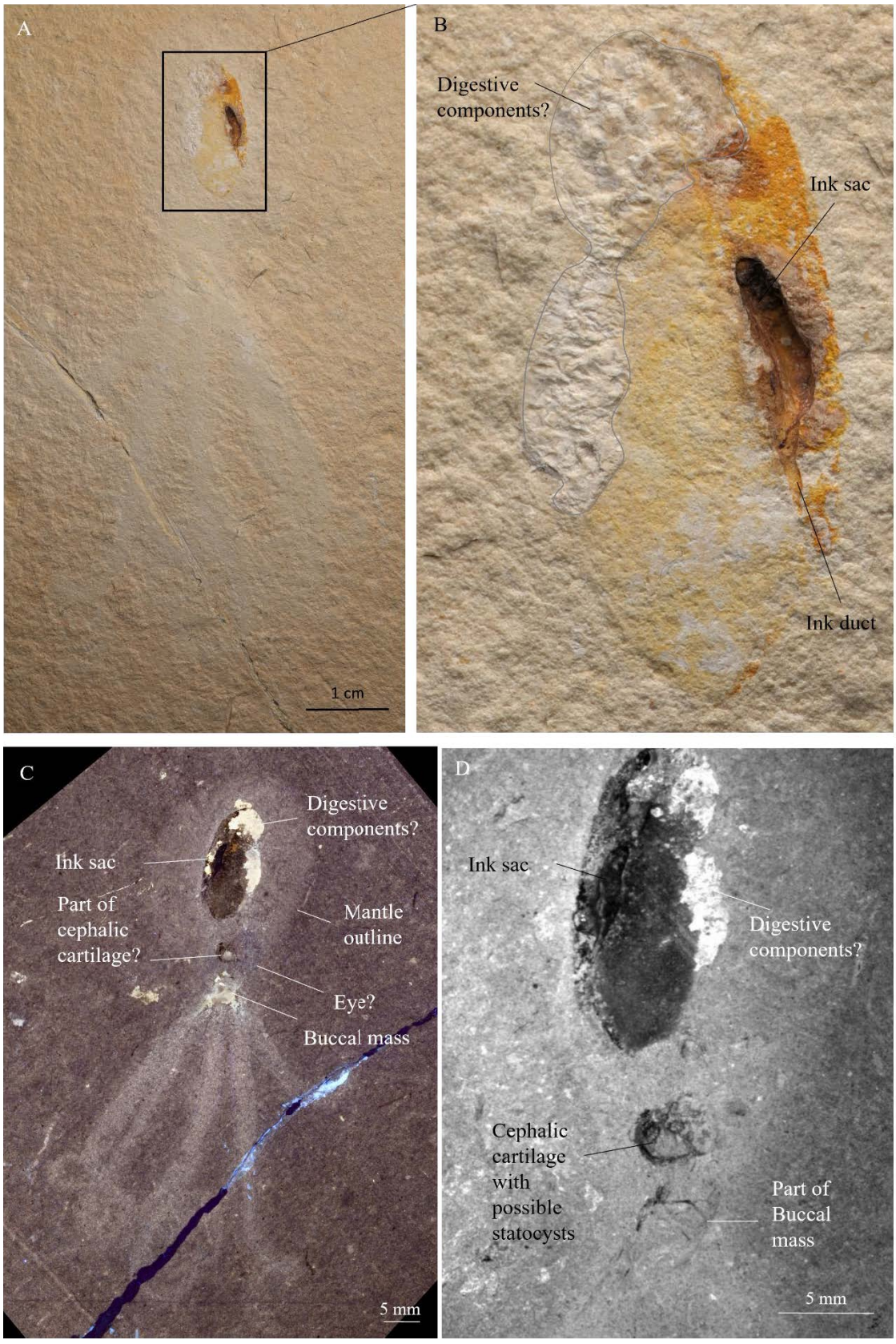

Figure 4.7: Photographs of AMNH 117083a, b in natural light (A, B), UV (C), and UV-visible-near infrared multi-spectral imaging (MSI), SOLEIL Synchrotron, Saint-Aubin, France (D). The close-up (B) is taken from a slice of an RTI image stack. The ink sac is clearly visible in natural light. The UV images reveal other structures including the buccal mass, cephalic cartilage, and possible statocysts. UV photograph by L. Cazes, MNHN.

4.6 PERSPECTIVES

Rowe *et al.* (in prep) in this chapter, and the preliminary study of the *Keuppia* specimens, clearly show the benefits of a complimentary array of 2D imaging techniques, and the structures they make visible. These methods enabled us to rectify previous anatomical misinterpretations, identify intraspecific variation, and resolve a number of phylogenetic character states of a key Mesozoic coleoid, leading to a redescription of the species, as well as the holotype. However, like much of the existing work on Lebanese fossil coleoids, it focused mainly on fossil systematics. Ultimately the study raised further questions about the taphonomic processes in the Lebanese Lagerstätten, and how they contribute to what preserves. The selectivity for preservation – what organs or soft tissues are more likely to fossilize, and how – is poorly explored, making it difficult to determine the amount of information that is potentially lost during fossilization, or how the same tissues may preserve, or not, under slightly different settings. This lack of information has implications for a variety of paleontological analysis, including systematics, the coding of phylogenetic characters, or palaeoecological interpretation. Assessing the anatomical and elemental variation expressed in fossilized soft tissue, would highlight the taphonomic biases in the Lebanese lithographic limestones.

As the most abundant species of gladius-bearing coleoid in the Lebanese Lagerstätte sediments, *D. syriaca* would be an ideal group to test the taphonomic signatures of multiple organs/tissues. The use of just one species removes the potential for interspecific bias and, as it is present in each of the outcrops, it can be studied over a 10 My period from slightly varied depositional environments.

The array of 2D imaging including μXRF and XAS utilized in the Rowe *et al.* (in prep) provides an optimal framework for this line of study. The panel of techniques have already been successfully applied to a selection of individuals in the existing sample. The methods can be extended to include more of the individuals as well as additional specimens from fieldwork and collection loans.

The creation of a dataset that contains the elemental traces of all the preserved soft tissues would form the basis for quantitative and qualitative statistical analyses and enable inquiry into taphonomic and preservational differences between the localities. In doing so, it would highlight implications for using just one Lagerstätte outcrop for paleontological studies. This would provide a reference not just for coleoids in the Lebanese Lagerstätte deposits but could be extrapolated as a framework on the variation of soft tissue preservation in other taxa.

BIBLIOGRAPHY

ALLISON, P. A. 1988. *Konservat-Lagerstätten:* cause and classification. *Paleobiology*, **14**, 331–344.

AUDO, D. & CHARBONNIER, S. 2012. Late Cretaceous crest-bearing shrimps from the Sahel Alma Lagerstätte of Lebanon. *Acta Palaeontologica Polonica*, **58**, 335–349.

———, ———, GARASSINO, A. and HYŽNÝ, M. 2017. *Fossil crustacea of Lebanon*. *Mémoires du Muséum national d'Histoire naturelle*, **210,** Paris.

BRIGGS, D.E. and WILBY, P.R., 1996. The role of the calcium carbonate-calcium phosphate switch in the mineralization of soft-bodied fossils. *Journal of the Geological Society*, **153**, 665-668.

BROCCHI, P. 1875. Note sur une nouvelle espèce de crustacé fossile (Penaeus libanensis). *Bulletin de la Société géologique de France*, **3**, 609–610.

CHARBONNIER, S., TERUZZI, G., AUDO, D., LASSERON, M., HAUG, C. and HAUG, J. T. 2017. New thylacocephalans from the Cretaceous Lagerstätten of Lebanon. *Bulletin de la Société géologique de France*, **188**, 19.

———., AUDO D., GARASSINO A. and HYŽNÝ M. 2017*a*. — *Fossil Crustacea of Lebanon. Mémoires du Muséum national d'Histoire naturelle*, **210,** Paris.

———., Teruzzi, G., Audo, D., Lasseron, M., Haug, C. and Haug, J.T., 2017*b*. New thylacocephalans from the Cretaceous Lagerstätten of Lebanon. *Bulletin de la Société géologique de France*, *188*(3).

DAVIS, J. W. 1887. *The Fossil Fishes of the Chalk of Mount Lebanon, in Syria*. Royal Dublin Society.

DOLLO, L. 1912. Les Céphalopodes adaptés à la vie nectique secondaire et benthique tertiaire. *Zoologisches Jahrbuch (Suppl.)* 15 (1): 105–140.

DONOVAN, D. T. & FUCHS, D. 2016. Treatise Online no. 73: Part M, Chapter 13: Fossilized Soft Tissues in Coleoidea. *Treatise Online*.

EL HOSSNY, T. & CAVIN, L. 2023. A New Enigmatic Teleost Fish from the Mid-Cretaceous of Lebanon. *Diversity*, **15**, 839.

ENGESER, T. and REITNER, J. 1985. Teuthiden aus dem Unterapt (»Töck«) von Helgoland (Schleswig-Holstein, Norddeutschland): Teuthids from the early aptian ("Töck") of heligoland (Schleswig-Holstein, North Germany). *Paläontologische Zeitschrift*, **59**, 245–260.

EUDES-DESLONGCHAMPS, M. 1835. Mémoire sur les Teudopsides, animaux fossiles, voisins des calmars. Mémoires de la Société Linnéenne de Normandie **5**:68–78.

D'ORBIGNY, A., 1835–1848. In A. Ferussac & A. D'Orbigny (eds) Histoire Naturelle Générale et Particuliere des Céphalopodes Acétabulifères Vivants et Fossils. 2 vols. *Text and Atlas*. Paris

FOREY, P. L., YI, L., PATTERSON, C. and DAVIES, C. E. 2003. Fossil fishes from the Cenomanian (Upper Cretaceous) of Namoura, Lebanon. *Journal of Systematic palaeontology*, **1**, 227.

FRAAS, O., 1878. *Geologisches aus dem Libanon*. Jahreshefte des Vereins für vaterländische Naturkunde in Württemberg **34**:257–391

FUCHS, D. 2006*b*. Morphology, taxonomy and diversity of vampyropod coleoids (Cephalopoda) from the Upper Cretaceous of Lebanon. *Memorie della Società italiana di Scienze naturali e del Museo civico di Storia naturale di Milano*, **34**, 1–28.

———. 2007. Coleoid cephalopods from the plattenkalks of the Upper Jurassic of Southern Germany and from the Upper Cretaceous of Lebanon A faunal comparison. *Neues Jahrbuch für Geologie und Paläontologie - Abhandlungen*, **245**, 59–69.

———. 2020. Treatise Online no. 138: Part M, Chapter 23G: Systematic Descriptions: Octobrachia. *Treatise Online*.

——— & WEIS, R. 2009. A new Cenomanian (Late Cretaceous) coleoid (Cephalopoda) from Hâdjoula, Lebanon. *Fossil Record*, **12**, 175–181.

——— & LARSON, N. 2011*a*. Diversity, morphology, and phylogeny of coleoid cephalopods from the Upper Cretaceous Plattenkalks of Lebanon-Part I: Prototeuthidina. *Journal of Paleontology*, **85**, 234–249.

——— & ———. 2011*b*. Diversity, Morphology, and Phylogeny of Coleoid Cephalopods from the Upper Cretaceous Plattenkalks of Lebanon–Part II: Teudopseina. *Journal of Paleontology*, **85**, 815–834.

———, BRACCHI, G. and WEIS, R. 2009. New Octopods (Cephalopoda: Coleoidea) from the Late Cretaceous (Upper Cenomanian) of Häkel and Hädjoula, Lebanon. *Palaeontology*, **52**, 65–81.

———, WILBY, P. R., VON BOLETZKY, S., ABI-SAAD, P., KEUPP, H. and IBA, Y. 2016. A nearly complete respiratory, circulatory, and excretory system preserved in small Late Cretaceous octopods (Cephalopoda) from Lebanon. *PalZ*, **90**, 299–305.

GRIMPE, G., 1916. Chunioteuthis: eine neue Cephalopodengattung. *Zoologischer Anzeiger*, **46,** 249.

GUERIAU, P., JAUVION, C. and MOCUTA, C. 2018. Show me your yttrium, and I will tell you who you are: implications for fossil imaging. *Palaeontology*, **61**, 981–990.

HAECKEL, E. H. P. A. 1866. *Generelle morphologie der organismen. Allgemeine grundzüge der organischen formen-wissenschaft, mechanisch begründet durch die von Charles Darwin reformirte descendenztheorie, von Ernst Haeckel.* G. Reimer, Berlin.

JATTIOT, R., BRAYARD, A., FARA, E. and CHARBONNIER, S. 2015. Gladius-bearing coleoids from the Upper Cretaceous Lebanese Lagerstätten: Diversity, morphology, and phylogenetic implications. *Journal of Paleontology*, **89**, 148–167.

JAUVION, C. 2020. *De la vie à la pierre: préservation exceptionnelle d'arthropodes marins fossiles*. (Doctoral dissertation. Muséum National d'Histoire Naturelle, Paris).

KLUG, C., DI SILVESTRO, G., HOFFMANN, R., SCHWEIGERT, GFUCHS, D., CLEMENTS, T. and GUERIAU, P., 2021 Taphonomic patterns mimic biologic structures: diagenetic Liesegang rings in Mesozoic coleoids and coprolites. *PeerJ*, **9**, e10703.

———., HOFFMANN, R., TISCHLINGER, H., FUCHS, D., POHLE, A., ROWE, A., ROUGET, I., and KRUTA, I., 2023. 'Arm brains' (axial nerves) of Jurassic coleoids and the evolution of coleoid neuroanatomy. *Swiss Journal of Paleontology* **142**, 22.

LEACH, W. E., 1817. Synopsis of the orders, families, and genera of the class Cephalopoda. *The Zoological Miscellany, being descriptions of new or interesting animals*, **3**, 137.

LUKENEDER, A. & HARZHAUSER, M., 2004. The Cretaceous coleoid Dorateuthis syriaca Woodward: morphology, feeding habits and phylogenetic implications. *Annalen des Naturhistorischen Museums in Wien. Serie A für Mineralogie und Petrographie, Geologie und Paläontologie, Anthropologie und Prähistorie*, **106**, 213–225.

MEYER, H.V., 1846. Mitteilungen an Prof. Bronn gerichtet (Brief). *Neues Jahrbuch für Mineralogie, Geologie und Paläontologie*, *1846*, pp.462-476.

NAEF, A., 1921. Das System der dibranchiaten Cephalopoden und die mediterranen Arten derselben. *Mitt. Zool. Stn. Neapel*, **22**, 527–542.

REGTEREN ALTENA, C. O. VAN 1949. Systematic catalogue of the palaeontological collection: Sixth supplement (Teuthoidea). Teyler's Museum

RÜPPELL, E., 1829. *Abbildung und Beschreibung einiger neuen oder wenig gekannten Versteinerungen aus der Kalkschieferformation von Solenhofen*. Verlag der Brönner'schen buchhandlung,(S. Schmerber).

STAROBOGATOV, Ya. I. 1983. Sistema Golovonogikh Molliuskov [Systematics of cephalopod molluscs]. In Ya. I. Starobogatov & Kir N. Nesis, eds., *Sistematika i Ekologiia Golovonogikh Molliuskov* [Taxonomy and Ecology of Cephalopod mollusks]. Zoological Institute of the USSR Academy of Sciences. Leningrad. p. 4–7

WOODWARD, H., 1883. I.—On a New Genus of Fossil "Calamary," from the Cretaceous Formation of Sahel Alma, near Beirût, Lebanon, Syria. *Geological Magazine*, **10**(1), 1–5.

———, 1896. On a Fossil Octopus (*Calais Newboldi*, J. De C. Sby. MS.) from the Cretaceous of Lebanon. *Quarterly Journal of the Geological Society*, **52**, 229-NP.

Specimen number	Reposited	Originally Assigned Genus	Locality	Age	XRF	XAS	MMI	RTI	UV	Photo	Figured	Notes
BMNH_C5017_HOLOTYPE	BMNH	*Dorateuthis syriaca*	Sahel Alma	Santonian	X			X	X	X	Woodward 1883; Fuchs 2006; Fuchs&Larson 2001; Fuchs 2006 (Thesis) 17I	
BNHM_No label	BMNH		Lebanon							X		
MNHN.F.A88588	MNHN		Hjoula	Cenomanian	X	X	X	X	X	X		
MNHN.F.A88589	MNHN		Hjoula	Cenomanian	X		X	X	X	X		
MNHN.F.A88590	MNHN		Hjoula	Cenomanian	X		X	X	X	X		
MNHN.F.A50394	MNHN	*Dorateuthis syriaca*	Sahel Alma	Santonian				X	X	X	Jattiot et al. 2015, Fig 5.1; 12	
MNHN.F.A50396	MNHN	*Dorateuthis syriaca*	Sahel Alma	Santonian	X			X	X	X	Jattiot et al. 2015, Fig 12	
MNHN.F.A50398	MNHN	*Dorateuthis syriaca*	Sahel Alma	Santonian				X	X	X	Jattiot et al. 2015, Fig 4.3; 5; 9; 10	
MNHN.F.A50400 (counter A69219)	MNHN	*Dorateuthis syriaca*	Sahel Alma	Santonian				X	X	X	Jattiot et al. 2015, Fig 7; 13	
MNHN.F.A50402 (counter A68475)	MNHN	*Dorateuthis syriaca*	Sahel Alma	Santonian					X	X	Jattiot et al. 2015, Fig 4.3; 13.2 and3 - ink sac: 13.2 "50402" - actually 69297. Fig. 13.3 "50401" - actually 50402.	
MNHN.F.A69297 (A50405?)	MNHN	*Belemnites sp.*	Haqel	Cenomanian							Jattiot et al. 2015, Fig 5.2, 11.1; 12	50405 is listed in the Figures - not sure which specimen this refers to - is this the same as MNHN.F.A69297? Fig 5.2 _ lateral fields? Fig 11.1 cephalic cartilage ? Not on A69297.
MNHN.F.A68491	MNHN	*Belemnites sp.*	Lebanon					X	X	X	Jattiot et al. 2015	Described, not figured
MNHN.F.R06746	MNHN	*Dorateuthis syriaca*	Sahel Alma	Santonian	X		X	X	X	X	Roger 1946, Planche IX: Jattiot et al. 2015, Fig 14: Donovan & Fuchs 2016 Fig 15	
NPL52121a&b	UT, Austin	*Dorateuthis*	Haqel	Cenomanian						X	Fuchs 2020	Fuchs 2020 Fig. 3. No spec. # listed. website: https://www.jsg.utexas.edu/npl/outreach/squids-the-cretaceous-ink-well/
BHI 2200	BHI	*Dorateuthis sp.*	Hjoula	Cenomanian					X	X		
BHI 2201	BHI	*Dorateuthis sp.*	Hjoula	Cenomanian					X	X	Fuchs & Larson 2011, Fig. 2	
BHI 2202	BHI	*Dorateuthis sp.*	Hjoula	Cenomanian					X	X		
BHI 2203	BHI	*Dorateuthis sp.*	Hjoula	Cenomanian					X	X		
BHI 2205	BHI	*Dorateuthis sp.*	Hjoula	Cenomanian	X				X	X	Fuchs & Larson 2011. Figs2&5	
BHI 2206	BHI	*Dorateuthis sp.*	Hjoula	Cenomanian						X		
BHI 2207	BHI	*Dorateuthis sp.*	Hjoula	Cenomanian					X	X	Fuchs & Larson 2011, Fig2 & 4; Fuchs et al 2016 (locomotion) fig. 9	
BHI 2208	BHI	*Dorateuthis sp.*	Hjoula	Cenomanian						X		
BHI 2209	BHI	*Dorateuthis sp.*	Hjoula	Cenomanian					X	X		
BHI 2210	BHI	*? Dorateuthis sp.*	Hjoula	Cenomanian					X	X	Fuchs & Larson 2011, Fig 2	

BHI 2212	BHI	*Dorateuthis sp.*	Hjoula	Cenomanian	X	X		
BHI 2213	BHI	*Dorateuthis sp.*	Hjoula	Cenomanian	X	X		
BHI 2214	BHI	*Dorateuthis sp.*	Hjoula	Cenomanian	X	X		
BHI 2215	BHI	*Dorateuthis sp.*	Hjoula	Cenomanian	X	X		
BHI 2216	BHI	*Dorateuthis sp.*	Hjoula	Cenomanian		X		
BHI 2217	BHI	*Dorateuthis sp.*	Hjoula	Cenomanian		X		
BHI 2219	BHI	*Dorateuthis sp.*	Hjoula	Cenomanian		X	Fuchs & Larson 2011 Fig.6	
BHI 2220	BHI	*Dorateuthis sp.*	Hjoula	Cenomanian	X	X	Fuchs & Larson 2011; Fuchs et al. 2016 (locomotion) fig. 1	
BHI 2221	BHI	*Dorateuthis sp.*	Hjoula	Cenomanian	X	X		
BHI 2222	BHI	*Dorateuthis sp.*	Hjoula	Cenomanian		X		
BHI 2223	BHI	*Dorateuthis sp.*	Hjoula	Cenomanian		X		
BHI 2225	BHI	*Dorateuthis sp.*	Hjoula	Cenomanian	X	X		
BHI 2226	BHI	*Dorateuthis sp.*	Hjoula	Cenomanian		X		
BHI 2227	BHI	*Dorateuthis sp.*	Hjoula	Cenomanian	X	X		
BHI 2228	BHI	*Dorateuthis sp.*	Hjoula	Cenomanian	X	X		
BHI 2229	BHI	*Dorateuthis sp.*	Hjoula	Cenomanian	X	X		
BHI 2232	BHI	*Dorateuthis sp.*	Hjoula	Cenomanian	X	X		
BHI 2233	BHI		Hjoula	Cenomanian	X	X	Fuchs & Larson2011 Fig 5.3	
BHI 5779	BHI	*Dorateuthis sp.*	Hjoula	Cenomanian	X	X	Larson 2010, Fig.1, 3A. Donovan & Fuchs 2016 Fig 12. Fuchs 2020 Fig.3,1b; Fuchs & Larson, 2011a, fig 4 & 10; Jattiot et al 2015, fig 11.4. Nixon 2015, fig 6	Listed in Fuchs & Larson 2011, fig 4.5 and 4.6 as BHI 5779 (ventral view); Fuchs 2020 as BHI 5579 (dorsal view)
Coll Nohra_New Image (DF)	Private collection	*Dorateuthis*	Lebanon			X		
RuSmith (DF)	Private collection		Hjoula	Cenomanian		X		
MSNMi_25128	MSNM		Lebanon			X		
MSNMi 24800	MSNM	*Dorateuthis syriaca*	Hjoula	Cenomanian		X	Fuchs 2006, P2	
MSNMi_25134	MSNM	*Dorateuthis syriaca*	Hjoula	Cenomanian		X	Fuchs 2006 Pl.III	
MSNMi 25144	MSNM	*Dorateuthis syriaca*	Hjoula	Cenomanian		X	Fuchs2006 Pl. 1a, b. Fuchs 2006 (Thesis) 17J	Noted as MSNM-251449 in Fuchs 2006 (Thesis)
NHMW1998z01050000	NHMW	*Dorateuthis syriaca*	Sahel Alma	Santonian			Fuchs & Larson2011 Fig 3: Lukeneder & Harzhauser 2004, fig 2, plates 1 & 2; Fuchs2006 Pl.II. Jattiot2015 Fig.12. Nixon 2015, fig. 6	
V_33 (DF)	Private collection		Lebanon			X		
V_54 (DF)	Private collection		Lebanon			X		
V_61 (DF)	Private collection		Lebanon			X		
MNHNL_CRE047	MNHNL	*Dorateuthis syriaca*	Haqel	Cenomanian		X	Jattiot et al. 2015 fig 11.2, Fuchs & Larson 2011 Fig. 4, Don&Fuchs2016 Fig.15.b	

NOT USING IN THIS STUDY	Reposited	Originally Assigned Genus	Locality	XRF	XAS	MMI	RTI	UV	Photo	Figured	Notes
BHI 2211	BHI	*Doratauthis*						X	X		
BHI 2230	BHI	*Doratauthis*	Haqel					X	X	Fuchs & Larson 2011 Fig. 6	
BHI 2231	BHI	*Doratauthis*	Haqel					X	X	Fuchs&Larson2011. Fig4; Fuchs2020, Fig3*; Don&Fuchs2016, Fig14	Listed in Fuchs 2020 as BHI 2132
BHI 5655	BHI	*Doratauthis*						X	X		
BHI 5718	BHI	*Rachiteuthis*	Haqel							Fuchs&Larson2011. Fig2; Larson2010 Fig 6	Listed in Larson 2010 as BHI 5718, Rachiteuthis. Listed in Fuchs & Larson 2011as BHI 5618 D. syriaca (juvenile).
BHI 5814	BHI	*Doratauthis*	Hjoula						X	Larson 2010 Fig 4; Fuchs 2020 Fig3	
BMNH (without reg. #)	BMNH	*Doratauthis syriaca*	Sahal Alma					X	X	Fuchs&Larson2011, Fig3; Donovan & Fuchs 2016	
BMNH C2919	BMNH	*P. fraasi*	Sahal Alma						X	Donovan & Fuchs 2016, Fig7; Fuchs&Larson2011, Fig3	
BNHM 89193	BMNH	*Doratauthis sp.*	Sahel Alma						X		
BNHM C7163	BMNH	*Doratauthis syriaca*	Sahel Alma						X		
BNHM C7163	BMNH	*Doratauthis syriaca*	Sahel Alma						X		
MNHN.F. A68481	MNHN	*Belemnites sp.*	Liban				X		X		
MNHN.F.68134 (counter MNHN.F.A68496)	MNHN	*Doratauthis syriaca*	Sahel Alma	X						Gueriau et al. 2018, fig. 5	MNHN.F.68134 figured. Counterpart not figured
MNHN.F.A50397	MNHN	*Doratauthis syriaca*	Sahal Alma				X	X	X	Jattiot et al. 2015, Fig 9; 13	Not Doratauthis.
MNHN.F.A50401	MNHN	*Doratauthis syriaca*	Sahal Alma						X	Jattiot 2015	
MNHN.F.A50403	MNHN	*Doratauthis syriaca*	Sahel Alma						X	Jattiot et al. 2015, Fig 11	
MNHN.F.A68478	MNHN	*1946-18-1432a Belemnites sp.*	Liban						X		
MNHN.F.A68480 (counter MNHN.F.A69114)	MNHN	*1946-18-1434a, b Belemnites sp.*	Haqel				X		X		
MNHN.F.A68492	MNHN	*1946-18-1425 Belemnites sp.*	Liban						X		
MNHN.F.A68494	MNHN	*1946-18-1419 Belemnites sp.*	Liban						X		
MNHN.F.A68500 (counter MNHN.F.A69219)	MNHN	*1946-18-1406a, b, Belemnites sp.*	Haqel			X			X		
MNHN.F.A68504	MNHN	*Belemnites sp.*	Liban	X		X		X	X		
MNHN.F.B18829	MNHN	*Doratauthis syriaca*	Sahal Alma	X		X		X	X	Roger 1946, Planche IV	
MNHN.F.R06751	MNHN	*Doratauthis syriaca*	Sahal Alma			X		X	X	Roger1946 Planche IV; Jattiot et al. 2015	Described in Jattiot et al. 2015, not figured
MNHN.F.XXXX Sahel alma Thomas office	MNHN		Sahal Alma						X		
MNHNL_CRE050	MNHNL	*Doratauthis syriaca*	Haqel						X		
MSNMi 23108	MSNM	*Doratauthis syriaca*	Sahal Alma						X	Fuchs 2006, P 1	
MSNMi24802	MSNM	*Doratauthis syriaca*	Hjoula						X	Fuchs & Larson2011 Fig 5.2	
MSNMi25133	MSNM	*Doratauthis syriaca*	Hjoula						X	Fuchs2006 Pl.IIB	
MSNMi26092	MSNM	*Doratauthis*							X		
RuSmith2 (DF)	Private collection	*Doratauthis*							X		
SMNS 26269	SMNS	*Doratauthis sahildalmae*	Sahal Alma						X	Fuchs2006 Pl. III	
V_39 (DF)	Private collection	*Doratauthis*							X		
V_59 (DF)	Private collection	*Doratauthis*							X		

Supplementary Table 1: The three pages included in this table show the specimens available for the study. The tables provide the collection numbers, repository information, the genus/species-level assignment, the locality information, if, and where, the specimens have been previously figured, and the type of imaging utilized. µXRF major-to-trace elemental mapping (XRF) was acquired at SOLEIL Synchrotron (PUMA Beamline), Saint-Aubin, France, Centre de Recherche sur la Conservation, MNHN, CNRS (M6 Jetstream Bruker XRF, UAR 3224) Paris, France, and the iXRF facility (ATLAS M benchtop microEDXRF (micro XRF) spectrometer), Austin, TX, USA. Reflectance Transformation Imaging (RTI) and UV light photography was completed at the MNHN, Paris, France; UV-visible-near infrared multi-spectral imaging (MSI) was acquired at SOLEIL Synchrotron (IPANEMA Platform), Saint-Aubin, France. X-ray absorption spectroscopy (XAS) was acquired at SOLEIL Synchrotron (PUMA Beamline), Saint-Aubin, France. The specimens shown in blue were not utilized for this study as the gladius was not preserved in such a way where measurements could be obtained.

Specimen number	Direct measurement (DM)/ Composite (C)/ Straightened (S)	GLADIUs WIDTH (median field)(~mm)	GLADIUS LENGTH (median field) (~mm)	APICAL (OPENING) ANGLE° (direct measurements)	LATERAL FIELDS: Posterior Width (~mm) If present	LATERAL FIELDS: Anterior length (~mm) If present	LATERAL FIELDS: Area (measured in ImageJ) approx mm²	MEDIAN FIELD area if lateral fields are present (~mm²)	CONUS LENGTH (~mm)	CONUS WIDTH (~mm)
BMNH_C5017_ HOLOTYPE	S	4.3	40	6.3						
BNHM_No label	DM	19	139.6	7.8						
MNHN.F.A88588	DM	6.9	83	4.7		66	32	305		
MNHN.F.A88589	DM	14	92	8.7						
MNHN.F.A88560	S	8.8	87	5.9						
MNHN.F.A50394	DM	4.5	45.2	5.6	3		20.7	116		
MNHN.F.A50396	DM	9.8	94	6.1						
MNHN.F.A50398	DM	8	114	4.3						
MNHN.F.A50400 (counter A69219)	C	24	140	9.5						
MNHN.F.A50402 (counter A68475)	S	31.8	241	7.3						
MNHN.F.A69297 (A50405?)	DM	15.4	105	8						
MNHN.F.A68491	S	2.2	47	2.6						
MNHN.F.R06746	S	13.4	81	9.4						
NPL52121a&b	S	11.9	87	7.8						
BHI 2200	S	11.8	95	7.1						
BHI 2201	S	18.6	123	8.7		101.5	237.8	980		
BHI 2202	S	17.6	145.2	6.9						
BHI 2203	S	14.1	113.8	6.6		93.4	48.2	771.3		
BHI 2205	DM	15.3	102.7	7.7						
BHI 2206	S	18.7	160.4	6.2						
BHI 2207	DM	14.5	124.6	6.6		99.8	144.8	836.5		
BHI 2208	C	15.2	149.5	5.4						
BHI 2209	S	8.1	130.3	3.1						
BHI 2210	S	18.8	175.1	6.3						
BHI 2212	DM	9.6	69.3	7.8						
BHI 2213	S	16	129.2	7.1						
BHI 2214	S	16.6	140	6.7						
BHI 2215	S	18.8	127	8.4						
BHI 2216	S	17.2	114.5	8.5		102.9	173.8	878.5		
BHI 2217	S	16.8	141.5	6.7		99	175.7	1053		
BHI 2219	DM	7.6	73.4	6						
BHI 2220	S	12.8	83.1	8.7						
BHI 2221	S	15.6	147.3	5.9						
BHI 2222	DM	18.7	112.2	9.6		95.7	254	819		
BHI 2223	S	13.1	95.6	7.8						
BHI 2225	S	9.1	68.9	7.5	5.1		30.4	321		
BHI 2226	S	17.7	127	7.6	9		226	1214		
BHI 2227	S	11.6	82	8.1						
BHI 2228	S	16.5	145.9	6.5						
BHI 2229	DM	21.5	139.2	8.8						
BHI 2232	S	18.7	138.9	7.5						
BHI 2233	DM	10.9	77	8.1	6.8		41.6	340		
BHI 5779	S	11.1	87.8	7.1						
Coll Nohra_New Image (DF)	S	18.7	133.6	7.9						
RuSmith (DF)	DM	12.3	123.8	5.7						
MSNMi_25128	S	19.8	125.6	9						
MSNMi 24800	S	7.9	108.9	4					5.3	6.6
MSNMi_25134	S	17.3	143.6	6.9						
MSNMi 25144	DM	8.4	67.6	7.2	3.1		16	254		
NHMW1998z010 50000	DM	7.4	95.7	4.4						
V_33 (DF)	S	9.7	92	5						
V_54 (DF)	DM	17.9	139.6	7.5					4.6	13.5
V_61 (DF)	S	7.3	106	3.8						
MNHNL_CRE047	DM	13.4	89.4	8.5						

Specimen number	ARMS: MAX arm length (~mm)	ARMS: Intermediate 'pair 1' length - (~mm)	ARMS: Intermediate 'pair 2'length - (~mm)	ARMS: MIN length - (~mm)	BUCCAL MASS (including beak) length (~mm)	BUCCAL MASS Width (~mm)	Beak angle°	SUCKER SIZE RANGE (~mm)	GILL LENGTH (inc. Brachial heart) (~mm)	EYES: Eye 1 - diameter 1 (mm) Smaller (~mm)	EYES: Eye 1 - diameter 2 (mm) Larger (~mm)	EYES: Eye 2 - Diameter 1 (mm) Smaller (~mm)	EYES: Eye 2 - Diameter 2 (mm) Larger (~mm)	EYES: Lens 1 -diameter 1 (~mm)	EYES: Lens 1 - diameter 2 (~mm)	EYES: Lens 2 -diameter 1 (~mm)	EYES: Lens 2 - diameter 2 (~mm)
BMNH_C5017_HOLOTYPE	21	20	18	18	4.4	23	81.8				9						
BNHM_No label					8	4	62										
MNHN.F.A88588					11.6	8.2	76			7.2	12.7	8.1	14.8				
MNHN.F.A88589	55	44	34		10.9	4.9											
MNHN.F.A88560	31																
MNHN.F.A50394					14	3	34			11.2	21.3	8.6	21.5				
MNHN.F.A50396	84	73			15	4	36										
MNHN.F.A50398	118	102 - 110	83 - 100	58 - 78	13	7	109										
MNHN.F.A50400 (counter A69219)	215	177	146-150	148	32	11.7	62			25.8	40	32.3	32.4				
MNHN.F.A50402 (counter A68475)																	
MNHN.F.A69297 (A50405?)	24	22	21		3.8	1.3	54							3.1	4		
MNHN.F.A68491	68	48-49	46		13.8	8.8	67			17.6	20.1						
MNHN.F.R06746					11	9											
NPL52121a&b	43				19	13	68										
BHI 2200					22.9	12											
BHI 2201																	
BHI 2202								0.9 - 1.4		11.2	17.8			3.2	3.3		
BHI 2203	50	39			14	9	82										
BHI 2205																	
BHI 2206																	
BHI 2207																	
BHI 2208	77				22	11.6				15.8	16.7						
BHI 2209																	
BHI 2210	41	33	26		10.7	5.6	61.4	1.3 - 1.6		13.5	16.6			2.5	4.2		4.1
BHI 2212	79				19	9	46	1.4 - 2.2		10.9	18.1	10.3	17.7			4	
BHI 2213	59	52-54			15	11		1-3									
BHI 2214					20	9	57										
BHI 2215									15.7								
BHI 2216					3.6	2.2	63.9			11.3	15.3	9.2	14.9				
BHI 2217					13.2	9.2				7.4	25	7.8	25				
BHI 2219	51				16.4	10.9				8.9	15.8	10.1	15.1				
BHI 2220					11	7.8	67										
BHI 2221										7.8	13.4	7.7	12.1				
BHI 2222					6.9	5.4	97										
BHI 2223								0.9-1.8									
BHI 2225	36									12.9	22.1	14.4	21.5				
BHI 2226					21.5	11.3	82.4			12.9	22.1	14.4	21.5				
BHI 2227	77	57-58			18.9	12.1	77.6	1.2-2.4		11.9	23.1	9	25				
BHI 2228	77	63	54-56		14	7.5	50.1										
BHI 2229																	
BHI 2232	50	36.4	32		10.2	7.1	87										
BHI 2233																	
BHI 5779					16.5	9.6	61.7										
Coll Nohra_New Image (DF)																	
RuSmith (DF)					17.1	11.9	71.2										
MSNMi_25128																	
MSNMi 24800																	
MSNMi_25134					12.5	5.1	53.6										
MSNMi 25144										13.5	13.6	13.4	13.5				
NHMW1998z 0105000	56	46-47	38-39	34													
V_33 (DF)	66													4.2	5.4		
V_54 (DF)	57	49-50								13.1	15.1						
V_61 (DF)	43																
MNHNL_CRE047																	

Supplementary Table 2: Summary of the measurements collected for the specimens used in the study.

Specimen number	GLADIUS LENGTH (median field) (~mm)	STATE: GLADIUS SIZE (small/med/large) (Fuchs 2020)	INDICES: MEDIAN FIELD WIDTH $_{MAX}$ (direct measure as Hyperbolar zones are either indistinct or absent in prototeuthids) (Fuchs 2020)	INDICES: OPENING ANGLE OF THE MEDIAN FIELD (Apical angle). Direct measurement only (Fuchs 2020)	STATE: OPENING ANGLE: <12°? (Fuchs 2020)	INDICES: GLADIUS WIDTH (Gladius width $_{max}$: Gladius length) (Fuchs 2020)	STATE: GLADIUS WIDTH V. small/Small/Medium/Large/V. large (Fuchs 2020)	INDICES: MEDIAN FIELD LENGTH (Median field length:Gladius Length) (Fuchs 2020)	LATERAL FIELDS: Posterior Width (~mm) If present	LATERAL FIELDS: Anterior length (~mm) If present	LATERAL FIELDS: Area (measured in ImageJ) approx mm² (Fuchs 2020)
BMNH_C5017 HOLOTYPE	40	v small	4.3	6.3	<12°	0.11	Slender	1			
BNHM_No label	139.6	small	19	7.8	<12°	0.14	Slender	1			
MNHN.F.A88588	83	small	6.9	4.7	<12°	0.08	V. Slender	1		66	32
MNHN.F.A88589	92	small	14	8.7	<12°	0.15	Slender	1			
MNHN.F.A88560	87	small	8.8	5.9	<12°	0.10	Slender	1			
MNHN.F.A50394	45.2	v small	4.5	5.6	<12°	0.10	Slender	1	3		20.7
MNHN.F.A50396	94	small	9.8	6.1	<12°	0.10	Slender	1			
MNHN.F.A50398	114	small	8	4.3	<12°	0.07	V. Slender	1			
MNHN.F.A50400 (counter A69219)	140	small	24	9.5	<12°	0.17	Slender	1			
MNHN.F.A50402 (counter A68475)	241	Medium	31.8	7.3	<12°	0.13	Slender	1			
MNHN.F.A69297 (A50405?)	105	Small	15.4	8	<12°	0.15	Slender	1			
MNHN.F.A68491	47	V. small	2.2	2.6	<12°	0.05	V. Slender	1			
MNHN.F.R06746	81	Small	13.4	9.4	<12°	0.17	Slender	1			
NPL52121a&b	87	Small	11.9	7.8	<12°	0.14	Slender	1			
BHI 2200	95	Small	11.8	7.1	<12°	0.12	Slender	1			
BHI 2201	123	Small	18.6	8.7	<12°	0.15	Slender	1		101.5	237.8
BHI 2202	145.2	Small	17.6	6.9	<12°	0.12	Slender	1			
BHI 2203	113.8	Small	14.1	6.6	<12°	0.12	Slender	1		93.4	48.2
BHI 2205	102.7	Small	15.3	7.7	<12°	0.15	Slender	1			
BHI 2206	160.4	Small	18.7	6.2	<12°	0.12	Slender	1			
BHI 2207	124.6	Small	14.5	6.6	<12°	0.12	Slender	1		99.8	144.8
BHI 2208	149.5	Small	15.2	5.4	<12°	0.10	Slender	1			
BHI 2209	130.3	Small	8.1	3.1	<12°	0.06	V. Slender	1			
BHI 2210	175.1	Small	18.8	6.3	<12°	0.11	Slender	1			
BHI 2212	69.3	Small	9.6	7.8	<12°	0.14	Slender	1			
BHI 2213	129.2	Small	16	7.1	<12°	0.12	Slender	1			
BHI 2214	140	Small	16.6	6.7	<12°	0.12	Slender	1			
BHI 2215	127	Small	18.8	8.4	<12°	0.15	Slender	1			
BHI 2216	114.5	Small	17.2	8.5	<12°	0.15	Slender	1		102.9	173.8
BHI 2217	141.5	Small	16.8	6.7	<12°	0.12	Slender	1		99	175.7
BHI 2219	73.4	Small	7.6	6	<12°	0.10	Slender	1			
BHI 2220	83.1	Small	12.8	8.7	<12°	0.15	Slender	1			
BHI 2221	147.3	Small	15.6	5.9	<12°	0.11	Slender	1			
BHI 2222	112.2	Small	18.7	9.6	<12°	0.17	Slender	1		95.7	254
BHI 2223	95.6	Small	13.1	7.8	<12°	0.14	Slender	1			
BHI 2225	68.9	Small	9.1	7.5	<12°	0.13	Slender	1	5.1		30.4
BHI 2226	127	Small	17.7	7.6	<12°	0.14	Slender	1	9		226
BHI 2227	82	Small	11.6	8.1	<12°	0.14	Slender	1			
BHI 2228	145.9	Small	16.5	6.5	<12°	0.11	Slender	1			
BHI 2229	139.2	Small	21.5	8.8	<12°	0.15	Slender	1			
BHI 2232	138.9	Small	18.7	7.5	<12°	0.13	Slender	1			
BHI 2233	77	Small	10.9	8.1	<12°	0.14	Slender	1	6.8		41.6
BHI 5779	87.8	Small	11.1	7.1	<12°	0.13	Slender	1			
Coll Nohra_New Image (DF)	133.6	Small	18.7	7.9	<12°	0.14	Slender	1			
RuSmith (DF)	123.8	Small	12.3	5.7	<12°	0.10	Slender	1			
MSNMi_25128	125.6	Small	19.8	9	<12°	0.16	Slender	1			
MSNMi 24800	108.9	Small	7.9	4	<12°	0.07	V. Slender	1			
MSNMi_25134	143.6	Small	17.3	6.9	<12°	0.12	Slender	1			
MSNMi 25144	67.6	Small	8.4	7.2	<12°	0.12	Slender	1	3.1		16
NHMW1998z01050000	95.7	Small	7.4	4.4	<12°	0.08	V. Slender	1			
V_33 (DF)	92	Small	9.7	5	<12°	0.11	Slender	1			
V_54 (DF)	139.6	Small	17.9	7.5	<12°	0.13	Slender	1			
V_61 (DF)	106	Small	7.3	3.8	<12°	0.07	V. Slender	1			
MNHNL_CRE047	89.4	Small	13.4	8.5	<12°	0.15	Slender	1			

Specimen number	INDICES: POSTERIOR LATERAL FIELDS (Gladius Width $_{max}$: Median Field Width$_{max}$) (Fuchs 2020)	STATE: POSTERIOR LATERAL FIELDS (Fuchs 2020)	INDICES: LATERAL FIELD LENGTH (lateral field length:gladius length)	INDICES: MEDIAN FIELD AREA (median field area:gladius area total) (Fuchs 2020)	STATE: MEDIAN FIELD AREA (Fuchs 2020)	INDICES: ARM LENGTH (Arm length $_{max}$:mantle length) (Fuchs 2020)	STATE: ARM LENGTH (Fuchs 2020)	TOTAL BODY LENGTH (only those that are on the border btwn two states, and holotype) (~mm)	STATE: TOTAL BODY SIZE (mantle + head + arms as per DF: 21/5/23)	INDICES: EYE DIAMETER (Eye diameter $_{max}$: Glad length $_{max}$)	INDICES: BUCCAL MASS (Buccal mass length $_{max}$: gladius length (Nixon 2015)
BMNH_C5017						0.53	Moderate	68	Small	0.23	0.11
HOLOTYPE											
BNHM_No label			0.80	0.9	Very large	0.60	Moderate		Small	0.16	0.10
MNHN.F.A88588											0.13
MNHN.F.A88589											0.13
MNHN.F.A88560	0.67	Slender	0.32	0.85	Very large	0.69	Moderate		Small	0.23	0.15
MNHN.F.A50394						0.74	Moderate	225	Medium		0.13
MNHN.F.A50396						0.84	Long		Medium		0.09
MNHN.F.A50398						0.89	Long		Large	0.17	0.13
MNHN.F.A50400											
(counter A69219)											
MNHN.F.A50402											
(counter A68475)											
MNHN.F.A69297											
(A50405?)						0.51	Moderate		Small		0.08
MNHN.F.A68491						0.84	Long		Small	0.25	0.17
MNHN.F.R06746											0.13
NPL52121a&b						0.45	Moderate		Small		
BH1 2200			0.83	0.8	Very large						0.19
BH1 2201										0.16	
BH1 2202			0.82	0.94	Very large	0.49	Moderate		Small		0.14
BH1 2203											
BH1 2205			0.80	0.85	Very large					0.13	0.15
BH1 2206						0.59	Moderate		Small		
BH1 2207										0.13	0.14
BH1 2208						0.56	Moderate		Medium		0.12
BH1 2209						0.46	Moderate	203.6	Medium		0.17
BH1 2210											
BH1 2212			0.90	0.84	Very large	0.59	Moderate		Medium	0.13	0.17
BH1 2213			0.70	0.86	Very large						
BH1 2214											0.05
BH1 2215										0.18	0.16
BH1 2216						0.35	Short	208	Medium	0.17	0.11
BH1 2217			0.85	0.76	Large					0.14	0.10
BH1 2219											
BH1 2220						0.44	Moderate		Small	0.19	0.10
BH1 2221			0.2 (minimum)	0.9	very large						
BH1 2222			0.42	0.84	very large						
BH1 2223						0.55	Moderate		Medium	0.15	0.15
BH1 2225	0.56	Slender				0.55	Moderate		Medium	0.16	0.14
BH1 2226	0.51	Slender								0.18	0.10
BH1 2227						0.57	Moderate		Small		0.12
BH1 2228											
BH1 2229			0.2 (minimum)	0.89	Very large						0.13
BH1 2232	0.62	Slender									
BH1 2233						0.59	Moderate		Small		0.13
BH1 5779						0.72	Moderate		Small	0.147826087	
Coll Nohra_New Image						0.41	Moderate	229	Medium		
(DF)						0.41	Moderate		Small	0.14245283	
RuSmith (DF)											
MSNM_25128											
MSNM_24800											
MSNM_25134	0.37	Slender	0.17	0.94	Very large						
MSNM_25144											
NHMW19982010500000											
V_33 (DF)											
V_54 (DF)											
V_61 (DF)											
MNHNL_CRE047											

Supplementary Table 3: Indices calculated for the specimens used in the study. Indices from Fuchs (2020).

Specimen number	Median field triangular: Yes/No	Widest section of the gladius is at the median field: Yes/No	Are lateral reinforcements (keels) present: Yes/No	Are the lateral reinforcements (keels) pronounced: Yes/No	The lateral reinforcements (keels) are continuous from anterior-posterior extremities: Yes/No	Is there a Central Median Field (Linear area in the central part of the median field)	Is there a Median reinforcement (Line or ridge) present: Yes/No	If Yes, is this a Line or Ridge. If No the cell is empty
BMNH_C5017_HOLOTYPE	Yes	Yes	Yes	Yes	Yes	No	Yes	Ridge
BNHM_No label	Yes	Yes	Yes	Yes	Yes	Yes	Yes	Line
MNHN.F.A88588	Yes	Yes	Yes	Yes	Yes	Yes	Yes	Line
MNHN.F.A88589	Yes	Yes	Yes	Yes	Yes	No	No	
MNHN.F.A88560	Yes	Yes	Yes	Yes	Yes	Yes	Yes	Line
MNHN.F.A50394	Yes	Yes	Yes	Yes	Yes	No	Yes	Ridge
MNHN.F.A50396	Yes	Yes	Yes	Yes	Yes	Yes	Yes	Line
MNHN.F.A50398	Yes	Yes	Yes	Yes	Yes	No	Yes	Ridge
MNHN.F.A50400 (counter A69219)	Yes	Yes	Yes	Yes	Yes	No	No	
MNHN.F.A50402 (counter A68475)	Yes	Yes	Yes	Yes	Yes	No	No	
MNHN.F.A50405? (A69297)	Yes	Yes	Yes	Yes	Yes	No	No	
MNHN.F.A68491	Yes	Yes	Yes	Yes	Yes	No	No	
MNHN.F.R06746	Yes	Yes	Yes	Yes	Yes	No	Yes	Ridge
NPL52121a&b /(Vinther_58)	Yes	Yes	Yes	Yes	Yes	Yes	Yes	Line
BHI2200	Yes	Yes	Yes	Yes	Yes	Yes	Yes	Line
BHI2201	Yes	Yes	Yes	Yes	Yes	Yes	No	
BHI2202	Yes	Yes	Yes	Yes	Yes	No	Yes	Ridge
BHI 2203	Yes	Yes	Yes	Yes	Yes	Yes	Yes	Line
BHI 2204 (2205) (fish in mouth)	Yes	Yes	Yes	Yes	Yes	Yes	Yes	Line
BHI 2206	Yes	Yes	Yes	Yes	Yes	No	No	
BHI 2207	Yes	Yes	Yes	Yes	Yes	Yes	Yes	Ridge
BHI 2208	Yes	Yes	Yes	Yes	Not visible	No	No	
BHI 2209	Yes	Yes	Yes	Yes	Yes	No	No	
BHI 2210	Yes	Yes	Yes	Yes	Yes	Yes	Yes	Ridge
BHI 2212	Yes	Yes	Yes	Yes	Yes	Yes	Yes	Line
BHI 2213	Yes	Yes	Yes	Yes	Yes	Yes	Yes	Ridge
BHI 2214	Yes	Yes	Yes	Yes	Yes	No	Yes	Ridge
BHI 2215	Yes	Yes	Yes	Yes	Yes	Yes	Yes	Line
BHI 2216	Yes	Yes	Yes	Yes	Yes	Yes	Yes	Line
BHI 2217	Yes	Yes	Yes	Yes	Yes	Yes	No	
BHI 2219	Yes	Yes	Yes	Yes	Yes	Yes	Yes	Line
BHI 2220	Yes	Yes	Yes	Yes	Yes	Yes	No	
BHI 2221	Yes	??	Yes	Yes	Yes	No	Yes	Line
BHI 2222	Yes	Yes	Yes	Yes	Yes	Yes	Yes	Ridge
BHI 2223	Yes	Yes	Yes	Yes	Yes	No	No	
BHI 2225	Yes	Yes	Yes	Yes	Yes	No	No	
BHI 2226	Yes	??	Yes	Yes	Yes	Yes	Yes	Line
BHI 2227	Yes	Yes	Yes	Yes	Yes	Yes	No	
BHI 2228	Yes	Yes	Yes	Yes	Yes	Yes	Yes	Line
BHI 2229	Yes	Yes	Yes	Yes	Yes	No	No	
BHI 2232	Yes	Yes	Yes	Yes	Yes	No	No	
BHI 2233	Yes	Yes	Yes	Yes	Yes	No	No	
BHI 5779	Yes	Yes	Yes	Yes	Yes	Yes	No	
Coll Nohra_New Image (DF)	Yes	Yes	Yes	Yes	Yes	No	No	
RuSmith (DF)	Yes	Yes	Yes	Yes	Yes	No	No	
MSNMi_25128	Yes	Yes	Yes	Yes	Yes	Yes	No	
MSNMi 24800	Yes	Yes	Yes	Yes	Yes	No	No	
MSNMi_25134	Yes	Yes	Yes	Yes	Yes	No	No	
MSNMi 25144	Yes	Yes	Yes	Yes	Yes	No	No	
NHMW1998z01050000	Yes	??	Yes	Yes	Yes	No	Yes	Ridge
V_33 (DF)	Yes	Yes	Yes	Yes	Yes	No	No	
V_54 (DF)	Yes	??	Yes	Yes	Yes	Yes	No	
V_61 (DF)	Yes	Yes	Yes	Yes	Yes	Yes	Yes	Line
MNHNL_CRE047	Yes	Yes	Yes	Yes	Yes	No	No	

Specimen number	If Yes, is this Unipartite or Bipartite. If No the cell is empty	Lateral Fields Present: Posterior/Anterior/Both/No	Is there a conus present: Yes/No	Is the cephalic cartilage visible? (Yes/No)	Cephalic cartilage orientation: Lateral/Dorsal/Ventral. If not present the cell is empty	Orientation	Ink sac	Paired structures Present	Gills preserved?	Stomach contents	Eye/s preserved	Beak/Cavity preserved	Suckers	Axial nerve	Fin Shape: (Name)
BMNH_C5017_HOLOTYPE_	Bipartite			Yes		Ventral	Yes	Yes	Yes?	Yes	Yes?	Yes			
BNHM_No label	Unipartite			Yes	Ventral	Ventral	Yes								
MNHN.F.A88588	Unipartite	Anterior		Yes	Dorsal	Dorsal	Yes					Yes			Oar-shaped
MNHN.F.A88589				Yes	Ventral		Yes	Yes	Yes	Yes	Yes	Yes			Oar-shaped
MNHN.F.A88560	Unipartite			Yes	Ventral	Dorsal	Yes		Yes	Yes		Yes			
MNHN.F.A50394	Bipartite	Posterior				Ventral	Yes	Yes				Yes			
MNHN.F.A50396	Unipartite					Ventral	Yes	Yes			Yes	Yes			
MNHN.F.A50398	Unipartite					Ventral	Yes					Yes			
MNHN.F.A50400 (counter A69219)						Dorsal/Ventral	Yes	Yes							
MNHN.F.A50402 (counter A68475)						Dorsal/Ventral	Yes			Yes	Yes	Yes			
MNHN.F.A50405? (A69297)						Ventral	Yes								
MNHN.F.A68491						Ventral	Yes			Yes		Yes			
MNHN.F.R06746	Bipartite			Yes	Dorsal	Dorsal/Ventral	Yes		Yes	Yes	Yes	Yes			
NPL52121a&b //(Vinther_58)	Unipartite			Yes	Dorsal	Dorsal/Ventral	Yes	Yes				Yes			"Oar-shaped"
BHI2200	Unipartite			Yes	Ventral	Dorsal	Yes		Yes			Yes			
BHI2201		Anterior		Yes	Ventral	Ventral	Yes					Yes			
BHI2202	Unipartite					Ventral	Yes			Yes					
BHI 2203	unipartite	Anterior				Dorsal and Ventral	Yes		Yes		Yes	Yes	Yes		
BHI 2204 (2205) (fish in mouth)	Unipartite			Yes	Ventral	Ventral	Yes			Yes	Yes	Yes			"Oar-shaped"
BHI 2206						Ventro-lateral	Yes								
BHI 2207	Unipartite	Anterior		Yes	Ventral	Ventral	Yes								
BHI 2208						Ventro-lateral	Yes								
BHI 2209				Yes	Ventro & dorso-lateral	Dorsal/Ventral	Yes				Yes	Yes			
BHI 2210	Unipartite					Dorsal	Yes								
BHI 2212	Unipartite			Yes	Dorsal?	Ventral	Yes					Yes	Yes		"Oar-shaped"
BHI 2213	Unipartite					Dorsal	Yes			Yes	Yes	Yes			
BHI 2214	Bipartite			Yes	Ventrol & dorso-lateral	Ventro & dorso-lateral	Yes				Yes	Yes	Yes		
BHI 2215	Unipartite			Yes	Ventro-lateral	Ventral	Yes				Yes	Yes	Yes		
BHI 2216	Unipartite	Anterior		Yes	Ventral	Ventral	Yes				Yes	Yes			
BHI 2217		Anterior				Ventral	Yes								
BHI 2219	Unipartite			Yes	Ventral	Ventral	Yes		Yes	Yes	Yes	Yes			
BHI 2220						Dorsal				Yes	Yes	Yes			
BHI 2221	Unipartite					Dorsal	Yes				Yes	Yes			
BHI 2222	Bipartite	Anterior		Yes	Ventral	Ventral	Yes	Yes			yes	Yes			
BHI 2223						Ventro-lateral	Yes					Yes			
BHI 2225		Posterior		Yes	Ventral	Ventral				Yes	Yes	Yes			
BHI 2226	Unipartite	Posterior				Dorsal	Yes								
BHI 2227				Yes	Ventral	Ventral	Yes					Yes	Yes		"Oar-shaped"
BHI 2228	Unipartite			Yes	ventral	Ventral				Yes	Yes	Yes			
BHI 2229				Yes	Ventral	Ventral	Yes			Yes	Yes	Yes	Yes		
BHI 2232						Dorsal (check not ventral?BHI)	Yes			Yes	Yes	Yes		Yes	
BHI 2233		Posterior				Ventral	Yes		Yes						
BHI 5779				Yes	Dorsal	Dorsal	Yes			Yes	Yes	Yes		Yes	
Coll Nohra_New Image (DF)						?	Yes		Yes						
RuSmith (DF)							Yes								
MSNM_25128							Yes					Yes			
MSNM_24800			Yes						Yes						
MSNM_25134						Lateral	Yes			Yes					
MSNM_25144						Lateral	Yes					Yes			
NHMW1998z0105000	Unipartite	Posterior				Ventral	Yes		Yes	Yes					
V_33 (DF)						Ventral	Yes	Yes		Yes		Yes			
V_54 (DF)			Yes	Yes	Dorsal and ventral	Dorsal/Ventral	Yes				Yes	Yes			
V_61 (DF)				Yes	Lateral	Dorsal	Yes		Yes		Yes	Yes			
MNHNL_CRE047				Yes	Ventral	Ventral	Yes		Yes			Yes			

Supplementary Table 4: Characters observed in the specimens in the study.

	Muscular Mantle	Head mantle fusion	Arms	Tentacles	Tentacular pockets	Circular Suckers	Onychites	Cirri-like appendages	Sucker rings	Arm web	Funnel	Fins	Cephalic Cartilage	Fin cartilage	Nucahl-and funel-locking cartilage	Buccal Mass
Donovan & Fuchs 2016	I		I									I	I			I
This study	I		I	X	X	I	X	X	X	X	I	I	I		?	I
Hadjoula	I		I			I					I	I	I			I
Hakel	I											I	I			I
Sahel Alma	I		I								I	I	I			I
Percentage	~70%		~48%			~11%						~13%	~46%			56%
Normal light	I		I			I						I	I			I
Visible as:	Stain/white coating		Not visible/stain/imprint/faint white coating			Not visible/faint white coating					Stain	Imprint/faint staining				Brown Mass/imprint
UV light	I		I			I						I	I			I
Visible as:	White coating		faint white coating										Faint staining			White coating
MMI																
Visible as:												Faint staining				White coating
µXRF	I		I									I				I
Visible as:	Yttrium		Faint Yttrium			-						Faint Yttrium				Faint Yttrium
n=	**38**		**26**			**6**						**7**	**25**			**30**

	Beak	Esophagus	Stomach	Crop	Respiratory system	Circulatory system	Excretory system	Reproductive system	Digestive system	Axial nerves	Eyes	Lens in eye	Brain/Optic lobes	Statoliths	Paired structures Present	Ink sac	Funnel
Donovan & Fuchs 2016	1	1	1	1	1			?									
This study	1	1	1	1	1 (Gills ~22%, branchial heart ~2%)	1 (blood vessels in eyes)	1 (Coprolite)	1 (Oviducts?)	1 (Digestive gland? ~2%, lower intestine ~2%)								
Hadjoula	1	1	1	1	1	1		1	1	1	1	1	1	1	1	1	1
Hakel	1				1	1									1	1	
Sahel Alma	1	1	1		1		i		1		1	1	1		1	1	
Percentage	~67%	~20%	~31%	~4%	~24%	~22%	~2%	~2%	~4%	~4%	~41%	~7%	~6%	~7%	~15%	~94%	~2%
Normal light	1	1	1	1	1	1			1	1	1	1	1	1	1	1	1
Visible as:	Contour/outline	Staining	Mass, or bones/fins etc.	bones/fins etc.	Imprints/stained lamellae (orange/black)	Orange filaments	Stained corresponding shape	Imprints	White coating (digestive gland), Black/brown corresponding shape.	Stain	ovoid imprints/stained orange	ovoid imprints/stained orange	Orange staining	Orange staining	Imprint/faint staining	Black/brown corresponding shape.	indicated by Black/brown corresponding shape of intestine
UV light	1	1			1	1			1	1			1	1	1		
Visible as:	Black triangular shape	White coating	Does not fluorescse	Does not fluoresce	Black filaments/lamellae with faint white coating	Black filaments	Does not fluorescse	Does not fluoresce	White coating (digestive gland), Black/brown corresponding shape.	Stain	Not visible	White coating	White coating	Black staining	Staining/white coating	Black/brown corresponding shape.	
MMI																	
Visible as:	Black triangular shape	White coating	Does not fluorescse	Does not fluoresce	lamellae with faint white coating	Not observed in MMI specimen					Faint black corresponding shape		White coating				
µXRF	1	1					1		1		1	1	1		1		
Visible as:	Yttrium, Titanium	Yttrium	No unique elemental trace	No unique elemental trace	No unique elemental trace	Not observed in µXRF specimen	Titanium		Yttrium	Not observed in µXRF specimen	Yttrium. Traces of iron, Titanium	Yttrium	Yttrium	No unique elemental trace	Yttrium	Black/brown corresponding shape.	
n=	**36**	**11**	**17**	**2**	**13**	**12**	**1**	**1**	**2**	**2**	**22**	**4**	**3**	**4**	**8**	**51**	**1**

Supplementary Table 5: Soft tissues preserved in the specimens, and how they appear in the different imaging techniques.

	Dorateuthis	*D. syriaca* (F&L'11)	This sample	*Boreopeltis*	*Plesioteuthis*	*Paraplesioteuthis*	*Senefelderiteuthis*	*Romaniteuthis*
Body size (Character)	Medium		Small - large	Medium	Medium	Medium	Medium	Medium
Body size (mm)	201 - 400 mm			201 - 400 mm	201 - 400 mm	202 - 400 mm	201 - 400 mm	202 - 400 mm
Gladius size (Character) (directly based on gladius length (mm)			Very small - Medium					
Gladius length (mm)			40 - 214					
Mantle outline		"Bullet- or torpedo-shaped mantle outline"	Torpedo, arrow, and rugby ball-shaped outline					torpedo-shaped
Gladius width (Character)	Slender	Slender	Very slender - slender	Slender - moderate	Very slender - slender	Slender - moderate	Very slender - slender	Very slender - slender
Gladius width (indices)	0.10-0.19		0.05 - 0.17	0.15-0.25	0.05–0.15	0.15 - 0.25	0.05-0.15	0.05-0.15
Median Field (Character)	Very slender		Same as gladius width indices	Slender	Slender	Slender - moderate	Very slender - slender	Very slender
Median Field (indices)			0.05 - 0.17	0.20-0.30	0.25-0.34	0.25-0.35	0.15-0.25	0.10-0.19
Median Field opening (apical) angle (°)	<12°	6 - 10°	2.6 - 9.6°	12 - 17°	12°–19°	14-20°	9-14°	<12°
Median Field area (Character)	Very Large			Large	Very Large	Large - Very large	Large - Very large	Large - Very large
Median Field area (indices) *Not specifically measured here as the lateral fields are so small.	>0.95			0.70-0.80	>0.90	0.75–0.85	0.75-0.85	0.75-0.85
Median reinforcements	No keel	Bipartite ridge ("delicate")	Line or Ridge (unipartite or bipartite), and/or Central median field	Broad median line, no keel	pronounced uni- or bipartite keel (posterior only)	bipartite median ridge	pronounced median keel absent except in conus region, broad reinforcement anteriorly.	Median keel
Anterior margin of Gladius	Lateral keels and central median field anteriorly projected	Possibly concave with short anterior projection of the median reinforcement	Convex	convex	weakly convex	Anterior projection of the median and lateral reinforcement		Poorly known
Lateral reinforcements (keels)	Pronounced. Continuous from anterior to posterior.	Pronounced. Continuous from anterior to posterior.	Pronounced. Continuous from anterior to posterior.	Anteriorly narrow, posteriorly wide	Anterior	present	*Pronounced. Continuous from* anterior to posterior.	
Lateral fields (Character)	Poorly known. "If present then both very short and very slender"	-		Slender	Slender	Slender	Moderate	Slender - moderate
Lateral fields (indices)	Poorly known. "If present then both very short and very slender"	-		0.55-0.80	0.65-0.75	0.85-0.95	1.00-1.10	0.95-1.05
Conus	Poorly known. "If present then both very short and very slender"	Poorly known		Pointed conus				
Hyperbolar zone (Character)		Unknown		Long	Very short - short	Moderate - long	Moderate	Short
Hyperbolar zone (indicies)		Unknown		0.5-0.7	0.05-0.15	0.45-0.55	0.35-0.45	0.20-0.29
Arm length (Character)	Moderate (0.40 - 0.80)			Unknown	Short	Poorly known	Moderate - long	Short
Arm length (indices)	~0.5			Unknown	~0.2	Poorly known	0.7-1.0	~0.25
Arm morphology	Dorsal arm pair elongated	8 arms. The longest and thickest are in dorsal position, The shortest and most delicate arms are ventral, and the ventrolateral and dorsolateral arm pairs are equal in length and thickness		Unknown	Dorsal arm pair elongated	Poorly known		
Fins	"oar-shaped"			Unknown		Poorly known		
Age	Lower - Upper Cretaceous			Upper Jurassic - Upper Cretaceous	Jurassic	Lower Jurassic	Upper Jurassic	Mid-Jurassic
Localities	Lebanon, Germany, Cape Verde Islands, Netherlands		Lebanon	Germany, France	Germany, France	Germany, France, Canada	Germany	France, (Germany, UK?)

Supplementary Table 6: Genera-level comparisons between *Dorateuthis* and other prototeuthids. *D. syriaca* is also included in the table. Genus-level data is taken from Fuchs (2020).

Character # Whalen & Landman 2022	1	2	3	4	5	6	7	8*	9	10	11	12	13	14	15	16	17	18	19	20	21	22	23	24	25	26	27	28	29	30	31	32	33	34	35
New Character in Whalen & Landman 2022						X								X	X							X													
Character # Sutton et al. 2016	0	1	2	3	5		7	4	8	9	11	12	13			15	14	16	17	20	19		22	23	23	24	25	26	29	34	35	38	38	38	39	40
	1	1	2	0	1	1	0	-	-	-	1	0	1	0	-	-	0	1	0	0	-	-	1	0	-	4	-	2	0	-	0	0	-	-	0
	1	1	2	?	1		0	?	?	?	1	0	1			-	0	1	0	?	?		?	?	?	5	-	0	-	-	?	2	2	-	0
#6, 10, 18, 21, 27, 28, 30, 31, 32, 33, 36, 37, 50, 77, not in w&l. In S, 0, 0, -, 0, 0, ?, -, -, -, -0, -, 0, 0,																																			
* = adapted																																			
Amended character states: this study													Two types																						
Character # Rowe et al. 2002	0	1	2	3	5		7	4	8	9	11	12	13			15	14	16	17	20	19		22	23	23	24	25	26	29	34	35	38	38	38	39	40
	1	1	2	?	1		0	?	?	?	1	0	1			?	0	1	0	?	?		?	?	?	5	?	0	?	?	?	2	2	?	0
Character # Kruta et al. 2016	0	1	2	3	5		7	4	8	9	11	12	13			15	14	16	17	20	19		22	23	23	24	25	26	29	34	35	38	38	38	39	40
	1	1	2	?	1		0	?	?	?	1	0	1			?	0	1	0	?	?		?	?	?	5	?	0	?	?	?	2	2	?	0

Shell/gladius/vestigial shell: absent (0); present (1)

Shell location in relation to the rest of the body: external (0); internal (1)

Shell extent along A-P axis: anterior half (0); posterior half (1); whole or most of the body length (2)

Shell extent along D-V axis: dorsal half (0); whole or most of the body height (1)

Discrete proostracum developed: no (0); yes (1)

Anterodorsally extended proostracum: absent (0); present (1)

Septate phragmocone: absent (0); present (1)

Mineralized phragmocone: absent (0); present (1)

Siphuncle linking chambers, or homologous structure: absent (0); present (1)

Position of siphuncle within the shell: ventral (0); central (1)

Median field (or homologous rachis): absent (0); present (1)

Median field (or homologous rachis): absent (0); present (1)

Lateral fields (or homologous wings): absent (0); present (1)

Primordial rostrum: absent (0); present (1)

Mineralized primordial rostrum: absent (0); present (1)

Primordial rostrum length: short, up to 25% of the shell length (0); strongly developed, 25% or more of the shell length (1)

Rostrum or guard: absent (0); present (1)

Conus (primary cone): absent (0); present (1)

Shell coiled: no (0); yes, endogastric (1); yes, exogastric (2)

Condition of the primary cone: funnel-like cone (0); cup-like cone (1)

Primary cone open ventrally: absent (0); present (1)

Patella: absent (0); present (1)

'Cone flags': absent (0); present (1)

Ventral folding of posterolateral gladius margin: flat, not folded (0); folded (1)

Ventral folding of posterolateral gladius margin: folded but not fused (e.g., 'pseudocone') (0); folded and fused ventrally ('secondary cone') (1)

Gladius length / gladius width: < 2 (0); ≥ 2 (1); ≥ 3 (2); ≥ 4 (3); ≥ 5 (4); ≥ 10 (5) [ordered character]

Vane length / rachis length: < 0.3 (0); ≥ 0.3 (1); ≥ 0.5 (2); ≥ 0.7 (3); ≥ 0.9 (4) [ordered character]

Wing length / rachis length: < 0.3 (0); ≥ 0.3(1); ≥ 0.5 (2); ≥ 0.7 (3); ≥ 0.9 (4) [ordered character]

Cone flags length / gladius length: < 0.3 (0); ≥ 0.3 (1)

Vane width / rachis width at vane: < 0.25 (0); < 0.75 (1); < 1.25 (2); < 2.5 (3); < 4 (4); ≥ 4 (5) [ordered character]

Wing width / rachis width at wing: < 0.25 (0); < 0.75 (1); < 1.25 (2); ≥ 2.5 (3) [ordered character]

Position of greatest width of median field / rachis: at extreme anterior (0); posterior to extreme anterior (1)

Position of greatest width of median field / rachis: anterior to hyperbolar zone / vane insertion but not at extreme anterior (0); at hyperbolar zone / vane insertion (1)

Rachis width at vane insertion / rachis width 2/3 of the way between vane insertion and the anterior: ≤ 1 (0); ≤ 1.5 (1); ≤ 2.5 (2); > 2.5 (3) [ordered character]

Concave inflexion or inflexions in median field / rachis: absent (0); present (1)

?	41	?	41		?	41	0		36	Outline of posterior margin of lateral field / wings: convex (0); straight (1); concave (2)
2	42	2	42		2	42	2		37	Shape of posterior end of median field / rachis: concave (0), flat (1), convex (2)
1	43	1	43		1	43	1		38	Nature of convex end: rounded (0); pointed (1)
0	44	0	44	2	0	44	0		39	Shape of anterior tip of median field: concave (0), flat (1), convex (2)
?	45	?	45	0	-	45	-		40	Nature of convex tip: rounded (0); pointed (1)
?	46	?	46		-	46	-		41	Inflexion in gladius outline where lateral asymptote intersects margin: absent (0); present (1)
?	46	?	46		-	46	-		42	Inflexion in gladius outline where lateral asymptote intersects margin: weak (0); strong/sharp (1)
?	47	?	47		-	47	-		43	Tapering of the hyperbolar zone / vane both anteriorly and posteriorly (forming a spindle shape): absent (0); present (1)
0	48	0	48		0	48	1		44	Angle between inner/median asymptote and midline: ≤ 5 degrees (0); > 5 and ≤ 10 degrees (1); > 10 and ≤ 15 degrees (2); > 15 and ≤ 20 degrees (3); > 20 degrees (4) [ordered character]
0	49	0	49		0	49	-		45	Angle between outer/lateral asymptote and midline: ≤ 5 degrees (0); > 5 and ≤ 10 degrees (1); > 10 and ≤ 15 degrees (2); > 15 and ≤ 20 degrees (3); > 20 degrees (4) [ordered character]
1	51	1	51		1	51	1		46	Ventral median field / rachis in transverse section: smooth (0); interrupted by a median or sub-median structure or structures ('interruption(s)') (1)
0	52	0	52		0	52	0		47	Form of ventral interruption(s): concave (0); convex (1)
0	52	0	52		0	52	-		48	Form of ventral interruption(s): line (0); rib/keel (1)
0	52	0	52		0	52	-		49	Form of ventral interruption(s): rib (0); keel (1)
2	53	2	53		2	53	1		50	Anterior ventral interruption(s): absent (0); present (1)
2	53	2	53		2	53	1		51	Posterior ventral interruption(s): absent (0); present (1)
?	54	?	54	1?	?	54	?		52	Ventral interruption bipartite (at any point anterior-posterior)?: no (0); yes (1)
1	55	1	55		1	55	1		53	Dorsal median field / rachis in transverse section: smooth (0); interrupted by a median or sub-median structure or structures ('interruption(s)') (1)
3	56	3	56		3	56	1		54	Form of dorsal interruption(s): concave (0); convex (1)
3	56	3	56	Keel not in Dora. Line/ Ridge	3	56	1		55	Form of dorsal interruption(s): line (0); rib/keel (1)
3	56	3	56		3	56	1		56	Form of dorsal interruption(s): rib (0); keel (1)
1	57	1	57		1	57	1		57	Dorsal interruption(s) at 25% of rachis length from anterior: not present (0); present (1)
1	57	1	57		1	57	0		58	Dorsal interruption(s) at 25% of rachis length from anterior: one structure, not split (0); split in two structures (1)
1	58	1	58		1	58	1		59	Dorsal interruption(s) at 75% length of rachis length from anterior: not present (0); present (1)
1	58	1	58		1	58	0		60	Dorsal interruption(s) at 75% length of rachis length from anterior: one structure, not split (0); split in two structures (1)
1	59	1	59		1	59	1		61	Lateral reinforcements on the median field / rachis: absent (0); present (1)
2	60	2	60		2	60	1		62	Extent of lateral reinforcements: anterior (0); majority/whole of the median field / rachis (1)
1	61	1	61		1	61	1		63	Lateral reinforcement position: not at edge of median field (0); at edge of median field (1)
0	62	0	62		0	62	0		64	Lateral reinforcements subdivided: no (0); yes (1)
0	63	0	63	1	0	63	0		65	Thin lateral plates on the dorsal median field/rachis: absent (0); present (1)
0	64	0	64		0	64	0		66	Granules (tubercles) on the gladius/proostracum: absent (0); present (1)
?	65	?	65		-	65	-		67	Arrangement of granules in the anterior half: regular (0); irregular (1)
?	66	?	66		-	66	-		68	Arrangement of granules in the posterior half: regular (0); irregular (1)
?	67	?	67		-	67	-		69	Granule size-change from posterior to anterior: decreasing (0); no change (1); increasing (2) [ordered character]
?	68	?	68		-	68	-		70	Granule size-change from midline towards lateral margin: decreasing (0); no change (1); increasing (2) [ordered character]
?	69	?	69		-	69	-		71	Row of relatively coarse granules along lateral edges of granulated area: absent (0); present (1)
?	70	?	70		-	70	-		72	Row of relatively coarse granules along median field / rachis: absent (0); present (1)
?	71	?	71		-	71	-		73	Lateral margins of the granulated area meet anteriorly at the anterior edge of the median field / rachis?: no (0); yes (1)
?	72	?	72		-	72	-		74	Lateral margins of posterior 1/3 of granulated area: straight (0); curved (1)
?	73	?	73		-	73	-		75	Width of granulated area at vane / rachis width at vane: < 0.5 (0); ≥ 0.5 (1)
1	74	1	74		1	74	1		76	Fins: absent (0); present (1)
0	75	0	75		0	75	0		77	Number of fin pairs: 1 pair (0); 2 pairs (1)
0	76	0	76	shape name	0	76	0		78	Shape of fins: lobate (0); rhomboidal (1); skirt-like (2)
0	78	0	78		0	78	0		79	Posterior fin termination: subterminal (0); terminal (1)
0	79	0	79		0	79	0		80	Maximum length of unmodified arms compared to mantle length: shorter (0); longer or approximately equivalent (1)
							?	X	152	Stellar ganglia connected by a commissure: absent (0); present (1)
							?	X	153	Development of a commissure between the mantle and visceral nerve: absent (0); present (1)

80	**Maximum length of unmodified arms compared to mantle length: shorter (0); longer or approximately equivalent (1)**	0		79	0		79	0	79	0
81	**Maximum length of unmodified arms compared to mantle length: approximately the same, ±10% (0); longer (1)**	-		79	0		79	0	79	0
82	**Number of appendage pairs: many (0); 4-5 (1)**	1		80	0		80	0	80	0
83	**Reduction of appendage pair II: not reduced (0), reduced to filaments or absent (1)**	1		81	?		81	?	81	?
84	**Loss of appendage pair II: retained (0); lost (1)**	?	X			1				
85	**Modification of appendage IV into a tentacle: absent (0); present (1)**	0		82	0		82	0	82	0
86	**Loss of tentacles in adulthood: no (0); yes (1)**	-	X							
87	**Retractile tentacles: absent (0); present (1)**	-	X							
88	**Tentacle suckers: in up to 4 rows (0); in more than 4 rows (1)**	-		83	-		83	?	83	?
89	**Tentacle locking apparatus: absent (0); present (1)**	-		84	-		84	?	84	?
90	**Tentacle locking apparatus: present on carpus only (0); present on manus and carpus (1)**	-		84	-		84	?	84	?
91	Interbrachial web: absent (0); present (1)	0		85	0		85	0	85	0
92	True arm hooks: absent (0); present (1)	0		86	0		86	0	86	0
93	Cirri or spines on arms: absent (0): present (1)	1		87	1	0	87	1	87	1
94	Suckers on any appendage: absent (0); present (1)	?		88	?	1	88	?	88	?
95	Sucker-hooks: absent (0); present (1)	0	X			0				
96	Sucker symmetry: radial (0); bilateral (1)	?		89	?	0	89	?	89	?
97	Sucker-stalk on arms: absent (sessile, unstalked) (0); present (1)	?		90	?		90	?	90	?
98	Sucker-stalk on arms: attached to arm muscles (0); not clearly attached to arm muscles (1)	?		90	?		90	?	90	?
99	Shape of stalks attached to the arm muscles: conical pillar with base and neck (0); cylinder (1)	?		91	?		91	?	91	?
100	Lining of arm suckers: neither horny nor cuticular ring (0); horny ring (1); cuticular ring (2)	?		92	?		92	?	92	?
101	Suckers (on arms) proximally: absent (0); present (1)	?		93	?	1	93	?	93	?
102	Suckers (on arms) proximally: 1 row (0); > 1 rows (1)	?		93	?	0	93	?	93	?
103	Suckers (on arms) proximally: 2 rows (0); > 2 rows (1)	?		93	?		93	?	93	?
104	Suckers (on arms) medially: absent (0); present (1)	?		94	?	1	94	?	94	?
105	Suckers (on arms) medially: 1 row (0); > 1 rows (1)	?		94	?	0	94	?	94	?
106	Suckers (on arms) medially: 2 rows (0); > 2 rows (1)	?		94	?		94	?	94	?
107	Suckers (on arms) distally: absent(0); present (1)	?		95	?	1	95	?	95	?
108	Suckers (on arms) distally: 1 row (0); > 1 rows (1)	?		95	?	0	95	?	95	?
109	Suckers (on arms) distally: 2 rows (0); > 2 rows (1)	?		95	?		95	?	95	?
110	Ink sac: absent (0); present (1)	1		96	1		96	1	96	1
111	Nuchal cartilage: absent (0); present (1)	?		97	?	?	97	?	97	?
112	Chromatophores: (0) absent; (1) present	?		98	?		98	?	98	?
113	Buccal crown: (0) absent; (1) present	?		99	?		99	?	99	?
114	Buccal membrane connective attachment to arm-pair V: dorsal (0); ventral (1)	?		100	?		100	?	100	?
115	Number of buccal lappets (supports): 6 (0); 7 (1); 8 (2); Many (3)	?		101	?		101	?	101	?
116	Suckers on buccal membrane: absent (0); present (1)	?		102	?		102	?	102	?

Supplementary Table 7: Existing matrix of Whalen & Landman 2022, and comparisons with Sutton *et al.* 2016. The minor modifications included in Kruta *et al.* 2016 and Rowe *et al.* 2022 are also included.

	MEASUREMENT: Gladius (median field) Length (mm)	Arm length (max) - approx (mm)	MEASUREMENT: Gladius (median field) Length (mm)	Arm length (max) - approx (mm)	MEASUREMENT: Gladius (median field) Length (mm)	Arm length (max) - approx (mm)	MEASUREMENT: Gladius (median field) Length (mm)	Arm length (max) - approx (mm)
Locality	Hâdjoula	Hâdjoula	Hâkel	Hâkel	Lebanon	Lebanon	Sahel Aalma	Sahel Aalma
N	36	12	3	0	7	4	8	7
Min	67.6	36	87		47	24	40	21
Max	175.1	79	105		139.6	57	241	215
Mean	114.6	57.9	93.8		111.9	45	106.4	84.7
Std. error	4.9	4.5	5.6		12.8	7.7	22.5	24.9
Stand. dev	29.2	15.7	9.8		33.8	15.4	63.7	66.0
Mode	127	77	NA		139.6	NA	NA	NA

Supplementary Table 8: Measurements statistics of *D. syriaca* associated with the 3 localities.

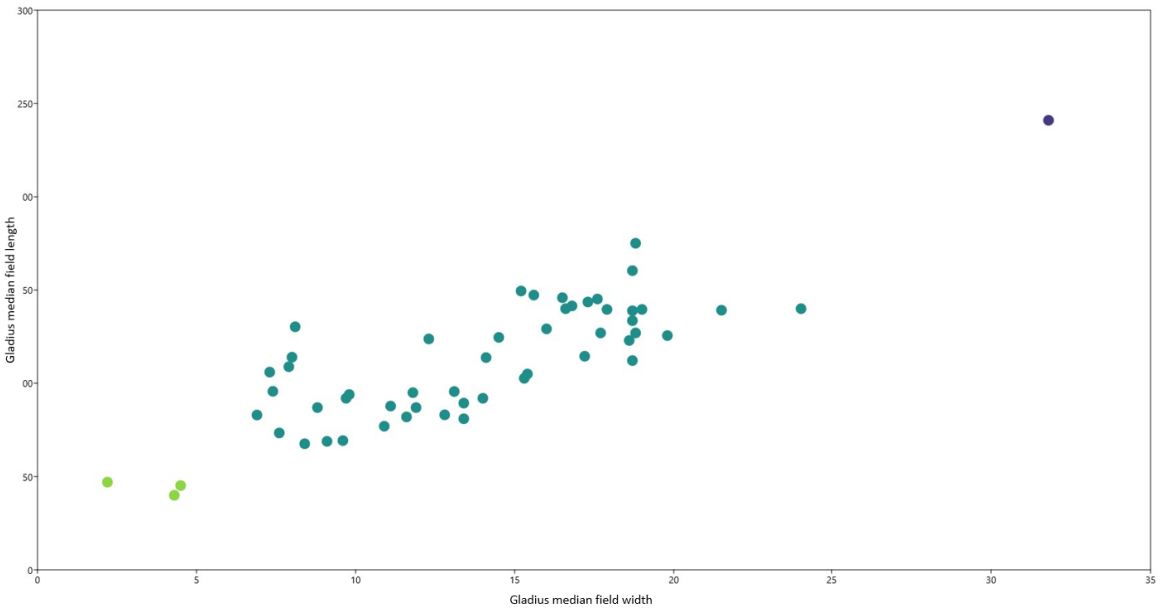

Supplementary Figure 1: Relative size of gladii in the sample. The three different colors represent the mantle size delineations from “small” to “very large” outlined in Fuchs (2020) and followed here. All the specimens of D. syriaca fall within the variation from "very small" to "medium". according to this categorization. Three specimens are “very small size (<50 mm)” are represented by the pale green points. The holotype is included in this group. The majority of specimens (dark green points) are “small (50 – 200 mm)”. Only one specimen (MNHN.F.A50402) is “medium (201–400 mm) (purple point) in size.

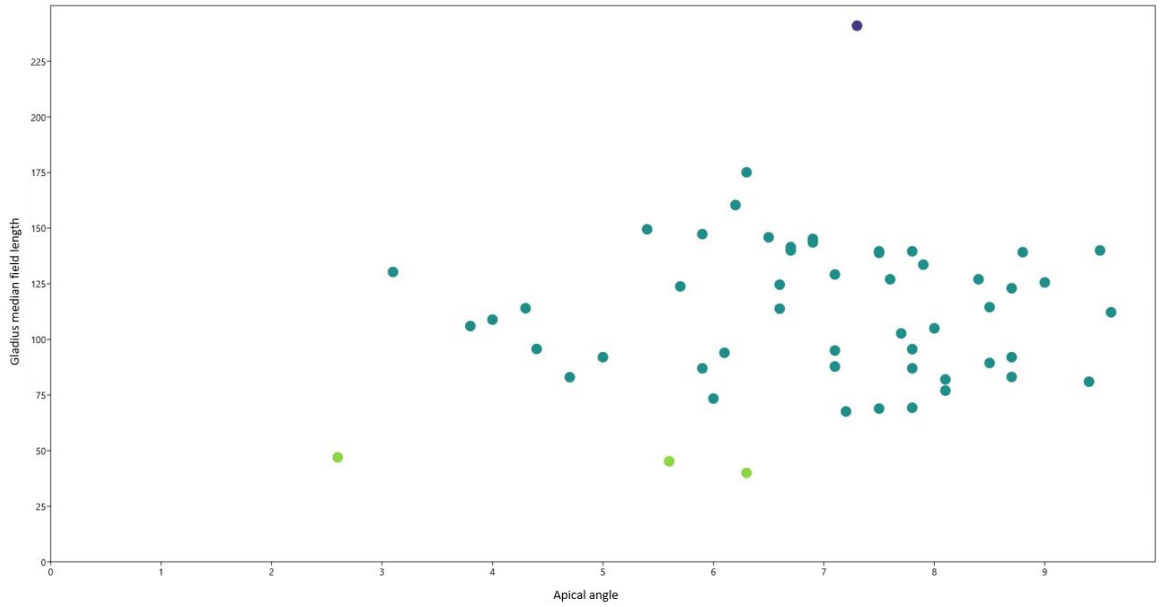

Supplementary Figure 2: The characteristic apical (opening) angle of the gladius is described as <12° for *D. syriaca* (Fuchs 2020), and between 6–10° for *D. syriaca* (Fuchs & Larson 2011). All the specimens in the sample reflect an apical angle smaller than the upper limit (10°) for the species, though some are smaller than the lower limit (6°). The smallest angle here (2.6°) belongs to MNHN.F.A68491 and the largest (9.6°) to BHI 2222. The holotype has an apical angle of 6.3°. The mean angle is 6.9° (Standard error: 0.2).

CONCLUSION AND PERSPECTIVES

Only a very small percentage of living organisms fossilize, and the fossil record is biased toward mineralized elements (e.g., shells, bones, and teeth), as well as taxa from marine environments. Much like today, soft-bodied forms probably dominated ancient marine ecosystems, though without exceptional circumstances enabling preservation, they are rarely encountered in the fossil record. Fortunately, sites of exceptional preservation (Lagerstätten) exist where the normal decay processes are interrupted, and the soft-tissue anatomy is retained. These Lagerstätten deposits provide unparalleled snapshots of fossil communities necessary to explore the evolution of ecological networks.

As discussed in Chapter 1, the fossil record of Mesozoic Octobrachiate coleoids is known almost entirely from these deposits, where rapid processes of mineralization preserved the normally decay-prone soft tissues. These extraordinary fossils have revealed unique insights into the morphological organization of Mesozoic coleoids, and greatly contributed to the current understanding of their evolutionary relationships.

The aim of the PhD was to increase what is known about the morphology of Mesozoic Octobrachiate coleoids by using multiple imaging techniques to reveal what was previously unobtainable with traditional methods. Fundamentally, this involved a good working knowledge of modern coleoid anatomy and comparative morphological analyses with fossil forms. Then, a variety of imaging methods were employed to capture the morphological data preserved in the fossils. The preservation of the specimens determined which methods were used for imaging. For example, digital imaging techniques such as the X-ray absorption methods of MRI and CT scanning, are particularly suited to specimens preserved in 3D, and enable the internal organs to be assessed in a non-destructive way. This is demonstrated in Chapter 3, which includes two articles utilizing these X-ray imaging methods to reveal previously unknown anatomical details of two vampyromorph species. The benefits of synchrotron X-ray fluorescence (XRF) are illustrated in Chapter 4 and show how elemental distributions can be mapped, revealing the properties of 'ghost' tissues. The work presented in Chapters 3 and 4 also benefits from the use of Reflectance Transformation Imaging (RTI), which allows high resolution observations of the surface of the coleoid specimens, enabling the contours of the organism to be seen in relief from the matrix.

By utilizing a combination of these imaging methods on the exceptionally preserved fossil Octobrachia specimens, it was possible to reappraise species with increased resolution. For example, these investigations identified significant morphological traits in *Vampyronassa rhodanica* that were previously unknown, and also identified a new taxon, *Vampyrofugiens*

atramentum, that was previously misinterpreted as *V. rhodanica*. The study on *Dorateuthis syriaca* is the largest of its kind to utilize these imaging methods in combination with morphological measurements. It allowed a reappraisal of both the holotype and species definition, identified more variability than was previously known and ontogenetic changes in the arm crown, and increased new soft tissue characters.

GETTING DEEP INTO THE SOFT TISSUE ANATOMY OF FOSSIL TAXA

The original description of *V. rhodanica* was published ~20 years ago. Current X-ray based imaging techniques provide an unprecedented opportunity for the first reassessment of the species, analyzing both the external and internal anatomy in a non-destructive way. The work completed in Chapter 3 using these techniques revealed details about the arm crown that have phylogenetic and ecological significance. The scans and 3D renderings confirmed the Octobrachiate affiliation of *Vampyronassa rhodanica*, with the presence of eight tapered arms of varying lengths, and the absence of retractable filaments. Significantly, the tomography revealed that the suckers of *V. rhodanica* have a combination of characteristics known from both modern Octobrachia and Decabrachia. These include a radial symmetry and infundibulum like that of modern Octobrachia, a conical sucker attachment of *Vampyroteuthis infernalis,* which is inserted into the base of the sucker (the acetabulum), like that of extant Decabrachia. The species also has distinctive dorsal arms, which are longer than the rest and have just two distal suckers flanked by sensory cirri. *Vampyrofugiens atramentum* also possessed these suckers and attachments, though the arm crown has a different organization.

The study of an unpublished specimen carried out in Chapter 3 revealed a number of morphological characters that had never before been documented in fossil vampyromorphs. These include the first images of the complete internal arm muscle configuration of a Jurassic species. It is clear they resemble those of Octobrachia, though would require comparisons of muscular anatomy with additional specimens to provide important functional information. Further, the X-ray tomography revealed an extinct character combination: a pair of luminous organs with anterior-posterior symmetry, which was previously undocumented in the fossil record. These were paired with an ink sac, which is an anti-predation strategy that was previously unknown in Mesozoic Octobrachiate coleoids.

The work presented here clearly shows the importance of a variety of imaging techniques for paleontological studies, and the increased resolution they can bring to the appraisal of specimens and discovery of new anatomical features and characters. A more complete understanding of fossil coleoid morphology also has wider implications for the improvement of the systematic assessment.

INFERRING THE ECOLOGY OF THE MESOZOIC OCTOBRACHIA

A significant outcome of this work has been the ecological interpretations inferred from the new morphological data. As discussed in Chapter 1, many important evolutionary changes occurred in the marine environment during the Mesozoic. The predatorial pressures of the Mesozoic Marine Revolution, and the emergence of ecosystems similar to those in the Modern, are reflected in the variety of characters observed in the described species of the Jurassic Vampyromorphs from La Voulte-sur-Rhône. Their morphologies were linked with active predation as well as evidence of predation avoidance, suggesting that co-occurring coleoids in this habitat exploited different lifestyle strategies. Though the arms of the *V. rhodanica* and *V. atramentum* both seem adapted to prey capture and manipulation, the absence of a differentiated arm crown in *V. atramentum* suggests less specialized usage. Additionally, this work has revealed that defense mechanisms known from extant coleoids (e.g., ink sacs, and luminous organs) were already present in the coleoids from La Voulte-sur-Rhône. The extent of the anatomical knowledge we now have on these taxa, and the inference on behaviors stemming from morphology, provide a much clearer picture of the ecosystems of La Voulte-sur-Rhône.

The lifestyle and behavior strategies described for each of the Mesozoic Octobrachiate species (Chapters 3 and 4) do not necessarily reflect those found in extant Octobrachia. The emergence and evolution of ecological niches occupied by coleoids remains poorly understood but reinterpretation of Jurassic fossils demonstrates their diversity early in the group history. Indeed, Lindgren *et al.* (2012) discussed various convergent structures in Recent Coleoidea (accessory nidamental glands, corneas, photophores, branchial canal, and a right oviduct) that are correlated with habitat and driven by similar selective pressures. Our results indicate that characters linked with habitat and lifestyle were also already found in the Mesozoic. For example, *V. rhodanica*, and other coleoids (*Proteroctopus, Gramadella*) from La Voulte-sur-Rhône, had elongated dorsal arms with terminal suckers, which indicates a specialized predatory function over species where the arm crown is more homogenous, such as *V.*

atramentum. The lack of ink sac and luminous organs in *V. rhodanica* indicates the species was subject to different predatory pressures than *V. atramentum,* who possessed both these organs. Despite these differences, both species had the same type of suckers and attachments, and their overall body shapes suggest they were adapted for swimming.

The morphology observed in *Dorateuthis syriaca* suggests they were hydrodynamic pelagic swimmers and visual predators, like some modern Decabrachia. This is supported by the slender gladius and overall body morphology, common muscular striations, large eyes, and remnants of fish in the digestive system. The three main species discussed in Chapters 3 and 4 represent two of the main Octobrachia lineages, Prototeuthina and Vampyromorpha, though some of their morphological characters and inferred behaviors are analogous with extant Decabrachia.

PHYLOGENETIC IMPLICATIONS

While coleoid anatomy provides key insights into Mesozoic ecologies, it is also a fundamental element to paleontological systematic analyses. As discussed in Chapters 1, 3, and 4, a few computed phylogenies have combined the morphologies of fossil and extant forms, though given the inherent issues with the available matrices there is no cephalopod phylogeny that is widely accepted. Some of the challenges faced by these phylogenies are the limited fossil record, and the need to better understand homologies between fossil and extant taxa.

Given the relatively low number of determinable soft tissue states in fossil forms, many of the characters are based on the gladius. As discussed in Chapters 1, 3, and 4, this structure contributes approximately half of the characters to the existing morphological matrix (fossil and extant). The work on *Dorateuthis syriaca* revealed undocumented variation in the gladius that is not currently reflected in the existing morphological matrix. Though there are multiple states for size ratios of gladius characters (e.g., #24 – 35 in Sutton *et al.* 215, and #26-31, 34, 44, 45, and 75 in Whalen & Landman (2022), there is no specific state to identify whether the lateral fields are in a posterior, or anterior position. Further, the *D. syriaca* sample included specimens that represented different ontogenetic stages. The species showed that the relative arm lengths varied depending on whether the individual was a juvenile, or an adult. However, the age of the specimen is not currently considered for character coding. Broadly speaking, future phylogenetic assessments would optimally address the intraspecies variation and be able to assess those with a phylogenetic signal.

PERSPECTIVES

The key to unlocking insights into the evolutionary history of coleoids is to be able to provide accurate and unambiguous character interpretations. Our current understanding of known characters is linked with preservational biases – knowing not just what *has* been preserved, but also what has *not* been preserved. Indeed, differences in taphonomic processes have a great impact on what fossilizes, which in turn affects our interpretations. This can be as simple as the preserved orientation, or more complex, like the fossilization pathways.

Large scale studies trying to understand these biases in coleoids from Lagerstätten deposits have yet to be conducted. However, as we have determined and discussed in Chapter 4, *D. syriaca* from the Lebanese localities provide an ideal opportunity by which to do so. The abundance of individuals from this single taxon includes specimens from various stages of ontogeny and encompass an approximate 9-10My timespan. Additionally, the depositional environments in which they were preserved vary somewhat in paleodepth between the oldest and youngest localities.

The recent advances in physio-chemical imagery (e.g., the XRF methods utilized in Chapter 4) provide new pathways by which to understand the tissues that are likely to preserve in this setting, and statistical analyses can inform us with what frequency. Furthermore, we can identify if there is variation in what preserves across the different depositional environments, and if each of these localities are subject to the same taphonomic processes.

ANNEX

ORDER	SUBORDER	FAMILY	GENERA	Time Bin
	PROTOTEUTHINA	PLESIOTEUTHIDAE	*Plesioteuthis*	Upper Jurassic (upper Kimmeridgian–lower Tithonian):
	PROTOTEUTHINA	PLESIOTEUTHIDAE	*Boreopeltis*	Upper Jurassic (lower Tithonian)– Upper Cretaceous (upper Cenomanian)
	PROTOTEUTHINA	PLESIOTEUTHIDAE	*Dorateuthis*	Lower Cretaceous (Barremian)–Upper Cretaceous (Maastrichtian)
	PROTOTEUTHINA	PLESIOTEUTHIDAE	*Eromangateuthis*	Upper Cretaceous (upper Albian)
	PROTOTEUTHINA	PLESIOTEUTHIDAE	*Nesisoteuthis*	Lower Cretaceous (lower Aptian)
	PROTOTEUTHINA	PLESIOTEUTHIDAE	*Normanoteuthis*	Lower Cretaceous (lower Albian)
	PROTOTEUTHINA	PLESIOTEUTHIDAE	*Paraplesioteuthis*	Lower Jurassic (upper Pliensbachian–lower Toarcian)
	PROTOTEUTHINA	PLESIOTEUTHIDAE	*Romaniteuthis*	Middle Jurassic (lower Callovian)
	PROTOTEUTHINA	PLESIOTEUTHIDAE	*Rhomboteuthis*	Middle Jurassic (lower Callovian)
	PROTOTEUTHINA	PLESIOTEUTHIDAE	*Senefelderiteuthis*	Upper Jurassic (upper Kimmeridgian–lower Tithonian)
	PROTOTEUTHINA	INCERTAE SEDIS	*Germanoteuthis*	Middle Triassic (lower Ladinian)
	PROTOTEUTHINA	INCERTAE SEDIS	*Reitneriteuthis*	Upper Triassic (upper Norian)
	LOLIGOSEPIINA	LOLIGOSEPIIDAE	*Loligosepia*	Lower Jurassic (lower Sinemurian– lower Toarcian)
VAMPYROMORPHA	LOLIGOSEPIINA	LOLIGOSEPIIDAE	*Jeletzkyteuthis*	Lower Jurassic (lower Toarcian)
VAMPYROMORPHA	LOLIGOSEPIINA	GEOPELTIDAE	*Geopeltis*	Lower Jurassic (upper Pliensbachian–lower Toarcian)
VAMPYROMORPHA	LOLIGOSEPIINA	GEOPELTIDAE	*Parabelopeltis*	Lower Jurassic (upper Pliensbachian, lower Toarcian)– Upper Jurassic (Tithonian)
VAMPYROMORPHA	LOLIGOSEPIINA	GEOPELTIDAE	*Vampyrofugiens*	Middle Jurassic (lower Callovian)
VAMPYROMORPHA	LOLIGOSEPIINA	LEPTOTHEUTHIDAE	*Leptotheuthis*	Upper Jurassic (upper Kimmeridge–lower Tithonian)
VAMPYROMORPHA	LOLIGOSEPIINA	LEPTOTHEUTHIDAE	*Donovaniteuthis*	Lower Cretaceous (lower Aptian)
VAMPYROMORPHA	LOLIGOSEPIINA	MASTIGOPHORIDAE	*Mastigophora*	Middle Jurassic (lower–upper Callovian)
VAMPYROMORPHA	LOLIGOSEPIINA	MASTIGOPHORIDAE	*Doryanthes*	Upper Jurassic (lower Tithonian)
VAMPYROMORPHA	LOLIGOSEPIINA	INCERTA SEDIS	*Bavaripeltis*	Upper Jurassic (lower Tithonian)
VAMPYROMORPHA	VAMPYROMORPHINA	VAMPYROMORPHINA	*Necroteuthis*	Oligocene
VAMPYROMORPHA	VAMPYROMORPHINA	INCERTAE SEDIS	*Nanaimoteuthis*	Upper Cretaceous (middle Turonian–lower Campanian)
VAMPYROMORPHA	VAMPYROMORPHINA	INCERTAE SEDIS	*Gramadella*	Middle Jurassic (lower Callovian)
VAMPYROMORPHA	VAMPYROMORPHINA	INCERTAE SEDIS	*Proteroctopus*	Middle Jurassic (lower Callovian)
VAMPYROMORPHA	VAMPYROMORPHINA	INCERTAE SEDIS	*Vampyronassa*	Middle Jurassic (lower Callovian)
VAMPYROMORPHA	VAMPYROMORPHINA	NOMEN DUBIUM	*Provampyroteuthis*	Upper Cretaceous, lower Santonian
OCTOPODA	TEUDOPSEINA	TEUDOPSEIDAE	*Teudopsis*	Lower Jurassic (lower–upper Toarcian, ?Callovian)
OCTOPODA	TEUDOPSEINA	TEUDOPSEIDAE	*Teudopsinia*	?Upper Jurassic (lower Tithonian), Upper Cretaceous (upper Cenomanian)
OCTOPODA	TEUDOPSEINA	TRACHYTEUTHIDAE	*Trachyteuthis*	Middle Jurassic (Callovian)–Upper Cretaceous (upper Cenomanian)
OCTOPODA	TEUDOPSEINA	TRACHYTEUTHIDAE	*Actinosepia*	Upper Cretaceous (Campanian– Maastrichtian)
OCTOPODA	TEUDOPSEINA	TRACHYTEUTHIDAE	*Glyphidopsis*	Upper Cretaceous (Cenomanian)
OCTOPODA	TEUDOPSEINA	TRACHYTEUTHIDAE	*Glyphiteuthis*	Upper Cretaceous (lower Cenomanian–Santonian)
OCTOPODA	TEUDOPSEINA	TRACHYTEUTHIDAE	*Paraglyphiteuthis*	Upper Cretaceous (upper Turonian)
OCTOPODA	TEUDOPSEINA	TRACHYTEUTHIDAE	*Styloteuthis*	Upper Cretaceous (upper Turonian)
OCTOPODA	TEUDOPSEINA	PALAEOLOLIGINIDAE	*Palaeololigo*	Upper Jurassic (lower Tithonian)
OCTOPODA	TEUDOPSEINA	PALAEOLOLIGINIDAE	*Marekites*	Upper Cretaceous (upper Cenomanian–upper Turonian)
OCTOPODA	TEUDOPSEINA	PALAEOLOLIGINIDAE	*Rachiteuthis*	Upper Cretaceous (upper Cenomanian)
OCTOPODA	TEUDOPSEINA	MUENSTERELLIDAE	*Muensterella*	Upper Jurassic (upper Kimmeridgian)–Upper Cretaceous middle Turonian)
OCTOPODA	TEUDOPSEINA	MUENSTERELLIDAE	*Celaenoteuthis*	Upper Jurassic (lower Tithonian)
OCTOPODA	TEUDOPSEINA	MUENSTERELLIDAE	*Engeseriteuthis*	Upper Jurassic (upper Kimmeridgian)
OCTOPODA	TEUDOPSEINA	MUENSTERELLIDAE	*Etchesia*	Upper Jurassic (lower Tithonian)
OCTOPODA	TEUDOPSEINA	MUENSTERELLIDAE	*Listroteuthis*	Upper Jurassic (lower Tithonian)
OCTOPODA	TEUDOPSEINA	MUENSTERELLIDAE	*Muensterellina*	Middle Jurassic (upper Callovian)
OCTOPODA	TEUDOPSEINA	MUENSTERELLIDAE	*Tyrionella*	Upper Jurassic (lower Tithonian)
OCTOPODA	TEUDOPSEINA	ENCHOTEUTHIDAE	*Enchoteuthis*	Lower Cretaceous (upper Albian)–Upper Cretaceous (upper Campanian)
OCTOPODA	TEUDOPSEINA	ENCHOTEUTHIDAE	*Niobrarateuthis*	Upper Cretaceous (upper Santonian–lower Campanian):
OCTOPODA	TEUDOPSEINA	INCERTA SEDIS	*Tusoteuthis*	Upper Cretaceous (upper Santonian– lower Campanian)
OCTOPODA	TEUDOPSEINA	PATELLOCTOPODIDAE	*Patelloctopus*	Upper Jurassic (upper Kimmeridgian)
OCTOPODA	TEUDOPSEINA	PATELLOCTOPODIDAE	*Pearceiteuthis*	Middle Jurassic (upper Callovian)
OCTOPODA	TEUDOPSEINA	PUTATIVE MUENSTERELLOIDEA	*Eoteuthoides*	Upper Cretaceous (upper Turonian)
OCTOPODA	CIRRATA	UNDETERMINED	*Paleocirroteuthis*	Upper Cretaceous (Santonian–lower Campanian)
OCTOPODA	INCIRRATA	PALAEOCTOPODIDAE	*Palaeoctopus*	Upper Cretaceous (Santonian)
OCTOPODA	INCIRRATA	PALAEOCTOPODIDAE	*Keuppia*	Upper Cretaceous (upper Cenomanian)
OCTOPODA	INCIRRATA	OCTOPODIDAE	*Styletoctopus*	Upper Cretaceous (Cenomanian)

Annex 1: Existing fossil Octobrachia and their systematic placement, adapted from Fuchs 2020, with the addition of *Vampyrofugiens* described in Rowe *et al.* 2023.

Virtual dissection of *Vampyroteuthis infernalis* provides the first 3-D comparative morphological study between fossil and extant Vampyromorpha

Alison J. Rowe[1], Isabelle Rouget[1], Henk-Jan Hoving[2], Neil H. Landman[3], Loïc Villier[1], Isabelle Kruta[1]

[1]Sorbonne Université-MNHN-CNRS-CR2P. [2]GEOMAR Helmholtz Center for Ocean Research Kiel. [3]American Museum of Natural History

Background:

X-ray imaging (CT scan- PPC SRμCT-scan) is a non-invasive imaging method that allows an in situ, 3-D visualisation of morphological features [1,2]. As the structures are imaged while the shape and dimensions of the sample are retained, the resulting reconstructions are realistic and offer a 'virtual dissection' of the specimen. This method can be applied on a large array of taxa - including both extant and fossil forms [4], with anatomical reconstructions easily accessible via morphological databases. This is specifically useful in determining soft tissue morphology of rare and precious specimens; an issue identified as one of the big challenges in cephalopod research[3].

Materials:

V. infernalis: Recent, Pacific Ocean. 2 Specimens: AMNH (# to be assigned); YPM IZ 18279.GP.

V. infernalis Illustration. Pickford 1948 [6]

V. rhodanica: 3 Specimens: MNHN.B.74247 (Holotype); MNHN.B.74243; MNHN.B.74244 (Jurassic, Callovian: ~166.1 – 163.5 Ma)

MNHN.B.74247 in lateral view. Photo: C. Loubry (CR2P)

Much attention has been focused on the systematic position and ecology of Vampyromorpha and its only living species, *Vampyroteuthis infernalis*. Here, we directly apply this imaging technique in a comparative anatomy study between extant and fossil Vampyromorph taxa: modern *V. infernalis*, and a supposed related species from the Jurassic, *Vampyronassa rhodanica* [5].

V. infernalis: Deep-sea habitat; opportunistic detritivore [7,8]

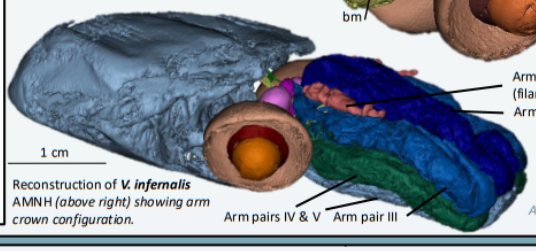

Reconstruction of ***V. infernalis*** AMNH *(above right) showing arm crown configuration.*

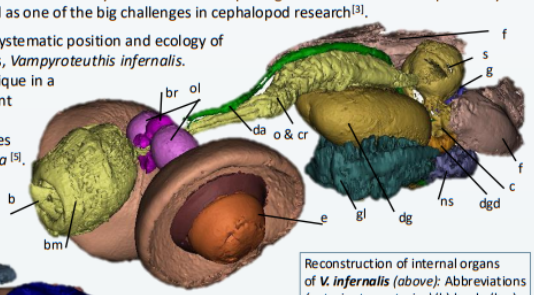

Reconstruction of internal organs of ***V. infernalis*** *(above):* Abbreviations *(anterior to posterior)* (b) beak, (bm) buccal mass, (br) brain, (ol) optic lobe, (e) eye, (da) dorsal aorta, (o & cr) oesophagus and crop, (gl) gill, (dg) digestive gland, (dgd) digestive gland duct, (ns) needhams sac, (s) stomach, (c) caecum, (g) gonad, (f) fin, (i) intestine. The same abbreviations are used below for ***V. rhodanica***.

Data Acquisition:

V. infernalis: μCT. Microscopy and Imaging Facility of the American Museum of Natural History (AMNH, New York, USA). Resulting voxel sizes: 38.40 μm (AMNH) and 18.25 μm (YPM IZ18279.GP). Specimens were stained in a 1% PTA solution prior to scanning [9]. ***V. rhodanica:*** Propagation phase-contrast X-ray synchrotron microtomography (PPC-SRμCT). European Synchrotron Radiation Facility Grenoble, France (ID19 beamline). Voxel size: 12.64 μm Final CT data were reduced in size (ImageJ software), and segmented using Mimics software. (Materialise NV, Belgium, Version 21.0). Contrasting tissue densities helped identify anatomical features for segmentation.

V. rhodanica:

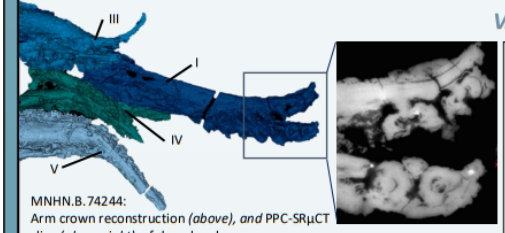

MNHN.B.74244: Arm crown reconstruction *(above), and* PPC-SRμCT slice *(above right)* of dorsal suckers

Reconstruction of sucker profile *(top)* PPC-SRμCT slice of sucker and attachment *(bottom)* MNHN.B.74244

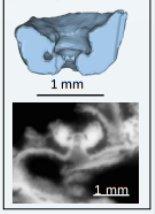

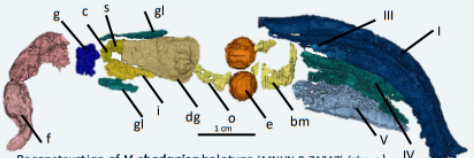

Reconstruction of ***V. rhodanica*** holotype (MNHN.B.74247) *(above)* showing arm crown (arm pair I, III, IV, and V) and other internal elements. *(See above for abbreviations)*

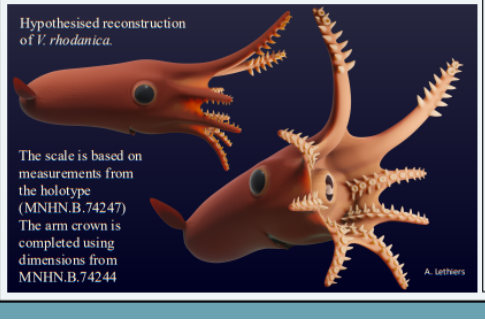

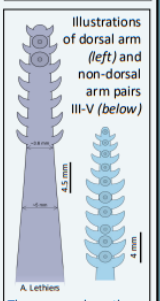

Illustrations of dorsal arm *(left)* and non-dorsal arm pairs III-V *(below)*

These arms show the uniserial suckers, lateral cirri, and variation in armature configuration between the dorsal and non-dorsal arms.

Key Findings:

→ Characters observed in *V. infernalis*, including the sucker attachments are present in Jurassic Vampyromorpha *(right)*.

→ New characters were coded and included in a phylogenetic matrix [4]. The resulting tree supported a sister group relationship between *V. infernalis* and *V. rhodanica*.

→ The mosaic of characters observed in *V. rhodanica* (including *sucker attachments, specialized arm crown, proportionally larger infundibulum, increased number and size of suckers and cirri, muscular streamlined mantle*) are consistent with the taxon having a pelagic predatory lifestyle which is in contrast to the modern form.

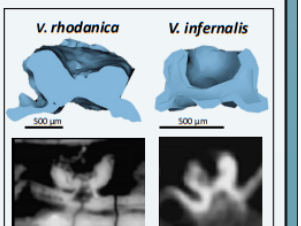

Reconstruction *(top), and* PPC-SRμCT slice *(bottom)* of suckers and the attachments of the two taxa

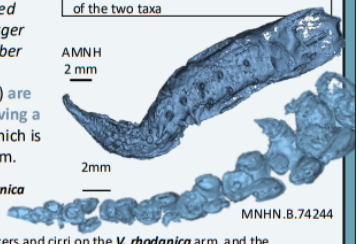

V. infernalis *(top right)* and ***V. rhodanica*** *(bottom right):* Reconstruction (of arm pair V, and 4 respectively) shows the increased number of suckers and cirri on the ***V. rhodanica*** arm, and the proportionately larger cirri and infundibulum of the suckers.

References: **1. Ziegler, A. & Sagorny, C.** Holistic description of new deep sea megafauna (Cephalopoda: Cirrata) using a minimally invasive approach. *BMC biology* **19**, 1–14 (2021). **2. Ziegler, A. *et al.*** Digital three-dimensional imaging techniques provide new analytical pathways for malacological research. *Am. Mal. Bull.* **36**, 248–273 (2018). **3. Xavier, J. C. *et al.*** Future challenges in cephalopod research. *Journal of the Marine Biological Association of the United Kingdom* **95**, 999–1015 (2015). **4. Kruta, I. *et al.*** *Proteroctopus ribeti* in coleoid evolution. *Palaeontology* **59**, 767–773 (2016). **5. Fischer, J.-C. & Riou, B.** *Vampyronassa rhodanica nov. gen. nov sp.*, vampyromorphe (Cephalopoda, Coleoidea) du Callovien inférieur de La Voulte-sur-Rhône (Ardèche, France). *Ann. De Paléontol.* **88**, 1–17 (2002). **6. Pickford, G. E.** *Vampyroteuthis infernalis* Chun -An archaic dibranchiate cephalopod. II. External anatomy. *Dana Rep.* **32**,1–132 (1949). **7. Hoving, H. J. T. & Robison, B. H.** Vampire squid: detritivores in the oxygen minimum zone. *Proc. R. Soc. B* **279**, 4559–4567 (2012). **8. Golikov, A. V. *et al.*** The first global deep-sea stable isotope assessment reveals the unique trophic ecology of Vampire Squid Vampyroteuthis infernalis (Cephalopoda). *Sci. Rep.* **9**, (2019). **9. Metscher, B. D.** MicroCT for comparative morphology: simple staining methods allow high-contrast 3D imaging of diverse non-mineralized animal tissues. *BMC physiology* **9**, 1–14 (2009).

Annex 2: Poster Presentation *Virtual dissection of Vampyroteuthis infernalis provides the first 3-D comparative morphological study between fossil and extant Vampyromorpha* (Cephalopod International Advisory Council, Sesimbra, Portugal, 2022)

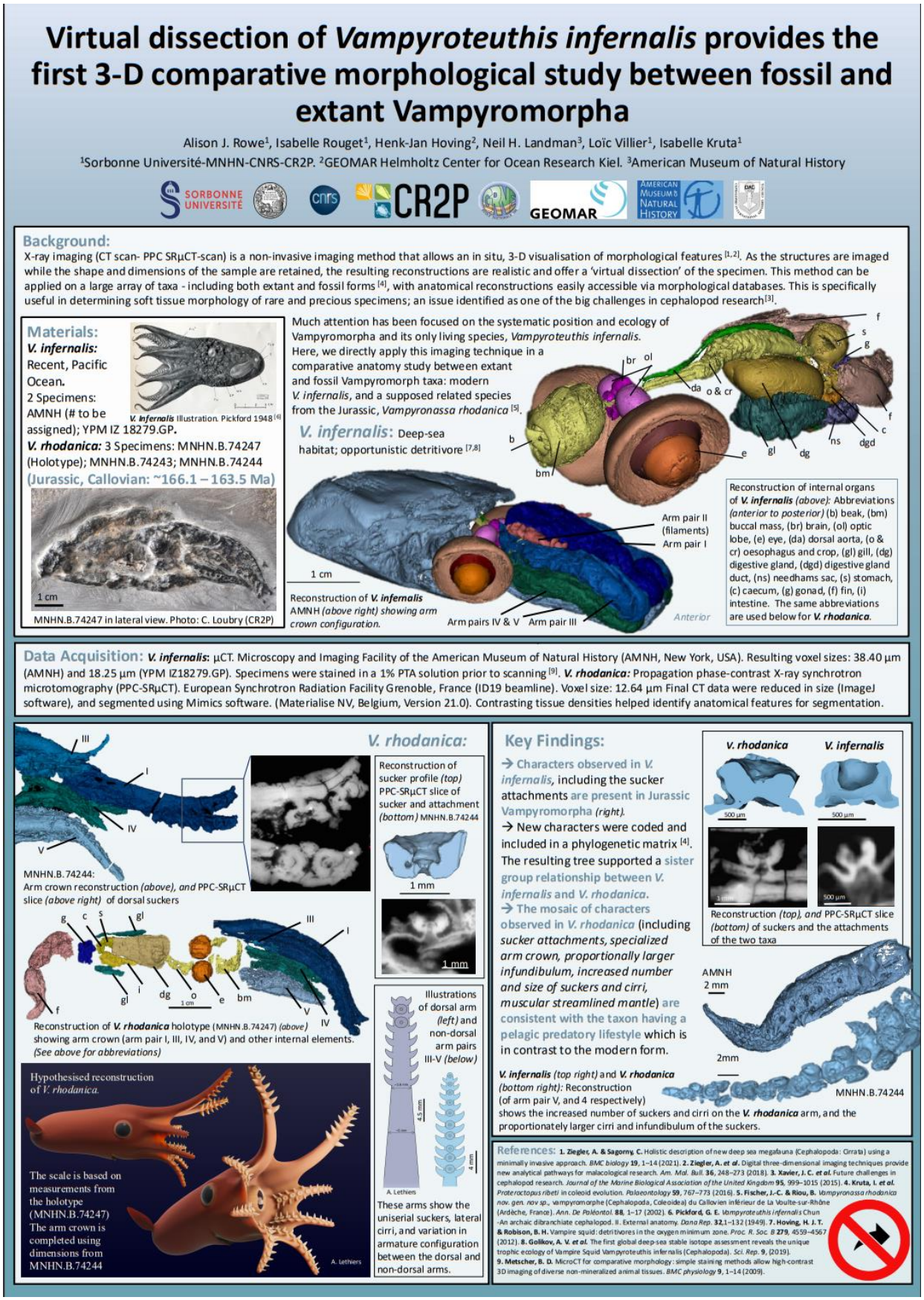

Annex 2: Poster Presentation *Virtual dissection of Vampyroteuthis infernalis provides the first 3-D comparative morphological study between fossil and extant Vampyromorpha* (Cephalopod International Advisory Council, Sesimbra, Portugal, 2022)

Multi-approach imaging techniques shed new light on Lebanese gladius-bearing coleoids

Alison Rowe[1], Isabelle Kruta[1], Pierre Gueriau[2], Aimie Doriath-Döhler[3], Robin Piguet-Ruinet[3], Isabelle Rouget[1]
[1]Sorbonne Université-Muséum national d'Histoire naturelle-CNRS-Centre de Recherche en Paléontologie, Paris, France.
[2] Muséum national d'Histoire naturelle, UAR3461 IPANEMA, Gif-sur-Yvette, France. [3]Sorbonne Université, Paris, France.

INTRODUCTION:

UV imaging is commonly used to study 2D fossils preserved in the Lebanese Lagerstätte sites of Hâkel, Hâdjoula, and Sahel Aalma. This method produces excellent results when identifying certain features, such as the remains of phosphatised soft tissues, and many descriptions of prototeuthid coleoids from these localities, including the genus *Dorateuthis* Woodward, 1883, have benefited from this imaging method[1, 2]. While *Dorateuthis* has defined parameters for body size, fin shape, arm crown proportions, and the morphological detail of the gladius[3], there remains variation expressed in fossil samples of the genus. Here, we analyse two previously undescribed specimens from the Hâdjoula Lagerstätte. We used both classical observations along with a suite of non-destructive imaging methods including UV and RTI photography, and X-ray fluorescence elemental mapping. The results obtained allowed us to visualize remains of tissues that are no longer visible to the naked eye. One of the studied specimens seems clearly to fit within the diagnosis of *Dorateuthis syriaca* Woodward, 1883. However, the other is more ambiguous and raises questions regarding the current systematic diagnosis of the genus.

GEOLOGIC SETTING:

Konservat–Lagerstätten in Lebanon are known for their well-preserved fossil coleoid specimens. To date, the four outcrops (Hâkel, Hâdjoula, En Nammoura, and Sahel Aalma) have revealed 10 genera, including two Prototeuthids, *Boreopeltis* and *Dorateuthis*.[1-2, 4-5]

Hâdjoula, Lebanon

- Lithographic limestones:
- Fossils are compressed within 2D slabs of matrix
- When preserved, soft tissues are typically phosphatised

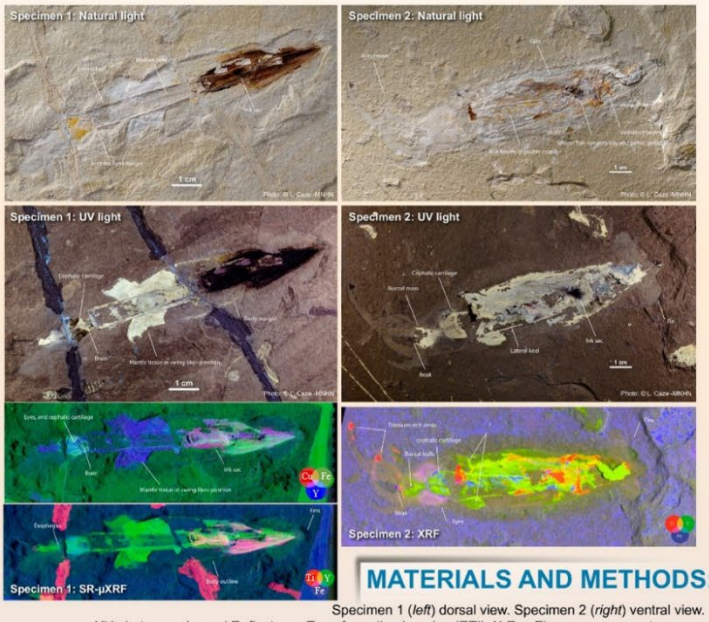

PROTOTEUTHID GLADIUS:
MORPHOLOGY & TERMINOLOGY

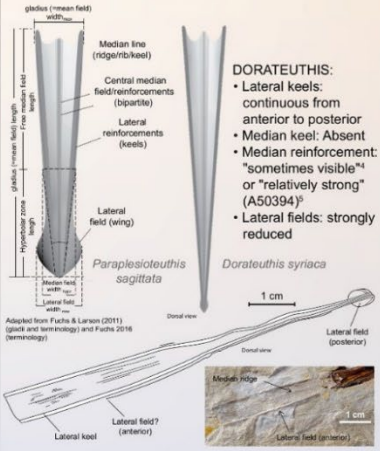

DORATEUTHIS:
- Lateral keels: continuous from anterior to posterior
- Median keel: Absent
- Median reinforcement: "sometimes visible"[4] or "relatively strong" (A50394)[5]
- Lateral fields: strongly reduced

Gladius illustration (*above left*) of specimen 1 (*above right*) showing the continuous lateral keels, the most anterior part of lateral field – this position is common to Plesioteuthis – as well as the posteriorly located median ridge.

MATERIALS AND METHODS:

Specimen 1 (*left*) dorsal view. Specimen 2 (*right*) ventral view.
UV photopgraphy and Reflectance Transformation Imaging (RTI), X-Ray Fluorescence spectroscopy:
Specimen 1 (Synchoroton Soleil, PUMA Beamline, µXRF major-to-trace ememental mapping).
Specimen 2: M6 Jetstream Bruker XRF (UAR 3224 CRC, MNHN).

RESULTS:

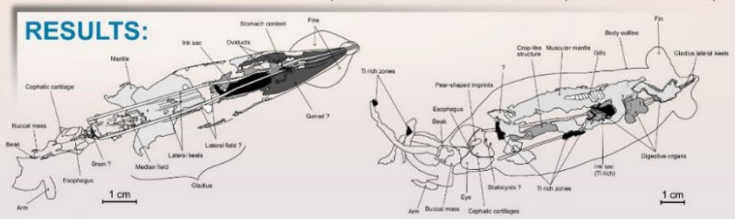

	gladius length (body size)	gladius width	gladius width max : length	median keel	median reinforcement	lateral Keels	opening angle	lateral field width max : med. field width max
Specimen 1 (dorsal view)	83 mm (Small*)	7mm	very slender (0.08)	present	visible	anterior – posterior	4.5°	lateral fields present?
Specimen 2 (ventral view)	90 mm (Small*)	14 mm	Slender (0.15)	absent	Not visible	anterior – posterior	7.7°	-
Doreteuthis (genus)	medium (201 – 400mm*)		slender (0.10 - 0.19*)	absent	bipartite "median ridge" sometimes visible[4] A50394: "Relatively strong median ridge"[5]	anterior – posterior	"6-10°[1] <12°[2]	poorly known/strongly reduced[1,2]

Data shown in red is not consistant with the *Dorateuthis* diagnosis
Based on the diagnosis of the genus *Dorateuthis* with additional variation described in the literature[1-5]

Two QR codes that link to short videos of the RTI images with the light moving around
Specimen 1 Specimen 2

EMERGING QUESTIONS:

- Is the variation expressed in the gladii of these two specimens representative of the genus?
- Can this variation be explained by dimorphism or ontogenetic change?
- Does the genus need to be redescribed to explain this variation?
- Do these specimens represent more than one species?

Acknowledgements:
Olivier Béthoux, Damien Germain, and Valentin Buffa for assistance with the RTI data collection. Marie Radepont and Ouifa Belhadj for XRF data acquisition. Alexandre Lethiers for the poster configuration and printing. Donald Davesne for the identification of fish remains, and Sebastian Schöder and Laurent Tranchant for assistance at the PUMA beam line.

References:

1. Fuchs, D. & Larson, N. Diversity, morphology, and phylogeny of coleoid cephalopods from the Upper Cretaceous Plattenkalks of Lebanon–Part I: Prototeuthina. J. Paleontol. 85, 234–249 (2011).
2. Donovan, D. T. & Fuchs, D. Treatise Online no. 73: Part M, Chapter 13: Fossilized Soft Tissues in Coleoids. Treatise Online (2016) doi:10.17161/to.v0i0.9875.
3. Fuchs, D. Treatise Online no. 136: Part M, Chapter 23G: Systematic Descriptions: Octobrachia. Treatise Online 1–52 (2020).
4. Fuchs, D. Treatise Online No. 53: Part M, Chapter 9B: The Gladius and Gladius Vestige in Fossil Coleoidea. Treatise Online (2016) doi:10.17161/to.v0i0.6466.
5. Jattiot, R., Bayard, A., Fara, E. & Charbonnier, S. Gladius-bearing coleoids from the Upper Cretaceous Lebanese Lagerstätten: Diversity, morphology, and phylogenetic implications. Journal of Paleontology 89, 148–167 (2015).
6. Lukeneder, A. & Harzhauser, M. The Cretaceous coleoid Dorateuthis syriaca Woodward: morphology, feeding habits and phylogenetic implications. Annalen des Naturhistorischen Museums in Wien. Serie A für Mineralogie und Petrographie, Geologie und Paläontologie,

Annex 3: Poster Presentation *Multi-approach imaging techniques shed new light on Lebanese gladius-bearing coleoids* (Awarded best poster prize, 11th International Symposium on Cephalopods Present and Past, London, 2022)

Swiss Journal of Palaeontology

RESEARCH ARTICLE

Open Access

'Arm brains' (axial nerves) of Jurassic coleoids and the evolution of coleoid neuroanatomy

Christian Klug[1*], René Hoffmann[2], Helmut Tischlinger[3,4], Dirk Fuchs[5], Alexander Pohle[1,2], Alison Rowe[6], Isabelle Rouget[6] and Isabelle Kruta[6]

Abstract

Although patchy, the fossil record of coleoids bears a wealth of information on their soft part anatomy. Here, we describe remains of the axial nerve cord from both decabrachian (*Acanthoteuthis, Belemnotheutis, Chondroteuthis*) and octobrachian (*Plesioteuthis, Proteroctopus, Vampyronassa*) coleoids from the Jurassic. We discuss some hypotheses reflecting on possible evolutionary drivers behind the neuroanatomical differentiation of the coleoid arm crown. We also propose some hypotheses on potential links between habitat depth, mode of life and the evolution of the Coleoidea.

Keywords Cephalopoda, Neuroanatomy, Nervous system, Ganglion, Brain, Konservat-Lagerstätte, Taphonomy

Introduction

The cephalopod arm crown is a fascinating body part, which inspires both researchers and artists, movie makers and authors of fiction. In recent years, the arm crown and other decentralized functions of cephalopod bodies, such as vision and the control of skin colouration, and arm movements independent of the central nervous systems have been widely discussed. For example, discussions regarding cephalopod vision and skin colouration (camouflage) are rooted in a debate between Hess and Frisch (Frisch, 1912; Hess, 1902, 1905, 1912), which was later resolved (Dröscher, 2016; Messenger, 1977; Messenger et al., 1973), although the discussion on the presence or absence of colour vision continues (Stubbs & Stubbs, 2016). Knowing the colour-blindness of octobrachians, their camouflaging capabilities are even more surprising. Kingston et al., (2015a, 2015b) found an explanation in the discoveries of dermal photoreception and of "Eye-independent, light-activated chromatophore expansion (LACE)" (i.e. colour change independent of the eyes; see Ramirez & Oakley, 2015; Katz et al., 2021). Independent of this discussion, the question for links between the neural equipment of the arms, overall neuroanatomy, and the (palaeo-) environment arises. Such links were found by, e.g., Chung et al., (2022a, 2022b) and are discussed here for extinct coleoids.

The neural equipment of cephalopod arms is linked with the organs of the arms such as suckers (Graziadei, 1962). Suckers are interesting sensory components of the coleoid arm crown, and likely originated in the Carboniferous, or even earlier (Fuchs et al., 2010, 2021; Kröger et al., 2011; Kruta et al., 2016; Tanner et al., 2017; Whalen & Landman, 2022). More than half a century ago, Wells, (1963, 1964) documented the presence of chemosensory and tactile receptors in *Octopus* (see also Chase & Wells, 1986; Lee, 1992; Maselli et al., 2020). Refined experiments confirmed the chemoreceptors to be located within their

Handling editor: Rakhi Dutta.

*Correspondence:
Christian Klug
chklug@pim.uzh.ch
[1] Paläontologisches Institut und Museum, Universität Zürich, Karl-Schmid-Strasse 4, 8006 Zurich, Switzerland
[2] Institute of Geology, Mineralogy, & Geophysics, Ruhr-Universität Bochum, 44801 Bochum, Germany
[3] 85134 Stammham, Germany
[4] Jura-Museum Eichstätt, Willibaldsburg, 85072 Eichstätt, Germany
[5] SNSB-Bayerische Staatssammlung für Paläontologie und Geologie, Richard-Wagner-Straße 10, 80333 Munich, Germany
[6] Centre de recherche en paléontologie - Paris, Sorbonne Université-MNHN-CNRS-CR2P, 4 Pl. Jussieu, 75005 Paris, France

suckers (Buresch et al., 2022). This is important in the generally dark, murky waters where they live as they use their arms to forage for prey in crevasses. Importantly, in octopods, the sensory information is processed initially by ganglia present in the suckers and then forwarded to the larger intrabrachial ganglia on the axial nerve cord (Graziadei, 1962; fig. 1; Young, 1971). Octopods have indeed a complex brachial nervous system related to their "*sophisticated use of their arm and their ability for tactile learning*" (Budelmann, 1995: p. 125).

Preservation of nervous systems is known only from fossil localities yielding exceptional preservation. The fossil record of soft tissues is best known among octobrachians (e.g., Clements et al., 2017; Fuchs et al., 2010; Fuchs, 2006a, 2006b; Klinghardt, 1932; Klug et al., 2015; Naef 1922; Rowe et al., 2022, 2023). Less is known about the soft tissues of decabrachians (Fuchs et al., 2010; Fuchs, 2006a, 2006b; Klug et al., 2016, 2019), and less still about externally shelled (ectocochleate) cephalopods such as ammonoids and nautiloids (De Baets et al., 2013; Klug & Lehmann, 2015; Klug et al., 2012, 2015, 2021a, 2021c). Some of these reports (Fuchs et al., 2010, 2021; Fuchs, 2006a, 2b; Klug et al., 2016, 2020; Kruta et al., 2016; Rowe et al., 2022, 2023) demonstrated the increased preservational potential for soft tissue anatomy in the coleoid arm crown, which are typically less common than the sclerotized elements such as arm hooks or sucker rings.

In contrast to many other soft-tissue details, descriptions of the nervous system of cephalopods have only occasionally found their way into the scientific literature (Fuchs & Larson, 2011a, 2011b; Fuchs, 2006a, 2006b; Jattiot et al., 2015; Klug et al., 2016, 2019, 2021a; Larson et al., 2010), mostly showing parts of the cephalic cartilage. Fossilized axial nerve cords that probably included the intrabrachial ganglia, the brain-like concentrations of neuronal tissues in the arms, have been documented only a few times (Kruta et al., 2016; Rowe et al., 2022, 2023) and once unknowingly (Klug et al., 2016, supplementary Fig. 5). This exceptional preservation is limited to conservation deposits (Seilacher, 1970) and, so far, have only been discovered in the German Posidonienschiefer (Toarcian, Early Jurassic, this paper), the French Callovian marls of La Boissine (La Voulte-sur-Rhône, Middle Jurassic; Kruta et al., 2016; Rowe et al., 2022, 2023) and the German platy limestones of the Solnhofen region (Late Jurassic; Klug et al., 2016). Remains of arms and axial nerve cords were also discovered in other Fossillagerstätten such as the English sites of Christian Malford (Middle Jurassic), and the Late Jurassic coastline (this paper) or the Cenomanian of Lebanon (Larson et al., 2010: figs. 3B and 5I) and, without axial nerves, in the Oligocene of Russia (Mironenko et al., 2021).

In this study, we describe some specimens showing phosphatized remains of arm soft-tissues from the Jurassic of France and Germany. We attempt a homologization of the visible structures and discuss their nature. Further, we put these structures into the evolutionary context of the origin of major coleoid clades. We assess potential links between habitat and neuroanatomy of these fossil coleoids.

Methods

As an independent test of our evolutionary hypotheses on habitat distribution, we performed Bayesian ancestral state reconstructions (Pagel et al., 2004). For this purpose, we used the ingroup of the time-calibrated phylogeny of Tanner et al., (2017), which is based on transcriptomic data from 26 extant cephalopod species. Fossil species were not included because timetrees uniting the relevant living and fossil taxa are currently not available. Each taxon was scored for their habitat distribution following Chung and Marshall, (2017), i.e. coastal (category GI) and pelagic (categories GII–III). We did not divide pelagic cephalopods further into deep pelagic and vertical migrating species because this trait is more variable, and a wider species coverage would be needed for accurate predictions. Nevertheless, at least within this dataset, pelagic species always are taxa that can regularly be found at depths of hundreds of metres or live permanently in the deep sea, while coastal species are restricted to depths of less than 200 m, mostly within the photic zone. Thus, it is conceivable that this habitat switch has important implications for the nervous system, as adaptations to low light conditions may be essential for pelagic species regardless of whether they are vertical migrants or deep-sea dwellers.

Ancestral state reconstructions were performed in RevBayes version 1.1.1 (Höhna et al., 2016), using the Mk model with equal transition rates (Lewis, 2001) and fixed tree topology. The prior on the transition rate and only parameter of the model was set to an exponential distribution. The MCMC algorithm was run for two independent replicates with 25,000 generations using a random move schedule, discarding 25% of the samples as burn-in. The output was then processed in R using the package RevGadgets version 1.1.0 (Tribble et al., 2022). The script for the analysis in RevBayes and its output are provided in Additional File 1.

The specimen of *Proteroctopus ribeti* (MNHN.F.R03801) and *Vampyronassa rhodanica* (MNHN.F.B74244) originally described by Fischer and Riou (1982, 2002), were reanalysed using propagation phase contrast synchrotron X-ray micro-computed tomography (PPC-SRμCT, ESRF-ID19) in Kruta et al., (2016) and Rowe et al., (2022, 2023). Acquisition details are provided in these publications. Additional PPC-SRμCT slices are illustrated here in order to show the

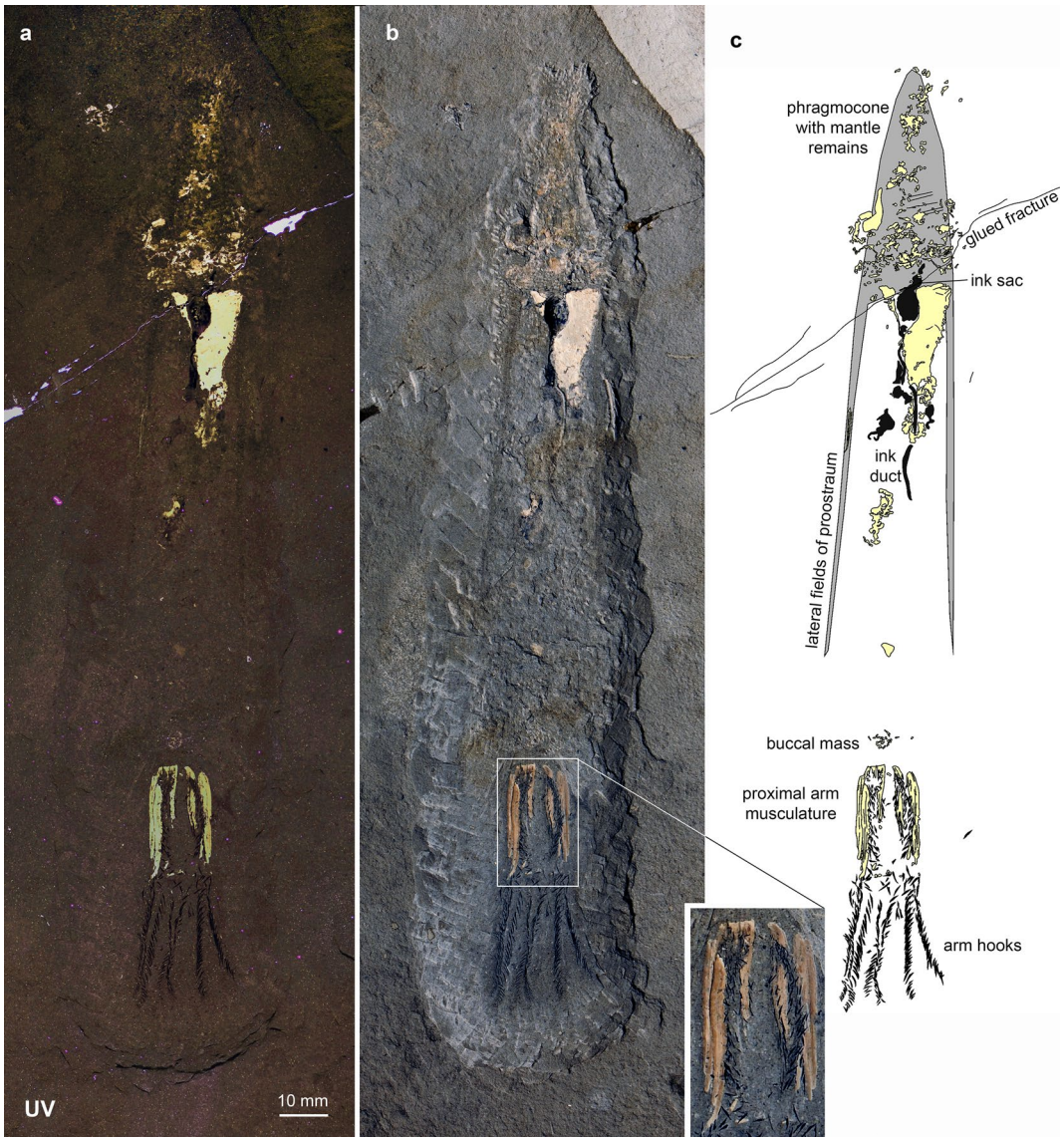

Fig. 1 *Sueviteuthis zellensis* Reitner & Engeser, 1982, GPIT Ce 1564/2,6/PV-67025, Toarcian, Fischer quarry, Zell, east of Ohmden. **a** UV-photo by R. Roth; **b** photo under white light (insert with magnification of the arm bases); **c** drawing after a

axial nerves in the specimens. Measurements were taken only where the section of axial nerve was visible in all three views (cross section, coronal, and longitudinal).

Results

Descriptions

Systematics and phylogeny are according to Hoffmann et al., (2022). We follow the order provided there on page 192. Below, we provide descriptions of the head-foot with a focus on the arm crown. Since all the specimens presented here show exceptional preservation, the number and shape of arms is more or less well known. In combination with the preserved hard parts, their placement within the decabrachians and octobrachians is quite well supported (e.g., Fuchs, 2006a, 2016; Haas, 1997; Jeletzky, 1966; Kröger et al., 2011; Tanner et al., 2017).

In some specimens, remains of the brachial nervous system (e.g., the axial nerve cord) are preserved. Others retain armature from which it is possible to infer function and therefore extrapolate the complexity of the central nervous system associated with the sensory tasks.

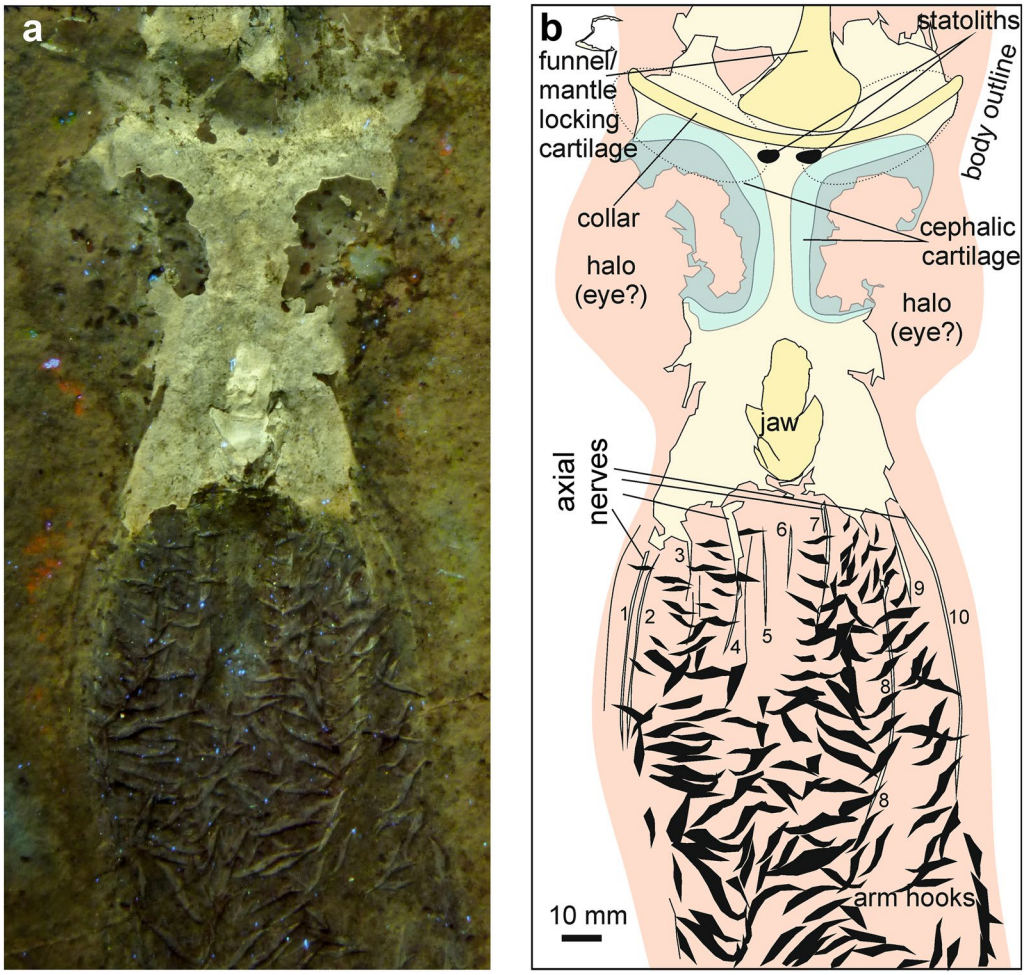

Fig. 2 *Acanthoteuthis speciosa* Münster, 1839, HT 02/2, latest Kimmeridgian, Öchselberg Quarry near Zandt, Bavaria (Germany). Figure modified after Klug et al., (2016, suppl. Fig. 5). **a** UV-photo by HT; **b** drawing after a

Crown group node Neocoleoidea Haas, 1997
Superorder Decabrachia Haeckel, 1866
Order Belemnitida Haeckel, 1866
Family Belemnotheutidae Zittel, 1884
Sueviteuthis zellensis Reitner & Engeser, 1982
(Fig. 1)

Specimen GPIT Ce 1564/2,6 (GPIT-PV-67025), paratype, original of Reitner and Engeser (1982:3, fig. 4, pl. 1).
Stratigraphy Posidonia Shales, Koblenzer, Semicelatum Subzone, Tenuicostatum Zone, Toarcian, Early Jurassic.
Locality Fischer quarry, east of Ohmden, Germany.
Description of arm crown The entire specimen is about 190 mm long. It preserves the complete phragmocone, most of the proostracum, the ink sac and most of the ink duct, and a complete arm crown with stretched out, subparallel arms. The arm crown is 53 mm long and preserves the remains of 391 small arm hooks. They are arranged in rows, which can be assigned to at least seven arms. The stylet-shaped arm hooks are of varying size, ranging up to 3.2 mm long. The proximal parts of the hook-rows are associated with elongated phosphatized fields. These fields are up to 25 mm long, between 1 and 2 mm wide, and bear very fine longitudinal striations which likely represent musculature. Depending on how these fields are counted (because the visible separation of the fields varies strongly), there are between six and nine distinct fields. When accepting the higher number, the maximum width is around 1 mm. There appears to be a gap between the distal end of these phosphatized fields and the distal 28 mm of the arms. This gap is present in all of the visible arms, suggesting a primary structure differentiating the proximal from the distal portions. A few arm hooks are present between these fields, though

the majority of aligned hooks are clustered in the distal section.

Acanthoteuthis speciosa Münster, 1839
(Fig. 2)

Specimen HT 02/2, original of Klug et al., (2016, supplement, p. 8, figs. S4, S5).
Stratigraphy Lithographic Limestones, Beckeri-zone, Ulmense subzone, Rebouletianum horizon, uppermost Kimmeridgian.
Locality Öchselberg Quarry near Zandt, Bavaria (Germany), Germany.
Description of arm crown The entire specimen measures 440 mm from the tips of the arms to the apex of the rostrum. The head foot-complex is exceptionally preserved, displaying statocysts with statoliths (Klug et al., 2016, supplement), cephalic cartilage, body outline, jaws and the arms. The arms are up to 120 mm long and nearly 300 hooks are discernible. The arm hooks belong to the *Acanthuncus* morphotype and show the characteristic changes from the proximal to distal parts of the arm crown. Proximally, the hooks are small and almost straight, while those in the mid-section are much larger, strongly curved and have a large uncinus. Distally, they become shorter again. Between the hook rows, UV-photos (Fig. 2a) show fine phosphatized lines that run parallel to the hook rows. These lines are up to 1.5 mm wide and between 15 and about 70 mm long. Traces of about 10 such lines are visible particularly in the proximal half of the arms. Several are linked with the phosphatized surface surrounding the jaws.

Acanthoteuthis sp.
(Fig. 3)

Specimen KI306, Etches collection.
Stratigraphy Kimmeridge Clay, Kimmeridgian.
Locality Kimmeridge Bay, United Kingdom.
Description of arm crown The body outline as indicated in Fig. 3b is about 180 mm long. The specimen preserves the ink sac and duct, an imprint of the phragmocone, phosphatized remains of the mantle musculature and parts of the arm crown. Four arms (up to 60 mm long) are reasonably complete with the majority of the arm hooks being preserved. The hooks look like those of *A. speciosa* and *Belemnotheutis antiquus* (*Acanthuncus* morphotype), an issue of systematics of these taxa that will need clarification in the future. The arm hooks are up to 6 mm long and display the characteristic change in size and shape from the arm base (smaller, less curved) to the middle hooks, which are the largest and most strongly curved back to the distal ones, which are gently curved sinusoidally and small. Between the arm hooks, phosphatized longitudinal structures are discernible. These are 1–2 mm wide and up to 16 mm long. Some are longitudinally striated (Fig. 3a insert). Based on these structures and the groupings of arm hooks, we identified remains of eight of the ten arms. The remaining two arms might be missing because the adjacent slab was likely already lost when the specimen was found.

Belemnotheutis antiquus Pearce, 1842
(Fig. 4)

Specimen NHMUK 25966, Natural History Museum, London; original of, e.g., Owen, (1844) and Pearce, (1847).
Stratigraphy Oxford Clay, Athleta Zone, upper Callovian,
Locality Christian Malford, Wiltshire, United Kingdom.
Description of arm crown This specimen is included for its excellent preservation and historical importance. It is also remarkable because it tells a story of the classical conflict between collectors and well-informed laypersons on the one hand (such as the amateur palaeontologists Mary Anning, who first discovered belemnotheutid materials in 1826, and Joseph Pearce, who introduced the genus and species in 1842) and professionals on the other hand, sometimes arrogant like Richard Owen, (1844) in this context, or correct such as Gideon Mantell, (1848). See Donovan and Crane, (1992) for a detailed historical report and description of the taxon.

The specimen is about 243 mm long. It is complete and preserves the phragmocone (72 mm long) with the proostracum, which is largely covered by the phosphatized mantle musculature (81 mm long and 48 mm wide in its flattened state). The head region is also phosphatized but is poor in anatomical detail. The centre displays a 10 mm wide crescent-shaped structure, which is tentatively interpreted as part of the jaw. The arm crown is very well preserved and shows the remains of at least seven arms with more than 240 distinct arm hooks, ranging between 1 mm (proximally and distally) and 5 mm (about 20–30 mm from the tips) in length, showing the previously mentioned shape change. Each double row of arm hooks is accompanied by an elongate phosphatized structure, which is 1–5 mm wide. It is unclear whether these structures represent the complete arms or parts thereof. Since it is a historic specimen, it is conceivable that parts of arm width were lost due to preparation efforts (for a photo see Clements et al., 2017).

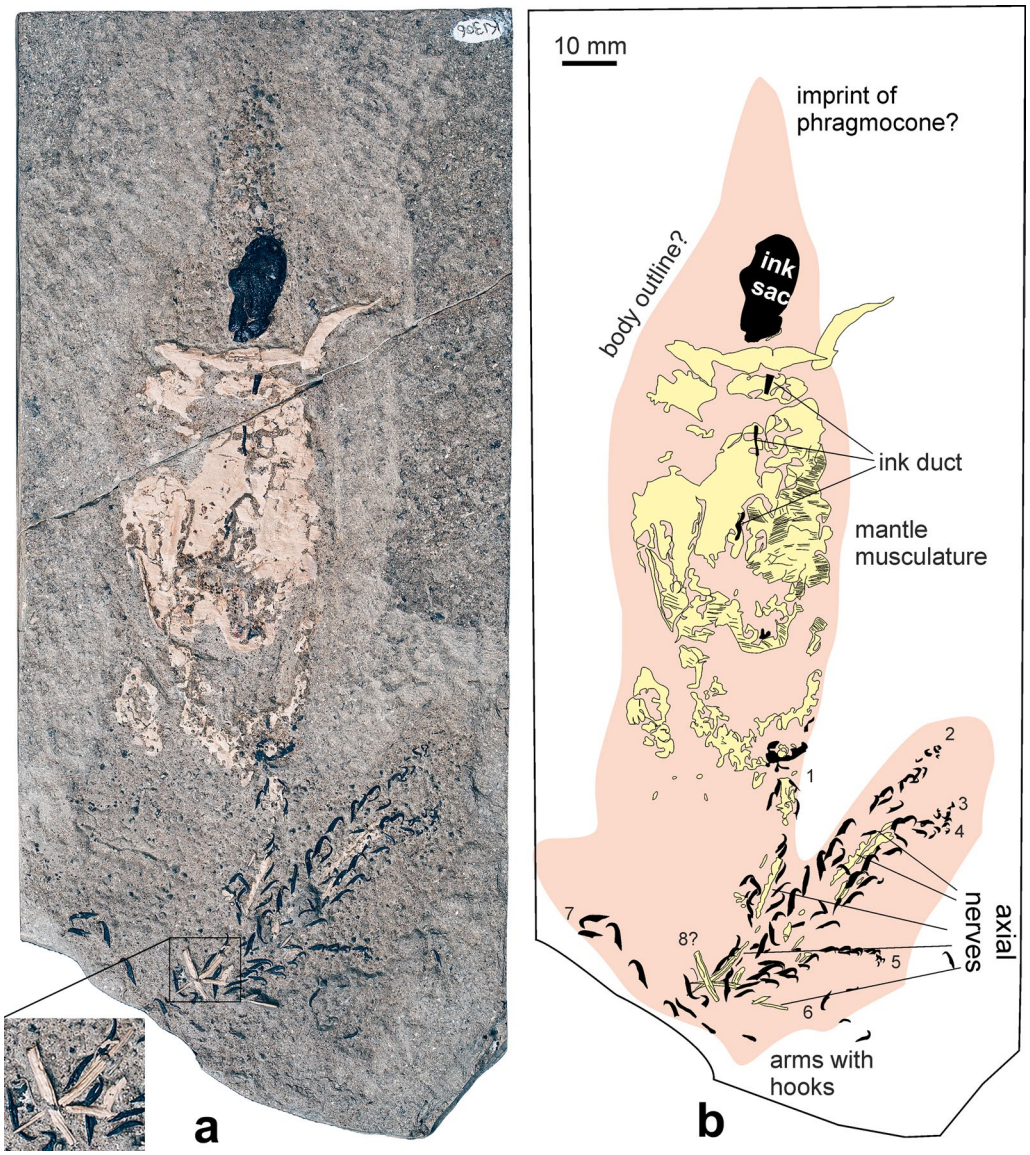

Fig. 3 *Acanthoteuthis* sp., KI306, Etches collection, Kimmeridgian, Kimmeridge Bay (United Kingdom). Photo by Terry Keenan. **a** photo of specimen, with magnified detail to show the striation of the axial nerves. **b** Sketch of the specimen

Order Diplobelida Jeletzky, 1965
Chondroteuthis wunnenbergi Bode, 1933
(Figs. 5, 6)

Specimen BGR MA 13436 (described in Hoffmann et al., 2017, specimen two therein).
Stratigraphy Posidonia Shale, Falciferum Zone, Toarcian, Early Jurassic.
Locality Hondelage near Brunswick, northern Germany.
Description of arm crown The specimen is complete and preserves the rostrum and phragmocone remains, imprints of parts of the proostracum, the ink sac with ink duct (Fig. 5) and a complete arm crown (Fig. 6). The entire specimen measures 170 mm from the apex of the rostrum to the tip of the arms. The arms are quite slender and up to 60 mm long. About 190 arm hooks are discernible, ranging between 0.2 and 3 mm in length, with the largest hooks in the middle of the arms. Typical for this taxon, the hooks are arranged in a single row (instead of biserial rows) and belong to four different hook morphotypes (see Hoffmann et al., 2017). The distal arm hooks appear to be missing, which is likely a taphonomic artefact. The larger hooks have a broad base and a long uncinus. These are visible in the overview photograph (Fig. 5), though to enhance the contrast, another more detailed

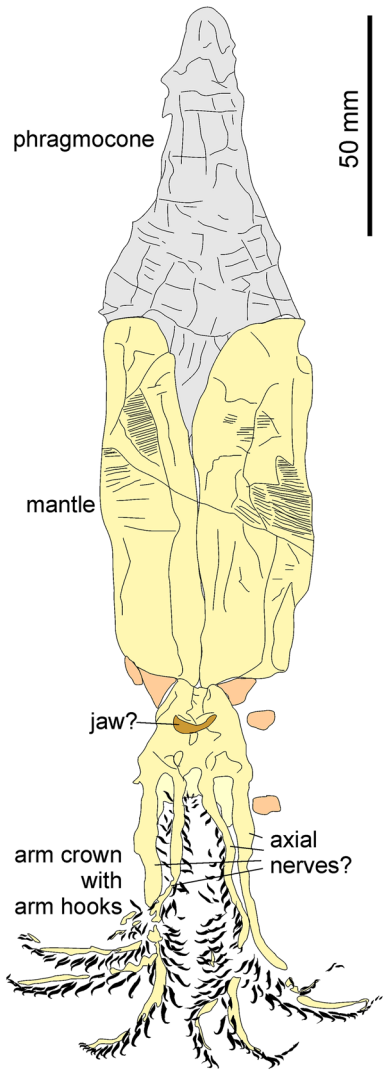

Fig. 4 *Belemnotheutis antiquus* Pearce, 1847; NHMUK 25966, Christian Malford, Wiltshire, England, Callovian Oxford Clay; entire animal with excellently preserved mantle and complete arm crown. Drawing after the holotype, refigured in Clements et al. (2017)

photograph was taken and inverted to obtain a negative image of the arm crown. This shows a set of pale stripes associated with the arm hook-series that likely represent faint remains of the arms. Within these faint outlines, light grey lines (Fig. 5, dark in Fig. 6a and light yellow in Fig. 6b) are visible, which can be traced from the base to the tip in some of the arms. In total, 10 arm traces could be identified, but only nine of which display the more distinct finer internal line. The arms seem aligned in two bundles. Between the bases of these two bundles, an oblique connecting line is visible (intrabrachial commissure in Fig. 6b).

Order Spirulida Haeckel, 1866
Spirula spirula (Linnaeus, 1758)
(Fig. 7)

Description The entire specimen is about 40 mm long. For CT-scanning, the extant specimen was stained with tungsten. Due to a subsequent staining with iodine, the specimen was unfortunately destroyed. The complete arm crown was preserved and composed of eight arms and two tentacles. All of these appendages curved inwards. The visible part of the arm crown is 6 mm long. It shows small biserial suckers that extend from the base to the middle section of the arms, before merging into a single row at the distal tips. Like the hooks in other species, the suckers decrease in diameter towards the arm tips but have their largest diameter at the first third of the arm. An orthoslice view cutting through the arm bases (Fig. 7) shows the central axial nerve cords surrounded by the arms musculature or slightly moved inwards as darker spots of 0.19–0.27 mm diameter (arm diameter/nerve diameter = ratio). For a list of measurements, see Table 1. The shell has a diameter of 14 mm and 26 chambers.

Fig. 5 *Chondroteuthis wunnenbergi* Bode, 1933, BGR MA 13436, Hondelage near Brunswick (Germany), Toarcian Posidonia Shale, entire animal with ink sac and duct as well as phragmocone and rostrum. The ammonite may be a hammatoceratid or harpoceratid. White light

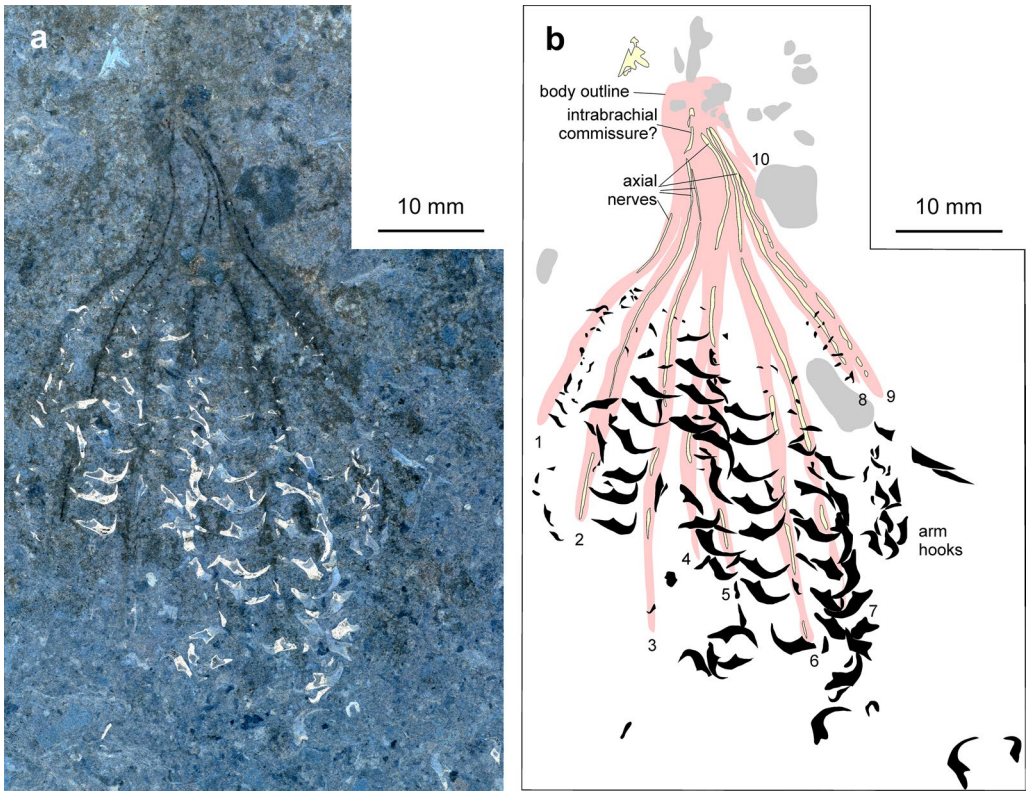

Fig. 6 *Chondroteuthis wunnenbergi* Bode, 1933, BGR MA 13436, Hondelage near Brunswick (Germany), Toarcian Posidonia Shale. **a** Arm crown, inverted white light photo by RH; arm hooks appear whitish, the axial nerves are dark. **b** Drawing after a. Pink—outlines of arms; black—arm hooks; light yellow—lightly phosphatized structures; grey—dark spots in the sediment

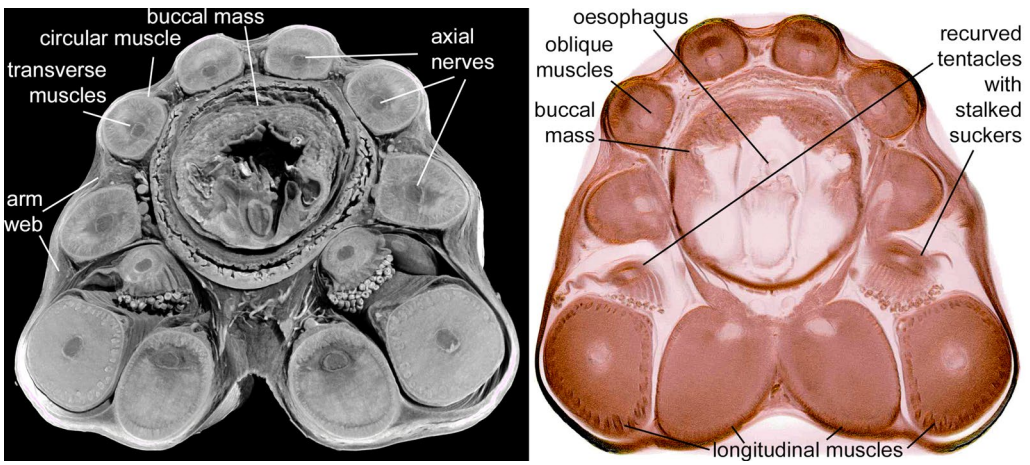

Fig. 7 Orthoslice made from a CT-data volume (left) and histological section (right) cutting through the arm bases and buccal mass of *Spirula spirula* (Linnaeus, 1758). The arm bases encircle the buccal mass. Each arm has longitudinal muscle fibres surrounding an indistinctive grey mass. The darker spot in the central or subcentral position represents the axial nerves. The ratio between arm diameter and nerve diameter varies between 6:1 in dorsal arms and 4:1 in ventral arms

Table 1 List of arm measurements and proportions of *Spirula spirula*

Arm	Arm diameter [mm]	Axial nerve diameter [mm]	Ratio arm/ nerve diameter
1	1.61	0.25	6.44
2	1.45	0.27	5.37
3	1.18	0.21	5.62
4	1.16	0.19	6.11
5	1.22	0.22	5.55
6	1.19	0.23	5.17
7	1.19	0.25	4.76
8	1.15	0.21	5.48
9	1.41	0.27	5.22
10	1.61	0.26	6.19

Superorder Octobrachia Haeckel, 1866
Order Vampyromorpha Robson, 1929

Remarks Here, we briefly summarize anatomical information about the arm crown as it was obtained in the initial descriptions by Fischer and Riou, (1982, 2002) as well as the re-descriptions using synchrotron data published by Kruta et al., (2016) and by Rowe et al., (2022, 2023).

Proteroctopus ribeti Fischer & Riou, 1982
(Fig. 8)

Specimen MNHN.F.R03801, holotype of Fischer and Riou, (1982).
Stratigraphy Koenigi Zone, early Callovian, Middle Jurassic.
Locality La Voulte-sur-Rhône, Ardèche, France.
Description of arm crown Like *Vampyronassa*, the holotype of *P. ribeti* is extremely well preserved, showing detail rarely seen in other coleoid fossils. The holotype measures about 120 mm in length with a 68 mm long mantle (Kruta et al., 2016: p. 2, Fig. 8a). Fins are clearly visible. The head is rather short with big eyes, though neither reveal a lot of anatomical detail. By contrast, the arm crown is complete and shows suckers and internal anatomical details. In fig. 1F of Kruta et al. (2016) and in Fig. 8b, c, the axial nerve cords are evident in the tomographic image. At an arm diameter of about 2.5 mm, the axial nerve is about 0.5 mm wide.

Vampyronassa rhodanica Fischer & Riou, 2002
(Fig. 9)

Specimen MNHN.F.B74244, paratype of Fischer and Riou (2002)

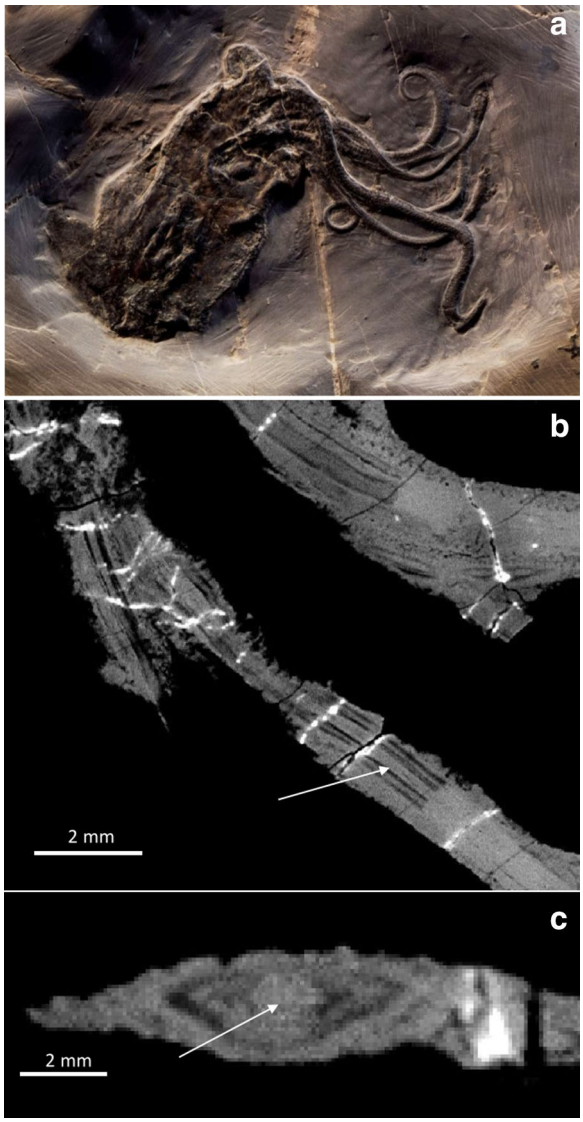

Fig. 8 *Proteroctopus ribeti* Fischer & Riou, 1982, MNHN.F.R03801. **A** Photograph by P. Loubry, reproduced with permission, CR2P. **B** PPC-SRμCT (ESRF-ID, ID 19, voxel size 44,5 μm) slice of arm crown showing axial nerve (coronal view). **C** Cross section of the arm crown. Arrow is pointing to the axial nerve seen at the centre of the arm musculature seen in B and C

Stratigraphy Koenigi Zone, early Callovian, Middle Jurassic.
Locality La Voulte-sur-Rhône, Ardèche, France.
Description of arm crown MNHN.F.B74244 has undergone some rotation and compaction prior to fossilization, though many of the original soft tissues are preserved in 3D (Rowe et al., 2022). The overall length (posterior-most tip of the mantle to the distal tip of the dorsal arms) of the specimen measures approximately 97 mm. There is no evidence that *V. rhodanica* possessed an ink sac. The

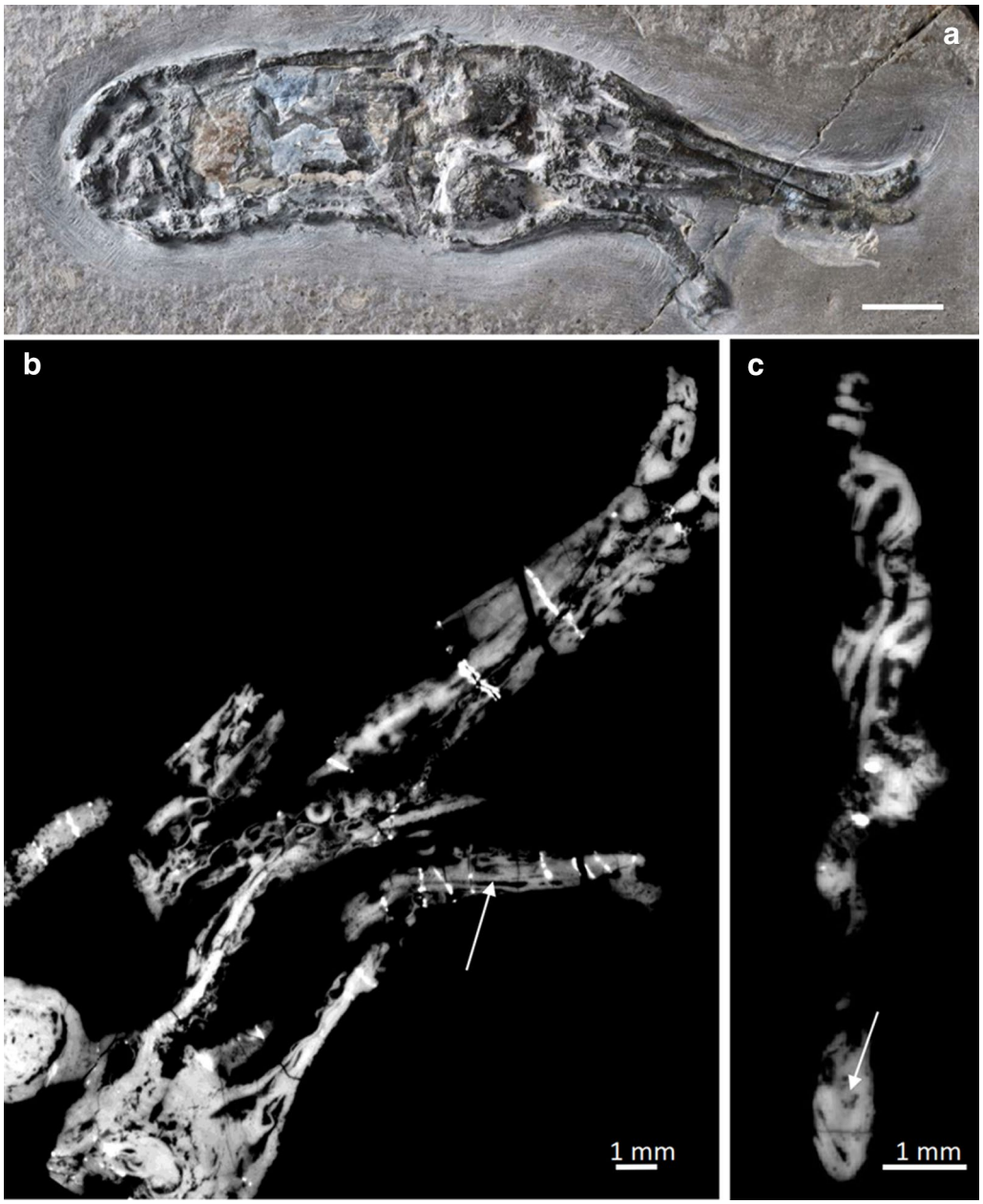

Fig. 9 *Vampyronassa rhodanica* Fischer & Riou, 2002, MNHN.F. R03801. **A** Photograph by P. Loubry, reproduced with permission, CR2P. **B** PPC-SRμCT (ESRF, ID 19, voxel size 25 μm) slice of arm crown showing axial nerve in the centre of the arm crown (coronal view). The suckers are also visible. **C** Cross section of the arm crown. Arrow is pointing to the axial nerve seen in b

head, which is fused to the mantle, preserves both eyes. Their position and subspherical shape (about 5–7 mm in diameter) likely reflect the compaction of the specimen.

Eight arms are visible in the arm crown (Fig. 9). The preserved length of the two dorsal arms is about 43 to 51 mm. This is approximately equivalent in length to the mantle (about 46 mm). The configuration of the armature on the dorsal arms comprises two distally positioned uniserial suckers, flanked by biserial cirri. The suckers are about 2 mm in diameter.

The six non-dorsal arms are shorter and their preserved length ranges from 24 to 36 mm. Up to ten uniserial suckers are visible per arm, and range in diameter from 1.6 mm (proximally) to 0.8 mm (distally). These are continuous along the length. Biserial cirri flank

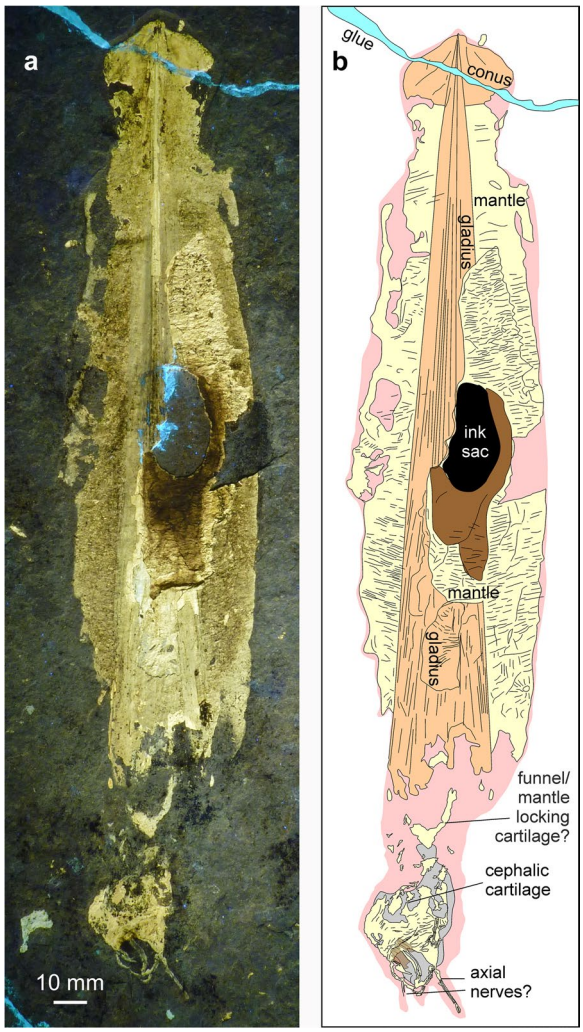

Fig. 10 *Plesioteuthis prisca* (Rüppell, 1829), HT 77/23, Daiting (Germany), Tithonian Moernsheim Formation. Specimen is 317 mm long

these suckers. They have a similar diameter and same tapering pattern as the suckers.

The axial nerves of each of the arms are visible in the PPC-SRμCT slices Fig. 9b, c. They are most prominent in the dorsal arms where, in the distal half of the arm, they range in diameter from about 0.2–0.6 mm. The width of the arms in this section varies from 1.6 to 2.9 mm. In the non-dorsal arms, the axial nerve size range is 0.3–0.7 mm and the arm width varies between 1.4 and 2.4 mm. It should be noted that the compression of the soft tissue prior to fossilization has likely altered the preserved diameter of these elements.

The suckers of *V. infernalis* are radially symmetrical, and each has a conical, *Vampyroteuthis*-like attachment. There is no clear attachment to the internal arm musculature.

Plesioteuthis prisca (Rüppell, 1829).
(Figs. 10, 11, 12)

Specimens HT 73/152, HT 77/23 (col. H. Tischlinger) .
Stratigraphy Moernsheim Formation, Moernsheimensis subzone, *Hybonotum* Zone, Lower Tithonian, Jurassic.
Locality Daiting near Monheim, Bavaria, Germany.
Description of arm crown Two specimens of *P. prisca* are discussed here because they both display a peculiarly preserved arm crown. HT 77/23 (Figs. 10, 11c, d) is a complete specimen measuring 317 mm from arm tip to the tip of the gladius. The mantle length is approximately 250 mm and partially covers the gladius. The conus is heavily phosphatized like the muscular mantle. The gladius is hardly phosphatized at its anterior edge and hence not well preserved there. The ink sac and duct are clearly visible. The head (Fig. 11c, d) is preserved on a slight angle, possibly due to necrolytical processes. It displays an oval structure, 13 mm long and 11 mm wide, which we interpret to be an imprint of the cephalic cartilage. The arm crown is preserved as seven phosphatized elongate structures of about 1 mm width each. All but one arm are curled inward, as seen in an exceptionally preserved specimen from the Kimmeridgian of Painten (BMMS 617a, Klug et al., 2015: fig. 2). The Painten-specimen, however, has much thicker arms, which display their cirri. In most other specimens, including those with landing marks (Klug et al., 2015: fig. 7) that sometimes accurately reflect arm proportions, the arms are much thicker proportionally (Additional File 1).

Specimen HT 73/152 is quite similarly preserved (Figs. 11a, b 12). It measures 320 mm from arm tip to gladius tip and also displays a strongly phosphatized mantle, the remains of an ink sac and duct, as well as the gladius. The head displays a limonitic stain on the phosphatic mass, which is here interpreted as jaw remains. Like in HT 77/23, this specimen preserves seven to eight fine, lightly phosphatized structures, which are about 1 mm wide. Correspondingly, these proportions support the interpretation that it is not the arms but rather the axial nerve cords, which are preserved here.

Ancestral state reconstructions

The analyses show a strong phylogenetic signal in the habitat distributions of crown group coleoids (Fig. 13). The oldest nodes (crown Cephalopoda and crown Coleoidea) contain the highest uncertainty, both slightly favouring a pelagic habitat with a probability of about

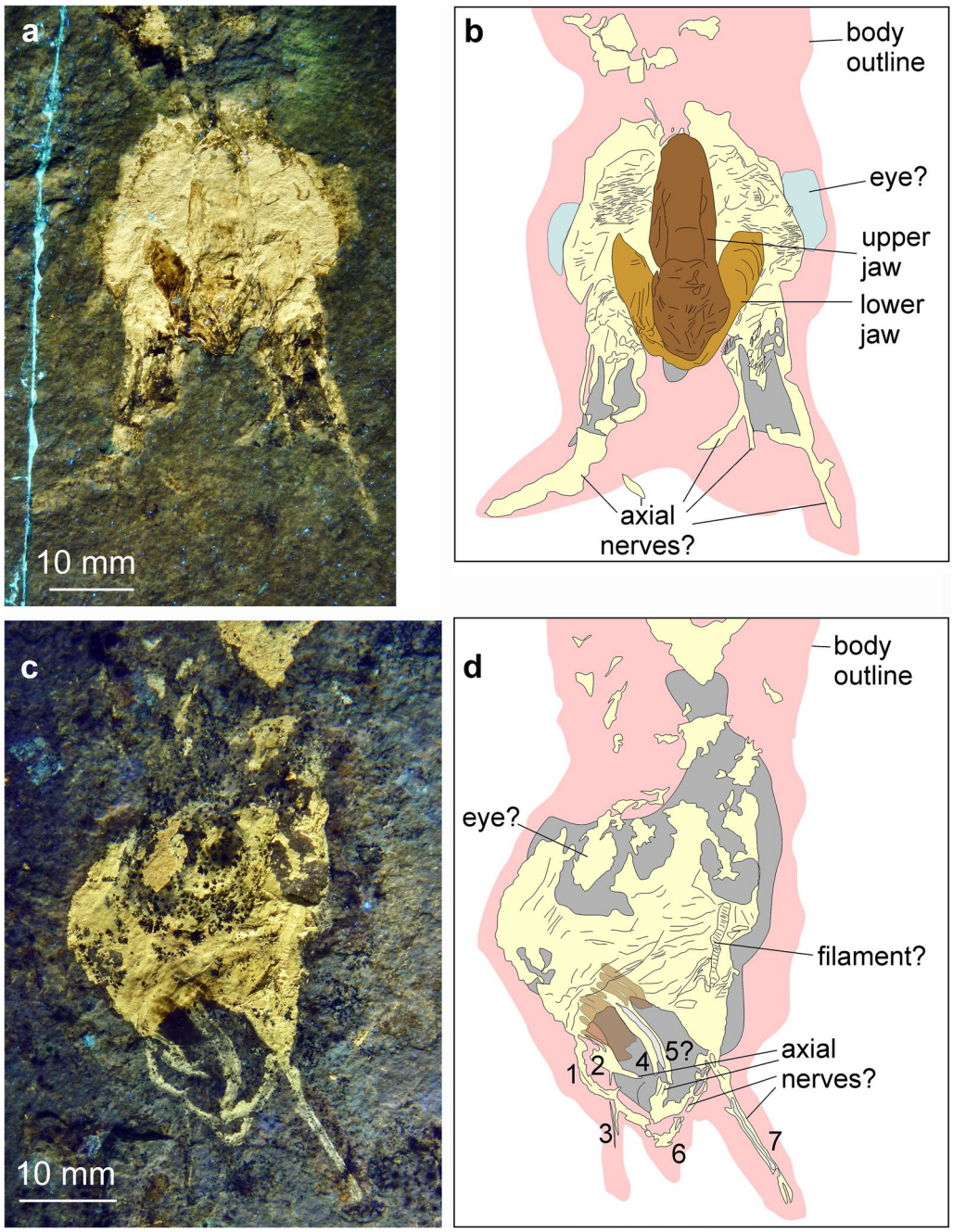

Fig. 11 *Plesioteuthis prisca* (Rüppell, 1829), Daiting (Germany), Tithonian Moernsheim Formation. **a**, **b** HT 73/152 **c**, **d** HT 77/23 detail of Fig. 8

2/3. This high uncertainty likely stems from the necessarily poor sampling of the *Nautilus* lineage, but also from the reconstruction of the basal coleoid dichotomy, where the crown octobrachian node is reconstructed with high probability (79%) as pelagic, while the most recent common ancestor of crown decabrachians most likely (88%) had a coastal habitat. Within both superorders, our analysis recovered a single habitat transition. Within Octobrachia, this switch occurred at the base of the Octopodidae, which is reconstructed as coastal with high probability (78%). Conversely, the transition between coastal and pelagic decabrachians was estimated at the node

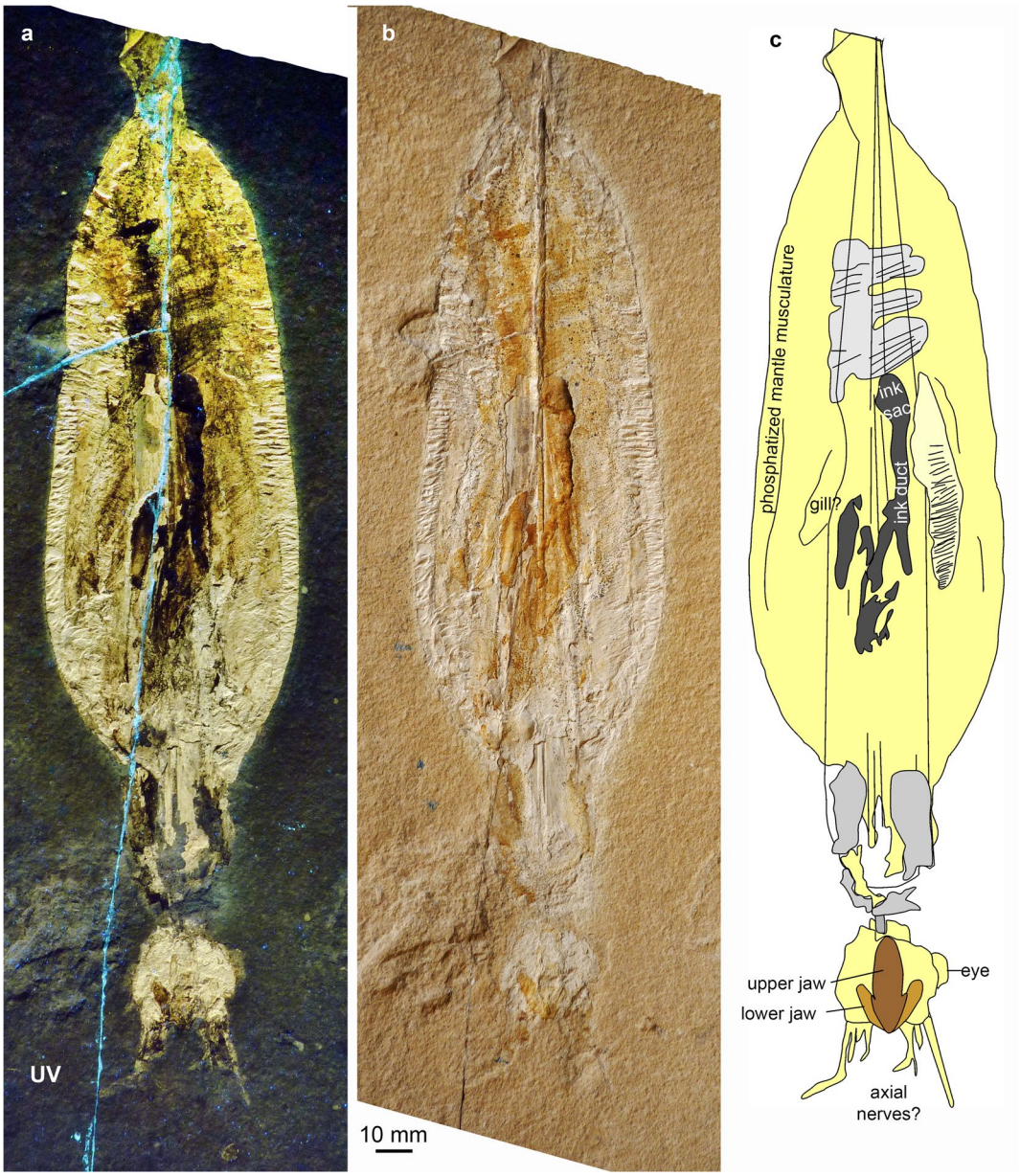

Fig. 12 *Plesioteuthis prisca* (Rüppell, 1829), HT 73/152, Daiting (Germany), Tithonian Moernsheim Formation. **a** UV-light. **b** White light. **c** Interpretative sketch

containing Oegopsida + Spirulida (74%). The transition rate for the change in habitat was estimated to a mean of 0.0019 per million years, with a median of 0.0017 and a 95% highest posterior density interval between 0.0002 and 0.0043. Thus, on average, a single lineage would be expected to transition between habitats only once in 500 million years, indicating a very slow transition rate.

Discussion

Taphonomy

In the past decades, experimental studies such as those of Clements et al., (2017) have shown the differential decay and preservation potential of coleoid organs. Clements et al., (2017: fig. 4) found that the mantle was quite resistant to decay, which coincides with the fact that it is often preserved in platy limestone Lagerstätten such as Solnhofen-Eichstätt (Germany), Hadjoula and Haqel (Lebanon), etc. They observed a significant difference

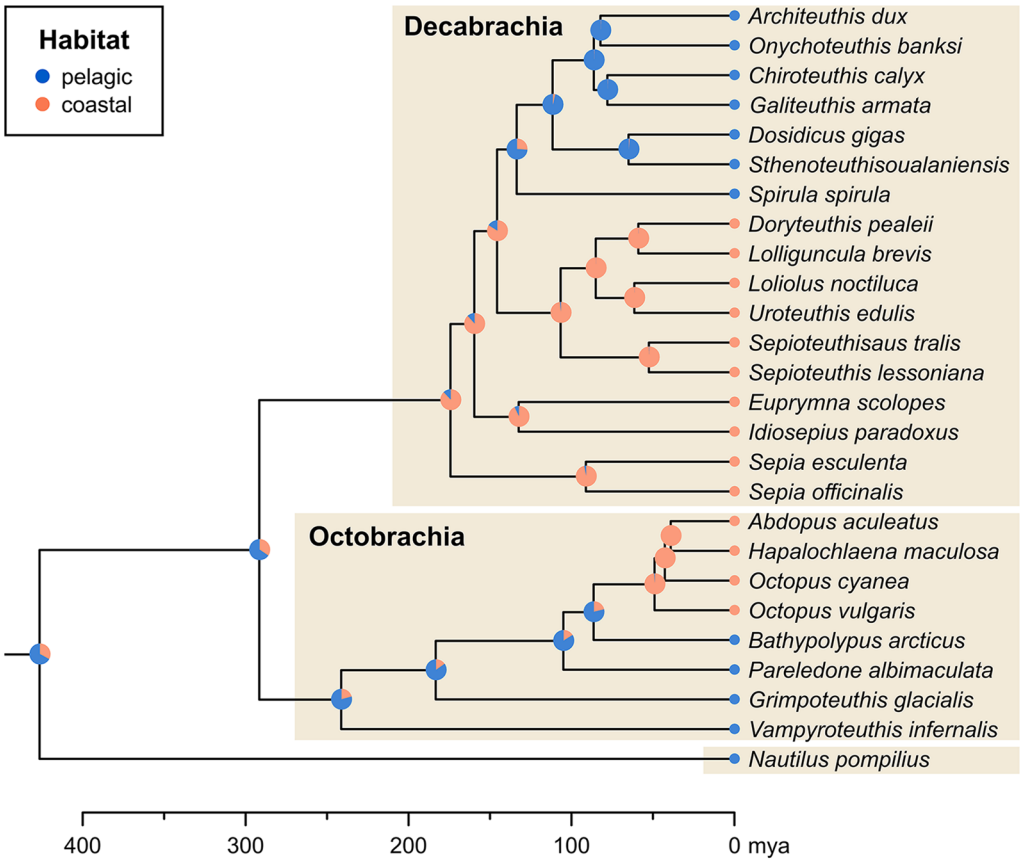

Fig. 13 Bayesian ancestral state reconstruction of cephalopod habitat distribution. Tree from Tanner et al., (2017) based on transcriptomic data. Pie charts at nodes represent posterior probabilities of states. Coastal habitats are essentially restricted to the photic zone, while pelagic species are either vertical migrants or deep-sea inhabitants. Note the independent secondary invasion of the pelagic habitat within decabrachians and the shift from pelagic to coastal habitat within octobrachians

in the rate of decay in the arms of octobrachians versus decabrachians. This was reflected in the pH levels, which stayed conducive to phosphatization in octobrachians, though was too high for preservation in the decabrachians (Clements et al., 2017: fig. 2). Interestingly, suckers of decabrachians were lost after three days, while octobrachians appear to be taphonomically more resilient. Despite the differences in necrolysis and the according character loss, a fast burial is still required to obtain the superior preservation seen in the coleoids from La Voulte-sur-Rhône (Fuchs & Hoffmann, 2017; Kruta et al., 2016; Rowe et al., 2022, 2023). The decabrachian tissue connecting the head and mantle decayed after about one week, and the mantle tissue supporting the anterior margin of the gladius broke down after about 10 days. These results are consistent with the states observed in the two *Plesioteuthis prisca* specimens depicted in Figs. 11 and 12 where the head in HT 77/23 is offset from the body, and the gladius extends anteriorly beyond the mantle in both specimens.

The selective preservation of axial nerves seen here is supported by the results of decay experiments on chordates by Sansom et al., (2010). They observed that the dorsal nerve chord, (i.e. nerve tissue), was preserved for 130 days. Accordingly, the preferential preservation of the principal arm nerves when compared with mantle tissue becomes understandable. The correctness of their interpretation is, to some degree, supported by the reasonably widespread preservation of the cephalopod cephalic cartilage in Mesozoic coleoids and maybe even in some exceptionally preserved ammonoids (e.g., Fuchs, 2006a, 2006b; Fuchs & Larson, 2011a, 2011b; Klug et al., 2012, 2016, 2019; Jattiot et al., 2015; Klug & Lehmann, 2015; Donovan & Fuchs, 2016; Lukeneder & Lukeneder, 2022).

Homologization of body parts

Identification and homologization of fossilized soft parts is often challenging. This is due, in part, to the selective preservation of tissues, the different modes of

preservation (including mineralization), and compression prior to fossilization, which is quite common in conservation deposits such as black shales and platy limestones. Hence, special attention must be paid to homologization.

The axial nerve cords can be identified based on their position, both the location within the arm crown and their association with the rows of arm hooks, as well as their structure, though this is more difficult to assess as nerve cells are not preserved and there are no surface structures to support the interpretation. Nevertheless, in these specimens, the number, diameter in relation to arm thickness, and the association with the head region suggest that both criteria are fulfilled. In the vampyromorphs from the Middle Jurassic of La Voulte-sur-Rhône, the axial nerve cords are actually preserved in three dimensions and still are surrounded by the arm musculature, thus confirming their nature (Kruta et al., 2016; Rowe et al., 2022, 2023). The criteria of embryology and continuity can only partially be evaluated. The embryonic development of the discussed fossil coleoids is unknown. Nevertheless, the presence of neuronal strands in the arms is well-documented in recent coleoid embryos (Shigeno et al., 2001: fig. 2). By contrast, continuity is given since the axial nerve cords are now documented from several important clades from the fossil record (Fig. 13).

Evolution of the arm crown and its nervous system

The oldest arm crowns of coleoids are those of *Gordoniconus beargulchensis* (AMNH 50267/AMNH 43264) from the Carboniferous of Montana (Klug et al., 2019 and references therein; Whalen & Landman, 2022). The early coleoid fossil *Syllipsimopodi bideni*, published by Whalen and Landman (2022: fig. 4), shares size, proportions, conch shape, preservation, locality and stratum with the conspecific *G. beargulchensis* as supposed by Klug et al. (in press). Their specimen (ROMIP 64897) preserves an arm crown, corroborating the finding of Klug et al. (2019) that this species had ten arms. It appears that the arm length was not uniform in this species (primarily or as a taphonomic artefact?), similar to the Middle Jurassic vampyromorphs from La Voulte-sur-Rhône (Kruta et al., 2016; Rowe et al., 2022). All arms were described with small suckers.

To date, no traces of the nervous system in fossilized arm crowns are known from the Palaeozoic (arm hooks: Doguzhaeva et al., 2007). Although phragmoteuthid arm crowns are reasonably well documented from the Triassic (Doguzhaeva et al., 2018; Fuchs & Donovan, 2018; Fuchs, 2006a; Lukeneder & Lukeneder, 2022; Rieber, 1970), they do not show the axial nerve cords. The oldest axial nerves described in the literature belong to the Toarcian *Chondroteuthis wunnenbergi* presented here.

The Middle Jurassic vampyromorphs from La Voulte-sur-Rhône (Kruta et al., 2016; Rowe et al., 2022, 2023) represent the most convincing examples of preserved axial nerves cords and provide the greatest anatomical detail. Although the intrabrachial ganglia are indiscernible in the fossil material, the morphology of the suckers in these specimens is now well documented; the large suckers with a large infundibulum might indicate the presence of ganglia in front of each sucker as in modern octobrachians. This suggests that these Jurassic forms already had the ability to coordinate precise movements. In contrast, nautilids lack the brain structure for an elaborate control of the arm (Budelmann, 1995). The digital tentacles and cirri of modern nautilids have an axial nerve cord (Kier, 2010; Nixon & Young, 2003) but lack suckers and the associated intrabrachial ganglia. Noteworthy, upon bait stimulation the grooved tentacle tips show a first initial chemosensory response followed by a tactile one (Nixon & Young, 2003). The type of arm armature and how the arms are used could therefore be related to the complexity and structure of the central nervous system. *Nautilus* is considered to have a much simpler nervous system compared with other cephalopods, while octobrachians have larger brachial and pedal lobes compared to decabrachians due to their advanced use of arms (Budelmann, 1995). Although fossil central nervous systems are rare, a complex arm armature could therefore provide indirect evidence for the complexity of the nervous system. The data on arm armature (suckers, hooks) and remnants of the axial nerve cords seem to indicate complex nervous systems were already present in the Palaeozoic.

Studies of the evolution of the nervous system in Palaeozoic cephalopods are hampered by the fact that even if arm crowns were discovered, the placement of the origin of the *Nautilus* lineage is uncertain (compare, e.g., Kröger et al., 2011; Pohle et al., 2022). This complicates interpretations of evolutionary transitions near the cephalopod crown group.

Ecological implications

Cephalopods are world-renowned for comprising some of the most intelligent invertebrates (e.g., Budelmann, 1995; Crook & Basil, 2008; Nixon & Young, 2003; Schnell et al., 2021). What ecological drivers brought molluscs to this point? We cannot provide a satisfying reply to that question yet. However, we hypothesize that a combination of factors was at play, including changes in locomotion, habitat, and the need to process sensory input from

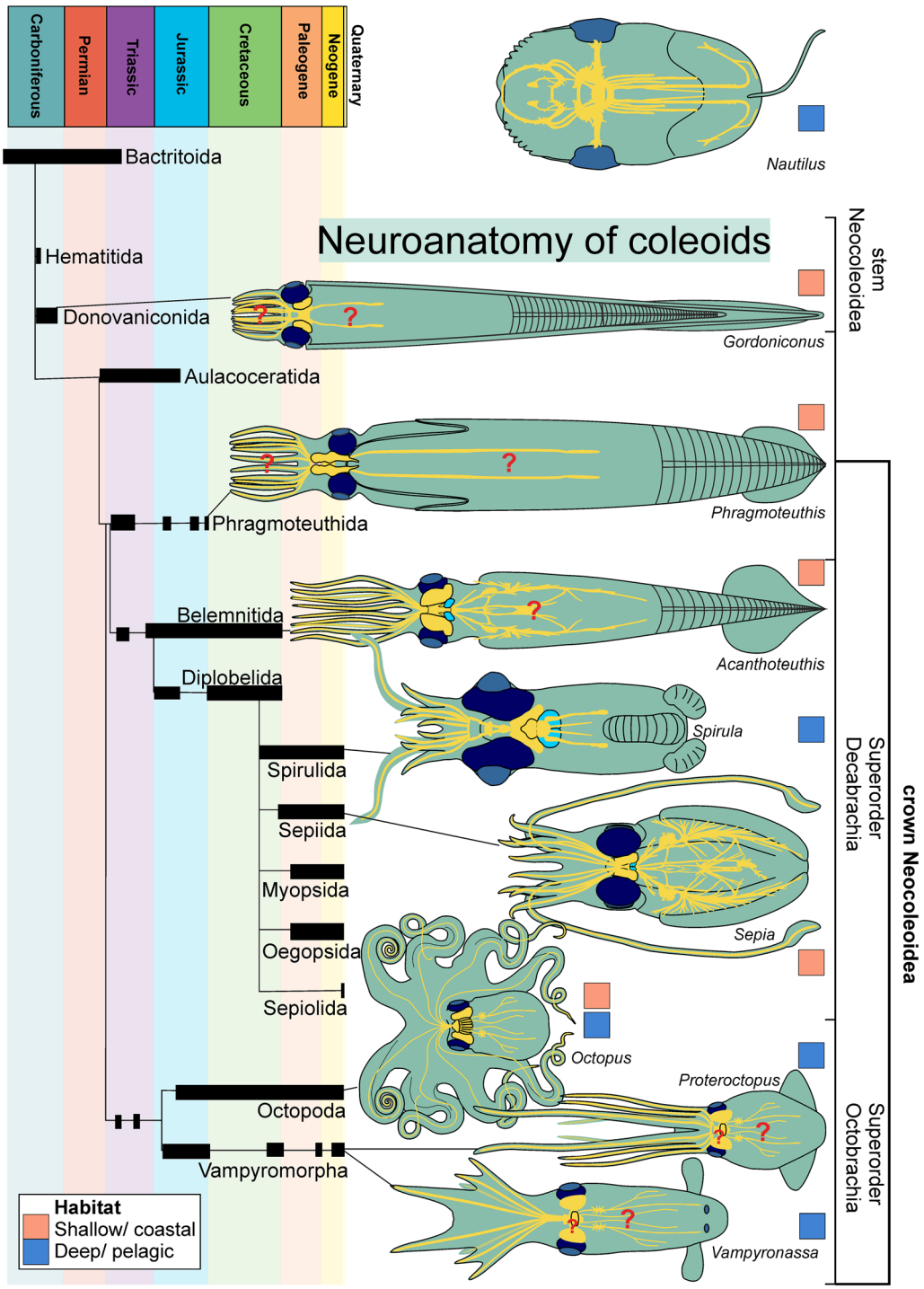

Fig. 14 Coleoid phylogeny (modified after Kröger et al., 2011) with illustrations of the nervous system (yellow), eyes (blue) and statocysts (turquoise) of some fossil and modern representatives of important coleoid clades. *Nautilus* after Budelmann (1996: fig. 4), *Gordoniconus* after Klug et al., (2019), *Phragmoteuthis* after Lukeneder and Lukeneder, (2022), *Acanthoteuthis* after material presented here and Klug et al., (2016), *Spirula* after Huxley and Pelseneer, (1895) and Trombke, (2016: fig. 2, 7–9), *Sepia* after Budelmann, (1996: fig. 1), *Octopus* after Haeckel (1904: pl. 54) and Chung et al., (2022a, 2022b: fig. 6, 7), *Proteroctopus* after Kruta et al., (2016), *Vampyronassa* after Rowe et al., (2022: fig. 1, 5)

an increased number of sensory cells, as well as ecological factors such as rising predatory pressure (e.g., Klug et al., 2017; Vermeij, 1977). The data on the axial nerve cords, which we present here, suggest that the nervous system was already highly evolved in early coleoids (see also Klug et al., 2019) far back in the Palaeozoic.

The axial nerve cords did not deliver much information regarding likely ecological drivers of coleoid evolution. Unsurprisingly, the brain has a larger potential there. As demonstrated by Nixon and Young, (2003), the brains of cephalopods are as diversified as the group itself. In Fig. 14, we present a first overview of the nervous systems of cephalopods including axial nerves and the brains with the optical lobes through phylogeny. So far, not much is known about the nervous system in the body, hence these were tentatively reconstructed based on close relatives. Eye-size varies quite substantially in relation to body size and of the depicted taxa: the deepest diver, *Spirula spirula*, has the largest eyes (e.g., Huxley & Pelseneer, 1895; Nixon & Young, 2003; Trombke, 2016). Surprisingly, the optic lobes vary much less in size than the eyes, although the brain of *Spirula* also appears large in relation to body size. When only the body chamber or soft body in the proostracum region is considered in phragmocone-bearing forms, they also have rather large brains in relation to body (chamber) size.

Remarkably, *Spirula* appears to have rather large statocysts when compared with other cephalopods (Huxley & Pelseneer, 1895; Trombke, 2016). This seems logical given they inhabit the deeper parts of the water column where orientation is hampered by low light conditions and the distance to the sea-floor. By contrast, one might hypothesize that phragmocone-bearing forms are permanently informed about their spatial orientation by their gas-filled phragmocone and thus orient themselves with the gas-filled space usually situated above (e.g., Denton & Gilpin-Brown, 1966; Hoffmann et al., 2015; Jacobs, 1996; Naglik et al., 2016; Peterman et al., 2021; Tajika et al., 2015; Ward, 1979, 1987; Ward & Martin, 1978). Of course, the statocysts also allow the animal to orient itself in the water, both for swimming direction and vertical movement. Hence, sensitive statocysts are more important for non-benthic forms that are nocturnal and/or migrate below the euphotic zone. In the case of *Spirula*, it was recently demonstrated that they occasionally swim with their head facing upward (Lindsay et al., 2020), which seems counter-intuitive since balancing on the gas-filled phragmocone must be difficult and an inefficient use of energy. Nevertheless, the spirulid phragmocone contains a considerable amount of chamber liquid, thereby facilitating these movements. Of course, a refined sense of spatial orientation helps minimize the energetic cost of such actions.

Chung et al., (2022a, 2022b) discovered relationships between brain structure in modern cephalopods and habitat as well as habit. According to these authors, octobrachians with subdivided optic lobes and 7-gyrus vertical lobes are characteristically diurnal species that inhabit the photic zone, while nocturnal species have bean-shaped optic lobes and 5-gyrus vertical lobes (Chung et al., 2022a). Similarly, croissant-shaped optic lobes are typical for diurnal sepiids, while they are bean-shaped in nocturnal species (Chung et al., 2022b). *Vampyroteuthis* has a simple vertical lobe and bean-shaped optic lobes and is a deep-sea dweller. This suggests that the bean-shaped optic lobes are typical for forms that live under low light conditions.

Transferring this knowledge of Chung et al., (2022a, 2022b) to extinct coleoids is hampered by the usually insufficient preservation of the neuroanatomy and the impossibility to observe their behaviour. Additionally, while the host rock of fossils informs us to some degree about the palaeoenvironment but it does not allow conclusions on the exact habitat depth especially when the species under consideration was not benthic or demersal. Our ancestral state reconstructions (Fig. 13) of habitat suggest that light conditions played an important role in coleoid evolution, as switches between shallow and at least partly deep habitats occurred relatively rarely. We are aware that the ancestral state reconstructions have several shortcomings such as the relatively low species coverage, reliance on a single tree despite considerable uncertainties in coleoid phylogenetics (see, e.g., Tanner et al., 2017; Sanchez et al., 2018; Anderson & Lindgren, 2021; Lindgren et al., 2022) and the use of a relatively simplistic model that assumes equal transition rates. Despite this, the signal for the transitions between coastal and pelagic species is quite strong. Therefore, we suggest that these factors do not greatly impact the overall result, though they might contribute a higher amount of uncertainty.

Although we did not include fossil taxa in the ancestral state reconstructions (Fig. 13), we can obtain some information on their habitats from the sediment and associated fauna. This can then be compared to their assumed phylogenetic positions as an independent test.

Concerning the oldest complete coleoid *Gordoniconus* (Klug et al., 2019), the associated fauna suggests a photic zone habitat (Horner & Hanson, 2020). Eyes are not preserved but fragments of the cephalic cartilage are. With some reservation, we suggest a pelagic and nocturnal mode of life, because we assume that their bactritid and orthocerid ancestors had a rather passive nektoplanktic

mode of life as vertical migrants (Kröger, 2003), which rose to shallower water during the night. A potential bias roots in drifting conchs (e.g., Wani et al., 2005; Yacobucci, 2018). However, *Gordoniconus* is fairly common, and several specimens preserve soft tissue-remains (Klug et al., 2019), which are unlikely to be preserved in drifted shells.

Phragmoteuthids are known from several Triassic localities in the Alps such as Polzberg (Lukeneder & Lukeneder, 2021, 2023). Fauna, flora and facies suggest an epipelagic to mesopelagic environment. Their widely accepted phylogenetic position as the last common ancestors of Decabrachia and Octobrachia coincides with the possibly predominantly coastal habitat of stem decabrachians recovered in our Bayesian ancestral state reconstruction of cephalopod habitat distribution (Fig. 13). The cephalic cartilage is unusually well preserved (Lukeneder & Lukeneder, 2022) and displays a quite constricted shape of the optic lobe, providing the anatomical interpretation of these strange cartilages are correct. Chung et al., (2022a, 2022b) found that diurnal octobrachians have distinctly constricted optic lobes while in nocturnal taxa, the optic lobes are more bean-shaped. Presuming the interpretation of its anatomy is correct, *Phragmoteuthis* would thus have been diurnal.

The cephalic cartilage of the stem decabrachiate *Acanthoteuthis* is reasonably well known (Klug et al., 2016: fig. 1b). It is quite constricted, suggesting a diurnal mode of life in the lagoons of the Solnhofen-Eichstätt-Nusplingen archipelago. The same likely applies to the Cretaceous stem octobrachiate *Dorateuthis syriaca* from Lebanon (Fuchs & Larson, 2011a, 2011b). The question arises whether diurnal vertical migration is likely in basins with oxygen impoverished bottom waters. This might be explained by the fact that some organisms do not sink below the twilight zone (Watanabe et al., 2006; Häfker et al., 2017; Kaartvedt et al., 2020), but of course, the lagoons of the Solnhofen archipelago were likely less deep (Kölbl-Ebert & Cooper, 2019). In any case, moving to deeper and thus darker parts of the sea during daylight still was an important strategy to escape predation. The more coastal habitat of many living decabrachians groups coincides with the coastal habitat of stem decabrachians of Germany and Lebanon.

In several respects, the vampyromorphs from the Middle Jurassic of La Voulte-sur-Rhône show the best soft tissue preservation currently known (Kruta et al., 2016; Rowe et al., 2022, 2023). However, their cephalic cartilage is hardly discernible in the tomography images. Despite this, the complex palaeoenvironment of La Voulte-sur-Rhône "*represents a bathyal ecosystem in an offshore environment with steep, fault-controlled bathymetric gradients*" (Rowe et al., 2022: p. 1; see also: Charbonnier, 2009; Charbonnier et al., 2014). Although the fossil assemblage has yielded rare arthropods that are adapted to (eu) photic conditions (Vannier et al., 2016), it is likely that the cephalopod species considered in the present study had a rather deep and certainly pelagic habitat. The general anatomical similarity of at least *Proteroctopus* and *Vampyronassa* to the modern *Vampyroteuthis* suggests a life below the photic zone although we lack direct evidence for the habitat depth (Charbonnier et al., 2014). The supposed photophores of *Vampyrofugiens atramentum* (Rowe et al., 2023) at least suggest a partially dark habitat like in modern *Vampyroteuthis*. Palaeobathymetry often suffers from poor evidence and in the case of the La Voulte-sur-Rhône Lagerstätte, the vampyromorphs have been used as evidence for a bathyal habitat. The different facies and palaeogeographic setting of the La Voulte-sur-Rhône and Solnhofen regions reflect the contrasting depositional depths of the two localities: the complex bathymetry and mix of habitats at La Voulte-sur-Rhône, and the shallow platy limestones of the Solnhofen region were laid down in shallower water. In turn, this suggests a certain diversity in habitat depths of extinct vampyromorphs (e.g., Košťák et al., 2021; Klug et al., 2021b), which is not surprising taking the higher diversity of Jurassic vampyromorphs (about four families with ten genera; see Fuchs et al., 2020) as opposed to the single living species into account.

Overall, neuroanatomical data of Palaeozoic and Mesozoic coleoids are still very patchy (Fig. 14). Based on this sparse evidence and the ancestral state reconstructions, we suggest the following hypotheses, which require more anatomical data of additional species to be adequately tested:

Hypothesis 1: The earliest coleoids (Hematitida, Donovaniconida,? Aulacoceratida) had a tube-like body chamber, which lacked a long forward projecting proostracum. Their bactritid ancestors were diurnal vertical migrants, possibly spending the days in the deep and the nights in shallower water.

Hypothesis 2: Proostracum-bearing predatory ten-armed coleoids (Phragmoteuthida, Belemnitida, Diplobelida) of the Triassic and Jurassic were diurnal and inhabited photic zone habitats.

Hypothesis 3: The neocoleoid crown group originated from diurnal forms of the photic zone.

Hypothesis 4: The split into decabrachians and octobrachians was initially linked with a preference for shallower habitats in decabrachians and for deeper habitats in octobrachians. Both clades diversified ecologically later with subclades living in coastal and pelagic habitats in both coleoid clades.

Conclusions

We document neuroanatomical details of several Mesozoic coleoid species, which were poorly known previously. For example, we portray the axial nerve cords of *Acanthoteuthis*, *Belemnotheutis*, *Chondroteuthis, Plesioteuthis, Proteroctopus, Sueviteuthis* and *Vampyronassa*. Axial nerve cord preservation varies from 3D in the material from la Voulte and flattened phosphatized lines in the other Jurassic materials. We discuss the preservation modes and taphonomy of the arm crown of Mesozoic coleoids.

The new data are combined with data from the literature to provide an overview of the neuroanatomy of several important extinct and extant coleoid clades. The comparison with modern octobrachians and ancestral state reconstructions suggest that a differentiation in habitat depth and diurnal versus nocturnal mode of life might have played an important role in the evolution of the Coleoidea. We propose four hypotheses concerning these evolutionary processes, which require further coleoid species preserved with neuroanatomical detail to test them.

Supplementary Information

The online version contains supplementary material available at https://doi.org/10.1186/s13358-023-00285-3.

Additional file 1. This folder contains all data used for an produced by the Bayesian ancestral state reconstructions of cephalopod habitat distribution.

Acknowledgements

Rosemarie Roth (Zürich) produced some of the UV-photos. Philippe Loubry (Paris) provided photos of the French material. Terry Keenan (Kimmeridge) photographed some specimens for us, which were made accessible by Steve Etches (Kimmeridge). K. Wiedenroth (Hanover) showed RH the illustrated *Chondroteuthis*, deposited at the Bundesanstalt für Geowissenschaften und Rohstoffe (BGR) in Hannover, Germany. We thank Martin Košťák (Prague) and an anonymous reviewer for their constructive criticism.

Author contributions

CK, RH, DF and AP had the idea to describe the material. RH, HT and AR photographed the specimens under white und UV-light. CK produced the figures using photos by HT, RH, and others. AP performed the Bayesian ancestral state reconstructions and made Fig. 13. All authors wrote parts of the text, proofread various versions including the final version and approved of it.

Funding

CK and AP were supported by the Swiss National Science Foundation SNSF (Project nr. 200021_169627). RH and AP received funding from the Deutsche Forschungsgemeinschaft DFG (Project nr. 507867999).

Availability of data and materials

The specimens are stored in the collections of the Geological Institute of the University of Tübingen, Germany (GPIT Ce 1564/2,6/PV-67025), in the collection of Helmut Tischlinger, Stammham, Germany (HT numbers; will be given to a public institution at a later date), in the Etches collection in Kimmeridge, UK (KI306), in the Natural History Museum, London, UK (NHMUK 25966) and in the Bundesanstalt für Geowissenschaften und Rohstoffe (BGR MA 13436). *Proteroctopus* (MNHN.F.R03801) and *Vampyronassa* (MNHN.F.B74244) are deposited in the Muséum national d'Histoire naturelle, Paris. Files for the Bayesian ancestral state reconstruction of cephalopod habitat distribution presented in Fig. 13 are available at XX.

Declarations

Competing interests

We have no competing interests.

Received: 22 May 2023 Accepted: 11 August 2023
Published online: 27 September 2023

References

Anderson, F. E., & Lindgren, A. R. (2021). Phylogenomic analyses recover a clade of large-bodied decapodiform cephalopods. *Molecular Phylogenetics and Evolution, 156*, 107038. https://doi.org/10.1016/j.ympev.2020.107038

Bode, A. (1933). *Chondroteuthis wunnenbergi* n. g., n. sp., eine neue Belemnoideenform, in günstiger Erhaltung. *Jahresbericht Des Niedersächsischen Geologischen Vereins Zu Hannover, 25*, 33–66.

Budelmann, B. U. (1995). The cephalopod nervous system: What evolution has made of the molluscan design. In O. Breidbach & W. Kutsch (Eds.), *The nervous systems of invertebrates: An evolutionary and comparative approach*. Birkhäuser: Basel.

Budelmann, B. U. (1996). Active marine predators: The sensory world of cephalopods. *Marine and Freshwater Behaviour and Physiology, 27*, 59–75.

Buresch, K. C., Sklar, K., Chen, J. Y., Madden, S. R., Mongil, A. S., Wise, G. V., FBoal, J. G., & Hanlon, R. T. (2022). Contact chemoreception in multi-modal sensing of prey by Octopus. *Journal of Comparative Physiology A, 208*, 435–442. https://doi.org/10.1007/s00359-022-01549-y

Charbonnier, S. (2009). *Le Lagerstätte de La Voulte: un environnement bathyal au Jurassique* (p. 272). Publications scientifiques du Muséum Paris.

Charbonnier, S., Audo, D., Caze, B., & Biot, V. (2014). The La Voulte-sur-Rhône Lagerstätte (Middle Jurassic, France). *Comptes Rendus Palevol, 13*, 369–381.

Chase, R., & Wells, M. J. (1986). Chemotactic behaviour in *Octopus*. *Journal of Comparative Physiology A, 158*, 375–381. https://doi.org/10.1007/BF00603621

Chung, W.-S., Kurniawan, N. D., & Marshall, N. J. (2022a). Comparative brain structure and visual processing in octopus from different habitats. *Current Biology, 32*, 97–110. https://doi.org/10.1016/j.cub.2021.10.070

Chung, W.-S., López-Galán, A., Kurniawan, N. D., & Marshall, N. J. (2022b). The brain structure and the neural network features of the diurnal cuttlefish *Sepia plangon*. *iScience, 26*, 105846. https://doi.org/10.1016/j.isci.2022.105846

Chung, W.-S., & Marshall, N. J. (2017). Complex visual adaptations in squid for specific tasks in different environments. *Frontiers in Physiology, 8*, 105. https://doi.org/10.3389/fphys.2017.00105

Clements, T., Colleary, C., De Baets, K., & Vinther, J. (2017). Buoyancy mechanisms limit preservation of coleoid cephalopod soft tissues in Mesozoic Lagerstätten. *Palaeontology, 60*, 1–14.

Crook, R., & Basil, J. (2008). A biphasic memory curve in the chambered nautilus, *Nautilus pompilius* L. (Cephalopoda: Nautiloidea). *Journal of Experimental Biology, 211*, 1992–1998. https://doi.org/10.1242/jeb.018531

De Baets, K., Klug, C., Korn, D., Bartels, C., & Poschmann, M. (2013). Emsian Ammonoidea and the age of the Hunsrück Slate (Rhenish Mountains, Western Germany). *Palaeontographica A, 299*, 1–114.

Denton, E. J., & Gilpin-Brown, J. B. (1966). On the buoyancy of the pearly Nautilus. *Journal of the Marine Biological Association UK, 46*, 723–759.

Doguzhaeva, L. A., Brayard, A., Goudemand, N., Krumenacker, L. J., Jenks, J. F., Bylund, K. G., Fara, E., Olivier, N., Vennin, E., & Escarguel, G. (2018). An Early Triassic gladius associated with soft tissue remains from Idaho, USA—a squid-like coleoid cephalopod at the onset of Mesozoic Era. *Acta Palaeontologica Polonica, 63*, 341–355.

Doguzhaeva, L. A., Mapes, R. H., & Mutvei, H. (2007). A Late Carboniferous coleoid cephalopod from the Mazon Creek Lagerstätte (USA), with a radula, arm hooks, mantle tissues, and ink. In N. H. Landman, R. A. Davis,

& R. H. Mapes (Eds.), *Cephalopods—present and past. New insights and fresh perspectives, 121-143*. The Netherlands: Springer.
Donovan, D. T., & Crane, M. D. (1992). The type material of the Jurassic Cephalopod *Belemnotheutis*. *Palaeontology, 35*, 273–296.
Donovan, D. T., & Fuchs, D. (2016). Fossilized soft tissues in Coleoidea. *Treatise Online Part M Chapter, 13*, 1–29.
Dröscher, A. (2016). Pioneering studies on cephalopod's eye and vision at the stazione zoologica Anton Dohrn (1883–1977). *Frontiers in Physiology, 7*(618), 1–5. https://doi.org/10.3389/fphys.2016.00618
Fischer, J. C., & Riou, B. (1982). Le plus ancien Octopode connu (Cephalopoda, Dibranchiata): Proteroctopus ribeti nov gen., nov. sp., du Callovien de l'Ardèche (France). *Comptes Rendus De L'académie Des Sciences, 295*(2), 277–280.
Fischer, J.-C., & Riou, B. (2002). *Vampyronassa rhodanica* nov. gen. nov sp., vampyromorphe (Cephalopoda, Coleoidea) du Callovien inférieur de La Voulte-sur-Rhône (Ardèche, France). *Annales De Paléontologie, 88*, 1–17.
Frisch, K. (1912). Über Färbung und Farbensinn der Tiere. *Sitzungs-Berichte Gesellschaft Für Morphologie Und Physiologie München, 1912*, 1–9.
Fuchs, D. (2006a). Fossil erhaltungsfähige Merkmalskomplexe der Coleoidea (Cephalopoda) und ihre phylogenetische Bedeutung. *Berliner Paläobiologische Abhandlungen, 8*, 1–122.
Fuchs, D. (2006b). Morphology, taxonomy and diversity of vampyropod coleoids (Cephalopoda) from the upper cretaceous of Lebanon. *Memorie Della Società Italiana Die Scienze Naturali, 34*, 3–27.
Fuchs, D. (2016). The gladius and gladius vestige in fossil Coleoidea. *Treatise Online Pt M Chapter, 9B*, 1–23. https://doi.org/10.17161/to.v0i0.6488
Fuchs, D., Boletzky, S. V., & Tischlinger, H. (2010). New evidence of functional suckers in belemnoid coleoids weakens support for the "Neocoleoidea" concept. *Journal of Molluscan Studies, 76*, 404–406.
Fuchs, D., & Donovan, D. T. (2018). Systematic descriptions: Phragmoteuthida. *Treatise Online Pt M Chapter, 23C*, 1–7.
Fuchs, D., & Hoffmann, R. (2017). Arm armature in belemnoid coleoids. *Treatise Online Pt M Chapter, 10*, 1–20.
Fuchs, D., Laptikhovsky, V., Nikolaeva, S., Ippolitov, A., & Rogov, M. 2020. Evolution of reproductive strategies in coleoid mollusks. *Paleobiology*, *46*, 82–103. https://doi.org/10.1017/pab.2019.41
Fuchs, D., Hoffmann, R., & Klug, C. (2021). Evolutionary development of the cephalopod arm armature: A review. *Swiss Journal of Palaeontology, 140*, 1–18. https://doi.org/10.1186/s13358-021-00241-z
Fuchs, D., & Larson, N. L. (2011a). Diversity, morphology, and phylogeny of coleoid cephalopods from the upper Cretaceous Plattenkalks of Lebanon—Part I: Prototeuthidina. *Journal of Paleontology, 85*, 234–249.
Fuchs, D., & Larson, N. L. (2011b). Diversity, morphology and phylogeny of coleoid cephalopods from the upper Cretaceous Plattenkalks of Lebanon—Part II: Teudopseina. *Journal of Paleontology, 85*, 815–834.
Graziadei, P. (1962). Receptors in the suckers of *Octopus*. *Nature, 195*, 57–59.
Haas, W. (1997). Der Ablauf der Entwicklugsgeschichte der Decabrachia (Cephalopoda, Coleoidea). *Palaeontographica A, 245*, 63–81. https://doi.org/10.1002/spp2.1511
Haeckel, E. (1866). *Generelle Morphologie der Organismen. Allgemeine Grundzüge der organischen Formen-wissenschaft, mechanisch begründet durch die von Charles Darwin reformirte Descendenztheorie*. Berlin: De Gruyter.
Haeckel, E. (1904). *Kunstformen der Natur*. Leipzig und Wien: Bibliographisches Institut.
Häfker, N. S., Meyer, B., Last, K. S., Pond, D. W., Hüppe, L., & Teschke, M. (2017). Circadian clock involvement in zooplankton diel vertical migration. *Current Biology, 27*, 2194–2201.
Hess, C. (1902). Über das Vorkommen von Sehpurpur bei Cephalopoden. *Centralblatt Physiologie, 16*, 91.
Hess, C. (1905). Beiträge zur Physiologie und Anatomie des Cephalopodenauges. *Pflügers Archiv Der Gesellschaft Für Physiologie, 109*, 393–439. https://doi.org/10.1007/BF01677979
Hess, C. (1912). *Vergleichende Physiologie des Gesichtssinnes*. Jena: G. Fischer.
Hoffmann, R., Howarth, M. K., Fuchs, D., Klug, C., & Korn, D. (2022). The higher taxonomic nomenclature of Devonian to Cretaceous ammonoids and Jurassic to Cretaceous ammonites including their authorship and publication. *Neues Jahrbuch Für Geologie Und Paläontologie, Abhandlungen, 305*, 187–197.
Hoffmann, R., Lemanis, R., Naglik, C., & Klug, C. (2015). Ammonoid buoyancy. In C. Klug, D. Korn, K. De Baets, I. Kruta, & R. H. Mapes (Eds.), *Ammonoid paleobiology, Volume I: from anatomy to ecology*. Dordrecht: Springer.
Hoffmann, R., Weinkauf, M. F. G., & Fuchs, D. (2017). Grasping the shape of belemnoid arm hooks—a quantitative approach. *Paleobiology, 43*, 304–320.
Höhna, S., Landis, M. J., Heath, T. A., Boussau, B., Lartillot, N., Moore, B. R., Huelsenbeck, J. P., & Ronquist, F. (2016). RevBayes: Bayesian phylogenetic inference using graphical models and an interactive model-specification language. *Systematic Biology, 65*, 726–736. https://doi.org/10.1093/sysbio/syw021
Horner, J. R., & Hanson, D. A. (2020). Vertebrate paleontology of Montana. MBMG Special Publication. *Geology of Montana, 122*(2), 1–46.
Huxley, T. H., & Pelseneer, P. (1895). *Zoölogy of the Voyage of H. M. S. Challenger: Part I., XXXII. Report on* Spirula. *VIII.*, 32 and 12, pp. 4, 6 pls
Jacobs, D. K. (1996). Chambered cephalopod shells, buoyancy, structure, and decoupling: History and red herrings. *Palaios, 11*, 610–614.
Jattiot, R., Brayard, A., Fara, E., & Charbonnier, S. (2015). Gladius-bearing coleoids from the upper Cretaceous Lebanese Lagerstätten: Diversity, morphology, and phylogenetic implications. *Journal of Paleontology, 89*, 148–167.
Jeletzky, J. A. (1966). Comparative morphology, phylogeny, and classification of fossil Coleoidea. *University of Kansas Paleontological Contributions, Mollusca, 7*, 162
Jeletzky, J. A. (1965). Taxonomy and phylogeny of fossil Coleoidea (=Dibranchiata). *Geological Survey of Canada Papers, 65–2*(42), 72–76.
Kaartvedt, S., Røstad, A., Christiansen, S., & Klevjer, T. A. (2020). Diel vertical migration and individual behavior of nekton beyond the ocean's twilight zone. *Deep-Sea Research I, 160*(103280), 1–6. https://doi.org/10.1016/j.dsr.2020.103280
Katz, I., Shomrat, T., & Nesher, N. (2021). Feel the light: sight-independent negative phototactic response in octopus arms. *Journal of Experimental Biology, 24*, jeb237529. https://doi.org/10.1242/jeb.237529
Kier, W. M. (2010). The functional morphology of the tentacle musculature of *Nautilus pompilius*. In W. B. Saunders & N. H. Landman (Eds.), *Nautilus: The biology and Paleobiology of a living fossil, reprint with additions*. Dordrecht: Springer Netherlands.
Kingston, A. C. N., Kuzirian, A. M., Hanlon, R. T., & Cronin, T. W. (2015a). Visual phototransduction components in cephalopod chromatophores suggest dermal photoreception. *The Journal of Experimental Biology, 218*, 1596–1602. https://doi.org/10.1242/jeb.117945
Kingston, A. C. N., Wardill, T. J., Hanlon, R. T., & Cronin, T. W. (2015b). An unexpected diversity of photoreceptor classes in the longfin squid Doryteuthis pealeii. *PLoS ONE, 10*(9), e0135381. https://doi.org/10.1371/journal.pone.0135381
Klinghardt, F. (1932). Über den methodischen Nachweis der Eingeweide bei fossilen Tintenfischen. *Paläontologische Zeitschrift, 14*, 160–164.
Klug, C., Davesne, D., Fuchs, D., & Argyriou, T. (2020). First record of non-mineralized cephalopod jaws and arm hooks from the latest Cretaceous of Eurytania Greece. *Swiss Journal of Palaeontology, 139*(9), 1–13.
Klug, C., Frey, L., Pohle, A., De Baets, K., & Korn, D. (2017). Palaeozoic evolution of animal mouthparts. *Bulletin of Geosciences*. https://doi.org/10.3140/bull.geosci.1648
Klug, C., Fuchs, D., Schweigert, G., Röper, M., & Tischlinger, H. (2015). New anatomical information on arms and fins from exceptionally preserved *Plesioteuthis* (Coleoidea) from the Late Jurassic of Germany. *Swiss Journal of Palaeontology, 134*, 245–255.
Klug, C., Landman, N. H., Fuchs, D., Mapes, R. H., Pohle, A., Gueriau, P., Reguer, S., & Hoffmann, R. (2019). Anatomy of the first Coleoidea and character evolution in the Carboniferous. *Communications Biology, 2*(280), 1–12. https://doi.org/10.1038/s42003-019-0523-2
Klug, C., & Lehmann, J. (2015). Soft part anatomy of ammonoids: reconstructing the animal based on exceptionally preserved specimens and actualistic comparisons. In C. Klug, D. Korn, K. I. De Baets, & R. H. Mapes (Eds.), *Ammonoid paleobiology, Volume I: from anatomy to ecology Topics in Geobiology*. Dordrecht: Springer.
Klug, C., Pohle, A., Roth, R., Hoffmann, R., Wani, R., & Tajika, A. (2021a). Preservation of nautilid soft parts inside and outside the conch interpreted as central nervous system, eyes, and renal concrements from the Lebanese Cenomanian. *Swiss Journal of Palaeontology, 140*, 11. https://doi.org/10.1186/s13358-021-00229-9
Klug, C., Riegraf, W., & Lehmann, J. (2012). Soft-part preservation in heteromorph ammonites from the Cenomanian-Turonian boundary

event (OAE 2) in the Teutoburger Wald (Germany). *Palaeontology, 55*, 1307–1331.
Klug, C., Schweigert, G., Fuchs, D., & De Baets, K. (2021b). Distraction sinking and fossilized Coleoid predatory behaviour from the German Early Jurassic. *Swiss Journal of Palaeontology, 140*, 1–12. https://doi.org/10.1186/s13358-021-00218-y
Klug, C., Schweigert, G., Fuchs, D., Kruta, I., & Tischlinger, H. (2016). Adaptations to squid-style high-speed swimming in Jurassic belemnitids. *Biology Letters, 12*, 20150877.
Klug, C., Schweigert, G., Tischlinger, H., & Pochmann, H. (2021c). Failed prey or peculiar necrolysis? Isolated ammonite soft body from the Late Jurassic of Solnhofen (Germany). *Swiss Journal of Palaeontology, 140*, 15. https://doi.org/10.1186/s13358-020-00215-7
Klug, C., Stevens, K., Hoffmann, R., Zaton, M., Košťák, M., Weis, R., De Baets, K., Lehmann, J., Fuchs, D., & Vinther, J. Revisiting the identification of *Syllipsimopodi bideni* and timing of the decabrachian-octobrachian divergence. *Nature Communications* **(in press)**.
Kölbl-Ebert, M., & Cooper, B. J. (2019). Solnhofener Plattenkalk: A heritage stone of international significance from Germany. *Geological Society London Special Publications, 486*, 103–113.
Kröger, B. (2003). The size of siphuncle in cephalopod evolution. *Senckenbergiana Lethaea, 83*, 39–52.
Kröger, B., Vinther, J., & Fuchs, D. (2011). Cephalopod origin and evolution: A congruent picture emerging from fossils, development and molecules. *BioEssays, 33*, 1–12.
Kruta, I., Rouget, I., Charbonnier, S., Bardin, J., Fernandez, V., Germain, D., Brayard, A., & Landman, N. H. (2016). *Proteroctopus ribeti* in coleoid evolution. *Palaeontology, 59*, 767–773.
Larson, N. L., Morton, R. W., Larson, P. L., & Bergmann, U. (2010). A new look at fossil cephalopods. In K. Tanabe, Y. Shigeta, T. Sasaki, & H. Hirano (Eds.), *Cephalopods—present and past* (pp. 303–314). Tokai University Press.
Lee, P. G. (1992). Chemotaxis by *Octopus maya* Voss et Solis in a Y-maze. *Journal of Experimental Marine Biology and Ecology, 156*, 53–67. https://doi.org/10.1016/0022-0981(92)90016-4
Lewis, P. O. (2001). A likelihood approach to estimating phylogeny from discrete morphological character data. *Systematic Biology, 50*, 913–925. https://doi.org/10.1080/106351501753462876
Lindgren, A. R., Pratt, A., Vecchione, M., & Anderson, F. E. (2022). Finding a home for the ram's horn squid: Phylogenomic analyses support *Spirula spirula* (Cephalopoda: Decapodiformes) as a close relative of Oegopsida. *Organisms Divsersity & Evolution, 23*, 91–101. https://doi.org/10.1007/s13127-022-00583-7
Lindsay, D. J., Hunt, J. C., McNeil, M., Beaman, R. J., & Vecchione, M. (2020). The first in situ observation of the ram's horn squid *Spirula spirula* turns "common knowledge" upside down. *Diversity, 12*(449), 6. https://doi.org/10.3390/d12120449
Linnaeus, C. (1758). *Systema Naturae per regna tria naturae, secundum classes, ordines, genera, species, cum characteribus, differentiis, synonymis, locis.* 10th revised edition, vol. 1: 824 pp. Laurentius Salvius: Holmiae.
Lukeneder, A., & Lukeneder, P. (2021). The upper Triassic Polzberg palaeobiota from a marine Konservat-Lagerstätte deposited during the Carnian Pluvial Episode in Austria. *Scientific Reports, 11*(16644), 1–14. https://doi.org/10.1038/s41598-021-96052-w
Lukeneder, A., & Lukeneder, P. (2023). New data on the marine upper Triassic palaeobiota from the Polzberg Konservat-Lagerstätte in Austria. *Swiss Journal of Palaeontology, 142*, 1–14. https://doi.org/10.1186/s13358-023-00269-3
Lukeneder, P., & Lukeneder, A. (2022). Mineralized belemnoid cephalic cartilage from the late Triassic Polzberg Konservat-Lagerstätte (Austria). *PLoS ONE, 17*(4), e0264595. https://doi.org/10.1371/journal.pone.0264595
Mantell, G. A. (1854). *The Medals of Creation: Or, First Lessons in Geology and the Study of Organic Remains*. H.G. Bohn, London.
Mantell, G. A. (1848). Observations on some belemnites and other fossil remains of Cephalopoda, discovered by Mr. Reginald Neville Mantell, C.E. in the Oxford Clay near Trowbridge, in Wiltshire. *Philosophical Transactions of the Royal Society, 138*, 171–182.
Maselli, V., Al-Soudy, A.-S., Buglione, M., Aria, M., Polese, G., & Di Cosmo, A. (2020). Sensorial hierarchy in Octopus vulgaris's food choice: chemical vs. visual. *Animals, 10*, 457. https://doi.org/10.3390/ani10030457
Messenger, J. B. (1977). Evidence that *Octopus* is colour-blind. *Journal of Experimental Biology, 70*, 49–55.
Messenger, J. B., Wilson, A. P., & Hedge, A. (1973). Some evidence for colour-blindness in *Octopus*. *Journal of Experimental Biology, 59*, 77–94.
Mironenko, A. A., Boiko, M. S., Bannikov, A. F., Arkhipkin, A. I., Bizikov, V. A., & Košťák, M. (2021). First discovery of the soft-body imprint of an Oligocene fossil squid indicates its piscivorous diet. *Lethaia, 54*, 793–805. https://doi.org/10.1111/let.12440
Münster, G. Zu, G. (1839). Decapoda Macroura Abbildung und Beschreibung der fossilen langschwänzigen Krebse in den Kalkschiefern von Bayern. In: Münster, G. Zu, G. (eds). Beiträge zur Petrefacten-Kunde
Naef, A. (1922). *Die fossilen Tintenfische. Eine paläozoologische Monographie.* Jena (Fischer). 322 pp.
Naglik, C., Rikhtegar, F. N., & Klug, C. (2016). Buoyancy in Palaeozoic ammonoids from empirical 3D-models and their place in a theoretical morphospace. *Lethaia, 49*, 3–12. https://doi.org/10.1111/let.12125
Nixon, M., & Young, J. Z. (2003). *The brains and lives of cephalopods* (p. 392). Oxford: Oxford University Press.
Owen, R. (1844). VI. A description of certain Belemnites, preserved, with a great proportion of their soft parts, in the Oxford Clay, at Christian-Malford, Wilts. *Transactions of the Royal Society of London, 5*, 65–85.
Pagel, M., Meade, A., & Barker, D. (2004). Bayesian estimation of ancestral character states on phylogenies. *Systematic Biology, 53*, 637–684. https://doi.org/10.1080/10635150490522232
Pearce, J. C. (1842). On the mouths of ammonites, and on fossil contained in laminated beds of the Oxford Clay, discovered in cutting the Great Western Railway, near Christian Malford in Wiltshire. *Proceedings of the Geological Society of London, 3*, 592–594.
Pearce, J. C. (1847). On the fossil Cephalopoda constituting the genus *Belemnotheutis*, Pearce. *London Geological Journal, 2*, 75–78.
Peterman, D. J., Ritterbush, K. A., Ciampaglio, C. N., Johnson, E. H., Inoue, S., Mikami, T., & Linn, T. J. (2021). Buoyancy control in ammonoid cephalopods refined by complex internal shell architecture. *Scientific Reports, 11*(8055), 12. https://doi.org/10.1038/s41598-021-87379-5
Pohle, A., Kröger, B., Warnock, R. C. M., King, A. H., Evans, D. H., Aubrechtová, M., Cichowolski, M., Fang, X., & Klug, C. (2022). Early cephalopod evolution clarified through Bayesian phylogenetic inference. *BMC Biology, 20*, 88.
Ramirez, M. D., & Oakley, T. H. (2015). Eye-independent, light-activated chromatophore expansion (LACE) and expression of phototransduction genes in the skin of *Octopus bimaculoides*. *The Journal of Experimental Biology, 218*, 1513–1520. https://doi.org/10.1242/jeb.110908
Reitner, J., & Engeser, T. (1982). Phylogenetic trends in phragmocone-bearing coeloids (Belemnomorpha). *Neues Jahrbuch Für Geologie Und Paläontologie, 164*, 156–162. https://doi.org/10.23689/fidgeo-2450
Rieber, H. (1970). *Phragmoteuthis*? *ticinensis* n. sp., ein Coleoidea-Rest aus der Grenzbitumenzone (Mittlere Trias) des Monte San Giorgio (Kt. Tessin, Schweiz). *Paläontologische Zeitschrift, 44*, 32–40.
Robson, G. C. (1929). On the rare abyssal octopod *Melanoteuthis beebei* (sp. n.): A contribution to the phylogeny of the Octopoda. *Proceedings of the Zoological Society of London, 3*, 469–486.
Rowe, A. J., Kruta, I., Landman, N. H., Villier, L., Fernandez, V., & Rouget, I. (2022). Exceptional soft-tissue preservation of Jurassic *Vampyronassa rhodanica* provides new insights on the evolution and palaeoecology of vampyroteuthids. *Scientific Reports, 12*, 8292. https://doi.org/10.1038/s41598-022-12269-3
Rowe, A. J., Kruta, I., Villier, L., & Rouget, I. (2023). A new vampyromorph species from the Middle Jurassic La Voulte-sur-Rhône Lagerstätte. *Papers in Palaeontology, 1511*, 1–17. https://doi.org/10.1002/spp2.1511
Rüppell, E. (1829). Abbildung und Beschreibung einiger neuer oder weniger bekannten Versteinerungen aus der Kalkschieferformation von Solnhofen (p. 12). Brönner: Frankfurt a. M.
Sanchez, G., Setiamarga, D. H. E., Tuanapaya, S., Tongtherm, K., Winkelmann, I. E., Schmidbaur, H., Umino, T., Albertin, C., Allcock, L., Perales-Raya, C., Gleadall, I., Strugnell, J. M., Simakov, O., & Nabhitabhata, J. (2018). Genus-level phylogeny of cephalopods using molecular markers: current status and problematic areas. *PeerJ, 6*, e4331. https://doi.org/10.7717/peerj.4331
Sansom, R. S., Gabbott, S. E., & Purnell, M. E. (2010). Non-random decay of chordate characters causes bias in fossil interpretation. *Nature, 463*, 797–800. https://doi.org/10.1038/nature08745
Schnell, A. K., Boeckle, M., Rivera, M., Clayton, N. S., & Hanlon, R. T. (2021). Cuttlefish exert self-control in a delay of gratification task. *Proceedings of the Royal Society B, 288*, 20203161. https://doi.org/10.1098/rspb.2020.3161

Seilacher, A. (1970). Begriff und Bedeutung der Fossil-Lagerstätten. *Neues Jahrbuch Für Geologie Und Paläontologie, Monatshefte, 1970*, 34–39.
Shigeno, S., Kidokoro, H., Tsuchiya, K., Segawa, S., & Yamamoto, M. (2001). Development of the brain in the oegopsid squid, *Todarodes pacificus*: An atlas up to the hatching stage. *Zoological Science, 18*, 527–541. https://doi.org/10.2108/zsj.18.527
Stubbs, A. L., & Stubbs, C. W. (2016). Spectral discrimination in color blind animals via chromatic aberration and pupil shape. *Proceedings of the National Academy of Science u.s.a, 113*, 8206–8211. https://doi.org/10.1073/pnas.1524578113
Tajika, A., Naglik, C., Morimoto, N., Pascual-Cebrian, E., Hennhöfer, D. K., & Klug, C. (2015). Empirical 3D-model of the conch of the Middle Jurassic ammonite microconch Normannites, its buoyancy, the physical effects of its mature modifications and speculations on their function. *Historical Biology, 27*, 181–191.
Tanner, A. R., Fuchs, D., Winkelmann, I. E., Gilbert, M. T. P., Pankey, M. S., Ribeiro, A. M., Kocot, K. M., Halanych, K. M., Oakley, T. H., da Fonseca, R. R., Pisani, D., & Vinther, J. (2017). Molecular clocks indicate turnover and diversification of modern coleoid cephalopods during the Mesozoic Marine Revolution. *Proceedings of the Royal Society B, 284*, 20162818. https://doi.org/10.1098/rspb.2016.2818
Tribble, C., Freyman, W. A., Landis, M. J., Lim, J. Y., Barido-Sottani, J., Kopperud, B. T., Höhna, S., & May, M. R. (2022). RevGadgets: An R package for visualizing Bayesian phylogenetic analyses from RevBayes. *Methods in Ecology and Evolution, 13*, 314–323. https://doi.org/10.1111/2041-210X.13750
Trombke, G. (2016). *Morphologische und volumetrische Analysen des Nervensystems und sensorischer Strukturen von* Spirula spirula *Linnaeus, 1758*. 49 pp. BSc thesis, Bonn University.
Vannier, J., Schoenemann, B., Gillot, B., Charbonnier, S., & Clarkson, E. (2016). Exceptional preservation of eye structure in arthropod visual predators from the Middle Jurassic. *Nature Commununications, 7*, 10320. https://doi.org/10.1038/ncomms10320
Vermeij, G. J. (1977). The Mesozoic marine revolution: Evidence from snails, predators and grazers. *Paleobiology, 3*, 245–258. https://doi.org/10.1017/S0094837300005352
Wani, R., Kase, T., Shigeta, Y., & De Ocampo, R. (2005). New look at ammonoid taphonomy, based on field experiments with modern chambered nautilus. *Geology, 33*, 849–852. https://doi.org/10.1131/G21712.1
Ward, P. D. (1979). Cameral liquid in *Nautilus* and ammonites. *Paleobiology, 5*, 40–49.
Ward, P. D. (1987). *The natural history of nautilus*. Allen and Unwin.
Ward, P. D., & Martin, A. W. (1978). On the buoyancy of the Pearly Nautilus. *Journal of Experimental Zoology, 205*, 5–12.
Watanabe, H., Kubodera, T., Moku, M., & Kawaguchi, K. (2006). Diel vertical migration of squid in the warm core ring and cold water masses in the transition region of the western North Pacific. *Marine Ecology Progress Series, 315*, 187–197.
Wells, M. J. (1963). Taste by touch: Some experiments with *Octopus*. *Journal of Experimental Biology, 40*, 187–193. https://doi.org/10.1242/jeb.40.1.187
Wells, M. J. (1964). Detour experiments with Octopuses. *Journal of Experimental Biology, 41*, 621–642. https://doi.org/10.1242/jeb.41.3.621
Whalen, C. D., & Landman, N. H. (2022). Fossil coleoid cephalopod from the Mississippian Bear Gulch Lagerstätte sheds light on early vampyropod evolution. *Nature Communications, 13*(1107), 1–11. https://doi.org/10.1038/s41467-022-28333-5
Yacobucci, M. M. (2018). Postmortem transport in fossil and modern shelled cephalopods. *PeerJ, 6*(e5909), 1–29. https://doi.org/10.7717/peerj.5909
Young, J. (1971). *The anatomy of the nervous systems of "Octopus Vulgaris."* Clarendon Press.
Zittel, K. A. (1884). *Handbuch der Palaeontologie. I. Abteilung Palaeozoologie. II. Band. Mollusca und Arthropoda*. 958 pp. München, (Oldenbourg).

Publisher's Note

Conservation exceptionnelle des tissus mous de céphalopodes coléoïdes mésozoïques : les clés d'une histoire

Résumé : Les coléoïdes (seiches, calmars et pieuvres) représentent 99 % des quelque 800 espèces de céphalopodes modernes et jouent un rôle clé dans les écosystèmes marins actuels. Comme ils sont principalement à corps mou, ils sont rarement conservés dans les archives fossiles et les relations entre les groupes fossiles et modernes restent floues. Cela empêche d'établir une chronologie bien étayée de l'origine des clades modernes et des changements de niches écologiques paléo- et modernes. Heureusement, certains Lagerstätten mésozoïques conservent des tissus mous et les progrès des techniques d'imagerie non destructives offrent de nouvelles voies pour les études anatomiques. Cette thèse se concentre sur les coléoïdes de deux Lagerstätten dont les paléoenvironnements et la préservation sont contrastés.
Les fossiles 3D uniques de l'environnement bathyal de La Voulte-sur-Rhône (Callovien, France) et les fossiles 2D des calcaires d'eau peu profonde du Crétacé supérieur (Cénomanien et Santonien) du Liban sont étudiés en utilisant une combinaison de techniques d'imagerie à haute résolution (par exemple, les scans µCT, XRF, RTI). Plusieurs spécimens de *Vampyronassa rhodanica* de La Voulte-sur-Rhône ont été imagés à l'aide de la microtomographie à rayons X, ce qui a permis de réexaminer l'anatomie des tissus mous. Les comparaisons entre les taxons fossiles et les taxons existants, y compris le seul membre de la famille existant, *Vampyroteuthis infernalis*, ont démontré que les caractères des *Vampyroteuthis* étaient présents dans les taxons jurassiques. Ces recherches ont également permis d'attribuer un nouveau taxon, *Vampyrofugiens atramentum*. *Dorateuthis syriaca* est abondant dans les affleurements libanais (~9 My). Une étude, la plus grande pour *D. syriaca*, combinant l'imagerie à haute résolution et des mesures complètes sur 54 individus, a permis de réévaluer l'holotype et l'espèce, révélant des informations systématiques et écologiques jusqu'alors inconnues. Ces techniques d'imagerie permettent une analyse comparative significative entre les coléoïdes mésozoïques et les coléoïdes existants et démontrent leur diversité écologique et leur importance au cours du Mésozoïque.

Abstract: Coleoids (cuttlefish, squid, and octopuses) represent 99% of the ~800 species of modern cephalopods and play key roles in modern marine ecosystems. As they are predominantly soft-bodied, they rarely preserve in the fossil record and relationships between fossil and modern groups remain unclear. This prevents a well-supported timeline outlining the origination of modern clades and shifts to paleo- and modern ecological niches. Fortunately, some Mesozoic Lagerstätten preserve soft tissues, and advances in non-destructive imaging techniques offer new pathways for anatomical studies. This thesis focuses on coleoids from two Lagerstätten with contrasting palaeoenvironments and preservation.
The unique 3D fossils of the bathyal La Voulte-sur-Rhône (Callovian, France), and the 2D fossils from the shallow-water limestones of the Upper Cretaceous (Cenomanian and Santonian) of Lebanon are studied using a combination of high-resolution imaging techniques (e.g., µCT scans, XRF, RTI). Multiple specimens of *Vampyronassa rhodanica* from La Voulte-sur-Rhône, were imaged using X-ray microtomography, enabling a re-examination of soft tissue anatomy. Comparisons between fossil and extant taxa, including its only extant family member, *Vampyroteuthis infernalis*, demonstrated that *Vampyroteuthis* characters were present in Jurassic taxa. These investigations also enabled the assignment of a new taxon, *Vampyrofugiens atramentum*. *Dorateuthis syriaca* is abundant in the Lebanese outcrops (~9 My). A study combining high-resolution imaging and comprehensive measurements on 54 individuals, the largest for *D. syriaca*, enabled the reappraisal of the holotype and species, revealing previously unknown systematic and ecological information. These imaging techniques enable meaningful comparative analysis between Mesozoic and extant coleoids and demonstrate their ecological diversity and importance during the Mesozoic.

Exceptional preservation of soft tissues in Mesozoic coleoid cephalopods: The keys to a story